Targeting fatty acid metabolism in prostate cancer

Chui Yan Mah

Supervisors: Professor Lisa Butler,
Dr. Zeyad Nassar and Professor David Lynn

Adelaide Medical School, Faculty of Health and Medical Sciences,
The University of Adelaide
&
Prostate Cancer Research Group
South Australian Health and Medical Research Institute

A thesis submitted in total fulfilment of the
requirements for the degree of Doctor of Philosophy (Medicine)

April 2021

Declaration

I certify that this work contains no material which has been accepted for the award of any other degree or diploma in my name, in any university or other tertiary institution and, to the best of my knowledge and belief, contains no material previously published or written by another person, except where due reference has been made in the text. In addition, I certify that no part of this work will, in the future, be used in a submission in my name, for any other degree or diploma in any university or other tertiary institution without the prior approval of the University of Adelaide and where applicable, any partner institution responsible for the joint-award of this degree.

I acknowledge that copyright of published works contained within this thesis resides with the copyright holder(s) of those works.

I also give permission for the digital version of my thesis to be made available on the web, via the University's digital research repository, the Library Search and also through web search engines, unless permission has been granted by the University to restrict access for a period of time.

I acknowledge the support I have received for my research through the provision of an Australian Government Research Training Program Scholarship.

Chui Yan Mah
South Australian Health and Medical Research Institute
Adelaide Medical School
The University of Adelaide

“For I know the plans I have for you,” declares the Lord, “plans to prosper you and not to harm you, plans to give you hope and a future.”

Jeremiah 29:11

To my late father who inspired my entire scientific journey,
this is for you.

Mah Wai Keong (1965 - 2008)

Acknowledgments

I honestly didn't think that writing the acknowledgements' section would be this hard. There are a lot of emotions going through my head, and memories that I can never forget, as I try my best to 'pen down' the thoughts in my head at this very moment. I am so, so incredibly thankful for the opportunity to pursue a PhD, and most importantly, for the people who have journeyed with me, stood by me, believed in me, encouraged me, and loved me – I just simply don't have the words to describe how immensely grateful I am for all of you (but I'll try!).

Lisa, you're such an inspiration! I remember listening to you speak as one of the guest lecturers for our third year undergraduate Biochemistry subject, that was when it hit me, "I want to be like her!", "She is goals!". At that time, I already knew I wanted to do a PhD and so I decided to email you in hopes that I could one day be a part of your lab and working with you. Thank you for saying 'yes' to taking me in as your student 4 years ago. Thank you for all your support and encouragements, for believing in me when I was doubting myself, for letting me cry in your office, for allowing me to speak up whenever I had problems/personal issues, and for helping me find solutions despite your busy schedule. Thank you for being so patient with me, especially when it comes to my last-minute requests/submissions. Thank you for all the opportunities you've given me that has made me the scientist I am today. Indeed, I couldn't have asked for a better supervisor!

Zeyad, I don't know where to start! When Lisa first introduced us, I thought to myself, "I hope he's friendly", probably because you kept a straight face when we first met. Low and behold, you were definitely not who I pictured you to be. Thank you for being a fun and easy-going, sometimes rather silly, supervisor. I remember you told me how you wanted to be like your previous PhD supervisor, Mo, who helped made your PhD an enjoyable and memorable one! Well, you did it alright. So here goes… Thank you for the car rides (to the beach and work), for letting me drive your car (because you wanted me to teach you how to drive and you needed the extra hours to get your driver's license), for the coffee and chats, for listening to my banters (and bantering with me), for the random ice cream pick-up (because for the very first time, our experiment worked on the first try!!!), for always saying that I'm your

‘best/brilliant student’ (well, I was your only student for the first couple of years), for being so patient with me (I know I can be very emotional), for believing in me even when I didn’t believe in myself (sometimes I can’t tell if you’re actually serious, because every single time I asked you if you think my work was good enough/am I capable enough, you would just say, “Yes, very good”, “It is brilliant”, “You’re amazing”, “You’re doing a great”), for being so supportive in (almost) everything that I do, and for giving me so many opportunities – all I can say is, thank you. I told you that I would write this in, about how during the 4 years of my PhD, I ‘watched you grow’ from a single man, to going on your first date (with my dating advice), to getting married and having your first child! I went a little off topic, but I just want you to know that you’re an awesome supervisor, and I wouldn’t have it any other way.

Thank you to David Lynn and Max Moldovan for guiding me with Bioinformatics. Special thanks to Max for being so patient with me while answering my bucket load of questions and helping me solve errors in my code. I would also like to thank Chung Hoow Kok for being my Bioinformatics 师父, thank you for always looking out for me, for your mentorship, and for your constant encouragements!

Thank you to my lab-partners-in-crime: Adel Aref, Shadrack Mutuku, Josephine Hinneh, Julia Scott, Deanna Miller, Joshua Hodgson, Jacob Truong, Elizabeth Collis, and my beloved Honours student, Takuto Nijiima. I have been fortunate to be involved in the supervision or mentorship of many (summer) students during the course of my PhD. Thanks to all the members of the Prostate Cancer Research Group, past and present, with special thanks to Natalie Ryan (my western blot queen), Swati Irani (my IHC queen), Nicole Moore (my grammar/review queen), Madison Helm (for animal studies), and Joanna Gillis. I’m incredibly grateful to be part of such a fantastic lab family!

Special thanks to the Fantastic 4 – Sabrina Ng, Joshua Chey and Arthur Yeow – for all your love and support, and for keeping me sane throughout my PhD. I don’t know what I’d do without you guys! Sabrina, thank you for sticking with me during some of the lowest points in my life, cheers to many more years of friendship! I would also like to thank Queenie Tangseefa for being such a sweetheart; we met during the EMBL PhD course when I first started my MPhil, thank you for helping me when I

was drowning in the sea of documentations and research proposals, and for being a friendly face around SAHMRI.

To my mother and sister, the pillars of my strength, I love you both and you mean the world to me. Dad passed away too early; you single-handedly raised two daughters on your own, but despite the financial hardships, you managed to send me overseas to pursue my science dream. There were many moments during my PhD when I wanted to quit, but you kept pushing me, encouraging me, and telling me that I'm capable enough to do anything once I put my mind to it. But somehow along the way, you started telling me, "It's okay if you want to quit, just come back home. I will not be disappointed or think that you're not good enough, I just don't want to see you suffer alone and overstressed/overworking yourself. If it's too hard for you, just come home" – this motivated me to become stronger and more resilient. Thank you, mum, and now I can say "I did it!". Thank you, mum, without you, this PhD wouldn't have been possible.

I've met a lot of people and made a lot of new friends throughout my years in Adelaide (be it in the lab, or outside the lab); some stayed till the end, and some left. To those that I may have missed acknowledging here, you have not been forgotten – in one way or another, whether big or small, you have made an impact in my life and that has shaped me to become the person I am today.

To God be the glory, Amen.

Abstract

Prostate cancer (PCa) is the most commonly diagnosed malignancy in men and the second leading cause of cancer-related mortality in the developed world. Prostate cancers are androgen-dependent and rely on androgen receptor signalling for growth and survival. Hence, the mainstay treatment for patients with advanced metastatic PCa is androgen deprivation therapy. Although initially effective, most patients eventually relapse with castrate-resistant prostate cancer (CRPC), and this stage of the disease is ultimately fatal. Despite the clinical development of more potent anti-androgens, these agents are not curative. Alternative treatment strategies are urgently sought to overcome treatment resistance and progression to CRPC. Targeting cancer metabolism has emerged as a promising therapeutic avenue for cancer treatment, especially by targeting upregulated metabolic pathways that promote cancer cell survival. Dysregulation of lipid metabolism is a prominent feature of prostate cancer, and overexpression of key enzymes involved in lipid metabolism is characteristic of both primary and advanced stages of the disease. Moreover, androgens have been shown to regulate lipid metabolism pathways, either directly or indirectly by coordinating with other oncogenic signalling or metabolic networks. Hence, lipid metabolism represents a promising therapeutic vulnerability for the treatment of PCa and could potentially circumvent treatment resistance. While most studies have focused on targeting de novo lipogenesis and, more recently, lipid uptake pathways in cancer, fatty acid oxidation (FAO) remains an underexplored aspect of lipid metabolism. FAO is the dominant bioenergetic pathway in prostate cancer, which has led to interest in exploiting FAO inhibitors as a potential therapeutic strategy to suppress cancer tumorigenesis and overcome treatment resistance. Despite promising preclinical data, FAO inhibitors (ie. etomoxir and perhexiline) used for metabolic diseases have seen rapid decline in their use due to their severe toxicity and side effects. This is attributed to their broad specificity and subsequent off-target effects by targeting the rate limiting enzyme of mitochondrial FAO, carnitine palmitoyltransferase 1 (CPT1). Therefore, it is important that we identify new and more selective targets of FAO. In this dissertation, we characterise two novel and potential targetable FAO enzymes, 2,4-Dienoyl CoA Reductase 1 and 2 (DECR1 and DECR2) respectively.

In Chapter 3, we identified DECR1 as a robustly overexpressed gene in prostate cancer compared to normal or benign tissues and associated with shorter relapse-free survival rates. DECR1 is an auxiliary enzyme involved in polyunsaturated fatty acid (PUFA) oxidation in the mitochondria. Intriguingly, DECR1 is an androgen-repressed gene and besides its fundamental function to produce energy from mitochondrial FAO, DECR1 plays an important role to protect prostate cancer cells from oxidative stress and lipid peroxidation-induced cell death, ferroptosis (caused by the accumulation of peroxidation-prone PUFAs). In Chapter 4, we investigated its peroxisomal counterpart, DECR2, an auxiliary enzyme involved in peroxisomal FAO. To date, there is very limited knowledge on the roles of peroxisomal FAO in PCa and its potential as a therapeutic target. We found that DECR2 is significantly upregulated in prostate cancer and markedly suppressed prostate tumour oncogenesis. Moreover, we uncovered an association between peroxisomal FAO and treatment resistance, as well as a novel link with mitochondrial FAO whereby mitochondrial respiration was maintained in DECR2 knockdown cells likely to support tumour survival. We also provide evidence of cell cycle arrest, a mechanism by which DECR2 or peroxisomal FAO inhibition attenuates prostate cancer cell growth. We utilised thioridazine, a peroxisomal FAO inhibitor as a proof-of-concept that targeting peroxisomal FAO is efficacious and a promising avenue for therapeutic targeting. In Chapter 5, we were also interested whether FAO could play a role as an adaptive survival response in the context of treatment resistance. We analysed a proteomics dataset of AUY922 (heat shock protein 90 inhibitor) treated prostate tumours and found that FAO was a significantly enriched pathway in response to treatment. We then proceeded to evaluate the efficacy of the combination treatment with AUY922 and a clinical FAO inhibitor, perhexiline, and demonstrated enhanced suppressive effects on prostate tumour proliferation compared with individual treatments alone. Taken together, the findings of this thesis support the notion that FAO is a critical survival pathway in PCa progression and treatment resistance. Moreover, targeting FAO represents an exciting and novel therapeutic avenue for PCa treatment and provides a strong rationale for further investigation and clinical development of specific DECR1/2 inhibitors. This thesis also provided novel insights into previously unexplored areas and links of cancer metabolism and opens up new opportunities or questions for future exploration.

Table of Contents

Declaration i
Acknowledgments vii
Abstract xi
Table of Contents xiii
List of Figures and Tables xvii
List of Abbreviations xix
Funding and Awards xxiii
List of Presentations xxv
List of Publications xxix
Chapter 1: General Introduction 1
1.1 Prostate cancer 2
1.1.1 Androgens and the androgen receptor 2
1.1.2 Current methods for the treatment of prostate cancer 2
1.2 Role of lipid metabolism in cancer 4
1.3 Androgens and lipid metabolism in prostate cancer 5
1.4 Fatty Acid Oxidation 20
1.5 Aims and Objectives of Thesis 24
Chapter 2: Materials and Methods 25
2.1 Materials and consumables 26
2.2 Buffers and solutions 29
2.3 Cell Culture 32
2.4 Short-interfering RNA (siRNA) transfection 32
2.5 Immunohistochemistry 33
2.6 Western blot analysis 33
2.7 RNA extraction and quantitative reverse-transcription PCR 34
Chapter 3: DECR1 is a key survival factor that protects prostate cancer cells from ferroptosis 35
3.1 Supplementary figures 73
3.2 Supplementary material for Chapter 3 81
3.2.1 Transcriptomic analysis of DECR1 knockdown LNCaP cells 81
3.2.2 Preparation of LNCaP cells for RNA sequencing 81
3.2.3 Data processing 81

3.2.4 Results: Exploratory data analysis 83
3.2.5 Results: Differential gene expression analysis 86
3.2.6 Results: Pathway enrichment analysis 87
3.2.7 Discussion 94
Chapter 4: Targeting peroxisomal fatty acid oxidation in advanced metastatic prostate cancer 97
4.1 Abstract 100
4.2 Introduction 101
4.3 Materials and methods 103
4.3.1 Cell lines and tissue culture 103
4.3.2 *Ex vivo* culture of human prostate tumours 103
4.3.3 Bioinformatics analysis 104
4.3.4 Western blotting 104
4.3.5 siRNA transfection 104
4.3.6 Generation of stable shDECR2 and hDECR2 LNCaP cells 104
4.3.7 Cell viability 105
4.3.8 Cell migration 105
4.3.9 Colony formation assay 105
4.3.10 Cell cycle analysis 106
4.3.11 Apoptosis assay 106
4.3.12 Neutral lipid content quantification 106
4.3.13 Lipid extraction 107
4.3.14 Mass Spectrometry 107
4.3.15 Data analysis 108
4.3.16 Seahorse extracellular flux assay 108
4.3.17 Membrane fluidity 108
4.3.18 Orthotopic tumour growth 109
4.3.19 Statistical analysis 109
4.4 Results 110
4.4.1 DECR2 is upregulated in clinical prostate tumours and treatment resistance 110
4.4.2 Targeting DECR2 inhibits prostate cancer cell proliferation 112
4.4.3 Inhibition of peroxisomal beta-oxidation by thioridazine suppresses prostate cancer oncogenesis 115

4.4.4 Peroxisomal beta-oxidation inhibition dysregulates lipid metabolism 118
4.4.5 Interplay between peroxisomal and mitochondrial beta oxidation 121
4.4.6 Targeting peroxisomal beta oxidation inhibits prostate cancer cell proliferation by inducing cell cycle arrest 124
4.5 Supplementary figures and tables 127
4.6 Discussion 134
4.7 References 143
Chapter 5: Fatty acid oxidation contributes to treatment resistance in prostate cancer 153
5.1 Introduction 154
Chapter 6: Phospholipid profiling of clinical prostate tumours 171
6.1 Introduction 172
6.2 Abstract 180
6.3 Introduction 181
6.4 Results 183
6.4.1 Tumor-specific lipid profiles are evident in clinical prostate tumors 183
6.4.2 Associations between Lipid Profiles and Malignancy 187
6.4.3 Lipid profile is altered by AR inhibition in patient-derived tumor explants 191
6.4.4 Targeting lipidomic changes in clinical tumors suppresses cellular proliferation 194
6.5 Discussion 197
6.6 Materials and Methods 201
6.6.1 Tissue collection 201
6.6.2 *Ex vivo* culture of primary prostate tissues 201
6.6.3 MALDI mass spectrometry imaging 202
6.6.4 ESI-MS/MS-based lipidomics 203
6.6.5 RNA extraction and sequencing 204
6.6.6 Immunohistochemical staining 205
6.6.7 Statistical analysis 205
6.7 References 224

Chapter 7: General Discussion **231**
7.1 Summary of findings 232
7.2 Fatty acid oxidation and molecular heterogeneity 235
7.3 Crosstalk between mitochondria and peroxisomes 237
7.4 Ferroptosis and polyunsaturated fatty acid metabolism 239
7.5 Cell cycle and lipid metabolism 243
7.5.1 Interplay of oncogenic signalling, cell cycle and metabolism 243
7.5.2 Possible mechanism for peroxisomal metabolism in cell cycle regulation 244
7.6 Lipid accumulation and remodelling: protects or kills? 245
7.7 Epigenetics and lipid metabolism 246
7.8 A role for DECR1/2 in neuroendocrine prostate cancer 248
7.9 From bench to bedside: strategies for fatty acid oxidation inhibition 252
7.10 Conclusion and future directions 253
7.10.1 Small molecule inhibitors of DECR1 254
7.10.2 Mechanistic insights of DECR2 and peroxisomal β-oxidation 254
Chapter 8: References **257**
Chapter 9: Appendices **273**
9.1 Appendix A: Nassar et al., 2018 BJU International 274
9.2 Appendix B: Centenera et al., 2021 Cancer Research 287
9.3 Appendix C: Butler et al., 2021 Cancer Research 303

List of Figures and Tables

Figures

Figure 1.1 Simplified overview of androgen receptor signalling. 3
Figure 1.2 Structural diversity of fatty acids. 20
Figure 1.3 Simplified overview of mitochondrial and peroxisomal β-oxidation.....21
Figure 7.1 GSEA correlation analysis of DECR2 revealed significant positive correlation with hallmark DNA repair pathway.....245
Figure 7.2 An overview of the findings discussed in Chapter 7. 250
Figure 7.3 An overview of possible stages of prostate cancer where fatty acid oxidation inhibition would be beneficial……254
Supplementary Figure 3.1 RNA-seq analysis pipeline. 82
Supplementary Figure 3.2 84
Supplementary Figure 3.3 Hierarchical clustering analysis. 85
Supplementary Figure 3.4 86
Supplementary Figure 3.5 Gene set enrichment analysis (GSEA) of DECR1 knockdown cells at 72 hrs. 92
Supplementary Figure 3.6 Gene set enrichment analysis (GSEA) of DECR1 knockdown cells at 96 hrs. 93

Tables

Table 1.1 Comparison between mitochondrial and peroxisomal β-oxidation 23
Table 2.1 List of materials and reagents used in this thesis 26
Table 2.2 List of buffers and solutions with compositions 29
Table 3.1 Top 50 upregulated DEGs in DECR1 knockdown cells at 72 hrs.....88
Table 3.2 Top 50 downregulated DEGs in DECR1 knockdown cells at 72 hrs ...89
Table 3.3 Top 50 upregulated DEGs in DECR1 knockdown cells at 96 hrs.....90
Table 3.4 Top 50 downregulated DEGs in DECR1 knockdown cells at 96 hrs ...91

List of Abbreviations

ABCD	ATP binding cassette subfamily D
ACC	Acetyl-CoA carboxylase
ACLY	ATP citrate lyase
ACOX	acyl-coenzyme A oxidase
ADT	Androgen deprivation therapy
AKT	serine/threonine protein kinase
AMACR	α-methylacyl-CoA racemase
AR	Androgen receptor
ARI	Androgen receptor inhibition
ATP	Adenosine triphosphate
BCFA	Branched chain fatty acid
BODIPY	Boron dipyrromethene
CAT	Catalase
CDK	Cyclin-dependent kinase
CE	Cholesteryl ester
Cer	Ceramide
CPT1	Carnitine palmitoyltransferase 1
CRISPR	Clustered regularly interspaced short palindromic repeats
CRPC	Castrate-resistant prostate cancer
DAG	Diacylglyceride
DECR1	2,4-Dienoyl CoA Reductase 1
DECR2	2,4-Dienoyl CoA Reductase 2
DHT	Dihydrotestosterone
DNA	Deoxyribonucleic acid
ECI2	Enoyl-CoA Delta Isomerase 2
ENZ	Enzalutamide
ER	Endoplasmic reticulum
ETC	Electron transport chain
ETX	Etomoxir
FA	Fatty acids
FAD	Flavin-adenine dinucleotide
FAO	Fatty acid oxidation

FASN	Fatty acid synthase
GAPDH	Glyceraldehyde-3-phosphate dehydrogenase
GFP	Green fluorescent protein
GSEA	Gene set enrichment analysis
HDAC	Histone deacetylase
LCFA	Long chain fatty acid
mTORC	Mammalian target of rapamycin complex
MUFA	Monounsaturated fatty acid
NAD	Nicotinamide adenine dinucleotide
NEPC	Neuroendocrine prostate cancer
OCR	Oxygen consumption rate
OXPHOS	Oxidative phosphorylation
PC	Phosphatidylcholine
PCa	Prostate cancer
PCR	Polymerase chain reaction
PDE	Patient-derived explant
PE	Phosphatidylethanolamine
PGC1-α	PPAR gamma coactivator 1-alpha
PI	Phosphatidylinositol
PI3K	Phosphatidylinositol 3-kinase
PL	Phospholipid
PMP70	Peroxisomal membrane protein 70
PPAR	Peroxisome proliferator-activated receptor
PS	Phosphatidylserine
PUFA	Polyunsaturated fatty acid
RB	Retinoblastoma protein
RFP	Red fluorescent protein
RIPA	Radioimmunoprecipitation assay buffer
RNA	Ribonucleic acid
ROS	Reactive oxygen species
SCD	Stearoyl CoA desaturase
SFA	Saturated fatty acid
SM	Sphingomyelin
SREBP	Sterol regulatory element-binding protein

TAG	Triacylglyceride
TCA	Tricarboxylic acid cycle
TDZ	Thioridazine
VLCFA	Very long chain fatty acid

Funding and Awards

Funding

Master of Philosophy (No Honours) International Scholarship, 2017-2020

Freemasons Centre for Male Health and Wellbeing Top-Up Scholarship, 2017-2020

Awards

Research Travel Awards

Adelaide Medical School Research Travel Awards (International), 2019

Adelaide Medical School Research Travel Awards (National), 2018

EMBL Australia Travel Grant, 2017

Conference Awards

Ross Wishart Memorial Award Finalist, 2020

John Barker Bequest Prize in Cancer Research, 2020

People's Choice Oral Presentation Award, 2019

Three Minute Thesis (3MT) competition Finalist, 2019

Platinum Level of Sponsorship for ABACBS and COMBINE Student Symposium, 2017

List of Presentations

National and Local Conference Poster Abstracts

Mah, C.Y., Nassar Z.D., Burvenich, I.J.G., Irani, S., Centenera, M.M., Moldovan M., Lynn D.J., Hoy, A.J., Swinnen, J.V. and Butler L.M. DECR1 is a key survival factor and protector of prostate cancer cells from ferroptosis, Florey Postgraduate Research Conference, September 2020.

Mah, C.Y., Nassar Z.D., Moldovan M., Lynn D.J. and Butler L.M. Targeting polyunsaturated fatty acid metabolism in prostate cancer, Lorne Cancer, February 2020.

Mah, C.Y., Nassar Z.D., Moldovan M., Lynn D.J. and Butler L.M. Targeting polyunsaturated fatty acid metabolism in prostate cancer, 13th Annual Florey International Postgraduate Research Conference, September 2019.

Mah, C.Y., Moldovan M., Nassar Z.D., Lynn D.J. and Butler L.M. Integrative analysis of lipid metabolic pathways in prostate cancer reveals DECR1 as a key cancer-related gene that promotes tumour cell survival, Australian Bioinformatics and Computational Biology Society and COMBINE Symposium, November 2017.

Mah, C.Y., Nassar Z.D. and Butler L.M. Androgenic Regulation of Lipid Metabolism in Prostate Cancer, 11th Annual Florey International Postgraduate Research Conference, September 2017.

Mah, C.Y., Nassar Z.D. and Butler L.M. Optimization of the hang drop assay for advanced prostate cancer cells, Australian Society for Medical Research, June 2017.

International Conference Poster Abstracts

Mah, C.Y., Nassar Z.D., Burvenich I.J.G., Irani S., Centenera M.M., Moldovan M., Lynn D.J., Hoy A.J., Swinnen J.V. and Butler L.M. DECR1: The rate limiting enzyme of polyunsaturated fatty acid metabolism and a novel therapeutic target in prostate cancer, American Association for Cancer Research Annual Meeting, April 2020.

Mah, C.Y., Nassar Z.D., Burvenich I.J.G., Irani S., Centenera M.M., Moldovan M., Lynn D.J., Hoy A.J., Swinnen J.V. and Butler L.M. DECR1 is a key survival factor and protector of prostate cancer cells from ferroptosis, Cold Spring Harbor Laboratory, Cancer: Mechanisms & Models meeting, August 2020.

Butler, L.M., **Mah, C.Y.**, Dehairs, J., Vincent, A., Mutuku, S., Spotbeen, X., Das, R., Nassar, Z.D., Selth, L.A., Trim, P., Snel, M., Lynn, D.J., Horvath, L.G., Tilley, W., Centenera, M.M. and Swinnen, J.V. Phospholipid profiling of clinical prostate tissues reveals targetable alterations in membrane lipid composition accompanying tumorigenesis, American Association for Cancer Research Annual Meeting, April 2020.

Shrestha, R.J., Townley, S., Hanson, A., Pickering, M., Nassar, Z.D., **Mah, C.Y.**, Ghodsi, M.A., Hoy, A.J., Quek, L.E., Tilley, W.D., Butler, L.M., and Selth L.A. ACSM1 and ACSM3 regulate fatty acid oxidation in prostate cancer to promote growth and protect against oxidative stress, AACR Special Virtual Conference on Epigenetics and Metabolism; October 2020.

Nassar, Z.D., Centenera, M.M., Machiels, J., Zinonos, I., Hanson, A., Bloch, K., **Mah, C.Y.**, Ryan, N.K., Williams, E.D., Evdokiou, A. and Tilley, W.D., 2019, September. Lipid elongation in prostate cancer: an androgen regulated process and a novel therapeutic target. In 7th International Pacific Rim (PacRim) Breast and Prostate Cancer Meeting (Vol. 1). BioScientifica, September 2019.

Oral Presentations

Mah, C.Y., Nassar, Z.D. and Butler L.M. DECR1 is a key survival factor that regulates PUFA oxidation to protect prostate cancer cells from ferroptosis, ASMR SA Scientific Meeting (Ross Wishart Memorial Award Finalist), November 2020.

Mah, C.Y., Nassar, Z.D. and Butler L.M. Targeting polyunsaturated fatty acid metabolism in prostate cancer, SAHMRI Precision Medicine Theme Seminar, October 2020.

Mah, C.Y., Centenera M.M., Machiels J., Vincent A., Spotbeen X., Mutuku S., Das R., Derua R., Waelkens E., Trim P., Snel M., Swinnen J.V. and Butler L.M. Unravelling the phospho-lipidome of prostate cancer, Australian Society for Medical Research, June 2019.

Mah C.Y., Centenera M.M., Machiels J., Vincent A., Spotbeen X., Mutuku S., Das R., Derua R., Waelkens E., Trim P., Snel M., Swinnen J.V. and Butler L.M. Unravelling the phospho-lipidome of prostate cancer, Australian Cancer and Metabolism Meeting, May 2019.

Mah C.Y., Nassar Z.D. and Butler L.M. Targeting polyunsaturated fatty acid metabolism in prostate cancer, Freemasons Foundation Centre for Men's Health Seminar, 2018.

3-Minute Thesis

Mah C.Y. Break-a-leg in the fight against prostate cancer, SAHMRI Annual Scientific Meeting, October 2019.

Mah C.Y. Brak-a-leg in the fight against prostate cancer. Faculty of Health and Medical Sciences 3MT Competition, The University of Adelaide, September 2019.

List of Publications

Publications arising from this work

Nassar, Z.D.,* **Mah, C.Y.**,* Dehairs, J., Burvenich, I.J., Irani, S., Centenera, M.M., Helm, M., Shrestha, R.K., Moldovan, M., Don, A.S., Holst, J., Scott, A.M., Horvath, L.G., Lynn, D.J., Selth, L.A., Hoy, A.J., Swinnen, J.V. and Butler, L.M. (2020) Human DECR1 is an androgen-repressed survival factor that regulates PUFA oxidation to protect prostate tumor cells from ferroptosis. ***eLife***, vol. 9, pp. e54166. doi: https://doi.org/10.7554/eLife.54166. **these authors contributed equally*

Mah, C.Y., Nassar, Z.D., Swinnen, J.V., and Butler, L.M. (2020) Lipogenic effects of androgen signaling in normal and malignant prostate. ***Asian Journal of Urology***, vol. 7(3), pp. 258–270. doi: https://doi.org/10.1016/j.ajur.2019.12.003.

Nassar, Z.D., **Mah, C.Y.**, Centenera, M.M., Irani, S., Sadowski, M.C., Scott, J.S., Nguyen, E.V., Nagarajan, S.R., Moldovan, M., Lynn, D.J., Daly, R.J., Hoy, A.J. and Butler, L.M. (2020) Fatty acid oxidation is an adaptive survival pathway induced in prostate tumors by heat shock protein 90 inhibition. ***Molecular Cancer Research***, advance online publication, doi: https://doi.org/10.1158/1541-7786.MCR-20-0570.

Publications arising in addition to this work

Butler, L.M., **Mah, C.Y.**, Machiels, J., Vincent, A.D., Irani, S., Mutuku, S.M., Spotbeen, X., Bagadi, M., Waltregny, D., Moldovan, M., Dehairs, J., Vanderhoydonc, F., Bloch, K., Das, R., Stahl, J., Kench, J.G., Gevaert, T., Derua, R., Waelkens, E., Nassar, Z.D., Selth, L.A., Trim, P.J., Snel, M.F., Lynn, D.J., Tilley, W.D., Horvath, L.G., Centenera, M.M., Swinnen, J.V. (2021) Lipidomic profiling of clinical prostate cancer reveals targetable alterations in membrane lipid composition. ***Cancer Research***. doi: 10.1158/0008-5472.CAN-20-3863.

Nassar, Z.D.,* Aref, A.T.,* Miladinovic, D., **Mah, C.Y.**, Raj, G.V., Hoy, A.J. and Butler, L.M. (2018) Peri-prostatic adipose tissue: the metabolic microenvironment of prostate cancer. ***BJU international***, vol. 121, pp. 9-21, doi: https://doi.org/10.1111/bju.14173. **these authors contributed equally*

Centenera, M., Scott, J., Machiels, J., Nassar, Z.D., Miller, D., Zininos, I., Dehairs, J., Burvenich, I., Zadra, G., Chetta, P., Bango, C., Evergreen, E., Ryan, N., Gillis, J., **Mah, C.Y.**, Tieu, T., Hanson, A., Carelli, R., Bloch, K., Panagopoulos, V., Waelkens, E., Derua, R., Williams, E., Evdokioou, A., Cifuentes, A.R., Voelcker, N., Mills, I., Tilley, W.D., Scott, A., Loda, M., Selth, L.A., Swinnen, J.V. and Butler, L.M. (2021) ELOVL5 is a critical and targetable fatty acid elongase in prostate cancer. ***Cancer Research***. doi: 10.1158/0008-5472.CAN-20-2511.

Other publications

Tangseefa, P., Martin, S.K., Chin, P.Y., Breen, J., **Mah, C.Y.**, Baldock, P.A., Wittert, G.A., Page, A.J., Proud, C.G., Fitter, S. and Zannettino, A.C. (2021) The mTORC1 complex in pre-osteoblasts regulates whole-body energy metabolism independently of osteocalcin. ***Bone research***, 9(1), pp.1-17.

Asare, P.F., Roscioli, E., Hurtado, P.R., Tran, H.B., **Mah, C.Y.** and Hodge, S. (2020) LC3-Associated Phagocytosis (LAP): A Potentially Influential Mediator of Efferocytosis-Related Tumor Progression and Aggressiveness. ***Frontiers in Oncology***, 10.

Schjenken, J.E., Green, E.S., Overduin, T.S., **Mah, C.Y.**, Russell, D.L. and Robertson, S.A. (2021) Exposure to endocrine disruptor compounds (EDCs)–a cause of aberrant maternal immune tolerance driving inflammatory disorders of pregnancy?. ***Frontiers in Endocrinology***, 12, p.4.

Chapter 1: General Introduction

1.1 Prostate cancer

Prostate Cancer (PCa) is the most commonly diagnosed malignancy and the second leading cause of cancer-related mortality in Western men (Siegel et al. 2019). Globally, it is estimated that nearly 1.3 million men were diagnosed with PCa and approximately 350,000 deaths (accounts for 3.8 % of cancer-related deaths in men) in 2018 (Bray et al. 2018). By 2040, it is estimated that there will be up to 2.3 million new PCa cases accompanied by 700,000 PCa-related deaths (McNevin et al. 2021). In Australia, it is estimated that approximately 16,000 men were diagnosed with PCa in 2020 and 3,100 PCa-specific deaths (Cancer Australia 2019).

1.1.1 Androgens and the androgen receptor

PCa is dependent on male sex hormones known as androgens which act through the androgen receptor (AR) transcription factor for malignant cell growth and survival. In the absence of androgens, the AR is located in the cytoplasm and is associated with heat shock proteins HSP90 and HSP70, and several other chaperones that maintain the AR in an inactive conformation to protect from proteolytic degradation (Albany and Hahn 2014). Upon androgen binding, the AR undergoes a conformational change and dissociates from HSP90, and subsequently translocates into the nucleus (Tan et al. 2015). AR binds to AR-response elements (ARE) in the DNA and recruits coregulators to drive the transcription of AR target genes that are involved in promoting growth and survival of prostate epithelial cells (Richter et al. 2007) (Figure 1.1).

1.1.2 Current methods for the treatment of prostate cancer

Therapeutic options for PCa vary depending on the stage of the disease upon diagnosis. For the majority of men with early stage or low-risk localised PCa, surgical removal of the tumour and/or radiotherapy is potentially curative (Pullar and Shah 2016). For men with locally recurrent and/or metastatic disease, hormonal manipulation, or androgen-deprivation therapy (ADT), has remained the frontline strategy since the 1940s due to the dependence of prostate cells on androgens for growth and survival (Huggins 1941). Therefore, the goal of ADT is to abolish AR signalling by (i) reducing circulating levels of androgens in the body (i.e.

orchidectomy or LHRH agonists); (ii) inhibiting the binding of androgens to the AR (i.e. bicalutamide); (iii) inhibiting translocation of AR into the nucleus (i.e. enzalutamide); or (iv) degradation of AR (i.e. UT-34 and ARD-61) (Ponnusamy et al. 2019; Kregel et al. 2020; Crawford et al. 2019) (Figure 1.1). Although ADT is initially effective, the majority of patients eventually proceed to become resistant (within 2-3 years) to ADT and relapse with castration-resistant PCa (CRPC) (Karantanos et al. 2013; Attard et al. 2016).

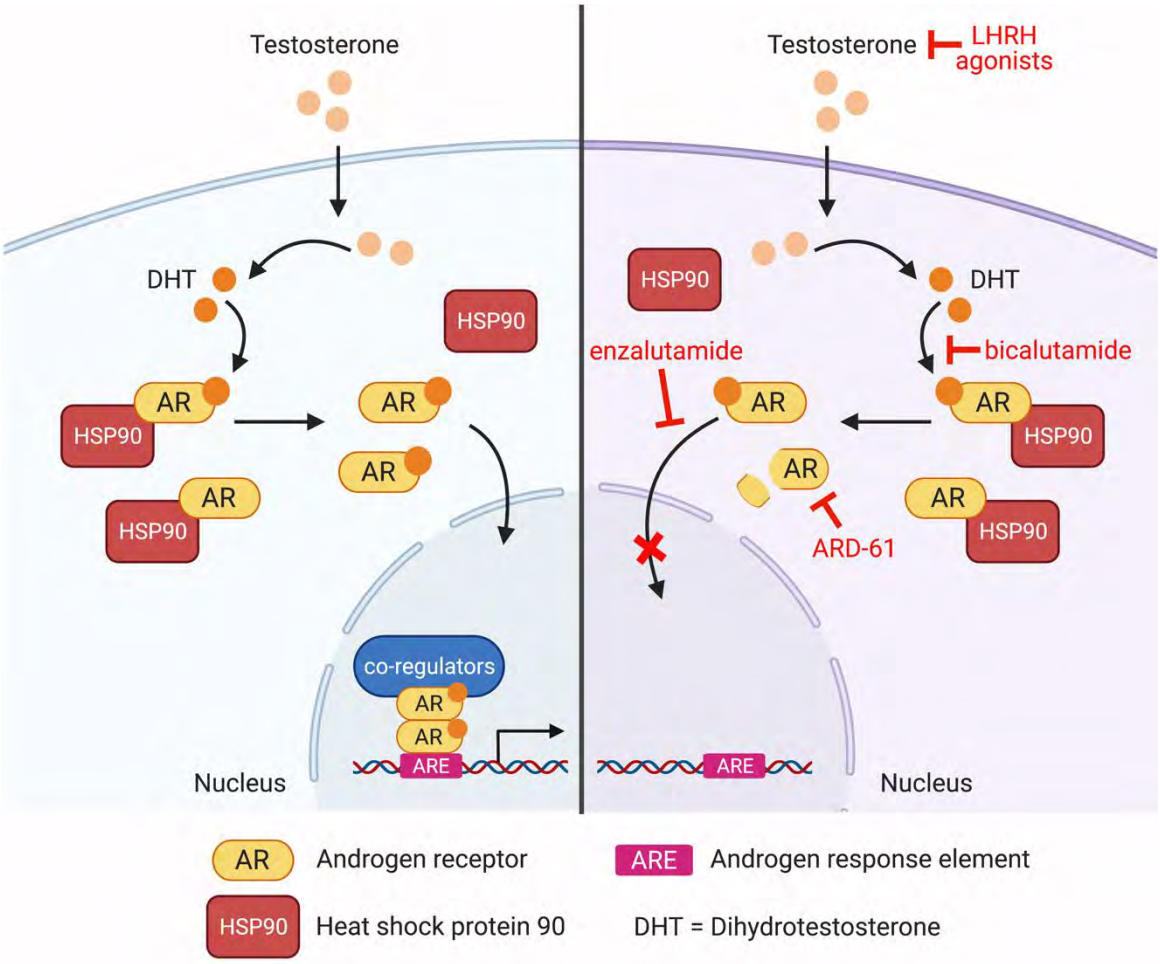

Figure 1.1 Simplified overview of androgen receptor signalling.
(Left) androgens (testosterone) are converted to DHT where it binds the AR and is translocated into the nucleus to stimulate growth promoting and survival genes. (Right) Mechanism of action of androgen deprivation therapy (ADT) to inhibit AR signalling.

To date, CRPC still remains incurable and has a median survival time of less than 2 years (Cookson et al. 2015). Failure of ADT is attributed to adaptive survival

pathways within PCa cells that result in persistent AR signalling despite the absence of androgens (Watson et al. 2015). Consequently, this led to the development of more potent 2nd generation AR-targeted therapies (i.e. abiraterone, enzalutamide and apalutamide) to overcome treatment resistance (Smith et al. 2018; Scher et al. 2012; de Bono et al. 2011). Despite the success in prolonging survival of men with CRPC (Hussain et al. 2018; Davis et al. 2019), these agents are still not curative. Therefore, alternative therapeutic strategies to subvert treatment resistance and prevent progression to CRPC are urgently sought

1.2 Role of lipid metabolism in cancer

Lipids have diverse biological roles and are key players in tumour biology. For instance, lipids can function as building blocks for biological membranes to support the high proliferative rate of cancer cells (Zadra et al. 2013). The bulk of cell membrane lipids are phospholipids (PLs) such as phosphatidylcholine (PC), phosphatidylethanolamine (PE), phosphatidylinositol (PI) and phosphatidylserine (PS). Other lipids include sterols (i.e. cholesterol), sphingolipid and lyso-PLs (Currie et al. 2013). Membranes function as barriers to separate and compartmentalise the cell's content and play crucial roles in numerous cellular processes (including cell proliferation and death, signalling, nutrient transport) (Butler et al. 2016). Moreover, these structural lipids facilitate the formation of detergent-resistant membrane microdomains (or lipid rafts) for oncogenic signal transduction, migration and intracellular trafficking required for cancer cells (Zadra et al. 2013; Swinnen et al. 2003). Lipids such as diacylglycerol (DAG), sphingosine-1-phosphate (S1P) and arachidonic acid (AA) can also serve as second messengers or lipid mediators to regulate numerous signalling or metabolic pathways that are crucial to support tumour growth, proliferation, migration and survival (Snaebjornsson et al. 2020). Moreover, lipids can also participate in post-translational modification of proteins, hence regulating its function, expression and localisation (Resh 2006). Finally, lipids synthesised endogenously or taken up exogenously can be catabolised via β-oxidation for energy production or stored in lipid droplets to protect against peroxidation or lipotoxicity (Liu et al. 2015; Bailey et al. 2015; Farese and Walther 2009).

In light of the above, it is not surprising that cancer cells actively exploit lipid metabolic pathways to support tumorigenesis. Altered lipid metabolism has been increasingly recognised as a hallmark of cancer, particularly in prostate cancer. The following section describes how androgenic regulation of lipid metabolic pathways are dysregulated during prostate cancer development and tumorigenesis, and why lipid metabolism represents an exciting and targetable avenue for therapeutic intervention.

1.3 Androgens and lipid metabolism in prostate cancer

This section of general introduction was published as a review article.

STATEMENT OF AUTHORSHIP

Title of Paper	Lipogenic effects of androgen signaling in normal and malignant prostate
Publication Status	☒ Published ☐ Submitted for Publication ☐ Accepted for Publication ☐ Unpublished and Unsubmitted work written in a manuscript style
Publication Details	Mah, CY, Nassar, ZD, Swinnen, JV, & Butler, LM 2020, 'Lipogenic effects of androgen signaling in normal and malignant prostate', *Asian journal of urology*, vol. 7(3), pp. 258–270, DOI: https://doi.org/10.1016/j.ajur.2019.12.003.

Principal Author

Name of Principal Author (Candidate)	Chui Yan Mah	
Contribution to the Paper	Conceptualization, Writing – Original and draft preparation, Writing – Review and editing	
Overall Percentage (%)	70 %	
Signature		Date: 26/03/2021

Co-Author Contributions

By signing the Statement of Authorship, each author certifies that:

i. the candidate's stated contribution to the publication is accurate (as detailed above);
ii. permission is granted for the candidate to include the publication in the thesis; and
iii. the sum of all co-author contributions is equal to 100% less than the candidate's stated contribution.

Name of Co-Author	Zeyad Nassar	
Contribution to the Paper	Conceptualization, Writing – Original and draft preparation, Writing – Review and editing	
Signature		Date: 26/03/2021

Name of Co-Author	Johannes Swinnen	
Contribution to the Paper	Conceptualization, Writing – Review and editing	
Signature		Date: 22 March 2021

Name of Co-Author	Lisa Butler	
Contribution to the Paper	Conceptualization, Writing – Review and editing	
Signature		Date: 01/04/2021

Asian Journal of Urology (2020) 7, 258–270

Available online at www.sciencedirect.com

ScienceDirect

journal homepage: www.elsevier.com/locate/ajur

Review

Lipogenic effects of androgen signaling in normal and malignant prostate

Chui Yan Mah [a,b], Zeyad D. Nassar [a,b], Johannes V. Swinnen [c], Lisa M. Butler [a,b,*]

[a] *Adelaide Medical School and Freemasons Foundation Centre for Men's Health, University of Adelaide, Adelaide, Australia*
[b] *South Australian Health and Medical Research Institute, Adelaide, Australia*
[c] *KU Leuven- University of Leuven, LKI- Leuven Cancer Institute, Department of Oncology, Laboratory of Lipid Metabolism and Cancer, Leuven, Belgium*

Received 8 May 2019; received in revised form 16 September 2019; accepted 5 November 2019
Available online 10 December 2019

KEYWORDS
Androgen receptor;
Fatty acids;
Metabolism;
Phospholipids;
Prostate gland

Abstract Prostate cancer is an androgen-dependent cancer with unique metabolic features compared to many other solid tumors, and typically does not exhibit the "Warburg effect". During malignant transformation, an early metabolic switch diverts the dependence of normal prostate cells on aerobic glycolysis for the synthesis of and secretion of citrate towards a more energetically favorable metabolic phenotype, whereby citrate is actively oxidised for energy and biosynthetic processes (*i.e. de novo* lipogenesis). It is now clear that lipid metabolism is one of the key androgen-regulated processes in prostate cells and alterations in lipid metabolism are a hallmark of prostate cancer, whereby increased *de novo* lipogenesis accompanied by overexpression of lipid metabolic genes are characteristic of primary and advanced disease. Despite recent advances in our understanding of altered lipid metabolism in prostate tumorigenesis and cancer progression, the intermediary metabolism of the normal prostate and its relationship to androgen signaling remains poorly understood. In this review, we discuss the fundamental metabolic relationships that are distinctive in normal versus malignant prostate tissues, and the role of androgens in the regulation of lipid metabolism at different stages of prostate tumorigenesis.
© 2020 Editorial Office of Asian Journal of Urology. Production and hosting by Elsevier B.V. This is an open access article under the CC BY-NC-ND license (http://creativecommons.org/licenses/by-nc-nd/4.0/).

* Corresponding author. Adelaide Medical School and Freemasons Foundation Centre for Men's Health, University of Adelaide, Adelaide, Australia.
E-mail address: lisa.butler@adelaide.edu.au (L.M. Butler).
Peer review under responsibility of Second Military Medical University.

https://doi.org/10.1016/j.ajur.2019.12.003
2214-3882/© 2020 Editorial Office of Asian Journal of Urology. Production and hosting by Elsevier B.V. This is an open access article under the CC BY-NC-ND license (http://creativecommons.org/licenses/by-nc-nd/4.0/).

1. Introduction

The prostate gland is exquisitely sensitive to androgenic hormones, and this dependence has been exploited to treat metastatic prostate cancer (PCa) since the 1930s. Whereas the interplay between androgen action and the unique lipid metabolic phenotype of PCa cells has been extensively studied [1—8], our knowledge of normal metabolism in the prostate lags considerably behind that of other tissues such as liver or heart. Understanding lipid metabolism in the normal prostate is essential to reveal the intermediary processes that mediate cell transformation, and in turn provide new insights into PCa detection, preventive and/or therapeutic strategies that are not evident from current experimental cancer models. This review article aims to provide a contemporary perspective on androgens and their impact on different aspects of lipid metabolism in normal and malignant prostate tissues, and highlight some recently identified metabolic vulnerabilities related to androgen action.

2. Normal prostate metabolism and androgens

The main function of the prostate is to produce and secrete prostatic fluid, which constitutes approximately one-third of the total volume of semen. Prostatic fluid is comprised of enzymes including prostate-specific antigen (PSA) that are responsible for liquefying semen, zinc, lipids and citrate. High citrate production and secretion are unique characteristics of the prostate; citrate concentration in prostate cells is about 1.0—3.0 mmol/L compared with only 0.1—0.5 mmol/L in other mammalian cells. Accordingly, citrate concentration in the prostatic fluid is about 24—130 mmol/L, which is 240—1 300-fold greater than that in blood plasma [9—11]. Typically, citrate is either retained and oxidized in the mitochondria to generate energy as an essential intermediate in the citric acid cycle, or is exported into the cytoplasm where it is cleaved by citrate lyase (ACLY) to generate acetyl-CoA, which is used for fatty acid synthesis. The complete oxidation of citrate via the citric acid cycle fuels the cell with 12 mol ATP/mol citrate and 24 mol ATP/mol glucose oxidized. However, as described above, the prostate secretes enormous quantities of citrate, depriving prostate cells of a major pool of energy. Although the function of citrate within the prostatic fluid is not fully understood, it presumably contributes to the seminal fluid buffering capacity, chelation of calcium, zinc and other cations, and as an energy source to maintain sperm viability and/or for capacitation processes [12—18].

Studies on human and rat ventral prostate tissues or isolated prostate epithelial cells have revealed the dependence of prostate cells on aerobic glycolysis [19—24]. The aerobic glycolysis metabolic phenotype in normal prostate tissues is accompanied by another phenotype of secretion of high citrate concentrations within the prostatic fluid. However, PCa cells exhibit a decrease in citrate concentration, which suggests a metabolic transformation from citrate producing cells into citrate oxidizing cells [11]. In support of this, it was recently reported that significantly lower levels of citrate were detected in PCa tissues compared with normal prostate tissues as evaluated using desorption electrospray ionization mass spectrometry (DESI-MSI) [25]. This switch in citrate fate is suggested to take place by inhibition of the m-aconitase enzyme by zinc (Fig. 1). M-aconitase is responsible for the stereo-specific isomerization of citrate to isocitrate. The citrate/isocitrate ratio in most mammalian tissues is 10:1 compared with 30:1 in prostate cells, suggesting an inhibition of this key enzymatic activity [26]. In addition to producing and secreting large concentrations of citrate, normal prostate tissues are further characterized by the ability to uptake and accumulate large concentrations of zinc [27—29]. Zinc concentration is 10-fold greater in normal prostate tissues compared with other soft tissues, and its concentration in the prostatic fluid is 500-fold greater than in blood plasma [30]. Zinc inhibits m-aconitase activity, paving the way for prostate cells to halt citrate oxidation [31,32]. In addition to the secretion of citrate, the prostate is also a source of cholesterol, which comprises a major proportion of the seminal fluid [33].

Few studies have focused on the impact of androgen receptor (AR) signaling in normal prostate cell metabolism [34—36], and have largely focused on the role of androgens in increasing the intracellular citrate pool and lipid biosynthesis. The former is accomplished by increasing citrate production via enhanced availability of citrate precursors, acetyl-CoA and oxaloacetic acid, and/or decreased citrate consumption. Androgens were found to induce pyruvate oxidation by increasing the expression of pyruvate dehydrogenase E1 component subunit alpha (PDHE1α) [37], resulting in an increase in acetyl-CoA. Androgens were also reported to induce aspartate uptake and transamination processes by inducing expression of the aspartate transporter (*EAAC1*) and aspartate aminotransferase (*mAAT*) genes [38—41], providing cells with oxaloacetic acid. Moreover, androgens can induce zinc uptake by the prostate [42,43], inhibiting citrate oxidation (Fig. 1). 5α-dihydrotestosterone (DHT) increased mAAT expression in PC3 cells expressing AR [44], and in isolated pig prostate epithelial cells [45]. Testosterone increases the levels of m-aconitase mRNA and the transcription rates of m-aconitase in rat ventral prostate cells, pig prostate cells, and human malignant prostate cells (LNCaP and AR-PC-3) [36]. Testosterone up-regulated EAAC1 expression in rat ventral prostate epithelial cells [46]. PDHE1α expression was stimulated in response to testosterone in ventral prostate epithelial cells, rat ventral prostate cells, and in PC3 cells transfected with AR [37,47]. In contrast with this induction of citrate accumulation, androgens were found to induce m-aconitase activities in normal and malignant prostate cells [34—36,48]. Using castrated mature monkey models, androgens were found to control enzymes involved in the citric acid cycle, such as isocitrate dehydrogenase (IDH) and malate dehydrogenase (MDH) [49]. It is plausible that this induction is not enough to counteract other processes that increase citrate levels in prostate cells. Of note, the effects of testosterone in rodents were lobe-specific; testosterone induced m-aconitase mRNA expression in rat ventral prostate lobes but not in the dorsal lobes and decreased m-aconitase mRNA expression in the lateral lobes [50]. There is no consensus as to which of these rodent lobes is the most similar to the human prostate peripheral zone, where most prostate tumours arise [24,51] and although there are some anatomical resemblances between the rodent dorsolateral lobe and the human peripheral zone, molecular comparison studies are warranted. In contrast to humans, rodents rarely develop spontaneous PCa

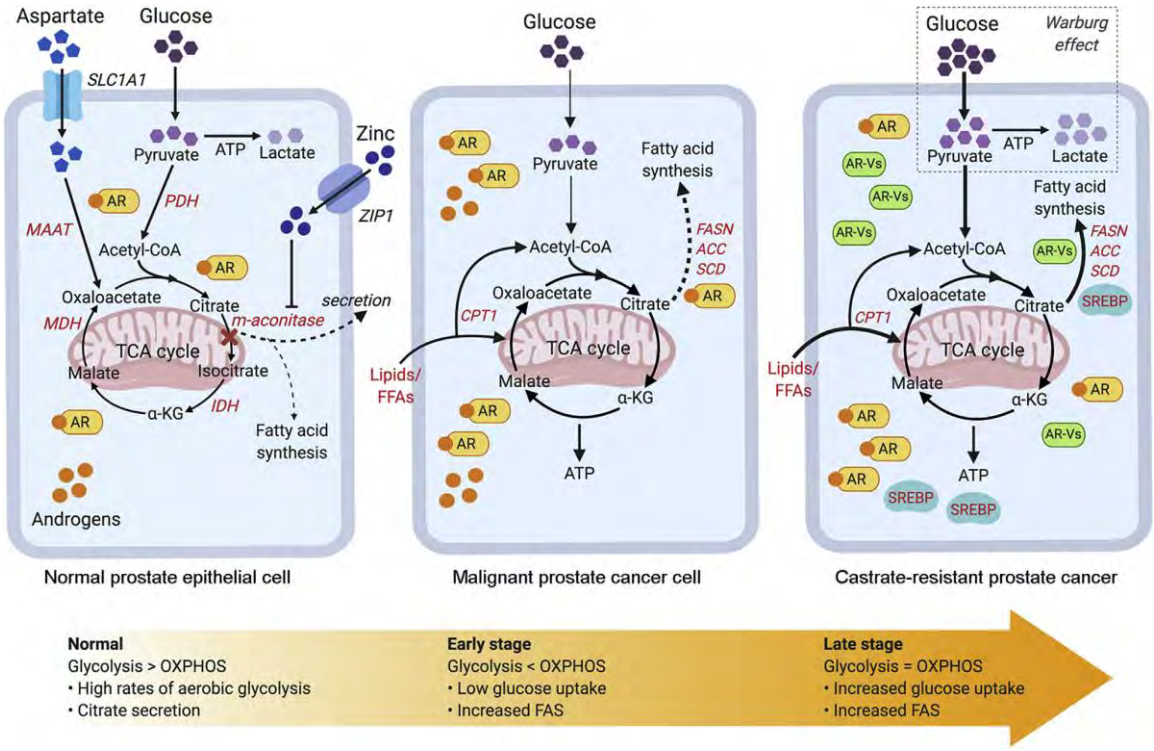

Figure 1 Metabolic landscape of prostate cancer progression (from normal prostate to malignant to metastatic/CRPC). Normal prostate epithelial cells exhibit high rates of aerobic glycolysis and low rates of oxidative phosphorylation. Glucose is used for citrate production and secretion, resulting in an impaired TCA cycle; this process is facilitated by zinc and aspartate through inhibition of *m-aconitase* and supply of metabolic precursors (*i.e.* oxaloacetate). Alternatively, citrate may be used for lipid biosynthesis through androgen-mediated activation of lipogenic enzymes. During malignant transformation, prostate cancer cells exhibit increased oxidative phosphorylation and hence, reactivate the TCA cycle to oxidize citrate for energy production. Instead of glucose, FFAs are the dominant bioenergetic substrates that feed into the TCA cycle for energy production. More importantly, *de novo* lipogenesis is enhanced at this stage of disease through the up-regulation of AR-regulated lipogenic enzymes. Despite initial positive responses to androgen-deprivation therapy, patients eventually progress to CRPC. AR signalling is maintained in CRPC; AR resistant mechanisms such as the AR-variants (AR-Vs) and/or indirect activation of alternative metabolic pathways (*i.e.* SREBP) play a role in driving the androgen-mediated lipogenic phenotype that may contribute to prostate cancer progression and treatment resistance. Notably, increased aerobic glycolysis or the Warburg effect is observed in advanced stages of the disease/CRPC. Words highlighted in red: AR-regulated genes. Thin/dotted lines: Baseline level; thick lines: Up-regulated. TCA, tricarboxylic acid cycle; PDH, pyruvate dehydrogenase; MAAT, aspartate aminotransferase; FASN, fatty acid biosynthesis; ACC, acetyl-CoA-carboxylase; SCD, stearoyl-CoA-desaturase; OXPHOS, oxidative phosphorylation; CRPC, castrate-resistant prostate cancer; AR, androgen receptor; FFAs, lipids or free fatty acids; MDH, malate dehydrogenase; α-KG, alpha ketoglutarate; AR-Vs, androgen receptor variants; CPT1, carnitine palmitoyltransferase 1; FAS, fatty acid synthesis. Created with BioRender.com.

[41], suggesting that rodent models should be supplemented with better human-mimic models.

Other studies on androgens and normal prostate tissue metabolism have focused on lipogenesis. Androgens were found to be essential in the prostate for lipid biosynthesis. Castration of the rat or monkey results in repression of lipogenic enzymes including ATP citrate lyase (ACLY), fatty acid synthase (FASN) and acetyl-CoA-carboxylase (ACC), and decreased total prostatic lipid content. Conversely, androgen administration after castration restored these lipogenic enzyme activities and lipid levels to baseline [49,52—55].

The metabolism of other nutrients such as fatty acids or amino acids in normal prostate tissues have not been examined thoroughly yet. It is surprising that our understanding of androgen regulation on prostate tissues is limited to relatively few processes and genes, given that androgens are the main orchestrator of prostate functions and physiology. Whereas prostate epithelial androgen receptor knockout (PEARKO) mouse models exist, to date there has been no investigation on the role of AR on prostate cell metabolism using these models. Similarly, little is known about the altered metabolic pathways in prostate cells during oncogenic transformation, and whether these alterations are driving malignancy or reflect changes to other genes or signaling pathways. One obvious manifestation of PCa is a striking decrease in citrate secretion into the prostatic fluid [11]. Redirecting citrate into the

mitochondria allows cell to use other nutrients to generate energy, including fatty acids. Fatty acid and lipid metabolism, with a focus on the androgen-regulated facets, will be discussed in the following sections.

3. Androgens and lipid metabolism in PCa

In the 1920s, Warburg [56,57] observed that rapidly proliferating tumor cells consume glucose at significantly higher rates compared to normal cells. Interestingly, most of the glucose-derived carbon was secreted as lactate rather than undergoing complete oxidation. This phenomenon is known as the "Warburg effect". This provides proliferating cancer cells several advantages including (1) rapid and abundant ATP/energy production and (2) essential intermediates/precursors needed for biosynthetic pathways [58,59]. More importantly, the Warburg effect has become the basis for the development of 18F-fluorodeoxyglucose positron emission tomography (FDG-PET) as a staging tool for diverse types of cancers.

The Warburg effect is a classic example of metabolic reprogramming in cancer. However, unlike most solid tumors, PCa typically does not exhibit the "glycolytic switch" (or Warburg effect) and is poorly detected with FDG-PET due to its weak avidity for glucose [60]. Given that rapid cell proliferation in malignant tumors requires increased energy supply, alternative sources of energy likely fuel PCa growth. Early studies revealed that primary PCa is associated with alterations in lipid metabolism (see below). Banerjee et al. [25] observed an increase in the glucose to citrate ratio in PCa tissues compared with benign prostate tissues using DESI-MSI. This difference was largely driven by the marked decrease in citrate levels in PCa while the increase in glucose signal intensity was less pronounced. The authors subsequently detected higher levels of lipids in PCa compared with normal prostate tissues and proposed the shunting of citrate into lipogenesis and oxidation in PCa [25]. Conversely, an increased aerobic glycolysis phenotype has been reported in advanced stages of PCa, while other studies have reported a spectrum in the degree of glycolysis between androgen-dependent and androgen-independent PCa [61,62]. Moreover, increased glucose utilization as indicated by higher FDG-PET avidity in PCa patients was able to predict biochemical recurrence and PCa progression to castrate-resistant PCa (CRPC) [63]. More recently, it was found that AR-dependent CRPC exhibited higher aerobic glycolysis *in vivo* using patient-derived xenograft models [64]. In addition, Bok et al. [65] demonstrated using transgenic mouse prostate models that an increased Warburg effect was essential to support tumour progression and metastasis, particularly in hypoxic conditions. Taken together, these findings suggest that the Warburg effect is still applicable in PCa and the binary notion that PCa is non-glycolytic should be reconsidered.

3.1. Role of the AR in lipid metabolism

The AR modulates multiple metabolic gene networks in PCa. In support of this, combined analysis of direct AR binding targets and androgen regulated genes revealed a significant enrichment of metabolic targets in LNCaP and VCaP PCa cells [66]. Interestingly, lipid metabolism has been identified as one of the key cellular processes affected by androgens. We previously reported that exposure of LNCaP cells to androgens induced a marked accumulation of lipids such as cholesteryl esters and triacylglycerols. Further analysis of the origins of the accumulated lipids revealed that the observed lipid accumulation was due to androgen stimulated *de novo* lipogenesis, rather than uptake from extracellular sources [67]. More importantly, this lipid accumulation was abrogated by treatment with an AR-antagonist and was not observed in AR-negative PC3 and DU-145 PCa cells. Subsequently, numerous studies have reported androgen stimulation of the expression of diverse lipogenic enzymes, including several additional enzymes involved in lipid binding, uptake, metabolism and transport [2,3] (Fig. 2). Androgenic regulation of these genes has also been validated in several cell line RNA microarray and sequencing studies [66,68,69]. Overall, these findings highlighted an anabolic program downstream of the AR signaling axis to facilitate PCa development and progression.

3.2. Androgens and lipid biosynthesis

Increased *de novo* lipogenesis is an early hallmark of PCa tumorigenesis and is significantly associated with PCa progression and poor disease survival outcomes [70—73]. More than half a century ago, it was demonstrated that cancer cells shunted glucose-derived carbons from the mitochondrial Kreb's cycle to the cytosol for fatty acid synthesis (FAS) despite an abundant supply of extracellular lipids [74]. In rapidly proliferating cells, citrate generated from glucose and glutamine metabolism is essential for the production of acetyl-CoA which is the building block for *de novo* lipogenesis. In line with this observation, candidate-gene expression studies have reported tumor-related overexpression of key enzymes involved in lipogenesis that are essential for development and progression of PCa [75]. Notably, androgens have been reported to regulate the expression of lipogenic and lipid-modifying enzymes [76,77], such as FASN, ACC and steroyl-CoA-desaturase (SCD), to meet the growing demands of PCa cells for lipids, which serve as building blocks for membrane production, energy supply and storage, and act as mediators of intracellular signaling [78]. FASN forms a fatty acid by catalysing successive condensation reactions from malonyl-CoA and acetyl-CoA substrates. Overexpression of FASN occurs at the early stages of PCa pathogenesis and has been correlated to poor prognosis and reduced disease-free survival [71,79]. Moreover, elevated expression of FASN has been associated with aggressive PCa and metastasis to the bone [70]. ACC catalyses the rate-limiting step in FAS by converting acetyl-CoA to malonyl-CoA. Two isoforms, ACC1 and ACC2 exist: (1) ACC1 primarily produces malonyl-CoA to serve as a substrate for FAS; (2) ACC2 produces malonyl-CoA primarily to inhibit fatty acid β-oxidation via allosteric inhibition of carnitine palmitoyltransferase 1 (CPT1) [80]. It has been demonstrated that depletion of ACC1 expression by siRNA inhibited cell proliferation and induced caspase-mediated apoptosis in PCa cells, but non-malignant cells were unaffected [81]. Similar results were observed through chemical inhibition of ACC1 and ACC2 by Soraphen

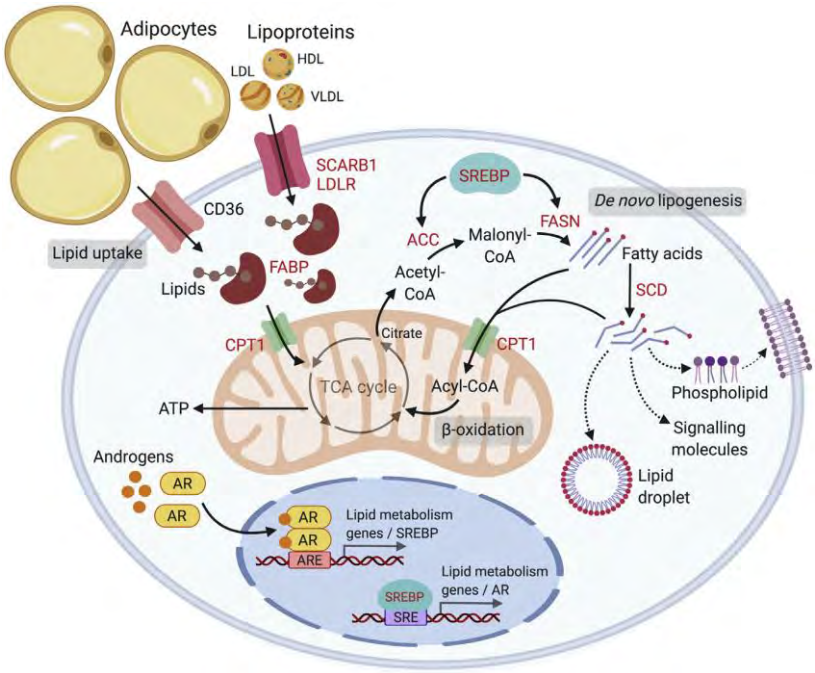

Figure 2 Overview of lipid metabolism in prostate cancer. Androgens regulate a number of lipid metabolic pathways in prostate cancer cells, including lipid uptake, biosynthesis and degradation. The AR directly (via binding of AR to the ARE) or indirectly (via activation of SREBP) regulates key lipid metabolic genes. Lipids can be derived from lipolysis of adipocytes or from circulating lipoproteins (LDL, HDL, VLDL). Alternatively, lipids can be synthesized endogenously by the cells via enzymes ACC and FASN. Androgens up-regulate lipid transporters that transport lipids or free fatty acids to the mitochondria for fatty acid oxidation (β-oxidation) or *de novo* lipogenesis. Free fatty acids are shuttled into the mitochondria as Acyl-CoAs by coupling with CPT1 (a mitochondrial transporter); a cyclical series of reactions result in the shortening of Acyl-CoA and the production of energy in the form of ATP via the TCA cycle. Citrate produced from the TCA cycle may also be cleaved to produce Acetyl-CoA, which is a precursor for *de novo* lipogenesis in the cytosol. Synthesized fatty acids may be further modified (*i.e.* degree of saturation via SCD) to generate a variety of lipids such as phospholipids that compose the plasma membranes, to promote lipid droplet production or to act as oncogenic signalling molecules to drive disease progression. Words in red = androgen-regulated genes. ARE, androgen response element; SRE, SREBP response element; AR, androgen receptor; LDL, low density lipoprotein; HDL, high density lipoprotein; VLDL, very low density lipoprotein; FASN, fatty acid biosynthesis; TCA, tricarboxylic acid cycle; SCD, stearoyl-CoA-desaturase; SREBP, sterol response element binding protein. Created with BioRender.com.

A in both androgen-dependent and androgen-independent PCa cells [82]. Generally, fatty acids are composed of a terminal carboxyl group and an alkyl chain which can undergo further modifications performed by desaturases or elongases. The rate-limiting enzyme SCD1 catalyses the biosynthesis of monounsaturated fatty acids (MUFA) from saturated fatty acids (SFA) by introducing a cis-double bond to the acyl chain, specifically palmitate and stearate to yield palmitoleate and oleate. It has been reported that PCa cells upregulate lipid biosynthesis to generate SFA and MUFA-rich phospholipids that partition into detergent-resistant lipid rafts to markedly alter signal transduction cascades, vesicular trafficking and cell migration [83,84]. Alterations in the desaturation index (MUFA to SFA ratio) affect phospholipid composition and hence, cancer cell behaviour [85]. One of the potential consequences of this altered desaturation ratio is changes to membrane fluidity [86]. Of note, Fritz et al. [87] reported an increase in MUFA/SFA ratio in human PCa patient tissues compared with normal prostate tissues. Consistent with this observation, the authors found enhanced expression of SCD1 in androgen-sensitive and resistant PCa cell lines and patient tissues. More importantly, SCD1 inhibition was shown to repress proliferation of androgen-dependent LNCaP and androgen-independent C4-2 PCa cells *in vitro* and in prostate tumor xenografts [87]. This was attributed to the inhibition of the AKT signaling pathway due to a decrease in the generation of phosphatidylinositols (precursors of a known AKT activator) following pharmacological inhibition of SCD1 (BZ36).

3.3. Androgens and fatty acid oxidation (FAO)

FAO is the dominant bioenergetic pathway in PCa [88,89]. The early "metabolic switch" towards citrate oxidation during PCa development coupled with the low glucose avidity of PCa (see above) diverts the focus away from glucose catabolism as the major source of energy/ATP to fatty acids. Mounting evidence suggests that FAO plays a

crucial role in (1) sensitizing cancer cells to apoptosis induction by pro-apoptotic agents [90], (2) impairing NADPH production resulting in oxidative stress-induced cell death [91], and (3) increasing resistance to radiation and chemotherapeutic agents [92]. Moreover, it was proposed that FAO could play a role in driving specific oncogenic pathways (*i.e.* Src signaling) associated with tumor progression and metastasis [93]. Altogether, these findings suggest that cancer cells depend on FAO for their survival and disease progression, particularly in cancers such as PCa which rely on FAO as a key energy source. In line with this observation, a recent study showed that knockdown of a FAO enzyme, enoyl-CoA-isomerase 2 (ECI2) inhibited PCa cell proliferation and activated cell death in LNCaP and VCaP PCa cells [4]. This study demonstrated that using ChIP-qPCR androgen stimulation resulted in a 6-fold increase in AR binding to the putative AR binding site of ECI2 and enhanced ECI2 mRNA expression [4]. While androgenic regulation of *de novo* lipogenesis has gained considerable attention, this suggests that androgens may also stimulate FAO for growth and survival. A previous study found that androgens promoted the complete oxidation of fatty acids in LNCaP and VCaP PCa cells, and inhibition of FAO via treatment with Etomoxir (inhibitor of CPT1) suppressed androgen-mediated PCa cell growth [94]. Overexpression of CPT1 (the rate-limiting enzyme of mitochondrial FAO) has been reported in several cancers, including PCa [88,95,96], and Etomoxir causes toxic lipid accumulation and, subsequently, the development of endoplasmic reticulum stress leading to PCa cell apoptosis [96]. Interestingly, this study also showed a reduction in expression AR-regulated genes (*PSA, NKX3.1*) following a significant decrease in AR as a result of FAO inhibition, suggesting a feed-forward loop to sustain PCa cell growth [96]. Overall, FAO is an important component of cancer metabolism that remains underexplored in PCa, and further study of this process may also inform new mechanisms of clinical resistance to androgen targeting therapies.

3.4. Androgens and lipid uptake

In light of enhanced *de novo* lipogenesis as a hallmark of PCa, and the fact that fatty acids are the dominant metabolic substrate for the development and progression of PCa, it was recently reported that exogenous lipids are the major contributor to lipid biosynthesis and oxidation in PCa [97]. Exogenous lipids can be derived from adipose tissue lipolysis or the breakdown of triglycerides contained in circulating lipoproteins. Moreover, the prostate is surrounded by peri-prostatic adipose tissue which has the capacity to directly supply substantial quantities of fatty acids [98,99]. In line with this, recent studies have demonstrated that increased lipid uptake in PCa cells can drive proliferation and potentially invasiveness [98,100]. Furthermore, PCa cells co-cultured with peri-prostatic derived adipocytes from obese mice showed enhanced migratory properties compared with lean mice [101]. Mechanistically, androgens have previously been reported as stimulating lipid uptake in androgen-responsive PCa cells through increased expression of FABPpm (a transporter protein) [102]. More recently, it was reported that androgens significantly increased cellular lipid uptake (including fatty acids, cholesterol and lipoproteins) in AR-positive PCa cells (LNCaP, VCaP, C4-2B and DuCaP) via direct AR-mediated induction of several lipid transporters [100]. This effect was abrogated when cells were co-treated with the AR antagonist enzalutamide. Notably, it was demonstrated that androgen-enhanced lipid uptake was maintained in LNCaP PCa cells under cell cycle arrest. This suggests that AR regulated lipid uptake is independent of cell cycle progression and proliferation, and is not indirectly caused by lipid biomass demand as a requirement for cell division [100]. Moreover, this study also confirmed the association of these lipid transporters with PCa progression from localized disease to bone metastatic disease [100]. In view of the critical roles for fatty acid uptake in PCa, CD36, a major transporter for exogenous fatty acids into cells, has been reported to play critical roles in cancer progression, metastasis and epithelial-to-mesenchymal transition in several tumour types [103—105]. In the context of PCa, it was shown that DHT significantly increased CD36 expression, and this effect was abrogated by enzalutamide treatment [100]. In addition, it was shown that CD36 was expressed at a higher level in metastatic disease (although there was no evidence for increased CD36 protein expression in tumor regions of human PCa tissues relative to benign regions, stromal and epithelial cells) and that high expression of CD36 was associated with reduced relapse-free survival in PCa [98]. It was demonstrated that CD36 blockade reduces fatty acid uptake, resulting in a reduction of cancer-mediated lipid biosynthesis from fatty acid precursors and accumulation of oncogenic lipid signaling molecules, ultimately attenuating PCa growth and progression in cultured cells (LNCaP and PC3) and patient-derived xenograft (PDX)-derived organoids [98]. Given that anti-tumor effects of inhibiting lipogenesis can be rescued by the addition of exogenous fatty acids, lipid uptake poses an important mechanism of treatment resistance to inhibitors of *de novo* lipogenesis. Accordingly, this study demonstrated in PDX-derived human organoids that CD36 blockade enhanced the efficacy of *de novo* lipogenesis inhibition [98].

3.5. Cross-talk between lipid metabolic processes in PCa

Taken together, the above findings suggest that androgens actively regulate different aspects of lipid metabolism—biosynthesis, degradation and uptake—that are essential for driving PCa tumorigenesis and disease progression. Intriguingly, androgens stimulate both FAO and FAS in PCa cells suggesting that an intricate balance may exist between these processes to provide both biomass generation and energy required to support PCa cell growth and survival [78]. It was previously considered that simultaneous mitochondrial FAO and cytosolic FAS are incompatible due to the inhibition of CPT1 by malonyl-CoA. However, studies have shown that genetic manipulation of ACC1 or ACC2 in cancer cells may exert different outcomes in terms of FAO and FAS [106]. ACC2-generated malonyl-CoA can inhibit CPT1, blocking fatty acid transport to the mitochondria and its subsequent β-oxidation, while

malonyl-CoA generated by ACC1 serves as an intermediate for FAS and exert no suppressive effects on CPT1 [107,108]. In addition, FAO can contribute to the accumulation of acetyl-CoA in the cytoplasm that is needed to initiate FAS, thereby supporting each other. On the basis of this idea, not only do the levels of acetyl-CoA and malonyl-CoA determine which metabolic pathways are activated, but also the ACC1 and ACC2 localization-dependent compartmentalization of these metabolites that allow FAO and FAS to occur simultaneously and independently from each other [95,107,109]. Alternatively, FAO may also play a protective role during conditions of metabolic stress such as hypoxia or glucose deprivation. Schlaepfer et al. [110] reported that LNCaP, C4-2B and DU-145 PCa cells were significantly enriched in triglycerides due to induction of lipogenic genes in response to hypoxic stress, and proposed that the accumulated lipids could support growth following reoxygenation. Accordingly, the inhibition of lipid utilization via treatment with etomoxir and shRNA-mediated CPT1 knockdown significantly compromised hypoxic PCa cell proliferation following reoxygenation. Altogether, these findings imply the importance of both FAO and FAS to promote tumour survival. In line with this observation, it has been shown that simultaneously targeting FAS and FAO significantly decreased PCa cell viability and AR expression [96]. Further research is needed to elucidate the precise mechanism of AR-mediated metabolic switching between *de novo* lipogenesis and FAO.

One possible explanation could be the cross-talk between AR and other metabolic or oncogenic pathways. A recent study reported that androgens induce mTOR relocalization to the nucleus to drive androgen-mediated metabolic reprogramming of PCa cells [111]. It was subsequently demonstrated that SREBF1, which acts as a downstream effector of the AR/mTOR signalling axis, helps regulate the balance between citrate consumption for mitochondrial energy production and as a carbon source for FAS in the cytoplasm [112]. These findings suggest that AR coordinates its actions with other transcription factors or oncogenes to establish or fine tune specific metabolic programs in PCa cells. Correspondingly, other transcriptional co-activators and signalling pathways that interplay with the AR signalling axis such as PGC-1a and estrogen related receptor gamma (ERRy) have also been described [94,113]. However, it remains to be determined how these metabolic pathways can be most optimally targeted in a setting of PCa.

3.6. Direct versus indirect regulation of lipid metabolic genes by AR

A major transcriptional regulator of lipogenic enzymes is the sterol response element binding protein 1 (SREBP1) transcription factor. Previous studies have shown that SREBP1 is androgen-regulated and that androgens activate SREBP1 expression via elevated expressions of the SREBP1 cleavage activating protein (SCAP) [3,114]. In line with this observation, androgen-induced lipogenic genes such as FASN harbor SREBP1-binding sites. Furthermore, SREBP1 induces fatty acid and lipid droplet formation and accumulation in AR-positive PCa cells. In contrast, several studies have shown that inhibition of SREBP1, achieved by shRNA knockdown or synthetic inhibitors (*i.e.* fatostatin) repressed expression of key lipogenic enzymes and suppressed growth of tumor xenografts [75,115,116]. Intriguingly, it was also shown that the expression of AR was, in turn, regulated by SREBP1 via binding of SREBP1 upstream of the AR gene [117]. This creates a positive feedback loop for the expression of lipogenic enzymes as well as AR expression and function. Collectively, these findings suggest that androgens can exert a coordinate control over lipogenesis that is regulated by the reciprocal relationship between AR and SREBP1 in support of PCa growth and survival (Fig. 2). While the androgenic regulation of SREBP1 has largely been reported in the context of PCa, little is known about the relationship between the AR and SREBP1 signaling, and the various roles of SREBP1 signaling in normal prostate cells. Elevated SREBP1 protein levels were reported in clinical human prostate tumours compared with normal prostate tissue or benign prostatic hypertrophy tissue [118]. Previous studies have shown that castration decreases expression of lipogenic enzymes in rat ventral prostate tissues, and that the effects were restored upon androgen treatment [52]. Given that these enzymes (*i.e.* FASN, ACLY, ACC) are known to be regulated by SREBP and that they harbour SREBP-binding sites, it is plausible that SREBPs may be involved in the coordinated activation of lipogenic gene expression by androgens in the normal prostate. Intriguingly, this study also demonstrated that androgen deprivation resulted in a marked decrease of mature nuclear-SREBP1 (nSREBP1) in the normal prostate *in vivo*; in contrast, readministration of testosterone completely restored nSREBP1 protein levels [52]. Nevertheless, the precise mechanism underlying the coordinated activation of the lipogenic phenotype by androgens and SREBP1 in the context of normal prostate cells remains to be elucidated.

Genome-wide analyses of AR binding and activity also suggest a distinct role for the AR in direct transcriptional regulation of lipogenic genes. Based on their proximity to AR binding sites [66,119] and their transcriptional regulation by androgens, genes involved in lipid metabolism and other key cellular metabolic processes have the potential to be directly regulated by the AR in malignant and non-malignant PCa cells [3]. This suggests that in addition to the effects of androgens on transcriptional activators such as SREBP1, androgens may also directly stimulate a coordinated metabolic network to regulate energy production and biosynthesis in PCa.

4. Effects of ADT on lipid metabolism

4.1. Metabolic effects of ADT

The current standard treatment for advanced and metastatic PCa is ADT [120]. This targets androgen signaling in PCa by reducing circulating levels of androgen or by blocking binding of androgens to the AR. Despite initial positive responses to ADT, the majority of patients eventually proceed to become resistant to ADT while maintaining functional AR signaling. This stage of cancer is termed CRPC. Several mechanisms of resistance to

ADT including AR-dependent mechanisms (*i.e.* AR overexpression, AR point mutations and constitutively active AR splice variants) and AR-independent mechanisms (*i.e.* glucocorticoid receptor [GR] activity) have been described. Accordingly, multiple clinical attempts to further suppress AR activity have been made. In spite of recent approval of novel AR-targeted therapies (*e.g.* enzalutamide), metastatic CRPC (mCRPC) remains incurable, with patients having a median survival of less than 2 years.

While there is abundant evidence that ADT has profound effects on systemic metabolism, few studies have examined the effects of ADT on lipid metabolism in PCa cells. An earlier study by Ettinger et al. [118] observed that androgen-regulated genes (*i.e. PSA*) including *SREBP1* were significantly decreased following androgen deprivation in prostate tumours. Given that *SREBP1* is a known transcriptional activator of genes involved in lipogenesis and cholesterol synthesis, androgen withdrawal resulted in a decrease in several genes involved in fatty acid biosynthesis (*FASN*), energy production (*ACBP*) and cholesterol synthesis (*FDPS*). Intriguingly, another study linked Siah2 (an E3 ubiquitin ligase) to regulation of AR target genes associated with sterol and lipid metabolism [121]. This was attributed to the finding that *SREBF1* was a Siah2-dependent androgen-responsive gene, consistent with their down-regulation in Siah2 knockdown PCa cells. Of note, Siah2 expression was significantly reduced after ADT and is required for PCa cell growth under androgen-deprivation conditions *in vitro* and *in vivo*, suggesting that Siah2-regulated lipid metabolism may contribute to CRPC [121]. More recently, Alsannawi et al. [122] investigated the role of *SLCO*-encoded transporters (proteins that transport bile acids, xenobiotics, steroid conjugates and drugs) in response of primary PCa to ADT. Despite the small sample sizes, the authors observed clear differences in *SLCO* expression levels suggesting that ADT-induced changes in PCa *SLCO* transporters may influence steroid uptake and response to ADT, including uptake and response to PCa therapies (*i.e.* abiraterone). Altogether, these studies have begun to shed light into the connection between ADT and lipid metabolism in PCa cells, but much more work is needed to distinguish between the systemic effects of ADT on patient metabolism that may also impact on PCa cell properties.

4.2. Resistance to ADT: The role of lipid metabolism

Overexpression of key lipid biosynthetic enzymes in PCa is characteristic of both primary and advanced disease [123]. In view of the relationship between androgens and lipid metabolism, several studies have reported that genes mediating the lipogenesis pathway (*i.e. FASN*, *SREBP1*) that were initially suppressed following castration were subsequently up-regulated or re-activated during the emergence of CRPC [70,118,124]. Indeed, AR-mediated lipogenesis is a highly-conserved metabolic feature of CRPC (Fig. 1), suggesting the potential of lipid metabolism as a key survival pathway that promotes resistance [124].

As AR signaling is initially repressed during ADT, it is plausible that other genes or pathways critical to survival (including metabolic adaptations) are activated to help facilitate progression to CRPC. This includes, but is not limited to, lipid metabolism; FAS and cholesterol synthesis provide CRPC cells with fatty acids for energy and membrane synthesis, and cholesterol allows intratumoral *de novo* synthesis of androgens. Previous studies have reported overexpression of a key enzyme in cholesterol synthesis, 3-hydroxy-3-methyl-glutaryl-CoA reductase (HMGCR) in enzalutamide-resistant PCa cells [125]. Notably, a combination of simvastin and enzalutamide significantly inhibited the growth of enzalutamide-resistant PCa cells *in vitro* and *in vivo* [125]. Another study demonstrated that silencing the expression of ELOVL7 (a fatty acid elongase enzyme) reduced growth of CRPC xenograft tumours in mice [124]. Furthermore, Flaig et al. [126] showed that targeting FAO via inhibition of CPT1A enhanced sensitivity of both androgen-dependent PCa (LNCaP) and CRPC (22Rv1) cells to enzalutamide, and that co-targeting the AR axis and FAO significantly inhibited PCa cell growth *in vitro* and in tumours. Altogether, these studies highlight the potential importance of lipid metabolism in CRPC. However, further research is required to understand the interactions of AR with lipid metabolism in driving treatment resistance and CRPC progression, particularly in more complex tumour environments containing multiple cell types.

One potential mechanism for the re-activation of lipid metabolic genes is the emergence of constitutively active AR splice variants (AR-Vs), such as AR-V7. AR-V7 lacks the C-terminal ligand-binding domain of the full-length AR and functions as a constitutively active, ligand-independent transcription factor that drives the growth of metastatic CRPC (mCRPC) cells *in vitro* and *in vivo* [127]. In support of this, AR-V7 was shown to be increased in patients resistant to the anti-androgen enzalutamide and abiraterone [128]. A recent study reported that pharmacological inhibition of FASN activity (IPI-9119) in CRPC not only suppressed fatty acid synthesis, but also inhibited full-length AR and AR-V7 expression in androgen-dependent and androgen-independent PCa cells [127]. Given that AR-V7 has the potential to re-activate lipid biosynthesis and is associated with treatment resistance, this suggests that AR-V7-mediated reactivation of lipid biosynthesis (Fig. 1) may drive disease recurrence and that targeting lipid metabolism pathways in combination with ADT and AR-directed therapies may be an effective therapeutic approach in CRPC (particularly for patients with high AR-V expression) or delay disease relapse.

Intriguingly, an AR blockade "bypass" mechanism was recently proposed as a prevalent mechanism of resistance. Upregulation of the GR was a common feature of drug-resistant tumours as evidenced from two preclinical models (LNCaP & VCaP) and was supported by correlative data showing increased GR expression in patients with enzalutamide resistance [129]. Importantly, comparative AR and GR transcriptome and ChIP-Seq studies have reported that a large majority of genes robustly regulated by GR are also regulated by AR [129,130]. Furthermore, a recent study revealed metabolic regulation of GR activation to stimulate enzalutamide resistance in PCa [131], which in turn, suggests a role for perturbed metabolic regulation in promoting tumour progression through activation of alternative steroid receptors. Finally, studies in non-prostatic tissues have reported that the GR directly activates several genes in lipid

metabolism (*i.e. FASN, ACC, SCD1*) [132]. In view of these findings, it is plausible that the upregulation of GR permits the re-expression of AR-responsive genes, including genes involved in lipid metabolism, to promote PCa progression or CRPC.

Likewise, SREBP1-mediated activation of lipid biosynthesis pathways is critical to survival and facilitates progression to androgen-independence or CRPC [50,118]. Previous study showed that overexpression of SREBP1 is sufficient to increase tumorigenicity and invasion of PCa *in vitro* and its activation promoted CRPC progression *in vivo* [116]. Given the reciprocal relationship between the AR and SREBP1, SREBP1 may provide a further level of complexity through its interactions with upstream effectors or oncogenic signalling pathways in conjunction with AR signaling to enable an SREBP1-dependent lipogenic program to drive CRPC [50,116,133]. Having said all the above, although these studies have enhanced our understanding of how several distinct mechanisms of AR resistance may drive PCa progression to CRPC, the opportunity now is to determine whether a coordinated signaling network exists between these previously unlinked mechanisms of AR resistance (*i.e.* AR-V7, SREBP1 and GR).

5. Conclusion and new opportunities

The landscape of PCa progression is intimately linked to androgen signaling and alterations in lipid metabolism. Androgens regulate a large repertoire of genes involved in lipid uptake, biosynthesis, remodeling and degradation to drive prostate cell transformation and tumor development. Accordingly, numerous groups have exploited this facet of metabolic reprogramming in PCa as a therapeutic vulnerability by co-targeting lipid metabolism pathways with ADT or anti-androgens (*i.e.* enzalutamide). In linking these observations, it is crucial that we understand the AR-driven metabolic changes (including, but not limited to, other lipid metabolism processes such as fatty acid elongation and desaturation) that occur during the malignant transformation of prostate epithelial cells in order to target the key processes hijacked by tumor cells to survive. Likewise, it is important to recognise that PCa is a highly heterogenous and multifocal disease and that major discrepancies exist between patient tissues and cell line models (particularly for metabolism) which may have significant impact on translational applications. Cancer metabolic reprogramming is profoundly impacted by spatial heterogeneity, a fundamental feature of the tumour microenvironment [134]. While the vast majority of research has been undertaken in the epithelial cells of the normal and malignant prostate, recent insights into the importance of metabolic reprogramming in the TME underscore the need to broaden our focus to different cell types in the prostate such as the stromal fibroblasts and infiltrating immune cells. These supporting players in the microenvironment can be co-opted or modified by cancer cells to enhance the proliferation and invasion of the tumor, and provide exciting new targeting strategies to improve clinical outcomes for patients with PCa. For this reason, there is an increasing need to integrate information on lipid metabolism with spatial information on gene expression and lipid abundance. Recent technologies such as spatial transcriptomics have enabled transcriptomic profiling of hundreds of locations within tissue sections with high spatial resolution to dissect spatial metabolic heterogeneity in the tumour microenvironment and uncover novel tumour specific metabolic vulnerabilities [135]. However, this still poses a challenge due to the complex metabolic landscape of cancer. Mass spectrometry imaging (MSI), on the other hand, has the potential to distinguish tumour regions of different grade within the same tissue specimen, and characterize histologically benign tissue adjacent to the tumour to assess field cancerization [136—138]. Accordingly, a study demonstrated using a high-resolution matrix-assisted laser desorption/ionization time-of-flight MSI (MALDI MSI) method for metabolomic/lipidomic analysis and imaging of PCa tissues to characterize metabolic signatures associated with different Gleason scores (GS) [138]. In addition, Morse et al. [139], used desorption electrospray ionization coupled to MSI (DESI-MSI) to identify metabolites with differential abundances between regions of benign and PCa tissues which also validated with pre-established metabolic pathways highlighting an importance in altered lipid metabolism in PCa. In future studies, the incorporation of patient-derived explants or xenograft models and, more recently, human PCa organoids offers the opportunity to elucidate the interactions between PCa and the tumour microenvironment in systems that more closely recapitulate the disease heterogeneity and complexity of the clinical tissue microenvironment to provide a more robust mechanistic basis by which lipid metabolism may drive PCa disease progression and treatment resistance [99].

Author contributions

Study concept and design: Chui Yan Mah, Zeyad D. Nassar, Johannes V. Swinnen, Lisa M. Butler.
Drafting of manuscript: Chui Yan Mah, Zeyad D. Nassar.
Critical revision of the manuscript: Johannes V. Swinnen, Lisa M. Butler.

Conflicts of interest

The authors declare no conflict of interest.

Acknowledgement

This work was supported by grants from the Movember Foundation and Prostate Cancer Foundation of Australia (MRTA3 to Lisa M. Butler, Johannes V. Swinnen), Prostate Cancer Foundation of Australia (NDDA2711 to Lisa M. Butler, Johannes V. Swinnen), the Research Foundation—Flanders (FWO G.0841.15 to Johannes V. Swinnen), the Stichting tegen Kanker (to Johannes V. Swinnen), KU Leuven (C16/15/073 and C32/17/052 to Johannes V. Swinnen), Interreg V-A (EMR23 "EURLIPIDS" to Johannes V. Swinnen). Chui Yan Mah is supported by a Master of Philosophy International Scholarship and a Top-Up Scholarship from the Freemasons Foundation Centre for Men's Health. Zeyad D. Nassar is supported by an Early Career Fellowship from the National Health and Medical Research Council of Australia

(1138648), a John Mills Young Investigator Award from the Prostate Cancer Foundation of Australia (YI 1417) and the Cure Cancer Australia Priority-driven Collaborative Cancer Research Scheme (1164798). Lisa M. Butler was supported by an ARC Future Fellowship (130101004) and Beat Cancer SA Beat Cancer Project Principal Cancer Research Fellowship (PRF1117).

References

[1] Gonthier K, Poluri RTK, Audet-Walsh É. Functional genomic studies reveal the androgen receptor as a master regulator of cellular energy metabolism in prostate cancer. J Steroid Biochem Mol Biol 2019;191:105367. https://doi.org/10.1016/j.jsbmb.2019.04.016.

[2] Barfeld SJ, Itkonen HM, Urbanucci A, Mills IG. Androgen-regulated metabolism and biosynthesis in prostate cancer. Endocr Relat Cancer 2014;21:T57—66. https://doi.org/10.1530/ERC-13-0515.

[3] Butler LM, Centenera MM, Swinnen JV. Androgen control of lipid metabolism in prostate cancer: novel insights and future applications. Endocr Relat Cancer 2016;23:R219—27. https://doi.org/10.1530/ERC-15-0556.

[4] Itkonen HM, Brown M, Urbanucci A, Tredwell G, Ho Lau C, Barfeld S, et al. Lipid degradation promotes prostate cancer cell survival. Oncotarget 2017;8:38264—75.

[5] Tamura K, Makino A, Hullin-Matsuda F, Kobayashi T, Furihata M, Chung S, et al. Novel lipogenic enzyme ELOVL7 is involved in prostate cancer growth through saturated long-chain fatty acid metabolism. Cancer Res 2009;69:8133—40.

[6] Lamont KR, Tindall DJ. Androgen regulation of gene expression. Adv Cancer Res 2010;107:137—62.

[7] Swinnen JV, Heemers H, van de Sande T, de Schrijver E, Brusselmans K, Heyns W, et al. Androgens, lipogenesis and prostate cancer. J Steroid Biochem Mol Biol 2004;92:273—9.

[8] Swinnen JV, Verhoeven G. Androgens and the control of lipid metabolism in human prostate cancer cells. J Steroid Biochem Mol Biol 1998;65:191—8.

[9] Costello LC, Franklin RB. Concepts of citrate production and secretion by prostate. 1. Metabolic relationships. Prostate 1991;18:25—46.

[10] Kavanagh JP. Sodium, potassium, calcium, magnesium, zinc, citrate and chloride content of human prostatic and seminal fluid. J Reprod Fertil 1985;75:35—41.

[11] Costello LC, Franklin RB. The intermediary metabolism of the prostate: a key to understanding the pathogenesis and progression of prostate malignancy. Oncology 2000;59:269—82.

[12] Hicks JJ, Martínez-Manautou J, Pedron N, Rosado A. Metabolic changes in human spermatozoa related to capacitation. Fertil Steril 1972;23:172—9.

[13] Arver S. Zinc and zinc ligands in human seminal plasma. III. The principal low molecular weight zinc ligand in prostatic secretion and seminal plasma. Acta Physiol Scand 1982;116:67—73.

[14] Tomlins AM, Foxall PJ, Lynch MJ, Parkinson J, Everett JR, Nicholson JK. High resolution 1H NMR spectroscopic studies on dynamic biochemical processes in incubated human seminal fluid samples. Biochim Biophys Acta 1998;1379:367—80.

[15] Searcy RL, Simms NM. A practical approach for acid-base characterization of human semen. Int J Fertil 1967;12:329—34.

[16] Ford WC, Harrison A. The role of citrate in determining the activity of calcium ions in human semen. Int J Androl 1984;7:198—202.

[17] Hori T, Masuda T, Kobayashi M, Kawakami E. Role of prostatic fluid in cooled canine epididymal sperm. Reprod Domest Anim 2017;52:655—60.

[18] Medrano A, Fernández-Novell JM, Ramió L, Alvarez J, Goldberg E, Montserrat Rivera M, et al. Utilization of citrate and lactate through a lactate dehydrogenase and ATP-regulated pathway in boar spermatozoa. Mol Reprod Dev 2006;73:369—78.

[19] Härkönen P. Androgenic control of glycolysis, the pentose cycle and pyruvate dehydrogenase in the rat ventral prostate. J Steroid Biochem 1981;14:1075—84.

[20] Müntzing J, Varkarakis MJ, Saroff J, Murphy GP. Comparison and significance of respiration and glycolysis of prostatic tissue from various species. J Med Primatol 1975;4:245—51.

[21] Farnsworth WE. Testosterone stimulation of citric acid synthesis in the rat prostate. Biochim Biophys Acta 1966;117:247—54.

[22] Härkönen P, Isotalo A, Santti R. Studies on the mechanism of testosterone action on glucose metabolism in the rat ventral prostate. J Steroid Biochem 1975;6:1405—13.

[23] Santti RS, Villee CA. Hormonal control of hexokinase in male sex accessory glands. Endocrinology 1971;89:1162—70.

[24] Costello LC, Akuffo V, Franklin RB. Net citrate production by isolated prostate epithelial cells. Enzyme 1988;39:125—33.

[25] Banerjee S, Zare RN, Tibshirani RJ, Kunder CA, Nolley R, Fan R, et al. Diagnosis of prostate cancer by desorption electrospray ionization mass spectrometric imaging of small metabolites and lipids. Proc Natl Acad Sci USA 2017;114:3334—9.

[26] Costello LC, Franklin R, Stacey R. Mitochondrial isocitrate dehydrogenase and isocitrate oxidation of rat ventral prostate. Enzyme 1976;21:495—506.

[27] Costello LC, Franklin RB, Narayan P. Citrate in the diagnosis of prostate cancer. Prostate 1999;38:237—45.

[28] Costello LC, Franklin RB. Novel role of zinc in the regulation of prostate citrate metabolism and its implications in prostate cancer. Prostate 1998;35:285—96.

[29] Costello LC, Feng P, Milon B, Tan M, Franklin RB. Role of zinc in the pathogenesis and treatment of prostate cancer: critical issues to resolve. Prostate Cancer Prostatic Dis 2004;7:111—7.

[30] Franklin RB, Milon B, Feng P, Costello LC. Zinc and zinc transporters in normal prostate and the pathogenesis of prostate cancer. Front Biosci 2005;10:2230—9.

[31] Costello LC, Franklin RB, Liu Y, Kennedy MC. Zinc causes a shift toward citrate at equilibrium of the m-aconitase reaction of prostate mitochondria. J Inorg Biochem 2000;78:161—5.

[32] Costello LC, Liu Y, Franklin RB, Kennedy MC. Zinc inhibition of mitochondrial aconitase and its importance in citrate metabolism of prostate epithelial cells. J Biol Chem 1997;272:28875—81.

[33] Eliasson R. Cholesterol in human semen. Biochem J 1966;98:242—3.

[34] Costello LC, Liu Y, Franklin RB. Testosterone stimulates the biosynthesis of m-aconitase and citrate oxidation in prostate epithelial cells. Mol Cell Endocrinol 1995;112:45—51.

[35] Costello LC, Liu Y, Franklin RB. Testosterone and prolactin stimulation of mitochondrial aconitase in pig prostate epithelial cells. Urology 1996;48:654—9.

[36] Costello LC, Liu Y, Zou J, Franklin RB. Mitochondrial aconitase gene expression is regulated by testosterone and prolactin in prostate epithelial cells. Prostate 2000;42:196—202.

[37] Costello LC, Liu Y, Zou J, Franklin RB. The pyruvate dehydrogenase E1 alpha gene is testosterone and prolactin regulated in prostate epithelial cells. Endocr Res 2000;26:23—39.

[38] Franklin RB, Brandly RL, Costello LC. Mitochondrial aspartate aminotransferase and the effect of testosterone on citrate production in rat ventral prostate. J Urol 1982;127:798—802.

[39] Franklin RB, Brandly RL, Costello LC. Effect of inhibitors of RNA and protein synthesis on mitochondrial aspartate

aminotransferase response to testosterone in rat ventral prostate. Prostate 1982;3:637—42.
[40] Franklin RB, Kahng MW, Akuffo V, Costello LC. The effect of testosterone on citrate synthesis and citrate oxidation and a proposed mechanism for regulation of net citrate production in prostate. Horm Metab Res 1986; 18:177—81.
[41] Costello LC, Akuffo V, Franklin RB. Testosterone stimulates net citrate production from aspartate by prostate epithelial cells. Horm Metab Res 1988;20:252—3.
[42] Costello LC, Liu Y, Zou J, Franklin RB. Evidence for a zinc uptake transporter in human prostate cancer cells which is regulated by prolactin and testosterone. J Biol Chem 1999; 274:17499—504.
[43] Liu Y, Franklin RB, Costello LC. Prolactin and testosterone regulation of mitochondrial zinc in prostate epithelial cells. Prostate 1997;30:26—32.
[44] Juang HH, Costello LC, Franklin RB. Androgen modulation of multiple transcription start sites of the mitochondrial aspartate aminotransferase gene in rat prostate. J Biol Chem 1995;270:12629—34.
[45] Qian K, Franklin RB, Costello LC. Testosterone regulates mitochondrial aspartate aminotransferase gene expression and mRNA stability in prostate. J Steroid Biochem Mol Biol 1993;44:13—9.
[46] Franklin RB, Zou J, Yu Z, Costello LC. EAAC1 is expressed in rat and human prostate epithelial cells; functions as a high-affinity L-aspartate transporter; and is regulated by prolactin and testosterone. BMC Biochem 2006;7:10. https://doi.org/10.1186/1471-2091-7-10.
[47] Costello LC, Liu Y, Franklin RB. Prolactin specifically increases pyruvate dehydrogenase E1 alpha in rat lateral prostate epithelial cells. Prostate 1995;26:189—93.
[48] Franklin RB, Juang HH, Zou J, Costello LC. Regulation of citrate metabolism by androgen in the LNCaP human prostate carcinoma cell line. Endocrine 1995;3:603—7.
[49] Arunakaran J, Balasubramanian K, Srinivasan N, Aruldhas MM, Govindarajulu P. Interaction of androgens and prolactin on prostatic enzymes of the pyruvate-malate cycle involved in lipogenesis in castrated mature monkey, Macaca radiata. Cytobios 1992;70:33—40.
[50] Chen M, Zhang J, Sampieri K, Clohessy JG, Mendez L, Gonzalez-Billalabeitia E, et al. An aberrant SREBP-dependent lipogenic program promotes metastatic prostate cancer. Nat Genet 2018;50:206—18.
[51] Choi SM, Kam SC. Metabolic effects of androgen deprivation therapy. Korean J Urol 2015;56:12—8.
[52] Heemers H, Vanderhoydonc F, Roskams T, Shechter I, Heyns W, Verhoeven G, et al. Androgens stimulate coordinated lipogenic gene expression in normal target tissues in vivo. Mol Cell Endocrinol 2003;205:21—31.
[53] Arunakaran J, Aruldhas MM, Govindarajulu P. Effects of prolactin and androgens on the prostatic lipids of castrated mature bonnet monkeys. Prostate 1990;17:247—60.
[54] Arunakaran J, Aruldhas MM, Govindarajulu P. Influence of castration and testosterone propionate on prostatic and seminal vesicular lipids in mature monkeys. Indian J Physiol Pharmacol 1987;31:184—9.
[55] Nyden SJ, Williams-Ashman HG. Influence of androgens on synthetic reactions in ventral prostate tissue. Am J Physiol 1953;172:588—600.
[56] Warburg O. On the origin of cancer cells. Science 1956;123: 309—14.
[57] Warburg O. Über den stoffwechsel der carcinomzelle. Naturwissenschaften 1924;12:1131—7.
[58] DeBerardinis RJ, Chandel NS. Fundamentals of cancer metabolism. Sci Adv 2016;2:e1600200. https://doi.org/10.1126/sciadv.1600200.
[59] DeBerardinis RJ, Lum JJ, Hatzivassiliou G, Thompson CB. The biology of cancer: metabolic reprogramming fuels cell growth and proliferation. Cell Metabol 2008;7:11—20.
[60] Jadvar H. Prostate cancer: PET with ^{18}F-FDG, ^{18}F- or ^{11}C-acetate, and ^{18}F- or ^{11}C-choline. J Nucl Med 2011;52:81—9.
[61] Li W, Cohen A, Sun Y, Squires J, Braas D, Graeber TG, et al. The role of CD44 in glucose metabolism in prostatic small cell neuroendocrine carcinoma. Mol Cancer Res 2016;14:344—53.
[62] Vaz CV, Alves MG, Marques R, Moreira PI, Oliveira PF, Maia CJ, et al. Androgen-responsive and nonresponsive prostate cancer cells present a distinct glycolytic metabolism profile. Int J Biochem Cell Biol 2012;44:2077—84.
[63] Lavallée E, Bergeron M, Buteau FA, Blouin AC, Duchesnay N, Dujardin T, et al. Increased prostate cancer glucose metabolism detected by ^{18}F-fluorodeoxyglucose positron emission tomography/computed tomography in localised gleason 8—10 prostate cancers identifies very high-risk patients for early recurrence and resistance to castration. Eur Urol Focus 2019;5:998—1006.
[64] Zacharias N, Lee J, Ramachandran S, Shanmugavelandy S, McHenry J, Dutta P, et al. Androgen receptor signaling in castration-resistant prostate cancer alters hyperpolarized pyruvate to lactate conversion and lactate levels *in vivo*. Mol Imaging Biol 2019;21:86—94.
[65] Bok R, Lee J, Sriram R, Keshari K, Sukumar S, Daneshmandi S, et al. The role of lactate metabolism in prostate cancer progression and metastases revealed by dual-agent hyperpolarized 13C MRSI. Cancers (Basel) 2019;11:E257. https://doi.org/10.3390/cancers11020257.
[66] Massie CE, Lynch A, Ramos-Montoya A, Boren J, Stark R, Fazli L, et al. The androgen receptor fuels prostate cancer by regulating central metabolism and biosynthesis. EMBO J 2011;30:2719—33.
[67] Swinnen JV, Van Veldhoven PP, Esquenet M, Heyns W, Verhoeven G. Androgens markedly stimulate the accumulation of neutral lipids in the human prostatic adenocarcinoma cell line LNCaP. Endocrinology 1996;137:4468—74.
[68] Nelson PS, Clegg N, Arnold H, Ferguson C, Bonham M, White J, et al. The program of androgen-responsive genes in neoplastic prostate epithelium. Proc Natl Acad Sci USA 2002; 99:11890—5.
[69] Ngan S, Stronach EA, Photiou A, Waxman J, Ali S, Buluwela L. Microarray coupled to quantitative RT-PCR analysis of androgen-regulated genes in human LNCaP prostate cancer cells. Oncogene 2009;28:2051—63.
[70] Rossi S, Graner E, Febbo P, Weinstein L, Bhattacharya N, Onody T, et al. Fatty acid synthase expression defines distinct molecular signatures in prostate cancer. Mol Cancer Res 2003;1:707—15.
[71] Swinnen JV, Roskams T, Joniau S, Van Poppel H, Oyen R, Baert L, et al. Overexpression of fatty acid synthase is an early and common event in the development of prostate cancer. Int J Cancer 2002;98:19—22.
[72] Swinnen JV, Vanderhoydonc F, Elgamal AA, Eelen M, Vercaeren I, Joniau S, et al. Selective activation of the fatty acid synthesis pathway in human prostate cancer. Int J Cancer 2000;88:176—9.
[73] Kuhajda FP, Jenner K, Wood FD, Hennigar RA, Jacobs LB, Dick JD, et al. Fatty acid synthesis: a potential selective target for antineoplastic therapy. Proc Natl Acad Sci USA 1994;91:6379—83.
[74] Medes G, Thomas A, Weinhouse S. Metabolism of neoplastic tissue. IV. A study of lipid synthesis in neoplastic tissue slices in vitro. Cancer Res 1953;13:27—9.
[75] Zadra G, Photopoulos C, Loda M. The fat side of prostate cancer. Biochim Biophys Acta 2013;1831:1518—32.
[76] Santos CR, Schulze A. Lipid metabolism in cancer. FEBS J 2012;279:2610—23.

[77] Swinnen JV, Brusselmans K, Verhoeven G. Increased lipogenesis in cancer cells: new players, novel targets. Curr Opin Clin Nutr Metab Care 2006;9:358—65.
[78] Zadra G, Loda M. Metabolic vulnerabilities of prostate cancer: diagnostic and therapeutic opportunities. Cold Spring Harb Perspect Med 2018;8:a030569. https://doi.org/10.1101/cshperspect.a030569.
[79] Shurbaji MS, Kalbfleisch JH, Thurmond TS. Immunohistochemical detection of a fatty acid synthase (OA-519) as a predictor of progression of prostate cancer. Hum Pathol 1996;27:917—21.
[80] Luo X, Cheng C, Tan Z, Li N, Tang M, Yang L, et al. Emerging roles of lipid metabolism in cancer metastasis. Mol Cancer 2017;16:76. https://doi.org/10.1186/s12943-017-0646-3.
[81] Brusselmans K, De Schrijver E, Verhoeven G, Swinnen JV. RNA interference-mediated silencing of the acetyl-CoA-carboxylase-alpha gene induces growth inhibition and apoptosis of prostate cancer cells. Cancer Res 2005;65:6719—25.
[82] Beckers A, Organe S, Timmermans L, Scheys K, Peeters A, Brusselmans K, et al. Chemical inhibition of acetyl-CoA carboxylase induces growth arrest and cytotoxicity selectively in cancer cells. Cancer Res 2007;67:8180—7.
[83] Staubach S, Hanisch FG. Lipid rafts: signaling and sorting platforms of cells and their roles in cancer. Expert Rev Proteomics 2011;8:263—77.
[84] Swinnen JV, Van Veldhoven PP, Timmermans L, De Schrijver E, Brusselmans K, Vanderhoydonc F, et al. Fatty acid synthase drives the synthesis of phospholipids partitioning into detergent-resistant membrane microdomains. Biochem Biophys Res Commun 2003;302:898—903.
[85] Deep G, Schlaepfer IR. Aberrant lipid metabolism promotes prostate cancer: role in cell survival under hypoxia and extracellular vesicles biogenesis. Int J Mol Sci 2016;17:E1061. https://doi.org/10.3390/ijms17071061.
[86] Barelli H, Antonny B. Lipid unsaturation and organelle dynamics. Curr Opin Cell Biol 2016;41:25—32.
[87] Fritz V, Benfodda Z, Rodier G, Henriquet C, Iborra F, Avancès C, et al. Abrogation of de novo lipogenesis by stearoyl-CoA desaturase 1 inhibition interferes with oncogenic signaling and blocks prostate cancer progression in mice. Mol Cancer Ther 2010;9:1740—54.
[88] Liu Y. Fatty acid oxidation is a dominant bioenergetic pathway in prostate cancer. Prostate Cancer Prostatic Dis 2006;9:230—4.
[89] Liu Y, Zuckier L, Ghesani N. Fatty acid rather than glucose metabolism is the dominant bioenergetic pathway in prostate cancer. J Nucl Med 2008;49(Suppl 1):104P.
[90] Samudio I, Harmancey R, Fiegl M, Kantarjian H, Konopleva M, Korchin B, et al. Pharmacologic inhibition of fatty acid oxidation sensitizes human leukemia cells to apoptosis induction. J Clin Investig 2010;120:142—56.
[91] Pike LS, Smift AL, Croteau NJ, Ferrick DA, Wu M. Inhibition of fatty acid oxidation by etomoxir impairs NADPH production and increases reactive oxygen species resulting in ATP depletion and cell death in human glioblastoma cells. Biochim Biophys Acta 2011;1807:726—34.
[92] Harper ME, Antoniou A, Villalobos-Menuey E, Russo A, Trauger R, Vendemelio M, et al. Characterization of a novel metabolic strategy used by drug-resistant tumor cells. FASEB J 2002;16:1550—7.
[93] Park JH, Vithayathil S, Kumar S, Sung PL, Dobrolecki LE, Putluri V, et al. Fatty acid oxidation-driven Src links mitochondrial energy reprogramming and oncogenic properties in triple-negative breast cancer. Cell Rep 2016;14:2154—65.
[94] Tennakoon JB, Shi Y, Han JJ, Tsouko E, White MA, Burns AR, et al. Androgens regulate prostate cancer cell growth via an AMPK-PGC-1α-mediated metabolic switch. Oncogene 2014;33:5251—61.
[95] Qu Q, Zeng F, Liu X, Wang QJ, Deng F. Fatty acid oxidation and carnitine palmitoyltransferase I: emerging therapeutic targets in cancer. Cell Death Dis 2016;7:e2226. https://doi.org/10.1038/cddis.2016.132.
[96] Schlaepfer IR, Rider L, Rodrigues LU, Gijón MA, Pac CT, Romero L, et al. Lipid catabolism via CPT1 as a therapeutic target for prostate cancer. Mol Cancer Ther 2014;13:2361—71.
[97] Balaban S, Nassar ZD, Zhang AY, Hosseini-Beheshti E, Centenera MM, Schreuder M, et al. Extracellular fatty acids are the major contributor to lipid synthesis in prostate cancer. Mol Cancer Res 2019;17:949—62.
[98] Watt MJ, Clark AK, Selth LA, Haynes VR, Lister N, Rebello R, et al. Suppressing fatty acid uptake has therapeutic effects in preclinical models of prostate cancer. Sci Transl Med 2019;11. https://doi.org/10.1126/scitranslmed.aau5758.
[99] Nassar ZD, Aref AT, Miladinovic D, Mah CY, Raj GV, Hoy AJ, et al. Peri-prostatic adipose tissue: the metabolic microenvironment of prostate cancer. BJU Int 2018;121(Suppl 3):9—21.
[100] Tousignant KD, Rockstroh A, Taherian Fard A, Lehman ML, Wang C, McPherson SJ, et al. Lipid uptake is an androgen-enhanced lipid supply pathway associated with prostate cancer disease progression and bone metastasis. Mol Cancer Res 2019;17:1166—79.
[101] Laurent V, Guérard A, Mazerolles C, Le Gonidec S, Toulet A, Nieto L, et al. Periprostatic adipocytes act as a driving force for prostate cancer progression in obesity. Nat Commun 2016;7:10230. https://doi.org/10.1038/ncomms10230.
[102] Pinthus JH, Lu JP, Bidaisee LA, Lin H, Bryskine I, Gupta RS, et al. Androgen-dependent regulation of medium and long chain fatty acids uptake in prostate cancer. Prostate 2007;67:1330—8.
[103] Nath A, Li I, Roberts LR, Chan C. Elevated free fatty acid uptake via CD36 promotes epithelial-mesenchymal transition in hepatocellular carcinoma. Sci Rep 2015;5:14752. https://doi.org/10.1038/srep14752.
[104] Pascual G, Avgustinova A, Mejetta S, Martín M, Castellanos A, Attolini CS, et al. Targeting metastasis-initiating cells through the fatty acid receptor CD36. Nature 2017;541:41—5.
[105] Hale JS, Otvos B, Sinyuk M, Alvarado AG, Hitomi M, Stoltz K, et al. Cancer stem cell-specific scavenger receptor CD36 drives glioblastoma progression. Stem Cells 2014;32:1746—58.
[106] Jeon S-M, Chandel NS, Hay N. AMPK regulates NADPH homeostasis to promote tumour cell survival during energy stress. Nature 2012;485:661—5.
[107] Abu-Elheiga L, Matzuk MM, Abo-Hashema KA, Wakil SJ. Continuous fatty acid oxidation and reduced fat storage in mice lacking acetyl-CoA carboxylase 2. Science 2001;291:2613—6.
[108] Wakil SJ, Abu-Elheiga LA. Fatty acid metabolism: target for metabolic syndrome. J Lipid Res 2009;50(Suppl):S138—43. https://doi.org/10.1194/jlr.R800079-JLR200.
[109] Carracedo A, Cantley LC, Pandolfi PP. Cancer metabolism: fatty acid oxidation in the limelight. Nat Rev Cancer 2013;13:227—32.
[110] Schlaepfer IR, Nambiar DK, Ramteke A, Kumar R, Dhar D, Agarwal C, et al. Hypoxia induces triglycerides accumulation in prostate cancer cells and extracellular vesicles supporting growth and invasiveness following reoxygenation. Oncotarget 2015;6:22836—56.
[111] Audet-Walsh É, Dufour CR, Yee T, Zouanat FZ, Yan M, Kalloghlian G, et al. Nuclear mTOR acts as a transcriptional

integrator of the androgen signaling pathway in prostate cancer. Genes Dev 2017;31:1228—42.
[112] Audet-Walsh É, Vernier M, Yee T, Laflamme C, Li S, Chen Y, et al. SREBF1 activity is regulated by an ar/mtor nuclear axis in prostate cancer. Mol Cancer Res 2018;16:1396—405.
[113] Audet-Walsh É, Yee T, McGuirk S, Vernier M, Ouellet C, St-Pierre J, et al. Androgen-dependent repression of ERRγ reprograms metabolism in prostate cancer. Cancer Res 2017; 77:378—89.
[114] Heemers HV, Verhoeven G, Swinnen JV. Androgen activation of the sterol regulatory element-binding protein pathway: current insights. Mol Endocrinol 2006;20:2265—77.
[115] Li X, Chen YT, Hu P, Huang WC. Fatostatin displays high antitumor activity in prostate cancer by blocking SREBP-regulated metabolic pathways and androgen receptor signaling. Mol Cancer Ther 2014;13:855—66.
[116] Huang WC, Li X, Liu J, Lin J, Chung LWK. Activation of androgen receptor, lipogenesis, and oxidative stress converged by SREBP-1 is responsible for regulating growth and progression of prostate cancer cells. Mol Cancer Res 2012;10:133—42.
[117] Huang WC, Zhau HE, Chung LWK. Androgen receptor survival signaling is blocked by anti-beta2-microglobulin monoclonal antibody via a MAPK/lipogenic pathway in human prostate cancer cells. J Biol Chem 2010;285:7947—56.
[118] Ettinger SL, Sobel R, Whitmore TG, Akbari M, Bradley DR, Gleave ME, et al. Dysregulation of sterol response element-binding proteins and downstream effectors in prostate cancer during progression to androgen independence. Cancer Res 2004;64:2212—21.
[119] Sharma NL, Massie CE, Ramos-Montoya A, Zecchini V, Scott HE, Lamb AD, et al. The androgen receptor induces a distinct transcriptional program in castration-resistant prostate cancer in man. Cancer Cell 2013;23:35—47.
[120] Pullar B, Shah N. Prostate cancer. Surgery (Oxford) 2016;34: 505—11.
[121] Qi J, Tripathi M, Mishra R, Sahgal N, Fazli L, Ettinger S, et al. The E3 ubiquitin ligase Siah2 contributes to castration-resistant prostate cancer by regulation of androgen receptor transcriptional activity. Cancer Cell 2013;23:332—46.
[122] Alsinnawi M, Zhang A, Bianchi-Frias D, Burns J, Cho E, Zhang X, et al. Association of prostate cancer SLCO gene expression with Gleason grade and alterations following androgen deprivation therapy. Prostate Cancer Prostatic Dis 2019;22:560—8.
[123] Shafi AA, Putluri V, Arnold JM, Tsouko E, Maity S, Roberts JM, et al. Differential regulation of metabolic pathways by androgen receptor (AR) and its constitutively active splice variant, AR-V7, in prostate cancer cells. Oncotarget 2015;6. 31997—2012.
[124] Han W, Gao S, Barrett D, Ahmed M, Han D, Macoska JA, et al. Reactivation of androgen receptor-regulated lipid biosynthesis drives the progression of castration-resistant prostate cancer. Oncogene 2018;37:710—21.
[125] Kong Y, Cheng L, Mao F, Zhang Z, Zhang Y, Farah E, et al. Inhibition of cholesterol biosynthesis overcomes enzalutamide resistance in castration-resistant prostate cancer (CRPC). J Biol Chem 2018;293:14328—41.
[126] Flaig TW, Salzmann-Sullivan M, Su LJ, Zhang Z, Joshi M, Gijón MA, et al. Lipid catabolism inhibition sensitizes prostate cancer cells to antiandrogen blockade. Oncotarget 2017;8:56051—65.
[127] Zadra G, Ribeiro CF, Chetta P, Ho Y, Cacciatore S, Gao X, et al. Inhibition of de novo lipogenesis targets androgen receptor signaling in castration-resistant prostate cancer. Proc Natl Acad Sci USA 2019;116:631—40.
[128] Antonarakis ES, Lu C, Wang H, Luber B, Nakazawa M, Roeser JC, et al. AR-V7 and resistance to enzalutamide and abiraterone in prostate cancer. N Engl J Med 2014;371: 1028—38.
[129] Arora VK, Schenkein E, Murali R, Subudhi SK, Wongvipat J, Balbas MD, et al. Glucocorticoid receptor confers resistance to antiandrogens by bypassing androgen receptor blockade. Cell 2013;155:1309—22.
[130] Sahu B, Laakso M, Pihlajamaa P, Ovaska K, Sinielnikov I, Hautaniemi S, et al. FoxA1 specifies unique androgen and glucocorticoid receptor binding events in prostate cancer cells. Cancer Res 2013;73:1570—80.
[131] Li J, Alyamani M, Zhang A, Chang KH, Berk M, Li Z, et al. Aberrant corticosteroid metabolism in tumor cells enables GR takeover in enzalutamide resistant prostate cancer. Elife 2017;6:e20183. https://doi.org/10.7554/eLife.20183.
[132] Wang JC, Gray NE, Kuo T, Harris CA. Regulation of triglyceride metabolism by glucocorticoid receptor. Cell Biosci 2012;2:19. https://doi.org/10.1186/2045-3701-2-19.
[133] Zhang Z, Hou X, Shao C, Li J, Cheng JX, Kuang S, et al. Plk1 inhibition enhances the efficacy of androgen signaling blockade in castration-resistant prostate cancer. Cancer Res 2014;74:6635—47.
[134] Yuan Y. Spatial heterogeneity in the tumor microenvironment. Cold Spring Harb Perspect Med 2016;6:a026583. https://doi.org/10.1101/cshperspect.a026583.
[135] Berglund E, Maaskola J, Schultz N, Friedrich S, Marklund M, Bergenstråhle J, et al. Spatial maps of prostate cancer transcriptomes reveal an unexplored landscape of heterogeneity. Nat Commun 2018;9:2419. https://doi.org/10.1038/s41467-018-04724-5.
[136] Curtius K, Wright NA, Graham TA. An evolutionary perspective on field cancerization. Nat Rev Cancer 2018;18: 19—32.
[137] De Vivar AD, Sayeeduddin M, Rowley D, Cubilla A, Miles B, Kadmon D, et al. Histologic features of stromogenic carcinoma of the prostate (carcinomas with reactive stroma grade 3). Hum Pathol 2017;63:202—11.
[138] Randall EC, Zadra G, Chetta P, Lopez BGC, Syamala S, Basu SS, et al. Molecular characterization of prostate cancer with associated Gleason Score using mass spectrometry imaging. Mol Cancer Res 2019;17:1155—65.
[139] Morse N, Jamaspishvili T, Simon D, Patel PG, Ren KYM, Wang J, et al. Reliable identification of prostate cancer using mass spectrometry metabolomic imaging in needle core biopsies. Lab Investig 2019;99:1561—71.

1.4 Fatty Acid Oxidation

Fatty acids are the main building blocks of several lipid species such as phospholipids, sphingolipids, and triglycerides. They are composed of a carboxylic group and a hydrocarbon chain of varying carbon lengths and degrees of unsaturation (number of double bonds) (Figure 1.2). Moreover, desaturation can occur at different positions of the fatty acid chain. To add to their complexity, fatty acids can also be channelled into other metabolic pathways to synthesise more complex lipid species including diacylglycerides, triacylglycerides, or converted into phosphoglycerides such as PE and PS (Koundouros and Poulogiannis 2020). As a result, fatty acids contribute to the vast structural diversity of the cellular lipid pool in order to regulate a plethora of biochemical processes including membrane biosynthesis and modulation of their fluidity, serving as signalling molecules, and as a source of fuel for energy production or storage (Beloribi-Djefaflia et al. 2016).

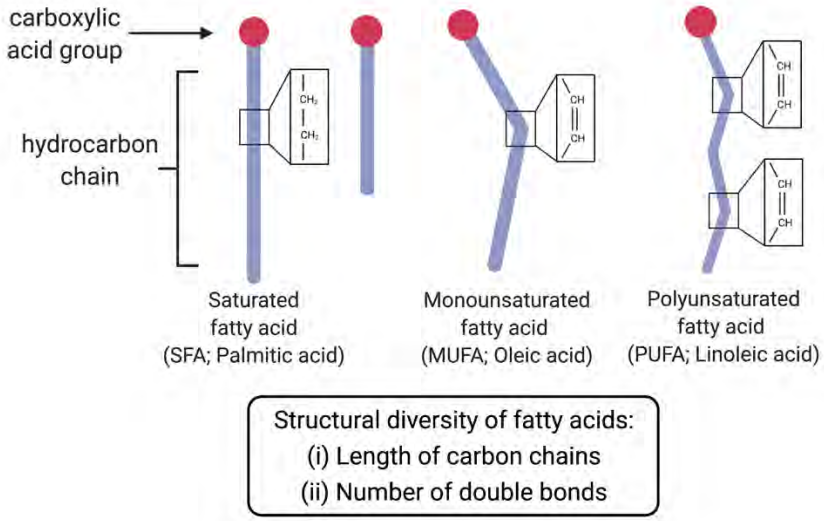

Figure 1.2 Structural diversity of fatty acids.

Simplified schematic of how fatty acids can vary in structure and their respective examples. SFAs = no double bond; MUFAs = one double bond; PUFAs = multiple double bonds.

Fatty acids can be acquired exogenously from circulation, through mobilisation of stored lipids or accumulating lipid droplets, or from *de novo* lipogenesis (Currie et al. 2013). Fatty acids are an extremely important source of energy. While the complete oxidation of a glucose molecule can generate up to 32 molecules of ATP,

complete degradation of a fatty acid molecule can yield up to 130 molecules of ATP (Röhrig and Schulze 2016). Generally, fatty acid oxidation maintains lipid homeostasis and supports mitochondrial tricarboxylic acid (TCA) cycle by generating acetyl-CoA for anabolic reactions and replenishing NADH and FADH pools (Barfeld et al. 2014). Moreover, fatty acid oxidation occurs in two distinct cellular compartments: the mitochondria and peroxisome (Table 1.1). Briefly, the mitochondria primarily functions to oxidise short, medium and long chain fatty acids (C13 – 21) whereas the peroxisome oxidises very long chain fatty acids (≥ C22) (Nagarajan et al. 2021). However, only the mitochondria are able to completely degrade fatty acids to generate energy/ATP due to the presence of the tricarboxylic acid (TCA) cycle and electron transport chain (ETC). Therefore, the main role of the peroxisome in regard to fatty acid β-oxidation is to shorten fatty acyl-CoAs before they are transported into the mitochondria for complete degradation and energy production (Wanders et al. 2015).

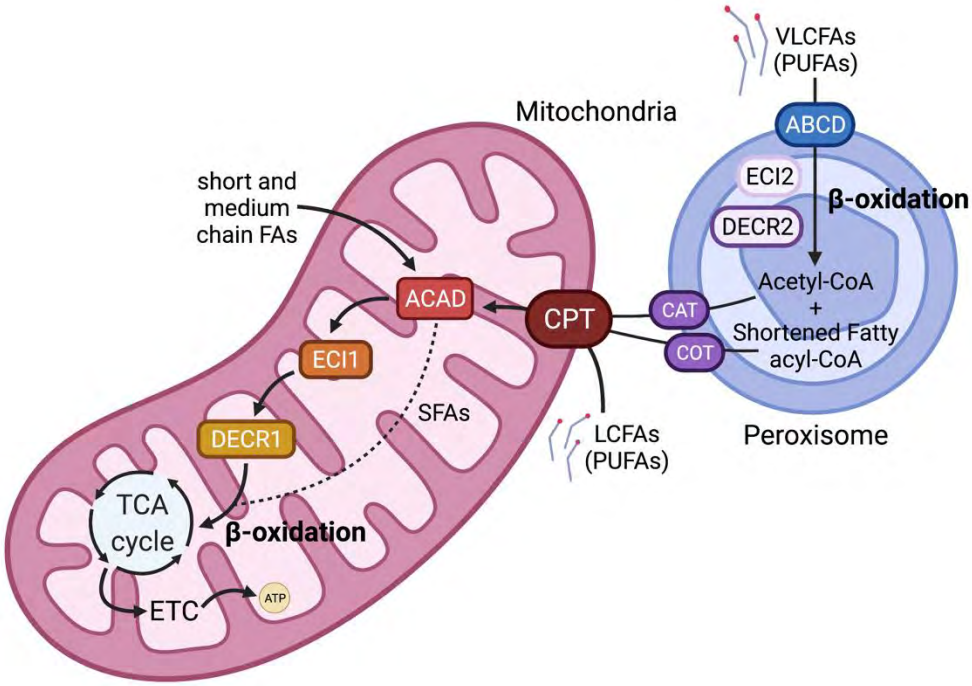

Figure 1.3 Simplified overview of mitochondrial and peroxisomal β-oxidation. Short and medium chain fatty acyl-CoAs diffuse freely into the mitochondria, whereas LCFAs are transported into the mitochondria via the CPT shuttle system. SFAs can directly enter β-oxidation (dotted line). MUFAs/PUFAs require auxiliary enzymes (i.e., DECR1/2) to process the double bonds before entering β-oxidation. ACADs represent the first step of mitochondrial β-oxidation. The end products of

mitochondrial β-oxidation are shortened fatty acyl-CoAs and acetyl-CoA, of which the latter is a substrate for mitochondrial TCA cycle to produce ATP. VLCFAs are transported into the mitochondria via ABCD transporters and undergo β-oxidation to produce shortened fatty acyl-CoAs, which are then converted to acyl-carnitines by COT and transported into the mitochondria for complete degradation. Peroxisomal acetyl-CoA can be converted to acetyl-carnitine by *CAT. COT = carnitine octanoyltransferase; CAT = carnitine acetyltransferase; LCFAs = long chain fatty acids; VLCFAs = very long chain fatty acids, SFA = saturated fatty acid; MUFA = monounsaturated fatty acid; PUFA = polyunsaturated fatty acid; ETC = electron transport chain; TCA = tricarboxylic acid cycle; CPT = carnitine palmitoyltransferase; DECR1/2 = 2,4-dienoyl-CoA reductase 1/2; ECI1/2 = enoyl-CoA delta isomerase 1/2; ACAD = acyl-CoA dehydrogenase*.

Despite their differences, the mitochondria and peroxisome share common and fundamental concepts of fatty acid oxidation such as (1) transportation of fatty acyl-CoAs into the organelle; (2) auxiliary enzymes for polyunsaturated fatty acid oxidation; and (3) production of acetyl-CoA (Demarquoy and Le Borgne 2015). Short and medium-chain fatty acids can freely diffuse through the mitochondrial membranes. In contrast, long and very long-chain fatty acids require a shuttle system for transport into the mitochondrial or peroxisomal matrix. The overall β-oxidation processes are similar in both the mitochondria and peroxisomes; this involves four consecutive reactions: (i) desaturation/oxidation; (ii) hydration; (iii) dehydrogenation; and (iv) thiolysis (Nagarajan et al. 2021). Ultimately, these reactions shorten fatty acyl-CoAs by two carbons to generate a shorten acyl-COA (which can re-enter the β-oxidation pathway) and acetyl-CoA. Of particular interest is polyunsaturated fatty acid (PUFA) oxidation. Unlike saturated and monounsaturated fatty acids (SFAs and MUFAs respectively), the presence of multiple double bonds in naturally occurring PUFAs poses a problem for both mitochondrial and peroxisomal beta oxidation. To resolve this, PUFA oxidation requires the participation of several auxiliary enzymes for example mitochondrial and peroxisomal enoyl-CoA delta isomerase 1 and 2 (ECI1 and 2), and 2,4-dienoyl-CoA reductase 1 and 2 (DECR1 and DECR2) respectively (Hiltunen and Qin 2000). These auxiliary enzymes allow the efficient break down of PUFAs by generating the

essential trans-2-enoyl-CoA intermediate which undergoes further and complete β-oxidation in the mitochondria to produce ATP (Hiltunen and Qin 2000).

Table 1.1 Comparison between mitochondrial and peroxisomal β-oxidation

	Mitochondria	**Peroxisome**
Substrates	Short, medium and long chain fatty acids (LCFA)	Very long chain fatty acids (VLCFA)
Shuttle system	Carnitine palmitoyltransferase 1 and 2 (CPT1/2)	ATP-binding cassette (ABC) transporters
End products	Acetyl-CoA, ATP (via electron transport chain), co-factors (NADH/FADH)	Shortened fatty acyl-CoA, Acetyl-CoA, co-factors, H_2O_2

While *de novo* lipogenesis has been the primary focus of most research studies, the relevance of fatty acid oxidation for cancer cell function has not been carefully examined. Owing to the rapid proliferation of malignant tumours, a net increase in fatty acid oxidation (and hence, increased ATP production) may offer prostate cancer cells a survival advantage, for instance, in nutrient-deprived conditions (Carracedo et al. 2013). To this end, fatty acid oxidation has been reported to be upregulated in several cancers including lung, breast, liver and prostate (Ma et al. 2018; Balaban et al. 2019). Notably, fatty acid oxidation is the dominant bioenergetic pathway in prostate cancer (Liu 2006). Emerging evidence suggests a role for fatty acid oxidation in cancers apart from ATP production. Besides promoting tumour growth and survival, fatty acid oxidation has been shown to drive resistance to radiation and chemotherapeutic agents and protection from oxidative stress (also discussed in section 1.2). Taken together, fatty acid oxidation represents a novel avenue to investigate new therapeutic approaches to prostate cancer treatment.

1.5 Aims and Objectives of Thesis

The overall goal of this work was to gain insights into the roles of lipid metabolism in driving prostate cancer oncogenesis, tumour progression and treatment resistance, and identify targetable pathways that could be exploited for therapeutic intervention. Currently, it is known that the tumour lipidome is dynamic and markedly altered during prostate cancer development and disease progression, and these cancer-related changes in lipid profiles provide a source of novel molecular therapeutic targets. Several aspects of targeting lipid metabolism have been well-studied over the recent years including *de novo* lipogenesis and fatty acid uptake, however fatty acid oxidation and its therapeutic potential remains an underexplored facet of lipid metabolism. More importantly, fatty acid oxidation is a way of targeting fatty acid metabolism that is irrespective of fatty acid source (i.e., synthesis or uptake). Here, we propose that fatty acid beta-oxidation is a metabolic and therapeutic vulnerability in prostate cancer tumorigenesis and treatment resistance. Notably, this work would further enhance our understanding on the role of fatty acid oxidation in driving prostate cancer development and disease progression, and facilitate the identification of new fatty acid oxidation targets that are more selective and safer to be translated into the clinic.

The work presented in this thesis is divided into two specific research aims:

Aim 1: To identify novel molecular targets of fatty acid beta-oxidation for the treatment of prostate cancer (Chapter 3 and 4).

Aim 2: To investigate a potential role for fatty acid beta-oxidation in driving treatment-resistance (Chapter 5).

Chapter 2: Materials and Methods

This Chapter contains the general materials and methods used throughout the thesis. More specific methods are described in Chapters 3, 4 and 5 respectively.

2.1 Materials and consumables

Reagents and materials that have been obtained commercially are listed below (Table 2.1).

Table 2.1 List of materials and reagents used in this thesis

Product	Supplier	Catalogue number
7-aminoactinomycin D (7-AAD)	Sigma-Aldrich	7240-37-1
Agarose, analytical grade	Sigma-Aldrich	9012-36-6
Acetonitrile (20%)	Sigma-Aldrich	75-05-8
Bradford assay reagent	BioRad	500-0006
BSA (bovine serum albumin)	Sigma-Aldrich	9048-46-8
Criterion precast gel (4-15%)	BioRad	5671084
Chloroform	Sigma-Aldrich	67-66-3
Citric acid monohydrate	Sigma-Aldrich	5949-29-1
Crystal violet	Sigma-Aldrich	548-62-9
Clarity Max western ECL substrate	BioRad	1705062
D-(+)-Glucose solution	Sigma-Aldrich	50-99-7
DAPI prolong gold mount media	Molecular Probes (Life Tech)	P26935
DHT (5α-dihydrotestosterone)	Sigma-Aldrich	521-18-6
DTT (dithiothreitol 0.1 M)	Invitrogen	27565-41-9
Dulbecco's Modified Eagle's Medium (DMEM)	Sigma-Aldrich	D5796
Dulbecco's Phosphate Buffered Saline (PBS)	Sigma-Aldrich	D8537
DMSO (dimethyl sulphoxide)	Sigma-Aldrich	67-68-5
Doxorubicin hydrochloride	Sigma-Aldrich	25316-40-9
Doxycycline hyclate	Sigma-Aldrich	10592-13-9
ECLTM western detection reagent	BioRad	170-5061
EtOH (ethanol), general use	Chem Supply	EA061
EtOH (ethanol), molecular grade	Sigma-Aldrich	64-17-5
Enzalutamide	Cayman Chemical	915087-33-1
Ethylenediamine-tetra acetic acid (EDTA)	Sigma-Aldrich	60-00-4
Etomoxir salt hydrate E1905	Sigma-Aldrich	828934-41-4

FBS (fetal bovine serum)	Sigma-Aldrich	
Formaldehyde	Chem Supply	50-00-0
Formalin 10%	Sigma-Aldrich	50-00-0
Haematoxylin Lillie/Mayer	Sigma-Aldrich	517-28-2
Hank's Balance Salt Solution	Sigma-Aldrich	H9394
HEPES (4-(2-hydroxyethyl)-1-piperazineethanesulphonic acid)	Sigma-Aldrich	7365-45-9
Hydrogen peroxide	Chem Supply	7722-84-1
iQ SYBR Green Supermix	BioRad	1708885
iScript cDNA synthesis kit	BioRad	170-8891
Luminespib (AUY922)	Novartis	747412-49-3
Lipofectamine RNAiMAX	Invitrogen	13778150
L-glutamine	Sigma-Aldrich	56-85-9
L-Carnitine hydrochloride	Sigma-Aldrich	6645-46-1
Linoleic acid	Sigma-Aldrich	60-33-3
MetOH (Methanol)	Chem Supply	67-56-1
MgCl2 (magnesium chloride)	Univar	296
MitoTracker Red CMXRos	ThermoFisher Scientific	M7512
MitoTracker Green FM	ThermoFisher Scientific	M7514
Nitrocelulose membrane (0.45 µm)	BioRad	162-0115
Nuclease-free water	Ambion Inc.	AM9937
Oleic acid	Sigma-Aldrich	112-80-1
Palmitic acid	Sigma-Aldrich	57-10-3
Perhexiline maleate 10 mM	Sigma-Aldrich	6724-53-4
PF 05175157 ACCi	Tocris	1301214-47-0
Ponceau S	Sigma-Aldrich	6226-79-5
Propidium Iodide	Sigma-Aldrich	25535-16-4
Protease Inhibitor Cocktail Tablet	Roche Applied Sciences	5892970001
Puromycin	Sigma-Aldrich	53-79-2
Potassium chloride	Sigma-Aldrich	7447-40-7
ProLong Gold Antifade Mountant with DAPI	ThermoFisher Scientific	P36941
Ribociclib Cdk4/6i	Cayman Chemical	1211441-98-3

RNeasy mini kit	Qiagen	74106
RPMI 1640 phenol red free	Sigma-Aldrich	R7509
SDS (sodium dodecyl sulphate)	Sigma-Aldrich	75746
Skim milk powder	Coles brand	N/A
Sodium hydroxide 5 M	Sigma-Aldrich	1310-73-2
Sodium chloride	Sigma-Aldrich	7647-14-5
Sodium pyruvate solution	Sigma-Aldrich	113-24-6
Tetracycline hydrochloride	Sigma-Aldrich	9002-93-1
Triton-X 100	Sigma-Aldrich	T8787
Trypsin EDTA solution	Sigma-Aldrich	T4049
Tween® 20	Sigma-Aldrich	9005-64-5
TRI reagent	Sigma-Aldrich	108-95-2, 593-84-0
Trolox	Tocris Bioscience	53188-07-1
Trypan blue 0.4 % liquid	Sigma-Aldrich	72-57-1
Xylene	Chem Supply	1330-20-7
Z-VAD-FMK	Sigma-Aldrich	161401-82-7

2.2 Buffers and solutions

Table 2.2 lists the compositions of buffers and solutions that have been made for experimentation in this thesis.

Table 2.2 List of buffers and solutions with compositions

Buffers and solutions	Composition
Citrate Buffer	0.525g Citric acid monohydrate Volume to 250mL with RO water pH 6.5
Dextran Coated Charcoal (DCC)	5g Charcoal 0.5g Dextran 20mL Glycerol Volume to 1L with TE buffer
Loading dye (6x) for western blot	7mL 4x Tris-Cl/SDS 3mL Glycerol 1g SDS 0.93g DTT 1.2mg Bromophenol blue Volume to 10mL with RO water Store at -20°C
Ponceau S stain	2g Ponceau S 30g Trichloracetic acid 30g Sulphosalycylic acid Volume to 100mL with RO water
RIPA buffer	10mM Tris 150mM NaCl 1mM EDTA 1% Triton X-100
Running buffer (10x)	77.5g Tris base 360g Glycine 25g SDS 2.5L RO water

Running buffer (1x)	1L 10x Running buffer 9L RO water
Seahorse substrate-limited media	Dulbecco's Modified Eagle's Medium (DMEM) 0.5mM Glucose 1.0mM Glutamine 0.5mM Carnitine 1% FBS
Seahorse fatty acid oxidation medium	111mM NaCl 4.7mM KCl 2.0mM $MgSO_4$ 1.2mM Na_2HPO_4 2.5mM Glucose 0.5mM Carnitine 5mM HEPES
SDS 20%	20g SDS Volume to 100mL with RO water
TBS (10x)	151.5g Tris 219g NaCl Volume to 2.5L with RO water pH 7.4
TBST (1x)	2.5mL Tween20 250mL 10x TBS 2.25L RO water
Transfer buffer (10x)	77.5g Tris 360g Glycine Volume to 2.5L with RO water
Transfer buffer (1x)	1% 10x Transfer buffer 20% Methanol Volume to 2.5L with RO water Store at 4°C

Tris 1M, pH 7.4	60.57g Tris Volume to 500mL with RO water pH 7.4
Tris-Cl/SDS (4x)	3.025g Tris-Cl Volume to 20mL with RO water pH 6.8 0.2g SDS Volume to 50mL with RO water

2.3 Cell Culture

Human normal prostate epithelial cell lines PNT1 and PNT2, and human prostate carcinoma cell lines, LNCaP, VCaP, 22Rv1 and C42B were obtained from the American Type Culture Collection (ATCC). Castrate resistant and enzalutamide resistant cell lines, V16D and MR49F, were derived from serial xenograft passages of LNCaP cells and were a kind gift from Professor Amina Zoubeidi's laboratory (Toren et al. 2016). Cell Bank Australia performed verification of all cell lines in 2018 via short-tandem repeat profiling. PNT1, PNT2, LNCaP, 22Rv1, C42B and V16D cell lines were maintained in RPMI-1640 media supplemented with 10 % Fetal Bovine Serum (FBS). VCaP cell line was maintained in Dulbecco's Modified Eagle's Medium (DMEM) supplemented with 10 % FBS and 1 nM dihydrotestosterone (DHT). MR49F cell line was maintained in RPMI-1640 media supplemented with 10 % FBS and 10 μM of enzalutamide.

To prepare cells for storage in liquid nitrogen, fully confluent T75 flasks were collected using trypsin, followed by centrifugation at 1,500 x g for 5 min. Pellets were resuspended in 4 mL of freezing mix (90 % FBS and 10 % DMSO). 1 mL of cell suspension was then aliquoted into each cryovial, labelled appropriately and placed in an isopropanol filled Mr. Frosty freezing container at -80 °C. Cells were then transferred to liquid nitrogen for long term storage. Human prostate cancer cell lines obtained from liquid nitrogen stored were thawed quickly by gentle agitation in a 37 °C water bath. Once thawed, the cell suspension was then mixed with 9 mL of cell line specific culture medium and centrifuge at 1,500 x g for 5 min. Pellets were resuspended in 10 mL of cell line specific culture medium, transferred directly into a T25 flask and incubated overnight in a 5 % CO_2 and 37 °C incubator. Cells were then passaged into a T75 flask after 48 h prior to use in experiments.

2.4 Short-interfering RNA (siRNA) transfection

To transfect siRNA, siRNA-Lipofectamine RNAiMAX complexes were prepared according to the manufacturer's instructions (Invitrogen). siRNA (5 nM) and Lipofectamine RNAiMAX were diluted in serum-free RPMI (phenol red-free) media and incubated for 5 min at RT. An equal volume of Lipofectamine RNAiMAX was added to the diluted siRNA, vortexed and incubated for 10 min at RT. The siRNA-

Lipofectamine RNAiMAX complexes were added to each well of a 6-well (250 µL), 24-well (50 µL), or 96-well plate (10 µL). 1 mL (6-well and 24-well plates) or 100 µL (96-well plate) of prostate cancer cell suspensions diluted in RPMI media supplemented with 10 % FBS were added to each well containing the siRNA-Lipofectamine RNAiMAX complexes and mixed gently by rocking the plate back and forth. Cells were incubated for 24 h to 96 h as indicated in a 5 % CO_2 and 37 °C incubator.

2.5 Immunohistochemistry

Prostate cancer explant tissues were cultured, processed and embedded in paraffin. 2 µm sections were cut onto superfrost ultra-plus slides using a microtome and placed on a heating block at 60 °C for at least 2 h. Tissue sections were then de-waxed in xylene, re-hydrated in ethanol, and washed in PBS before proceeding to block endogenous peroxidase activity with 1 % hydrogen peroxide for 5 min. Antigen retrieval was performed using citrate buffer (0.525 g in 250 mL RO-water, pH 6.5), with a Biocare Medical Decloaking Chamber V3.7.2.2 (110 °C for 15 min). Sections were blocked for 30 min at room temperature (RT) with 10 % goat serum (DAKO) in a humidifier box. Sections were incubated with primary antibodies diluted in blocking solution overnight at 4 °C. Cells were then washed and incubated with secondary antibody for 1 h at RT, followed by a 1 h incubation at RT with streptavidin. 3,3'-diaminobenzidine was used as the substrate for streptavidin-biotin peroxidase detection (DAKO). Counterstaining (90 sec haematoxylin, 2 min tap water) was then performed, followed by dehydration and clearing in ethanol, and de-waxing in xylene. Coverslipping was done using DPX mounting media. Slides were imaged with a Nanozoomer digital slide scanner (Hamamatsu) and viewed with NDPview software. Staining quantification was performed using video image analysis. Manual counting was performed by two separate researchers for quantification of Ki67 staining.

2.6 Western blot analysis

Cells were washed with 1x PBS and lysed in 150 µL of ice-cold RIPA buffer containing protease inhibitors and phosphatase inhibitors. After the addition of RIPA buffer, cells were collected by scrapping and homogenised using an ultra-fine insulin syringe. Samples were then centrifuged (10,000 x g, 10 min at 4 °C) and total protein

concentration was quantified using Bradford assay on a FLUOstar Omega microplate reader (BMG LABTECH). Aliquots of each sample (20 µg protein) were mixed with 6x loading dye and milliQ water, and heated at 95 °C for 5 min. Proteins were then separated by SDS-PAGE using a 4 – 15 % gradient gel (BioRad) in 1x SDS running buffer, and transferred to nitrocellulose membranes (BioRad) by wet-transfer (BioRad Criterion Blotter) in transfer buffer. Membranes were blocked with milk (3 % skim milk powder in 1x TBST) before being probed overnight with primary antibodies at 4 °C. The following day, membranes with washed with TBST and probed with HRP-conjugated secondary antibodies for 1.5 h at RT. For detection, membranes were incubated with ECL (BioRad) for 1 min and imaged on a BioRad Chemidoc MP imaging system and processed using Image Lab Software.

2.7 RNA extraction and quantitative reverse-transcription PCR

RNA was isolated from cells using the RNeasy Mini kit (Qiagen) together with an on-column DNAse treatment (Qiagen), according to the manufacturer's protocol. cDNA was synthesised with the iScript™ Reverse Transcription kit (BioRad) using a thermal cycler (5 min at 42 °C, 30 min at 42 °C, 5 min at 85 °C), and diluted with milliQ water (1:10). Quantitative reverse-transcription (RT)-PCR was performed in triplicate with BioRad C1000 Touch™ Thermal Cycler and CFX384™ Real-Time System using SYBR Green PCR Master Mix (BioRad) together with sequence-specific primers. Expression analysis was performed using CFX Manager Software Version 3.0 (BioRad). RNA expression of target genes was expressed as relative to reference genes (*GUSB* and *L19*).

Chapter 3: DECR1 is a key survival factor that protects prostate cancer cells from ferroptosis

This Chapter includes a publication, followed by a supplementary chapter that complements the work in this Chapter as part of this PhD. Additional figures included at the end of this chapter display data produced during preparation of this manuscript that has not been included in the final publication.

STATEMENT OF AUTHORSHIP

Title of Paper	Human DECR1 is an androgen-repressed survival factor that regulates PUFA oxidation to protect prostate tumor cells from ferroptosis
Publication Status	☒ Published ☐ Submitted for Publication ☐ Accepted for Publication ☐ Unpublished and Unsubmitted work written in a manuscript style
Publication Details	Nassar, ZD*, Mah, CY*, Dehairs, J, Burvenich, IJ, Irani, S, Centenera, MM, Helm, M, Shrestha, RK, Moldovan, M, Don, AS, Holst, J, Scott, AM, Horvath, LG, Lynn, DJ, Selth, LA, Hoy, AJ, Swinnen, JV & Butler, LM 2020, 'Human DECR1 is an androgen-repressed survival factor that regulates PUFA oxidation to protect prostate tumor cells from ferroptosis', *eLife*, vol. 9, pp. e54166, DOI: https://doi.org/10.7554/eLife.54166.

Principal Author

Name of Principal Author (Candidate)	Chui Yan Mah		
Contribution to the Paper	Methodology, Formal analysis, Investigation, Data curation, Validation, Visualization, Writing – Original and draft preparation, Writing – Review and editing		
Overall Percentage (%)	35 %		
Signature		Date:	26/03/2021

Name of Principal Author	Zeyad Nassar		
Contribution to the Paper	Conceptualization, Methodology, Formal analysis, Investigation, Data curation, Supervision, Funding acquisition, Writing – Original and draft preparation, Writing – Review and editing		
Signature		Date:	26/03/2021

Co-Author Contributions

By signing the Statement of Authorship, each author certifies that:

i.! the candidate's stated contribution to the publication is accurate (as detailed above);
ii.! permission is granted for the candidate to include the publication in the thesis; and
iii.! the sum of all co-author contributions is equal to 100% less than the candidate's stated contribution.

Name of Co-Author	Jonas Dehairs		
Contribution to the Paper	Data curation, Methodology, Writing – Review and editing		
Signature		Date:	22/03/2021

Name of Co-Author	Ingrid Burvenich		
Contribution to the Paper	Methodology, Investigation, Writing – Review and editing		
Signature		Date:	22/03/2021

Name of Co-Author	Swati Irani		
Contribution to the Paper	Methodology, Investigation, Writing – Review and editing		
Signature		Date:	30/03/2021

Name of Co-Author	Margaret Centenera		
Contribution to the Paper	Supervision, Methodology, Writing – Review and editing		
Signature		Date:	30/03/2021

Name of Co-Author	Madison Helm		
Contribution to the Paper	Methodology, Investigation		
Signature		Date:	22/3/21

Name of Co-Author	Raj Shrestha		
Contribution to the Paper	Investigation, Writing – Review and editing		
Signature		Date:	22/03/2021

Name of Co-Author	Max Moldovan		
Contribution to the Paper	Formal analysis, Investigation, Writing – Review and editing		
Signature		Date:	24 Mar 2021

Name of Co-Author	Anthony Don		
Contribution to the Paper	Methodology, Investigation, Writing – Review and editing		
Signature		Date:	22/03/2021

Name of Co-Author	Jeff Holst		
Contribution to the Paper	Methodology, Writing – Review and editing		
Signature		Date:	22/03/2021

Name of Co-Author	Andrew Scott		
Contribution to the Paper	Supervision, Writing – Review and editing		
Signature		Date:	22/3/2021
Name of Co-Author	Lisa Horvath		
Contribution to the Paper	Methodology, Writing – Review and editing		
Signature		Date:	22/3/21
Name of Co-Author	David Lynn		
Contribution to the Paper	Data curation, Supervision, Methodology, Formal analysis, Writing – Review and editing		
Signature		Date:	22/3/21
Name of Co-Author	Luke Selth		
Contribution to the Paper	Data curation, Supervision, Investigation, Visualization, Methodology, Formal analysis, Writing – Review and editing		
Signature		Date:	22/03/2021
Name of Co-Author	Andrew Hoy		
Contribution to the Paper	Data curation, Supervision, Investigation, Methodology, Writing – Review and editing		
Signature		Date:	22 March 2021
Name of Co-Author	Johannes Swinnen		
Contribution to the Paper	Conceptualization, Data curation, Supervision, Funding acquisition, Methodology, Writing – Review and editing		
Signature		Date:	22 March 2021
Name of Co-Author	Lisa Butler		
Contribution to the Paper	Conceptualization, Resources, Data curation, Supervision, Funding acquisition, Writing – Original and draft preparation, Project administration, Writing – Review and editing		
Signature		Date:	01/04/2021

eLife

RESEARCH ARTICLE

Human DECR1 is an androgen-repressed survival factor that regulates PUFA oxidation to protect prostate tumor cells from ferroptosis

Zeyad D Nassar[1,2†], Chui Yan Mah[1,2†], Jonas Dehairs[3], Ingrid JG Burvenich[4], Swati Irani[1,2], Margaret M Centenera[1,2], Madison Helm[1,2], Raj K Shrestha[5], Max Moldovan[2], Anthony S Don[6], Jeff Holst[7], Andrew M Scott[4], Lisa G Horvath[8], David J Lynn[2,9], Luke A Selth[1,5,9], Andrew J Hoy[10], Johannes V Swinnen[3], Lisa M Butler[1,2]*

[1]University of Adelaide Medical School and Freemasons Foundation Centre for Men's Health, University of Adelaide, Adelaide, Australia; [2]South Australian Health and Medical Research Institute, Adelaide, Australia; [3]KU Leuven- University of Leuven, LKI- Leuven Cancer Institute, Department of Oncology, Laboratory of Lipid Metabolism and Cancer, Leuven, Belgium; [4]Tumour Targeting Laboratory, Olivia Newton-John Cancer Research Institute, and School of Cancer Medicine, La Trobe University, Melbourne, Australia; [5]Dame Roma Mitchell Cancer Research Laboratories, University of Adelaide, Adelaide, Australia; [6]NHMRC Clinical Trials Centre, and Centenary Institute, The University of Sydney, Camperdown, Australia; [7]Translational Cancer Metabolism Laboratory, School of Medical Sciences and Prince of Wales Clinical School, UNSW Sydney, Sydney, Australia; [8]Garvan Institute of Medical Research, NSW 2010; University of Sydney, NSW 2006; and University of New South Wales, Darlinghurst, Australia; [9]College of Medicine and Public Health, Flinders University, Bedford Park, Australia; [10]Discipline of Physiology, School of Medical Sciences, Charles Perkins Centre, Faculty of Medicine and Health, The University of Sydney, Camperdown, Australia

***For correspondence:** lisa.butler@adelaide.edu.au

[†]These authors contributed equally to this work

Competing interests: The authors declare that no competing interests exist.

Funding: See page 20

Received: 04 December 2019
Accepted: 16 July 2020
Published: 20 July 2020

Reviewing editor: Nima Sharifi, Cleveland Clinic, United States

© Copyright Nassar et al. This article is distributed under the terms of the Creative Commons Attribution License, which permits unrestricted use and redistribution provided that the original author and source are credited.

Abstract Fatty acid β-oxidation (FAO) is the main bioenergetic pathway in human prostate cancer (PCa) and a promising novel therapeutic vulnerability. Here we demonstrate therapeutic efficacy of targeting FAO in clinical prostate tumors cultured ex vivo, and identify *DECR1*, encoding the rate-limiting enzyme for oxidation of polyunsaturated fatty acids (PUFAs), as robustly overexpressed in PCa tissues and associated with shorter relapse-free survival. *DECR1* is a negatively-regulated androgen receptor (AR) target gene and, therefore, may promote PCa cell survival and resistance to AR targeting therapeutics. DECR1 knockdown selectively inhibited β-oxidation of PUFAs, inhibited proliferation and migration of PCa cells, including treatment resistant lines, and suppressed tumor cell proliferation and metastasis in mouse xenograft models. Mechanistically, targeting of DECR1 caused cellular accumulation of PUFAs, enhanced mitochondrial oxidative stress and lipid peroxidation, and induced ferroptosis. These findings implicate PUFA oxidation via DECR1 as an unexplored facet of FAO that promotes survival of PCa cells.

Introduction

Prostate cancer (PCa) is the most prevalent male cancer and the second leading cause of cancer deaths in men in Western societies (**Bray et al., 2018**). For patients with locally-recurrent and/or metastatic disease, androgen deprivation therapy (ADT) has remained the frontline strategy for clinical management since the 1940s (**Huggins and Hodges, 1941**), due to the dependence of PCa cells on androgens for growth and survival. Although ADT is initially effective in most patients, ultimately all will relapse with castration resistant prostate cancer (CRPC), which remains incurable. The failure of ADT is attributed to the emergence of adaptive survival pathways that reprogram androgen signaling and/or activate alternative tumor survival pathways. Consequently, the development and FDA approval of agents that more effectively target androgen signaling, including enzalutamide (ENZ, Xtandi; an AR antagonist) (**Tran et al., 2009**; **Cai and Balk, 2011**; **Rodrigues et al., 2014**), has expanded the therapeutic options for CRPC. Nevertheless, even these approaches cannot durably control tumor growth and there is considerable variability in the nature and duration of responses between different patients (**Tran et al., 2009**; **Scher et al., 2012**; **Davis et al., 2019**). Thus, alternative therapeutic strategies that enhance response to ADT, and thereby prevent or delay PCa progression to CRPC, are essential.

Increasingly, targeting cancer cell metabolism is a focus of research efforts (**Hanahan and Weinberg, 2011**). While fundamental differences in cellular metabolism pathways between normal and malignant cells were detected by Warburg in the 1920s (**Warburg et al., 1927**), clinical targeting of cancer metabolism has not kept pace with the research advances in understanding metabolic features of cancer cells. PCa is mainly dependent on lipid metabolism for energy production (**Liu, 2006**). The overexpression of genes involved in lipid metabolism is characteristic of PCa at both early and advanced stages (**Wu et al., 2014**; **Chen et al., 2018**; **Swinnen et al., 2002**; **Zadra et al., 2013**; **Zadra and Loda, 2018**; **Ettinger et al., 2004**; **Nomura et al., 2011**), while recent proteomic analyses of primary PCa and bone metastases have shown clear associations between levels of lipid metabolic enzymes, PCa initiation and progression (**Iglesias-Gato et al., 2016**; **Iglesias-Gato et al., 2018**). These observations suggest that PCa may be particularly amenable to metabolic targeting strategies. Despite this, the role and complexity of lipid/fatty acid (FA) metabolism in PCa and its potential as a target for therapy remains underexplored, particularly in the context of a more complex tumor microenvironment.

Until recently, most attention has focused on the therapeutic targeting of de novo FA synthesis and, most recently, uptake of FAs in PCa to limit their availability as a source of energy and cell membrane phospholipids (**Zadra et al., 2013**; **Zadra and Loda, 2018**; **Watt et al., 2019**). However, it has become evident in work from our group and others that β-oxidation of FAs, as the ultimate fate of FAs in the energy production cycle, is upregulated in PCa cells, stimulated by a lipid-rich extracellular environment and critical for viability (**Liu, 2006**; **Schlaepfer et al., 2014**; **Balaban et al., 2019**). In this study, we evaluated the targeting of FA β-oxidation (FAO) in patient-derived prostate tumor explants (PDE) to provide the first clinically-relevant evidence that targeting this pathway is efficacious. We subsequently identify DECR1, a rate-limiting enzyme in an auxiliary pathway for polyunsaturated fatty acid (PUFA) β-oxidation, as a promising novel therapeutic vulnerability for PCa. Importantly, we show that DECR1 is an androgen-repressed gene induced in PCa cells in response to ADT and/or AR-targeted therapies, implicating PUFA oxidation as an adaptive survival response that may contribute to emergence of CRPC and treatment resistance.

Results

Targeting FA oxidation is efficacious in patient-derived PCa explants

In addition to our recent report of enhanced FAO in PCa cells (**Balaban et al., 2019**), an accumulating body of evidence supports the efficacy of targeting key enzymes involved in FAO using in vitro and in vivo models of PCa (**Itkonen et al., 2017**; **Schlaepfer et al., 2014**; **Flaig et al., 2017**). However, to date there is limited evidence that targeting this pathway would be clinically efficacious, which prompted us to target this pathway in clinical tumors. Using our well-defined patient derived explant (PDE) model that recapitulates the complexity of the clinical tissue microenvironment (**Centenera et al., 2012**), we targeted the rate-limiting enzyme in mitochondrial FAO, carnitine palmitoyltransferase-1 (CPT-1), in cultured PDEs using the chemical inhibitor etomoxir. Consistent with

literature reports, etomoxir had weak activity against the LNCaP PCa cell line in vitro, with an IC50 of 170 µM (***Figure 1—figure supplement 1A***), but was considerably potent in the PDEs, in which a dose of 100 µM inhibited cell proliferation by an average of 48.4 ± 16.6% (n = 13 patients; p<0.05) (***Figure 1A***). Etomoxir effectively inhibited FAO in the tissues, evidenced by a significant decrease in multiple acylcarnitines in the conditioned medium (***Figure 1B***).

In order to prioritize key functional genes involved in PCa progression, we conducted a meta-analysis of the expression of 735 genes involved in lipid metabolism (as identified from REACTOME) in four clinical datasets with malignant and matched normal RNA sequencing data (***Nikitina et al., 2017***; ***Ren et al., 2012***; ***Ding et al., 2016***). Genes were rank-ordered on the basis of their *meta effect size* scores in PCa malignant versus matched normal tissues (***Figure 1—figure supplement 1B***). The meta-analysis revealed a strikingly consistent deregulation of lipid metabolism genes, including genes involved in FAO (***Figure 1C***), despite the predicted high inter-individual heterogeneity of patient PCa tissues. We conducted disease-relapse survival analysis using TCGA data for each of the top 20 genes from the meta-analysis. This identified *DECR1*, a rate-limiting enzyme in the mitochondrial β-oxidation of polyunsaturated fatty acids, as a robustly overexpressed gene in PCa tissues that is associated with shorter relapse-free survival rates.

DECR1 is upregulated in clinical prostate tumors

Consistently, *DECR1* mRNA expression was significantly higher in malignant compared to benign prostate tissues in ten independent expression datasets of PCa tissues versus non-malignant tissues (***Figure 1D***, ***Figure 1—figure supplement 1C***). Further analysis of the TCGA data revealed increased *DECR1* expression with increased Gleason score or in with advanced disease stage (***Figure 1E***). Consistent with our observation of increased DECR1 mRNA expression in PCa, *DECR1* gene copy gain was evident in several clinical datasets accessed via cBioPortal (***Cerami et al., 2012***; ***Figure 1F***). Interestingly, the top three cancer types exhibiting increased *DECR1* copy gain were hormone-dependent tumors (uterine, breast and prostate), suggestive of a relationship between DECR1 expression and hormone signaling (***Figure 1G***). *DECR1* mRNA expression was associated with shorter relapse-free survival rates and overall survival rates (***Figure 1H***), and in the TCGA dataset, *DECR1* amplification was significantly associated with shorter recurrence-free survival rates (***Figure 1I***).

We confirmed overexpression of DECR1 protein in clinical PCa using two independent proteomic datasets (***Figure 2A***). We observed overexpression of DECR1 in PCa tissues (n = 8) compared with benign tissues (n = 3) (***Figure 2B***), and increased expression was evident in high grade versus low grade cancer tissue. Quantitative IHC staining analysis revealed a significant increase of DECR1 expression in malignant *vs* benign tissues. Furthermore, intra-tissue analysis exposed a significant increase of DECR1 expression in malignant regions *vs* benign ones within the same core (***Figure 2C***). DECR1 expression was markedly increased in a panel of hormone-dependent and -independent cancer cell lines compared with non-malignant PNT1 and PNT2 prostate cell lines (***Figure 2D***). Consistent with its function, DECR1 localises to the mitochondria, confirmed using immunocytochemistry and Western blot of nuclear, cytoplasmic and mitochondrial cell fractions (***Figure 2E***). Together, the mRNA and protein findings suggest that expression of DECR1 is closely linked to PCa progression and patient outcomes, and therefore might represent an unexplored therapeutic target.

DECR1 is a directly androgen-repressed gene in PCa

The relationship between androgen receptor (AR) signaling and lipid metabolic genes is well established. Many studies have reported a marked stimulatory effect of AR on key lipid metabolism pathways either directly or indirectly through activation of a family of transcription factors called sterol regulatory element-binding proteins (SREBPs) (***Butler et al., 2016***). We therefore investigated the relationship between AR and DECR1 using a panel of in vitro, ex vivo and in vivo models. DECR1 expression is notably more abundant in AR-negative cells (PC3) than in AR-expressing cells (***Figure 2D***), consistent with negative regulation of DECR1 expression by AR. We confirmed that androgen (5α-dihydrotestosterone) significantly decreased DECR1 expression in androgen-dependent LNCaP and VCaP cell lines at both mRNA and protein levels (***Figure 3A***). Data mining of publicly available microarray datasets also revealed downregulation of DECR1 in LNCaP cells after treatment with DHT or the synthetic androgen R1881 (***Figure 3—figure supplement 1A***); GSE7868,

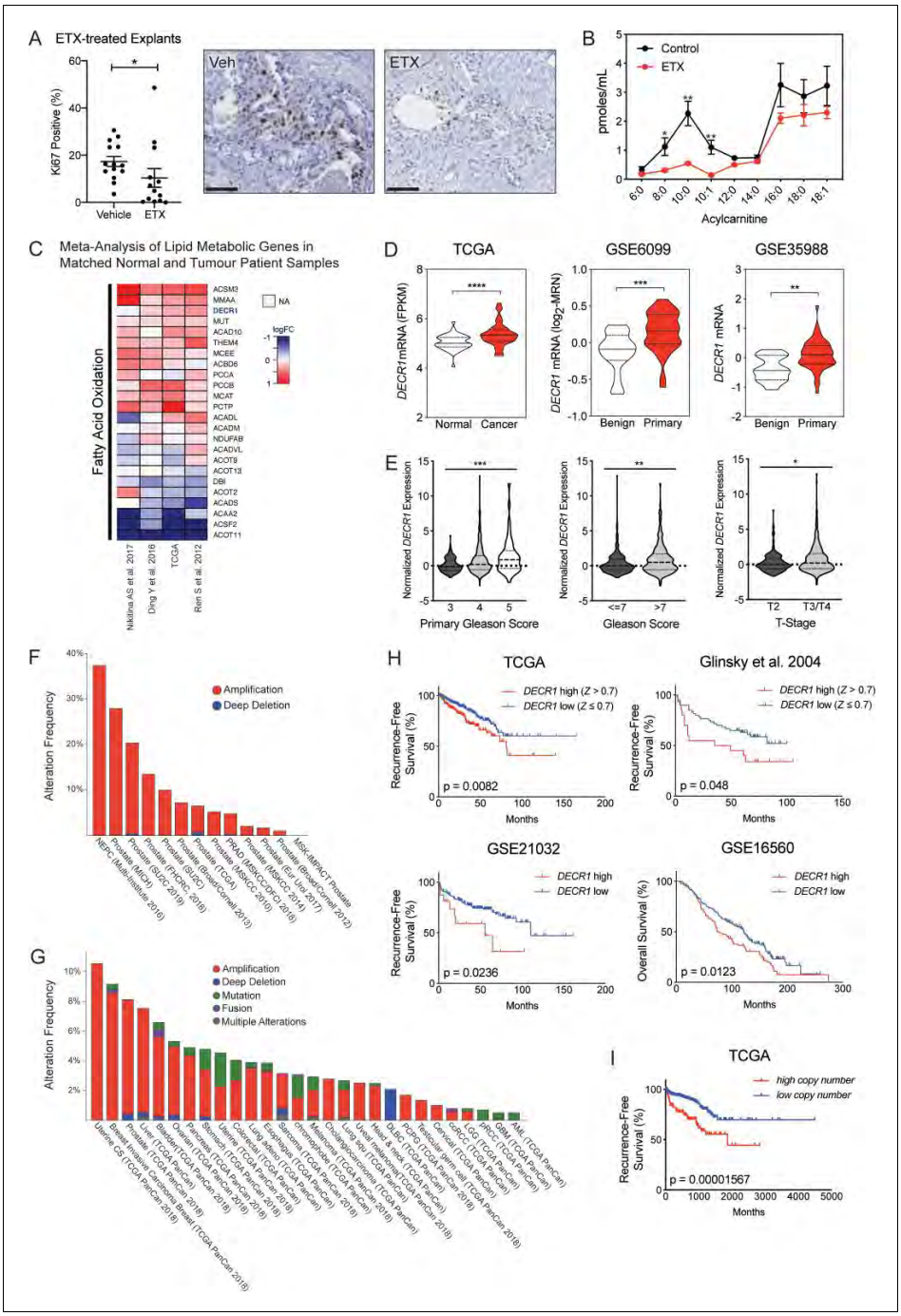

Figure 1. Fatty acid β-oxidation genes are overexpressed in prostate cancer and targeting this process is effective in patient-derived human prostatic ex vivo tumor explants. (**A**) Etomoxir reduced cell proliferation in patient-derived human prostatic ex vivo tumor explants. Tissues were treated with 100 µM etomoxir for 72 hr, sections were fixed in formalin, paraffin embedded and stained against the proliferative marker Ki67 (n = 13) (scale bar = 50 µm). (**B**) Etomoxir (100 µM) decreased acylcarnitine species, the products of CPT1 activity. Acylcarnitines secreted to the conditioned medium were

Figure 1 continued on next page

Figure 1 continued

measured after 72 hr treatment of PDEs (n = 9). (**C**) A meta-analysis of fatty acid oxidation genes using four clinical datasets with malignant and matched normal RNA-sequencing data (n = 122). Genes were rank-ordered on the basis of their *meta effect size* scores in PCa malignant tissues versus matched normal tissues. (**D**) Violin plots demonstrate DECR1 mRNA overexpression in PCa primary/malignant tissues compared to normal/benign tissues in three independent datasets. (**E**) DECR1 mRNA expression is associated with PCa primary Gleason score, total Gleason score (>7) and diseases stage (T-stage). Data were extracted from TCGA PCa dataset. (**F**) Histogram displaying DECR1 mutation and copy-number amplification frequency across 13 PCa genomic datasets, and (**G**) across 28 tumor types. Histograms were obtained from CbioPortal platform. (**H**) DECR1 mRNA expression is associated with shorter relapse-free survival in TCGA PCa, ***Glinsky et al., 2005*** and GSE21032 datasets, and shorter overall survival rates in GSE16560 dataset. (**I**) DECR1 copy number amplification frequency is associated with shorter relapse-free survival in TCGA PCa dataset. Data in (**A**) are represented as as the mean ± s.e.m and were statistically analysed using a Wilcoxon matched-pairs signed rank test. Data in (**B**) are represented as the mean ± s.e.m and were statistically analysed using two-tailed Student's *t*-test. Data in (**D**) and (**E**) are represented as violin plots in GraphPad prism: the horizontal line within the violin represents the median, and were statistically analysed using a Mann-Whitney two-tailed t-test. Data in (**H**) and (**I**) were statistically analysed using a two-sided log-rank test. *p<0.05, **p<0.01, ***p<0.001 and ****p<0.0001.
The online version of this article includes the following figure supplement(s) for figure 1:

Figure supplement 1. Fatty acid metabolism is consistently altered in clinical prostate tumors.

GSE22606). In contrast to the effect of androgens, AR-targeted therapies increase DECR1 expression. LNCaP and VCaP cell treatment with the androgen antagonist enzalutamide (ENZ) significantly increased DECR1 expression at both mRNA and protein levels (***Figure 3B***). In vivo, LNCaP tumors exhibited increased DECR1 expression in mice treated with ENZ (10 mg/kg) or castration, which was enhanced further in mice treated with both ENZ and castration (***Figure 3C***). Our observations were supported by published microarray datasets which showed that treatment of LNCaP or VCaP cells with ENZ increases *DECR1* mRNA expression (***Figure 3—figure supplement 1B***; GSE69249). In vivo, castration of mice increased DECR1 expression in prostate (***Figure 3—figure supplement 1C***; GSE5901), while in LNCaP/AR xenografts treatment with the AR antagonist ARN-509 (apalutamide) for 4 days significantly increased DECR1 expression (***Figure 3—figure supplement 1D***; GSE52169). To confirm androgenic regulation of DECR1 in a clinical context, we validated these data using PDEs. ENZ treatment of PDEs significantly increased DECR1 expression whereas, as expected, mRNA levels of the well-characterized AR target genes *KLK3* and *KLK2* were decreased (***Figure 3D, E***). To determine whether AR directly represses *DECR1*, we interrogated published chromatin immunoprecipitation (ChIP) sequencing data. In VCaP cells, AR bound strongly to the *DECR1* promoter in response to DHT treatment, but not when co-treated with AR antagonists (***Figure 3F***; GSE55064). Moreover, AR binding was enriched at the *DECR1* promoter in benign and malignant prostate tissues (***Figure 3—figure supplement 1E***; GSE56288). A site-specific ChIP-qPCR assay revealed DHT-stimulated AR occupancy at this region in LNCaP cells (***Figure 3G***). Collectively, these data reveal *DECR1* as a novel AR-repressed gene.

Targeting DECR1 disrupts PUFA oxidation in PCa cells

FAs are metabolized mainly in mitochondria through the β-oxidation process to generate acetyl-CoA, which enters the tricarboxylic acid cycle (TCA) and produces ATP and NADH as energy for the cell. Unlike saturated FAs, all unsaturated FAs with double bonds originating at even-numbered positions, and some unsaturated FAs with double bonds originating at odd-numbered positions, require three auxiliary enzymes to generate intermediates that are harmonious with the standard β-oxidation pathway (***Hiltunen and Qin, 2000***; ***Shoukry and Schulz, 1998***): Enoyl CoA isomerase (ECI1), 2,4 Dienoyl-CoA reductase (DECR1) and Dienoyl CoA isomerase (ECH1) (***Figure 4A***). DECR1 catalyses the rate limiting step in this pathway (***Alphey et al., 2005***). Given the critical role of DECR1 in PUFA metabolism, we studied the consequences of DECR1 downregulation on β-oxidation of PUFAs in PCa cells. DECR1 knockdown was achieved successfully (>80% downregulation) using two different siRNAs (***Figure 4B***). DECR1 knockdown resulted in an increase in linoleic acid (***Figure 4C***) as well as an accumulation of 2-trans,4-cis-decadienoylcarnitine (acylcarnitine 10:2; ***Figure 4D***), an intermediate of linoleic acid metabolism, indicating incomplete PUFA β-oxidation. Mitochondrial β-oxidation provides reducing equivalents that drive ATP production. LNCaP cells increased ATP levels in response to exogenous linoleic acid supplementation when cultured in glucose-free media containing the lipase inhibitor diethylumbelliferyl phosphate (DEUP), to prevent the cells from using intracellular FAs (***Figure 4E***). However, cells transfected with DECR1-targeting

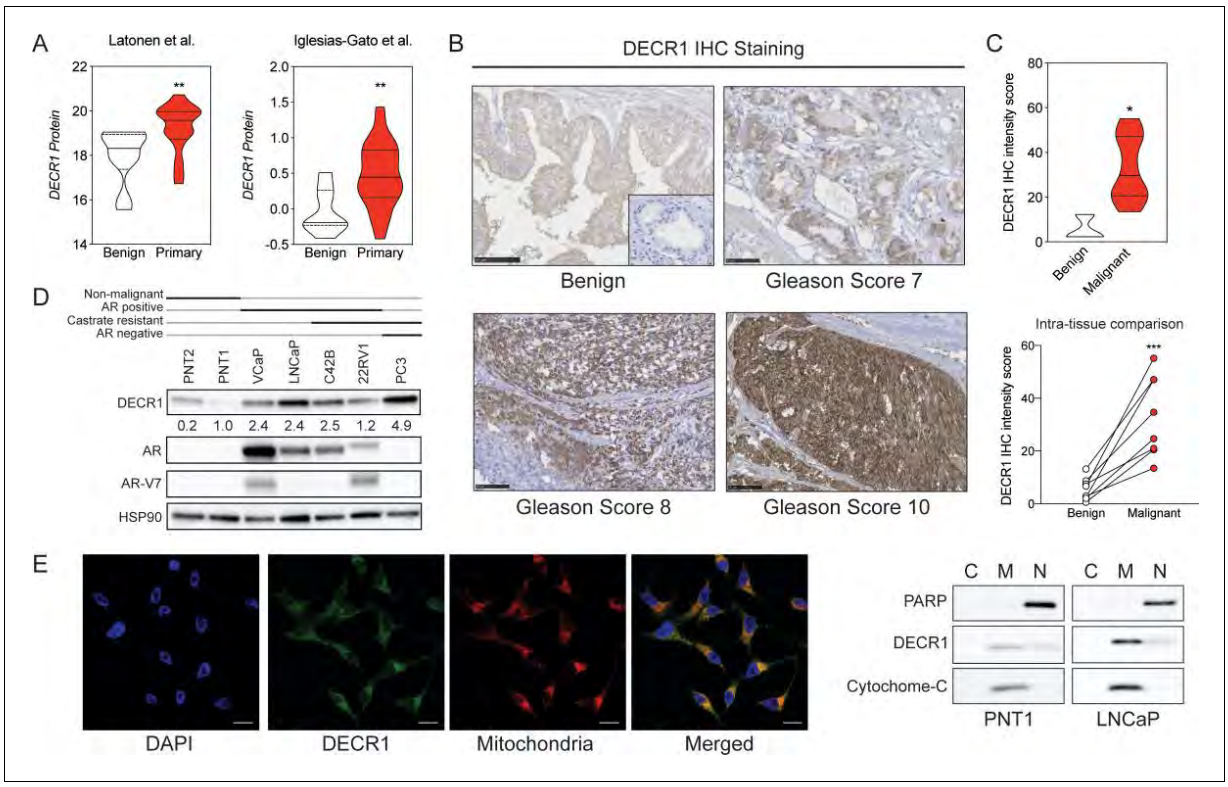

Figure 2. DECR1 protein in overexpressed in malignant prostate cells/tissues. (**A**) Violin plots of DECR1 protein overexpression in primary PCa tissues compared to benign prostate tissues in two independent datasets. (**B**) Representative DECR1 IHC staining of benign prostate tissues and PCa tissues (negative control stain included in bottom right box). Scale bar, 50 µm. (**C**) Violin plot of DECR1 protein expression in a validation cohort consisting of benign prostate tissues (n = 3) and PCa tissues (n = 8) (*top panel*). Intra-tissue IHC analysis of DECR1 expression in PCa tissues (n = 8) (*bottom panel*). (**D**) DECR1 protein expression in non-malignant prostate cell lines (PNT1 and PNT2) and PCa cell lines (LNCaP, VCaP, 22RV1, C42B and PC3). (**E**) Immunocytochemistry staining of LNCaP cells to determine the subcellular localization of DECR1: nuclei were labelled using DAPI; mitochondria were labelled using MitoTracker Red; and DECR1 proteins were labelled using Alexa Fluor 488 secondary antibody, (Scale bar = 10 µm). Immunoblot of PNT1 and LNCaP cells separated into cytosolic, mitochondrial and nuclear fractions and incubated with poly (ADP-ribose) polymerase (PARP) and cytochrome-C antibodies to mark nuclear and mitochondrial fractions. Data are represented as violin plots in GraphPad prism: the horizontal line within the violin represents the median. Statistical analysis was performed using a Mann-Whitney two-tailed t-test (A and C *top panel*), or two-tailed paired t-test (C *bottom panel*): *p<0.05, **p<0.01 and ***p<0.001.

siRNAs failed to increase ATP levels with linoleic acid supplementation (***Figure 4E***), indicating impaired capacity to metabolize PUFAs.

Next, we employed extracellular flux analysis to determine the intrinsic rate and capacity of PCa cells to oxidise PUFAs in conditions where other exogenous substrates were limiting. Exogenous linoleic acid stimulated basal oxygen consumption rates (OCR), as a measure of mitochondrial oxidative phosphorylation, and maximal respiration, ATP production, and mitochondrial spare capacity (***Figure 4F***, ***Figure 4—figure supplement 1A***) as determined by consecutive cell exposure to respiration chain inhibitors and uncouplers. This supports the observed increased in total ATP levels in response to linoleic acid supplementation (***Figure 4E***). Importantly, DECR1 knockdown prevented the exogenous linoleic acid induction of basal and maximal respiration, ATP production, and mitochondrial spare capacity (***Figure 4F***, ***Figure 4—figure supplement 1A***). In contrast, DECR1 knockdown has no impact on mitochondrial metabolism of the saturated FA, palmitate (***Figure 4G***). Further, DECR1 knockdown increased glycolysis, as determined by ECAR (***Figure 4H***, ***Figure 4—figure supplement 1B***), as well as decreased glucose and fructose concentrations (***Figure 4I***), to sustain

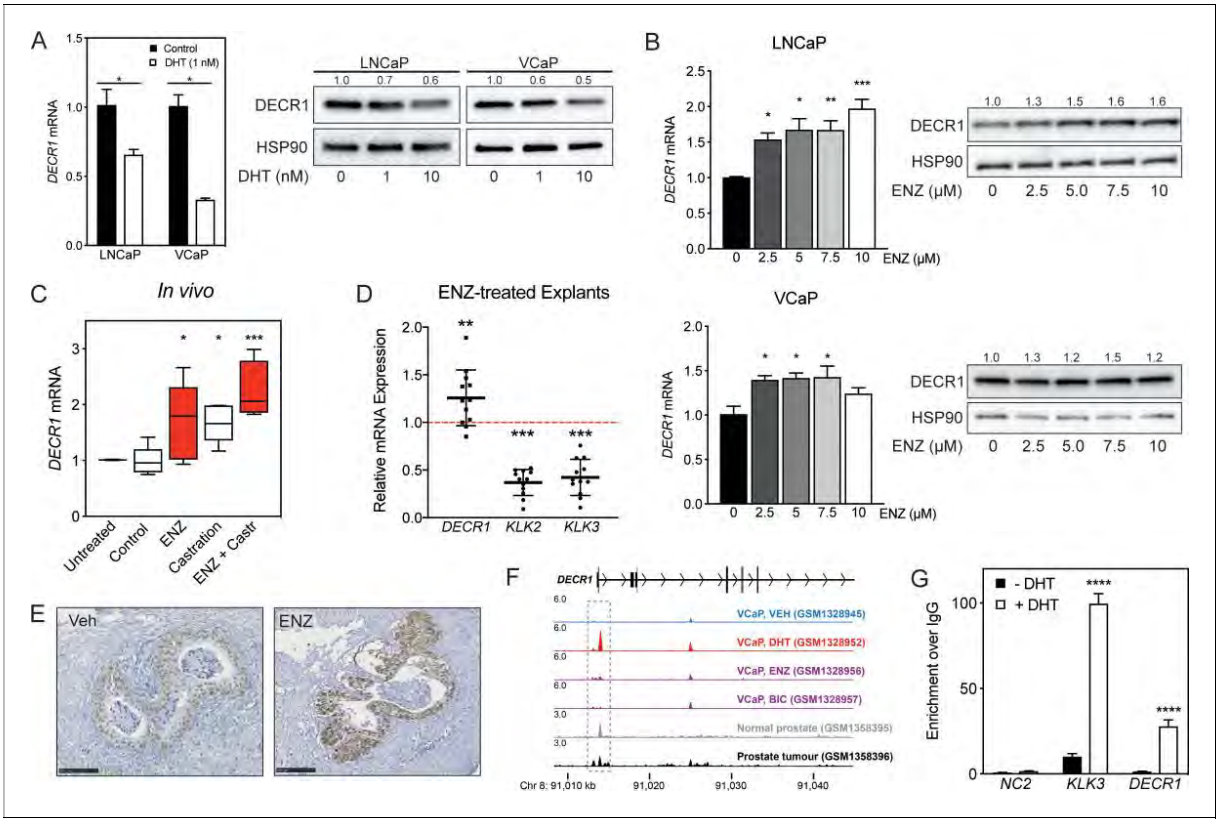

Figure 3. DECR1 is an androgen-repressed gene. (**A**) DECR1 mRNA and protein was measured by qRT-PCR and western blot analysis after PCa cell treatment with dihydrotestosterone (DHT), or (**B**) enzalutamide (ENZ). Relative mRNA expression of *DECR1* was calculated using comparative CT method, where the cells treated with vehicle (control) were set to one and normalised to the geometric mean CT value of *GUSB* and *L19* (housekeeping genes). Densitometry quantification of relative DECR1 protein expression was normalized to the HSP90 internal control. *n* = 3 independent experiments. (**C**) qRT-PCR analysis of *DECR1* mRNA expression in LNCaP-derived tumors treated with enzalutamide (ENZ) and/or castration (Castr). (**D**) qRT-PCR analysis of *DECR1* and androgen regulated genes *KLK2* and *KLK3* mRNA expression in a cohort of 10 patient-derived human prostatic ex vivo tumor explants treated with enzalutamide (ENZ, 10 μM). Relative mRNA expression was calculated using comparative CT method, where the matched untreated tissue from the same patient was set to one and normalized to the geometric mean CT value of *TUBA1B*, *PPIA* and *GAPDH*. (**E**) Representative DECR1 IHC staining of patient-derived human prostatic ex vivo tumor explants treated with enzalutamide (ENZ, 10 μM). Scale bar, 100 μm. (**F**) AR ChIP-sequencing data from VCaP cells (top panel), normal human prostate and primary human prostate tumor specimens (bottom panel). Data from GSE55064 and GSE56288. (**G**) ChIP-qPCR analysis demonstrates AR binding at *DECR1* locus in LNCaP cells after treatment with DHT. Data in bar graphs (A, B and G) are represented as the mean ± s.e.m. Data in (**C**) are represented as box plots using the Tukey method in GraphPad prism. Statistical analysis was performed using two-tailed Student's *t*-test (A, C, D and G) or one-way ANOVA, followed by Dunnett's multiple comparisons test (**B**): *p<0.05, **p<0.01, ***p<0.001 and ****p<0.0001.

The online version of this article includes the following figure supplement(s) for figure 3:

Figure supplement 1. Androgenic regulation of DECR1 expression.

TCA cycle intermediate levels (***Figure 4J***) as a consequence of disruption of PUFA β-oxidation. While DECR1 exhibited selectivity in inhibition of PUFA metabolism, as expected, etomoxir inhibited both PUFA and saturated fatty acids (***Figure 4—figure supplement 1C***). There was no effect of ETX treatment on DECR1 expression (***Figure 4—figure supplement 1D***). Collectively, these results demonstrate that DECR1 is critical for PUFA metabolism in LNCaP PCa cells.

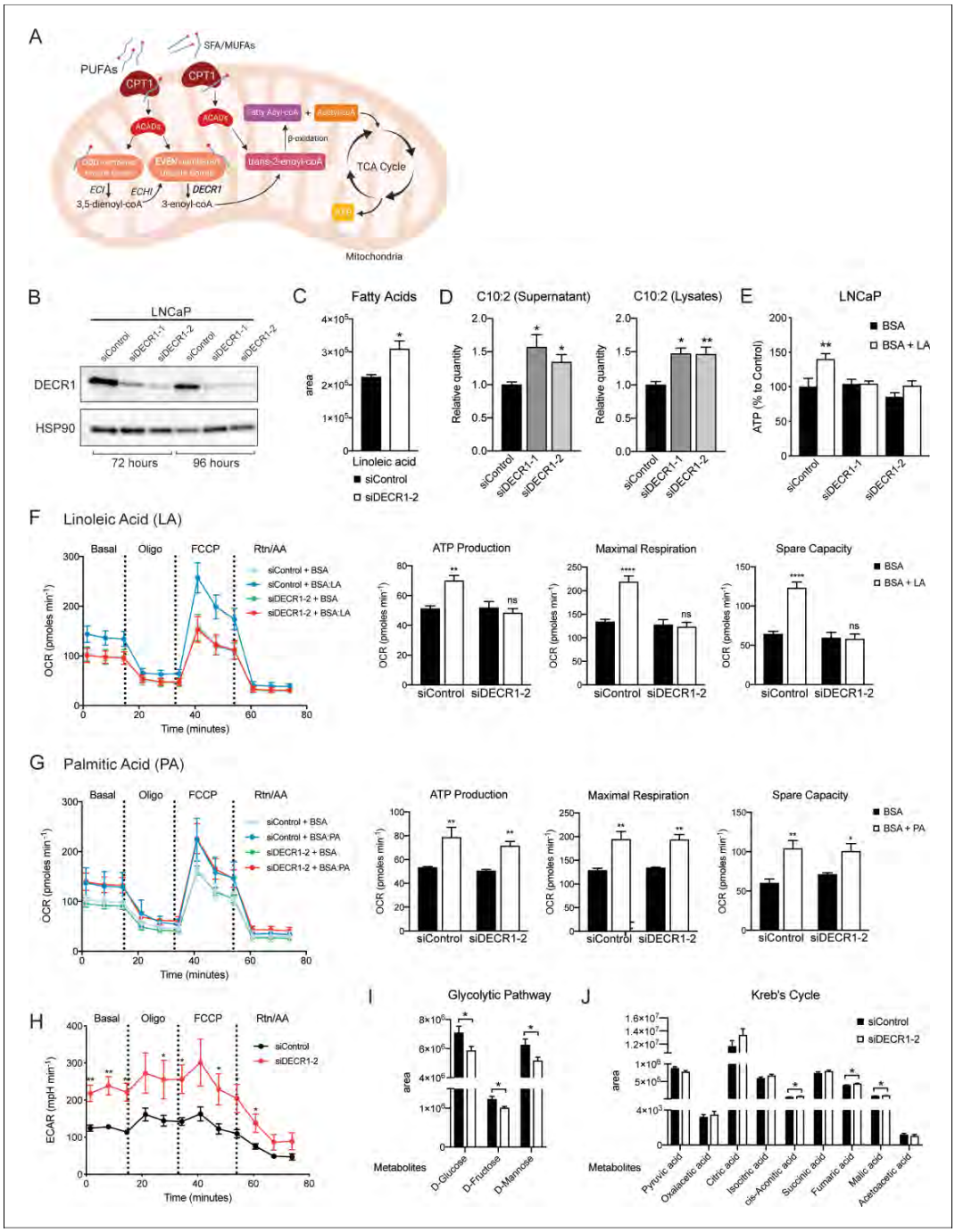

Figure 4. DECR1 knockdown interrupts PUFA β-oxidation in PCa cells. (**A**) Schematic of DECR1 function in fatty acid (FA) β-oxidation. In order to translocate FAs into the mitochondria, CPT1 converts long-chain acyl-CoA species to their corresponding long-chain acylcarnitine species. This is followed by a dehydrogenation step mediated by acyl CoA dehydrogenase (ACAD) to generate trans-2-enoyl-CoA, the only intermediate that can be processed by downstream enzymes in the β-oxidation process. Many FAs have unsaturated bonds either on an odd-numbered carbon or in the cis-

Figure 4 continued on next page

Figure 4 continued

configuration, resulting in the generation of enoyl-CoA intermediates that cannot be directly processed via the downstream β-oxidation enzymes. These FAs require the activity of 3 auxiliary enzymes, ECI1, ECH1 and DECR1 in order to form trans-2-enoyl-CoA before undergoing β-oxidation. DECR1 catalyzes the conversion of either 2-trans,4-cis-dienoyl or 2-trans,4-trans-dienoyl-CoA to 3-trans-enoyl-CoA. A complete cycle of β-oxidation results in the release of the first two carbon units as acetyl-CoA, and a fatty-acyl-CoA minus two carbons. The acetyl-CoA enters the TCA cycle to produce energy (ATP). The shortened fatty-acyl-CoA is processed again starting with the ACADs to form trans-2-enoyl-CoA either directly or with the aid of the auxiliary enzymes depending on the presence of double bonds. This process continues until all carbons in the fatty acid chain are turned into acetyl-CoA. (**B**) DECR1 protein expression after 72 hr or 96 hr siRNA transfection. Densitometry quantification of relative DECR1 protein expression was normalized to the HSP90 internal control. (**C**) Linoleic acid level in LNCaP cells quantified in following 96 hr DECR1 knockdown using GC QQQ targeted metabolomics. (**D**) Relative quantities of the C10:2 acylcarnitine species in LNCaP cell conditioned medium (left) or cell lysates (right) (n = 3). (**E**) Quantification of ATP levels in LNCaP cell lysates. LNCaP cells were transfected with DECR1 siRNAs for 48 hr and then starved in no-glucose medium and treated with the lipolysis inhibitor DEUP (100 μM) in the presence (BSA-LA) or absence (BSA) of the PUFA linoleic acid for 48 hr before measuring ATP levels. (**F**) Oxygen consumption rate (OCR) was assessed in LNCaP cells supplemented with the PUFA linoleic acid (LA) or (**G**) the saturated fatty acid palmitic acid (PA). Each data point represents an OCR measurement. ATP production, maximal mitochondrial respiration and mitochondrial spare capacity were assessed. (**H**) Extracellular acidification rate (ECAR) was assessed in LNCaP cells. Each data point represents an ECAR measurement. For experiments (**F-H**) LNCaP cells were transfected with DECR1 siRNAs for 72 hr, then starved in substrate limited medium for 24 hr; the assay was run in FAO assay medium. (**I and J**) Metabolites were quantified in LNCaP cells following 96 hr DECR1 knockdown using GC QQQ targeted metabolomics. Data in bar graphs are represented as the mean ± s.e.m (n = 3). Statistical analysis was performed using two-tailed Student's *t*-test: *p<0.05, **p<0.01 and ****p<0.0001.

The online version of this article includes the following figure supplement(s) for figure 4:

Figure supplement 1. Effects of DECR1 on prostate cancer cellular metabolism.

Targeting DECR1 suppresses PCa oncogenesis

The consistently increased expression of DECR1 in PCa tissue and its association with shorter-relapse times and survival rates (***Figure 1*** and ***2***), taken together with its impact on PUFA metabolism (***Figure 4***), suggested that it may contribute to PCa cell viability and invasive behaviour. We evaluated the impact of DECR1 downregulation or overexpression on various oncogenic properties of PCa cells using a series of in vitro and in vivo experiments. While there was no effect of DECR1 downregulation on the non-malignant prostate cell line PNT1, a significant attenuation of PCa proliferation and induction of cell death was observed in a panel of PCa lines (***Figure 5A***), comprising androgen-dependent (VCaP and LNCaP), CRPC (22RV1 and V16D) and acquired ENZ-resistant cells (MR49F). Notably, this effect on PCa cell viability was lost when cells were cultured in lipid-depleted media (***Figure 5—figure supplement 1***), suggesting that the observed effect is due to interference with FA metabolism. Likewise, stable DECR1 knockdown using a short hairpin vector attenuated LNCaP cell line viability and induced cell death (***Figure 5B***) In contrast, stable DECR1 overexpression significantly enhanced LNCaP cell viability (***Figure 5C***) and colony formation ability (***Figure 5D***), while stable DECR1 knockdown markedly decreased colony formation (***Figure 5E***). DECR1 knockdown also decreased LNCaP growth in 3D spheroids (***Figure 5F***), which better mimic in vivo conditions than 2-dimensional cell culture (***Duval et al., 2017***). In addition, DECR1 knockdown reduced LNCaP, 22RV1 and MR49F cell migration by ~50% (***Figure 5G***) and 22RV1 invasion by ~65% (***Figure 5H***). In vivo, LNCaP cells stably depleted of DECR1 showed highly variable growth rates in a subcutaneous model (***Figure 5—figure supplement 2A***), but inspection of the resultant tumors revealed significantly reduced cellular proliferation compared to control cells, concomitant with reduced DECR1 expression (***Figure 5I***, ***Figure 5—figure supplement 2B***). To study the effect of DECR1 downregulation on PCa in the prostate microenvironment, we undertook a second study using LNCaP orthotopic xenografts. DECR1 knockdown significantly retarded tumor growth (***Figure 5K***, (***Figure 5—figure supplement 2C,D,E***), and significantly inhibited lung metastasis in the orthotopic tumor model (***Figure 5L***).

DECR1 targeting induces lipid peroxidation and cellular ferroptosis

DECR1 knockdown resulted in inhibition of PUFA β-oxidation and led to accumulation of PUFAs in phospholipids (***Figure 6A***). Inspection of the phospholipid profile revealed accumulation of PUFAs in the PC, PI and PS classes (***Figure 6B***) with no impact on total saturated or MUFA phospholipids (***Figure 6—figure supplement 1A***). PUFA are highly susceptible to peroxidation, so we next assessed the effect of DECR1 knockdown on lipid peroxidation. DECR1 knockdown increased levels of

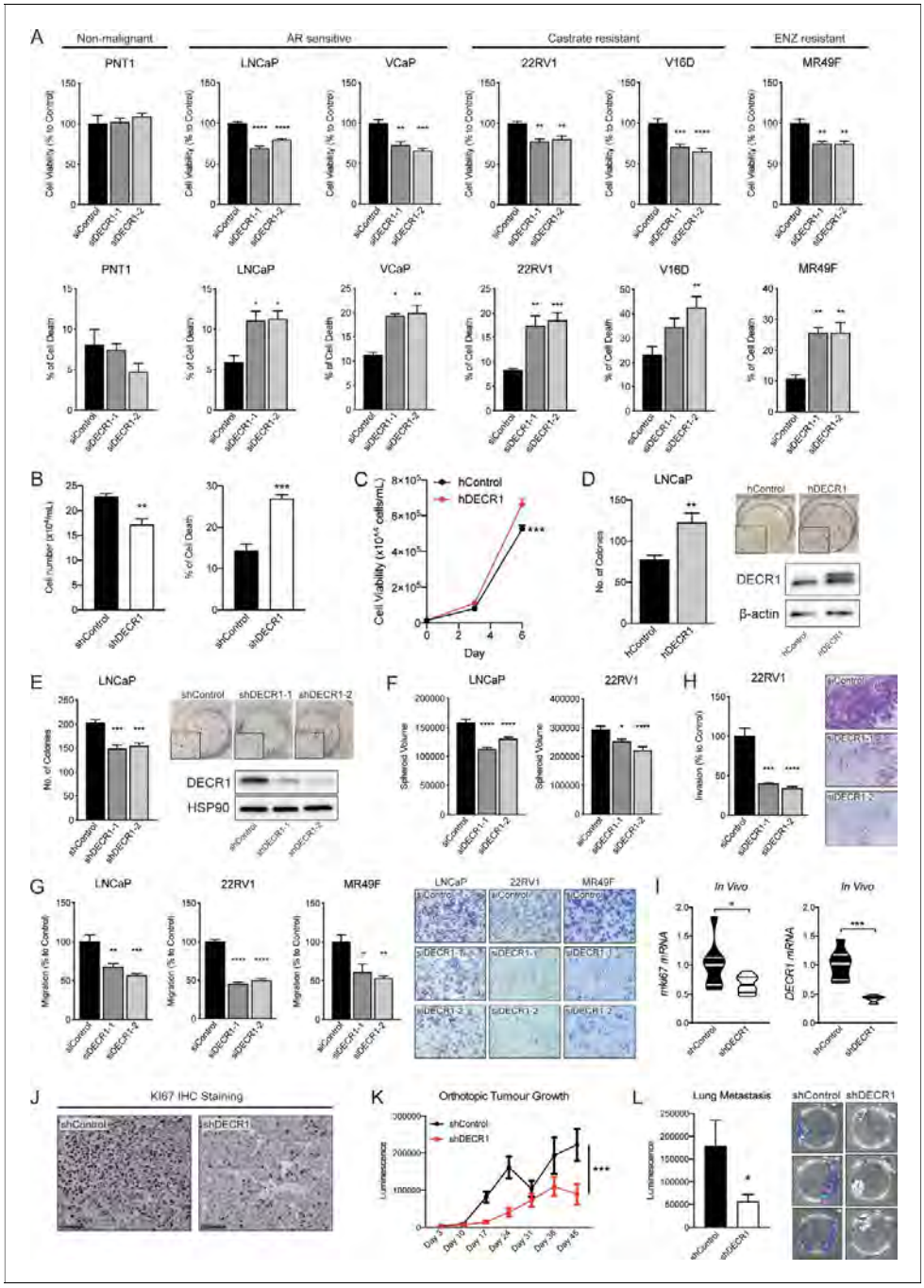

Figure 5. DECR1 knockdown suppresses oncogenic phenotypes of PCa cells. (**A**) Cell viability after DECR1 knockdown in non-malignant PNT1 prostate cells; hormone-responsive PCa cell lines (LNCaP and VCaP); castrate-resistant V16D and 22RV1 cell lines and enzalutamide-resistant MR94F cells cultured in full serum media. (**B**) Cell viability and cell death of stable DECR1 knockdown LNCaP cells cultured in full serum media. (**C**) Cell viability of stable DECR1-overexpressed LNCaP cells cultured in full serum media. Cell viability and cell death were measured using trypan blue exclusion

Figure 5 continued on next page

Figure 5 continued

following 96 hr DECR1 knockdown. Percentages are represented relative to the control siRNA; *n* = 3 independent experiments per cell line. (**D**) Clonogenic cell survival of LNCaP cells was assessed using colony formation assay. Stable DECR1-overexpressed cells or (**E**) stable DECR1 knockdown was achieved using two different short hairpin (sh) vectors and DECR1 expression was confirmed using western blot. Cells were cultured for 2 weeks, washed with PBS, fixed with paraformaldehyde and stained with 1% crystal violet for 30 min. Colonies with more than 50 cells were counted manually; data shown is representative of *n* = 2 independent experiments. (**F**) LNCaP and 22RV1 cell growth in 3D spheres. Spheroids were prepared using the hang drop assay following 48 hr DECR1 knockdown. Spheroid volumes were determined after five days of culturing the cells in 20 µl drops; at least 25 spheres per cell line were assessed using the ReViSP software, *n* = 3 independent experiments per cell line. (**G**) LNCaP, 22RV1 and MR49F cell migration and (**H**) 22RV1 cell invasion were assessed using a transwell migration/invasion assay. Cells were transfected with DECR1 siRNA or control siRNA for 48 hr prior to the assay; data shown is representative of *n* = 3 independent experiments. (**I**) Violin plots of mKi67 and DECR1 mRNA expression in subcutaneous LNCaP tumors (n = 5 mice, shControl; n = 4 mice, shDECR1). (**J**) Representative Ki67 IHC staining of subcutaneous LNCaP tumors. Scale bar, 100 µm. Data in bar graphs are represented as the mean ± s.e.m. Statistical analysis was performed using one-way ANOVA, followed by Dunnett's multiple comparisons test: *p<0.05, **p<0.01, ***p<0.001 and ****p<0.0001. (**K**) Tumor growth of intraprostatically injected LNCaP cells (shControl and shDECR1). (**J**) Lung luminescence readings following DECR1 knockdown in mice. Data are presented as mean ± s.e.m. Statistical analysis was performed using two-way ANOVA or two-tailed student's t-test: *p<0.05 and ***p<0.001.
The online version of this article includes the following figure supplement(s) for figure 5:

Figure supplement 1. Depletion of extracellular lipids prevents antiproliferative effects of DECR1 in prostate cancer cells.
Figure supplement 2. DECR1 suppresses growth of prostate tumor xenografts in mice.
Figure supplement 3. The sequence of the DECR1 shRNA and hDECR1 vectors.

malondialdehyde, a marker of lipid peroxidation (***Gaweł et al., 2004***; ***Figure 6C***). In contrast, DECR1 overexpression markedly decreased cellular malondialdehyde levels (***Figure 6C***). We observed enhanced mitochondrial oxidative stress measured using MitoSOX, a mitochondrial superoxide indicator (***Figure 6D***), in response to DECR1 knockdown. Moreover, DECR1 knockdown resulted in significant accumulation of phospholipid hydroperoxides, a hallmark of ferroptosis (***Figure 6E***). In contrast, DECR1 overexpression significantly decreased mitochondrial oxidative stress under basal (***Figure 6F***) and linoleic acid-induced conditions (***Figure 6G***). Lipid peroxidation is a major driver of ferroptosis, an iron-dependent non-apoptotic form of cell death (***Dixon et al., 2012***). Cell treatment with the ferroptosis inhibitors, deferoxamine or ferrostatin, abolished the effect of DECR1 knockdown on PCa cell death (***Figure 6H–I***), while cell treatment with the ferroptosis inducers, erastin, FIN56 or ML210, enhanced the cytotoxic action of DECR1 downregulation (***Figure 6J–K***, ***Figure 6—figure supplement 1B***). Supporting ferroptosis as the cell death mechanism, DECR1 knockdown did not induce apoptosis (***Figure 6—figure supplement 2A***), and the apoptosis inhibitor ZVAD did not rescue the cells from cell death induced by DECR1 depletion (***Figure 6—figure supplement 2B***). Collectively, these results suggest that DECR1 expression protect cells from oxidative stress and that DECR1 knockdown-induced cell death is primarily mediated by induction of ferroptosis.

Discussion

Metabolic rewiring is both a hallmark feature of cancer cells and a promising therapeutic vulnerability. Several anabolic and catabolic metabolism pathways have been explored, however, few agents have been investigated clinically. This can at least partly be explained by the relatively recent appreciation of cancer metabolism as a target, the high toxicity, particularly hepatotoxicity, expected to be associated with targeting certain metabolic pathways, the predictable metabolic heterogeneity within and between patients and the lack of intermediate pre-clinical models that can predict clinically efficacious outcomes. Previous research has largely focused on studying and targeting FA synthetic pathways in PCa. Major lipogenic enzymes such as ATP citrate lyase (ACLY), acetyl-CoA carboxylase (ACC) and fatty acid synthase (FASN) are all overexpressed in PCa compared to benign tissue (***Wu et al., 2014***; ***Rossi et al., 2003***; ***Shurbaji et al., 1996***). While many first-generation FA synthesis inhibitors (e.g. FASN inhibitors) showed promising preclinical efficacy against PCa, unfavorable drug solubility and pharmacokinetics profiles, off-target effects and side effects including weight loss have hindered clinical development of this agent class (***Zadra et al., 2013***). In addition to de novo synthesis of FAs, PCa cells depend on lipid uptake from the circulation, and from stromal adipocytes (***Watt et al., 2019***; ***Kuemmerle et al., 2011***; ***Gazi et al., 2007***). We showed previously that extracellular FAs are the major contributor to lipid synthesis in PCa (***Balaban et al., 2019***).

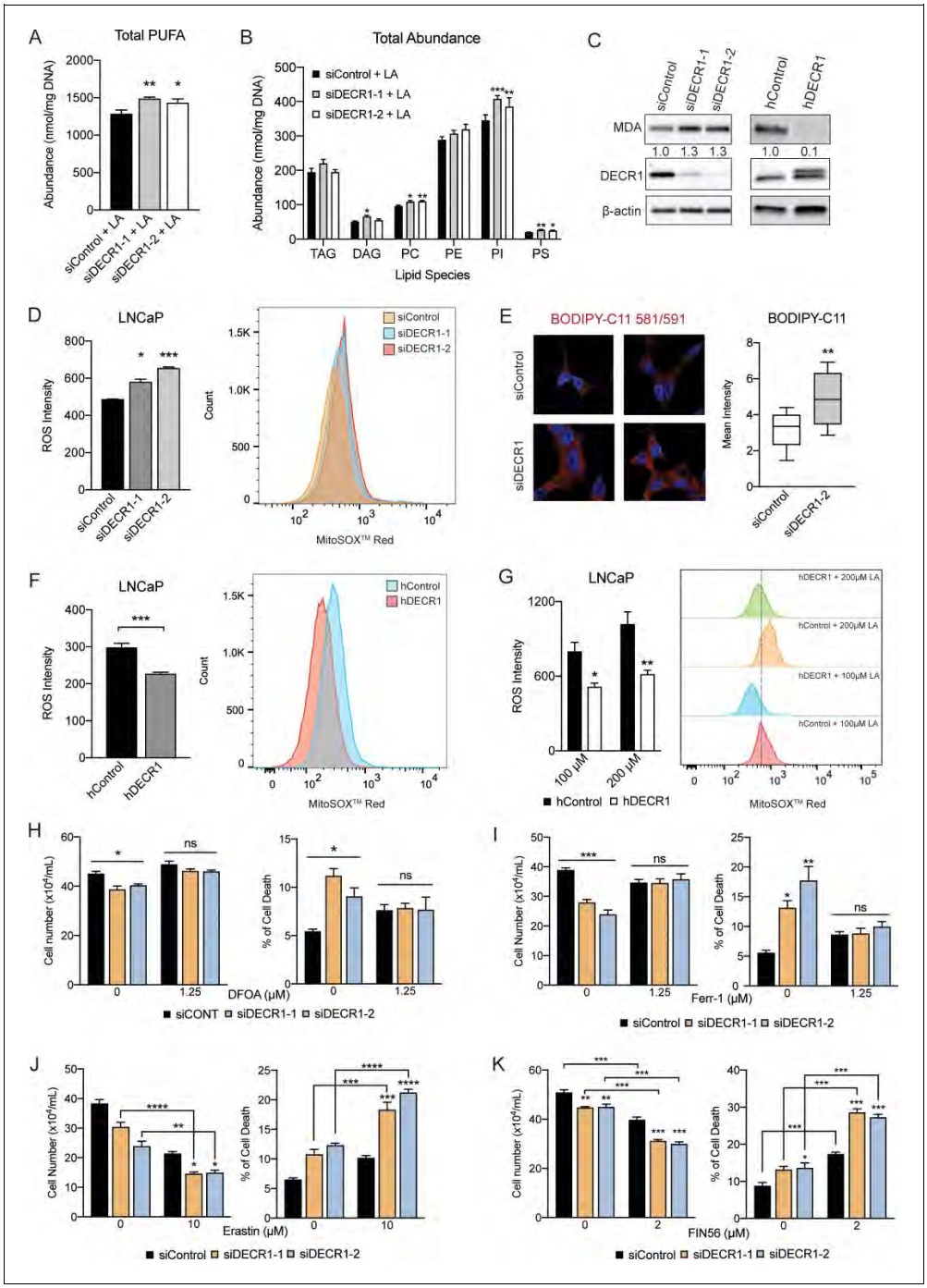

Figure 6. DECR1 knockdown induces PUFA accumulation, lipid peroxidation and ferroptosis. (**A**) Abundance of total PUFAs and (**B**) total abundance of lipid species in phospholipids from control and DECR1 knockdown cells supplemented with linoleic acid (LA). (**C**) Malondialdehyde (MDA), an oxidative stress marker, was measured by western blot in LNCaP cells transfected with DECR1 siRNAs and in DECR1-overexpressed LNCaP cells. (**D**) Mitochondrial superoxide levels were quantified following 96 hr DECR1 knockdown using MitoSOX red stain. Fluorescent intensity was quantified using

Figure 6 continued on next page

Figure 6 continued

flow cytometry and ROS levels presented as mean fluorescent intensity. (**E**) Fluorescent images of BODIPY-C11 stained LNCaP cells following DECR1 knockdown (left). Fluorescent intensity was quantified using ImageJ and presented as mean fluorescent intensity (right). (F) Mitochondrial superoxide levels were quantified in stable DECR1-overexpressing LNCaP cells using MitoSOX red stain under basal or (**G**) linoleic acid (100 μM or 200 μM) conditions. Fluorescence intensity was quantified using flow cytometry and ROS levels were presented as mean fluorescent intensity. Cell viability of LNCaP cells after 48 hr DECR1 knockdown, treated with (**H**) deferoxamine (DFOA, 1.25 μM), (**I**) ferrostatin (Ferr-1, 1.25 μM), (**J**) erastin (10 μM), or (**K**) FIN56 (2 μM). Data in bar graphs are represented as the mean ± s.e.m. Statistical analysis was performed using two-tailed Student's *t*-test (**A-G**) or one-way ANOVA, followed by Holm-Sidak's multiple comparisons test (**H-K**): ns, not significant, *p<0.05, **p<0.01, ***p<0.001 and ****p<0.0001. TAG: triacylglycerol; DAG: diacylglycerol; PC: phosphotidylcholine; PE: phosphotidylethanolamine; PI: phosphatidylinositol; PS: phosphotidylserine.
The online version of this article includes the following figure supplement(s) for figure 6:

Figure supplement 1. Depletion of DECR1 sensitizes prostate cancer cells to ferroptosis inducing agents.
Figure supplement 2. Targeting DECR1 does not induce apoptosis of prostate cancer cells.

Moreover, targeting FA uptake using an antibody against CD36, a major transporter for exogenous FAs into the cells, reduced cancer severity in patient-derived xenografts, and *CD36* deletion slowed cancer progression in prostate-specific *PTEN*$^{-/-}$ mice. However, it is increasingly evident that PCa exhibits plasticity in attaining FAs and that crosstalk between de novo synthesis and FA uptake requires dual targeting of the two pathways to achieve maximal efficacy (***Watt et al., 2019***), an approach that would likely be associated with greater toxicity. In this study, we focused on another understudied aspect of FA metabolism in PCa, β-oxidation, to evaluate its therapeutic potential.

We showed previously (***Balaban et al., 2019***), as have others (***Schlaepfer et al., 2014***; ***Schlaepfer et al., 2015***), that PCa cells exhibit increased FAO compared to prostate epithelial PNT-1 cells, or benign epithelial cells BPH-1 and WPMY-1. This metabolic phenotype is a vulnerability for PCa cells (***Schlaepfer et al., 2014***; ***Itkonen et al., 2017***; ***Flaig et al., 2017***). FAO inhibitors such as etomoxir, perhexiline or ranolazin inhibited tumor growth in vitro and in vivo (***Schlaepfer et al., 2014***; ***Itkonen et al., 2017***; ***Flaig et al., 2017***) and sensitized cells to ENZ treatment (***Itkonen et al., 2017***; ***Flaig et al., 2017***). However, all of these studies were undertaken using immortalized cell line models of PCa, and as cancer metabolism is markedly influenced by the tumor microenvironment (***Martinez-Outschoorn et al., 2012***; ***Nieman et al., 2011***; ***Nassar et al., 2018***), employing preclinical models and primary tissues that retain the complexity of this microenvironment as a stepping stone to clinical trials may accelerate clinical translation and avoid futile targeting strategies or agents. In this study, we evaluated the efficacy of the FAO inhibitor, etomoxir, using our established PDE model. Remarkably, etomoxir inhibited effectively cell proliferation in PDEs (***Figure 1A***), strengthening the case that targeting FA oxidation may be a promising clinical strategy. Interestingly, etomoxir was more potent in inhibition of cell proliferation in PDEs than in vitro 2-dimensional growth of LNCaP cells, emphasizing that in vitro models based on 2D cultured cells alone are suboptimal when evaluating anti-metabolism agents. This problem is compounded by the fact that standard growth media is rich in sugar and proteins, but contains low levels of lipids. As the clinical development of etomoxir was terminated due to severe hepatotoxicity associated with treatment (***Holubarsch et al., 2007***), we sought to identify new β-oxidation targets in PCa. As DECR1 is a directly androgen-repressed gene, its expression increases after castration or treatment with anti-androgens and is hypothesized to maintain tumor cell survival under castration conditions. Androgen-repressed genes are markedly understudied compared with androgen-induced genes, despite the fact that they possibly mediate adaptive survival pathways when androgen signalling is perturbed, and have already yielded novel therapeutic targets (***Kregel et al., 2013***; ***Tse et al., 2017***).

Surprisingly, very little is known about the biological role of DECR1 in cancer. Human DECR1 deficiency is lethal, with patients exhibiting hypocarnitinemia, decreased cellular oxygen consumption, increased lactic acidosis, and unusual accumulation of FA intermediates in urine and blood due to incomplete β-oxidation (***Roe et al., 1990***; ***Houten et al., 2014***). DECR1-null mice exhibit impaired lipid metabolism, hypoglycemia and activation of ketogenesis, and cold intolerance (***Miinalainen et al., 2009***; ***Mäkelä et al., 2019***). These phenotypes highlight the critical role of DECR1 in lipid metabolism. We confirmed the metabolic activities of DECR1 in PCa cells using a panel of metabolomic and lipidomic analyses. DECR1 knockdown increased levels of certain acylcarnitine species, indicating inhibition of β-oxidation. These results are consistent with previous studies reporting acylcarnitine accumulation in *Decr1*$^{-/-}$ mice and *DECR1*-deficient patients (***Roe et al.,***

1990; Miinalainen et al., 2009). We showed that DECR1 knockdown selectively inhibited PUFA catabolism, accompanied by an increase in glycolysis rate, which is also consistent with previous reports of FAO inhibition or impaired mitochondrial function leading to enhanced glucose uptake and glycolysis (Schlaepfer et al., 2015; Houten et al., 2014). Lipidomic analysis showed that DECR1 knockdown increased the abundance of PUFAs and certain lipids, particularly PE and PI phospholipid species, accompanied by increased levels of mitochondrial oxidative stress and particularly lipid peroxidation. In contrast to MUFAs, PUFAs are highly susceptible to peroxidation, thereby enhancing free radical generation and accumulation of toxic lipid peroxides (Das, 2011; Magtanong et al., 2019). Consistent with a role for PUFA oxidation in DECR1 function, ectopic DECR1 overexpression decreased mitochondrial oxidative stress. An important cellular protective response to excess intracellular lipid peroxides is the induction of ferroptosis, an iron-dependent form of cell death that is triggered by lipid peroxidation. Here, we show that the ferroptosis inhibitors ferrostatin and deferoxamine or the ferroptosis inducers erastin, FIN56 and ML210 abolished and augmented the effect of DECR1 on PCa cell death, respectively. These findings are consistent with a mechanism by which DECR1 knockdown-induced cell death is a ferroptosis-mediated process caused by PUFA accumulation, a conclusion that was independently validated in human prostate cancer during revision of this article (Blomme et al., 2020). It is therefore possible that PCa cells commonly select for DECR1 overexpression, not only to enhance ATP production to fulfil energy requirements, but also to protect cells from the tumoricidal effects of excess PUFAs.

PUFAs are essential FAs that cannot be synthesized in mammals and are only obtained from the diet. Dietary fat not only promotes obesity, but also PCa progression and disease aggressiveness. Several preclinical PCa studies have compared high-fat (or Western-style diets) versus low fat diet and reported that the former promotes AKT and ERK activity, tumor growth, tumor incidence in genetically engineered/transgenic mouse models, tumor progression to CRPC and metastasis (reviewed in Narita et al., 2019). Clinical case-control studies indicated saturated fat is associated with an increased risk of advanced PCa (Bairati et al., 1998; Stéfani et al., 2000; Slattery et al., 1990; Whittemore et al., 1995). Several underlying mechanisms were proposed to explain the association between dietary fat and PCa development and progression, including growth factor signalling (such as IGF-1), inflammation, and endocrine modulation (Narita et al., 2019). While the evidence supporting the negative impacts of saturated dietary FAs are more consistent, the effect of dietary PUFAs on PCa aggressiveness remains inconclusive and differences between omega-3 and omega-6 have been reported (Bairati et al., 1998; Stéfani et al., 2000; Park et al., 2009; Fu et al., 2015). In contrast to omega-3 PUFAs, which are reported to inhibit PCa progression (Wang et al., 2012), omega-6 PUFAs (Khankari et al., 2016; Brown et al., 2010), and higher omega-6/omega-3 PUFA ratio, increase PCa risk (Williams et al., 2011; Apte et al., 2013). Dietary intervention by decreasing total fat intake and increasing omega-3 PUFAs was found to improve PCa survivorship (Epstein et al., 2012; Colli and Colli, 2005; Davies et al., 2011; Ornish et al., 2005). It is unclear whether there is a preference for n-6 or n-3 PUFA β-oxidation in PCa cells, however both require DECR1 for complete β-oxidation.

Although FAO is a complex process that requires the activity of several enzymes, to date the entire focus of drug development strategies has been inhibitors against CPT1, the rate-limiting step of FA β-oxidation. CPT1 is responsible for synthesizing fatty acyl-carnitines from fatty acyl-CoAs which are then transported from the cytoplasm into the mitochondria by carnitine acylcarnitine translocase for subsequent processing then entry into the β-oxidation pathway. Even though targeting CPT1 is efficient in inhibiting FA β-oxidation, the clinical use of CPT1 inhibitors is challenging. Based on our current findings, we propose that DECR1 is an attractive alternative target to CPT1. CPT1 inhibition would suppress β-oxidation of all long FA species (saturated FA, MUFA and PUFA), whilst in contrast DECR1 is specific for PUFA. Homozygous *CPT1* deficiency, of either the liver or muscle isoform, is lethal in mice (Nyman et al., 2005; Ji et al., 2008; Haynie et al., 2014), but *Decr1*$^{-/-}$ mice are viable, and clinical symptoms arose only after metabolic stress (Miinalainen et al., 2009; Mäkelä et al., 2019). The marked overexpression of DECR1 in prostate tumors across multiple clinical cohorts, potentially coupled to PUFA-related dietary interventions, may lend further selectivity to targeting strategies. Of note, the crystal structure of DECR1 active site has been solved (Alphey et al., 2005), and thus developing DECR1 inhibitors is feasible.

In summary, herein we strengthen the evidence base for the critical importance of FAO and, specifically, PUFA oxidation in PCa, thereby identifying a promising new therapeutic candidate, DECR1.

Materials and methods

Meta-Analysis of lipid metabolism genes

Individual RNA-sequencing (RNA-seq) datasets composed of matched normal versus tumor prostate cancer patient tissue samples were acquired and are listed as follows: (**Bray et al., 2018**) The Cancer Genome Atlas (TCGA, n = 53); (**Huggins and Hodges, 1941**) Nikitina AS et al. (GSE89223, n = 10) (**Nikitina et al., 2017**; **Tran et al., 2009**) Ren S et al. (n = 14) (**Ren et al., 2012**; and (**Cai and Balk, 2011**) Ding Y et al. (GSE89194, n = 45) (**Ding et al., 2016**). Before the meta-analysis, RNA-seq data was quality controlled and analysed using the R limma voom-*eBayes pipeline* (**Law et al., 2016**). Effect sizes (log-fold changes) and corresponding variances were collected from the differential expression analysis under the matched-pairs design. Meta-analysis was performed by applying a restricted maximum-likelihood estimator (REML) within a random-effects model using the *rma* function from the R *metafor* package. At most one missing observation out of four was allowed per gene. Next, the retained genes were intersected with the list of pre-selected 735 genes involved in lipid metabolism as identified from REACTOME. Finally, the remaining genes were rank-ordered on the basis of their *meta effect size* scores across all four RNA-seq datasets. Top 20 candidate genes were selected for further disease-free survival association analyses from well-characterized clinical cohorts.

Clinical datasets

Transcriptomic data was downloaded from The Cancer Genome Atlas (TCGA) data portal, cBioPortal (**Cerami et al., 2012**), and GEO; GSE21032 **Taylor et al., 2010**; GSE35988 **Grasso et al., 2012**; GSE6099 **Tomlins et al., 2007**; GSE16560 (**Sboner et al., 2010**). Proteomics data was extracted from **Iglesias-Gato et al., 2018**.

Cell lines and tissue culture

The human normal prostate epithelial cell lines PNT1 and PNT2 were obtained from the European Collection of Authenticated Cell Cultures (ECACC), and prostate carcinoma cells LNCaP, VCaP, and 22RV1 were obtained from the American Type Culture Collection (ATCC; Rockville, MD, USA). Castrate resistant V16D and enzalutamide resistant MR49F cells were derived through serial xenograft passage of LNCaP cells (**Toren et al., 2016**) were a kind gift from Prof. Amina Zoubeidi laboratory. Cell lines were verified in 2018 via short tandem repeat profiling (Cell Bank Australia). Cell lines were maintained in RPMI-1640 medium containing 10% fetal bovine serum (FBS; Sigma-Aldrich, NSW, Australia) in 5% CO_2 in a humidified atmosphere at 37˚C. Prior to androgen treatment, cells were seeded in medium supplemented with 5% dextran charcoal coated FBS (DCC-FBS) and after 24 hr, 1 nM or 10 nM of dihydrotestosterone (DHT) was added. For anti-androgen treatment, cells were cultured in growth medium supplemented with 2.5 µM, 5 µM, 7.5 µM or 10 µM Enzalutamide (dissolved in dimethyl sulfoxide, DMSO; Sigma Aldrich). The sources and experimental conditions for primary antibodies used in this study are listed in the Key Resources Table. Primers were obtained from Sigma-Aldrich and their sequences are detailed in the Key Resources Table.

Ex vivo culture of human prostate tumors

Patient derived-explant culture was carried out according to techniques established in our laboratory and as described previously (**Armstrong et al., 2016**; **Centenera et al., 2018**; **Centenera et al., 2013**). 6 mm/8 mm biopsy cores were collected from men undergoing robotic radical prostatectomy at St. Andrew's Hospital (Adelaide, South Australia) with written informed consent through the Australian Prostate Cancer BioResource. The tissue was dissected into smaller 1 mm^3 pieces and cultured on Gelfoam sponges (80 × 125 mm Pfizer 1205147) in 24-well plates pre-soaked in 500 µl RPMI-1640 with 10% FBS, antibiotic/antimycotic solution. Etomoxir (100 µM) or Enzalutamide (10 µM) was added into each well and the tissues were cultured in 5% CO_2 in a humidified atmosphere at 37˚C for 48 hr, then snap frozen in liquid nitrogen and stored at −80˚C, or formalin-fixed and paraffin-embedded.

Immunohistochemistry (IHC)

Paraffin-embedded tissue sections (2–4 μm) were deparaffinized in xylene, rehydrated through graded ethanol, and blocked for endogenous peroxidase before being subjected to heat-induced epitope retrieval (**Armstrong et al., 2016**). IHC staining was performed using DECR1 (HPA023238, Sigma Aldrich, diluted 1:500) antibody and the 3,3′-Diaminobenzidine (DAB) Enhanced Liquid Substrate System tetrahydrochloride (Sigma Aldrich) as described previously (**Armstrong et al., 2016**). Intensity of DECR1 immunostaining was measured by video image analysis (**Armstrong et al., 2016**).

Western blotting

Protein lysates were collected in RIPA lysis buffer (10 mM Tris, 150 mM NaCl, 1 mM EDTA, 1% Triton X-100, 10% protease inhibitor). Western blotting on whole cell protein lysates were performed as previously described (**Armstrong et al., 2016**). *Cell Fractionation.* Protein lysates from each subcellular fraction (cytoplasm, mitochondria, and nucleus) were obtained from PNT1 and LNCaP cells using the cell fractionation kit (Abcam, VIC, Australia) according to the manufacturer's protocol.

Quantitative Real-Time PCR (qPCR)

RNA was extracted from cells using the RNeasy RNA extraction kit (Qiagen), followed by the iScript cDNA Synthesis kit (Bio-Rad, NSW, Australia). qPCR was performed with a 1:10 dilution of cDNA using SYBR Green (Bio-Rad) on a CFX384 Real-Time System (Bio-Rad). Relative gene expression was calculated using the comparative Ct method and normalized to the internal control genes *GUSB* and *L19* for prostate cancer cells and LNCaP-derived tumors, or *TUBA1B*, *PPIA* and *GAPDH* for PDEs.

Analysis of published ChIP-seq data

AR ChIP-seq data from published external datasets, GSE56288 (clinical specimens; seven normal prostate and 13 primary tumors) (**Pomerantz et al., 2015**) and GSE55064 (VCaP cell line; Veh, DHT treated, MDV3100 treated and Bicalutamide treated) (**Asangani et al., 2014**) were obtained from GEO and visualized using the Integrated Genome Browser (IGV).

Chromatin immunoprecipitation (ChIP)

LNCaP cells were seeded at 3×10^6 cells/plate in 15 cm plates in RPMI-1640 medium containing 10% DCC-FBS for 3 days, then treated for 4 hr with 10 nM DHT or Vehicle (ethanol). AR ChIP was performed as described previously (**Paltoglou et al., 2017**).

Transient RNA interference

The human DECR1 ON-TARGET plus small interfering RNAs (siRNAs) and control siRNA (D-001810-01-20 ON-TARGET plus Non-targeting siRNA #1) were purchased from Millennium Science (VIC, Australia). Four siRNA were tested and the two most effective were selected for our experimentation: siDECR1-1 (J-009642-05-0002) and siDECR1-2 (J-009642-06-0002). The siRNAs at a concentration of 5 nM were reverse transfected using Lipofectamine RNAiMAX transfection reagent (Invitrogen, VIC, Australia) according to the manufacturer's protocol. DECR1 downregulation (>80%) was confirmed on mRNA and protein levels.

Generation of stable shDECR1 and hDECR1 LNCaP cells

Short hairpin lentiviral expression vector

LNCaP cells were transduced with the universal negative control shRNA lentiviral particles (shControl), DECR1 shRNA lentiviral particles (shDECR1) or hDECR1 (GFP-Puro) designed by GenTarget Inc (San Diego, CA, USA) according to the manufacturer's protocol (**Figure 5—figure supplement 3**).

Functional assays

Cell viability

Cells were seeded in triplicates in 24-well plates at a density of 3.0×10^4–6.0×10^4 cells/well and reverse transfected with siRNA overnight. Cells were manually counted using a hemocytometer 96

hr post-siRNA knockdown and viability was assessed by Trypan Blue exclusion as described previously (*Armstrong et al., 2016*).

Cell migration

Transwell migration assays were performed using 24-well polycarbonate Transwell inserts (3422, Sigma Aldrich). LNCaP, 22RV1 and MR49F cells transfected overnight with siRNA were seeded into the upper chamber of the Transwell at a density of 8×10^4–2.5×10^5 cells/well in serum-free medium. 650 µl of medium containing 5% FBS was added to the bottom chamber. Cells were incubated at 37˚C for 48 hr. Non-migrated cells were gently removed using a cotton-tipped swab. The inserts were fixed in 4% paraformaldehyde for 20 min and stained with 1% crystal violet for 30 min. The images of migrated cells were captured using the Axio Scope A1 Fluorescent Microscope (Zeiss) at 40X magnification. The number of migrated cells were counted manually and presented as percentages relative to control cells ± SEM.

Cell invasion

Cell invasion were assessed using 24-well-plate BD Biocoat Matrigel Invasion Chambers (In Vitro Technologies, NSW, Australia) according to the supplier instructions. After 48 hr of siRNA transfection, 650 µl of medium containing 10% FBS was added to the bottom chamber, and equal number of cells within 1% FBS-contained medium were transferred to the upper chamber. After incubation at 37˚C, 5% CO_2 for 48 hr, non-invading cells as well as the Matrigel from the interior of the inserts were gently removed using a cotton-tipped swab. The inserts were fixed in 4% paraformaldehyde for 20 min and stained with 1% crystal violet for 30 min. The images of invaded cells were captured using the Axio Scope A1 Fluorescent Microscope (Zeiss) at 40X magnification. The number of invaded cells were counted manually and presented as percentages relative to control cells ± SEM.

Colony formation assay

DECR1 stable knockdown cells (shDECR1) or negative control cells (shControl) were prepared in a single-cell suspension before being plated in 6-well plates (500 cells/well). Cells were incubated for 2 weeks at 37˚C and medium was replenished every 3–7 days. After 3 weeks, cells were washed with PBS, fixed with 4% paraformaldehyde and stained with 1% crystal violet for 30 min. Colonies were counted manually, and results were reported as number of colonies ± SEM.

3D Spheroid growth assay

LNCaP and 22RV1 cells were transfected with siRNA in 6-well plates for 48 hr. Cells were collected and prepared at a concentration of 7.5×10^4 cells/ml. Cell suspensions (1500 cells in 20 µl) were pipetted onto the inside of a petri dish lid, and 15 ml of PBS was added to the dish to prevent the drops from drying. The petri dishes were reassembled and incubated at 37˚C for 5 days. Photos of the formed spheres were captured, and the sphere volume was determined using ReViSP software (*Piccinini et al., 2015*).

Seahorse extracellular flux analysis

Cells were plated on XF96 well cell culture microplates (Agilent, VIC, Australia) at equal densities in substrate-limited medium (DMEM with 0.5 mM glucose, 1.0 mM glutamine, 0.5 mM carnitine and 1% FBS) and incubated overnight. One hour before the beginning of OCR measurement, the cells were changed into FAO Assay Medium (111 mM NaCl, 4.7 mM KCl, 2.0 mM $MgSO_4$, 1.2 mM Na_2HPO_4, 2.5 mM glucose, 0.5 mM carnitine and 5 mM HEPES). After baseline OCR is stabilized in FAO Assay Medium, 200 µM of linoleic-acid (LA) or palmitic acid (PA) were added before initializing measurements. Extracellular flux analysis was performed using the Seahorse XF Cell Mitochondrial Stress Test kit (Seahorse Bioscience) according to the manufacturer's protocol. Extracellular flux experiments were performed on a Seahorse XF96 Analyzer and results were analysed using Seahorse Wave software for XF analyzers. The OCR values were normalized to cell numbers in each well.

Metabolomics

LNCaP cells were transfected with siRNA for 96 hr in no glucose medium (containing 10% FBS) supplemented with 2.5 mM glucose in 6-well plates. Cells were washed with 1 ml of 37˚C Milli-Q water

on the shaker for 2 s. The plate was placed in sufficient volumes of liquid nitrogen, enough to cover the surface of the plate and was briefly stored on dry ice. 600 µl of ice cold 90% 9:1 methanol:chloroform (MeOH:$CHCl_3$) extraction solvent containing the internal standards (0.5 µl/samples) was added onto each well and allowed to incubate for 10 min. Cells were collected into 1.5 ml Eppendorf tubes, incubated on ice for 5 min, and centrifuged at 4˚C for 5 min at 16,100 g. The supernatant was then transferred into a fresh 1.5 ml Eppendorf tube and allowed to dry in a Speedvac. Dried samples were derivatised with 20 µl methoxyamine (30 mg/ml in pyridine, Sigma Aldrich) and 20 µl N,O-Bis(trimethylsilyl)trifluoroacetamide (BSTFA) + 1% Trimethylchlorosilane (TMCS). The derivatised samples were analysed using GC QQQ targeted metabolomics as described in ***Best et al., 2018***.

Lipidomics

Lipid extraction

700 µl of sample (4 µl of plasma diluted in water, or 700 µl of homogenized cells) was mixed with 800 µl 1 N HCl:CH3OH 1:8 (v/v), 900 µl CHCl3 and 200 µg/ml of the antioxidant 2,6-di-tert-butyl-4-methylphenol (BHT; Sigma Aldrich). 3 µl of SPLASH LIPIDOMIX Mass Spec Standard (#330707, Avanti Polar Lipids) was spiked into the extract mix. The organic fraction was evaporated using a Savant Speedvac spd111v (Thermo Fisher Scientific) at room temperature and the remaining lipid pellet was stored at - 20˚C under argon.

Mass spectrometry

Lipid pellets were reconstituted in 100% ethanol. Lipid species were analyzed by liquid chromatography electrospray ionization tandem mass spectrometry (LC-ESI/MS/MS) on a Nexera X2 UHPLC system (Shimadzu) coupled with hybrid triple quadrupole/linear ion trap mass spectrometer (6500+ QTRAP system; AB SCIEX). Chromatographic separation was performed on a XBridge amide column (150 mm ×4.6 mm, 3.5 µm; Waters) maintained at 35˚C using mobile phase A [1 mM ammonium acetate in water-acetonitrile 5:95 (v/v)] and mobile phase B [1 mM ammonium acetate in water-acetonitrile 50:50 (v/v)] in the following gradient: (0–6 min: 0% B → 6% B; 6–10 min: 6% B → 25% B; 10–11 min: 25% B → 98% B; 11–13 min: 98% B → 100% B; 13–19 min: 100% B; 19–24 min: 0% B) at a flow rate of 0.7 mL/min which was increased to 1.5 mL/min from 13 min onwards. SM, CE, CER, DCER, HCER, LCER were measured in positive ion mode with a precursor scan of 184.1, 369.4, 264.4, 266.4, 264.4 and 264.4 respectively. TAG, DAG and MAG were measured in positive ion mode with a neutral loss scan for one of the fatty acyl moieties. PC, LPC, PE, LPE, PG, LPG, PI, LPI, PS and LPS were measured in negative ion mode by fatty acyl fragment ions. Lipid quantification was performed by scheduled multiple reactions monitoring (MRM), the transitions being based on the neutral losses or the typical product ions as described above. The instrument parameters were as follows: Curtain Gas = 35 psi; Collision Gas = 8 a.u. (medium); IonSpray Voltage = 5500 V and −4,500 V; Temperature = 550˚C; Ion Source Gas 1 = 50 psi; Ion Source Gas 2 = 60 psi; Declustering Potential = 60 V and −80 V; Entrance Potential = 10 V and −10 V; Collision Cell Exit Potential = 15 V and −15 V. The following fatty acyl moieties were taken into account for the lipidomic analysis: 14:0, 14:1, 16:0, 16:1, 16:2, 18:0, 18:1, 18:2, 18:3, 20:0, 20:1, 20:2, 20:3, 20:4, 20:5, 22:0, 22:1, 22:2, 22:4, 22:5 and 22:6 except for TGs which considered: 16:0, 16:1, 18:0, 18:1, 18:2, 18:3, 20:3, 20:4, 20:5, 22:2, 22:3, 22:4, 22:5, 22:6.

Data analysis

Peak integration was performed with the MultiQuant software version 3.0.3. Lipid species signals were corrected for isotopic contributions (calculated with Python Molmass 2019.1.1) and were normalized to internal standard signals. Unpaired T-test p-values and FDR corrected p-values (using the Benjamini/Hochberg procedure) were calculated in Python StatsModels version 0.10.1.

Mitochondrial ROS measurement

LNCaP cells were transfected with siRNA for 96 hr in 6-well plates. Cells were collected into fluorescence-activated cell sorting (FACS) tubes and stained with 2.5 µM of MitoSOX Red stain (Thermo Fisher Scientific, VIC, Australia) for 30 min in a 37˚C water bath. Cells were centrifuged at 1,500 rpm for 5 min, washed twice with 500 µl of PBS, and resuspended in 500 µl of pre-warmed PBS before the samples are read on a BD FACSymphony flow cytometer.

Acylcarnitine measurement

Total lipids were extracted from cells using two-phase extraction with methyl-tert-butyl-ether (MTBE)/methanol/water (10:3:2.5, v/v/v) (**Matyash et al., 2008**). Cell pellets were frozen in 8:1 methanol/water prior to extraction with the above solvent mixture; for cell culture supernatant samples, the cell culture medium replaced the water component. Deuterated (D3)-palmitoylcarnitine was included as an internal standard (200 pmole/sample for LNCaP samples; 20 pmole/sample for tumor explant samples). Samples were reconstituted in 200 µL of the HPLC starting condition, defined below.

Acylcarnitines were quantified by liquid chromatography-tandem mass spectrometry using a Q-Exactive HF-X mass spectrometer with heated electrospray ionization and a Vantage HPLC system (ThermoFisher Scientific). Extracts were resolved on a 2.1 × 100 mm Waters Acquity C18 UPLC column (1.7 µm pore size), using an 18 min binary gradient at 0.28 mL/min flow rate, as follows: 0 min, 80:20 A/B; 3 min, 80:20 A/B; 6 min, 57:43 A/B; 8 min, 35:65 A/B; 9 min, 0:100 A/B; 14 min, 0:100 A/B; 14.5 min, 80:20 A/B; 18 min, 80:20 A/B. Solvent A: 10 mM ammonium formate, 0.1% formic acid in acetonitrile:water (60:40); Solvent B: 10 mM ammonium formate, 0.1% formic acid in isopropanol: acetonitrile (90:10). Data was acquired in positive ion mode with data-dependent acquisition (full scan resolution 70,000 FWHM, scan range 220–1600 *m/z*). The ten most abundant ions in each cycle were subjected to fragmentation (collision energy 30 eV, resolution 17,500 FWHM). An exclusion list of background ions was used based on a solvent blank. TraceFinder v5.0 (Thermo Fisher Scientific) was used for peak detection and integration, based on exact precursor ion mass (*m/z* tolerance four ppm) and *m/z* 85.0 acylcarnitine product ion. Peak areas were normalised to the D3-palmitoylcarnitine internal standard.

Lipid peroxidation analysis by imaging

For imaging, LNCaP cells following DECR1 knockdown were plated at 5×10^3 cells/well in a 8-well chamber slide. Cells were then washed with Hank's balanced salt solution (HBSS) and incubated with 5 µM BODIPY-581/591 C11 stain (Thermo Fisher Scientific). Cells were washed and fixed with 4% paraformaldehyde (PFA), and mounted with Prolong Gold anti-fade solution with DAPI (Thermo Fisher Scientific). Cells were imaged at 60 X magnification using a Olympus FV3000 Confocal Microscope. Quantification of BODIPY-C11 stain was performed using ImageJ analysis software.

In vivo experiments

Castration + ENZ study

LNCaP cells (5×10^6 cells in 50 µL 10% FBS/RPMI 1640 medium) were co-injected subcutaneously with 50 µL Matrigel in 6-week-old NOD Scid Gamma male mice (Bioresource Facility, Austin Health, Heidelberg, Australia). When tumors reached ~200 mm^3, mice were randomized in different therapy groups. One group was left untreated (n = 5), one group was treated with vehicle control (10% DMSO/PBS; n = 5), one group was treated with enzalutamide (10 mg/kg MDV3100 in 10% DMSO/PBS) and one group was castrated by surgical castration under isofluorane anesthesia (n = 9). Five of the ten castrated mice were then treated daily with enzalutamide (10 mg/kg MDV3100 in 10% DMSO/PBS) by oral gavage for 7 days. Enzalutamide therapy of castrated mice started five days after surgery.

Subcutaneous tumor growth

DECR1 stable knockdown cells (shDECR1) or negative control cells (shControl) (5×10^6 cells in 50 µL 10% FBS/RPMI 1640 medium) were co-injected subcutaneously with 50 µL matrigel in 6-week-old NOD Scid Gamma male mice. Tumors were measured using callipers and their volumes were calculated using the formula length × $width^2/2$.

Orthotopic tumor growth

Ten microliter containing 1×10^6 DECR1 stable knockdown cells (shDECR1) or negative control cells (shControl) were -injected intraprostatically in 8 week old NOD/SCID male mice. Whole-body imaging to monitor luciferase-expressing LNCaP cells was performed at day 3 of the injection and once weekly after that using the IVIS Spectrum In Vivo Imaging System (PerkinElmer). D-luciferin (potassium salt, PerkinElmer) was dissolved in sterile deionized water (0.03 g/ml) and injected

subcutaneously (3 mg/20 g of mouse body weight) before imaging. Bioluminescence is reported as the sum of detected photons per second from a constant region of interest. After the animals were sacrificed, lungs and livers were excised for ex vivo imaging using the IVIS system.

After each study, tumors were excised and half was snap frozen for RNA extraction while the other half was formalin fixed and paraffin embedded. All animal procedures were carried out in accordance with the guidelines of the National Health and Medical Research Council of Australia, with subcutaneous xenograft studies approved by the Austin Health Animal Ethics Committee (approval number A2015/05311) and orthotopic xenograft studies approved by the University of Adelaide Animal Ethics Committee (approval number M-2019–037).

Statistical analysis

Results are reported as mean ± S.E.M. Statistical analysis was performed using GraphPad Prism (V7.0 for Windows). Differences between treatment groups were compared by T-test or one-way ANOVA followed by Tukey or Dunnett post hoc test. Significance is expressed as *$p < 0.05$, **$p < 0.01$, ***$p < 0.001$, ****$p < 0.0001$.

Acknowledgements

The results published here are in part based on data generated by The Cancer Genome Atlas, established by the National Cancer Institute and the National Human Genome Research Institute, and we are grateful to the specimen donors and relevant research groups associated with this project. Tissues for the patient-derived explants used in the study were collected with informed consent via the Australian Prostate Cancer BioResource and we thank the doctors, patients and health care professionals involved. We acknowledge expert technical assistance in the study from Natalie Ryan, Joanna Gillis, Kayla Bremert, Samira Khabbazi, Nhi Huynh, and Holly P McEwen. Flow cytometry analysis was performed at the South Australian Health Medical Research Institute (SAHMRI) in the ACRF Cellular Imaging and Cytometry Core Facility. The Facility is generously supported by the Australian Cancer Research Foundation (ACRF), Detmold Hoopman Group and Australian Government through the Zero Childhood Cancer Program. Animal studies were performed at the Bioresource Facilities at Austin Health, Heidelberg, Australia and the South Australian Health and Medical Research Institute. The authors thank Metabolomics Australia, Bio21 Institute, and Adelaide Microscopy (University of Adelaide).

Additional information

Funding

Funder	Grant reference number	Author
National Health and Medical Research Council	1138648	Zeyad D Nassar
National Health and Medical Research Council	1121057	Luke A Selth
National Health and Medical Research Council	1100626	Anthony S Don
National Health and Medical Research Council	1084178	Andrew M Scott
Prostate Cancer Foundation of Australia	YI 1417	Zeyad D Nassar
Cure Cancer Australia Foundation	1164798	Zeyad D Nassar
EMBL Australia	Group Leader Award	David J Lynn
University of Sydney	Robinson Fellowship	Andrew J Hoy
Fonds Wetenschappelijk Onderzoek	Project Grants G.0841.15 and G.0C22.19N	Johannes V Swinnen

KU Leuven	Project Grants C16/15/073 and C32/17/052	Johannes V Swinnen
Australian Research Council	FT130101004	Lisa M Butler
Cancer Council South Australia	PRF1117	Lisa M Butler
Movember Foundation	MRTA3	Lisa M Butler
Freemasons Foundation Centre for Men's Health, University of Adelaide		Lisa M Butler

The funders had no role in study design, data collection and interpretation, or the decision to submit the work for publication.

Author contributions

Zeyad D Nassar, Conceptualization, Data curation, Formal analysis, Supervision, Funding acquisition, Investigation, Methodology, Writing - original draft, Writing - review and editing; Chui Yan Mah, Data curation, Formal analysis, Validation, Investigation, Visualization, Methodology, Writing - original draft, Writing - review and editing; Jonas Dehairs, Data curation, Methodology, Writing - review and editing; Ingrid JG Burvenich, Swati Irani, Anthony S Don, Investigation, Methodology, Writing - review and editing; Margaret M Centenera, Supervision, Methodology, Writing - review and editing; Madison Helm, Investigation, Methodology; Raj K Shrestha, Investigation, Writing - review and editing; Max Moldovan, Formal analysis, Investigation, Writing - review and editing; Jeff Holst, Lisa G Horvath, Methodology, Writing - review and editing; Andrew M Scott, Supervision, Writing - review and editing; David J Lynn, Data curation, Formal analysis, Supervision, Methodology, Writing - review and editing; Luke A Selth, Data curation, Formal analysis, Supervision, Investigation, Visualization, Methodology, Writing - review and editing; Andrew J Hoy, Data curation, Supervision, Investigation, Methodology, Writing - review and editing; Johannes V Swinnen, Conceptualization, Data curation, Supervision, Funding acquisition, Methodology, Writing - review and editing; Lisa M Butler, Conceptualization, Resources, Data curation, Supervision, Funding acquisition, Writing - original draft, Project administration, Writing - review and editing

Author ORCIDs

Zeyad D Nassar http://orcid.org/0000-0002-7779-2697
Chui Yan Mah http://orcid.org/0000-0002-8820-4037
Lisa M Butler https://orcid.org/0000-0003-2698-3220

Ethics

Human subjects: Fresh and archival prostate tissue specimens were collected from men undergoing robotic radical prostatectomy at St Andrew's Hospital (Adelaide, South Australia) with written informed consent through the Australian Prostate Cancer BioResource. Ethical Approval was provided by the Human Research Ethics Committees of the University of Adelaide (H-2012-016) and St Andrew's Hospital.
Animal experimentation: Animal studies were approved by the Austin Health Animal Ethics Committee (approval number A2015/05311), Heidelberg, Australia, and the University of Adelaide Animal Ethics Committee (approval number M-2019-037), and were carried out in accordance with the recommendations of the National Health and Medical Research Council of Australia.

Decision letter and Author response

Decision letter https://doi.org/10.7554/eLife.54166.sa1
Author response https://doi.org/10.7554/eLife.54166.sa2

Additional files

Supplementary files

- Transparent reporting form

Data availability

All data generated or analysed during this study are included in the manuscript and supporting files.

The following previously published datasets were used:

Author(s)	Year	Dataset title	Dataset URL	Database and Identifier
Nikitina AS, Sharova EI, Danilenko SA, Butusova TB, Vasiliev AO, Govorov AV, Prilepskaya EA, Pushkar DY, Kostryukova ES	2017	Novel RNA biomarkers of prostate cancer revealed by RNA-seq analysis of formalin-fixed samples obtained from Russian patients	https://www.ncbi.nlm.nih.gov/geo/query/acc.cgi?acc=GSE89223	NCBI Gene Expression Omnibus, GSE89223
Ding Y, Wu H, Warden C, Steele L, Liu X, Iterson MV, Wu X, Nelson R, Liu Z, Yuan YC, Neuhausen SL	2016	Age-Related Gene Expression Changes in Prostate Cancer Patients	https://www.ncbi.nlm.nih.gov/geo/query/acc.cgi?acc=GSE89194	NCBI Gene Expression Omnibus, GSE89194
Ren S, Peng Z, Mao JH, Yu Y, Yin C, Gao X, Cui Z, Zhang J, Yi K, Xu W, Chen C, Wang F, Guo X, Lu J, Yang J, Wei M, Tian Z, Guan Y, Tang L, Xu C, Wang L, Tian W, Wang J, Yang H, Sun Y	2012	RNA-seq analysis of prostate cancer in the Chinese population identifies recurrent gene fusions, cancer-associated long noncoding RNAs and aberrant alternative splicings	https://www.ncbi.nlm.nih.gov/pubmed/22349460	Pubmed, 22349460
TCGA	2019	The Cancer Genome Atlas Prostate Adenocarcinoma (TCGA-PRAD)	https://portal.gdc.cancer.gov/projects/TCGA-PRAD	National Cancer Institute, TCGA-PRAD
Tomlins SA, Mehra R, Rhodes DR, Cao X, Wang L, Dhanasekaran SM, Kalyana-Sundaram S, Wei JT, Rubin MA, Pienta KJ, Shah RB, Chinnaiyan AM	2006	Integrative Molecular Concepts Modeling of Prostate Cancer Progression	https://www.ncbi.nlm.nih.gov/geo/query/acc.cgi?acc=GSE6099	NCBI Gene Expression Omnibus, GSE6099
Grasso CS, Wu YM, Robinson DR, Cao X, Dhanasekaran SM, Khan AP, Quist MJ, Jing X, Lonigro RJ, Brenner JC, Asangani IA, Ateeq B, Chun SY, Siddiqui J, Sam L, Anstett M, Mehra R, Prensner JR, Palanisamy N, Ryslik GA, Vandin F, Raphael BJ, Kunju LP, Rhodes DR, Pienta KJ, Chinnaiyan AM, Tomlins SA	2012	The Mutational Landscape of Lethal Castrate Resistant Prostate Cancer	https://www.ncbi.nlm.nih.gov/geo/query/acc.cgi?acc=GSE35988	NCBI Gene Expression Omnibus, GSE35988
Taylor BS, Schultz N, Hieronymus H, Gopalan A, Xiao Y, Carver BS, Arora VK, Kaushik P, Cerami E, Reva B, Antipin Y, Mitsiades N, Landers T, Dolgalev I, Major JE, Wilson M, Socci	2010	Integrative genomic profiling of human prostate cancer	https://www.ncbi.nlm.nih.gov/geo/query/acc.cgi?acc=GSE21032	NCBI Gene Expression Omnibus, GSE21032

ND, Lash AE, Heguy A, Eastham JA, Scher HI, Reuter VE, Scardino PT, Sander C, Sawyers CL, Gerald WL				
Sboner A, Demichelis F, Calza S, Pawitan Y, Setlur SR, Hoshida Y, Perner S, Adami HO, Fall K, Mucci LA, Kantoff PW, Stampfer M, Andersson SO, Varenhorst E, Johansson JE, Gerstein MB, Golub TR, Rubin MA, Andrén O	2010	Molecular Sampling of Prostate Cancer: a dilemma for predicting disease progression	https://www.ncbi.nlm.nih.gov/geo/query/acc.cgi?acc=GSE16560	NCBI Gene Expression Omnibus, GSE16560
Wang Q, Li W, Liu XS, Carroll JS, Jänne OA, Keeton EK, Chinnaiyan AM, Pienta KJ, Brown M	2007	A hierarchical network of transcription factors governs androgen receptor-dependent prostate cancer growth	https://www.ncbi.nlm.nih.gov/geo/query/acc.cgi?acc=GSE7868	NCBI Gene Expression Omnibus, GSE7868
Heemers HV, Schmidt LJ, Sun Z, Regan KM, Anderson SK, Duncan K, Wang D, Liu S, Ballman KV, Tindall DJ	2011	Identification of an SRF- and androgen-dependent gene signature in prostate cancer	https://www.ncbi.nlm.nih.gov/geo/query/acc.cgi	NCBI Gene Expression Omnibus, GSE22606
Asangani IA, Dommeti VL, Wang X, Malik R, Cieslik M, Yang R, Escara-Wilke J, Wilder-Romans K, Dhanireddy S, Engelke C, Iyer MK, Jing X, Wu YM, Cao X, Qin ZS, Wang S, Feng FY, Chinnaiyan AM	2014	Therapeutic Targeting of BET Bromodomain Proteins in Castration-Resistant Prostate Cancer	https://www.ncbi.nlm.nih.gov/geo/query/acc.cgi?acc=GSE55064	NCBI Gene Expression Omnibus, GSE55064
Li L, Karanika S, Yang G, Wang J, Park S, Broom BM, Manyam GC, Wu W, Luo Y, Basourakos S, Song JH, Gallick GE, Karantanos T, Korentzelos D, Azad AK, Kim J, Corn PG, Aparicio AM, Logothetis CJ, Troncoso P, Heffernan T, Toniatti C, Lee HS, Lee JS, Zuo X, Chang W, Yin J, Thompson TC	2016	Genome-wide analysis of enzalutamide- and/or olaparib-responsive gene expression in prostate cancer cells	https://www.ncbi.nlm.nih.gov/geo/query/acc.cgi?acc=GSE69249	NCBI Gene Expression Omnibus, GSE69249
Wang X, Wang B, Soriano R, Zha J, Zhang Z, Modrusan Z, Cunha GR, Gao W	2006	Expression profiling of the mouse prostate after castration and hormone replacement	https://www.ncbi.nlm.nih.gov/geo/query/acc.cgi?acc=GSE5901	NCBI Gene Expression Omnibus, GSE5901
Arora VK, Schenkein E, Murali R, Subudhi SK, Wongvipat J, Balbas MD, Shah N, Cai L, Efstathiou E,	2013	Glucocorticoid Receptor Confers Resistance to Anti-Androgens by Bypassing Androgen Receptor Blockade	https://www.ncbi.nlm.nih.gov/geo/query/acc.cgi?acc=GSE52169	NCBI Gene Expression Omnibus, GSE52169

Logothetis C, Zheng D, Sawyers CL				
Pomerantz MM, Li F, Takeda D, Chonkar A, Chabot M, Li Q, Cejas P, Vazquez F, Shivdasani RA, Seo J, Bowden M, Lis R, Hahn WC, Kantoff PW, Brown M, Loda M, Long HW, Freedman ML	2015	Androgen receptor programming in human tissue implicates HOXB13 in prostate pathogenesis [ChIP-Seq]	https://www.ncbi.nlm.nih.gov/geo/query/acc.cgi?acc=GSE56288	NCBI Gene Expression Omnibus, GSE56288
Glinsky GV, Glinskii AB, Stephenson AJ, Hoffman RM, Gerald WL	2004	Gene expression profiling predicts clinical outcome of prostate cancer	https://www.ncbi.nlm.nih.gov/pubmed/15067324	Pubmed, 15067324
Latonen L, Afyounian E, Jylhä A, Nättinen J, Aapola U, Annala M, Kivinummi KK, Tammela TTL, Beuerman RW, Uusitalo H, Nykter M, Visakorpi T	2018	Integrative proteomics in prostate cancer uncovers robustness against genomic and transcriptomic aberrations during disease progression	https://www.nature.com/articles/s41467-018-03573-6#Sec31	Peptide Atlas repository, PASS01126
Iglesias-Gato D, Thysell E, Tyanova S, Crnalic S, Santos A, Lima TS, Geiger T, Cox J, Widmark A, Bergh A, Mann M, Flores-Morales A, Wikström P	2018	The Proteome of Prostate Cancer Bone Metastasis Reveals Heterogeneity with Prognostic Implications	https://clincancerres.aacrjournals.org/content/24/21/5433	ProteomeXchange, PXD009868

References

Alphey MS, Yu W, Byres E, Li D, Hunter WN. 2005. Structure and reactivity of human mitochondrial 2,4-dienoyl-CoA reductase: enzyme-ligand interactions in a distinctive short-chain reductase active site. *The Journal of Biological Chemistry* **280**:3068–3077. DOI: https://doi.org/10.1074/jbc.M411069200, PMID: 15531764

Apte SA, Cavazos DA, Whelan KA, Degraffenried LA. 2013. A low dietary ratio of omega-6 to omega-3 fatty acids may delay progression of prostate Cancer. *Nutrition and Cancer* **65**:556–562. DOI: https://doi.org/10.1080/01635581.2013.775316, PMID: 23659447

Armstrong HK, Koay YC, Irani S, Das R, Nassar ZD, Selth LA, Centenera MM, McAlpine SR, Butler LM, Australian Prostate Cancer BioResource. 2016. A novel class of Hsp90 C-Terminal modulators have Pre-Clinical efficacy in prostate tumor cells without induction of a heat shock response. *The Prostate* **76**:1546–1559. DOI: https://doi.org/10.1002/pros.23239, PMID: 27526951

Asangani IA, Dommeti VL, Wang X, Malik R, Cieslik M, Yang R, Escara-Wilke J, Wilder-Romans K, Dhanireddy S, Engelke C, Iyer MK, Jing X, Wu YM, Cao X, Qin ZS, Wang S, Feng FY, Chinnaiyan AM. 2014. Therapeutic targeting of BET bromodomain proteins in castration-resistant prostate Cancer. *Nature* **510**:278–282. DOI: https://doi.org/10.1038/nature13229, PMID: 24759320

Bairati I, Meyer F, Fradet Y, Moore L. 1998. Dietary fat and advanced prostate Cancer. *Journal of Urology* **159**:1271–1275. DOI: https://doi.org/10.1016/S0022-5347(01)63579-1, PMID: 9507851

Balaban S, Nassar ZD, Zhang AY, Hosseini-Beheshti E, Centenera MM, Schreuder M, Lin HM, Aishah A, Varney B, Liu-Fu F, Lee LS, Nagarajan SR, Shearer RF, Hardie RA, Raftopulos NL, Kakani MS, Saunders DN, Holst J, Horvath LG, Butler LM, et al. 2019. Extracellular fatty acids are the major contributor to lipid synthesis in prostate Cancer. *Molecular Cancer Research* **17**:949–962. DOI: https://doi.org/10.1158/1541-7786.MCR-18-0347, PMID: 30647103

Best SA, De Souza DP, Kersbergen A, Policheni AN, Dayalan S, Tull D, Rathi V, Gray DH, Ritchie ME, McConville MJ, Sutherland KD. 2018. Synergy between the KEAP1/NRF2 and PI3K pathways drives Non-Small-Cell lung Cancer with an altered immune microenvironment. *Cell Metabolism* **27**:935–943. DOI: https://doi.org/10.1016/j.cmet.2018.02.006, PMID: 29526543

Blomme A, Ford CA, Mui E, Patel R, Ntala C, Jamieson LE, Planque M, McGregor GH, Peixoto P, Hervouet E, Nixon C, Salji M, Gaughan L, Markert E, Repiscak P, Sumpton D, Blanco GR, Lilla S, Kamphorst JJ, Graham D, et al. 2020. 2,4-dienoyl-CoA reductase regulates lipid homeostasis in treatment-resistant prostate Cancer. *Nature Communications* **11**:2508. DOI: https://doi.org/10.1038/s41467-020-16126-7, PMID: 32427840

Bray F, Ferlay J, Soerjomataram I, Siegel RL, Torre LA, Jemal A, statistics G. 2018. GLOBOCAN estimates of incidence and mortality worldwide for 36 cancers in 185 countries. *CA: A Cancer Journal for Clinicians* **68**:394–424. DOI: https://doi.org/10.3322/caac.21492

Brown MD, Hart C, Gazi E, Gardner P, Lockyer N, Clarke N. 2010. Influence of omega-6 PUFA arachidonic acid and bone marrow adipocytes on metastatic spread from prostate Cancer. *British Journal of Cancer* **102**:403–413. DOI: https://doi.org/10.1038/sj.bjc.6605481, PMID: 19997104

Butler LM, Centenera MM, Swinnen JV. 2016. Androgen control of lipid metabolism in prostate Cancer: novel insights and future applications. *Endocrine-Related Cancer* **23**:R219–R227. DOI: https://doi.org/10.1530/ERC-15-0556, PMID: 27130044

Cai C, Balk SP. 2011. Intratumoral androgen biosynthesis in prostate Cancer pathogenesis and response to therapy. *Endocrine-Related Cancer* **18**:R175–R182. DOI: https://doi.org/10.1530/ERC-10-0339, PMID: 21712345

Centenera MM, Gillis JL, Hanson AR, Jindal S, Taylor RA, Risbridger GP, Sutherland PD, Scher HI, Raj GV, Knudsen KE, Yeadon T, Tilley WD, Butler LM, Australian Prostate Cancer BioResource. 2012. Evidence for efficacy of new Hsp90 inhibitors revealed by ex vivo culture of human prostate tumors. *Clinical Cancer Research* **18**:3562–3570. DOI: https://doi.org/10.1158/1078-0432.CCR-12-0782, PMID: 22573351

Centenera MM, Raj GV, Knudsen KE, Tilley WD, Butler LM. 2013. Ex vivo culture of human prostate tissue and drug development. *Nature Reviews Urology* **10**:483–487. DOI: https://doi.org/10.1038/nrurol.2013.126, PMID: 23752995

Centenera MM, Hickey TE, Jindal S, Ryan NK, Ravindranathan P, Mohammed H, Robinson JL, Schiewer MJ, Ma S, Kapur P, Sutherland PD, Hoffmann CE, Roehrborn CG, Gomella LG, Carroll JS, Birrell SN, Knudsen KE, Raj GV, Butler LM, Tilley WD. 2018. A patient-derived explant (PDE) model of hormone-dependent Cancer. *Molecular Oncology* **12**:1608–1622. DOI: https://doi.org/10.1002/1878-0261.12354, PMID: 30117261

Cerami E, Gao J, Dogrusoz U, Gross BE, Sumer SO, Aksoy BA, Jacobsen A, Byrne CJ, Heuer ML, Larsson E, Antipin Y, Reva B, Goldberg AP, Sander C, Schultz N. 2012. The cBio Cancer genomics portal: an open platform for exploring multidimensional Cancer genomics data. *Cancer Discovery* **2**:401–404. DOI: https://doi.org/10.1158/2159-8290.CD-12-0095, PMID: 22588877

Chen M, Zhang J, Sampieri K, Clohessy JG, Mendez L, Gonzalez-Billalabeitia E, Liu XS, Lee YR, Fung J, Katon JM, Menon AV, Webster KA, Ng C, Palumbieri MD, Diolombi MS, Breitkopf SB, Teruya-Feldstein J, Signoretti S, Bronson RT, Asara JM, et al. 2018. An aberrant SREBP-dependent lipogenic program promotes metastatic prostate Cancer. *Nature Genetics* **50**:206–218. DOI: https://doi.org/10.1038/s41588-017-0027-2, PMID: 29335545

Colli JL, Colli A. 2005. Comparisons of prostate Cancer mortality rates with dietary practices in the united states. *Urologic Oncology: Seminars and Original Investigations* **23**:390–398. DOI: https://doi.org/10.1016/j.urolonc.2005.03.020, PMID: 16301115

Das UN. 2011. Essential fatty acids enhance free radical generation and lipid peroxidation to induce apoptosis of tumor cells. *Clinical Lipidology* **6**:463–489. DOI: https://doi.org/10.2217/clp.11.34

Davies NJ, Batehup L, Thomas R. 2011. The role of diet and physical activity in breast, colorectal, and prostate Cancer survivorship: a review of the literature. *British Journal of Cancer* **105 Suppl 1**:S52–S73. DOI: https://doi.org/10.1038/bjc.2011.423, PMID: 22048034

Davis ID, Martin AJ, Stockler MR, Begbie S, Chi KN, Chowdhury S, Coskinas X, Frydenberg M, Hague WE, Horvath LG, Joshua AM, Lawrence NJ, Marx G, McCaffrey J, McDermott R, McJannett M, North SA, Parnis F, Parulekar W, Pook DW, et al. 2019. Enzalutamide with standard First-Line therapy in metastatic prostate Cancer. *New England Journal of Medicine* **381**:121–131. DOI: https://doi.org/10.1056/NEJMoa1903835, PMID: 31157964

Ding Y, Wu H, Warden C, Steele L, Liu X, Iterson MV, Wu X, Nelson R, Liu Z, Yuan YC, Neuhausen SL. 2016. Gene expression differences in prostate cancers between young and old men. *PLOS Genetics* **12**:e1006477. DOI: https://doi.org/10.1371/journal.pgen.1006477, PMID: 28027300

Dixon SJ, Lemberg KM, Lamprecht MR, Skouta R, Zaitsev EM, Gleason CE, Patel DN, Bauer AJ, Cantley AM, Yang WS, Morrison B, Stockwell BR. 2012. Ferroptosis: an iron-dependent form of nonapoptotic cell death. *Cell* **149**:1060–1072. DOI: https://doi.org/10.1016/j.cell.2012.03.042, PMID: 22632970

Duval K, Grover H, Han LH, Mou Y, Pegoraro AF, Fredberg J, Chen Z. 2017. Modeling physiological events in 2D vs. 3D cell culture. *Physiology* **32**:266–277. DOI: https://doi.org/10.1152/physiol.00036.2016, PMID: 28615311

Epstein MM, Kasperzyk JL, Mucci LA, Giovannucci E, Price A, Wolk A, Håkansson N, Fall K, Andersson SO, Andrén O. 2012. Dietary fatty acid intake and prostate Cancer survival in Orebro county, Sweden. *American Journal of Epidemiology* **176**:240–252. DOI: https://doi.org/10.1093/aje/kwr520, PMID: 22781428

Ettinger SL, Sobel R, Whitmore TG, Akbari M, Bradley DR, Gleave ME, Nelson CC. 2004. Dysregulation of sterol response element-binding proteins and downstream effectors in prostate Cancer during progression to androgen independence. *Cancer Research* **64**:2212–2221. DOI: https://doi.org/10.1158/0008-5472.CAN-2148-2, PMID: 15026365

Flaig TW, Salzmann-Sullivan M, Su LJ, Zhang Z, Joshi M, Gijón MA, Kim J, Arcaroli JJ, Van Bokhoven A, Lucia MS, La Rosa FG, Schlaepfer IR. 2017. Lipid catabolism inhibition sensitizes prostate Cancer cells to antiandrogen blockade. *Oncotarget* **8**:56051–56065. DOI: https://doi.org/10.18632/oncotarget.17359, PMID: 28915573

Fu YQ, Zheng JS, Yang B, Li D. 2015. Effect of individual omega-3 fatty acids on the risk of prostate Cancer: a systematic review and dose-response meta-analysis of prospective cohort studies. *Journal of Epidemiology* **25**:261–274. DOI: https://doi.org/10.2188/jea.JE20140120, PMID: 25787237

Gaweł S, Wardas M, Niedworok E, Wardas P. 2004. [Malondialdehyde (MDA) as a lipid peroxidation marker]. *Wiadomosci Lekarskie* **57**:453–455. PMID: 15765761

Gazi E, Gardner P, Lockyer NP, Hart CA, Brown MD, Clarke NW. 2007. Direct evidence of lipid translocation between adipocytes and prostate Cancer cells with imaging FTIR microspectroscopy. *Journal of Lipid Research* **48**:1846–1856. DOI: https://doi.org/10.1194/jlr.M700131-JLR200, PMID: 17496269

Glinsky GV, Berezovska O, Glinskii AB. 2005. Microarray analysis identifies a death-from-cancer signature predicting therapy failure in patients with multiple types of Cancer. *Journal of Clinical Investigation* **115**:1503–1521. DOI: https://doi.org/10.1172/JCI23412, PMID: 15931389

Grasso CS, Wu YM, Robinson DR, Cao X, Dhanasekaran SM, Khan AP, Quist MJ, Jing X, Lonigro RJ, Brenner JC, Asangani IA, Ateeq B, Chun SY, Siddiqui J, Sam L, Anstett M, Mehra R, Prensner JR, Palanisamy N, Ryslik GA, et al. 2012. The mutational landscape of lethal castration-resistant prostate Cancer. *Nature* **487**:239–243. DOI: https://doi.org/10.1038/nature11125, PMID: 22722839

Hanahan D, Weinberg RA. 2011. Hallmarks of Cancer: the next generation. *Cell* **144**:646–674. DOI: https://doi.org/10.1016/j.cell.2011.02.013, PMID: 21376230

Haynie KR, Vandanmagsar B, Wicks SE, Zhang J, Mynatt RL. 2014. Inhibition of carnitine palymitoyltransferase1b induces cardiac hypertrophy and mortality in mice. *Diabetes, Obesity and Metabolism* **16**:757–760. DOI: https://doi.org/10.1111/dom.12248, PMID: 24330405

Hiltunen JK, Qin Y. 2000. beta-oxidation - strategies for the metabolism of a wide variety of acyl-CoA esters. *Biochimica Et Biophysica Acta (BBA) - Molecular and Cell Biology of Lipids* **1484**:117–128. DOI: https://doi.org/10.1016/S1388-1981(00)00013-5, PMID: 10760462

Holubarsch CJ, Rohrbach M, Karrasch M, Boehm E, Polonski L, Ponikowski P, Rhein S. 2007. A double-blind randomized multicentre clinical trial to evaluate the efficacy and safety of two doses of etomoxir in comparison with placebo in patients with moderate congestive heart failure: the ERGO (etomoxir for the recovery of glucose oxidation) study. *Clinical Science* **113**:205–212. DOI: https://doi.org/10.1042/CS20060307, PMID: 17319797

Houten SM, Denis S, Te Brinke H, Jongejan A, van Kampen AH, Bradley EJ, Baas F, Hennekam RC, Millington DS, Young SP, Frazier DM, Gucsavas-Calikoglu M, Wanders RJ. 2014. Mitochondrial NADP(H) deficiency due to a mutation in NADK2 causes dienoyl-CoA reductase deficiency with hyperlysinemia. *Human Molecular Genetics* **23**:5009–5016. DOI: https://doi.org/10.1093/hmg/ddu218, PMID: 24847004

Huggins C, Hodges CV. 1941. Studies on prostatic Cancer. I. the effect of castration, of estrogen and of androgen injection on serum phosphatases in metastatic carcinoma of the prostate. *Cancer Research* **1**:293–297. DOI: https://doi.org/10.3322/canjclin.22.4.232

Iglesias-Gato D, Wikström P, Tyanova S, Lavallee C, Thysell E, Carlsson J, Hägglöf C, Cox J, Andrén O, Stattin P, Egevad L, Widmark A, Bjartell A, Collins CC, Bergh A, Geiger T, Mann M, Flores-Morales A. 2016. The proteome of primary prostate Cancer. *European Urology* **69**:942–952. DOI: https://doi.org/10.1016/j.eururo.2015.10.053, PMID: 26651926

Iglesias-Gato D, Thysell E, Tyanova S, Crnalic S, Santos A, Lima TS, Geiger T, Cox J, Widmark A, Bergh A, Mann M, Flores-Morales A, Wikström P. 2018. The proteome of prostate Cancer bone metastasis reveals heterogeneity with prognostic implications. *Clinical Cancer Research* **24**:5433–5444. DOI: https://doi.org/10.1158/1078-0432.CCR-18-1229, PMID: 30042207

Itkonen HM, Brown M, Urbanucci A, Tredwell G, Ho Lau C, Barfeld S, Hart C, Guldvik IJ, Takhar M, Heemers HV, Erho N, Bloch K, Davicioni E, Derua R, Waelkens E, Mohler JL, Clarke N, Swinnen JV, Keun HC, Rekvig OP, et al. 2017. Lipid degradation promotes prostate Cancer cell survival. *Oncotarget* **8**:38264–38275. DOI: https://doi.org/10.18632/oncotarget.16123, PMID: 28415728

Ji S, You Y, Kerner J, Hoppel CL, Schoeb TR, Chick WS, Hamm DA, Sharer JD, Wood PA. 2008. Homozygous carnitine palmitoyltransferase 1b (muscle isoform) deficiency is lethal in the mouse. *Molecular Genetics and Metabolism* **93**:314–322. DOI: https://doi.org/10.1016/j.ymgme.2007.10.006, PMID: 18023382

Khankari NK, Murff HJ, Zeng C, Wen W, Eeles RA, Easton DF, Kote-Jarai Z, Al Olama AA, Benlloch S, Muir K, Giles GG, Wiklund F, Gronberg H, Haiman CA, Schleutker J, Nordestgaard BG, Travis RC, Donovan JL, Pashayan N, Khaw KT, et al. 2016. Polyunsaturated fatty acids and prostate Cancer risk: a mendelian randomisation analysis from the PRACTICAL consortium. *British Journal of Cancer* **115**:624–631. DOI: https://doi.org/10.1038/bjc.2016.228, PMID: 27490808

Kregel S, Kiriluk KJ, Rosen AM, Cai Y, Reyes EE, Otto KB, Tom W, Paner GP, Szmulewitz RZ, Vander Griend DJ. 2013. Sox2 is an androgen receptor-repressed gene that promotes castration-resistant prostate Cancer. *PLOS ONE* **8**:e53701. DOI: https://doi.org/10.1371/journal.pone.0053701, PMID: 23326489

Kuemmerle NB, Rysman E, Lombardo PS, Flanagan AJ, Lipe BC, Wells WA, Pettus JR, Froehlich HM, Memoli VA, Morganelli PM, Swinnen JV, Timmerman LA, Chaychi L, Fricano CJ, Eisenberg BL, Coleman WB, Kinlaw WB. 2011. Lipoprotein lipase links dietary fat to solid tumor cell proliferation. *Molecular Cancer Therapeutics* **10**:427–436. DOI: https://doi.org/10.1158/1535-7163.MCT-10-0802, PMID: 21282354

Law CW, Alhamdoosh M, Su S, Smyth GK, Ritchie ME. 2016. RNA-seq analysis is easy as 1-2-3 with limma, glimma and edgeR. *F1000Research* **5**:1408. DOI: https://doi.org/10.12688/f1000research.9005.1

Liu Y. 2006. Fatty acid oxidation is a dominant bioenergetic pathway in prostate Cancer. *Prostate Cancer and Prostatic Diseases* **9**:230–234. DOI: https://doi.org/10.1038/sj.pcan.4500879, PMID: 16683009

Magtanong L, Ko PJ, To M, Cao JY, Forcina GC, Tarangelo A, Ward CC, Cho K, Patti GJ, Nomura DK, Olzmann JA, Dixon SJ. 2019. Exogenous monounsaturated fatty acids promote a Ferroptosis-Resistant cell state. *Cell Chemical Biology* **26**:420–432. DOI: https://doi.org/10.1016/j.chembiol.2018.11.016, PMID: 30686757

Mäkelä AM, Hohtola E, Miinalainen IJ, Autio JA, Schmitz W, Niemi KJ, Hiltunen JK, Autio KJ. 2019. Mitochondrial 2,4-dienoyl-CoA reductase (Decr) deficiency and impairment of thermogenesis in mouse Brown adipose tissue. *Scientific Reports* **9**:12038. DOI: https://doi.org/10.1038/s41598-019-48562-x, PMID: 31427678

Martinez-Outschoorn UE, Lin Z, Whitaker-Menezes D, Howell A, Lisanti MP, Sotgia F. 2012. Ketone bodies and two-compartment tumor metabolism: stromal ketone production fuels mitochondrial biogenesis in epithelial Cancer cells. *Cell Cycle* **11**:3956–3963. DOI: https://doi.org/10.4161/cc.22136, PMID: 23082721

Matyash V, Liebisch G, Kurzchalia TV, Shevchenko A, Schwudke D. 2008. Lipid extraction by methyl-tert-butyl ether for high-throughput lipidomics. *Journal of Lipid Research* **49**:1137–1146. DOI: https://doi.org/10.1194/jlr.D700041-JLR200, PMID: 18281723

Miinalainen IJ, Schmitz W, Huotari A, Autio KJ, Soininen R, Ver Loren van Themaat E, Baes M, Herzig KH, Conzelmann E, Hiltunen JK. 2009. Mitochondrial 2,4-dienoyl-CoA reductase deficiency in mice results in severe hypoglycemia with stress intolerance and unimpaired ketogenesis. *PLOS Genetics* **5**:e1000543. DOI: https://doi.org/10.1371/journal.pgen.1000543, PMID: 19578400

Narita S, Nara T, Sato H, Koizumi A, Huang M, Inoue T, Habuchi T. 2019. Research evidence on High-Fat Diet-Induced prostate Cancer development and progression. *Journal of Clinical Medicine* **8**:597. DOI: https://doi.org/10.3390/jcm8050597

Nassar ZD, Aref AT, Miladinovic D, Mah CY, Raj GV, Hoy AJ, Butler LM. 2018. Peri-prostatic adipose tissue: the metabolic microenvironment of prostate Cancer. *BJU International* **121**:9–21. DOI: https://doi.org/10.1111/bju.14173

Nieman KM, Kenny HA, Penicka CV, Ladanyi A, Buell-Gutbrod R, Zillhardt MR, Romero IL, Carey MS, Mills GB, Hotamisligil GS, Yamada SD, Peter ME, Gwin K, Lengyel E. 2011. Adipocytes promote ovarian Cancer metastasis and provide energy for rapid tumor growth. *Nature Medicine* **17**:1498–1503. DOI: https://doi.org/10.1038/nm.2492, PMID: 22037646

Nikitina AS, Sharova EI, Danilenko SA, Butusova TB, Vasiliev AO, Govorov AV, Prilepskaya EA, Pushkar DY, Kostryukova ES. 2017. Novel RNA biomarkers of prostate Cancer revealed by RNA-seq analysis of formalin-fixed samples obtained from russian patients. *Oncotarget* **8**:32990–33001. DOI: https://doi.org/10.18632/oncotarget.16518, PMID: 28380430

Nomura DK, Lombardi DP, Chang JW, Niessen S, Ward AM, Long JZ, Hoover HH, Cravatt BF. 2011. Monoacylglycerol lipase exerts dual control over endocannabinoid and fatty acid pathways to support prostate Cancer. *Chemistry & Biology* **18**:846–856. DOI: https://doi.org/10.1016/j.chembiol.2011.05.009, PMID: 21802006

Nyman LR, Cox KB, Hoppel CL, Kerner J, Barnoski BL, Hamm DA, Tian L, Schoeb TR, Wood PA. 2005. Homozygous carnitine palmitoyltransferase 1a (liver isoform) deficiency is lethal in the mouse. *Molecular Genetics and Metabolism* **86**:179–187. DOI: https://doi.org/10.1016/j.ymgme.2005.07.021, PMID: 16169268

Ornish D, Weidner G, Fair WR, Marlin R, Pettengill EB, Raisin CJ, Dunn-Emke S, Crutchfield L, Jacobs FN, Barnard RJ, Aronson WJ, McCormac P, McKnight DJ, Fein JD, Dnistrian AM, Weinstein J, Ngo TH, Mendell NR, Carroll PR. 2005. Intensive lifestyle changes may affect the progression of prostate Cancer. *Journal of Urology* **174**:1065–1070. DOI: https://doi.org/10.1097/01.ju.0000169487.49018.73, PMID: 16094059

Paltoglou S, Das R, Townley SL, Hickey TE, Tarulli GA, Coutinho I, Fernandes R, Hanson AR, Denis I, Carroll JS, Dehm SM, Raj GV, Plymate SR, Tilley WD, Selth LA. 2017. Novel androgen receptor coregulator GRHL2 exerts both oncogenic and antimetastatic functions in prostate Cancer. *Cancer Research* **77**:3417–3430. DOI: https://doi.org/10.1158/0008-5472.CAN-16-1616, PMID: 28473532

Park SY, Wilkens LR, Henning SM, Le Marchand L, Gao K, Goodman MT, Murphy SP, Henderson BE, Kolonel LN. 2009. Circulating fatty acids and prostate Cancer risk in a nested case-control study: the multiethnic cohort. *Cancer Causes & Control* **20**:211–223. DOI: https://doi.org/10.1007/s10552-008-9236-4, PMID: 18821021

Piccinini F, Tesei A, Arienti C, Bevilacqua A. 2015. Cancer multicellular spheroids: volume assessment from a single 2D projection. *Computer Methods and Programs in Biomedicine* **118**:95–106. DOI: https://doi.org/10.1016/j.cmpb.2014.12.003, PMID: 25561413

Pomerantz MM, Li F, Takeda DY, Lenci R, Chonkar A, Chabot M, Cejas P, Vazquez F, Cook J, Shivdasani RA, Bowden M, Lis R, Hahn WC, Kantoff PW, Brown M, Loda M, Long HW, Freedman ML. 2015. The androgen receptor cistrome is extensively reprogrammed in human prostate tumorigenesis. *Nature Genetics* **47**:1346–1351. DOI: https://doi.org/10.1038/ng.3419, PMID: 26457646

R Development Core Team. 2019. R: A language and environment for statistical computing. Vienna, Austria, R Foundation for Statistical Computing. https://www.R-project.org/

Ren S, Peng Z, Mao JH, Yu Y, Yin C, Gao X, Cui Z, Zhang J, Yi K, Xu W, Chen C, Wang F, Guo X, Lu J, Yang J, Wei M, Tian Z, Guan Y, Tang L, Xu C, et al. 2012. RNA-seq analysis of prostate Cancer in the chinese population identifies recurrent gene fusions, cancer-associated long noncoding RNAs and aberrant alternative splicings. *Cell Research* **22**:806–821. DOI: https://doi.org/10.1038/cr.2012.30, PMID: 22349460

Rodrigues DN, Butler LM, Estelles DL, de Bono JS. 2014. Molecular pathology and prostate Cancer therapeutics: from biology to bedside. *The Journal of Pathology* **232**:178–184. DOI: https://doi.org/10.1002/path.4272, PMID: 24108540

Roe CR, Millington DS, Norwood DL, Kodo N, Sprecher H, Mohammed BS, Nada M, Schulz H, McVie R. 1990. 2, 4-Dienoyl-coenzyme A reductase deficiency: a possible new disorder of fatty acid oxidation. *Journal of Clinical Investigation* **85**:1703–1707. DOI: https://doi.org/10.1172/JCI114624, PMID: 2332510

Rossi S, Graner E, Febbo P, Weinstein L, Bhattacharya N, Onody T, Bubley G, Balk S, Loda M. 2003. Fatty acid synthase expression defines distinct molecular signatures in prostate Cancer. *Molecular Cancer Research : MCR* **1**:707–715. PMID: 12939396

Sboner A, Demichelis F, Calza S, Pawitan Y, Setlur SR, Hoshida Y, Perner S, Adami HO, Fall K, Mucci LA, Kantoff PW, Stampfer M, Andersson SO, Varenhorst E, Johansson JE, Gerstein MB, Golub TR, Rubin MA, Andrén O. 2010. Molecular sampling of prostate Cancer: a dilemma for predicting disease progression. *BMC Medical Genomics* **3**:8. DOI: https://doi.org/10.1186/1755-8794-3-8, PMID: 20233430

Scher HI, Fizazi K, Saad F, Taplin ME, Sternberg CN, Miller K, de Wit R, Mulders P, Chi KN, Shore ND, Armstrong AJ, Flaig TW, Fléchon A, Mainwaring P, Fleming M, Hainsworth JD, Hirmand M, Selby B, Seely L, de Bono JS, AFFIRM Investigators. 2012. Increased survival with enzalutamide in prostate Cancer after chemotherapy. *New England Journal of Medicine* **367**:1187–1197. DOI: https://doi.org/10.1056/NEJMoa1207506, PMID: 22894553

Schlaepfer IR, Rider L, Rodrigues LU, Gijón MA, Pac CT, Romero L, Cimic A, Sirintrapun SJ, Glodé LM, Eckel RH, Cramer SD. 2014. Lipid catabolism via CPT1 as a therapeutic target for prostate Cancer. *Molecular Cancer Therapeutics* **13**:2361–2371. DOI: https://doi.org/10.1158/1535-7163.MCT-14-0183, PMID: 25122071

Schlaepfer IR, Glodé LM, Hitz CA, Pac CT, Boyle KE, Maroni P, Deep G, Agarwal R, Lucia SM, Cramer SD, Serkova NJ, Eckel RH. 2015. Inhibition of lipid oxidation increases glucose metabolism and enhances 2-Deoxy-2-[(18)F]Fluoro-D-Glucose uptake in prostate Cancer mouse xenografts. *Molecular Imaging and Biology* **17**:529–538. DOI: https://doi.org/10.1007/s11307-014-0814-4, PMID: 25561013

Shoukry K, Schulz H. 1998. Significance of the reductase-dependent pathway for the beta-oxidation of unsaturated fatty acids with odd-numbered double bonds. Mitochondrial metabolism of 2-trans-5-cis-octadienoyl-CoA. *The Journal of Biological Chemistry* **273**:6892–6899. DOI: https://doi.org/10.1074/jbc.273.12.6892, PMID: 9506993

Shurbaji MS, Kalbfleisch JH, Thurmond TS. 1996. Immunohistochemical detection of a fatty acid synthase (OA-519) as a predictor of progression of prostate Cancer. *Human Pathology* **27**:917–921. DOI: https://doi.org/10.1016/S0046-8177(96)90218-X, PMID: 8816886

Slattery ML, Schumacher MC, West DW, Robison LM, French TK. 1990. Food-consumption trends between adolescent and adult years and subsequent risk of prostate Cancer. *The American Journal of Clinical Nutrition* **52**:752–757. DOI: https://doi.org/10.1093/ajcn/52.4.752, PMID: 2403069

Stéfani ED, Deneo-Pellegrini H, Boffetta P, Ronco A, Mendilaharsu M. 2000. α-Linolenic acid and risk of prostate Cancer: a Case-Control study in Uruguay. *Cancer Epidemiology Biomarkers & Prevention* **9**:335–338. DOI: https://doi.org/10.1007/s11745-004-1315-2

Swinnen JV, Roskams T, Joniau S, Van Poppel H, Oyen R, Baert L, Heyns W, Verhoeven G. 2002. Overexpression of fatty acid synthase is an early and common event in the development of prostate Cancer. *International Journal of Cancer* **98**:19–22. DOI: https://doi.org/10.1002/ijc.10127, PMID: 11857379

Taylor BS, Schultz N, Hieronymus H, Gopalan A, Xiao Y, Carver BS, Arora VK, Kaushik P, Cerami E, Reva B, Antipin Y, Mitsiades N, Landers T, Dolgalev I, Major JE, Wilson M, Socci ND, Lash AE, Heguy A, Eastham JA, et al. 2010. Integrative genomic profiling of human prostate Cancer. *Cancer Cell* **18**:11–22. DOI: https://doi.org/10.1016/j.ccr.2010.05.026, PMID: 20579941

Tomlins SA, Mehra R, Rhodes DR, Cao X, Wang L, Dhanasekaran SM, Kalyana-Sundaram S, Wei JT, Rubin MA, Pienta KJ, Shah RB, Chinnaiyan AM. 2007. Integrative molecular concept modeling of prostate Cancer progression. *Nature Genetics* **39**:41–51. DOI: https://doi.org/10.1038/ng1935, PMID: 17173048

Toren P, Kim S, Johnson F, Zoubeidi A. 2016. Combined AKT and MEK pathway blockade in Pre-Clinical models of Enzalutamide-Resistant prostate Cancer. *PLOS ONE* **11**:e0152861. DOI: https://doi.org/10.1371/journal.pone.0152861, PMID: 27046225

Tran C, Ouk S, Clegg NJ, Chen Y, Watson PA, Arora V, Wongvipat J, Smith-Jones PM, Yoo D, Kwon A, Wasielewska T, Welsbie D, Chen CD, Higano CS, Beer TM, Hung DT, Scher HI, Jung ME, Sawyers CL. 2009. Development of a second-generation antiandrogen for treatment of advanced prostate Cancer. *Science* **324**:787–790. DOI: https://doi.org/10.1126/science.1168175, PMID: 19359544

Tse BWC, Volpert M, Ratther E, Stylianou N, Nouri M, McGowan K, Lehman ML, McPherson SJ, Roshan-Moniri M, Butler MS, Caradec J, Gregory-Evans CY, McGovern J, Das R, Takhar M, Erho N, Alshalafa M, Davicioni E, Schaeffer EM, Jenkins RB, et al. 2017. Neuropilin-1 is upregulated in the adaptive response of prostate tumors to androgen-targeted therapies and is prognostic of metastatic progression and patient mortality. *Oncogene* **36**:3417–3427. DOI: https://doi.org/10.1038/onc.2016.482, PMID: 28092670

Wang S, Wu J, Suburu J, Gu Z, Cai J, Axanova LS, Cramer SD, Thomas MJ, Perry DL, Edwards IJ, Mucci LA, Sinnott JA, Loda MF, Sui G, Berquin IM, Chen YQ. 2012. Effect of dietary polyunsaturated fatty acids on castration-resistant Pten-null prostate Cancer. *Carcinogenesis* **33**:404–412. DOI: https://doi.org/10.1093/carcin/bgr290

Warburg O, Wind F, Negelein E. 1927. The metabolism of tumors in the body. *The Journal of General Physiology* **8**:519–530. DOI: https://doi.org/10.1085/jgp.8.6.519, PMID: 19872213

Watt MJ, Clark AK, Selth LA, Haynes VR, Lister N, Rebello R, Porter LH, Niranjan B, Whitby ST, Lo J, Huang C, Schittenhelm RB, Anderson KE, Furic L, Wijayaratne PR, Matzaris M, Montgomery MK, Papargiris M, Norden S, Febbraio M, et al. 2019. Suppressing fatty acid uptake has therapeutic effects in preclinical models of prostate Cancer. *Science Translational Medicine* **11**:eaau5758. DOI: https://doi.org/10.1126/scitranslmed.aau5758, PMID: 30728288

Whittemore AS, Kolonel LN, Wu AH, John EM, Gallagher RP, Howe GR, Burch JD, Hankin J, Dreon DM, West DW. 1995. Prostate Cancer in relation to diet, physical activity, and body size in blacks, whites, and asians in the united states and Canada. *JNCI Journal of the National Cancer Institute* **87**:652–661. DOI: https://doi.org/10.1093/jnci/87.9.652, PMID: 7752270

Williams CD, Whitley BM, Hoyo C, Grant DJ, Iraggi JD, Newman KA, Gerber L, Taylor LA, McKeever MG, Freedland SJ. 2011. A high ratio of dietary n-6/n-3 polyunsaturated fatty acids is associated with increased risk of prostate Cancer. *Nutrition Research* **31**:1–8. DOI: https://doi.org/10.1016/j.nutres.2011.01.002, PMID: 21310299

Wu X, Daniels G, Lee P, Monaco ME. 2014. Lipid metabolism in prostate Cancer. *American Journal of Clinical and Experimental Urology* **2**:111–120. DOI: https://doi.org/10.3390/ijms20112626, PMID: 25374912

Zadra G, Photopoulos C, Loda M. 2013. The fat side of prostate Cancer. *Biochimica Et Biophysica Acta* **1831**: 1518–1532. DOI: https://doi.org/10.1016/j.bbalip.2013.03.010

Zadra G, Loda M. 2018. Metabolic vulnerabilities of prostate Cancer: diagnostic and therapeutic opportunities. *Cold Spring Harbor Perspectives in Medicine* **8**:a030569. DOI: https://doi.org/10.1101/cshperspect.a030569, PMID: 29229664

Appendix 1

Key Resources Table

Appendix 1—key resources table

Reagent type (species) or resource	Designation	Source or reference	Identifiers	Additional information
Strain, strain background (*M. musculus*, male,)	NOD scid Gamma (*M. musculus*, male,) Mice	The Jackson Laboratory/Interbred at SAHMRI Bioresources	NOD.Cg-Prkdcscid/J RRID:IMSR_JAX:001303	
Cell line (*Homo sapiens*)	LNCaP	ATCC	ATCC CRL-1740 RRID:CVCL_1379	
Cell line (*Homo sapiens*)	VCaP	ATCC	ATCC CRL-2876 RRID:CVCL_2235	
Cell line (*Homo sapiens*)	22RV1	ATCC	ATCC CRL-2505 RRID:CVCL_1045	
Cell line (*Homo sapiens*)	PNT1A	The European Collection of Authenticated Cell Cultures (ECACC)	Cat# 95012614 RRID:CVCL_2163	
Cell line (*Homo sapiens*)	PNT2	The European Collection of Authenticated Cell Cultures (ECACC)	Cat# 95012613 RRID:CVCL_2164	
Cell line (*Homo sapiens*)	V16D	PMID:27046225	Kind gift from Prof. Amina Zoubeidi	
Cell line (*Homo sapiens*)	MR49F	PMID:27046225	Kind gift from Prof. Amina Zoubeidi	
Transfected construct (*Homo sapiens*)	control siRNA	Dharmacon	D-001810-01-20 ON-TARGET plus Non-targeting siRNA #1	transfected construct (human)
Transfected construct (*Homo sapiens*)	siDECR1-1	Dharmacon	J-009642-05-0002	transfected construct (human)
Transfected construct (*Homo sapiens*)	siDECR1-2	Dharmacon	J-009642-06-0002	transfected construct (human)
Transfected construct (*Homo sapiens*)	DECR1 shRNA lentivector	GenTargrt	LVS-1002	Lentiviral construct to transfect and express the shRNA.

Appendix 1—key resources table continued

Reagent type (species) or resource	Designation	Source or reference	Identifiers	Additional information
Transfected construct (*Homo sapiens*)	hDECR1 Overexpressing Lentivector	GenTargrt	LVS-2002	Lentiviral construct to transfect and overexpress DECR1.
Transfected construct (*Homo sapiens*)	Negative control shRNA lentivector	GenTargrt	LVS-1002	Lentiviral construct to transfect and express the shRNA.
Antibody	Anti-human β-Actin (Mouse monoclonal)	Sigma-Aldrich	Cat#: A5441 RRID:AB_476744	(WB 1:2000)
Antibody	Anti-human-HSP90 (Rabbit Polyclonal)	Cell Signalling Technology	Cat#: 48745 RRID:CVCL_E547	(WB 1:1000)
Antibody	Anti-human DECR1 (Rabbit Polyclonal)	Prestige Antibodies (Sigma-Aldrich)	Cat#: HPA023238 RRID:AB_1847587	(WB 1:1000) (IHC: 1:500)
Antibody	Anti-human Malondialdehyde (Rabbit Polyclonal)	Abcam	Cat#: ab6463 RRID:AB_305484	(WB 1:1000)
Antibody	Anti- human Androgen receptor (Rabbit Polyclonal)	Santa Cruz Biotechnology	Cat#: sc-816 RRID:AB_1563391	(WB 1:1000)
Antibody	Anti-human PARP (Rabbit Polyclonal)	Cell Signalling Technology	Cat#: 9542 RRID:AB_592473	(WB 1:1000)
Antibody	Anti-human Cytochrome C (Rabbit Polyclonal)	Abcam	Cat#: ab90529 RRID:AB_10673869	(WB 1:2000)
Other	MitoTracker Red CMXRos	Thermo Fisher Scientific	Cat#: M7512	ICC 1:1000
Other	MitoSOX Red Mitochondrial Superoxide Indicator	Thermo Fisher Scientific	Cat#: M36008	Flow Cytometry: 2.5 µM
Other	3,3′-Diaminobenzidine (DAB) Enhanced Liquid Substrate System tetrahydrochloride	Sigma Aldrich	Cat#: D3939	
Other	BODIPY-C11	Thermo Fisher Scientific	Cat#: D3861	Imaging: 5 µM
Antibody	Anti-human KI67 (Mouse monoclonal)	DAKO	Cat#: M7240 RRID:AB_2142367	(IHC 1:200)
Antibody	Anti-human AR (Rabbit polyclonal)	Santa Cruz	Cat#: sc-816 RRID:AB_1563391	(WB 1:1000)
Sequence-based reagent	DECR1_F	This paper	PCR primers	CTAAATGGCACAGCCTTCGT

Appendix 1—key resources table continued

Reagent type (species) or resource	Designation	Source or reference	Identifiers	Additional information
Sequenced-based reagent	DECR1_R	This paper	PCR primers	AACCTGAACCAG TCTCAGCA
Sequence-based reagent	GAPDH_F	This paper	PCR primers	TGCACCACCAAC TGCTTAGC
Sequenced-based reagent	GAPDH_R	This paper	PCR primers	GGCATGGACTG TGGTCATGAG
Sequence-based reagent	PPIA_F	This paper	PCR primers	GCATACGGGTCC TGGCAT
Sequence-based reagent	PPIA_R	This paper	PCR primers	ACATGCTTGCCA TCCAACC
Sequence-based re-agent	TUBA1B _F	This paper	PCR primers	CCTTCGCCTCC TAATCCCTA
Sequence-based reagent	TUBA1B _R	This paper	PCR primers	CCGTGTTCCAGG-CAGTAGA
Sequence-based reagent	MKI67_F	This paper	PCR primers	GCCTGC TCGACCCTACA-GA
Sequence-based reagent	MIK67_R	This paper	PCR primers	GCTTGTCAAC TGCGGTTGC
Sequence-based reagent	L19_F	This paper	PCR primers	TGCCAG TGGAAAAA TCAGCCA
Sequence-based reagent	L19_R	This paper	PCR primers	CAAAGCAAATC TCGACACCTTG
Sequence-based reagent	GUSB_F	This paper	PCR primers	CGTCCCACCTA-GAATCTGCT
Sequence-based reagent	GUSB_R	This paper	PCR primers	TTGCTCA-CAAAGGTCA-CAGG
Sequence-based reagent	DECR1_F	This paper	ChIP-qPCR	TTCTGGAGCGC TAAGAGAGC
Sequence-based reagent	DECR1_R	This paper	ChIP-qPCR	AGGGCTTCATC TGACAGTGG
Sequence-based reagent	KLK3_F	This paper	ChIP-qPCR	GCCTGGATCTGA-GAGAGATATCA TC
Sequence-based reagent	KLK3_R	This paper	ChIP-qPCR	ACACC TTTTTTTTTCTGGA TTGTTG
Sequence-based reagent	NC2_F	This paper	ChIP-qPCR	GTGAGTGCCCAG TTAGAGCATCTA

Appendix 1—key resources table continued

Reagent type (species) or resource	Designation	Source or reference	Identifiers	Additional information
Sequence-based reagent	NC2_R	This paper	ChIP-qPCR	GGAACCAGTGGG TCTTGAAGTG
Chemical compound, drug	Etomoxir	Sigma Aldrich	Cat#: E1905	
Chemical compound, drug	Dihydrotestosterone	Sigma Aldrich	Cas#: 521-18-6	
Chemical compound, drug	Enzalutamide	Sapphire Bioscience	Cat#: S1250	
Chemical compound, drug	Bovine-serum albumin	Bovostar	Cat#: BSAS-AU	
Chemical compound, drug	Linoleic acid	Sigma Aldrich	Cat#: L1376	
Chemical compound, drug	Palmitic acid	Sigma Aldrich	Cat#: P0500	
Chemical compound, drug	D-Luciferin	PerkinElmer	Cat#: 122799	3 mg/20 g
Chemical compound, drug	Deferoxamine	Sigma Aldrich	Cat#: D9533	
Chemical compound, drug	Ferrostatin	Sigma Aldrich	Cat#: SML0583	
Chemical compound, drug	Erastian	Sigma Aldrich	Cat#: E7781	
Chemical compound, drug	ML210	Tocris Bioscience	Cat#: 6429	
Chemical compound, drug	FIN56	Tocris Bioscience	Cat#: 6280	
Chemical compound, drug	cell fractionation kit	Abcam	Cat#: ab109719	
Chemical compound, drug	RNeasy RNA extraction kit	Qiagen	Cat#: 74136	
Chemical compound, drug	iScript cDNA Synthesis kit	Bio-Rad	Cat#: 1708890	
Chemical compound, drug	Seahorse XF Cell Mito chondrial Stress Test kit	Agilent	Cat#: 103015–100	
Software, algorithm	GraphPad Prism	GraphPad Software, Inc	Prism V7 RRID:SCR_002798	

Appendix 1—key resources table continued

Reagent type (species) or resource	Designation	Source or reference	Identifiers	Additional information
Software, algorithm	R	***R Development Core Team, 2019***	R version 3.6.2 RRID:SCR_001905	
Software, algorithm	ReViSP	PMID:25561413	ReViSP	Volume assessment of cancer spheroids
Software, algorithm	IVIS Spectrum In Vivo Imaging System	PerkinElmer	IVIS Spectrum In Vivo Imaging System RRID:SCR_018621	Tumor volume analysis
Other	Lipofectamine RNAiMAX transfection reagent	Thermo Fisher Scientific	13778075	
Software, algorithm	ImageJ analysis software	NIH	ImageJ RRID:SCR_003070	
Software, algorithm	TraceFinder v5.0	Thermo Fisher Scientific	OPTON-30688	

3.1 Supplementary figures

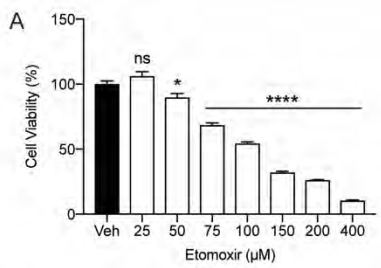

C

Dataset	Fold Change	P value	No. of Tissues	
			Normal	Malignant
TCGA	1.44	0.0001	499	51
Ding	1.12	0.0002	45	45
Tomlins	2.389	1.81E-04	23	30
Luo	1.404	0.001	15	15
Vanaja	1.9	5.57E-07	15	15
Grasso	1.311	5.25E-05	28	59
Areedouani	1.311	9.00E-03	8	13
Lapointe	1.068	0.062	41	62
Singh	2.294	2.55E-04	50	52
Weslh	1.419	1.00E-03	9	25

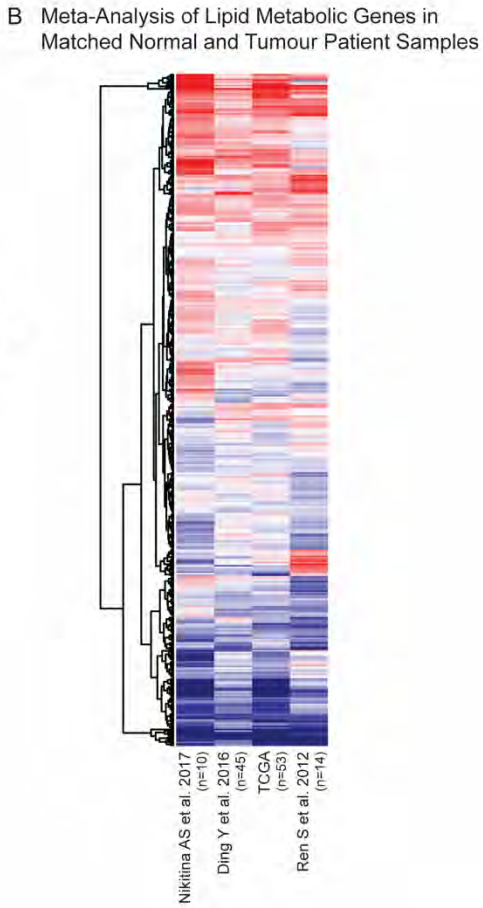

Figure 1-figure supplement 1 Fatty acid metabolism is consistently altered in clinical prostate tumors. (A) Cell viability of LNCaP cells treated with indicated concentrations of etomoxir for 72 hr. Cell viability was determined using CyQUANT Cell Assay. **(B)** A meta-analysis of 735 lipid metabolism genes using four clinical datasets with malignant and matched normal RNA-sequencing data (n = 122). Genes were rank-ordered on the basis of their *meta effect size* scores in PCa malignant tissues versus matched normal. **(C)** Fold change of DECR1 mRNA expression in malignant tissues compared to benign/normal tissues. Data were obtained from Oncomine.

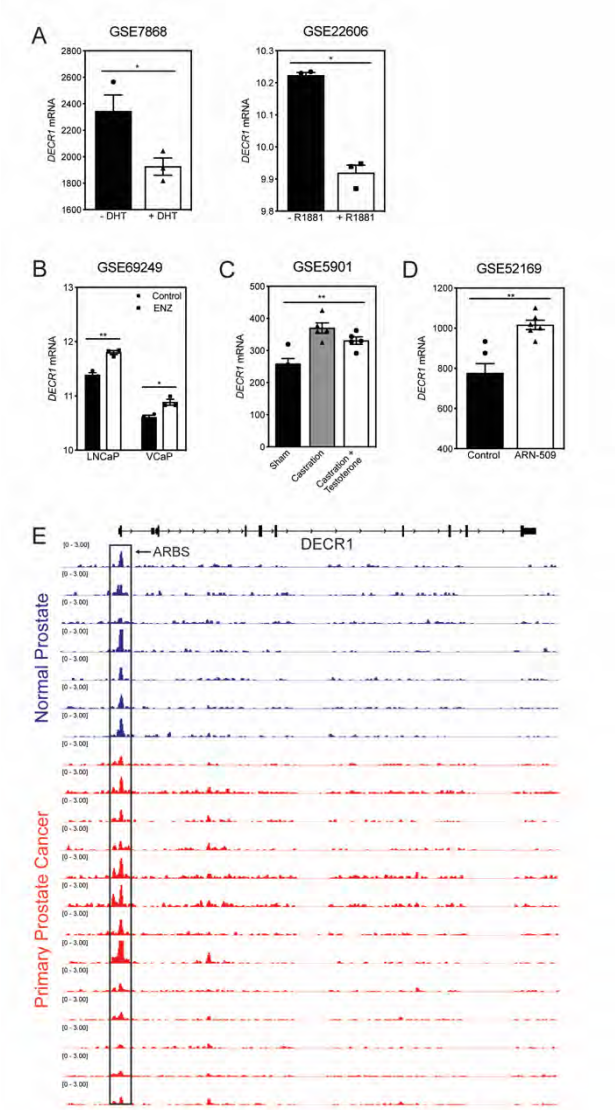

Figure 3-figure supplement 1 Androgenic regulation of DECR1 expression. (A) Bar graphs of DECR1 mRNA expression in two publically available datasets shows DECR1 mRNA expression decreased after LNCaP treatment with DHT (GSE7868) or R1881 (GSE22606). **(B)** DECR1 expression increased in LNCaP and VCaP upon treatment with Enzalutamide (GSE69249). **(C)** DECR1 mRNA expression increased in mouse prostate gland after castration but decreased after testosterone administration. **(D)** ARN-509 (Apalutamide) treatment of LNCaP/AR xenograft increased DECR1 mRNA expression (GSE52169). **(E)** AR ChIP-sequencing data from normal human prostate and primary human prostate tumor specimens (normal, n = 7; tumor, n = 13). Data from GSE56288. Statistical analysis was performed using two-tailed Student's *t*-test: *p<0.05, **p<0.01 and ****p<0.0001.

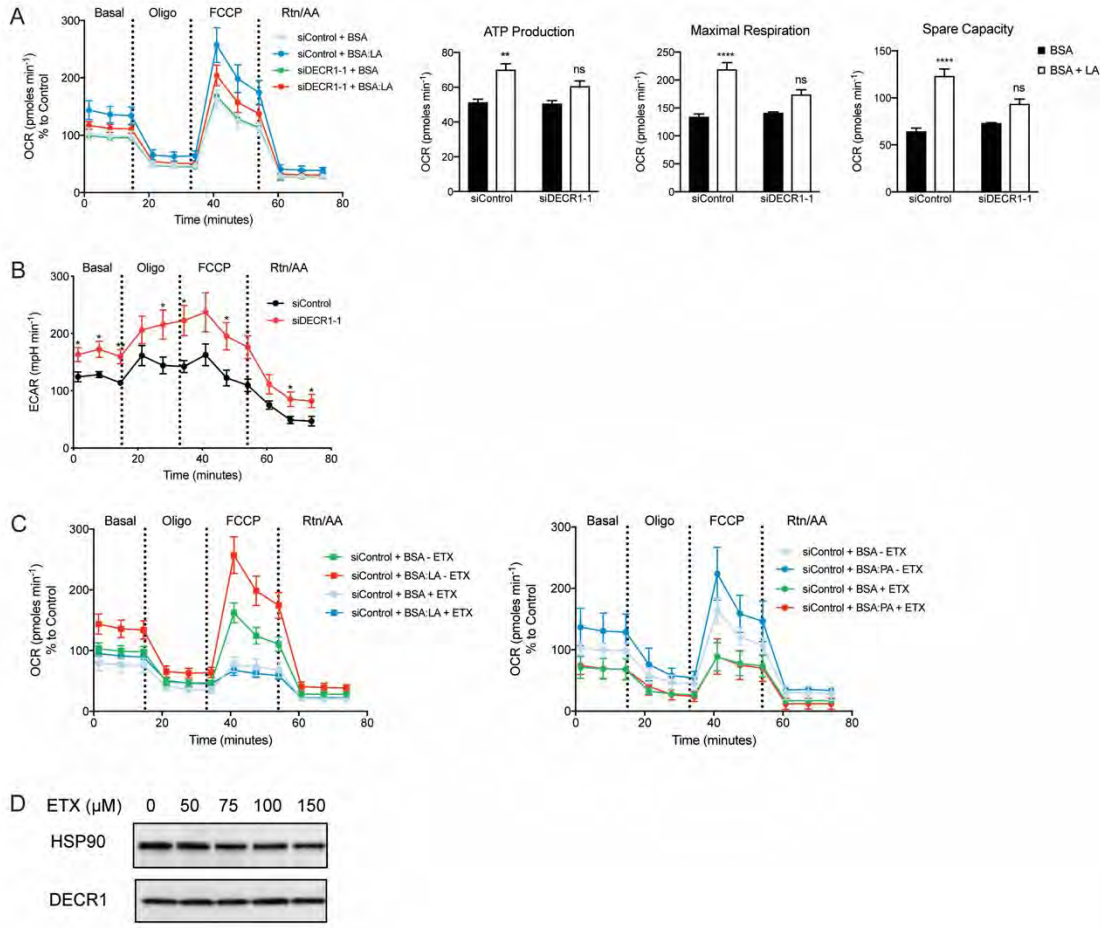

Figure 4-figure supplement 1 Effects of DECR1 on prostate cancer cellular metabolism. (A) Oxygen consumption rate (OCR) was assessed in LNCaP cells supplemented with the PUFA linoleic acid (LA). Each data point represents an OCR measurement. ATP production, maximal mitochondrial respiration and mitochondrial spare capacity were assessed. **(B)** Extracellular acidification rate (ECAR) was assessed in LNCaP cells. Each data point represents an ECAR measurement. **(C)** OCR of LNCaP cells supplemented with PUFA LA (top) or palmitic acid (PA, bottom) treated with etomoxir (ETX, 100 μM). Each data point represents an OCR measurement. **(D)** DECR1 protein expression after 48 hr treatment with varying concentrations of etomoxir. Statistical analysis was performed using two-tailed Student's *t*-test: *p<0.05, **p<0.01 and ****p<0.0001.

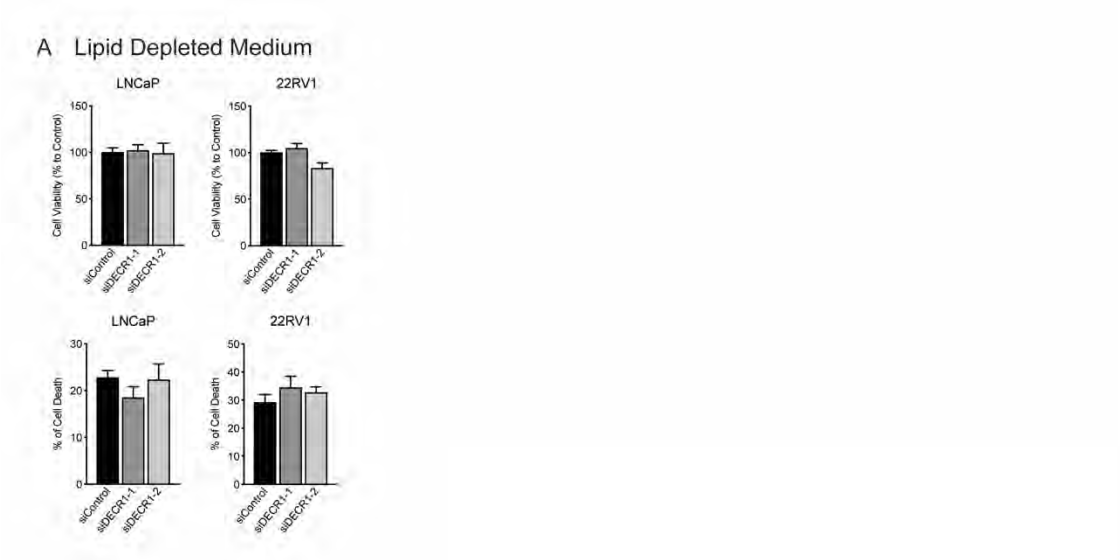

Figure 5-figure supplement 1 Depletion of extracellular lipids prevents antiproliferative effects of DECR1 in prostate cancer cells. (A) Cell viability and cell death after DECR1 knockdown in LNCaP and 22RV1 cultured in full serum media. Cell viability and cell death were measured using trypan blue exclusion following 96 hr DECR1 knockdown. Percentages are represented relative to the control siRNA; n = 3 independent experiments per cell line.

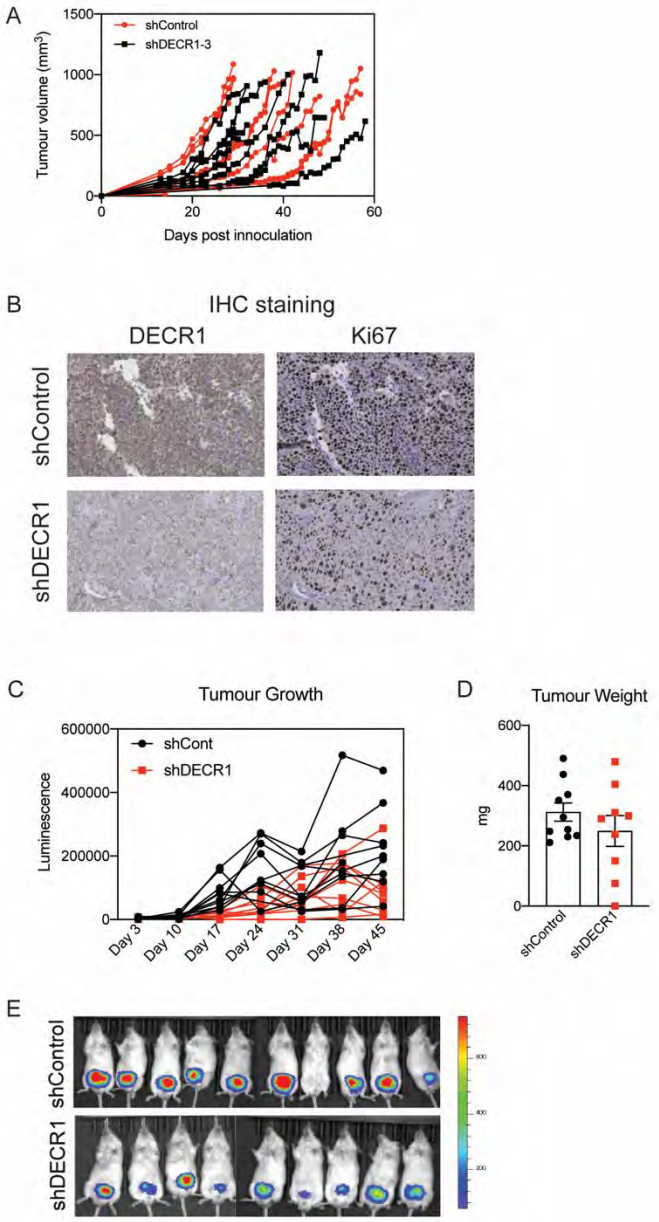

Figure 5-figure supplement 2 DECR1 suppresses growth of prostate tumor xenografts in mice. (A) Individual tumor growth of shControl and shDECR1 cells in LNCaP-xenograft tumors. **(B)** Representative DECR1 and KI67 IHC staining of consecutive sections of LNCaP-xenograft tumors. **(C)** Individual tumor growth and **(D)** tumour weight of shControl and shDECR1 cells in LNCaP-xenograft tumors from the second cohort of mice. **(E)** Tumor growth was monitored based on luciferase activity over time as indicated by IVIS imaging (n = 10 mice, shControl; n = 9 mice, shDECR1).

shControl sequence: GTCTCCACGCGCAGTACATTT
cloned shRNA hairpin sequence:

GTCTCCACGCGCAGTACATTTcgagAAATGTACTGCGCGTGGAGAC

shDECR1-1 sequence: GGTAAAGGAATGACAACTCTT
cloned shRNA hairpin sequence:

GGTAAAGGAATGACAACTCTTcgagAAGAGTTGTCATTCCTTTACC

blue: sense
black: loop
red: anti-sense

shDECR1-2 sequence: GTGATTCAACCAGGGCCTATA
cloned shRNA hairpin sequence:

GTGATTCAACCAGGGCCTATAcgagTATAGGCCCTGGTTGAATCAC

hDECR1
sub-cloned human target coding sequences:

Human DECR1
atgtcaggactggggaagaagcatctcctgctcatgggggagtttttcagttatgggacaaaaatattatatcaaaacactgaagcttt
gcaatctaaattcttttcacctcttcaaaaagcgatgctaccacctaatagttttcaaggaaaagtggcattcattactgggggaggtact
ggccttggtaaaggaatgacaactcttctgtccagcctaggtgctcagtgcgtgatagccagccggaagatggatgttttgaaagctac
cgcagaacaaatttcttctcaaactggaaataaggttcatgcaattcagtgtgatgtgagggatcctgatatggttcaaaacactgtgtc
agaactgatcaaagttgcaggacatcctaatattgtgataaacaatgcagcagggaattttatttctcctactgaaagactttctcctaat
gcttggaaaaccataactgacatagttctaaatggcacagccttcgtgacactagaaattggaaaacaactaattaaagcacagaaag
gagcagcatttctttctattactactatctatgctgagactggttcaggttttgtagtaccaagtgcttctgccaaagcaggtgtggaagcc
atgagcaagtctcttgcagctgaatggggtaaatatggaatgcgattcaatgtgattcaaccagggcctataaaaaccaaaggtgcctt
tagccgtctggacccaactggaacatttgagaaagaaatgattggcagaattccctgtggtcgcctggggactgtagaagaactcgca
aatcttgctgctttcctttgtagtgattatgcttcttggattaatggagcagtcattaaatttgacggtggagaggaagtacttatttcaggg
gaattcaacgacctgagaaaggtcaccaaggagcagtgggacaccatagaagaactcatcaggaagacaaaaggttcc

Figure 5-figure supplement 3 Sequence of the DECR1 shRNA and hDECR1 vectors.

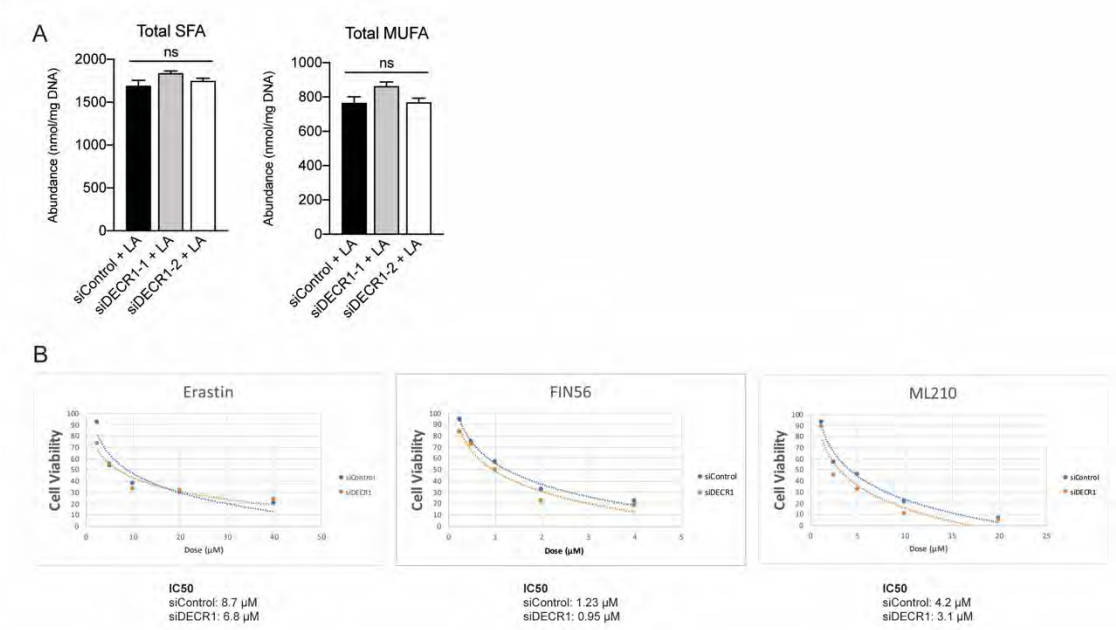

Figure 6-figure supplement 1 Depletion of DECR1 sensitizes prostate cancer cells to ferroptosis inducing agents. (A) Abundance of total SFA and **(B)** MUFA species in phospholipids from control and DECR1 knockdown cells supplemented with linoleic acid (LA). **(C)** Abundance of total SFAs (left) and MUFAs (right) in Control and DECR1 knockdown cells supplemented with LA. **(D)** IC50 values of ferroptosis inducers were determined in Control and DECR1 knockdown cells. Statistical analysis was performed using two-tailed Student's *t*-test: *p<0.05, **p<0.01 and ***p<0.001.

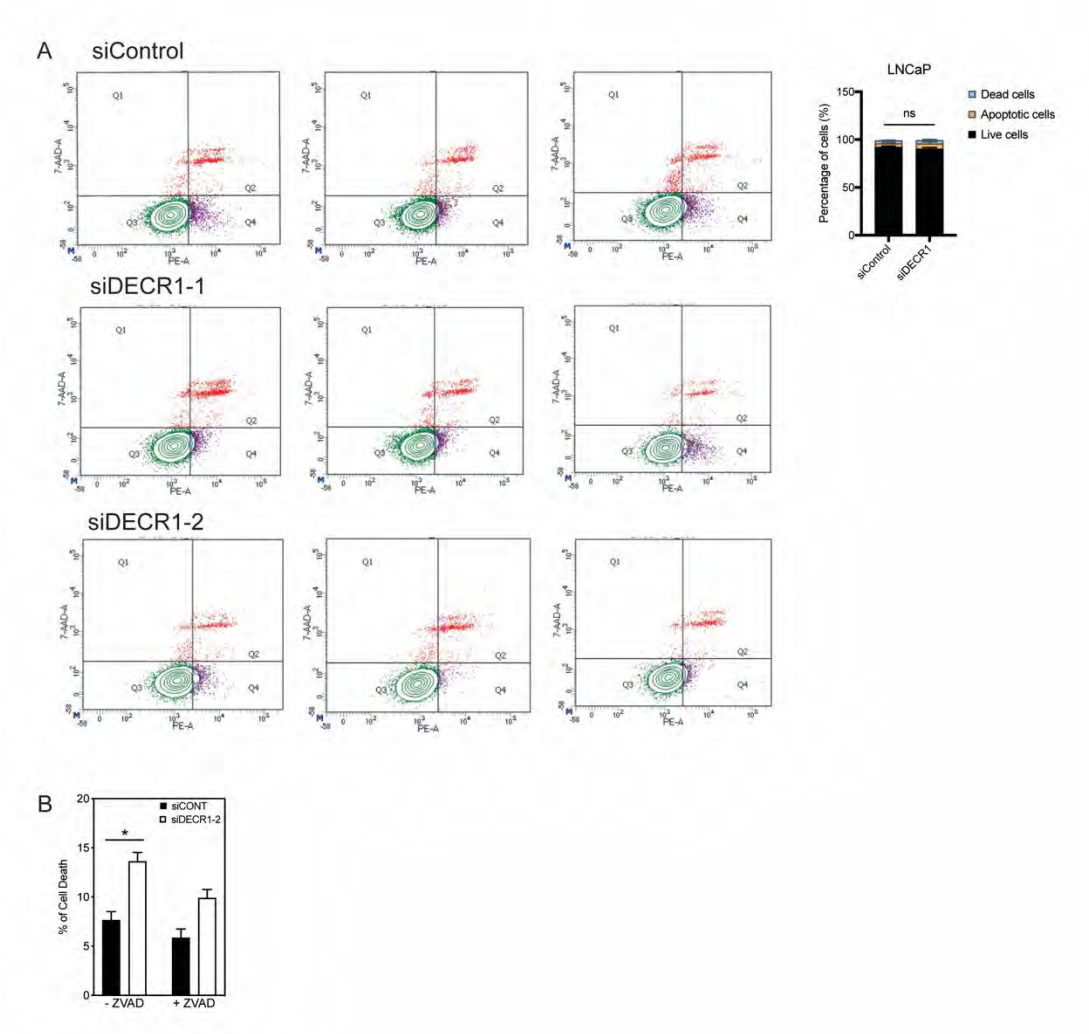

Figure 6-figure supplement 2 Targeting DECR1 does not induce apoptosis of prostate cancer cells. (A) LNCaP cells were stained with AnnexinV-Phycoerythrin (PE)/7-Aminoactinomycin D (7-AAD) followed by flow cytometry analysis after 96 hr DECR1 knockdown to detect apoptotic cells. **(B)** Cell death after DECR1 knockdown in LNCaP cells treated with or without the caspase inhibitor (ZVAD) measured using trypan blue exclusion.

3.2 Supplementary material for Chapter 3

This section contains supplementary materials for Chapter 3 that was not included in the publication.

3.2.1 Transcriptomic analysis of DECR1 knockdown LNCaP cells

Transcriptomic analysis was performed to characterise the changes in gene expression in response to DECR1 knockdown in LNCaP prostate cancer cells and delineate the molecular pathways that may be perturbed due to DECR1 inhibition. We aim to expand our current understanding of how polyunsaturated fatty acid oxidation enzymes, specifically DECR1, promotes prostate cancer progression and provide novel evidence of molecular mechanisms underlying the effects of DECR1 knockdown on prostate cancer oncogenesis.

3.2.2 Preparation of LNCaP cells for RNA sequencing

LNCaP cells were subjected to siRNA-mediated DECR1 knockdown (siDECR1-1 and siDECR1-2) in RPMI-1640 medium supplemented with 10 % FBS and incubated at 37 °C for 72 or 96 hrs (Supplementary figure 3.1A). The time points were selected based on optimal downregulation of DECR1 protein expression. Total RNA was isolated from each sample (n = 5 replicates) and DNase treated, then quality assessed. RNA was poly-A enriched, reverse transcribed, barcoded and sequenced on the Illumina NextSeq 500, and up to 40 million single-end reads (75 bp) obtained per sample (David Gunn Genomics Facility, SAHMRI).

3.2.3 Data processing

Raw single-end reads were assessed for quality using FastQC and summarised with MultiQC. Reads were filtered to remove low-quality sequences and trimmed to remove Illumina universal adapter sequences using Trimmomatic (minimum PHRED score 20, sliding window size 4 with average quality of 15). Reads were aligned or mapped to the human reference genome (GRCh38; at least 75 % alignment rates) using the STAR aligner, exported as *bam* files and quality assessed using FastQC. Raw counts were generated using featureCounts and imported into R for differential expression analysis. Prior to multi-dimensional scaling and

differential gene expression analysis, gene-annotated counts were filtered to remove low abundance genes (hence, reduce background noise) by removing genes that are < 1 count per million (cpm) in more than four samples and normalised using the trimmed mean of M-values (TMM) method in edgeR (Supplementary figure 3.1B).

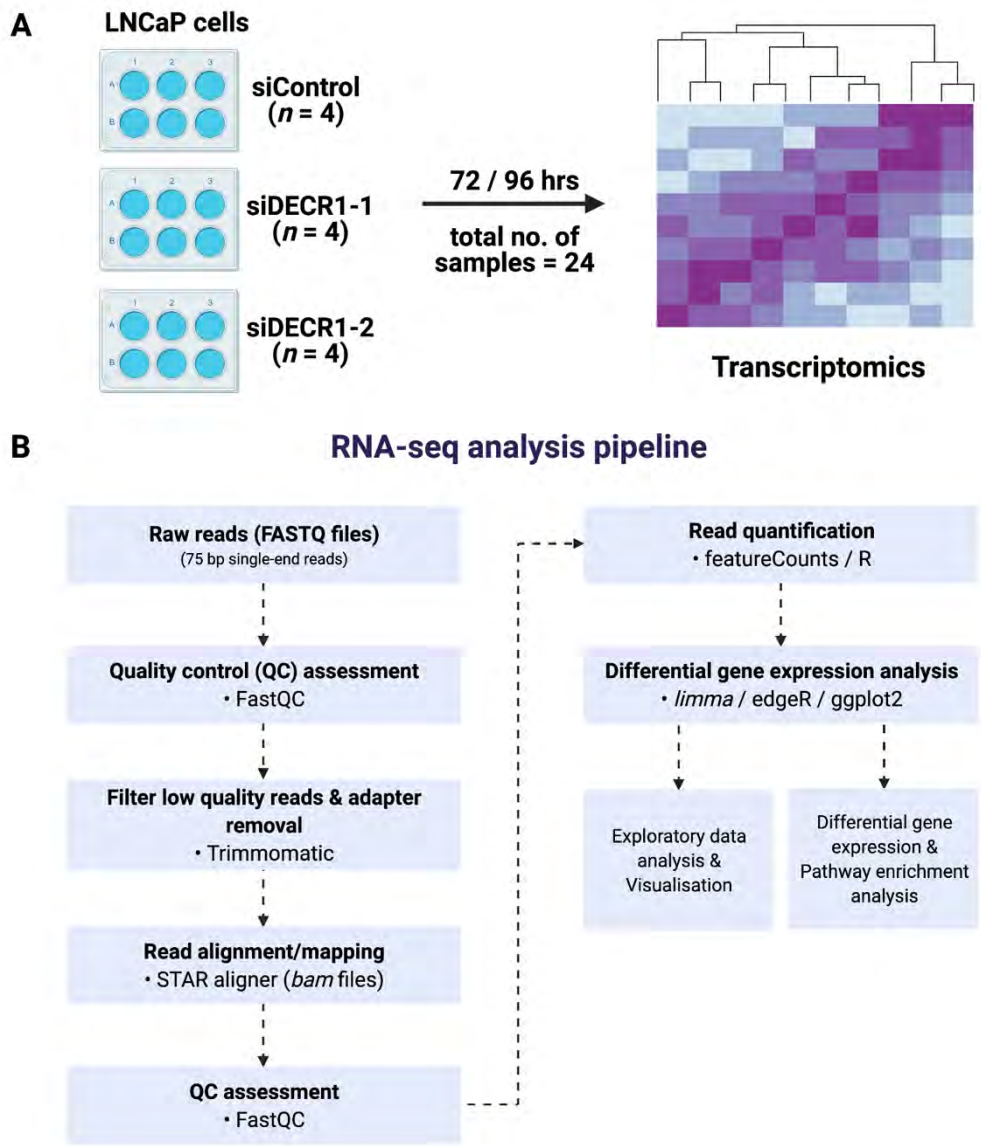

Supplementary Figure 3.1 RNA-seq analysis pipeline.

(A) Schematic showing RNA-seq experimental design. **(B)** RNA-seq analysis pipeline.

3.2.4 Results: Exploratory data analysis

Unsupervised clustering was performed using principal component analysis (PCA) to determine the amount of variation between samples and groups (Supplementary figure 3.2). Biological replicates for each experimental condition (Control, DECR1-1, DECR1-2) were clustered together, indicating high levels of similarity within these samples. Interestingly, the control samples for each time point were clustered further away from each other compared to DECR1 knockdown samples (DECR1-1 and DECR1-2). Notably, the control samples were clustered away from the DECR1 knockdown samples within each time point, suggesting altered transcriptomic profiles after DECR1 inhibition. We confirmed this by performing hierarchical clustering analysis, as represented by the heatmap in Supplementary figure 3.3. Similarly, the DECR1-1 and DECR1-2 knockdown samples clustered closely together at both the 72 and 96 hr time point, suggesting that the two siRNA expression vectors produced similar gene expression patterns. As expected, the control and DECR1 knockdown samples at both time points belong in separate clusters, indicating differences in their gene expression patterns after DECR1 inhibition. All aspects of the RNA-seq analysis (including data processing, differential gene expression analysis, and pathway analysis) as described in Supplementary figure 3.1B were performed by the candidate under guidance from supervisor, Professor David Lynn.

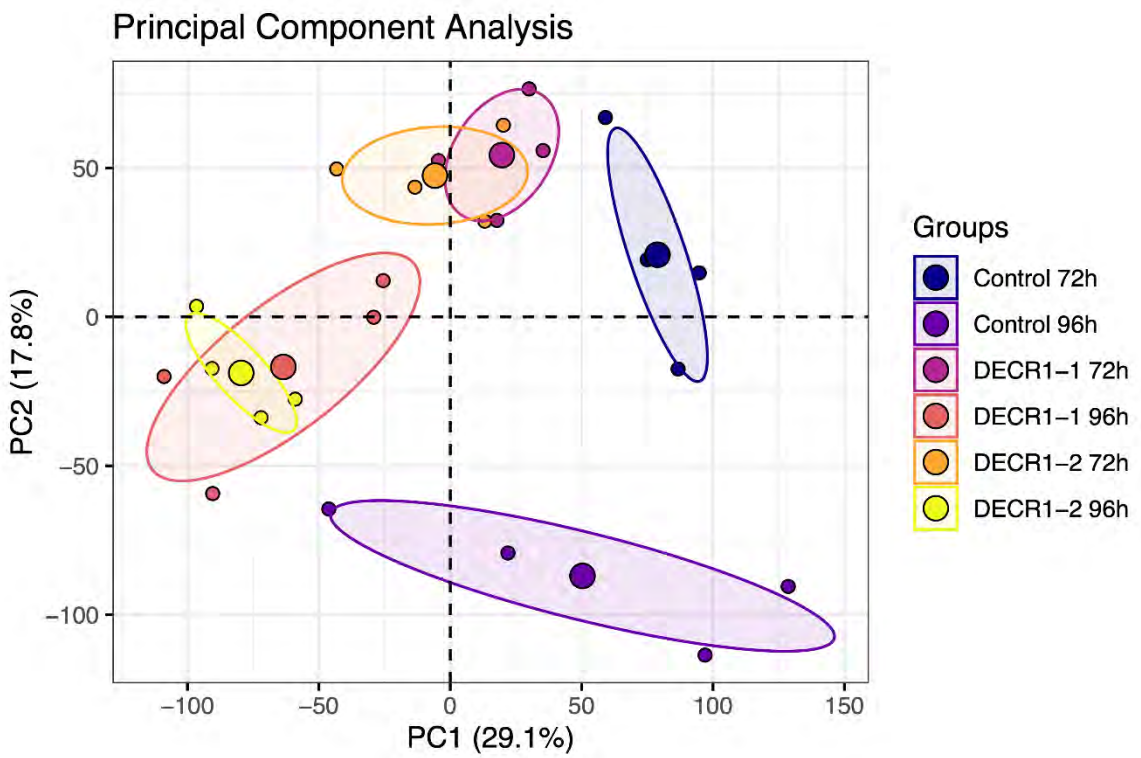

Supplementary Figure 3.2

Principal component analysis (PCA) plot of normalised data for all RNA-seq samples (n = 24). PCA plot was generated using *FactoMineR* and *factoextra* packages. The axis labels represent the amount of variation (%) retained by each principal component (PC).

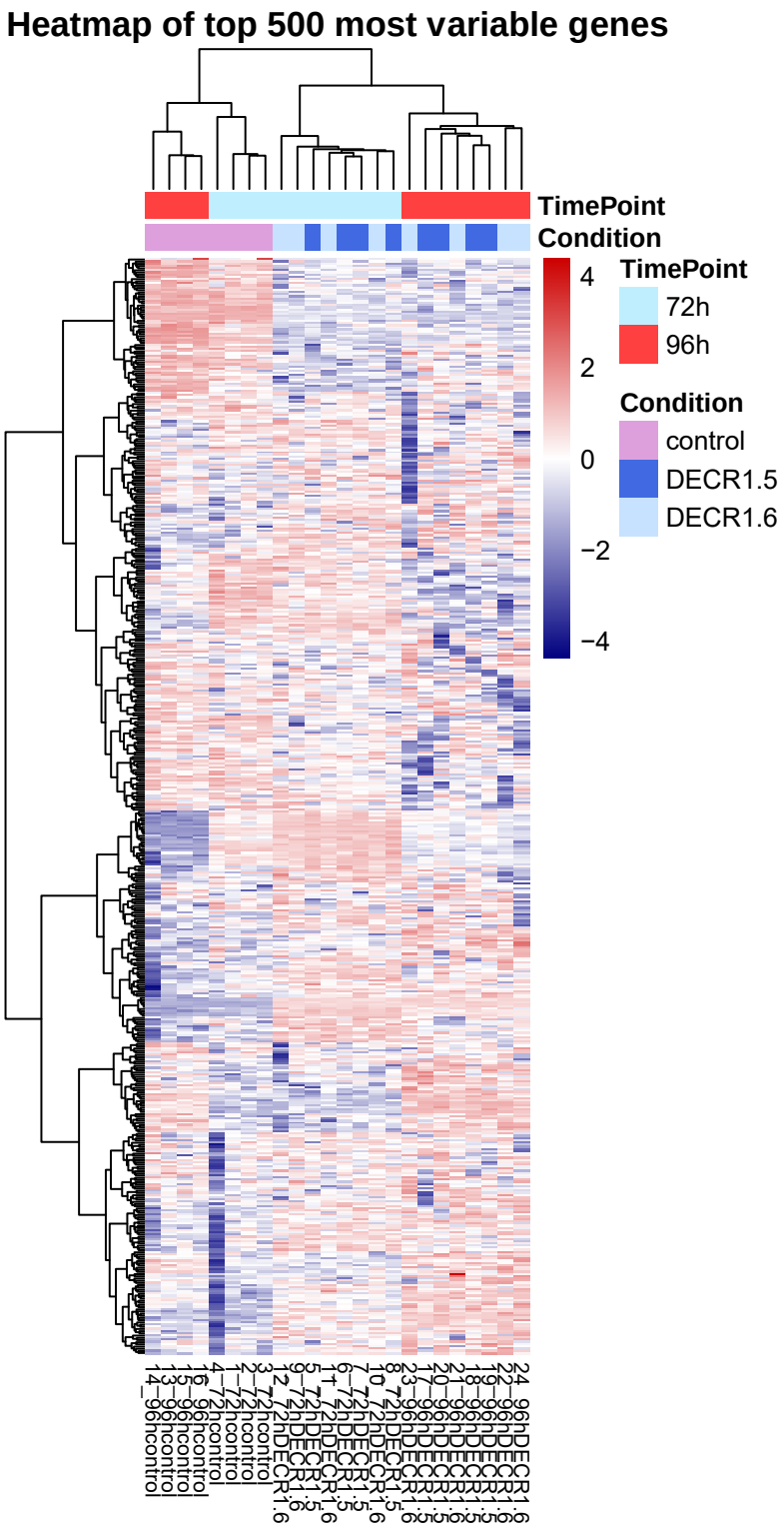

Supplementary Figure 3.3 Hierarchical clustering analysis.

Heatmap of the top 500 most variable genes. Data plotted as log2-cpm. Each row represents one gene, and samples with similar expression patterns are clustered together as represented by the dendogram on the y-axis.

3.2.5 Results: Differential gene expression analysis

Differential gene expression (DGE) analysis was performed between control and DECR1 knockdown cells to determine differentially expressed genes (DEGs; *p*-value < 0.05, log2-fold change ≥ 1) in response to DECR1 inhibition at both 72 and 96 hrs. A total of 378 DEGs (upregulated: 245 DEGs; downregulated: 133 DEGs) were identified in control versus DECR1 knockdown cells at 72 hrs (Supplementary figure 3.4A). Furthermore, a total of 729 DEGs (upregulated: 489 DEGs; downregulated: 240 DEGs) were identified in control versus DECR1 knockdown cells at 96 hrs (Supplementary figure 3.4B). To further confirm that *DECR1* mRNA was indeed knockdown in the samples, the volcano plot showed that DECR1 was one of the most significantly downregulated genes in DECR1 knockdown samples at both time points (Supplementary figure 3.4).

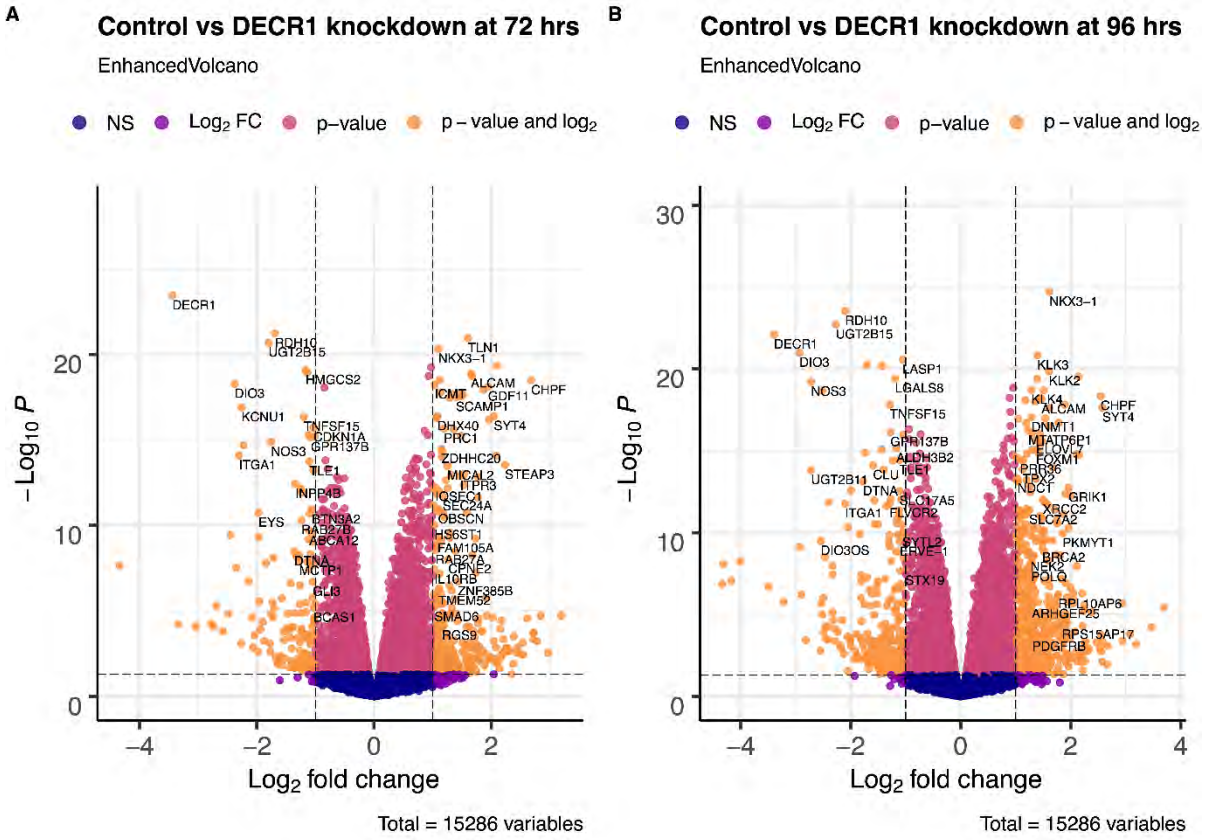

Supplementary Figure 3.4

Volcano plot of all 15286 genes in Control versus DECR1 knockdown samples. Orange dot: DEGs (defined as *p*-value < 0.05 and Log_2 fold change ≥ 1); NS (blue dot) = non-significant; Log_2 fold change ≥ 1 (purple dot); *p*-value > 0.05 (pink dot).

A list of the top 50 most differentially expressed genes (up- and down-regulated) in control versus DECR1 knockdown cells at 72 or 96 hrs are presented in Table 3.1 to Table 3.4. To our surprise, AR regulated genes such as *NKX3-1*, *KLK3*, *KLK2* and *ELOVL7* were upregulated in DECR1 knockdown cells compared to control cells at both 72 and 96 hr time points (Table 3.1 and 3.3).

3.2.6 Results: Pathway enrichment analysis

We then proceed to perform Gene Set Enrichment Analysis (GSEA) in order to identify molecular pathways or processes that may be enriched or perturbed in DECR1 knockdown cells (Supplementary figure 3.5 and 3.6). Surprisingly, this analysis identified several growth or cell proliferation promoting pathways such as ‘DNA replication’ and ‘Cell cycle’ (particularly at 96 hrs) that were upregulated in response to DECR1 inhibition. Moreover, pathways such as ‘Glycosaminoglycan biosynthesis chondroitin sulfate’ and ‘One carbon pool by folate’ were positively enriched in DECR1 knockdown cells compared to control cells at both time points, suggesting potential functional mitochondrial activity or biosynthetic processes. Unlike the positively enriched pathways, the negatively enriched pathways identified by GSEA in DECR1 knockdown cells were more consistent between the 72 and 96 hr time points and are composed of more metabolically related pathways. Of particular interest, drug metabolism pathways, ‘Starch and sucrose metabolism’, ‘Steroid hormone biosynthesis’, ‘PPAR signalling’ and ‘Fatty acid metabolism’ pathways were downregulated at both time points.

Table 3.1 Top 50 upregulated DEGs in DECR1 knockdown cells at 72 hrs

Ensembl ID	Symbol	Gene Name	Log2FC
ENSG00000137076	TLN1	talin 1	1.602519205
ENSG00000167034	NKX3-1	NK3 homeobox 1	1.097707118
ENSG00000136159	NUDT15	nudix hydrolase 15	2.100235273
ENSG00000170017	ALCAM	activated leukocyte cell adhesion molecule	1.652380991
ENSG00000186063	AIDA	axin interactor, dorsalization associated	1.673940012
ENSG00000142515	KLK3	kallikrein related peptidase 3	1.122405834
ENSG00000123989	CHPF	chondroitin polymerizing factor	2.681861081
ENSG00000116237	ICMT	isoprenylcysteine carboxyl methyltransferase	1.033825663
ENSG00000135414	GDF11	growth differentiation factor 11	1.946199312
ENSG00000128245	YWHAH	tyrosine 3-monooxygenase/tryptophan 5-monooxygenase activation protein eta	1.868499582
ENSG00000137815	RTF1	RTF1 homolog, Paf1/RNA polymerase II complex component	1.129966526
ENSG00000167751	KLK2	kallikrein related peptidase 2	1.314895584
ENSG00000164181	ELOVL7	ELOVL fatty acid elongase 7	1.482358996
ENSG00000168268	NT5DC2	5'-nucleotidase domain containing 2	1.517399023
ENSG00000184428	TOP1MT	DNA topoisomerase I mitochondrial	1.489765877
ENSG00000085365	SCAMP1	secretory carrier membrane protein 1	1.39778656
ENSG00000130816	DNMT1	DNA methyltransferase 1	1.282671357
ENSG00000132872	SYT4	synaptotagmin 4	2.046201995
ENSG00000108406	DHX40	DEAH-box helicase 40	1.079371454
ENSG00000007202	KIAA0100	KIAA0100	1.067925216
ENSG00000213853	EMP2	epithelial membrane protein 2	1.961803415
ENSG00000198901	PRC1	protein regulator of cytokinesis 1	1.190779012
ENSG00000099250	NRP1	neuropilin 1	1.357741526
ENSG00000110422	HIPK3	homeodomain interacting protein kinase 3	1.484399213
ENSG00000180776	ZDHHC20	zinc finger DHHC-type containing 20	1.150558035
ENSG00000133065	SLC41A1	solute carrier family 41 member 1	1.163799992
ENSG00000181104	F2R	coagulation factor II thrombin receptor	2.089783357
ENSG00000158813	EDA	ectodysplasin A	1.156292343
ENSG00000115107	STEAP3	STEAP3 metalloreductase	2.235008126
ENSG00000133816	MICAL2	microtubule associated monooxygenase, calponin and LIM domain containing 2	1.251170226
ENSG00000003989	SLC7A2	solute carrier family 7 member 2	1.533838394
ENSG00000174749	FAM241A	family with sequence similarity 241 member A	1.315848515
ENSG00000096433	ITPR3	inositol 1,4,5-trisphosphate receptor type 3	1.468911883
ENSG00000082556	OPRK1	opioid receptor kappa 1	1.777043052
ENSG00000119314	PTBP3	polypyrimidine tract binding protein 3	1.225739664
ENSG00000067798	NAV3	neuron navigator 3	1.530506878
ENSG00000144711	IQSEC1	IQ motif and Sec7 domain 1	1.044181081
ENSG00000075223	SEMA3C	semaphorin 3C	1.256865308
ENSG00000142188	TMEM50B	transmembrane protein 50B	1.015398209
ENSG00000188257	PLA2G2A	phospholipase A2 group IIA	1.108565397
ENSG00000204070	SYS1	SYS1, golgi trafficking protein	1.071728948
ENSG00000113615	SEC24A	SEC24 homolog A, COPII coat complex component	1.170105701
ENSG00000113272	THG1L	tRNA-histidine guanylyltransferase 1 like	1.770067173
ENSG00000080493	SLC4A4	solute carrier family 4 member 4	1.017581068
ENSG00000154358	OBSCN	obscurin, cytoskeletal calmodulin and titin-interacting RhoGEF	1.095560583
ENSG00000198300	PEG3	paternally expressed 3	1.051904671
ENSG00000090857	PDPR	pyruvate dehydrogenase phosphatase regulatory subunit	1.141069876
ENSG00000171189	GRIK1	glutamate ionotropic receptor kainate type subunit 1	1.586495575
ENSG00000180785	OR51E1	olfactory receptor family 51 subfamily E member 1	1.18163088

Table 3.2 Top 50 downregulated DEGs in DECR1 knockdown cells at 72 hrs

Ensembl ID	Symbol	Gene Name	Log2FC
ENSG00000104325	DECR1	2,4-dienoyl-CoA reductase 1	-3.4425996
ENSG00000121039	RDH10	retinol dehydrogenase 10	-1.6940079
ENSG00000196620	UGT2B15	UDP glucuronosyltransferase family 2 member B15	-1.8023073
ENSG00000134240	HMGCS2	3-hydroxy-3-methylglutaryl-CoA synthase 2	-1.168322
ENSG00000116977	LGALS8	galectin 8	-1.1398827
ENSG00000197406	DIO3	iodothyronine deiodinase 3	-2.3799737
ENSG00000215262	KCNU1	potassium calcium-activated channel subfamily U member 1	-2.2602932
ENSG00000181634	TNFSF15	TNF superfamily member 15	-1.1994212
ENSG00000124762	CDKN1A	cyclin dependent kinase inhibitor 1A	-1.0349582
ENSG00000132746	ALDH3B2	aldehyde dehydrogenase 3 family member B2	-1.1176633
ENSG00000124145	SDC4	syndecan 4	-1.0111562
ENSG00000077585	GPR137B	G protein-coupled receptor 137B	-1.077481
ENSG00000164867	NOS3	nitric oxide synthase 3	-1.7567578
ENSG00000213759	UGT2B11	UDP glucuronosyltransferase family 2 member B11	-2.224669
ENSG00000213949	ITGA1	integrin subunit alpha 1	-2.3066659
ENSG00000196781	TLE1	TLE family member 1, transcriptional corepressor	-1.1042998
ENSG00000153721	CNKSR3	CNKSR family member 3	-1.0368661
ENSG00000109452	INPP4B	inositol polyphosphate-4-phosphatase type II B	-1.3446099
ENSG00000120885	CLU	clusterin	-1.2488196
ENSG00000167799	NUDT8	nudix hydrolase 8	-1.2313558
ENSG00000186470	BTN3A2	butyrophilin subfamily 3 member A2	-1.0619053
ENSG00000188107	EYS	eyes shut homolog	-1.9724059
ENSG00000049130	KITLG	KIT ligand	-1.1000074
ENSG00000041353	RAB27B	RAB27B, member RAS oncogene family	-1.2383906
ENSG00000144452	ABCA12	ATP binding cassette subfamily A member 12	-1.1073707
ENSG00000122012	SV2C	synaptic vesicle glycoprotein 2C	-1.0556795
ENSG00000087128	TMPRSS11E	transmembrane serine protease 11E	-2.4539699
ENSG00000246375	PPM1K-DT	PPM1K divergent transcript	-1.9666942
ENSG00000236699	ARHGEF38	Rho guanine nucleotide exchange factor 38	-1.1180016
ENSG00000230882	AC005077.4	hypothetical protein LOC285908 (LOC285908) pseudogene	-1.0529327
ENSG00000134769	DTNA	dystrobrevin alpha	-1.3619816
ENSG00000163898	LIPH	lipase H	-1.0836143
ENSG00000255346	NOX5	NADPH oxidase 5	-1.2776612
ENSG00000176563	CNTD1	cyclin N-terminal domain containing 1	-1.3235373
ENSG00000114248	LRRC31	leucine rich repeat containing 31	-1.714312
ENSG00000175471	MCTP1	multiple C2 and transmembrane domain containing 1	-1.2730386
ENSG00000142871	CYR61	cellular communication network factor 1	-1.1411755
ENSG00000111885	MAN1A1	mannosidase alpha class 1A member 1	-1.087277
ENSG00000152766	ANKRD22	ankyrin repeat domain 22	-1.8456981
ENSG00000178750	STX19	syntaxin 19	-1.0232765
ENSG00000198092	TMPRSS11F	transmembrane serine protease 11F	-4.3424759
ENSG00000236345	SCAT8	S-phase cancer associated transcript 8	-2.356726
ENSG00000183508	FAM46C	terminal nucleotidyltransferase 5C	-1.1126606
ENSG00000147041	SYTL5	synaptotagmin like 5	-2.1428273
ENSG00000106571	GLI3	GLI family zinc finger 3	-1.0466785
ENSG00000127324	TSPAN8	tetraspanin 8	-1.4238095
ENSG00000267259	ERVE-1	endogenous retrovirus group E member 1	-1.2619221
ENSG00000249392	AC096588.1	novel transcript	-1.0528548
ENSG00000146592	CREB5	cAMP responsive element binding protein 5	-1.5738332

Table 3.3 Top 50 upregulated DEGs in DECR1 knockdown cells at 96 hrs

Ensembl ID	Symbol	Gene Name	Log2FC
ENSG00000167034	NKX3-1	NK3 homeobox 1	1.61425643
ENSG00000142515	KLK3	kallikrein related peptidase 3	1.39406692
ENSG00000167751	KLK2	kallikrein related peptidase 2	1.60724367
ENSG00000136159	NUDT15	nudix hydrolase 15	2.14145938
ENSG00000137076	TLN1	talin 1	1.38851842
ENSG00000167749	KLK4	kallikrein related peptidase 4	1.28670615
ENSG00000184428	TOP1MT	DNA topoisomerase I mitochondrial	1.51087336
ENSG00000123989	CHPF	chondroitin polymerizing factor	2.54581335
ENSG00000085365	SCAMP1	secretory carrier membrane protein 1	1.45745608
ENSG00000170017	ALCAM	activated leukocyte cell adhesion molecule	1.46823413
ENSG00000137815	RTF1	RTF1 homolog, Paf1/RNA polymerase II complex component	1.17652187
ENSG00000133639	BTG1	BTG anti-proliferation factor 1	1.35186163
ENSG00000128245	YWHAH	tyrosine 3-monooxygenase/tryptophan 5-monooxygenase activation protein eta	1.89208141
ENSG00000132872	SYT4	synaptotagmin 4	2.57632405
ENSG00000186063	AIDA	axin interactor, dorsalization associated	1.60931593
ENSG00000130816	DNMT1	DNA methyltransferase 1	1.28661575
ENSG00000099250	NRP1	neuropilin 1	1.53847202
ENSG00000124225	PMEPA1	prostate transmembrane protein, androgen induced 1	1.0458745
ENSG00000135414	GDF11	growth differentiation factor 11	1.78003775
ENSG00000080709	KCNN2	potassium calcium-activated channel subfamily N member 2	1.18996169
ENSG00000101057	MYBL2	MYB proto-oncogene like 2	1.60174485
ENSG00000248527	MTATP6P1	MT-ATP6 pseudogene 1	1.23124318
ENSG00000176890	TYMS	thymidylate synthetase	1.29753962
ENSG00000168268	NT5DC2	5'-nucleotidase domain containing 2	1.44535354
ENSG00000164181	ELOVL7	ELOVL fatty acid elongase 7	1.36996258
ENSG00000110422	HIPK3	homeodomain interacting protein kinase 3	1.44873702
ENSG00000198901	PRC1	protein regulator of cytokinesis 1	1.47586985
ENSG00000166851	PLK1	polo like kinase 1	1.44637152
ENSG00000198840	MT-ND3	mitochondrially encoded NADH:ubiquinone oxidoreductase core subunit 3	1.29896801
ENSG00000111206	FOXM1	forkhead box M1	1.36778218
ENSG00000174749	FAM241A	family with sequence similarity 241 member A	1.41906783
ENSG00000180776	ZDHHC20	zinc finger DHHC-type containing 20	1.20527704
ENSG00000165244	ZNF367	zinc finger protein 367	2.11191952
ENSG00000213853	EMP2	epithelial membrane protein 2	2.15624506
ENSG00000109576	AADAT	aminoadipate aminotransferase	1.0002351
ENSG00000183248	PRR36	proline rich 36	1.07869539
ENSG00000105290	APLP1	amyloid beta precursor like protein 1	1.13261075
ENSG00000188257	PLA2G2A	phospholipase A2 group IIA	1.67113779
ENSG00000088325	TPX2	TPX2, microtubule nucleation factor	1.12693464
ENSG00000058804	NDC1	NDC1 transmembrane nucleoporin	1.03435685
ENSG00000137804	NUSAP1	nucleolar and spindle associated protein 1	1.36529136
ENSG00000151025	GPR158	G protein-coupled receptor 158	1.19570643
ENSG00000164442	CITED2	Cbp/p300 interacting transactivator with Glu/Asp rich carboxy-terminal domain 2	1.0208728
ENSG00000133065	SLC41A1	solute carrier family 41 member 1	1.0429964
ENSG00000142945	KIF2C	kinesin family member 2C	1.25713273
ENSG00000171189	GRIK1	glutamate ionotropic receptor kainate type subunit 1	1.96309612
ENSG00000080493	SLC4A4	solute carrier family 4 member 4	1.26566371
ENSG00000110492	MDK	midkine	1.89669514
ENSG00000181104	F2R	coagulation factor II thrombin receptor	2.00650261

Table 3.4 Top 50 downregulated DEGs in DECR1 knockdown cells at 96 hrs

Ensembl ID	Symbol	Gene Name	Log2FC
ENSG00000121039	RDH10	retinol dehydrogenase 10	-2.1021534
ENSG00000196620	UGT2B15	UDP glucuronosyltransferase family 2 member B15	-2.2711346
ENSG00000104325	DECR1	2,4-dienoyl-CoA reductase 1	-3.3898713
ENSG00000197406	DIO3	iodothyronine deiodinase 3	-2.929963
ENSG00000002834	LASP1	LIM and SH3 protein 1	-1.0560672
ENSG00000134240	HMGCS2	3-hydroxy-3-methylglutaryl-CoA synthase 2	-1.7021952
ENSG00000197888	UGT2B17	UDP glucuronosyltransferase family 2 member B17	-1.428103
ENSG00000116977	LGALS8	galectin 8	-1.1915697
ENSG00000164867	NOS3	nitric oxide synthase 3	-2.7184213
ENSG00000215262	KCNU1	potassium calcium-activated channel subfamily U member 1	-2.5199938
ENSG00000181634	TNFSF15	TNF superfamily member 15	-1.2852226
ENSG00000077585	GPR137B	G protein-coupled receptor 137B	-1.2752783
ENSG00000116260	QSOX1	quiescin sulfhydryl oxidase 1	-1.0459653
ENSG00000132746	ALDH3B2	aldehyde dehydrogenase 3 family member B2	-1.1668991
ENSG00000136235	GPNMB	glycoprotein nmb	-1.4358519
ENSG00000111885	MAN1A1	mannosidase alpha class 1A member 1	-1.7359486
ENSG00000196781	TLE1	TLE family member 1, transcriptional corepressor	-1.1134899
ENSG00000153721	CNKSR3	CNKSR family member 3	-1.2315297
ENSG00000120885	CLU	clusterin	-1.5890402
ENSG00000090402	SI	sucrase-isomaltase	-1.4026116
ENSG00000213759	UGT2B11	UDP glucuronosyltransferase family 2 member B11	-2.720716
ENSG00000134769	DTNA	dystrobrevin alpha	-1.7753309
ENSG00000188107	EYS	eyes shut homolog	-1.9925448
ENSG00000119899	SLC17A5	solute carrier family 17 member 5	-1.1108493
ENSG00000236699	ARHGEF38	Rho guanine nucleotide exchange factor 38	-1.269694
ENSG00000150764	DIXDC1	DIX domain containing 1	-1.082307
ENSG00000041353	RAB27B	RAB27B, member RAS oncogene family	-1.5696739
ENSG00000146592	CREB5	cAMP responsive element binding protein 5	-2.3992892
ENSG00000119686	FLVCR2	feline leukemia virus subgroup C cellular receptor family member 2	-1.2912049
ENSG00000213949	ITGA1	integrin subunit alpha 1	-2.1011359
ENSG00000167799	NUDT8	nudix hydrolase 8	-1.3508669
ENSG00000149972	CNTN5	contactin 5	-1.1201984
ENSG00000177125	ZBTB34	zinc finger and BTB domain containing 34	-1.1151665
ENSG00000109452	INPP4B	inositol polyphosphate-4-phosphatase type II B	-1.1552416
ENSG00000230882	AC005077.4	hypothetical protein LOC285908 (LOC285908) pseudogene	-1.1632894
ENSG00000175471	MCTP1	multiple C2 and transmembrane domain containing 1	-1.5629547
ENSG00000144452	ABCA12	ATP binding cassette subfamily A member 12	-1.5094201
ENSG00000130589	HELZ2	helicase with zinc finger 2	-1.0698645
ENSG00000133019	CHRM3	cholinergic receptor muscarinic 3	-2.0497878
ENSG00000137501	SYTL2	synaptotagmin like 2	-1.0590467
ENSG00000114248	LRRC31	leucine rich repeat containing 31	-1.8361822
ENSG00000186470	BTN3A2	butyrophilin subfamily 3 member A2	-1.1346759
ENSG00000167552	TUBA1A	tubulin alpha 1a	-1.0662577
ENSG00000143036	SLC44A3	solute carrier family 44 member 3	-1.289425
ENSG00000049130	KITLG	KIT ligand	-1.0035483
ENSG00000258498	DIO3OS	DIO3 opposite strand upstream RNA	-2.5425968
ENSG00000180178	FAR2P1	fatty acyl-CoA reductase 2 pseudogene 1	-1.3051881
ENSG00000267259	ERVE-1	endogenous retrovirus group E member 1	-1.1073075
ENSG00000163898	LIPH	lipase H	-1.293288

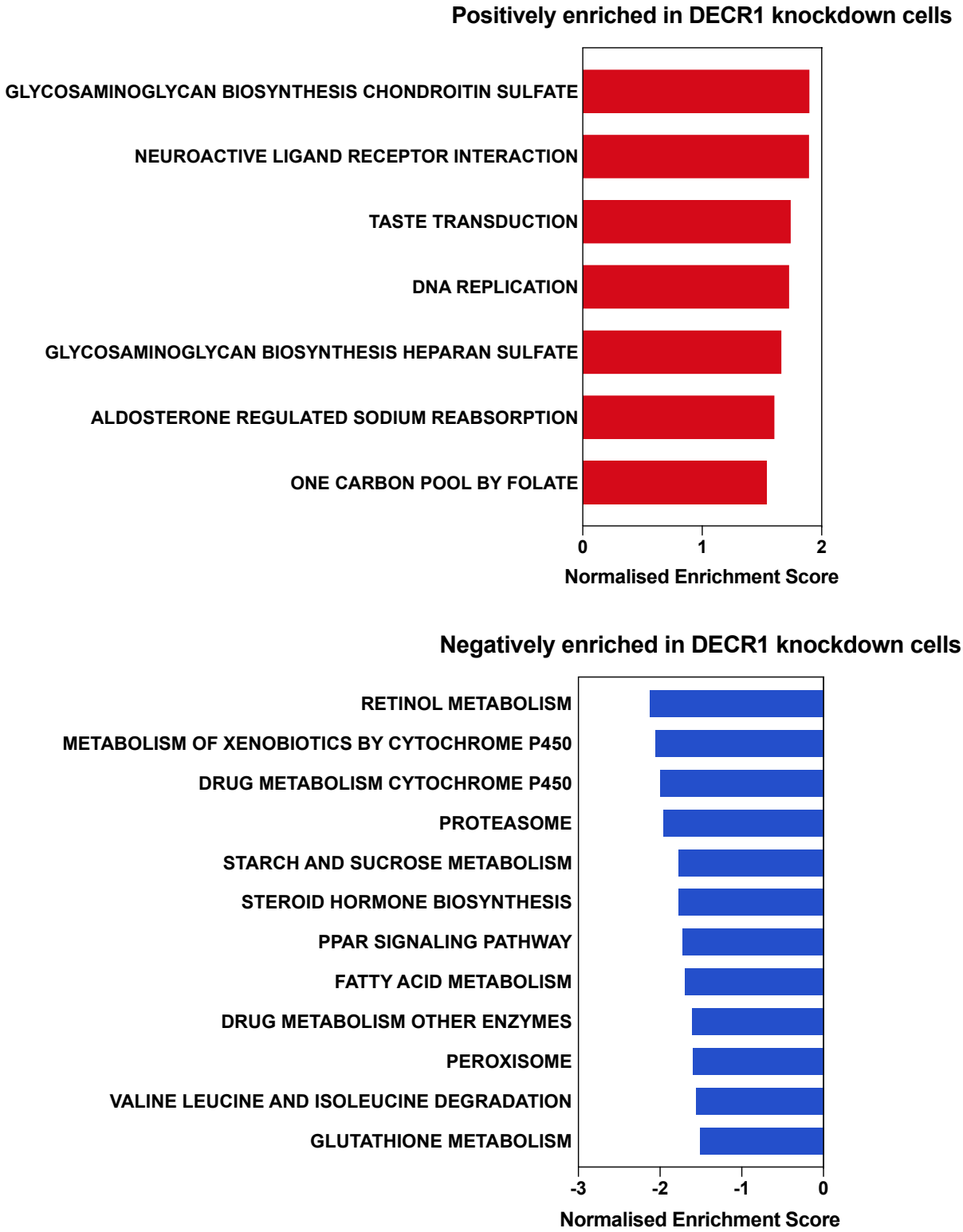

Supplementary Figure 3.5 Gene set enrichment analysis (GSEA) of DECR1 knockdown cells at 72 hrs.

(A) Top positively enriched (upregulated) and **(B)** top negatively enriched (downregulated) KEGG pathways in DECR1 knockdown cells at 72 hrs. Gene sets returning an FDR adjusted p-value < 25 % were selected as statistically enriched**.**

Supplementary Figure 3.6 Gene set enrichment analysis (GSEA) of DECR1 knockdown cells at 96 hrs.

(A) Top positively enriched (upregulated) and **(B)** top negatively enriched (downregulated) KEGG pathways in DECR1 knockdown cells at 96 hrs. Gene sets returning an FDR adjusted p-value < 25 % were selected as statistically enriched.

3.2.7 Discussion

In Chapter 3, we identified DECR1 (an auxiliary enzyme involved in polyunsaturated fatty acid oxidation) and characterised its role and function in prostate cancer tumorigenesis and disease progression. We showed that DECR1 is an androgen-repressed gene, and that DECR1 knockdown significantly suppressed prostate cancer oncogenesis *in vitro* and *in vivo*. Herein, we discuss the transcriptomic study that was initially performed in order to further understand the mechanism of action of DECR1 and its role in prostate cancer.

Our data showed several AR regulated genes such as *NKX3-1*, *KLK3*, *KLK2* and *ELOVL7* were significantly upregulated in DECR1 knockdown cells compared to control cells. Although we have shown that DECR1 expression is upregulated in response to AR inhibition (via castration or enzalutamide) and that DHT is able to decrease expression of DECR1, it is unclear whether DECR1 inhibition would cause the reverse effect whereby AR signalling is activated to promote cancer cell survival pathways. In line with this observation, GSEA analysis identified several growth or cell proliferation promoting pathways that were upregulated in response to DECR1 inhibition. Moreover, pathways such as 'Glycosaminoglycan biosynthesis chondroitin sulfate (CS)' whereby elevated levels of CS was previously reported to be predictive of poor prognosis in prostate cancer patients was upregulated in DECR1 knockdown cells (Ricciardelli et al. 1999; Ricciardelli et al. 1997). We would also like to highlight that mitochondrial-related pathways such as 'One carbon pool by folate' and 'Oxidative phosphorylation' were positively enriched in DECR1 knockdown cells compared to control cells. One carbon (1C) metabolism mediated by the cofactor, folate, plays a role in biosynthetic processes, amino acid homeostasis, epigenetic maintenance and redox defense (reviewed in (Ducker and Rabinowitz 2017)). It is plausible that mitochondrial activity or TCA cycle is maintained by other nutrient sources such as glucose due to the inability of the cells to oxidise PUFAs after DECR1 inhibition. This could, in part, explain why we observed an increase in glycolysis in DECR1 knockdown cells compared to control cells (Figure 3.4H). Given that we observed significant attenuation in cell viability and tumour growth after DECR1 inhibition, it is unclear why DNA replication and cell cycle pathway genes were upregulated in DECR1 knockdown cells. Arguably, we did not study the effect of DECR1 knockdown on cell cycle progression and whether

mRNA expression of cell cycle genes reflect biological outcomes phenotypically remains to be elucidated (Zopf et al. 2013).

Intriguingly, DECR1 knockdown cells showed a significant negative enrichment in ‘drug metabolism pathways by cytochrome P450’, ‘starch and sucrose metabolism’ and ‘steroid hormone biosynthesis’. Further interrogation of these gene sets revealed downregulation of several UDP-glucuronosyltransferase (UGT) genes (ie. *UGT2B10*, *11*, *15* and *17*), cytochrome P450 family 1 subfamily A member 1 (CYP1A1) and glutathione S-transferase (GST) genes (ie. *GSTA4* and *GSTK1*). UGTs catalyse the covalent addition of sugars from nucleotide UDP-sugar donors to hydroxyl, carboxyl or amino groups of various endogenous metabolites and toxic exogenous chemicals (Guillemette et al. 2014). Besides an important mechanism of drug resistance in cancer, UGTs also play a key role in modulating steroid levels as well as levels of pro and anti-oncogenic metabolites (retinoic acid, linoleic acid or arachidonic acid) by mediating their inactivation and elimination (Allain et al. 2020; Turgeon et al. 2003). GSTs are detoxifying enzymes that play important roles in cellular defense by conjugating toxic or carcinogenic compounds to glutathione, and is upregulated in prostate cancer (Liu et al. 2017). Interestingly, these groups of enzymes (CYPs, UGTs and GSTs) form the ‘xenobiotic detoxification program (XDP)’, and downregulation of these genes in DECR1 knockdown cells suggests that these cells are unable to cope with oxidative stress after DECR1 inhibition. This supports our findings that DECR1 knockdown increases mitochondrial oxidative stress (Figure 3.6D), further resulting in lipid peroxidation and cell death.

GSEA analysis also showed downregulation of fatty acid metabolism and PPAR signalling pathways, and further analysis showed a decrease in fatty acid oxidation pathway genes (ie. *CPT1A*, *ACOX1*, *SCD*, *ACSL1*) in DECR1 knockdown cells compared to control cells. Notably, peroxisomal metabolism genes were significantly and negatively enriched in DECR1 knockdown cells. Unlike the mitochondria, peroxisomes function to oxidise very long chain fatty acids (VLCFAs). Given that the cells already accumulate PUFAs due to DECR1 knockdown, the cells may cease production of VLCFAs thereby making peroxisomes redundant or limit peroxisomal activity to conserve energy and other TCA metabolic requirements for survival. It would be interesting to investigate the connection between mitochondrial and peroxisomal metabolism.

Taken together, these findings provide a foundation for which future research can be built upon. More importantly, these results will need to be confirmed in independent knockdown experiments with quantitative PCR (qPCR) to further validate our findings. While transcriptomic studies are beneficial to infer changes in biological processes, it cannot fully encapsulate the various biological or molecular networks that are going on in the cell (i.e., protein function and post-translational modifications). Further studies are still needed to elucidate these and other aspects of DECR1 inhibition in order to facilitate the development of DECR1 targeted therapies to prevent disease recurrence and treatment resistance.

Chapter 4: Targeting peroxisomal fatty acid oxidation in advanced metastatic prostate cancer

This Chapter includes unpublished work written in manuscript format.

STATEMENT OF AUTHORSHIP

Title of Paper	Peroxisomal fatty acid oxidation is an exploitable therapeutic avenue in advanced metastatic prostate cancer
Publication Status	☐ Published ☐ Submitted for Publication ☐ Accepted for Publication ☒ Unpublished and Unsubmitted work written in a manuscript style
Publication Details	Mah, CY, Nijiima, T, Dehairs, J, Helm, M, Swinnen, JV, Nassar, ZD & Butler, LM 2021, 'Peroxisomal fatty acid oxidation is an exploitable therapeutic avenue in advanced metastatic prostate cancer'.

Principal Author

Name of Principal Author (Candidate)	Chui Yan Mah	
Contribution to the Paper	Conceptualization, Methodology, Formal analysis, Investigation, Data curation, Validation, Visualization, Writing – Original and draft preparation, Writing – Review and editing	
Overall Percentage (%)	60 %	
Signature		Date: 26/03/2021

Co-Author Contributions

By signing the Statement of Authorship, each author certifies that:

i. the candidate's stated contribution to the publication is accurate (as detailed above);
ii. permission is granted for the candidate to include the publication in the thesis; and
iii. the sum of all co-author contributions is equal to 100% less than the candidate's stated contribution.

Name of Co-Author	Takuto Nijiima	
Contribution to the Paper	Investigation, Writing – Review and editing	
Signature		Date: 22/03/2021

Name of Co-Author	Jonas Dehairs	
Contribution to the Paper	Data curation, Methodology, Writing – Review and editing	
Signature		Date: 22/03/2021

Name of Co-Author	Madison Helm	
Contribution to the Paper	Methodology, Investigation	
Signature		Date: 22/3/21

Name of Co-Author	Johannes Swinnen		
Contribution to the Paper	Data curation, Methodology, Writing – Review and editing		
Signature		Date:	22 March 2021

Name of Co-Author	Zeyad Nassar		
Contribution to the Paper	Conceptualization, Resources, Data curation, Supervision, Funding acquisition, Project administration, Writing – Review and editing		
Signature		Date:	26/03/2021

Name of Co-Author	Lisa Butler		
Contribution to the Paper	Conceptualization, Resources, Data curation, Supervision, Funding acquisition, Project administration, Writing – Review and editing		
Signature		Date:	01/04/2021

Peroxisomal fatty acid oxidation is an exploitable therapeutic avenue in advanced metastatic prostate cancer

Chui Yan Mah[1,2], Takuto Nijiima[1], Jonas Dehairs[3], Madison Helm[1,2], Johannes V. Swinnen[3], Zeyad D. Nassar[1,2] and Lisa M. Butler[1,2]

[1] Adelaide Medical School and Freemasons Centre for Male Health and Wellbeing, University of Adelaide, Adelaide, Australia
[2] South Australian Health and Medical Research Institute, Adelaide, Australia
[3] KU Leuven, University of Leuven, LKI – Leuven Cancer Institute, Department of Oncology, Laboratory of Lipid Metabolism and Cancer, Leuven, Belgium

4.1 Abstract

Herein, we highlight a role for peroxisomal beta oxidation and a previously unexplored peroxisomal beta oxidation enzyme, 2,4-dienoyl CoA reductase 2 (DECR2) in CRPC. DECR2 is robustly overexpressed in prostate cancer tissues and is associated with poor overall survival. Previous proteomic analysis revealed an association between peroxisome metabolism and resistance to AR inhibitors. Inhibition of peroxisomal beta oxidation, either by molecular targeting of DECR2 or pharmacological inhibition using thioridazine (TDZ) significantly suppressed proliferation and migration of castrate-resistant and treatment-resistant prostate cancer cells *in vitro*. DECR2 knockdown or TDZ treatment induced lipid accumulation and cell cycle arrest. Moreover, DECR2 depleted cells maintained functional mitochondrial oxidative phosphorylation, suggesting an intimate link between mitochondrial and peroxisomal beta oxidation to promote prostate cancer cell survival. Notably, DECR2 knockdown and TDZ sensitises CRPC and enzalutamide-resistant cells to the androgen receptor antagonist, enzalutamide and cyclin-dependent kinase (Cdk) 4/6 inhibitor, ribociclib. Taken together, our data supports peroxisomal beta oxidation and more specifically, DECR2 as a promising novel therapeutic target for CRPC.

4.2 Introduction

Prostate cancer is the most commonly diagnosed malignancy in men, and a leading cause of cancer-related deaths in men globally (Siegel et al., 2019). Prostate cancer is mainly dependent on androgens which act through the androgen receptor (AR; transcription factor) for growth and survival. Consequently, androgen deprivation therapy (ADT) has remained the frontline strategy for clinical management of patients with advanced or metastatic prostate cancer since the 1940s (Huggins and Hodges, 1972). Although initially effective, the majority of patients eventually develop resistance to currently available therapies and relapse with castrate resistant prostate cancer (CRPC) which is ultimately fatal. Despite the development of more potent anti-androgens, including enzalutamide (ENZ) (Scher et al., 2012; Tran et al., 2009), these agents are still not curative and alternative therapeutic strategies to combat treatment resistance are urgently sought.

Targeting cancer metabolism has gained increasing attention. In conjunction with the fact that the AR plays key roles in modulating cancer metabolism (Mah et al., 2020; Massie et al., 2011), it has emerged as an attractive strategy to overcome resistance to AR-targeted therapies (Blomme et al., 2020; Li et al., 2016; Nambiar et al., 2014; Schulte et al., 2018; Zacharias et al., 2017; Zadra et al., 2019). Moreover, prostate cancer presents a unique metabolic phenotype that is mainly dependent on lipids and mitochondrial metabolism for energy production at early stages of the disease (Liu, 2006). Prostate cancer is also characterised by the dysregulation of genes and proteins involved in lipid metabolism during disease initiation and progression (Ettinger et al., 2004; Iglesias-Gato et al., 2018; Swinnen et al., 2004; Wu et al., 2014; Zadra and Loda, 2018), suggesting that this lipid rewiring may represent a promising therapeutic vulnerability for the treatment of CRPC (Butler et al., 2020).

While most studies have focused on therapeutic targeting of de novo lipogenesis and lipid uptake in prostate cancer (Watt et al., 2019; Zadra et al., 2019), recent work from our group and others have shown that fatty acid beta-oxidation (FAO) is upregulated in prostate cancer and is critical for cell survival and may contribute to emergence of CRPC and treatment resistance (Balaban et al., 2019; Nassar et al.,

2020b, 2020a; Schlaepfer et al., 2014). FAO occurs mainly in the mitochondria, and hence a lot of effort has been made into developing mitochondrial FAO inhibitors, particularly against carnitine palmitoyltransferase 1 (CPT1; an enzyme that facilitates transport of long chain fatty acids into the mitochondria) such as perhexiline and etomoxir (Dheeraj et al., 2018; Flaig et al., 2017; Schlaepfer et al., 2014; Zaugg et al., 2011). Despite promising pre-clinical data, mitochondrial FAO inhibitors have seen rapid decline in their approved clinical use due to severe toxicity and side effects. Having said that, FAO also occurs in the peroxisomes and both processes cooperate to produce energy (Islinger et al., 2018). In view of our recent discovery of mitochondrial DECR1, an auxiliary enzyme involved in polyunsaturated fatty acid oxidation (Blomme et al., 2020; Nassar et al., 2020b), we sought to investigate and characterise its peroxisomal counterpart, DECR2, and its role in prostate cancer.

Peroxisomal beta oxidation is a comparatively underexplored area of lipid metabolism particularly in the context of prostate cancer. Unlike mitochondrial beta oxidation, peroxisomal beta oxidation does not directly contribute to energy production. Instead, very long chain fatty acids (VLCFAs) or branched chain fatty acids are initially oxidised to shorter fatty acyl chains in the peroxisomes and transported into the mitochondria for complete degradation and subsequent energy production (Islinger et al., 2018; Wu et al., 2014). Herein, we showed that DECR2 is robustly overexpressed in advanced and metastatic prostate cancer tissues and provided evidence that peroxisomal beta oxidation or DECR2 may contribute to treatment resistance in prostate cancer. We also identified a potential clinical candidate agent and peroxisomal beta oxidation inhibitor, thioridazine (TDZ; anti-psychotic agent previously used to treat schizophrenia) (Van den Branden and Roels, 1985). The aim of this study was to evaluate the efficacy of targeting peroxisomal beta oxidation via DECR2 or the clinically available inhibitor TDZ, and to examine its role in CRPC and treatment resistance.

4.3 Materials and methods

4.3.1 Cell lines and tissue culture

Human normal prostate epithelial cell lines PNT1 and PNT2 were obtained from the European Collection of Authenticated Cell Cultures (ECACC). Prostate carcinoma cells LNCaP and 22RV1 were obtained from the American Type Culture Collection (ATCC; Rockville, MD, USA). Castrate-resistant V16D and enzalutamide-resistant MR49F cell lines were derived through serial xenograft passage of LNCaP cells (Toren et al., 2016) and were a kind gift from Professor Amina Zoubeidi's laboratory. Cell lines were verified in 2019 via short tandem repeat profiling (Cell Bank Australia). Cells were cultured in RPMI-1640 medium containing 10 % fetal bovine serum (FBS; Sigma-Aldrich, NSW, Australia) in a 5 % CO_2 humidified atmosphere at 37 °C. For thioridazine (TDZ) treatment, cells were cultured in growth medium supplemented with 2.5 μM, 5 μM, 7.5 μM, 10 μM or 15 μM TDZ (dissolved in dimethyl sulfoxide, DMSO; Sigma-Aldrich). For ribociclib (Rib) treatment, cells were cultured in growth medium supplemented with 0.1 μM or 0.25 μM ribociclib (dissolved in DMSO). The sources and experimental conditions for primary antibodies used in this study are listed in Supplementary Table 4.2.

4.3.2 *Ex vivo* culture of human prostate tumours

Patient derived-explant (PDE) culture was carried out according to techniques established in our laboratory, as described previously (Centenera et al., 2018). Briefly, 6 mm/8 mm biopsy cores were collected from men undergoing robotic radical prostatectomy at St. Andrew's Hospital (Adelaide, South Australia) with written informed consent through the Australia Prostate Cancer BioResource. Tissues were dissected into smaller 1 mm^3 pieces and cultured on Gelfoam sponges (80 x 125 mm Pfizer 1205147) in 24-well plates pre-soaked in 500 μL RPMI-1640 medium supplemented with 10 % FBS and antibiotic/antimycotic solution. TDZ (10 μM or 20 μM) was added into each well and the tissues were cultured in 5 % CO_2 in humidified atmosphere at 37 °C for 48 hrs, then snap frozen in liquid nitrogen and stored at -80 °C, or formalin-fixed and paraffin-embedded.

4.3.3 Bioinformatics analysis

Gene expression data were downloaded from The Cancer Genome Atlas (TCGA) data portal, cBioPortal (SU2C and MSKCC), and the GEO website; GSE6099 (Tomlin et al); GSE35988 (Grasso et al); GSE21034 (Taylor et al). Proteomics data (raw MaxQuant files) was downloaded from the ProteomeXchange Consortium via the PRIDE partner repository using the dataset identifier PXD016836 and analysed independently using the R software. For lipidomic analysis, heatmaps and volcano plots were generated in R version 3.6.3 using the pheatmap and ggplot2 package respectively. GSEA correlation analysis was performed using TCGA dataset and our laboratory's RNA-sequencing data.

4.3.4 Western blotting

Protein lysates were collected in RIPA lysis buffer (10 mM Tris, 150 mM NaCl, 1 mM EDTA, 1 % Triton X-100, 10 % protease inhibitor). Western blotting on whole cell protein lysates were performed as previously described (Armstrong et al., 2016).

4.3.5 siRNA transfection

Human DECR2 ON-TARGET plus SMART pool (L-009627-00-0005) small interfering RNAs (siRNAs) and control siRNA (D-001810-01-20 ON-TARGET plus non-targeting siRNA #1) were purchased from Millennium Science (VIC, Australia). siRNAs (5 nM) were reverse transfected using Lipofectamine RNAiMAX transfection reagent (Invitrogen, VIC, Australia) according to manufacturer's instructions.

4.3.6 Generation of stable shDECR2 and hDECR2 LNCaP cells

LNCaP cells were transduced with the universal negative control shRNA lentiviral particles (shControl) or hControl (GFP-Puro), DECR2 shRNA inducible lentiviral particles (shDECR2, RFP-Puro) designed by Horizon Discovery (Cambridge, UK), or hDECR2 (GFP-Puro) designed by GenTarget Inc (San Diego, CA, USA) according to manufacturer's instructions.

Functional assays

4.3.7 Cell viability

Cells were seeded in triplicate in 24-well plates at a density of 2.5 x 10^4 – 6.0 x 10^4 cells/well and reverse transfected with siRNA overnight or treated with drug-supplemented medium. Cells were manually counted using a hemocytometer 96 hrs post-siRNA knockdown or treatment and cell viability was assessed by Trypan Blue exclusion as described previously (Armstrong et al., 2016).

4.3.8 Cell migration

Transwell migration assays were performed using 24-well polycarbonate Transwell inserts (3422, Sigma-Aldrich). C42B and 22RV1 cells transfected overnight with siRNA were seeded into the upper chamber of the Transwell at a density of 9.0 x 10^4 – 1.5 x 10^5 cells/well in serum-free medium. 650 µL of medium containing 10 % FBS was added to the bottom chamber. Cells were incubated at 37 °C for 48 hrs. For TDZ treatment, medium in both the upper and lower chambers were supplemented with TDZ (2.5 µM). Inserts were washed with PBS and non-migrated cells were gently removed using a cotton-tipped swab. The inserts were then fixed in 4 % paraformaldehyde for 20 min and stained with 1 % crystal violet for 30 min. Images of migrated cells were captured using the Axio Scope A1 Fluorescent Microscope (Zeiss) at 40 X magnification. The number of migrated cells were counted manually and presented as percentages relative to control cells ± SEM.

4.3.9 Colony formation assay

DECR2 stable knockdown (shDECR2) cells or DECR2 overexpression (hDECR2) cells were prepared in a single-cell suspension before seeding in 6-well plates at a density of 500 cells/well. For TDZ treatment, C42B, V16D and MR49F cells were seeded overnight and gently treated with drug-supplemented medium. Cells were incubated for 2 weeks at 37 °C with medium being replenished every 3-7 days. After 2 weeks, cells were washed with PBS and fixed with 4 % paraformaldehyde, then stained with 1 % crystal violet for 30 min. Colonies were counted manually and results were reported as number of colonies ± SEM.

Flow cytometry

4.3.10 Cell cycle analysis

Cells were seeded in triplicate in 6-well plates at a density of 3 x 10^5 – 6 x 10^5 cells/well and reverse transfected with siRNA overnight or treated with drug-supplemented medium. Cells were collected into fluorescence-activated cell sorting (FACS) tubes and centrifuged at 1,500 rpm for 5 min, then fixed in cold 70 % ethanol for 2 hrs. Samples were stained with 50 µg/mL of propidium iodide (PI, Sigma-Aldrich) and 100 µg/mL Ribonuclease A from bovine pancreas (Sigma-Aldrich) for 30 min at room temperature. Cells were analysed using a BD LSRFortessa X-20 Flow Cytometer (BD Biosciences). Data were evaluated using FlowJo version 10.

4.3.11 Apoptosis assay

Cells were seeded in triplicate in 6-well plates at a density of 3 x 10^5 – 6 x 10^5 cells/well and reverse transfected with siRNA overnight or treated with drug-supplemented medium. Cells were collected into FACS tubes and centrifuged at 1,500 rpm for 5 min, then resuspended in FACS Binding Buffer (94 % Hank's Balanced Salt Solution, 1 % HEPES, 5 % $CaCl_2$), 7-AAD (Thermo Fisher Scientific) and Annexin-V PE (BD) for 30 min in the dark. Cells were analysed using a BD LSRFortessa X-20 Flow Cytometer (BD Biosciences). Data were evaluated using FlowJo version 10.

4.3.12 Neutral lipid content quantification

Cells were seeded in triplicate in 24-well plates at a density of 3 x 10^5 – 6 x 10^5 cells/well and reverse transfected with siRNA overnight or treated with drug-supplemented medium. Cells were collected into FACS tubes and centrifuged at 1,500 rpm for 5 min, then resuspended in 2 µM of fluorescent neutral lipid dye BODIPY 493/503 (Thermo Fisher Scientific) for 15 min at 37 °C. Cells were resuspended in 300 µL FACS Binding Buffer and analysed using a BD LSRFortessa X-20 Flow Cytometer (BD Biosciences). Data were evaluated using FlowJo version 10.

Lipidomics

4.3.13 Lipid extraction

700 µL of sample (4 µL of plasma diluted in water, or 700 µL of homogenized cells) was mixed with 800 µL 1 N HCl:CH_3OH 1:8 (v/v), 900 µL $CHCl_3$ and 200 µg/mL of the antioxidant 2,6-di-tert-butyl-4-methylphenol (BHT; Sigma Aldrich). 3 µL of SPLASH LIPIDOMIX Mass Spec Standard (#330707, Avanti Polar Lipids) was spiked into the extract mix. The organic fraction was evaporated using a Savant Speedvac spd111v (Thermo Fisher Scientific) at room temperature and the remaining lipid pellet was stored at -20 °C under argon.

4.3.14 Mass Spectrometry

Lipid pellets were reconstituted in 100 % ethanol. Lipid species were analyzed by liquid chromatography electrospray ionization tandem mass spectrometry (LC-ESI/MS/MS) on a Nexera X2 UHPLC system (Shimadzu) coupled with hybrid triple quadrupole/linear ion trap mass spectrometer (6500+ QTRAP system; AB SCIEX). Chromatographic separation was performed on a XBridge amide column (150 mm x 4.6 mm, 3.5 µm; Waters) maintained at 35 °C using mobile phase A [1 mM ammonium acetate in water-acetonitrile 5:95 (v/v)] and mobile phase B [1 mM ammonium acetate in water-acetonitrile 50:50 (v/v)] in the following gradient: (0–6 min: 0 % B → 6 % B; 6–10 min: 6 % B → 25 % B; 10–11 min: 25 % B → 98 % B; 11–13 min: 98 % B → 100 % B; 13–19 min: 100 % B; 19–24 min: 0 % B) at a flow rate of 0.7 mL/min which was increased to 1.5 mL/min from 13 min onwards. SM, CE, CER, DCER, HCER, LCER were measured in positive ion mode with a precursor scan of 184.1, 369.4, 264.4, 266.4, 264.4 and 264.4 respectively. TAG, DAG and MAG were measured in positive ion mode with a neutral loss scan for one of the fatty acyl moieties. PC, LPC, PE, LPE, PG, LPG, PI, LPI, PS and LPS were measured in negative ion mode by fatty acyl fragment ions. Lipid quantification was performed by scheduled multiple reactions monitoring (MRM), the transitions being based on the neutral losses or the typical product ions as described above. The instrument parameters were as follows: Curtain Gas = 35 psi; Collision Gas = 8 a.u. (medium); IonSpray Voltage = 5500 V and -4,500 V; Temperature = 550 °C; Ion Source Gas 1 = 50 psi; Ion Source Gas 2 = 60 psi; Declustering Potential = 60 V

and -80 V; Entrance Potential = 10 V and -10 V; Collision Cell Exit Potential = 15 V and -15 V. The following fatty acyl moieties were taken into account for the lipidomic analysis: 14:0, 14:1, 16:0, 16:1, 16:2, 18:0, 18:1, 18:2, 18:3, 20:0, 20:1, 20:2, 20:3, 20:4, 20:5, 22:0, 22:1, 22:2, 22:4, 22:5 and 22:6 except for TGs which considered: 16:0, 16:1, 18:0, 18:1, 18:2, 18:3, 20:3, 20:4, 20:5, 22:2, 22:3, 22:4, 22:5, 22:6.

4.3.15 Data analysis

Peak integration was performed with the MultiQuant software version 3.0.3. Lipid species signals were corrected for isotopic contributions (calculated with Python Molmass 2019.1.1) and were normalized to internal standard signals. Unpaired T-test p-values and FDR corrected p-values (using the Benjamini/Hochberg procedure) were calculated in Python StatsModels version 0.10.1.

4.3.16 Seahorse extracellular flux assay

Cells were plated on a XF96 well cell culture microplate (Agilent, Victoria, Australia) at equal densities in substrate-limited medium and incubated overnight. Prior to oxygen consumption rate (OCR) measurements, cells were washed and incubated in FAO assay medium supplemented with or without 200 µM of linoleic acid (LA). Extracellular flux analysis was performed using the Seahorse XF Mito Stress Test kit (Seahorse Bioscience) according to the manufacturer's protocol. Measurements were taken on the Seahorse XF96 Analyzer and results were analysed using the Seahorse Wave software. OCR values were normalized to cell numbers per well.

4.3.17 Membrane fluidity

Cells transfected with siRNA for 48 hours were reseeded onto a Nunc Glass Bottom dish (Thermo Fisher Scientific) and incubated overnight. Cells were then washed with PBS prior to incubation for 1 hr with 2.5 µM Laurdan dye diluted in phenol-red free RPMI-1640 media at 37 °C. Laurdan dye was excited under a 405 nm laser, and two Laurdan intensity images were recorded simultaneously with emissions read at 430 – 470 nm and 485 – 515 nm. The measure of membrane fluidity was obtained using the Generalized Polarization (GP) value, calculated using both Laurdan intensity images according to the equation $GP = I_{(450-500)} / I_{(450+500)}$, where I

represents the intensity of the pixels captured in the 430 – 470 nm and 485 – 515 nm spectral channels respectively, as measured using the ImageJ software.

In vivo studies

4.3.18 Orthotopic tumour growth

10 µL containing 1 x 10^6 DECR2 overexpression cells (hDECR2) or negative control cells (hControl) were injected intraprostatically in 8 week old NOD/SCID male mice. Whole-body imaging to monitor luciferase-expressing LNCaP cells was performed at day 3 of the injection and once weekly after that using the In Vivo Imaging System (IVIS, PerkinElmer). D-luciferin (potassium salt, PerkinElmer) was dissolved in sterile deionized water (0.03 g/mL) and injected subcutaneously (3 mg/20 g of mouse body weight) before imaging. Bioluminescence is reported as the sum of detected photons per second from a constant region of interest. After the animals were sacrificed, lungs and livers were excised for *ex vivo* imaging using the IVIS system.

After each study, tumours that were excised were snap frozen for RNA extraction and formalin fixed and paraffin embedded. All animal procedures were carried out in accordance with the guidelines of the National Health and Medical Research Council of Australia. The orthotopic xenograft studies were approved by the University of Adelaide Animal Ethics Committee (approval number M-2019-037).

4.3.19 Statistical analysis

Results are reported as mean ± SEM. Statistical analysis was performed using GraphPad Prism (V9.0 for Mac). The differences between treatment groups were compared by T-test or one-way ANOVA followed by Tukey or Dunnett post hoc test. Significance is expressed as *$p < 0.05$, **$p < 0.01$, ***$p < 0.001$, ****$p < 0.0001$.

4.4 Results

4.4.1 DECR2 is upregulated in clinical prostate tumours and treatment resistance

DECR2 mRNA expression was significantly higher in malignant prostate cancer tissues (primary and metastatic) compared to normal or benign prostate tissues in four independent gene expression datasets comprising of non-malignant and prostate cancer tissues (Figure 1A,B). Furthermore, DECR2 mRNA expression was higher in CRPC / neuroendocrine prostate cancer (NEPC) compared to benign or primary tumours (Figure 1B). In line with this observation, DECR2 gene copy number gain was evident in several clinical prostate cancer datasets (acquired from cBioportal) (Supplementary figure 1A). DECR2 mRNA expression was associated with shorter relapse-free survival and overall survival rates (Figure 1C). At the protein level, DECR2 expression was markedly increased in castrate-resistant and treatment-resistant prostate cancer cell lines compared with non-malignant PNT1 and PNT2 prostate cell lines (Figure 1D). Consistent with its known function, DECR2 localises to the peroxisome as confirmed using immunocytochemistry (Supplementary figure 1B). A recent proteomics study by Blomme et al characterised the changes associated with acquired resistance to AR inhibition (ARI) (Blomme et al., 2020). Here, we independently analysed the proteomics dataset and found that peroxisomal hallmark and KEGG pathway genes were strongly associated with acquired apalutamide and enzalutamide resistance (Figure 1E; Supplementary figure 1C). Notably, DECR2 protein was robustly and most consistently upregulated in ARI-resistant cells and organoids (Figure 1E; Supplementary figure 1C). Taken together, these findings suggest that DECR2 expression is closely linked to prostate cancer progression and may be associated with treatment-resistance.

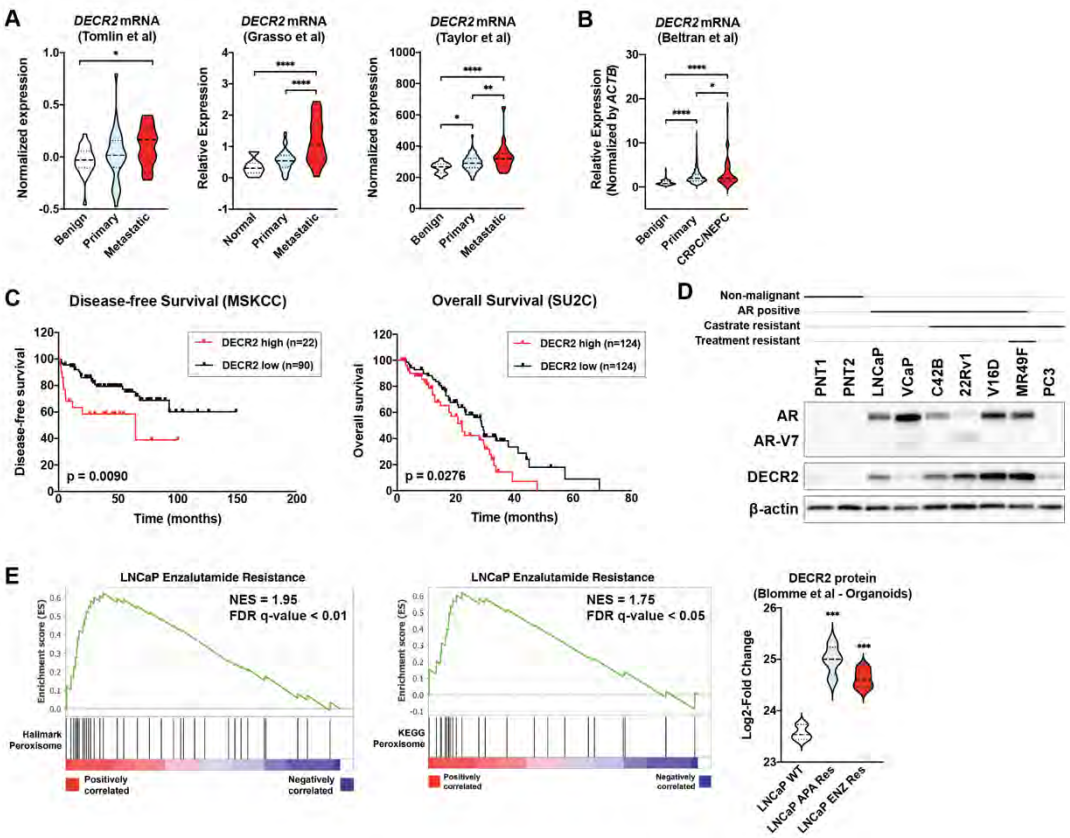

Figure 4.1 Peroxisomal beta-oxidation enzyme, DECR2, is upregulated in advanced and treatment-resistant prostate cancer. (A) DECR2 mRNA expression in normal or benign prostate tissue compared to primary or metastatic prostate cancer in three independent datasets; and **(B)** relative to primary or castrate-resistant and neuroendocrine prostate cancer. **(C)** DECR2 mRNA is associated with shorter disease-free survival (MSKCC) and shorter overall survival rates (SU2C). **(D)** DECR2 protein expression in non-malignant prostate cell lines (PNT1 and PNT2) and prostate cancer cell lines (LNCaP, VCaP, C42B, 22Rv1, V16D, PC3), including enzalutamide-resistant prostate cancer cell line (MR49F). **(E)** Peroxisomal genes are positively correlated with acquired resistance to enzalutamide as assessed by GSEA. DECR2 protein expression is significantly increased in LNCaP acquired apalutamide and enzalutamide resistance organoids compared to wildtype LNCaP organoids. Data are represented as violin plots in GraphPad prism. Statistical analysis was performed using ordinary one-way ANOVA. Data in (C) were statistically analysed using a two-sided log-rank test. *p<0.05, **p<0.01, ***p<0.001 and ****p<0.0001.

4.4.2 Targeting DECR2 inhibits prostate cancer cell proliferation

The overexpression of DECR2 in metastatic prostate cancer tissues and its association with shorter relapse time and overall survival rates suggests that DECR2 may contribute to prostate cancer cell proliferation and invasiveness. DECR2 knockdown significantly attenuated prostate cancer cell viability and induced cell death in androgen-dependent (LNCaP), castrate-resistant (C42B) and acquired enzalutamide-resistant (MR49F) cells; while no effect was observed in non-malignant PNT1 prostate cells (Figure 2A; Supplementary figure 2A). Similarly, stable knockdown of DECR2 significantly attenuated LNCaP prostate cancer cell viability (Figure 2B). In contrast, constitutive DECR2 overexpression (hDECR2) in LNCaP cells significantly enhanced cell viability compared to control (hControl; Figure 2C). Stable knockdown of DECR2 markedly decreased colony formation ability while stable overexpression of DECR2 increased colony formation (Figure 2D,E; Supplementary figure 1B). Likewise, DECR2 knockdown significantly reduced cell migration of C42B and 22Rv1 prostate cancer cells; whereas stable DECR2 overexpression increased LNCaP cell migration (Figure F-H). Consistently, stable overexpression of DECR2 increased tumour growth compared to hControl cells in an orthotopic tumour model (Figure I). In addition, analysis of detectable tumours from hDECR2 (n=6) and hControl (n=10) mice revealed a significant increase in tumour weight and lung metastasis of stable DECR2 overexpression cells (Supplementary figure 2D). Given that DECR2 may be associated with acquired ARI resistance, we wanted to test whether DECR2 knockdown could sensitize enzalutamide-resistant cells to enzalutamide. Indeed, DECR2 knockdown in combination with enzalutamide further decreased cell viability of enzalutamide-resistant MR49F cells compared to DECR2 knockdown or enzalutamide alone (Figure 2J). In contrast, stable DECR2 overexpression LNCaP cells were significantly more resistant to ENZ treatment (Figure 2K).

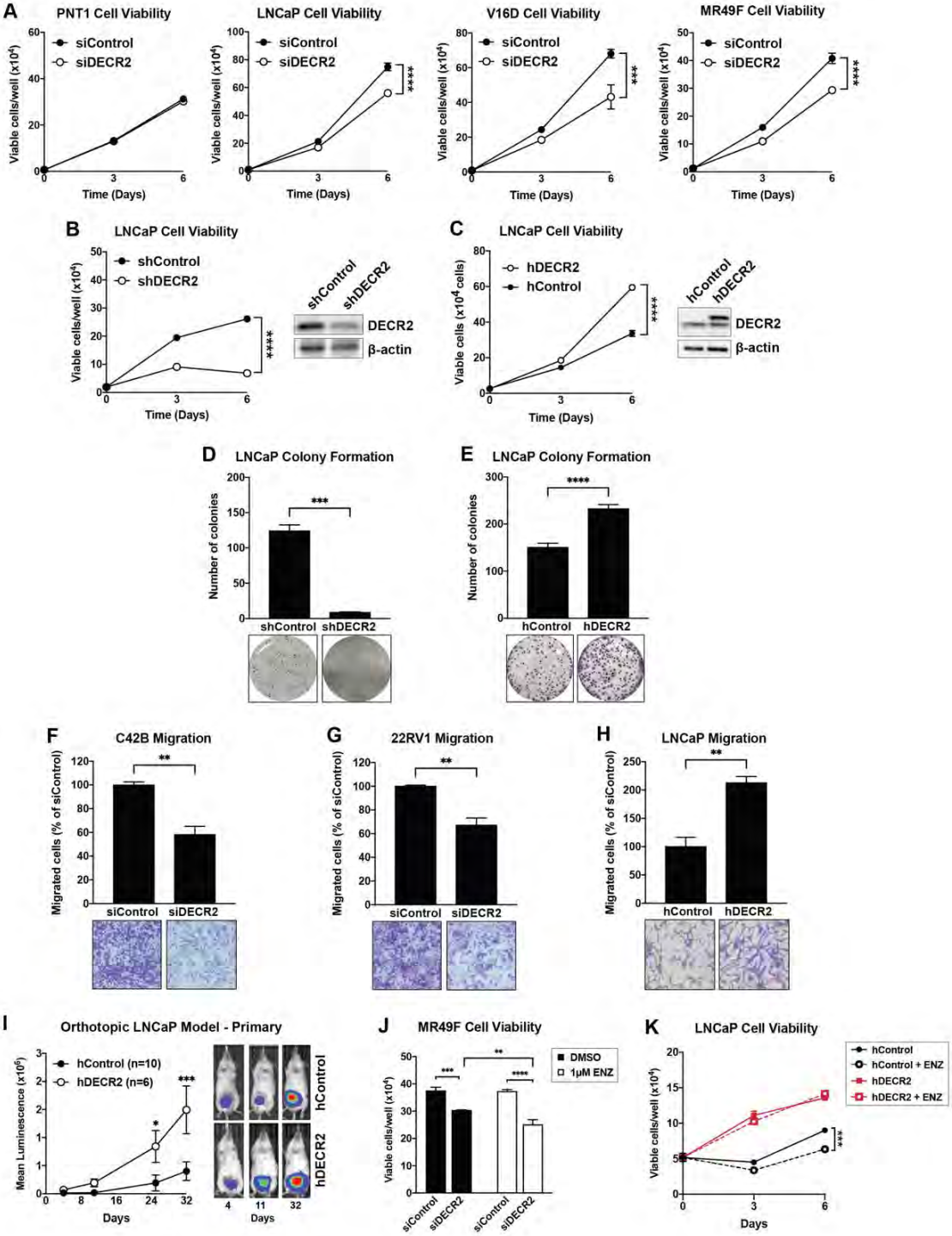
A
PNT1 Cell Viability
LNCaP Cell Viability
V16D Cell Viability
MR49F Cell Viability
siControl
siDECR2
Viable cells/well (x10⁴)
Time (Days)
B
LNCaP Cell Viability
shControl
shDECR2
DECR2
β-actin
C
LNCaP Cell Viability
hDECR2
hControl
Viable cells (x10⁴ cells)
D
LNCaP Colony Formation
Number of colonies
E
LNCaP Colony Formation
F
C42B Migration
Migrated cells (% of siControl)
G
22RV1 Migration
H
LNCaP Migration
I
Orthotopic LNCaP Model - Primary
hControl (n=10)
hDECR2 (n=6)
Mean Luminescence (x10⁶)
Days
J
MR49F Cell Viability
DMSO
1μM ENZ
K
LNCaP Cell Viability
hControl
hControl + ENZ
hDECR2
hDECR2 + ENZ

Figure 4.2 DECR2 knockdown inhibits prostate cancer cell growth. (A) Cell viability of normal prostate PNT1 cell line, androgen-dependent LNCaP, castrate-resistant V16D and enzalutamide-resistant MR49F prostate cancer cell lines subjected to siRNA-mediated DECR2 knockdown. **(B)** Cell viability of LNCaP cells with stable/inducible shRNA DECR2 knockdown (shDECR2). **(C)** Cell viability of LNCaP cells with stable overexpression of DECR2 (hDECR2). **(D-E)** LNCaP colony formation was evaluated in cells with stable/inducible shRNA DECR2 knockdown (shDECR2) or stable DECR2 overexpression (hDECR2). **(F-H)** C42B and 22Rv1 prostate cancer cell lines subjected to siRNA-mediated DECR2 knockdown, and LNCaP stable DECR2 overexpression (hDECR2) cell lines were assessed for cell migration using a transwell migration assay. **(I)** LNCaP cells with stable overexpression of DECR2 (hDECR2, n = 6) or control (hControl, n = 10) were analysed for orthotopic LNCaP tumour growth in mice, and representative bioluminescent tumour images (right). **(J)** Cell viability of enzalutamide-resistant MR49F cells subjected to siRNA-mediated DECR2 knockdown, with or without enzalutamide (1 μM) treatment. **(K)** Cell viability of stable DECR2 overexpression LNCaP cells with or without enzalutamide treatment (1 μM). All data is representative of at least 2 independent experiments and presented as mean ± s.e.m of triplicate wells. Statistical analysis was performed using ordinary one-way ANOVA or two-tailed student's t-test: *$p<0.05$, **$p<0.01$, ***$p<0.001$ and ****$p<0.0001$.

4.4.3 Inhibition of peroxisomal beta-oxidation by thioridazine suppresses prostate cancer oncogenesis

Our results support that targeting peroxisomal beta-oxidation via DECR2 is efficacious *in vitro*. However, no DECR2 inhibitors exist and little is known about targeting this pathway and its clinical exploitability. Accordingly, we identified a potential clinical candidate agent and selective peroxisomal beta-oxidation inhibitor, thioridazine (TDZ), and proceeded to evaluate its efficacy in castrate and treatment-resistant prostate cancer cells. TDZ induced a dose-dependent reduction in cell viability of castrate-resistant C42B and V16D cells and acquired enzalutamide-resistant MR49F cells (Figure 3A). Furthermore, TDZ significantly and dose-dependently decreased the colony formation ability of C42B, V16D and MR49F cells compared to vehicle-treated cells (Figure 3B). Next, TDZ significantly reduced cell migration of C42B and 22Rv1 prostate cancer cells at a low dose of 2.5 μM (Figure 3C). TDZ dose-dependently induced apoptosis and cell death in C42B, V16D and MR49F cells, more notably at 10 μM doses compared to vehicle-treated cells (Figure 3D). Our recent report demonstrated the efficacy of targeting mitochondrial FAO using the chemical inhibitor, etomoxir, using our well-defined patient derived explant (PDE) model that recapitulates the complexity of the clinical tissue microenvironment. Here, we evaluated the efficacy of targeting peroxisomal beta-oxidation using TDZ in PDE tissues (n = 11) and observed an overall significant decrease in the expression of the proliferative marker Ki67 (Figure 3E), with only 2 patients showing no response. It is worth noting that while basal proliferation rates of prostate tumours are relatively low (<10%), this increases substantially during *ex vivo* culture. Similar to what we demonstrated above for DECR2; we also examined the effects of peroxisomal beta oxidation inhibition using TDZ in combination with ENZ on prostate cancer cell viability. Consistently, we showed that TDZ in combination with ENZ further attenuated cell viability in C42B, V16D and most notably, enzalutamide-resistant MR49F cells compared to TDZ or enzalutamide alone (Figure 3F).

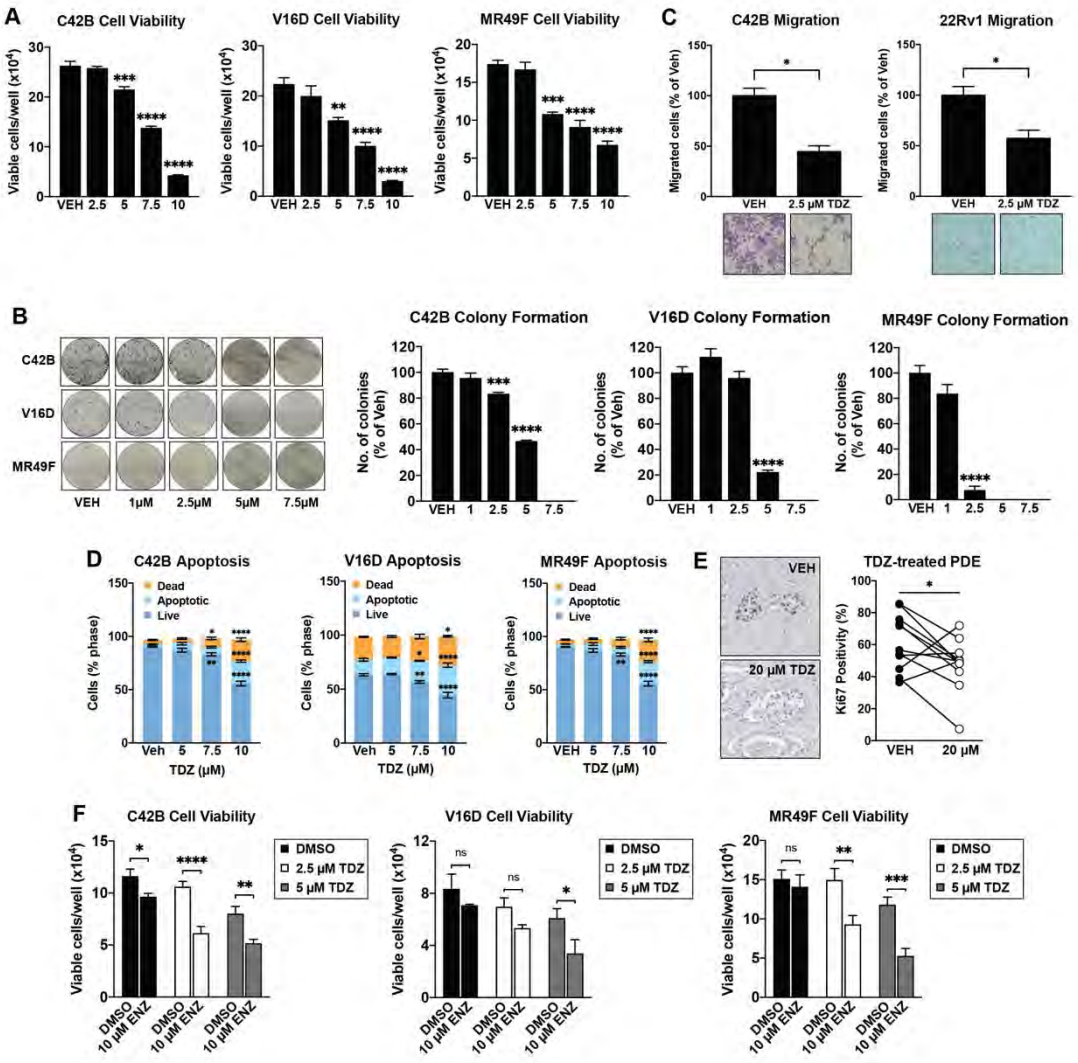

Figure 4.3 Thioridazine suppresses oncogenic phenotypes of prostate cancer cells. Cell viability of **(A)** castrate-resistant C42B and V16D, and enzalutamide-resistant MR49F prostate cancer cell lines across a range of TDZ doses. **(B)** C42B, V16D and MR49F colony formation was evaluated at the indicated TDZ doses. **(C)** C42B and 22Rv1 prostate cancer cell lines treated with TDZ (2.5 μM) were assessed for cell migration using transwell migration assay. **(D)** C42B, V16D and MR49F prostate cancer cells were treated with TDZ for 48 hrs and assessed for apoptotic and dead cells via flow cytometry. Data presented as percentage of cells in each live, apoptotic, or dead state per sample. **(E)** Immunostaining for proliferative marker Ki67 in untreated (VEH) or TDZ-treated (20 μM) patient-derived explants (PDEs). A decrease in proliferative marker Ki67 expression can be seen when PDE tissues are treated with TDZ (n = 10). **(F)** Cell viability of C42B, V16D and MR49F cells with or without enzalutamide treatment (10 μM). All data is representative of at

least 2 independent experiments and presented as mean ± s.e.m of triplicate wells. Statistical analysis was performed using ordinary one-way ANOVA or two-tailed student's t-test: ns = non-significant, *$p<0.05$, **$p<0.01$, ***$p<0.001$ and ****$p<0.0001$.

4.4.4 Peroxisomal beta-oxidation inhibition dysregulates lipid metabolism

Inspection of the lipid profiles of LNCaP, V16D and MR49F prostate cancer cells after DECR2 knockdown revealed a profound remodelling of the cellular lipidome (Figure 4A). All three cell lines displayed a strong and consistent accumulation of multiple lipid classes, in particular cholesteryl ester (CE), triacylglycerol (TAG), diacylglycerol (DAG), and several classes of phospholipids such as phosphotidylethanolamine (PE) and phosphatidylinositol (PI; Figure 4A, Supplementary figure 3A). Of note, DECR2 knockdown resulted in a significant accumulation of monounsaturated fatty acid (MUFA) and polyunsaturated fatty acid (PUFA) species, but not saturated lipid species (Figure 4B). Multiple sphingolipid species, and to a lesser extent some phospholipid species, were also significantly enriched in DECR2 knockdown cells compared to control (Figure 4C). Consistently, DECR2 knockdown significantly induced neutral lipid accumulation in V16D and MR49F cells, suggesting storage of lipids in lipid droplets (Figure 4D). Likewise, TDZ dose-dependently increased neutral lipid accumulation in C42B, V16D and MR49F cells (Figure 4E). Changes in lipid composition have been implicated to alter membrane properties, and certain lipids such as cholesterol and SM have been reported to profoundly influence membrane fluidity. Indeed, we found that DECR2 knockdown significantly decreased V16D and MR49F cell membrane fluidity, as measured using the generalized polarisation (GP) property of the fluorescent probe Laurdan (Figure 4F).

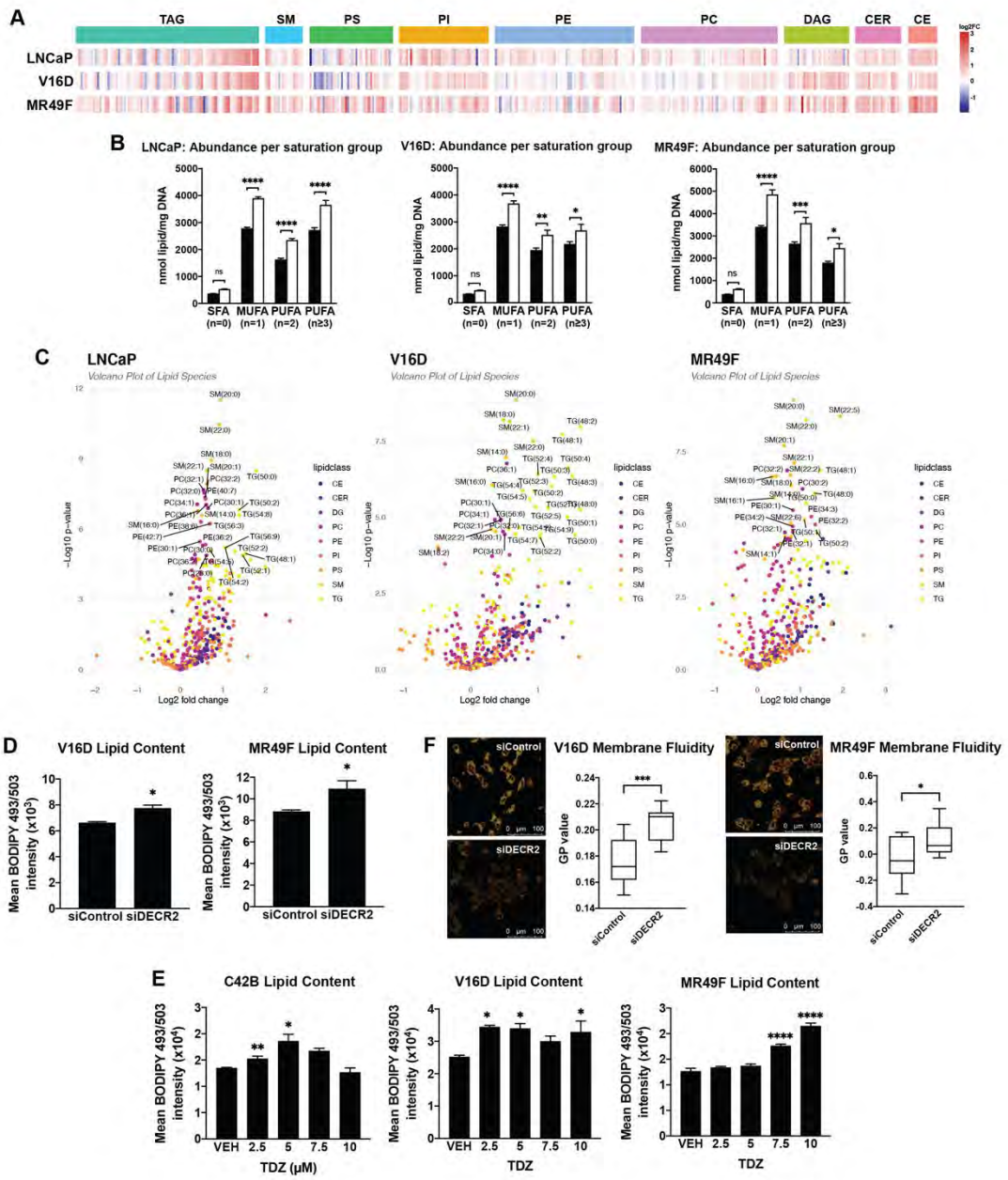

Figure 4.4 DECR2 knockdown and peroxisomal beta-oxidation inhibition by Thioridazine induces lipid accumulation. (A) Heatmap represents average log2 fold change of abundance of selected lipid classes in LNCaP, V16D and MR49F prostate cancer cells subjected to siRNA-mediated DECR2 knockdown (n = 6 per sample, per cell line). TAG: triacylglycerol; SM: sphingomyelin; PS: phosphotidylserine; PI: phosphatidylinositol; PE: phosphotidylethanolamine; PC: phosphotidylcholine; DAG: diacylglycerol; CER: ceramide; CE: cholesteryl ester. **(B)** Quantitative abundance per saturation group in LNCaP, V16D and MR49F cells. **(C)** Volcano plots of all lipid species in LNCaP, V16D and MR49F cells after DECR2 knockdown. Top 20-30 enriched lipid species ($p < 0.05$) were annotated. **(D)** V16D

and MR49F prostate cancer cells subjected to siRNA-mediated DECR2 knockdown were assessed for neutral lipid content via flow cytometry. **(E)** C42B, V16D and MR49F prostate cancer cells were treated with TDZ for 48 hrs and assessed for neutral lipid content via flow cytometry. **(F)** Membrane fluidity in DECR2-knockdown V16D and MR49F prostate cancer cells as measured by fluorescent Laurdan assay. For this assay, GP value is inversely correlated to membrane fluidity. All data is representative of at least 2 independent experiments and presented as mean ± s.e.m of triplicate wells. Statistical analysis was performed using ordinary one-way or two-way ANOVA, or two-tailed student's t-test: *$p<0.05$, **$p<0.01$, ***$p<0.001$ and ****$p<0.0001$.

4.4.5 Interplay between peroxisomal and mitochondrial beta oxidation

Little is known about the relationship that exists between the peroxisome and mitochondria despite their well-recognised fundamental roles in fatty acid oxidation. Gene-set enrichment analysis (GSEA) revealed that DECR2 expression was positively correlated with genes involved in oxidative phosphorylation in two independent clinical datasets (TCGA and local RNAseq patient cohort; Figure 5A). Accordingly, we sought to evaluate the effect of DECR2 knockdown on mitochondrial activity. DECR2 knockdown in castrate-resistant V16D and enzalutamide-resistant MR49F prostate cancer cells increased cellular ATP levels (Figure 5B). To determine if this was due, in part, to functional mitochondrial respiration, we employed the Seahorse Extracellular Flux assay to determine the rate and capacity of prostate cancer cells to oxidise fatty acids in conditions where nutrients are limiting. Our results revealed that DECR2 knockdown had similar to no effect in their oxygen consumption rates (OCR) when compared to control cells (Figure 5C). Having said that, exogenous supplementation of linoleic acid further stimulated the OCR of DECR2 knockdown cells suggesting that mitochondrial activity remains functional despite the impairment of peroxisomal beta oxidation via DECR2 knockdown (Figure 5C). Although there were slight variations in the results between the two cell lines, overall DECR2 knockdown increased the basal respiration rate, ATP production, maximal respiration and mitochondrial spare capacity compared to control cells (Figure 5C). In support of this, etomoxir treatment further potentiated the effect of DECR2 knockdown in V16D and MR49F cells compared to etomoxir treatment or DECR2 knockdown alone, indicating that mitochondrial oxidative phosphorylation may be essential to promote prostate cancer cell survival in response to DECR2 inhibition (Figure 5D).

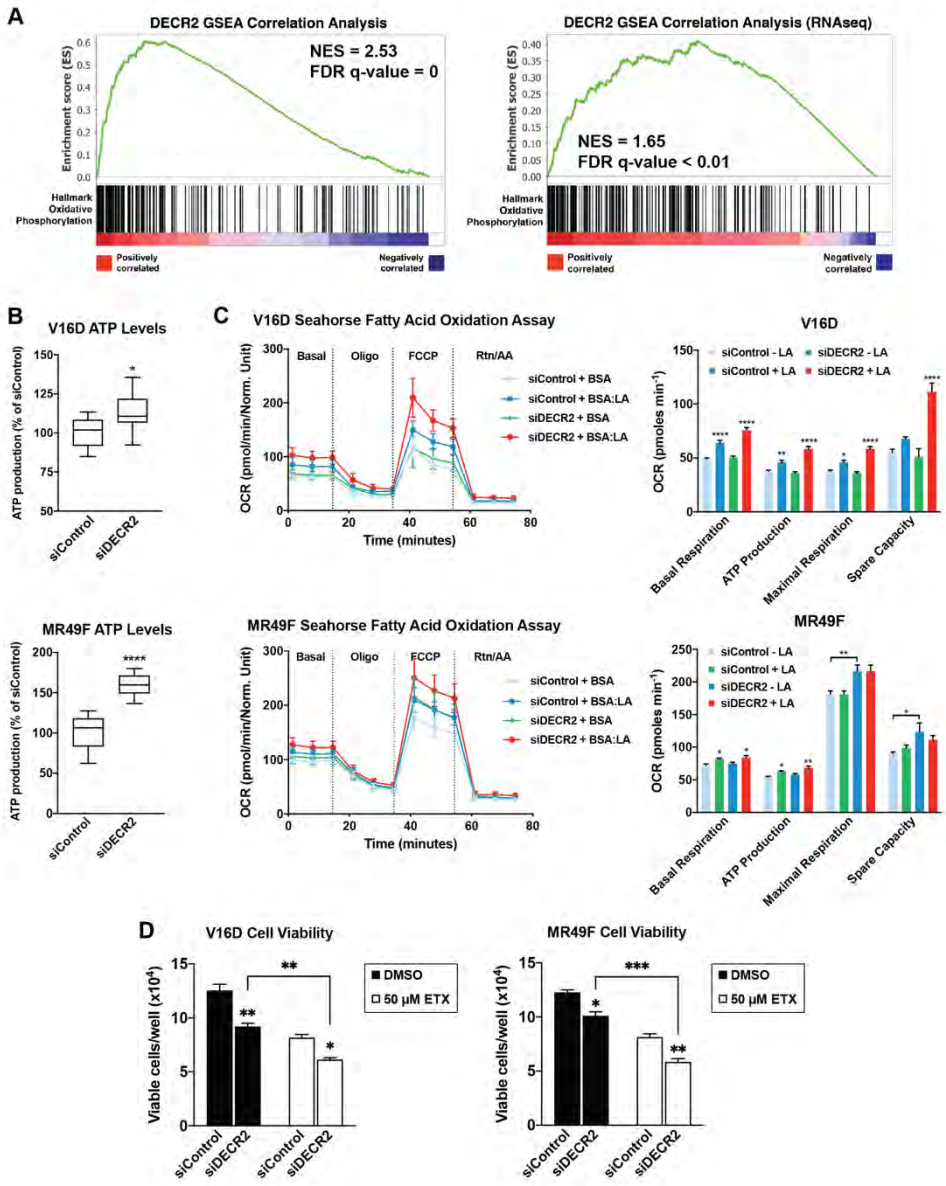

Figure 4.5 Mitochondrial oxidative phosphorylation remains functional in DECR2 knockdown cells. (A) DECR2 expression is positively correlated with genes involved in oxidative phosphorylation in prostate cancer tissues as assessed by GSEA; TCGA dataset (left) and personal RNAseq dataset (right). **(B)** Quantification of ATP levels in castrate-resistant V16D (top) and enzalutamide-resistant MR49F (bottom) prostate cancer cells subjected to siRNA-mediated DECR2 knockdown. **(C)** Oxygen consumption rate (OCR) of V16D and MR49F cells supplemented with linoleic acid (LA) were assessed using Seahorse Extracellular Flux assay. Each data point represents an OCR measurement. Basal respiration, ATP production, maximal respiration and spare capacity were evaluated (right). **(D)** Cell viability of V16D and MR49F cells treated with or without Etomoxir (ETX; 50

μM). All data is representative of at least 2 independent experiments and presented as mean ± s.e.m of triplicate wells. Statistical analysis was performed using two-tailed student's t-test (B) or two-way ANOVA (C-D): *$p<0.05$, **$p<0.01$, ***$p<0.001$ and ****$p<0.0001$.

4.4.6 Targeting peroxisomal beta oxidation inhibits prostate cancer cell proliferation by inducing cell cycle arrest

To investigate the mechanism by which prostate cancer cell growth and proliferation was attenuated by DECR2 knockdown or thioridazine, we examined the effect of DECR2 knockdown on cell cycle profile by flow cytometry. DECR2 knockdown induced cell cycle arrest at the G1/S phase in C42B, V16D and MR49F cells (Figure 6A; Supplementary figure 4A). In contrast, stable DECR2 overexpression in LNCaP cells showed the opposite effect where there was less inhibition of cell cycle progression, consistent with its increase in cell viability (Figure 6B; Figure 1C). Likewise, TDZ induced G1/S phase cell cycle arrest dose-dependently in C42B, V16D and MR49F cells, particularly at the 10 µM dose (Figure 6C). In light of these findings, we assessed the effect of DECR2 knockdown on several cell cycle-related proteins/regulators in V16D and MR49F cells. We observed an increase in cyclin-dependent kinase inhibitors p21 and p27, and a decrease in cyclin-dependent kinase CDK4. In addition, we observed a decrease in phosphorylated retinoblastoma (pRb) tumour suppressor protein in DECR2 knockdown cells compared to control (Figure 6D). We also examined the effects of TDZ treatment on cell cycle proteins and observed some similar effects, particularly for p21, p27 and cyclin D1 (Supplementary figure 4D). Interestingly, we observed some changes in histone H3 acetylation and proceeded to test the effect of HDAC inhibition using vorinostat (SAHA) in DECR2 knockdown V16D and MR49F cells. Overall, no significant effect was observed (Supplementary figure 4F). We then tested whether the cyclin-dependent kinase (CDK) 4/6 inhibitor, ribociclib (Rib) could further enhance the effect of DECR2 knockdown in the cells. Indeed, Rib further abrogated V16D and MR49F cell viability in DECR2 knockdown cells (Figure 6E; Supplementary figure 4B). In contrast, stable DECR2 overexpression in LNCaP cells experienced less cell growth inhibition when treated with Rib compared to hControl cells (Figure 6F; Supplementary figure 4C). Finally, we examined the effect of peroxisomal beta-oxidation inhibition via TDZ in combination with Rib on cell viability. We found that TDZ further abrogated C42B, V16D and MR49F cell viability when treated in combination with Rib compared to vehicle-treated cells or Rib alone (Figure 6G; Supplementary 4E).

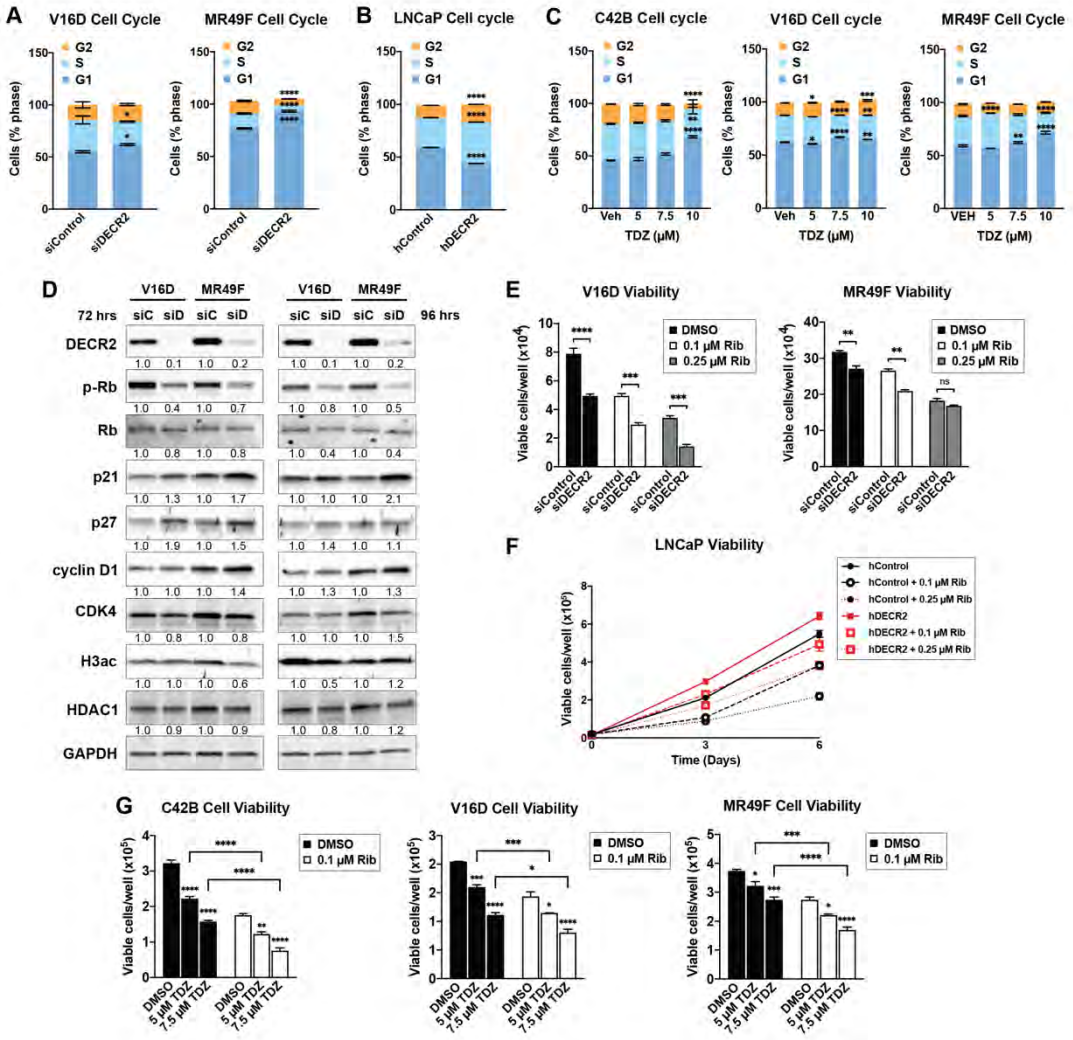

Figure 4.6 DECR2 knockdown and thioridazine induce cell cycle arrest and further abrogates prostate cancer cell growth in combination with ribociclib. **(A)** V16D and MR49F cell cycle distribution 96 hrs after siRNA-mediated DECR2 knockdown; **(B)** LNCaP cells with stable overexpression of DECR2 cell cycle distribution; and **(C)** C42B, V16D and MR49F cell cycle distribution 48 hrs after TDZ treatment was evaluated by flow cytometric analysis. Data presented as percentage of cells in each G1, S or G2 phase per sample. **(D)** Western blot analysis of a panel cell cycle-related protein markers in V16D and MR49F cells 72 and 96 hrs after DECR2 knockdown. GAPDH was used as loading control. Cell viability of **(E)** V16D and MR49F prostate cancer cells after DECR2 knockdown, and **(F)** LNCaP cells with stable overexpression of DECR2, treated with ribociclib (Rib; 0.1 μM and 0.25 μM). **(G)** Cell viability of C42B, V16D and MR49F prostate cancer cells treated with TDZ (5 μM and 7.5 μM) and/or in combination with Rib (0.1 μM). All data is representative of at least 2 independent experiments and presented as mean ±

s.e.m of triplicate wells. Statistical analysis was performed using ordinary one-way or two-way ANOVA: ns = non-significant, *$p<0.05$, **$p<0.01$, ***$p<0.001$ and ****$p<0.0001$.

4.5 Supplementary figures and tables

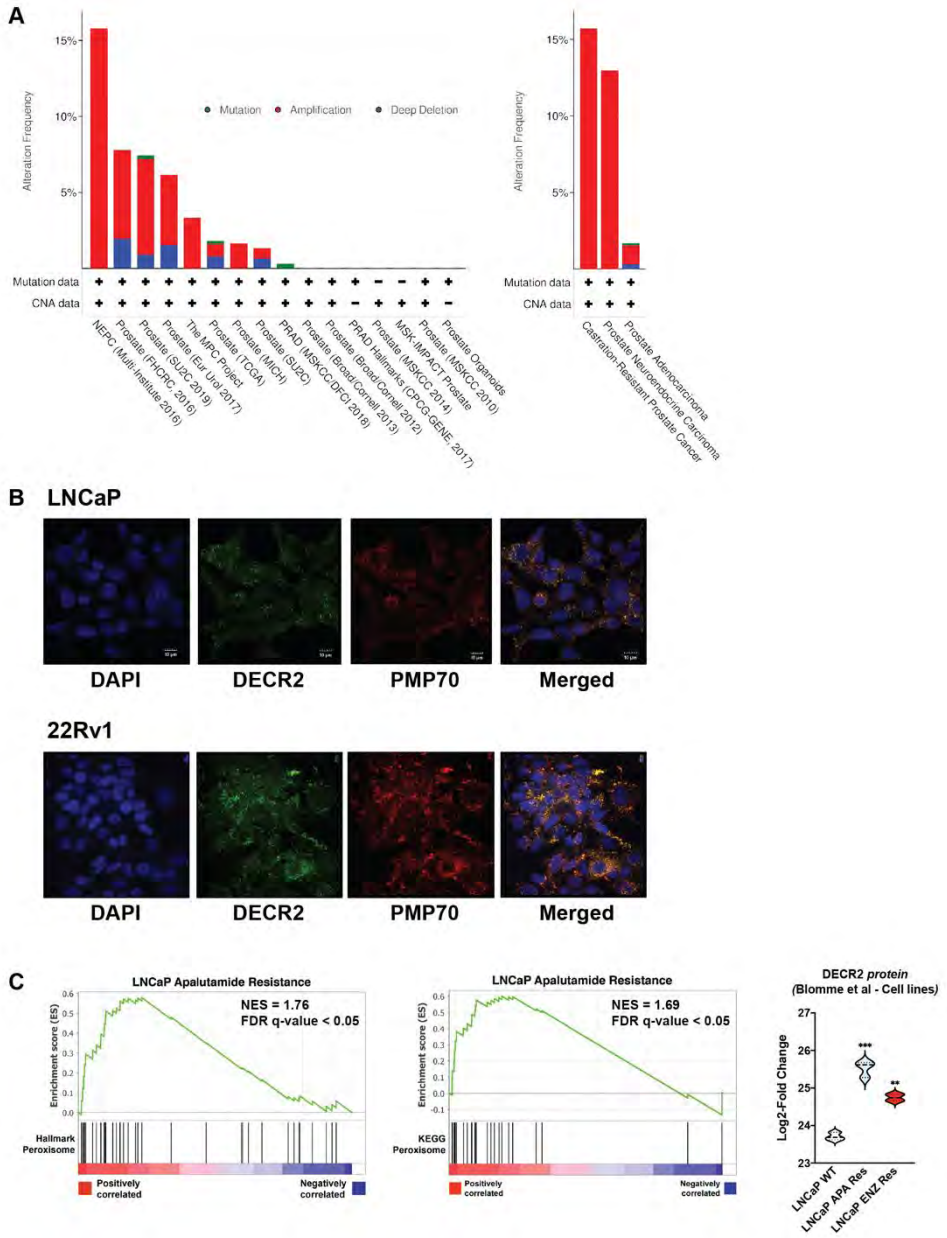

Supplementary Figure 4.1 (A) Histogram displaying DECR2 mutation and copy-number alteration frequency across 9 prostate cancer genomic datasets (left), and across 3 prostate cancer subtypes (right). **(B)** Immunocytochemistry staining of LNCaP and 22Rv1 cells to determine subcellular localization of DECR2. DAPI: nuclei; Alexa Fluor 488 secondary antibody: DECR2; Peroxisome: Alexa Fluor 594 secondary antibody (PMP70), scale bar = 10 µm. **(C)** Peroxisomal genes are positively correlated with acquired resistance to apalutamide as assessed by GSEA. DECR2 protein expression is significantly increased in LNCaP acquired apalutamide and enzalutamide resistance cells compared to wildtype LNCaP cells

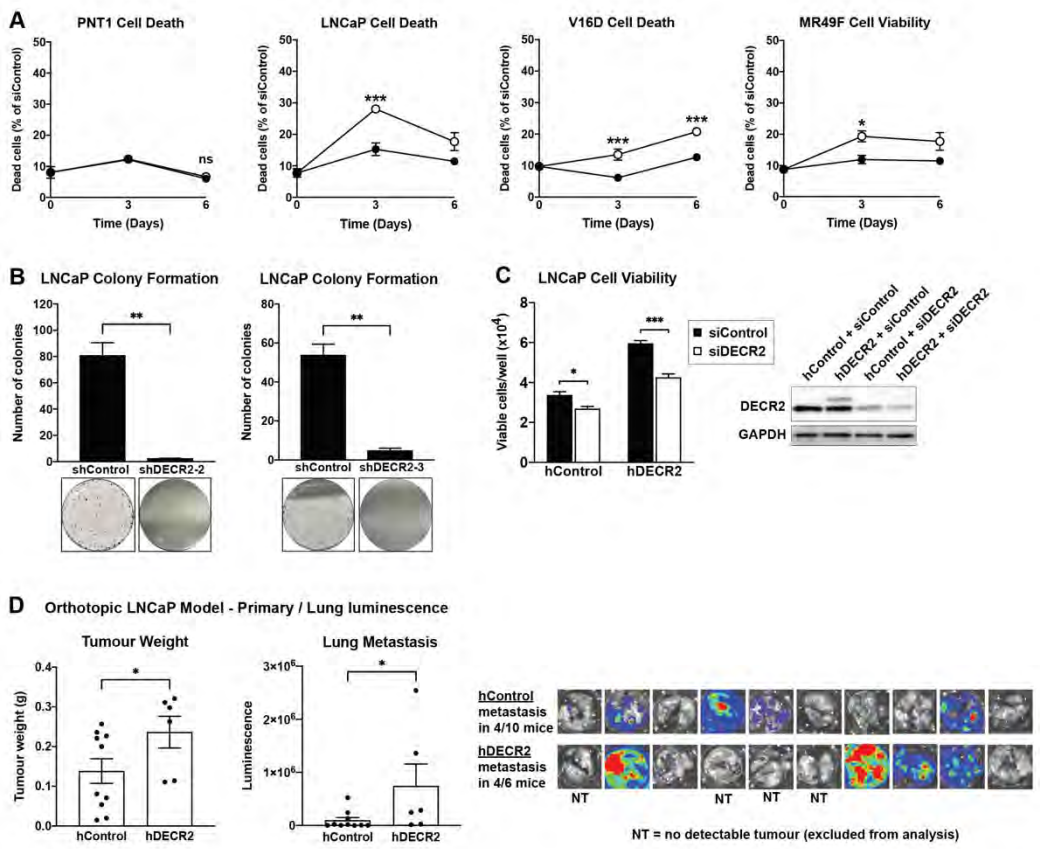

Supplementary Figure 4.2 (A) Cell death of normal prostate PNT1 cell line, androgen-dependent LNCaP, castrate-resistant V16D and enzalutamide-resistant MR49F prostate cancer cell lines subjected to siRNA-mediated DECR2 knockdown. **(B)** LNCaP colony formation was evaluated in cells with stable/inducible shRNA (vectors 2 and 3) DECR2 knockdown (shDECR2-2 and shDECR2-3). **(C)** Cell viability of LNCaP cells with stable DECR2 overexpression or control (hControl) subjected to siRNA-mediated DECR2 knockdown or control (siControl). DECR2 protein expression after 96 hrs siRNA transfection (right). GAPDH was used as loading control. **(D)** Tumour weight (left) and lung luminescence of tumour metastasis to the lungs (right) of detectable tumour after dissection (hControl, n = 10; hDECR2, n = 6). Bioluminescent images of metastatic spread to the lungs of all hControl (n = 10) and hDECR2 (n = 10) mice. *NT = non-detectable tumour excluded from analysis*.

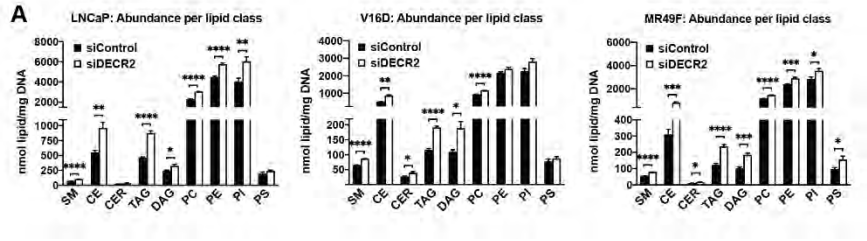

Supplementary Figure 4.3 (A) Quantitative abundance per lipid class of LNCaP, V16D and MR49F cells after DECR2 knockdown, representative bar graphs from Figure 4A. Statistical analysis was performed using two-tailed student's t-test: *p<0.05, **p<0.01, ***p<0.001 and ****p<0.0001.

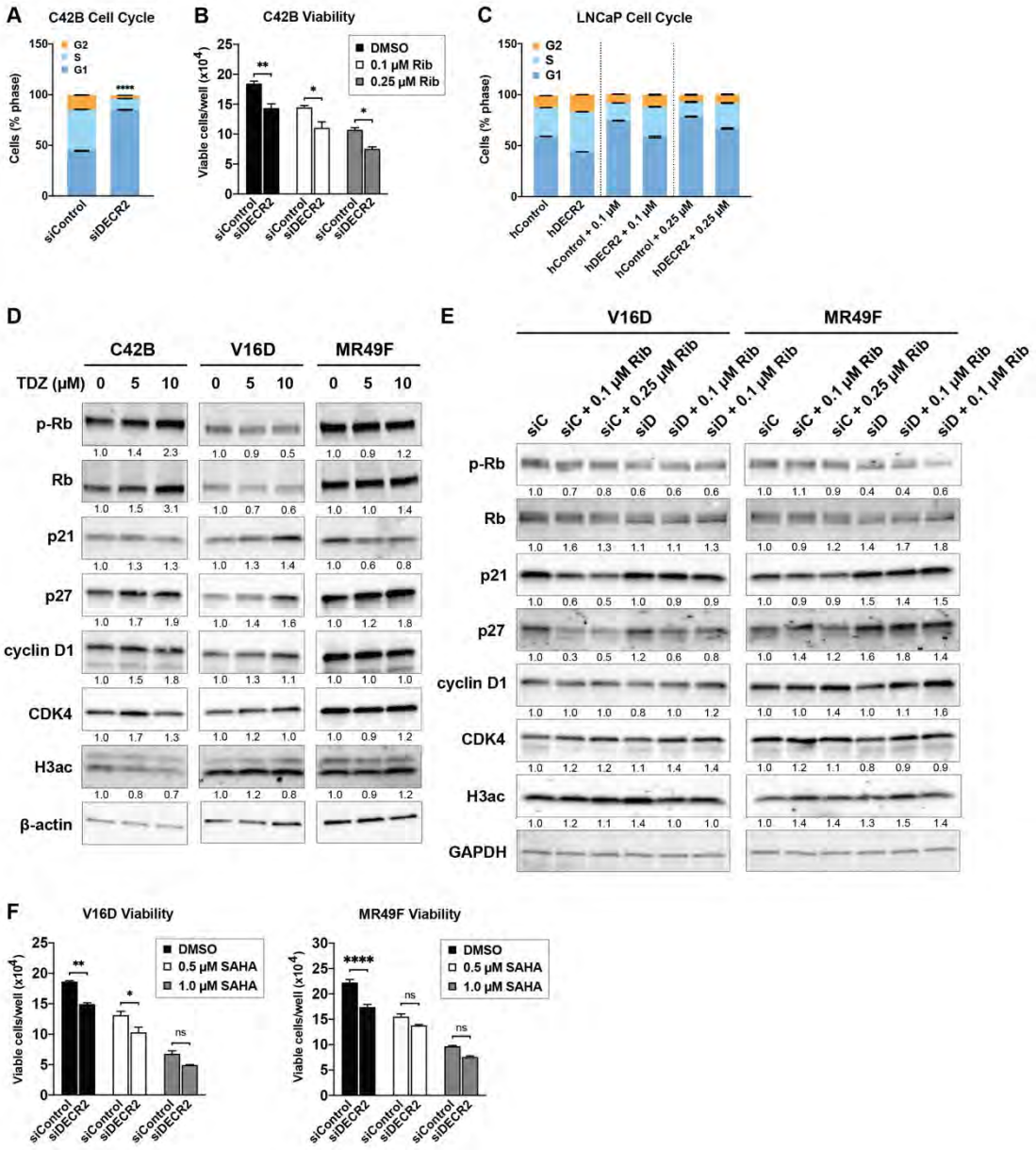

Supplementary Figure 4.4 (A) C42B cell cycle distribution 96 hrs after siRNA-mediated DECR2 knockdown was evaluated by flow cytometric analysis. **(B)** Cell viability of C42B prostate cancer cells after DECR2 knockdown, treated with ribociclib (Rib; 0.1 μM and 0.25 μM). **(C)** Cell cycle distribution of LNCaP cells with stable DECR2 overexpression treated with or without Rib (0.1 μM and 0.25 μM) was evaluated by flow cytometric analysis. **(D)** Western blot analysis of a panel of cell cycle-related protein markers (as in Figure 5D) in C42B, V16D and MR49F cells 24 hrs after TDZ treatment (0 μM, 5 μM or 10 μM). **(E)** Western blot analysis of a panel cell cycle-related protein markers (as in Figure 5D) in V16D and MR49F cells 96 hrs after DECR2 knockdown with or without Rib (0.1 μM and 0.25 μM) treatment. GAPDH was used as loading control. **(F)** Cell viability of V16D and MR49F prostate

cancer cells after DECR2 knockdown treated with or without HDAC inhibitor, SAHA (0.5 μM and 1.0 μM).

Table 4.1 Sequence of shDECR2 and hDECR2 expression vector

Expression target	**Sequence**
Human DECR2 shRNA	shDECR2-1 mature antisense: CAGCAATTCTCTTTAATCC shDECR2-2 mature antisense: ACAAGTCTCGGGATCCATG shDECR2-3 mature antisense: AAACGCACTAGCAAGATTG
Human DECR2: subcloned human target coding sequence (GenTarget Inc)	atggcccagccgccgcccgacgtggagggggacgactgtctccccgcgtaccgcc acctcttctgcccggacctgctgcgggacaaagtggccttcatcacaggaggcggct ctgggattgggttccggattgctgagattttcatgcggcacggctgccatacggtgattg ccagtaggagcctgccgcgagtgctgacggccgccaggaagctggctggggccac cggccggcgctgcctccctctctctatggacgtccgagcgcccccagctgtcatggcc gccgtggaccaggctctgaaggagtttggcagaatcgacattctcattaactgtgcgg ccgggaacttcctgtgccccgctggcgccttgtccttcaacgccttcaagaccgtgatg gacatcgataccagcggcaccttcaatgtgtctcgtgtgctctatgagaagttcttccgg gaccacggaggggtgatcgtgaacatcactgccaccctggggaaccgggggcag gcgctccaggtgcatgcaggctccgccaaggccgctgtggacgcgatgacgcggc acttggctgtggagtggggtccccaaaacatccgcgtcaacagcctcgcccctggcc ccatcagtggcacagaggggctccggcgactgggtggccctcaggccagcctgag caccaaggtcactgccagcccgctgcagaggctggggaacaagaccgagatcgc ccacagcgtgctctacctggccagccctctggcttcctacgtgacgggggccgtgctg gtggccgatggcggggcatggttgacgttcccaaacggtgtcaaagggctgccggat ttcgcatccttctctgctaagctc

Table 4.2 List of antibodies

Antibody	Conjugate	Species	Identifier	Supplier
β-actin	None	Mouse	A5441	Sigma-Aldrich
HSP90	None	Rabbit	4874S	Cell Signalling Technology
DECR2	None	Rabbit	ab153849	Abcam
AR	None	Rabbit	sc-816	Santa Cruz
PMP70	None	Mouse	SAB4200181	Sigma-Aldrich
Rb	None	Mouse	9309	Cell Signalling Technology
pRb	None	Rabbit	ab184796	Abcam
p21	None	Rabbit	SC-317	Santa Cruz
p27	None	Rabbit	SC-528	Santa Cruz
cyclin D1	None	Rabbit	M3642	DAKO
CDK4	None	Rabbit	SC-260	Santa Cruz
H3ac	None	Rabbit	06-599	Upstate
HDAC1	None	Rabbit	SC-7872	Santa Cruz
GAPDH	Rhodamine	Rabbit	12004167	BioRad
Ki67		Mouse	M7240	DAKO
Rabbit	HRP	Rabbit		DAKO
Mouse	HRP	Mouse		DAKO

Table 4.3 The clinicopathologic features of PCa patients included in this study

Patient ID	Age at RP	Pre-OP PSA	Gleason Score (Pre-OP)	1° GG	2° GG	3° GG	Pathological Staging
33975R	65.3	5.00	7	4	3		PT3A
33976LA	82.5	7.60	7	4	3		PT2
33985L	61.2	5.30	7	3	4		PT3A
33986L	73.6	7.90	7	4	3		PT3A
33987L	70.5	9.14	6	3	3		PT3A
33988RB	70.1	5.17	7	3	4		PT2
33989RA	69.1	6.60	7	4	3		PT2
33992L	74.0	6.16	7	3	4		PT2
33993L	70.5	10.50	6	3	3		PT2
33994R	58.2	8.75	8	4	4	3	PT2

4.6 Discussion

In this study, we provide novel evidence for a role of peroxisomal beta oxidation in prostate cancer progression. We report that the peroxisomal beta oxidation auxiliary enzyme, DECR2 (related to mitochondrial DECR1), is a robustly overexpressed gene in advanced prostate cancer tissues and is closely linked to clinical resistance to AR inhibition. Our data demonstrate that targeting of peroxisomal beta oxidation significantly suppressed prostate cancer cell growth and metastatic potential *in vitro* and *in vivo*. Moreover, we demonstrate that molecular targeting of DECR2 led to profound changes in lipid content and composition, and modulation of critical cell cycle regulatory pathways. Our findings provide new insights into the role of DECR2 in prostate cancer, extending our knowledge beyond the previous focus on mitochondrial beta oxidation and identify peroxisomal beta oxidation as a potential therapeutic target for advanced metastatic prostate cancer.

Altered lipid metabolism is a well-characterised hallmark of prostate cancer and, accordingly, significant research efforts have been made to target de novo lipogenesis and lipid uptake pathways. However, there is a growing body of evidence that supports fatty acid oxidation as a critical aspect of lipid metabolism that drives prostate cancer progression and contributes to treatment resistance (Flaig et al., 2017; Nassar et al., 2020b, 2020a; Schlaepfer et al., 2014; Zaugg et al., 2011). Despite the complexity of the fatty acid oxidation pathway, most drug development approaches have focused entirely on targeting mitochondrial CPT1, the rate-limiting enzyme of beta oxidation. Our previous study demonstrated therapeutic efficacy in targeting mitochondrial beta oxidation using a pharmacological agent, etomoxir (CPT1 inhibitor) in our established patient-derived explant (PDE) model (Nassar et al., 2020b). Although CPT1 inhibitors showed remarkable efficacy in attenuating cancer cellular proliferation *in vitro* and *in vivo*, its clinical use remains challenging due to the off-target effects that may underlie the severe toxicity (Holubarsch et al., 2007; Ma et al., 2020). For this reason, we sought to identify alternative targets involving beta oxidation and discovered DECR1, the rate-limiting auxiliary enzyme of mitochondrial polyunsaturated fatty acid metabolism (Nassar et al., 2020b). Interestingly, we also discovered peroxisomal 2,4-dienoyl CoA reductase 2 (DECR2), a peroxisomal beta oxidation enzyme

analogous to mitochondrial DECR1. Besides residing in different cellular compartments, DECR1 and 2 are both critical NADPH-dependent auxiliary enzymes that play key roles in polyunsaturated fatty acid (PUFA) oxidation (Alphey et al., 2005). Unlike mitochondrial DECR1, which functions primarily to oxidise PUFAs for energy, peroxisomal DECR2 is more selective for very long chain fatty acids (VLCFAs) and functions to chain-shorten VLCFA substrates before being transported into the mitochondria for complete degradation. Intriguingly, another study reported that DECR2 may also be involved in the degradation of short and medium chain substrates as well as docosahexaenoic acid (DHA) (De Nys et al., 2001), which warrants further investigation into the specific function and reactivity of peroxisomal DECR2.

Peroxisomal beta oxidation is an understudied aspect of fatty acid metabolism in prostate cancer. Unlike mitochondrial beta oxidation, where short to long chain fatty acid oxidation takes place, peroxisomal beta oxidation involves the breakdown of very long chain and branched chain fatty acids (VLCFAs and BCFAs). VLCFAs undergo peroxisomal beta oxidation to produce shorter fatty acyl-CoAs before they are transported into the mitochondria for complete degradation and energy production (Islinger et al., 2018; Lodhi and Semenkovich, 2014). The changes in peroxisomal gene and protein expression and metabolic flux in cancer cells relative to normal cells, and whether these changes are reflected in their lipid profiles, remains an area ripe for further investigation. To date, the most studied peroxisomal beta oxidation enzyme in prostate cancer is α-methylacyl-CoA racemase (AMACR; catalyses BCFA oxidation). AMACR is consistently overexpressed in prostate cancer and is associated with increased prostate cancer risk (Ananthanarayanan et al., 2005). More importantly, AMACR is highly specific for prostate cancer, and hence has been exploited as a specific prostate cancer biomarker (Ananthanarayanan et al., 2005; Jiang et al., 2004). In another study, it was reported that a peroxisomal beta oxidation enzyme, ECI2, was significantly overexpressed in human prostate cancers and is associated with poor overall patient survival. The authors showed that ECI2 knockdown attenuated prostate cancer cell growth and tumorigenicity, accompanied by an accumulation of fatty acids and cell cycle-related genes, analogous to the current study findings (Itkonen et al., 2017). A more recent study reported increased expression of several peroxisomal proteins (including but

not limited to ACOX1/3, ABCD1, CAT and PECI) in castrate-resistant 22Rv1 prostate cancer cells relative to non-malignant cells, accompanied by a significant increase in C26:0 oxidation (Valença et al., 2020). Interrogation of clinical datasets showed that DECR2 was significantly increased in malignant prostate cancer tissues, particularly metastatic samples, compared to normal or benign tissues and was associated with poorer overall survival. When comparing DECR2 protein expression across a range of prostate cancer cell lines, DECR2 expression was highest in castrate-resistant V16D and enzalutamide-resistant MR49F prostate cancer cells. This prompted us to investigate whether peroxisomal beta oxidation or DECR2 could pose a metabolic vulnerability in the context of treatment resistance. We independently analysed a proteomics dataset by Blomme et al where they characterised the changes associated with acquired resistance to AR inhibition (ARI) (Blomme et al., 2020). This analysis showed that peroxisomal pathway genes were strongly associated with acquired apalutamide and enzalutamide resistance and DECR2 was consistently upregulated in ARI-resistant cells and organoids. Consistently, we showed that DECR2 knockdown was able to sensitise enzalutamide-resistant MR49F cells to enzalutamide and that DECR2 overexpression cells showed no effect towards enzalutamide treatment. Collectively, these data are consistent with peroxisomal beta oxidation and DECR2 specifically playing a key role in treatment resistance. Intriguingly, it was found that the expression levels of several peroxisomal proteins (PMP70, PEX5/19, CAT) were decreased in androgen-independent PC3 cells; while those involved in peroxisomal beta oxidation (ACOX1 and PECI) were increased in PC3 cells when compared to 22Rv1 cells (Valença et al., 2020). In contrast, our data showed that DECR2 protein expression was lower in PC3 cells. This suggests that certain aspects of peroxisomal metabolism may play distinct roles at different stages of the disease, and that its metabolism may be rewired to meet specific needs or demands at various tumour stages. However, this warrants further investigation and needs to be confirmed in human clinical samples. It was reported in a recent study that BRAF mutant melanoma ‘persister’ cells resistant to BRAF/MEK inhibition switch their metabolism from glycolysis to oxidative phosphorylation that is predominantly dependent on peroxisomal beta oxidation compared to mitochondrial beta oxidation (Shen et al., 2020). Unlike DECR2, mitochondrial DECR1 was notably more abundant in AR-negative PC3 cells suggesting that PC3 cells may be more reliant

on mitochondrial beta oxidation relative to peroxisomal. Future studies will still be needed to understand the diversity of mechanisms involved in the regulation of peroxisomal metabolism or DECR2 during CRPC development.

Phenotypically, targeting DECR2 had profound effects on prostate cancer cell viability, colony formation and migration *in vitro*. In contrast, DECR2 overexpression showed evidence of increased tumour growth and metastasis *in vivo*. In future studies, we will assess the effects of DECR2 knockdown on tumour growth and metastasis *in vivo.* So far, our findings suggest that targeting peroxisomal beta oxidation may be an exploitable therapeutic target. To provide proof of principle, and circumvent the time and resources required to develop and test new drug treatments, we reappropriated an existing clinically available pharmacological agent to explore the efficacy and clinical exploitability of inhibiting peroxisomal beta oxidation, using thioridazine (TDZ) (Van den Branden and Roels, 1985). TDZ is a first-generation antipsychotic drug. Despite global market withdrawal in 2005 due to a well-defined risk of cardiac arrythmias, TDZ continues to be used off-label for patients with severe or chronic schizophrenia who are refractory to other treatment options (Purhonen et al., 2012). Recently, TDZ has been demonstrated to inhibit proliferation and induce apoptosis in several cancer cell types including brain (Johannessen et al., 2019), lung (Yue et al., 2016), colon (Zhang et al., 2017), ovarian (Yong et al., 2017) and breast cancers (Tegowski et al., 2018). However, less is known about its anti-tumorigenic effects in prostate cancer. We demonstrated that, much like targeting DECR2, inhibition of peroxisomal beta oxidation by TDZ significantly attenuated prostate cancer cell growth, colony formation and migration, and induced cell death by apoptosis. Moreover, we demonstrated that TDZ significantly attenuated cellular proliferation in PDEs, suggesting that peroxisomal beta oxidation inhibition may be a promising treatment strategy. Interestingly, PDEs from certain patients responded more strongly to TDZ than others; an important future avenue will be to identify biomarkers to aid in the selection of optimal patients for treatment with TDZ. Of note, the enhanced effect of TDZ on prostate cancer cell viability when treated in combination with enzalutamide suggests that targeting peroxisomal beta oxidation may circumvent the development of resistance. While TDZ has been claimed to suppress peroxisomal beta oxidation (Van den Branden and Roels 1985; Shi et al. 2012), it is important to note that there is currently no

evidence demonstrating the specificity of TDZ for peroxisomal beta oxidation, or whether TDZ directly targets DECR2. TDZ was primarily used to treat patients with severe schizophrenia by blocking the dopamine receptor 2 (DRD2) (Feinberg et al. 2021). Alternatively, TDZ is also a substrate of the cytochrome P450 enzymes and inhibits CYP2D6 *in vitro*, and CYP1A2 and CYP3A4 in rats (Gervasini et al. 2013; Daniel et al. 2001). Cytochrome P450 enzymes have been implicated to play a role in polyunsaturated fatty acid metabolism (Sarparast et al. 2020; Konkel and Schunck 2011), suggesting that TDZ may inhibit fatty acid oxidation via its inhibitory effects on cytochrome P450 enzymes (Shen et al. 2020). While more work is needed to investigate the specificities of TDZ for peroxisomal beta oxidation, our findings corroborate the concept of targeting peroxisomal beta oxidation and the development of more selective targets of FAO such as DECR2 for prostate cancer therapy.

To date, very little is known about the role of DECR2 in cancer. In light of this, we wanted to investigate the role of DECR2 in lipid metabolism in more detail. We showed that DECR2 knockdown had profound effects on the cellular lipidome of LNCaP, V16D and MR49F prostate cancer cells, most evidently an overall accumulation of multiple lipid classes particularly CE, TAG, DAG and several phospholipid classes such as PE and PI. Similar to what was observed in another study, in which the authors also reported lipid accumulation in response to ECI2 (a peroxisomal beta oxidation enzyme) knockdown prostate cancer cells. Surprisingly, DECR2 knockdown cells accumulated high levels of both monounsaturated and polyunsaturated lipids and low levels of saturated lipids compared to control cells. Of note, we observed a consistent increase of C16:0/C16:1 and C18:0/C18:1 long chain fatty acid in several lipid classes (data not shown). Our lipidomic analysis suggest the accumulation of lipid droplets in DECR2-deficient cells and we confirmed this by BODIPY 493/503 neutral lipid staining with flow cytometry. Furthermore, we also evaluated lipid droplet content in prostate cancer cells treated with TDZ and observed a similar phenotype. It is unclear why DECR2 or peroxisomal beta oxidation inhibition would lead to increased lipid (droplet) accumulation. Evidence suggests that peroxisomes are intimately associated with lipid droplets (Lodhi and Semenkovich, 2014). One possibility is that excess VLCFAs are channelled and stored in lipid droplets to prevent lipid peroxidation or

lipotoxicity. Alterations in lipid composition have been also implicated to alter membrane properties such as membrane fluidity, in a way that promotes survival and treatment resistance in cancer cells (Rysman et al., 2010). It is also worth noting that the majority of significantly enriched lipid species in DECR2 knockdown cells were sphingomyelin (SM) species and to a lesser extent, phosphatidylcholine (PC) and phosphatidylethanolamine (PE) species. Impediment of drug uptake via passive diffusion and/or endocytosis has been linked to reduced membrane fluidity and represents a hallmark of chemo-resistant cancer cells. This can be attributed to changes in the desaturation ratio of membrane lipids, increased sphingomyelin and/or cholesterol content, and the formation of detergent-resistant membrane domains that can activate multi-drug efflux transporters (Kopecka et al., 2020; Mannechez et al., 2005; Swinnen et al., 2003; Veldman et al., 2002; Zhuang et al., 2005). Accordingly, we showed that DECR2 knockdown significantly decreased membrane fluidity in V16D and MR49F prostate cancer cells. Membrane fluidity has previously been shown to play important roles in modulating critical membrane features such as signalling domains (lipid rafts), protein channels and membrane receptors, and metastatic capacity (Edmond et al., 2015; Zhao et al., 2016; Zhuang et al., 2005). Taken together, these results suggest that DECR2 may be required for lipid homeostasis in prostate cancer cells. Future studies are still needed to elucidate the precise role of peroxisomal beta oxidation in cancer-related changes to lipid metabolism and how this may be exploited by prostate cancer cells to drive disease progression and treatment resistance. A particularly novel and interesting aspect of this study was the relationship observed between peroxisomal and mitochondrial metabolic activities. It is clear that the peroxisome and mitochondria are closely intertwined as both organelles play a central role in regulating both energy and lipid metabolism and cellular redox signalling (reviewed in (Fransen et al., 2017). It was previously reported in C. elegans that cooperation between peroxisomes and mitochondria is required to maintain mitochondrial network homeostasis and oxidative phosphorylation (Weir et al., 2017). Moreover, melanoma resistant cells (as mentioned above) utilise both mitochondrial and peroxisomal beta oxidation to promote cell survival and treatment resistance (Shen et al., 2020). Hence, it is reasonable to speculate that cancer-related alterations in peroxisomal beta oxidation, and its therapeutic targeting, may have an impact on mitochondrial metabolism (Tanaka et al., 2019). Intriguingly, oxidative

phosphorylation or mitochondrial respiration was maintained in DECR2 knockdown cells as demonstrated using the seahorse metabolic assay. It is possible that excess intracellular fatty acids are being oxidised in the mitochondria to compensate for the loss of beta oxidation capacity in the peroxisomes and prevent toxic lipid accumulation in the cells. In line with this concept, a study reported that peroxisomal beta oxidation inhibition by TDZ selectively kills melanoma cells via steatosis (excess lipid accumulation)-induced cell death (Shen et al., 2020). Alternatively, mitochondrial oxidative phosphorylation or the TCA cycle could also be supported by input from other nutrient sources such as glucose or amino acids. Our findings suggest that mitochondrial fatty acid oxidation may be essential for metabolic adaptation in DECR2 knockdown cells for survival. However, the underlying mechanism remains to be elucidated. With that being said, it would be worth investigating the connection between DECR1 and DECR2. Considering that DECR2 is the peroxisomal counterpart of DECR1, it is plausible that there may be a compensatory increase in DECR1 expression to protect cells from the consequences of DECR2 knockdown/inhibition, and dual targeting may elicit a more effective response. Having said that, one important limitation of this study is the lack of evidence validating peroxisomal beta oxidation inhibition after DECR2 knockdown or by TDZ. To do this, one of the methods we would be employing is the measurement of acyl carnitines, as we had previously demonstrated in DECR1 knockdown cells accumulation of certain acyl carnitine species, indicative of beta oxidation inhibition (Nassar et al., 2020b).

One of the cellular processes most markedly affected by DECR2 or peroxisomal beta oxidation inhibition was cell cycle progression. Consistent with a previous study on the related enzyme ECI2 (Itkonen et al., 2017), we report that DECR2 knockdown or peroxisomal beta oxidation inhibition by TDZ markedly arrested cell cycle progression in particular at the G1 phase, while overexpression of DECR2 showed an accelerated rate of cell cycle progression. To further investigate this, we analysed protein expression of key cell cycle-related proteins and regulators involved in the G1-to-S phase transition. Notably, we observed an increase in cyclin-dependent kinase inhibitors p21 and p27 and cyclin D1, and a decrease in cyclin-dependent kinase CDK4 and phosphorylated retinoblastoma (pRb) tumour suppressor protein in DECR2 knockdown cells compared to control cells. It is not known whether these

effects are caused directly by DECR2 or are downstream effects arising from peroxisomal beta oxidation inhibition. Nonetheless, we demonstrated that Ribociclib (a CDK4/6 inhibitor) could further suppress prostate cancer cell viability after DECR2 knockdown or in combination with TDZ, which suggests a novel combinatorial strategy. It was surprising that DECR2-induced lipid accumulation did not promote prostate cancer cell proliferation, as rapidly proliferating cells have an increased need for lipids (Cruz et al., 2019). There is emerging evidence that there exists an interplay between cellular metabolism and the cell cycle machinery (Huber et al., 2020; Kaplon et al., 2015). Of particular interest is the connection between lipid metabolism and cell cycle progression (Huber et al., 2020; Kaplon et al., 2015). Certain lipid species such as DAG, SM or Cer that can act as second messengers, as well as changes in acyl chain composition of membrane lipids such as PCs are known to impact the regulation of oncogenic signalling pathways (Francis et al., 2020). Some studies have linked Rb/pRb to the control of lipid metabolism, including but not limited to modulation of mitochondrial oxidative phosphorylation (Sanidas et al., 2019) and lipid remodelling (ie. elongation and desaturation) (Muranaka et al., 2017). In addition, Rb/pRb is able to cooperate with various metabolic pathways (ie. mTORC1, SREBP, PI3K/AKT) to facilitate homeostatic control of cellular metabolism (Takahashi et al., 2012). More extensive work will be needed to determine the relationship between DECR2 or peroxisomal beta oxidation inhibition induced lipid dysregulation and cell cycle progression most likely mediated by upstream oncogenic signalling pathways. While it is important to investigate the expression levels of cell cycle-related genes and proteins, the activation or inactivation of cell cycle-related proteins are mainly influenced by their phosphorylation state. Future studies should include analysis of protein phosphorylation and potentially other post-translational modifications to further confirm these observations. To this end, an interesting observation from our cell cycle study is the fluctuation in protein levels of histone H3 acetylation in DECR2 knockdown and TDZ-treated cells suggesting a link between peroxisomal beta oxidation inhibition and epigenetic modifications, potentially driven by acetyl-CoA availability. Hence, we examined the effect of DECR2 knockdown in cells treated with the histone deacetylase (HDAC) inhibitor, suberoylanilide hydroxamic acid (SAHA). A previous study demonstrated that peroxisomes are able to protect lymphoma cells from HDAC inhibitor-mediated apoptosis by upregulating

peroxisome abundance (Dahabieh et al., 2017). Although our data remains inconclusive, we should not overlook the relevance of our current observations to epigenetics.

Limited studies have examined the role of peroxisomal beta oxidation in prostate cancer progression and ARI resistance. Herein we explored the effects of peroxisomal beta oxidation inhibition (either by molecular targeting of DECR2 or pharmacological inhibition by thioridazine) on lipid metabolism and shed light on potential mechanisms or functional roles that may facilitate our understanding of peroxisomal beta oxidation in cancer progression and treatment resistance. In addition, we provide evidence that targeting peroxisomal beta oxidation is a promising new therapeutic avenue for the treatment of prostate cancer and that DECR2 represents an exciting novel candidate that may afford greater selectivity in targeting this critical cellular process.

4.7 References

1. Alphey, M.S., Yu, W., Byres, E., Li, D., Hunter, W.N., 2005. Structure and reactivity of human mitochondrial 2,4-dienoyl-CoA reductase: enzyme-ligand interactions in a distinctive short-chain reductase active site. J. Biol. Chem. 280, 3068–3077. doi:10.1074/jbc.M411069200
2. Ananthanarayanan, V., Deaton, R.J., Yang, X.J., Pins, M.R., Gann, P.H., 2005. Alpha-methylacyl-CoA racemase (AMACR) expression in normal prostatic glands and high-grade prostatic intraepithelial neoplasia (HGPIN): association with diagnosis of prostate cancer. Prostate 63, 341–346. doi:10.1002/pros.20196
3. Armstrong, H.K., Koay, Y.C., Irani, S., Das, R., Nassar, Z.D., Australian Prostate Cancer BioResource, Selth, L.A., Centenera, M.M., McAlpine, S.R., Butler, L.M., 2016. A Novel Class of Hsp90 C-Terminal Modulators Have Pre-Clinical Efficacy in Prostate Tumor Cells Without Induction of a Heat Shock Response. Prostate 76, 1546–1559. doi:10.1002/pros.23239
4. Balaban, S., Nassar, Z.D., Zhang, A.Y., Hosseini-Beheshti, E., Centenera, M.M., Schreuder, M., Lin, H.-M., Aishah, A., Varney, B., Liu-Fu, F., Lee, L.S., Nagarajan, S.R., Shearer, R.F., Hardie, R.-A., Raftopulos, N.L., Kakani, M.S., Saunders, D.N., Holst, J., Horvath, L.G., Butler, L.M., Hoy, A.J., 2019. Extracellular fatty acids are the major contributor to lipid synthesis in prostate cancer. Mol. Cancer Res. 17, 949–962. doi:10.1158/1541-7786.MCR-18-0347
5. Blomme, A., Ford, C.A., Mui, E., Patel, R., Ntala, C., Jamieson, L.E., Planque, M., McGregor, G.H., Peixoto, P., Hervouet, E., Nixon, C., Salji, M., Gaughan, L., Markert, E., Repiscak, P., Sumpton, D., Blanco, G.R., Lilla, S., Kamphorst, J.J., Graham, D., Faulds, K., MacKay, G.M., Fendt, S.-M., Zanivan, S., Leung, H.Y., 2020. 2,4-dienoyl-CoA reductase regulates lipid homeostasis in treatment-resistant prostate cancer. Nat. Commun. 11, 2508. doi:10.1038/s41467-020-16126-7
6. Butler, L.M., Mah, C.Y., Machiels, J., Vincent, A.D., Irani, S., Mutuku, S., Spotbeen, X., Bagadi, M., Waltregny, D., Moldovan, M., Dehairs, J., Vanderhoydonc, F., Bloch, K., Das, R., Stahl, J., Kench, J., Gevaert, T., Derua, R., Waelkens, E., Nassar, Z.D., Selth, L.A., Trim, P.J., Snel, M.F., Lynn, D.J., Tilley, W.D., Horvath, L.G., Centenera, M.M., Swinnen, J.V., 2020. Lipidomic

profiling of clinical prostate cancer reveals targetable alterations in membrane lipid composition. BioRxiv. doi:10.1101/2020.10.27.356634

7. Centenera, M.M., Hickey, T.E., Jindal, S., Ryan, N.K., Ravindranathan, P., Mohammed, H., Robinson, J.L., Schiewer, M.J., Ma, S., Kapur, P., Sutherland, P.D., Hoffmann, C.E., Roehrborn, C.G., Gomella, L.G., Carroll, J.S., Birrell, S.N., Knudsen, K.E., Raj, G.V., Butler, L.M., Tilley, W.D., 2018. A patient-derived explant (PDE) model of hormone-dependent cancer. Mol. Oncol. 12, 1608–1622. doi:10.1002/1878-0261.12354
8. Cruz, A.L.S., Carrossini, N., Teixeira, L.K., Ribeiro-Pinto, L.F., Bozza, P.T., Viola, J.P.B., 2019. Cell cycle progression regulates biogenesis and cellular localization of lipid droplets. Mol. Cell. Biol. 39. doi:10.1128/MCB.00374-18
9. Dahabieh, M.S., Ha, Z., Di Pietro, E., Nichol, J.N., Bolt, A.M., Goncalves, C., Dupéré-Richer, D., Pettersson, F., Mann, K.K., Braverman, N.E., Del Rincón, S.V., Miller, W.H., 2017. Peroxisomes protect lymphoma cells from HDAC inhibitor-mediated apoptosis. Cell Death Differ. 24, 1912–1924. doi:10.1038/cdd.2017.115
10. Daniel, W.A., Syrek, M., Ryłko, Z. and Kot, M. 2001. Effects of phenothiazine neuroleptics on the rate of caffeine demethylation and hydroxylation in the rat liver. Polish journal of pharmacology 53(6), pp. 615–621.
11. De Nys, K., Meyhi, E., Mannaerts, G.P., Fransen, M., Van Veldhoven, P.P., 2001. Characterisation of human peroxisomal 2,4-dienoyl-CoA reductase. Biochim. Biophys. Acta 1533, 66–72. doi:10.1016/s1388-1981(01)00141-x
12. Dheeraj, A., Agarwal, C., Schlaepfer, I.R., Raben, D., Singh, R., Agarwal, R., Deep, G., 2018. A novel approach to target hypoxic cancer cells via combining β-oxidation inhibitor etomoxir with radiation. Hypoxia (Auckl) 6, 23–33. doi:10.2147/HP.S163115
13. Edmond, V., Dufour, F., Poiroux, G., Shoji, K., Malleter, M., Fouqué, A., Tauzin, S., Rimokh, R., Sergent, O., Penna, A., Dupuy, A., Levade, T., Theret, N., Micheau, O., Ségui, B., Legembre, P., 2015. Downregulation of ceramide synthase-6 during epithelial-to-mesenchymal transition reduces plasma membrane fluidity and cancer cell motility. Oncogene 34, 996–1005. doi:10.1038/onc.2014.55
14. Ettinger, S.L., Sobel, R., Whitmore, T.G., Akbari, M., Bradley, D.R., Gleave, M.E., Nelson, C.C., 2004. Dysregulation of sterol response element-binding proteins

and downstream effectors in prostate cancer during progression to androgen independence. Cancer Res. 64, 2212–2221.

15. Feinberg, S.M., Fariba, K. and Saadabadi, A. 2021. Thioridazine. In: StatPearls. Treasure Island (FL): StatPearls Publishing.
16. Flaig, T.W., Salzmann-Sullivan, M., Su, L.-J., Zhang, Z., Joshi, M., Gijón, M.A., Kim, J., Arcaroli, J.J., Van Bokhoven, A., Lucia, M.S., La Rosa, F.G., Schlaepfer, I.R., 2017. Lipid catabolism inhibition sensitizes prostate cancer cells to antiandrogen blockade. Oncotarget 8, 56051–56065. doi:10.18632/oncotarget.17359
17. Francis, M., Abou Daher, A., Azzam, P., Mroueh, M., Zeidan, Y.H., 2020. Modulation of DNA Damage Response by Sphingolipid Signaling: An Interplay that Shapes Cell Fate. Int. J. Mol. Sci. 21. doi:10.3390/ijms21124481
18. Fransen, M., Lismont, C., Walton, P., 2017. The Peroxisome-Mitochondria Connection: How and Why? Int. J. Mol. Sci. 18. doi:10.3390/ijms18061126
19. Gervasini, G., Caballero, M.J., Carrillo, J.A. and Benitez, J. 2013. Comparative cytochrome p450 in vitro inhibition by atypical antipsychotic drugs. ISRN pharmacology 2013, p. 792456.
20. Holubarsch, C.J.F., Rohrbach, M., Karrasch, M., Boehm, E., Polonski, L., Ponikowski, P., Rhein, S., 2007. A double-blind randomized multicentre clinical trial to evaluate the efficacy and safety of two doses of etomoxir in comparison with placebo in patients with moderate congestive heart failure: the ERGO (etomoxir for the recovery of glucose oxidation) study. Clin. Sci. 113, 205–212. doi:10.1042/CS20060307
21. Huber, K., Mestres-Arenas, A., Fajas, L., Leal-Esteban, L.C., 2020. The multifaceted role of cell cycle regulators in the coordination of growth and metabolism. FEBS J. doi:10.1111/febs.15586
22. Huggins, C., Hodges, C.V., 1972. Studies on prostatic cancer. I. The effect of castration, of estrogen and androgen injection on serum phosphatases in metastatic carcinoma of the prostate. CA Cancer J Clin 22, 232–240. doi:10.3322/canjclin.22.4.232
23. Iglesias-Gato, D., Thysell, E., Tyanova, S., Crnalic, S., Santos, A., Lima, T.S., Geiger, T., Cox, J., Widmark, A., Bergh, A., Mann, M., Flores-Morales, A., Wikström, P., 2018. The Proteome of Prostate Cancer Bone Metastasis Reveals

Heterogeneity with Prognostic Implications. Clin. Cancer Res. 24, 5433–5444. doi:10.1158/1078-0432.CCR-18-1229

24. Islinger, M., Voelkl, A., Fahimi, H.D., Schrader, M., 2018. The peroxisome: an update on mysteries 2.0. Histochem. Cell Biol. 150, 443–471. doi:10.1007/s00418-018-1722-5
25. Itkonen, H.M., Brown, M., Urbanucci, A., Tredwell, G., Ho Lau, C., Barfeld, S., Hart, C., Guldvik, I.J., Takhar, M., Heemers, H.V., Erho, N., Bloch, K., Davicioni, E., Derua, R., Waelkens, E., Mohler, J.L., Clarke, N., Swinnen, J.V., Keun, H.C., Rekvig, O.P., Mills, I.G., 2017. Lipid degradation promotes prostate cancer cell survival. Oncotarget 8, 38264–38275. doi:10.18632/oncotarget.16123
26. Jiang, Z., Woda, B.A., Wu, C.-L., Yang, X.J., 2004. Discovery and clinical application of a novel prostate cancer marker: alpha-methylacyl CoA racemase (P504S). Am. J. Clin. Pathol. 122, 275–289. doi:10.1309/EJUY-UQPE-X1MG-68MK
27. Johannessen, T.-C., Hasan-Olive, M.M., Zhu, H., Denisova, O., Grudic, A., Latif, M.A., Saed, H., Varughese, J.K., Røsland, G.V., Yang, N., Sundstrøm, T., Nordal, A., Tronstad, K.J., Wang, J., Lund-Johansen, M., Simonsen, A., Janji, B., Westermarck, J., Bjerkvig, R., Prestegarden, L., 2019. Thioridazine inhibits autophagy and sensitizes glioblastoma cells to temozolomide. Int. J. Cancer 144, 1735–1745. doi:10.1002/ijc.31912
28. Kaplon, J., van Dam, L., Peeper, D., 2015. Two-way communication between the metabolic and cell cycle machineries: the molecular basis. Cell Cycle 14, 2022–2032. doi:10.1080/15384101.2015.1044172
29. Konkel, A. and Schunck, W.-H. 2011. Role of cytochrome P450 enzymes in the bioactivation of polyunsaturated fatty acids. Biochimica et Biophysica Acta 1814(1), pp. 210–222.
30. Kopecka, J., Trouillas, P., Gašparović, A.Č., Gazzano, E., Assaraf, Y.G., Riganti, C., 2020. Phospholipids and cholesterol: Inducers of cancer multidrug resistance and therapeutic targets. Drug Resist Updat 49, 100670. doi:10.1016/j.drup.2019.100670
31. Li, W., Cohen, A., Sun, Y., Squires, J., Braas, D., Graeber, T.G., Du, L., Li, G., Li, Z., Xu, X., Chen, X., Huang, J., 2016. The role of CD44 in glucose metabolism in prostatic small cell neuroendocrine carcinoma. Mol. Cancer Res. 14, 344–353. doi:10.1158/1541-7786.MCR-15-0466

32. Liu, Y., 2006. Fatty acid oxidation is a dominant bioenergetic pathway in prostate cancer. Prostate Cancer Prostatic Dis. 9, 230–234. doi:10.1038/sj.pcan.4500879
33. Lodhi, I.J., Semenkovich, C.F., 2014. Peroxisomes: a nexus for lipid metabolism and cellular signaling. Cell Metab. 19, 380–392. doi:10.1016/j.cmet.2014.01.002
34. Ma, Y., Wang, W., Devarakonda, T., Zhou, H., Wang, X.-Y., Salloum, F.N., Spiegel, S., Fang, X., 2020. Functional analysis of molecular and pharmacological modulators of mitochondrial fatty acid oxidation. Sci. Rep. 10, 1450. doi:10.1038/s41598-020-58334-7
35. Mah, C.Y., Nassar, Z.D., Swinnen, J.V., Butler, L.M., 2020. Lipogenic effects of androgen signaling in normal and malignant prostate. Asian Journal of Urology 7, 258–270. doi:10.1016/j.ajur.2019.12.003
36. Mannechez, A., Reungpatthanaphong, P., de Certaines, J.D., Leray, G., Le Moyec, L., 2005. Proton NMR visible mobile lipid signals in sensitive and multidrug-resistant K562 cells are modulated by rafts. Cancer Cell Int. 5, 2. doi:10.1186/1475-2867-5-2
37. Massie, C.E., Lynch, A., Ramos-Montoya, A., Boren, J., Stark, R., Fazli, L., Warren, A., Scott, H., Madhu, B., Sharma, N., Bon, H., Zecchini, V., Smith, D.-M., Denicola, G.M., Mathews, N., Osborne, M., Hadfield, J., Macarthur, S., Adryan, B., Lyons, S.K., Brindle, K.M., Griffiths, J., Gleave, M.E., Rennie, P.S., Neal, D.E., Mills, I.G., 2011. The androgen receptor fuels prostate cancer by regulating central metabolism and biosynthesis. EMBO J. 30, 2719–2733. doi:10.1038/emboj.2011.158
38. Muranaka, H., Hayashi, A., Minami, K., Kitajima, S., Kohno, S., Nishimoto, Y., Nagatani, N., Suzuki, M., Kulathunga, L.A.N., Sasaki, N., Okada, N., Matsuzaka, T., Shimano, H., Tada, H., Takahashi, C., 2017. A distinct function of the retinoblastoma protein in the control of lipid composition identified by lipidomic profiling. Oncogenesis 6, e350. doi:10.1038/oncsis.2017.51
39. Nambiar, D.K., Deep, G., Singh, R.P., Agarwal, C., Agarwal, R., 2014. Silibinin inhibits aberrant lipid metabolism, proliferation and emergence of androgen-independence in prostate cancer cells via primarily targeting the sterol response element binding protein 1. Oncotarget 5, 10017–10033. doi:10.18632/oncotarget.2488

40. Nassar, Z.D., Mah, C.Y., Centenera, M.M., Irani, S., Sadowski, M.C., Scott, J.S., Nguyen, E.V., Nagarajan, S.R., Moldovan, M., Lynn, D.J., Daly, R.J., Hoy, A.J., Butler, L.M., 2020a. Fatty acid oxidation is an adaptive survival pathway induced in prostate tumors by HSP90 inhibition. Mol. Cancer Res. 18, 1500–1511. doi:10.1158/1541-7786.MCR-20-0570
41. Nassar, Z.D., Mah, C.Y., Dehairs, J., Burvenich, I.J., Irani, S., Centenera, M.M., Helm, M., Shrestha, R.K., Moldovan, M., Don, A.S., Holst, J., Scott, A.M., Horvath, L.G., Lynn, D.J., Selth, L.A., Hoy, A.J., Swinnen, J.V., Butler, L.M., 2020b. Human DECR1 is an androgen-repressed survival factor that regulates PUFA oxidation to protect prostate tumor cells from ferroptosis. Elife 9. doi:10.7554/eLife.54166
42. Purhonen, M., Koponen, H., Tiihonen, J., Tanskanen, A., 2012. Outcome of patients after market withdrawal of thioridazine: a retrospective analysis in a nationwide cohort. Pharmacoepidemiol Drug Saf 21, 1227–1231. doi:10.1002/pds.3346
43. Rysman, E., Brusselmans, K., Scheys, K., Timmermans, L., Derua, R., Munck, S., Van Veldhoven, P.P., Waltregny, D., Daniëls, V.W., Machiels, J., Vanderhoydonc, F., Smans, K., Waelkens, E., Verhoeven, G., Swinnen, J.V., 2010. De novo lipogenesis protects cancer cells from free radicals and chemotherapeutics by promoting membrane lipid saturation. Cancer Res. 70, 8117–8126. doi:10.1158/0008-5472.CAN-09-3871
44. Sanidas, I., Morris, R., Fella, K.A., Rumde, P.H., Boukhali, M., Tai, E.C., Ting, D.T., Lawrence, M.S., Haas, W., Dyson, N.J., 2019. A Code of Mono-phosphorylation Modulates the Function of RB. Mol. Cell 73, 985–1000.e6. doi:10.1016/j.molcel.2019.01.004
45. Sarparast, M., Dattmore, D., Alan, J. and Lee, K.S.S. 2020. Cytochrome P450 metabolism of polyunsaturated fatty acids and neurodegeneration. Nutrients 12(11).
46. Scher, H.I., Fizazi, K., Saad, F., Taplin, M.-E., Sternberg, C.N., Miller, K., de Wit, R., Mulders, P., Chi, K.N., Shore, N.D., Armstrong, A.J., Flaig, T.W., Fléchon, A., Mainwaring, P., Fleming, M., Hainsworth, J.D., Hirmand, M., Selby, B., Seely, L., de Bono, J.S., AFFIRM Investigators, 2012. Increased survival with enzalutamide in prostate cancer after chemotherapy. N. Engl. J. Med. 367, 1187–1197. doi:10.1056/NEJMoa1207506

47. Schlaepfer, I.R., Rider, L., Rodrigues, L.U., Gijón, M.A., Pac, C.T., Romero, L., Cimic, A., Sirintrapun, S.J., Glodé, L.M., Eckel, R.H., Cramer, S.D., 2014. Lipid catabolism via CPT1 as a therapeutic target for prostate cancer. Mol. Cancer Ther. 13, 2361–2371. doi:10.1158/1535-7163.MCT-14-0183
48. Schulte, M.L., Fu, A., Zhao, P., Li, J., Geng, L., Smith, S.T., Kondo, J., Coffey, R.J., Johnson, M.O., Rathmell, J.C., Sharick, J.T., Skala, M.C., Smith, J.A., Berlin, J., Washington, M.K., Nickels, M.L., Manning, H.C., 2018. Pharmacological blockade of ASCT2-dependent glutamine transport leads to antitumor efficacy in preclinical models. Nat. Med. 24, 194–202. doi:10.1038/nm.4464
49. Shen, S., Faouzi, S., Souquere, S., Roy, S., Routier, E., Libenciuc, C., André, F., Pierron, G., Scoazec, J.-Y., Robert, C., 2020. Melanoma Persister Cells Are Tolerant to BRAF/MEK Inhibitors via ACOX1-Mediated Fatty Acid Oxidation. Cell Rep. 33, 108421. doi:10.1016/j.celrep.2020.108421
50. Shi, R., Zhang, Y., Shi, Y., Shi, S. and Jiang, L. 2012. Inhibition of peroxisomal β-oxidation by thioridazine increases the amount of VLCFAs and Aβ generation in the rat brain. Neuroscience Letters 528(1), pp. 6–10.
51. Siegel, R.L., Miller, K.D., Jemal, A., 2019. Cancer statistics, 2019. CA Cancer J Clin 69, 7–34. doi:10.3322/caac.21551
52. Swinnen, J.V., Heemers, H., van de Sande, T., de Schrijver, E., Brusselmans, K., Heyns, W., Verhoeven, G., 2004. Androgens, lipogenesis and prostate cancer. J. Steroid Biochem. Mol. Biol. 92, 273–279. doi:10.1016/j.jsbmb.2004.10.013
53. Swinnen, J.V., Van Veldhoven, P.P., Timmermans, L., De Schrijver, E., Brusselmans, K., Vanderhoydonc, F., Van de Sande, T., Heemers, H., Heyns, W., Verhoeven, G., 2003. Fatty acid synthase drives the synthesis of phospholipids partitioning into detergent-resistant membrane microdomains. Biochem. Biophys. Res. Commun. 302, 898–903. doi:10.1016/s0006-291x(03)00265-1
54. Takahashi, C., Sasaki, N., Kitajima, S., 2012. Twists in views on RB functions in cellular signaling, metabolism and stem cells. Cancer Sci. 103, 1182–1188. doi:10.1111/j.1349-7006.2012.02284.x
55. Tanaka, H., Okazaki, T., Aoyama, S., Yokota, M., Koike, M., Okada, Y., Fujiki, Y., Gotoh, Y., 2019. Peroxisomes control mitochondrial dynamics and the

mitochondrion-dependent apoptosis pathway. J. Cell Sci. 132. doi:10.1242/jcs.224766

56. Tegowski, M., Fan, C., Baldwin, A.S., 2018. Thioridazine inhibits self-renewal in breast cancer cells via DRD2-dependent STAT3 inhibition, but induces a G1 arrest independent of DRD2. J. Biol. Chem. 293, 15977–15990. doi:10.1074/jbc.RA118.003719
57. Toren, P., Kim, S., Johnson, F., Zoubeidi, A., 2016. Combined AKT and MEK Pathway Blockade in Pre-Clinical Models of Enzalutamide-Resistant Prostate Cancer. PLoS One 11, e0152861. doi:10.1371/journal.pone.0152861
58. Tran, C., Ouk, S., Clegg, N.J., Chen, Y., Watson, P.A., Arora, V., Wongvipat, J., Smith-Jones, P.M., Yoo, D., Kwon, A., Wasielewska, T., Welsbie, D., Chen, C.D., Higano, C.S., Beer, T.M., Hung, D.T., Scher, H.I., Jung, M.E., Sawyers, C.L., 2009. Development of a second-generation antiandrogen for treatment of advanced prostate cancer. Science 324, 787–790. doi:10.1126/science.1168175
59. Valença, I., Ferreira, A.R., Correia, M., Kühl, S., van Roermund, C., Waterham, H.R., Máximo, V., Islinger, M., Ribeiro, D., 2020. Prostate cancer proliferation is affected by the subcellular localization of MCT2 and accompanied by significant peroxisomal alterations. Cancers (Basel) 12. doi:10.3390/cancers12113152
60. Van den Branden, C., Roels, F., 1985. Thioridazine: a selective inhibitor of peroxisomal beta-oxidation in vivo. FEBS Lett. 187, 331–333. doi:10.1016/0014-5793(85)81270-9
61. Veldman, R.J., Klappe, K., Hinrichs, J., Hummel, I., van der Schaaf, G., Sietsma, H., Kok, J.W., 2002. Altered sphingolipid metabolism in multidrug-resistant ovarian cancer cells is due to uncoupling of glycolipid biosynthesis in the Golgi apparatus. FASEB J. 16, 1111–1113. doi:10.1096/fj.01-0863fje
62. Watt, M.J., Clark, A.K., Selth, L.A., Haynes, V.R., Lister, N., Rebello, R., Porter, L.H., Niranjan, B., Whitby, S.T., Lo, J., Huang, C., Schittenhelm, R.B., Anderson, K.E., Furic, L., Wijayaratne, P.R., Matzaris, M., Montgomery, M.K., Papargiris, M., Norden, S., Febbraio, M., Risbridger, G.P., Frydenberg, M., Nomura, D.K., Taylor, R.A., 2019. Suppressing fatty acid uptake has therapeutic effects in preclinical models of prostate cancer. Sci. Transl. Med. 11. doi:10.1126/scitranslmed.aau5758

63. Weir, H.J., Yao, P., Huynh, F.K., Escoubas, C.C., Goncalves, R.L., Burkewitz, K., Laboy, R., Hirschey, M.D., Mair, W.B., 2017. Dietary restriction and AMPK increase lifespan via mitochondrial network and peroxisome remodeling. Cell Metab. 26, 884–896.e5. doi:10.1016/j.cmet.2017.09.024
64. Wu, X., Daniels, G., Lee, P., Monaco, M.E., 2014. Lipid metabolism in prostate cancer. Am. J. Clin. Exp. Urol. 2, 111–120.
65. Yong, M., Yu, T., Tian, S., Liu, S., Xu, J., Hu, J., Hu, L., 2017. DR2 blocker thioridazine: A promising drug for ovarian cancer therapy. Oncol. Lett. 14, 8171–8177. doi:10.3892/ol.2017.7184
66. Yue, H., Huang, D., Qin, L., Zheng, Z., Hua, L., Wang, G., Huang, J., Huang, H., 2016. Targeting Lung Cancer Stem Cells with Antipsychological Drug Thioridazine. Biomed Res. Int. 2016, 6709828. doi:10.1155/2016/6709828
67. Zacharias, N.M., McCullough, C., Shanmugavelandy, S., Lee, J., Lee, Y., Dutta, P., McHenry, J., Nguyen, L., Norton, W., Jones, L.W., Bhattacharya, P.K., 2017. Metabolic differences in glutamine utilization lead to metabolic vulnerabilities in prostate cancer. Sci. Rep. 7, 16159. doi:10.1038/s41598-017-16327-z
68. Zadra, G., Loda, M., 2018. Metabolic vulnerabilities of prostate cancer: diagnostic and therapeutic opportunities. Cold Spring Harb. Perspect. Med. 8. doi:10.1101/cshperspect.a030569
69. Zadra, G., Ribeiro, C.F., Chetta, P., Ho, Y., Cacciatore, S., Gao, X., Syamala, S., Bango, C., Photopoulos, C., Huang, Y., Tyekucheva, S., Bastos, D.C., Tchaicha, J., Lawney, B., Uo, T., D'Anello, L., Csibi, A., Kalekar, R., Larimer, B., Ellis, L., Butler, L.M., Morrissey, C., McGovern, K., Palombella, V.J., Kutok, J.L., Mahmood, U., Bosari, S., Adams, J., Peluso, S., Dehm, S.M., Plymate, S.R., Loda, M., 2019. Inhibition of de novo lipogenesis targets androgen receptor signaling in castration-resistant prostate cancer. Proc. Natl. Acad. Sci. USA 116, 631–640. doi:10.1073/pnas.1808834116
70. Zaugg, K., Yao, Y., Reilly, P.T., Kannan, K., Kiarash, R., Mason, J., Huang, P., Sawyer, S.K., Fuerth, B., Faubert, B., Kalliomäki, T., Elia, A., Luo, X., Nadeem, V., Bungard, D., Yalavarthi, S., Growney, J.D., Wakeham, A., Moolani, Y., Silvester, J., Ten, A.Y., Bakker, W., Tsuchihara, K., Berger, S.L., Hill, R.P., Jones, R.G., Tsao, M., Robinson, M.O., Thompson, C.B., Pan, G., Mak, T.W., 2011. Carnitine palmitoyltransferase 1C promotes cell survival and tumor growth under

conditions of metabolic stress. Genes Dev. 25, 1041–1051. doi:10.1101/gad.1987211

71. Zhang, C., Gong, P., Liu, P., Zhou, N., Zhou, Y., Wang, Y., 2017. Thioridazine elicits potent antitumor effects in colorectal cancer stem cells. Oncol. Rep. 37, 1168–1174. doi:10.3892/or.2016.5313
72. Zhao, W., Prijic, S., Urban, B.C., Tisza, M.J., Zuo, Y., Li, L., Tan, Z., Chen, X., Mani, S.A., Chang, J.T., 2016. Candidate antimetastasis drugs suppress the metastatic capacity of breast cancer cells by reducing membrane fluidity. Cancer Res. 76, 2037–2049. doi:10.1158/0008-5472.CAN-15-1970
73. Zhuang, L., Kim, J., Adam, R.M., Solomon, K.R., Freeman, M.R., 2005. Cholesterol targeting alters lipid raft composition and cell survival in prostate cancer cells and xenografts. J. Clin. Invest. 115, 959–968. doi:10.1172/JCI1993

Chapter 5: Fatty acid oxidation contributes to treatment resistance in prostate cancer

This Chapter contains a publication that makes up a portion of the work completed as part of this PhD.

5.1 Introduction

Fatty acid oxidation represents a metabolic vulnerability that is exploitable for prostate cancer therapy. As demonstrated in Chapters 3 and 4, (mitochondrial and peroxisomal) fatty acid oxidation pathways are significantly upregulated in prostate cancer compared to normal prostate cells. Previous studies have shown that fatty acid oxidation inhibition sensitises prostate cancer cells to AR-targeted therapies. Furthermore, we showed in Chapter 3 that DECR1 is an androgen-repressed gene that is elevated in response to castration and enzalutamide treatment suggesting that DECR1 may contribute to treatment resistance. Similarly in Chapter 4, we reported a close association between peroxisomal pathway genes (or DECR2) and acquired resistance to AR inhibition. Therefore, it is plausible that fatty acid oxidation pathways are upregulated in response to AR inhibition as an adaptive survival pathway to promote prostate cancer cell survival and potentially drive treatment resistance. In Chapter 5, the aim was to investigate the potential of fatty acid oxidation to drive treatment resistance in prostate cancer.

STATEMENT OF AUTHORSHIP

Title of Paper	Fatty acid oxidation is an adaptive survival pathway induced in prostate tumors by heat shock protein 90 inhibition
Publication Status	☒ Published ☐ Submitted for Publication ☐ Accepted for Publication ☐ Unpublished and Unsubmitted work written in a manuscript style
Publication Details	Nassar, ZD, Mah, CY, Centenera, MM, Irani, S, Sadowski, MC, Scott, JS, Nguyen, EV, Nagarajan, SR, Moldovan, M, Lynn, DJ, Daly, RJ, Hoy, AJ & Butler, LM 2020, 'Fatty acid oxidation is an adaptive survival pathway induced in prostate tumors by heat shock protein 90 inhibition', *Molecular Cancer Research*, advance online publication, DOI: https://doi.org/10.1158/1541-7786.MCR-20-0570.

Principal Author

Name of Principal Author	Zeyad Nassar	
Contribution to the Paper	Conceptualization, Investigation, Data curation, Funding acquisition, Visualization, Writing – Original and draft preparation, Writing – Review and editing	
Signature		Date: 26/03/2021

Co-Author Contributions

By signing the Statement of Authorship, each author certifies that:

i. the candidate's stated contribution to the publication is accurate (as detailed above);
ii. permission is granted for the candidate to include the publication in the thesis; and
iii. the sum of all co-author contributions is equal to 100% less than the candidate's stated contribution.

Name of Co-Author (Candidate)	Chui Yan Mah	
Contribution to the Paper	Investigation, Visualisation, Writing – Review and editing	
Overall Percentage (%)	25 %	
Signature		Date: 26/03/2021

Name of Co-Author	Margaret Centenera	
Contribution to the Paper	Supervision, Funding acquisition, Methodology, Writing – Review and editing	
Signature		Date: 25/03/2021

Name of Co-Author	Swati Irani		
Contribution to the Paper	Investigation, Methodology, Writing – Review and editing		
Signature		Date:	30/03/2021

Name of Co-Author	Martin Sadowski		
Contribution to the Paper	Investigation, Writing – Review and editing		
Signature		Date:	28/03/2021

Name of Co-Author	Julia Scott		
Contribution to the Paper	Investigation, Writing – Review and editing		
Signature		Date:	22/03/2021

Name of Co-Author	Elizabeth Nguyen		
Contribution to the Paper	Resources, Investigation, Writing – Review and editing		
Signature		Date:	01/04/2021

Name of Co-Author	Shilpa Nagarajan		
Contribution to the Paper	Investigation, Writing – Review and editing		
Signature		Date:	01/04/2021

Name of Co-Author	Max Moldovan		
Contribution to the Paper	Data curation, Formal analysis, Investigation, Writing – Review and editing		
Signature		Date:	24 Mar 2021

Name of Co-Author	David Lynn		
Contribution to the Paper	Data curation, Formal analysis, Supervision, Writing – Review and editing		
Signature		Date:	22/3/21

Name of Co-Author	Roger Daly		
Contribution to the Paper	Resources, Funding acquisition, Writing – Review and editing		
Signature		Date:	23.03.2021

Name of Co-Author	Andrew Hoy		
Contribution to the Paper	Conceptualization, Supervision, Funding acquisition, Investigation, Writing – Review and editing		
Signature		Date:	22 March 2021

Name of Co-Author	Lisa Butler		
Contribution to the Paper	Conceptualization, Resources, Supervision, Funding acquisition, Writing – Original and draft preparation, Project administration, Writing – Review and editing		
Signature		Date:	01/04/2021

Published OnlineFirst July 15, 2020; DOI: 10.1158/1541-7786.MCR-20-0570

MOLECULAR CANCER RESEARCH | METABOLISM

Fatty Acid Oxidation Is an Adaptive Survival Pathway Induced in Prostate Tumors by HSP90 Inhibition

Zeyad D. Nassar[1,2,3], Chui Yan Mah[1,2,3], Margaret M. Centenera[1,2,3], Swati Irani[1,3], Martin C. Sadowski[4], Julia S. Scott[1,2,3], Elizabeth V. Nguyen[5], Shilpa R. Nagarajan[6], Max Moldovan[3], David J. Lynn[3,7], Roger J. Daly[5], Andrew J. Hoy[6], and Lisa M. Butler[1,2,3]

ABSTRACT

HSP90 is a molecular chaperone required for stabilization and activation of hundreds of client proteins, including many known oncoproteins. AUY922 (luminespib), a new-generation HSP90 inhibitor, exhibits potent preclinical efficacy against several cancer types including prostate cancer. However, clinical use of HSP90 inhibitors for prostate cancer has been limited by toxicity and treatment resistance. Here, we aimed to design an effective combinatorial therapeutic regimen that utilizes subtoxic doses of AUY922, by identifying potential survival pathways induced by AUY922 in clinical prostate tumors. We conducted a proteomic analysis of 30 patient-derived explants (PDE) cultured in the absence and presence of AUY922, using quantitative mass spectrometry. AUY922 significantly increased the abundance of proteins involved in oxidative phosphorylation and fatty acid metabolism in the PDEs. Consistent with these findings, AUY922-treated prostate cancer cell lines exhibited increased mitochondrial mass and activated fatty acid metabolism processes. We hypothesized that activation of fatty acid oxidation is a potential adaptive response to AUY922 treatment and that cotargeting this process will sensitize prostate cancer cells to HSP90 inhibition. Combination treatment of AUY922 with a clinical inhibitor of fatty acid oxidation, perhexiline, synergistically decreased viability of several prostate cancer cell lines, and had significant efficacy in PDEs. The novel drug combination treatment induced cell-cycle arrest and apoptosis, and attenuated the heat shock response, a known mediator of HSP90 treatment resistance. This combination warrants further preclinical and clinical investigation as a novel strategy to overcome resistance to HSP90 inhibition.

Implications: Metabolic pathways induced in tumor cells by therapeutic agents may be critical, but targetable, mediators of treatment resistance.

Introduction

Prostate cancer is the most common cancer and the second leading cause of cancer-related deaths in men in developed countries (1). In the last decade, second-generation antiandrogen drugs have been clinically approved, and significant advances in disease detection and imaging techniques have been introduced. Nevertheless, men continue to succumb to this disease as all tumors develop resistance to current available drugs, and approximately 360,000 men worldwide died of prostate cancer in 2018 (1). Suggested strategies to overcome the emergence of drug resistance include targeting several oncogenic pathways simultaneously by inhibition of a single upstream central regulatory protein (2). Another strategy is to use combinations of drugs in which one targets the adaptive survival pathways elicited by the other/s (3). In this study, we applied both strategies; the former by targeting molecular chaperone HSP90 using AUY922 (luminespib, structure published in ref. 4), and the latter by identifying and targeting possible AUY922 treatment adaptive pathways.

HSP90 is a chaperone protein that plays an important role in stabilization, activation, and posttranslational maturation of more than 400 client proteins (https://www.picard.ch/downloads/hsp90interactors.pdf). Many HSP90 clients are oncoproteins, cell-cycle regulators, steroid hormone receptors, and transcription factors. HSP90 is overexpressed in many types of cancer including prostate cancer (5), and is thought to address the high level of cellular stress induced by hypoxia, production of reactive oxygen species (ROS), increased DNA damage, and accumulation of misfolded and aggregated proteins (6). Inhibition of HSP90 activity stimulates proteasomal degradation of its client proteins, and consequently induces cell death. Among its many client proteins, HSP90 is essential for the late-stage maturation, stability, and function of the androgen receptor (AR), the main driver of prostate tumorigenesis and diseases progression, and HSP90 inhibitors are efficient in degrading the AR (7). Since the discovery of geldanamycin in early 1990s, numerous HSP90 inhibitors were developed and more than 18 distinct inhibitors have entered phase I and II clinical trials (8); however, most clinical trials failed because of pharmacokinetic and toxicity complications. A second generation of HSP90 inhibitors with improved toxicity and solubility profiles were developed to enhance clinical efficacy. One of the most potent second-generation HSP90 inhibitors, AUY922, a synthetic resorcinylic isoxazole amide, showed modest efficacy against myeloma,

[1]Adelaide Medical School, University of Adelaide, Adelaide, South Australia, Australia. [2]Freemasons Foundation Centre for Men's Health, Adelaide, South Australia, Australia. [3]South Australian Health and Medical Research Institute, Adelaide, South Australia, Australia. [4]Australian Prostate Cancer Research Centre-Queensland, Institute of Health and Biomedical Innovation, School of Biomedical Sciences, Faculty of Health, Queensland University of Technology, Princess Alexandra Hospital, Translational Research Institute, Brisbane, Queensland, Australia. [5]Cancer Program, Biomedicine Discovery Institute and Department of Biochemistry and Molecular Biology, Monash University, Clayton, Melbourne, Australia. [6]Discipline of Physiology, School of Medical Sciences, Charles Perkins Centre, Faculty of Medicine and Health, The University of Sydney, Sydney, New South Wales, Australia. [7]College of Medicine and Public Health, Flinders University, Bedford Park, Adelaide, South Australia, Australia.

Note: Supplementary data for this article are available at Molecular Cancer Research Online (http://mcr.aacrjournals.org/).

Corresponding Author: Lisa M. Butler, University of Adelaide, School of Medicine and Freemasons Foundation Centre for Men's Health, North Terrace, Adelaide, South Australia 5001, Australia. Phone: 618-8128-4360; E-mail: lisa.butler@adelaide.edu.au

Mol Cancer Res 2020;18:1500–11

doi: 10.1158/1541-7786.MCR-20-0570

©2020 American Association for Cancer Research.

Downloaded from mcr.aacrjournals.org on January 25, 2021. © 2020 American Association for Cancer Research.

Published OnlineFirst July 15, 2020; DOI: 10.1158/1541-7786.MCR-20-0570

lung, gastrointestinal stromal tumors, and breast cancers (9–12). Preclinical studies demonstrated that AUY922 was a potent antitumor agent in prostate cancer (13, 14) and more effective than the first-generation HSP90 inhibitor, 17AAG (13). We reported that AUY922 perturbs prostate cancer cell invasion *in vitro* (15) and inhibits cell proliferation in patient-derived explants (PDE; ref. 13).

Despite this promising preclinical efficacy, AUY922 along with other HSP90 inhibitors induces heat shock response (HSR) genes via activation of the transcription factor, heat shock factor 1 (HSF1). Measurement of HSR gene induction is one of the most consistent pharmacodynamic markers of HSP90 inhibition used clinically (8). HSR genes encode a diverse set of chaperone proteins such as HSP27 and HSP70 that demonstrate cytoprotective activities (16), and their induction is a key mechanism of resistance to HSP90 inhibitors (8). Although AUY922 was considered well-tolerated in many clinical trials at dose of 70 mg/m^2 (9, 10, 12), using MTDs concomitantly increases the HSR and consequently treatment resistance. Using HSP90 inhibitors as a component in a combination regime might enable the use of lower doses of AUY922, lead to reduced activation of HSR, and result in better clinical outcomes. Only a few studies have investigated cotargeting HSP90 in prostate cancer (14, 17, 18), and little is known about effective combination therapy involving new-generation agents such as AUY922 in prostate cancer.

In our previous study, using cultured human prostate tumors, referred to as PDEs, we identified response protein biomarkers correlating with the antiproliferative response to AUY922 (19). In this study, we used this model system to identify possible survival pathways activated in response to AUY922 treatment and identified fatty acid oxidation as one of the prominent activated pathways. We then evaluated the efficacy of cotargeting HSP90 and fatty acid oxidation using prostate cancer cell lines *in vitro* and *ex vivo* PDEs. Our results suggest that targeting fatty acid oxidation sensitizes prostate cancer cells to HSP90 inhibition.

Materials and Methods

Cell lines and reagents

The human nonmalignant prostate epithelial cell line PNT1 was from the European Collection of Authenticated Cell Cultures. The prostate carcinoma cell lines LNCaP, C4-2B, and 22RV1 were obtained from the ATCC. Cell lines were authenticated by short tandem repeat profiling in March 2018 (Cell Bank Australia), and were regularly tested for *Mycoplasma* using PCR-based detection methods. The cells were propagated in RPMI1640 medium containing 10% FBS purchased from Sigma-Aldrich. Cells were cultured in 5% CO_2 in a humidified atmosphere at 37°C. New batches of cells were thawed after approximately 15 passages. All chemicals were purchased from Sigma-Aldrich, unless otherwise mentioned. AUY922 (Novartis), perhexiline, etomoxir, 2-bromopalmitate, and metformin were dissolved in DMSO. The sources and experimental conditions for the stains and primary antibodies are listed in Supplementary Table S1. Primers were obtained from Sigma-Aldrich and their sequences are detailed in Supplementary Table S2.

Ex vivo culture of human prostate tumors

PDE culture was carried out according to techniques established in our laboratory and as described previously (20). In brief, 6-mm biopsy cores were collected from men undergoing robotic radical prostatectomy at St. Andrew's Hospital (Adelaide, South Australia, Australia). The study was conducted in accordance with the Declaration of Helsinki and a written informed consent by each patient was obtained through the Australian Prostate Cancer BioResource, with ethical approval from the Human Research Ethics Committees of St Andrew's Hospital (Adelaide, South Australia, Australia) and the University of Adelaide (Adelaide, South Australia, Australia, approval H-2012-016). Clinicopathologic details of the deidentified patients are included in Supplementary Table S3. To determine the tissue tumor content, a longitudinal section of the entire tissue core was collected for hematoxylin and eosin analysis. The tissue was then dissected into small pieces (1 mm^3) and cultured on Gelatin Sponges (Gelfoam, Pfizer) presoaked in 500 μL of the cultural medium (RPMI1640 with 10% FBS, antibiotic/antimycotic solution, 0.01 mg/mL hydrocortisone, and 0.01 mg/mL insulin) in 24-well plates. Treatments were then added into each well with another 500 μL of the culture medium, and the plates were kept in 5% CO_2 in a humidified atmosphere at 37°C. After 48 hours, tissues were snap frozen in liquid nitrogen and stored at −80°C, or formalin-fixed and paraffin-embedded until further analysis.

Protein preparation and mass spectrometry analysis

Protein was extracted and prepared for mass spectrometry (MS) analysis from PDEs cultured in the absence or presence of AUY922 (500 nmol/L) as described previously (19). Samples were analyzed on an UltiMate 3000 RSLC Nano LC System (Thermo Fisher Scientific) coupled to an LTQ-Orbitrap Mass Spectrometer (LTQ-Orbitrap, Thermo Fisher Scientific).

Pathway overrepresentation analysis

Pathway overrepresentation analysis was conducted using annotations from Molecular Signatures Database v6.1 (21). To assess statistical significance, a hypergeometric test was implemented using the fisher.test function in the R v3.5.0 "stats" package. Pathways/gene sets returning an FDR adjusted $P < 5\%$ were accepted as statistically enriched, and are listed in Supplementary Table S4. Heatmaps and enrichment plots were generated using the heatmap.2 and ggplot functions from gplots and ggplot2 R packages, respectively.

IHC

Immunostaining for paraffin-embedded tissues for Ki67 and cleaved caspase-3 was conducted as described previously (20). A manual counting of at least 400 malignant cells from 10–20 randomly selected fields of view at 40× magnification was used to determine the percent of Ki67 and CC-3 positively stained nuclei.

Measurement of cell viability

Cell viability was determined using two methods, the CyQUANT Cell Proliferation Assay (Thermo Fisher Scientific) according to the manufacturer's protocol, or live imaging microscopy with the IncuCyte FLR and Zoom System (Essen BioScience). Synergism scores were determined using the SynergyFinder web application (22).

Fatty acid oxidation assay

Prostate cancer cells seeded in 6-well plates were pretreated with AUY922 for 24 hours, then washed with PBS to remove AUY922 and serum, and then incubated with freshly prepared low glucose DMEM containing [1-^{14}C] Oleate (0.5 μCi/mL; PerkinElmer), 0.5 mmol/L Oleate (Sigma-Aldrich), 1 mmol/L L-carnitine, and 2% w/v fatty acid–free BSA (BovaGen) for 4 hours. Afterwards, $^{14}CO_2$ was liberated by transferring the media into glass vials containing 1 mol/L perchloric acid and trapped in microcentrifuge tubes containing 1 M NaOH for 2 hours. NaOH was transferred to scintillation vials with 3 mL of Scintillation Cocktail (Ultima Gold, PerkinElmer). Aliquots of media

Downloaded from mcr.aacrjournals.org on January 25, 2021. © 2020 American Association for Cancer Research.

Published OnlineFirst July 15, 2020; DOI: 10.1158/1541-7786.MCR-20-0570

were transferred into scintillation vials to measure the specific activity. The radioactivity was measured using a Tri-Carb 2810TR liquid scintillation counter. Readings were normalized to total cellular protein content. Results were reported as mean pmol/minute/mg of protein ± SEM.

Flow cytometric analysis of cell cycle, apoptosis, mitochondrial mass, and cellular ROS

Prostate cancer cells were cultured in 6-well plates at a density of 3.5×10^5 per well. Cells were allowed to attach overnight, then the medium was replaced with fresh one containing treatments. Floating and adherent cells were collected and washed with ice-cold PBS. For mitochondria mass determination, cells were incubated with MitoTracker Green FM (for 30 minutes at 37°C before cell collection). For cell-cycle analysis, cells were fixed with 70% ethanol for 30 minutes at 4°C and then resuspended in 1 mL of PBS containing 100 μg/mL ribonuclease A and propidium iodide (PI). Cells were incubated in the dark for 30 minutes at room temperature before analysis. For apoptosis analysis, after washing with cold PBS, cells were resuspended in 200 μL of binding buffer (Hank's Balanced Salt Solution, 1% HEPES, and 5 Mm $CaCl_2$), Annexin V-PE, and the viability stain 7AAD. Cellular ROS were analyzed using the CellROX Deep Red Assay Kit (Thermo Fisher Scientific) according to the manufacturer's instructions. Cells were analyzed using a LSRFortessa X-20 (BD Biosciences). Data were evaluated using FlowJo version 10.

RNA isolation and quantitative real-time reverse-transcription PCR

Total RNA was isolated, and cDNA was synthesized as described previously (23). Quantitative reverse transcription PCR (RT-qPCR) was performed with a 1:10 dilution of cDNA using SYBR Green (Bio-Rad) on a CFX384 Real-Time System (Bio-Rad). Data were analyzed using the comparative C_t method and normalized by geometric averaging of internal control genes *GUSB* and *L19*.

Immunoblotting

The expression of cellular proteins of interest was measured using Western blotting as described previously (20). Protein level was normalized to the matching densitometric value of the internal control HSP90.

Statistical analysis

Results are reported as mean ± SEM. Statistical analysis was performed using GraphPad Prism (V7.0 for Windows). Differences between treatment groups were compared by one-way ANOVA followed by Tukey or Dunnett *post hoc* test. $P < 0.05$ was considered significant.

Results

AUY922 induces fatty acid oxidation and mitochondrial respiration pathways in clinical prostate tumors

Hyper reaction monitoring (HRM), a novel data-independent analysis (DIA) MS workflow, was previously performed on a cohort of 30 individual PDEs to identify novel protein markers of AUY922 activity in clinical tumors (**Fig. 1A**; ref. 19). Here, we performed pathway and gene ontology (GO) overrepresentation analysis to identify AUY922-upregulated pathways that may contribute to treatment resistance. Oxidative phosphorylation and fatty acid metabolism pathways were the top upregulated pathways in AUY922-treated explants (**Fig. 1B**). GO overrepresentation analysis confirmed the overexpression of key fatty acid pathways (Supplementary Fig. S1A). Notwithstanding the predicted high interindividual heterogeneity inherent to PDEs, heatmaps of each pathway revealed consistent activation of members of these pathways at an individual patient level (**Fig. 1C**).

We validated our results by analyzing the effect of AUY922 treatment on the expression of candidate genes involved in fatty acid metabolism in three human prostate cancer cell lines, LNCaP, C4-2B, and 22RV1. AUY922 treatment significantly induced the expression of *CPT1A, DECR1, ECH1*, and *ACADM* genes ($P < 0.05$; Supplementary Fig. S1B). We measured fatty acid β-oxidation in the prostate cancer cell lines using radiolabeled oleate. Basal levels of fatty acid oxidation in LNCaP and C4-2B cells were 3-fold higher than in PNT1 nonmalignant prostate cells (**Fig. 2A**). Consistent with the observed induction of fatty acid oxidation gene expression, treatment of the cancer cells with AUY922 significantly increased fatty acid oxidation as indicated by the increased CO_2 generation from extracellular oleate. However, AUY922 treatment did not significantly increase fatty acid oxidation in nonmalignant PNT1 cells (**Fig. 2B**).

We next measured mitochondrial mass as a surrogate marker for increased mitochondrial biogenesis, which is associated with increased cellular oxidation capacity (24). MitoTracker Green FM was used as its accumulation in mitochondria is independent of mitochondrial membrane potential. AUY922-treated LNCaP, C4-2B, and 22RV1 cells exhibited a significant increase in mitochondrial mass compared with vehicle control, suggesting an increase in mitochondrial biogenesis (**Fig. 2C**; Supplementary Fig. S1C). Furthermore, AUY922-treated cells also exhibited an increase in ROS, which is linked to increased mitochondrial mass (**Fig. 2D**; Supplementary Fig. S1D; refs. 25, 26).

Fatty acid oxidation inhibition sensitizes prostate cancer cells to AUY922 treatment

We next tested whether pharmacologic inhibition of fatty acid oxidation could sensitize prostate cancer cells to AUY922 treatment. Cells were cotreated with fatty acid oxidation inhibitors (etomoxir, perhexiline, or 2-bromopalmitate), or a mitochondrial respiratory chain complex I inhibitor (metformin). All of these tested agents sensitized cells to AUY922 treatment (Supplementary Fig. S2). We selected perhexiline for further evaluation, as an approved clinical agent. The combination of AUY922 and perhexiline significantly reduced LNCaP, C4-2B, and 22RV1 prostate cancer cell viability (**Fig. 3A**; Supplementary Fig. S3). Synergy testing using the Bliss, Zero Interaction Potency (ZIP), and Highest Single Agent (HSA) methodologies revealed synergistic activity for the AUY922 and perhexiline at multiple concentrations and timepoints (**Fig. 3B** and **C**; Supplementary Fig. S3). Although the nonmalignant prostate PNT1 cell line was less affected by the combination treatment after 24 hours of treatment, the combination acted synergistically and significantly inhibited cell viability by 48 and 72 hours (Supplementary Fig. S4). For subsequent mechanistic evaluations of the combination treatment, concentrations of 10 nmol/L for AUY922 and 10 μmol/L for perhexiline were selected, as these doses showed strong synergy and robustly inhibited fatty acid β-oxidation (Supplementary Fig. S5).

Perhexiline and AUY922 combination treatment induces cell-cycle arrest and apoptosis

AUY922 cotreatment with perhexiline decreased mRNA gene expression of many cell-cycle proteins to a greater extent than each individual drug treatment. In LNCaP cells, the combinational treatment decreased CDK4, CDK6, AURKB, CCD20, CCND1,

Downloaded from mcr.aacrjournals.org on January 25, 2021. © 2020 American Association for Cancer Research.

Published OnlineFirst July 15, 2020; DOI: 10.1158/1541-7786.MCR-20-0570

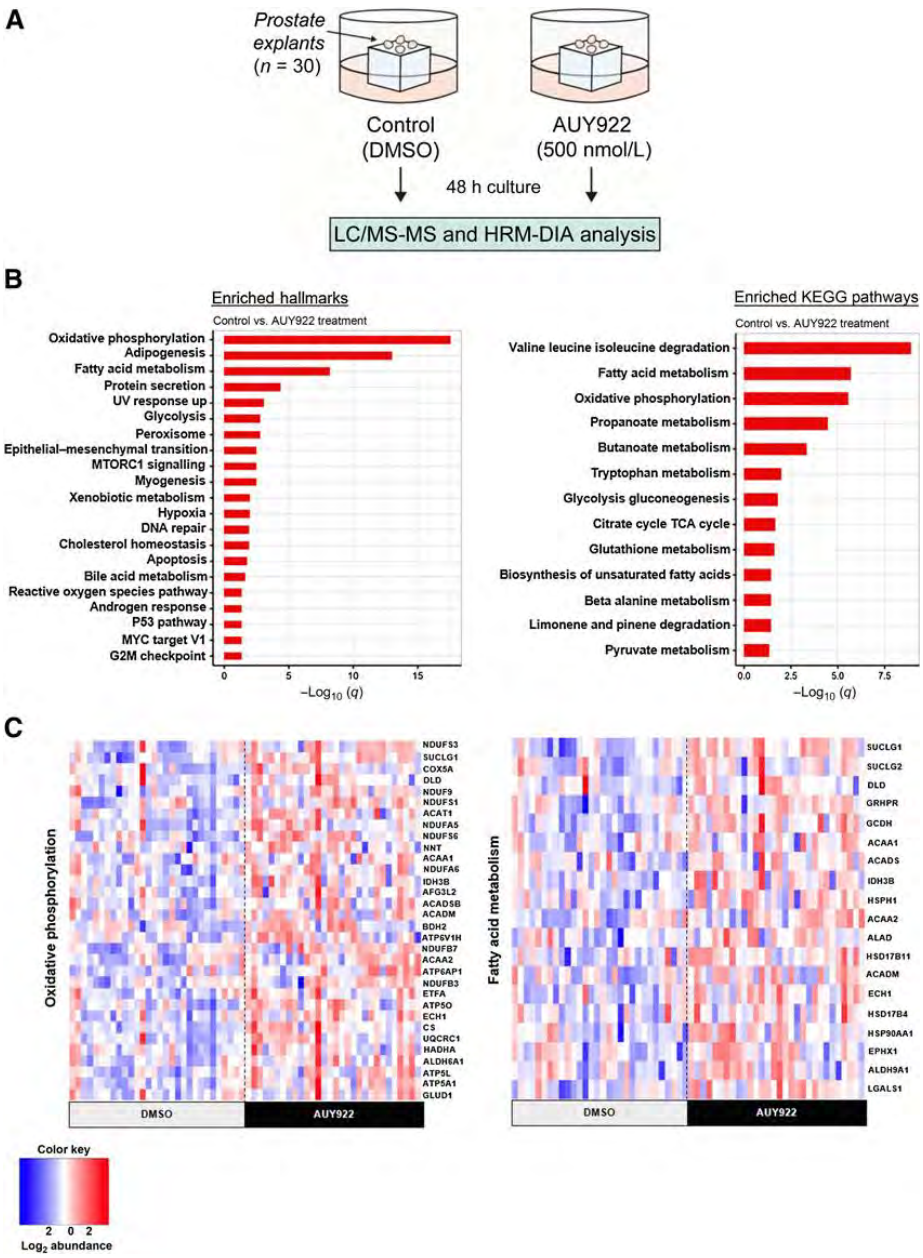

Figure 1.

AUY922 induces the expression of proteins in the fatty acid metabolism and oxidative phosphorylation pathways. **A,** HRM, a novel DIA MS was performed on 30 PDEs treated with control (DMSO) or AUY922 (500 nmol/L) for 48 hours. **B,** Pathway and GO overrepresentation analysis of proteins significantly upregulated in AUY922-treated PDEs. Pathways/GO terms with an FDR < 0.05 were considered to be statistically enriched. **C,** Heatmaps showing normalized protein abundance in PDEs treated with DMSO or AUY922. Differentially abundant proteins in the "oxidative phosphorylation" and "fatty acid metabolism" Molecular Signatures Database "Hallmarks" gene sets are shown for matched control- and AUY922-treated PDEs ($n = 30$). KEGG, Kyoto Encyclopedia of Genes and Genomes.

Downloaded from mcr.aacrjournals.org on January 25, 2021. © 2020 American Association for Cancer Research.

Published OnlineFirst July 15, 2020; DOI: 10.1158/1541-7786.MCR-20-0570

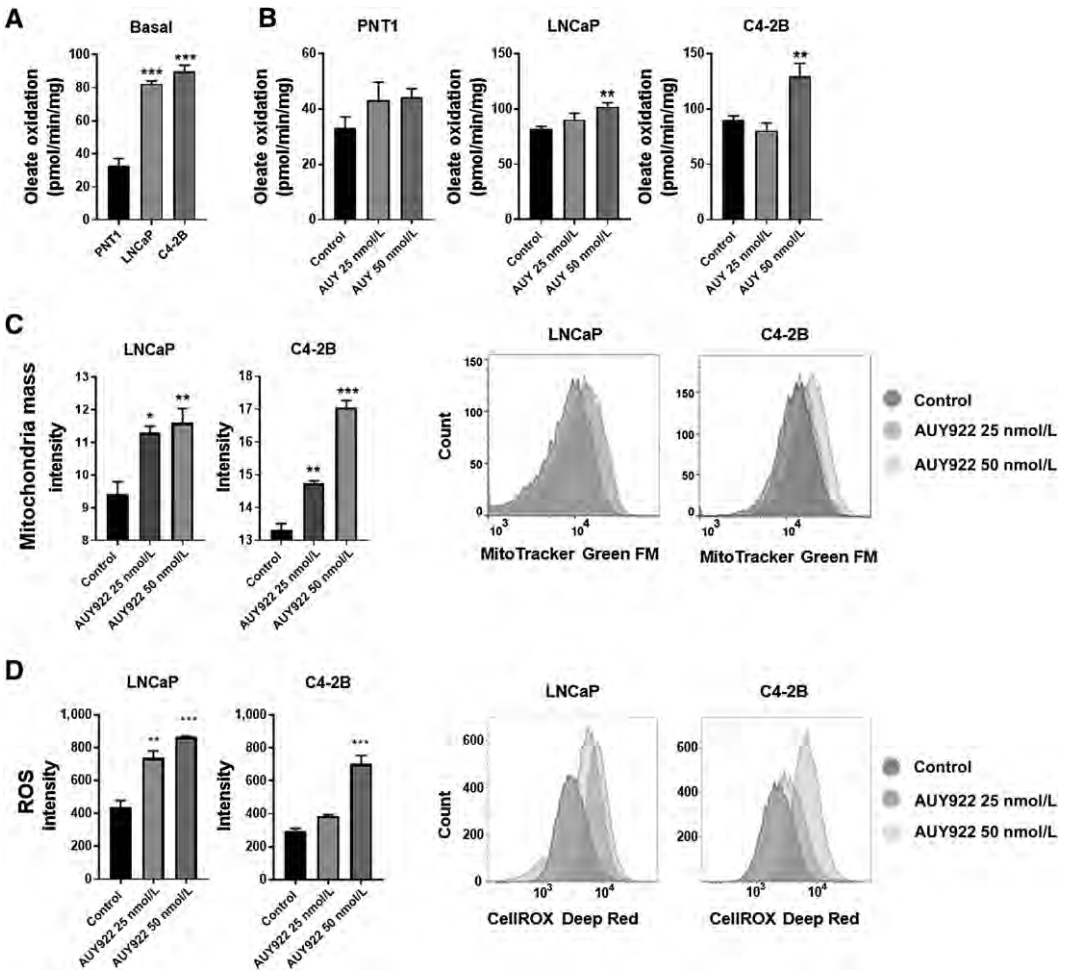

Figure 2.

AUY922 induces fatty acid metabolism in prostate cancer cells and is associated with increased prostate cancer mitochondrial mass and cellular ROS. **A,** Comparison of ^{14}C-oleate oxidation in nonmalignant and prostate cancer cells. **B,** Effect of AUY922 treatment on ^{14}C-oleate oxidation in nonmalignant and prostate cancer cells. **C,** Flow cytometry analysis of mitochondrial mass using MitoTracker Green FM. **D,** Flow cytometry analysis of cellular ROS with CellROX Deep Red. Cells were treated with control (DMSO) or AUY922 at the indicated concentration for 24 hours. Data are presented as mean ± SEM (*, $P < 0.05$; **, $P < 0.01$; ***, $P < 0.001$; $n = 3$).

CCNE2, and E2F1 mRNA expression significantly compared with the control and with each individual drug treatment (**Fig. 4A**). In C4-2B cells, the combination treatment decreased CDK4, CDK6, CCND1, and E2F1 and increased mRNA expression of the cyclin/CDK complex inhibitor CDKN1A (p21) significantly compared with the control and with each individual drug treatment (**Fig. 4A**). CDK4 was selected to prove that the changes at the mRNA level translated to protein levels. The expression of CDK4 protein level decreased markedly in both cancer cell lines when treated with the combination treatment compared with the control and with each individual drug treatment (**Fig. 4A**). Investigation of key cellular proliferation and survival signaling pathways showed modest downregulation of pERK and pAKT (Ser473) in C4-2B cells compared with the control (Supplementary Fig. S6). The marked cell death induced by the combination treatment was characteristic of apoptosis, as evidenced by increased levels of cleaved PARP compared with all other treatment groups (**Fig. 4A**).

Consistent with the changes observed in cell-cycle gene expression, the combination treatment arrested the cells in G_1-phase to a greater extent than each individual drug treatment. Specifically, combination-treated LNCaP cells exhibited a significant increase of cells in the G_0–G_1-phase from 55.6% to 85% when compared with control treatment ($P < 0.001$), and compared with AUY922 (58.7%; $P < 0.001$) or perhexiline (78.1%; $P < 0.05$), individually (**Fig. 4B**). Similarly, the cotreatment increased the C4-2B G_0–G_1-phase population significantly from 40.7% to 78.6% ($P < 0.001$), significantly more than single

Downloaded from mcr.aacrjournals.org on January 25, 2021. © 2020 American Association for Cancer Research.

Published OnlineFirst July 15, 2020; DOI: 10.1158/1541-7786.MCR-20-0570

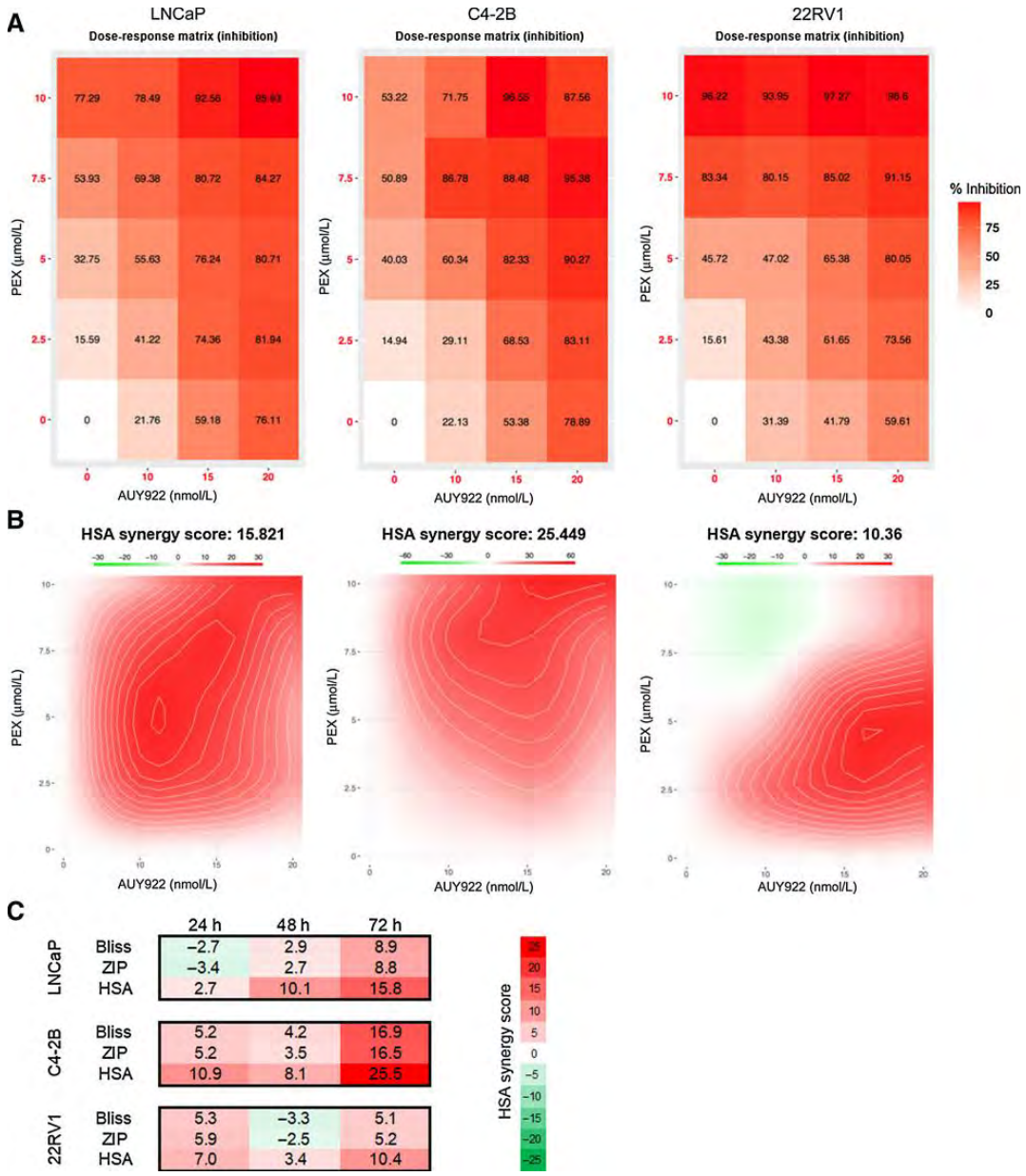

Figure 3.

AUY922 and perhexiline (PEX) act synergistically on prostate cancer cells. **A,** LNCaP, C4-2B, and 22RV1 cells were treated for 72 hours at the indicated concentrations. Cell viability was measured using CyQUANT cell proliferation assay. The percent of cell viability inhibition compared with the control is visualized as a heatmap ($n = 3$). **B,** The landscapes of the combination responses for AUY922 and perhexiline based on HSA model. **C,** Average synergy scores based on Bliss, ZIP, and HSA were calculated using the SynergyFinder software. Cells were treated with AUY922 and perhexiline for 24, 48, and 72 hours. Synergy scores >0 indicate synergism (red regions) and scores <0 indicate antagonism (green regions).

Downloaded from mcr.aacrjournals.org on January 25, 2021. © 2020 American Association for Cancer Research.

Published OnlineFirst July 15, 2020; DOI: 10.1158/1541-7786.MCR-20-0570

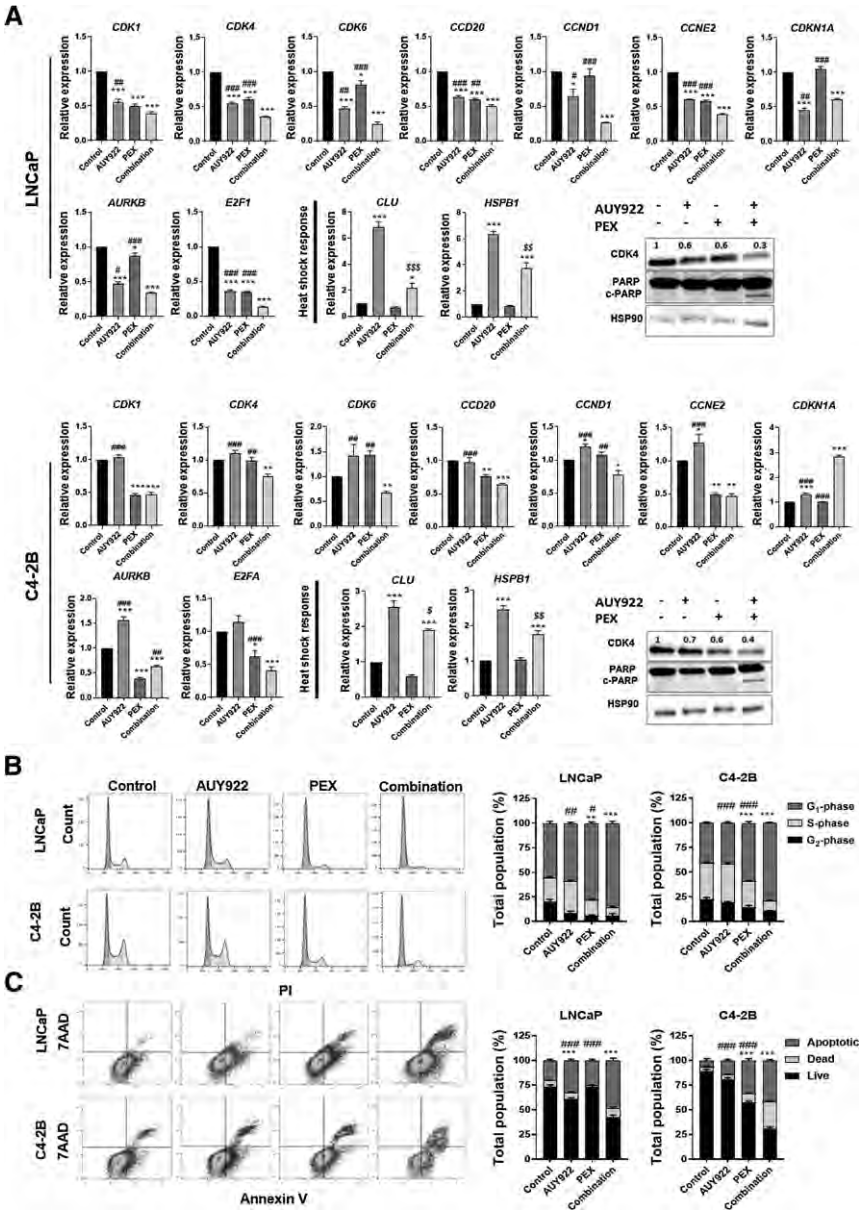

Figure 4.

AUY922 and perhexiline (PEX) combination treatment induces apoptosis and cell-cycle arrest. **A,** qRT-PCR analysis of key markers of cell cycle, HSR, and apoptosis in LNCaP and C4-2B prostate cancer cells (left). Western blot analysis of the cell-cycle marker CDK4 and the apoptosis marker c-PARP (right). Cells were treated with vehicle control (DMSO), AUY922 (10 nmol/L), perhexiline (10 μmol/L) alone, or in a combination of the two drugs at the same concentration. Densitometry was used to quantify protein expression levels relative to HSP90 loading control. Values are presented as fold change relative to control treatment. Results are presented as mean ± SEM; *, $P < 0.05$; **, $P < 0.01$; ***, $P < 0.001$ versus control; #, $P < 0.05$; ##, $P, < 0.01$; ###, $P < 0.001$ versus combination, and in HSR markers $, $P < 0.05$; $$, $P < 0.01$; $$$, $P < 0.001$ AUY922 versus AUY922 treatment. Flow cytometry analysis of cell-cycle distribution using PI staining (**B**) and analysis of apoptosis by Annexin V/7AAD double staining (**C**). Cells were treated with vehicle control (DMSO), AUY922 (10 nmol/L), perhexiline (10 μmol/L) alone, or in a combination of the two drugs at the same concentration for 24 hours. Results are presented as mean ± SEM; **, $P < 0.01$; ***, $P < 0.001$ versus control. #, $P < 0.05$; ##, $P < 0.01$; ###, $P < 0.001$ versus the combination treatment ($n = 3$).

Downloaded from mcr.aacrjournals.org on January 25, 2021. © 2020 American Association for Cancer Research.

Published OnlineFirst July 15, 2020; DOI: 10.1158/1541-7786.MCR-20-0570

treatment with AUY922 (40.1%; $P < 0.001$) or perhexiline (58.4%; $P < 0.001$; **Fig. 4B**).

Levels of Annexin V/7AAD in LNCaP cells were increased from 20.2% to 48.0% when cells were exposed to the cotreatment ($P < 0.05$), compared with AUY922 (32.5%; $P < 0.001$) or perhexiline (25.2%; $P < 0.001$) single-drug treatment (**Fig. 4C**). Likewise, the cotreatment significantly increased apoptotic C4-2B cells, as evidenced by increased levels of Annexin V/7AAD, to 41.8% compared with 7% in control-treated cells ($P < 0.001$), and this was higher than single-drug treatment with AUY922 (14.7%; $P < 0.001$) or perhexiline (30.7%; $P < 0.001$; **Fig. 4C**). We further validated the combined AUY922 and perhexiline–induced apoptotic cell death on the 22RV1 cell line (Supplementary Fig. S7A) and the nonmalignant prostate PNT1 cell line (Supplementary Fig. S7B). Collectively, this demonstrates that the combined targeting of HSP90 and fatty acid oxidation inhibition activates apoptosis.

Perhexiline and AUY922 combination treatment minimizes AUY922-induced resistance mechanisms

Clinical resistance to HSP90 inhibitors (including AUY922) is commonly attributed to the induction of the HSR in tumor cells. Reducing the HSR may prevent or delay resistance to AUY922 and thereby enhance its clinical efficacy. Consistent with previous studies (18, 20), AUY922 increased mRNA expression levels of the HSR elements CLU and HSPB1 by approximately 7-fold in LNCaP cells and by 2.5-fold in C4-2B cells (**Fig. 4A**). Combining AUY922 with perhexiline markedly attenuated *HSR* gene expression; *CLU* and *HSPB1* gene expression decreased significantly from 6.9-fold and 6.3-fold in AUY922-treated cells to 2.1-fold and 3.74-fold in combination-treated cells, respectively ($P < 0.05$; **Fig. 4A**). Similarly, *CLU* and *HSPB1* gene expression in C4-2B cells decreased significantly from 2.6-fold and 2.5-fold in AUY922-treated cells to 1.9-fold and 1.7-fold in combination-treated cells, respectively ($P < 0.01$; **Fig. 4A**).

Perhexiline and AUY922 combination treatment exhibits proapoptotic and antiproliferative effects in clinical prostate tumors cultured *ex vivo*

We previously reported the pronounced antiproliferative properties of AUY922 (500 nmol/L) in *ex vivo* cultured human prostate tumors (13). To investigate whether perhexiline could enhance the efficacy of AUY922, we opted to use a lower concentration of AUY922 (i.e., 250 nmol/L) than in our previous report (**Fig. 5A**). The clinicopathologic features of patients with prostate cancer who had undergone radical prostatectomy are provided in Supplementary Table S4. Individual Ki67 proliferative index (percent) values for each individual patient and treatment are depicted in **Fig. 5B**, and the mean inhibition of cell proliferation for the 9 patients is shown in **Fig. 5C**. AUY922 treatment inhibited cell proliferation by 64.0% ± 27% in eight of nine prostate tissue explants derived from 9 different patients ($P < 0.01$). In contrast, perhexiline (10 μmol/L) showed no efficacy in six of nine explants and only weak efficacy in three of the nine explants. The mean inhibition of cell proliferation by perhexiline alone was 17.9% ± 9.3%. Notably, the combination treatment was effective in all tested explants (9/9), significantly inhibiting cell proliferation (82.4% ± 15.5%; $P < 0.0001$). This demonstrates that the combination treatment reduced cell viability more than the individual drug treatments in eight of nine of the PDEs, and in six of these, there was more than 10% enhancement in cell proliferation inhibition. We also investigated the effect of the combinational treatment on the induction of apoptosis in human prostate cancer tissues (**Fig. 5A** and **C**; Supplementary Fig. S8). Perhexiline failed to induce apoptosis compared with vehicle control. In contrast, AUY922 single treatment and the combination treatment significantly increased the percentage of CC-3–positive cells by 283% ($P < 0.05$) and 335% ($P < 0.01$), respectively.

Discussion

The results of this study emphasize the important role of lipid metabolic pathways in prostate cancer progression, and reinforce the emerging preclinical evidence of the therapeutic benefit of lipid metabolism inhibitors in combinatorial regimens with other clinically available drugs (27–29). In addition, it proposes a new strategy to maximize the clinical benefit of HSP90 inhibitors, which showed promising preclinical activities but modest clinical efficacy.

Despite the development and regulatory approval of potent antiandrogen drugs over the past decade, advanced prostate cancer is still not curable. HSP90 inhibitors are rational therapeutics for advanced prostate cancer as they cause AR destabilization and degradation, a distinct mechanism of action against AR than current clinically available AR antagonists. In addition, HSP90 inhibitors maintain their efficacy in cells expressing AR variants that mediate advanced, castration-resistant prostate cancer (CRPC), and are capable of degrading glucocorticoid receptor (30), which confers resistance against AR antagonists (31). However, the very promising preclinical activities of HSP90 inhibitors have not translated well into clinical activity due to drug resistance and unfavorable pharmacokinetic and toxicity profiles. Although AUY922 showed improved solubility and tolerated toxicity, it induces the HSR which can mediate drug resistance. We hypothesized that AUY922 clinical use would be more successful if a lower drug concentration could be achieved within a therapeutic regimen by coapplying an agent that prevents AUY922-induced survival pathways, and thus elicits less activation of the HSR and sensitizes cancer cells to AUY922 treatment.

In an attempt to improve clinical performance of AUY922, here we identified novel survival pathways induced by AUY922 in cultured clinical prostate tumors using quantitative proteomic MS. In contrast to previous resistance studies utilizing cell line–based models of prostate cancer, we opted to include PDEs alongside cell lines as PDEs recapitulates disease heterogeneity and complexity of the clinical tissue microenvironment, in which cancer cells coexist with fibroblasts, immune cells, adipocytes, and endothelial cells. The tumor stroma plays essential roles in cancer development, progression, and therapeutic response via cell–cell interactions mediated by autocrine and paracrine signals, and can mediate drug resistance by hindering drug delivery into the cancer cells, by modifying tumor cell metabolism, and by secreting cytokines, hormones, growth factors, and apoptosis inhibitors (32, 33). Using PDEs is, therefore, a powerful approach to not only evaluate drug efficacy in cancer cells, but to anticipate and target potential stromal-promoting resistance pathways. This may in turn allow selection of the most promising treatments and combinations for subsequent clinical evaluation.

While the culture times in this study were only 2 days, short-term adaptive changes in response to androgen deprivation therapy (ADT) have been proven to be significant mediators of CRPC and antiandrogen resistance. For instance, overexpression of the glucocorticoid receptor, an established mechanism of CRPC and ADT resistance, takes place within days of antiandrogen treatment *in vivo* or after mouse castration (31, 34). In addition, the activation of HSR genes in response to HSP90 inhibition takes place rapidly and is suggested to mediate drug resistance against these agents. In this study, pathway overrepresentation analysis of proteomics data generated from 30

Downloaded from mcr.aacrjournals.org on January 25, 2021. © 2020 American Association for Cancer Research.

Published OnlineFirst July 15, 2020; DOI: 10.1158/1541-7786.MCR-20-0570

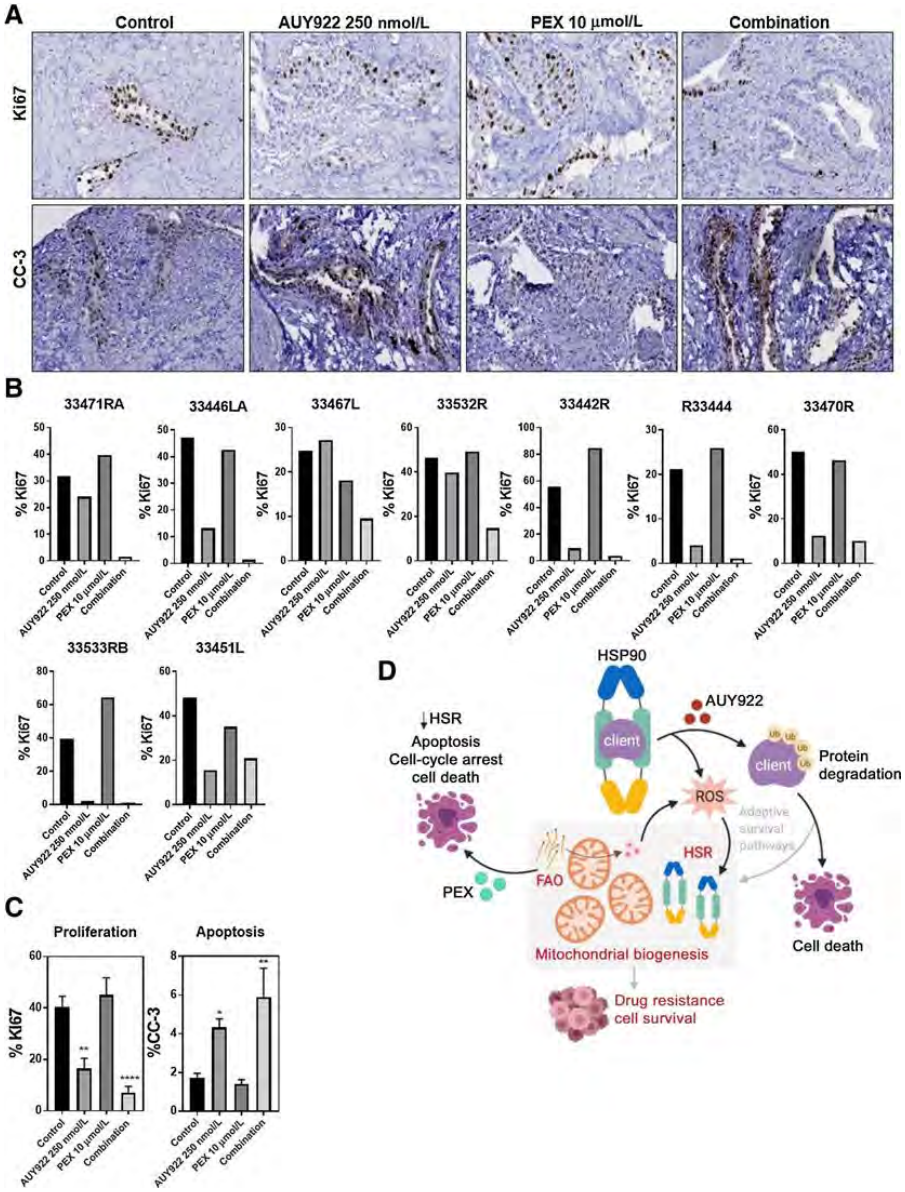

Figure 5.

AUY922 and perhexiline (PEX) combination treatment induces apoptosis and decreases cell proliferation in cultured primary prostate tumors. **A,** Representative immunostaining in sections of cultured primary prostate tumors using the proliferation marker Ki67 and the apoptosis marker CC-3. **B,** Percentages of Ki67-positive cells are reported for each individual patient included in this study. Quantification of positively stained nuclei of at least 400 cells/sample are shown. **C,** Mean percent of Ki67- and CC-3-positive cells of 9 patients is shown. Tumor tissue explants were treated with control (DMSO), AUY922 (250 nmol/L), perhexiline (10 µmol/L) alone, or in combination for 48 hours. Results are presented as the mean percentage of positive cells ±SEM; *, $P < 0.05$; **, $P < 0.01$; ****, $P < 0.0001$. $n = 9$. **D,** Proposed mechanistic model for fatty acid oxidation (FAO) targeting in sensitizing prostate cancer cells to HSP90 inhibition by AUY922. AUY922 treatment induces HSP90 chaperone complex remodeling, resulting in polyubiquitination and proteasomal degradation of HSP90 client proteins, and ultimately cell death. In clinical prostate tumors, the HSR, FAO, and mitochondrial biogenesis are all activated as survival pathways to minimize the efficacy of AUY922 and mediate drug resistance. Combination treatment with perhexiline blocks FAO, decreases ROS production, and subsequently minimizes HSR, thereby leading to cell-cycle arrest and induction of apoptosis. The diagram was created with BioRender.com.

Downloaded from mcr.aacrjournals.org on January 25, 2021. © 2020 American Association for Cancer Research.

Published OnlineFirst July 15, 2020; DOI: 10.1158/1541-7786.MCR-20-0570

PDEs revealed a striking overexpression of lipid metabolism and mitochondrial respiration pathways in response to AUY922 treatment (**Fig. 1**). Consistent with this, *in vitro* cell treatment with AUY922 significantly increased prostate cancer cell fatty acid oxidation, cytosolic ROS production, and mitochondrial mass (**Fig. 2**). Mitochondrial fatty acid β-oxidation is associated with the production of ROS, and previous reports have shown an increase in ROS to be linked to an increase in mitochondrial mass (25, 26), as a potential adaptive mechanism to facilitate maximum oxygen uptake and a higher production of energy within the cell (35, 36). Increased mitochondrial mass has been linked to drug resistance and shown to be overcome by inhibition of oxidative phosphorylation (37, 38). These observations led us to hypothesize that these activated pathways serve to provide the cells with more energy to help the cells survive the considerable stress of HSP90 inhibition, and that targeting these pathways will sensitize cells to AUY922 treatment.

It has become established that altered metabolic pathways are a hallmark of cancer cells and that a rewired metabolism is crucial for cancer growth and progression. An accumulating body of evidence demonstrates the impact of metabolism rewiring on cancer cell responses to established first-line chemotherapy in various types of cancer, suggesting that the alteration of metabolic pathways mediates cancer cells' drug resistance and these could be therapeutically targetable (39–41). Prostate cancer cells have a distinct metabolic phenotype as they depend on fatty acid oxidation as a predominant source of energy (42). The overexpression of lipid metabolism enzymes is a characteristic of both early and late stages of prostate cancer (43). Proteomic analyses of primary and bone metastatic prostate tumors have revealed fatty acid oxidation as a significant mediator of prostate cancer initiation and progression (44, 45), suggesting that targeting lipid metabolism pathways may be particularly relevant in prostate cancer compared with other type of tumors. Targeting fatty acid synthesis has been a major focus of research attention, but with limited clinical success to date due to serious adverse effects. Recently, targeting fatty acid oxidation and uptake has started to gain more attention (27, 46, 47). An emerging body of evidence shows that targeting lipid or cholesterol metabolism enzymes such as CPT1A or HMG-CoA reductase could be effective in CRPC or enzalutamide-resistant prostate cancer cells (27–29). Notably, numerous inhibitors of lipid metabolism pathways have been developed for liver and heart diseases, and several are approved for clinical use with established toxicity profiles, which facilitates drug repurposing and rapid clinical integration of these drugs into prostate cancer management.

In this study, we used the fatty acid oxidation inhibitor and clinically approved antianginal agent, in Australia and New Zealand, perhexiline (Pexsig). The clinical use of perhexiline as an antianginal agent is based on its ability to shift myocardial metabolism from fatty acid oxidation to glucose consumption. Although its selectivity for CPT1 is questionable (48), perhexiline inhibits oxidative phosphorylation and oxidation of short, medium, and long-chain fatty acids *in vitro* and *in vivo* (49). Importantly, when we tested other inhibitors of fatty acid oxidation (etomoxir and 2-bromopalmitate), both drugs acted very similarly to perhexiline and significantly sensitized prostate cancer cells to the AUY922 treatment, strengthening the case that fatty acid oxidation is the key target for this combination. We further showed that the perhexiline and AUY922 combination effect on cell viability is mediated by induction of apoptosis and cell-cycle arrest pathways. Although the cell death mechanism by the other two inhibitors (etomoxir and 2-bromopalmitate) and the oxidative phosphorylation inhibitor (metformin) in combination with AUY922 is expected to be similar to perhexiline, further characterization of cell death–mediated pathways induced by these combinations is warranted.

Perhexiline has previously demonstrated preclinical activity against several types of cancer (50, 51), while in prostate cancer, perhexiline suppressed cancer cells growth *in vitro* and *in vivo*, and sensitized prostate cancer cells to enzalutamide treatment (27). Although the cotreatment was less toxic on the nonmalignant PNT1 prostate cells than malignant cells after 24 hours, the cotreatment also inhibited PNT1 cell viability. However, as *in vitro* viability is not an indication of toxicity/safety of the combination, further *in vivo* experiments are needed to evaluate its potential therapeutic safety. Collectively with previous studies, these findings suggest that targeting fatty acid oxidation might be beneficial with other established first- and second-line AR-targeting strategies. While the use of perhexiline has been associated with adverse effects such as peripheral neuropathy, papilledema, hypoglycemia, and weight loss, perhexiline is tolerated with regular monitoring of liver function, and glucose and drug plasma concentrations (52).

In addition to its ability to prevent fatty acid oxidation induced by AUY922 treatment, we found that perhexiline surprisingly reduced the AUY922-induced HSR (**Fig. 4A**). In considering potential mechanisms for this observation, it is likely that production of ROS is a key factor. Mitochondrial respiration is the major source of intracellular ROS (53), and the cell responds to increased levels of ROS by activation of the HSR (54). Perhexiline has been reported to inhibit ROS production (55) and, presumably by this mechanism, minimizes HSR activation while inhibiting fatty acid oxidation (**Fig. 5D**).

In summary, we provide evidence that fatty acid oxidation is not only a primary source of energy for prostate cancer cells, but can also be enhanced as an adaptive survival pathway in response to drug treatment. In addition, our findings reinforce the use of patient-derived preclinical models to discover adaptive survival pathways that may contribute to clinical drug resistance, and to design efficacious combinational therapeutic regimens that overcome these adaptive responses.

Disclosure of Potential Conflicts of Interest

No potential conflicts of interest were disclosed.

Authors' Contributions

Z.D. Nassar: Conceptualization, data curation, funding acquisition, investigation, visualization, writing-original draft, writing-review and editing. **C.Y. Mah:** Investigation, visualization, writing-review and editing. **M.M. Centenera:** Supervision, funding acquisition, methodology, writing-review and editing. **S. Irani:** Investigation, methodology, writing-review and editing. **M.C. Sadowski:** Investigation, writing-review and editing. **J.S. Scott:** Investigation, writing-review and editing. **E.V. Nguyen:** Resources, investigation, writing-review and editing. **S.R. Nagarajan:** Investigation, writing-review and editing. **M. Moldovan:** Data curation, formal analysis, investigation, writing-review and editing. **D.J. Lynn:** Data curation, formal analysis, supervision, writing-review and editing. **R.J. Daly:** Resources, funding acquisition, writing-review and editing. **A.J. Hoy:** Conceptualization, supervision, funding acquisition, investigation, writing-review and editing. **L.M. Butler:** Conceptualization, resources, supervision, funding acquisition, writing-original draft, project administration, writing-review and editing.

Acknowledgments

Z.D. Nassar was supported by an Early Career Fellowship from the National Health and Medical Research Council of Australia (1138648), a John Mills Young Investigator Award from the Prostate Cancer Foundation of Australia (YI 1417), and the Cure Cancer Australia Priority-driven Collaborative Cancer Research Scheme (1164798). C.Y. Mah was supported by a Master of Philosophy International Scholarship and a Top-Up Scholarship from the Freemason's Foundation Centre

Downloaded from mcr.aacrjournals.org on January 25, 2021. © 2020 American Association for Cancer Research.

Published OnlineFirst July 15, 2020; DOI: 10.1158/1541-7786.MCR-20-0570

for Men's Health. J.S. Scott was supported by University of Adelaide George Fraser Scholarship and a Top-Up Scholarship from the Freemason's Foundation Centre for Men's Health. L.M. Butler was supported by an Australian Research Council Future Fellowship (130101004) and a Cancer Council SA Beat Cancer Project Principal Cancer Research Fellowship (PRF1117). A.J. Hoy was supported by a Robinson Fellowship and funding from the University of Sydney. D.J. Lynn was supported by an EMBL Australia Group Leader award. R.J. Daly was supported by an NHMRC Principal Research Fellowship (1058540). This research was supported by funding from the Movember Foundation and the Prostate Cancer Foundation of Australia (MRTA3, to L.M. Butler and A.J. Hoy and MRTA1, to M.C. Sadowski), and from Cancer Australia (1085471, to L.M. Butler, M.M. Centenera, and R.J. Daly). The authors thank the Monash Biomedical Proteomics Facility and SAHMRI Flow and Laser Scanning Cytometry Facility.

The costs of publication of this article were defrayed in part by the payment of page charges. This article must therefore be hereby marked *advertisement* in accordance with 18 U.S.C. Section 1734 solely to indicate this fact.

Received June 26, 2020; revised July 9, 2020; accepted July 13, 2020; published first July 15, 2020.

References

1. Bray F, Ferlay J, Soerjomataram I, Siegel RL, Torre LA, Jemal A. Global cancer statistics 2018: GLOBOCAN estimates of incidence and mortality worldwide for 36 cancers in 185 countries. CA Cancer J Clin 2018;68:394–424.
2. Reddy AS, Zhang S. Polypharmacology: drug discovery for the future. Exp Rev Clin Pharmacol 2013;6:41–7.
3. Al-Lazikani B, Banerji U, Workman P. Combinatorial drug therapy for cancer in the post-genomic era. Nat Biotechnol 2012;30:679–92.
4. Eccles SA, Massey A, Raynaud FI, Sharp SY, Box G, Valenti M, et al. NVP-AUY922: a novel heat shock protein 90 inhibitor active against xenograft tumor growth, angiogenesis, and metastasis. Cancer Res 2008;68:2850–60.
5. Cardillo MR, Ippoliti F. IL-6, IL-10 and HSP-90 expression in tissue microarrays from human prostate cancer assessed by computer-assisted image analysis. Anticancer Res 2006;26:3409–16.
6. Schopf FH, Biebl MM, Buchner J. The HSP90 chaperone machinery. Nat Rev Mol Cell Biol 2017;18:345–60.
7. Vanaja DK, Mitchell SH, Toft DO, Young CY. Effect of geldanamycin on androgen receptor function and stability. Cell Stress Chaperones 2002; 7:55–64.
8. Yuno A, Lee MJ, Lee S, Tomita Y, Rekhtman D, Moore B, et al. Clinical evaluation and biomarker profiling of Hsp90 inhibitors. In Calderwood SK, Prince TL, editors. Chaperones: methods and protocols. New York, NY: Springer; 2018. p. 423–41.
9. Felip E, Barlesi F, Besse B, Chu Q, Gandhi L, Kim SW, et al. Phase 2 study of the HSP-90 inhibitor AUY922 in previously treated and molecularly defined patients with advanced non-small cell lung cancer. J Thorac Oncol 2018;13: 576–84.
10. Kong A, Rea D, Ahmed S, Beck JT, Lopez Lopez R, Biganzoli L, et al. Phase 1B/2 study of the HSP90 inhibitor AUY922 plus trastuzumab in metastatic HER2-positive breast cancer patients who have progressed on trastuzumab-based regimen. Oncotarget 2016;7:37680–92.
11. Bendell JC, Bauer TM, Lamar R, Joseph M, Penley W, Thompson DS, et al. A phase 2 study of the hsp90 inhibitor AUY922 as treatment for patients with refractory gastrointestinal stromal tumors. Cancer Invest 2016;34: 265–70.
12. Seggewiss-Bernhardt R, Bargou RC, Goh YT, Stewart AK, Spencer A, Alegre A, et al. Phase 1/1B trial of the heat shock protein 90 inhibitor NVP-AUY922 as monotherapy or in combination with bortezomib in patients with relapsed or refractory multiple myeloma. Cancer 2015;121:2185–92.
13. Centenera MM, Gillis JL, Hanson AR, Jindal S, Taylor RA, Risbridger GP, et al. Evidence for efficacy of new Hsp90 inhibitors revealed by ex vivo culture of human prostate tumors. Clin Cancer Res 2012;18:3562–70.
14. Ku S, Lasorsa E, Adelaiye R, Ramakrishnan S, Ellis L, Pili R. Inhibition of Hsp90 augments docetaxel therapy in castrate resistant prostate cancer. PLoS One 2014; 9:e103680.
15. Armstrong HK, Gillis JL, Johnson IRD, Nassar ZD, Moldovan M, Levrier C, et al. Dysregulated fibronectin trafficking by Hsp90 inhibition restricts prostate cancer cell invasion. Sci Rep 2018;8:2090.
16. McCollum AK, TenEyck CJ, Stensgard B, Morlan BW, Ballman KV, Jenkins RB, et al. P-Glycoprotein-mediated resistance to Hsp90-directed therapy is eclipsed by the heat shock response. Cancer Res 2008;68:7419–27.
17. Chen L, Li J, Farah E, Sarkar S, Ahmad N, Gupta S, et al. Cotargeting HSP90 and its client proteins for treatment of prostate cancer. Mol Cancer Ther 2016;15: 2107–18.
18. Centenera MM, Carter SL, Gillis JL, Marrocco-Tallarigo DL, Grose RH, Tilley WD, et al. Co-targeting AR and HSP90 suppresses prostate cancer cell growth and prevents resistance mechanisms. Endocr Relat Cancer 2015; 22:805–18.
19. Nguyen EV, Centenera MM, Moldovan M, Das R, Irani S, Vincent AD, et al. Identification of novel response and predictive biomarkers to hsp90 inhibitors through proteomic profiling of patient-derived prostate tumor explants. Mol Cell Proteomics 2018;17:1470–86.
20. Armstrong HK, Koay YC, Irani S, Das R, Nassar ZD, Selth LA, et al. A novel class of hsp90 c-terminal modulators have pre-clinical efficacy in prostate tumor cells without induction of a heat shock response. Prostate 2016;76: 1546–59.
21. Liberzon A, Subramanian A, Pinchback R, Thorvaldsdóttir H, Tamayo P, Mesirov JP. Molecular signatures database (MSigDB) 3.0. Bioinformatics 2011;27:1739–40.
22. Ianevski A, He L, Aittokallio T, Tang J. SynergyFinder: a web application for analyzing drug combination dose-response matrix data. Bioinformatics 2017;33: 2413–5.
23. Nassar ZD, Hill MM, Parton RG, Francois M, Parat MO. Non-caveolar caveolin-1 expression in prostate cancer cells promotes lymphangiogenesis. Oncoscience 2015;2:635–45.
24. Costello LC, Franklin R, Stacey R. Mitochondrial isocitrate dehydrogenase and isocitrate oxidation of rat ventral prostate. Enzyme 1976;21:495–506.
25. Lee CF, Liu CY, Hsieh RH, Wei YH. Oxidative stress-induced depolymerization of microtubules and alteration of mitochondrial mass in human cells. Ann N Y Acad Sci 2005;1042:246–54.
26. Limoli CL, Giedzinski E, Morgan WF, Swarts SG, Jones GD, Hyun W. Persistent oxidative stress in chromosomally unstable cells. Cancer Res 2003; 63:3107–11.
27. Flaig TW, Salzmann-Sullivan M, Su LJ, Zhang Z, Joshi M, Gijón MA, et al. Lipid catabolism inhibition sensitizes prostate cancer cells to antiandrogen blockade. Oncotarget 2017;8:56051–65.
28. Kong Y, Cheng L, Mao F, Zhang Z, Zhang Y, Farah E, et al. Inhibition of cholesterol biosynthesis overcomes enzalutamide resistance in castration-resistant prostate cancer (CRPC). J Biol Chem 2018;293:14328–41.
29. Zadra G, Ribeiro CF, Chetta P, Ho Y, Cacciatore S, Gao X, et al. Inhibition of de novo lipogenesis targets androgen receptor signaling in castration-resistant prostate cancer. Proc Natl Acad Sci U S A 2019;116:631.
30. Agyeman AS, Jun WJ, Proia DA, Kim CR, Skor MN, Kocherginsky M, et al. Hsp90 inhibition results in glucocorticoid receptor degradation in association with increased sensitivity to paclitaxel in triple-negative breast cancer. Horm Cancer 2016;7:114–26.
31. Arora VK, Schenkein E, Murali R, Subudhi SK, Wongvipat J, Balbas MD, et al. Glucocorticoid receptor confers resistance to antiandrogens by bypassing androgen receptor blockade. Cell 2013;155:1309–22.
32. Trédan O, Galmarini CM, Patel K, Tannock IF. Drug resistance and the solid tumor microenvironment. J Natl Cancer Inst 2007;99:1441–54.
33. Son B, Lee S, Youn H, Kim E, Kim W, Youn B. The role of tumor microenvironment in therapeutic resistance. Oncotarget 2017;8:3933–45.
34. Davies P, Rushmere NK. Association of glucocorticoid receptors with prostate nuclear sites for androgen receptors and with androgen response elements. J Mol Endocrinol 1990;5:117–27.
35. Yang PS, Hsu YC, Lee JJ, Chen MJ, Huang SY, Cheng SP. Heme oxygenase-1 inhibitors induce cell cycle arrest and suppress tumor growth in thyroid cancer cells. Int J Mol Sci 2018;19:2502.
36. Liu J, Hanavan PD, Kras K, Ruiz YW, Castle EP, Lake DF, et al. Loss of SETD2 induces a metabolic switch in renal cell carcinoma cell lines toward enhanced oxidative phosphorylation. J Proteome Res 2019;18:331–40.
37. Farnie G, Sotgia F, Lisanti MP. High mitochondrial mass identifies a sub-population of stem-like cancer cells that are chemo-resistant. Oncotarget 2015;6:30472–86.

Downloaded from mcr.aacrjournals.org on January 25, 2021. © 2020 American Association for Cancer Research.

Published OnlineFirst July 15, 2020; DOI: 10.1158/1541-7786.MCR-20-0570

38. Cruz-Bermudez A, Laza-Briviesca R, Vicente-Blanco RJ, Garcia-Grande A, Coronado MJ, Laine-Menendez S, et al. Cisplatin resistance involves a metabolic reprogramming through ROS and PGC-1alpha in NSCLC which can be overcome by OXPHOS inhibition. Free Radic Biol Med 2019;135:167–81.
39. Zaal EA, Berkers CR. The influence of metabolism on drug response in cancer. Frontiers Oncol 2018;8:500.
40. Locasale JW. Metabolic rewiring drives resistance to targeted cancer therapy. Molecular Systems Biol 2012;8:597.
41. Zhao Y, Butler EB, Tan M. Targeting cellular metabolism to improve cancer therapeutics. Cell Death Dis 2013;4:e532.
42. Liu Y. Fatty acid oxidation is a dominant bioenergetic pathway in prostate cancer. Prostate Cancer Prostatic Dis 2006;9:230–4.
43. Wu X, Daniels G, Lee P, Monaco ME. Lipid metabolism in prostate cancer. Am J Clin Exp Urol 2014;2:111–20.
44. Iglesias-Gato D, Wikstrom P, Tyanova S, Lavallee C, Thysell E, Carlsson J, et al. The proteome of primary prostate cancer. Eur Urol 2016;69:942–52.
45. Iglesias-Gato D, Thysell E, Tyanova S, Crnalic S, Santos A, Lima TS, et al. The proteome of prostate cancer bone metastasis reveals heterogeneity with prognostic implications. Clin Cancer Res 2018;24:5433–44.
46. Watt MJ, Clark AK, Selth LA, Haynes VR, Lister N, Rebello R, et al. Suppressing fatty acid uptake has therapeutic effects in preclinical models of prostate cancer. Sci Transl Med 2019;11:eaau5758.
47. Schlaepfer IR, Rider L, Rodrigues LU, Gijon MA, Pac CT, Romero L, et al. Lipid catabolism via CPT1 as a therapeutic target for prostate cancer. Mol Cancer Ther 2014;13:2361–71.
48. George CH, Mitchell AN, Preece R, Bannister ML, Yousef Z. Pleiotropic mechanisms of action of perhexiline in heart failure. Expert Opin Ther Pat 2016;26:1049–59.
49. Deschamps D, DeBeco V, Fisch C, Fromenty B, Guillouzo A, Pessayre D. Inhibition by perhexiline of oxidative phosphorylation and the beta-oxidation of fatty acids: possible role in pseudoalcoholic liver lesions. Hepatology 1994;19:948–61.
50. Vella S, Penna I, Longo L, Pioggia G, Garbati P, Florio T, et al. Perhexiline maleate enhances antitumor efficacy of cisplatin in neuroblastoma by inducing overexpression of NDM29 ncRNA. Sci Rep 2015;5:18144.
51. Ren XR, Wang J, Osada T, Mook RA Jr, Morse MA, Barak LS, et al. Perhexiline promotes HER3 ablation through receptor internalization and inhibits tumor growth. Breast Cancer Res 2015;17:20.
52. Phuong H, Choi BY, Chong CR, Raman B, Horowitz JD. Can perhexiline be utilized without long-term toxicity? A clinical practice audit. Ther Drug Monit 2016;38:73–8.
53. St-Pierre J, Buckingham JA, Roebuck SJ, Brand MD. Topology of superoxide production from different sites in the mitochondrial electron transport chain. J Biol Chem 2002;277:44784–90.
54. Niforou K, Cheimonidou C, Trougakos IP. Molecular chaperones and proteostasis regulation during redox imbalance. Redox Biol 2014;2:323–32.
55. Gatto GJ Jr, Ao Z, Kearse MG, Zhou M, Morales CR, Daniels E, et al. NADPH oxidase-dependent and -independent mechanisms of reported inhibitors of reactive oxygen generation. J Enzyme Inhib Med Chem 2013;28:95–104.

Downloaded from mcr.aacrjournals.org on January 25, 2021. © 2020 American Association for Cancer Research.

Published OnlineFirst July 15, 2020; DOI: 10.1158/1541-7786.MCR-20-0570

AACR American Association for Cancer Research

Molecular Cancer Research

Fatty Acid Oxidation Is an Adaptive Survival Pathway Induced in Prostate Tumors by HSP90 Inhibition

Zeyad D. Nassar, Chui Yan Mah, Margaret M. Centenera, et al.

Mol Cancer Res 2020;18:1500-1511. Published OnlineFirst July 15, 2020.

Updated version	Access the most recent version of this article at: doi:10.1158/1541-7786.MCR-20-0570
Supplementary Material	Access the most recent supplemental material at: http://mcr.aacrjournals.org/content/suppl/2020/07/15/1541-7786.MCR-20-0570.DC1

Cited articles	This article cites 54 articles, 15 of which you can access for free at: http://mcr.aacrjournals.org/content/18/10/1500.full#ref-list-1

E-mail alerts	Sign up to receive free email-alerts related to this article or journal.
Reprints and Subscriptions	To order reprints of this article or to subscribe to the journal, contact the AACR Publications Department at pubs@aacr.org.
Permissions	To request permission to re-use all or part of this article, use this link http://mcr.aacrjournals.org/content/18/10/1500. Click on "Request Permissions" which will take you to the Copyright Clearance Center's (CCC) Rightslink site.

Downloaded from mcr.aacrjournals.org on January 25, 2021. © 2020 American Association for Cancer Research.

Chapter 6: Phospholipid profiling of clinical prostate tumours

This Chapter includes a manuscript that is submitted and currently under revision. A portion of this work was completed as part of this PhD. In addition to lab work and data analysis, all figures included in the manuscript were prepared by the candidate.

August 2021: Manuscript was accepted and in press at Cancer Research.

6.1 Introduction

This is a stand-alone chapter of this dissertation.

Chapter 6 aims to provide a comprehensive overview of the lipidomic changes that occur in clinical prostate tumours accompanying prostate cancer development or in response to treatment. To address this, we employed mass spectrometry-based quantitation of phospholipids in prostate tumours and benign tissues, as well as primary prostate explants treated with an AR antagonist. We also asked whether these cancer-related lipid alterations identified in this study are targetable using pharmacological agents. Overall, this Chapter corroborates the rationale of exploiting lipid metabolism pathways for therapeutic intervention.

STATEMENT OF AUTHORSHIP

Title of Paper	Lipidomic profiling of clinical prostate cancer reveals targetable alterations in lipid composition
Publication Status	☐ Published ☒ Submitted for Publication ☐ Accepted for Publication ☐ Unpublished and Unsubmitted work written in a manuscript style
Publication Details	Butler, LM, Mah, CY, Machiels, J, Vincent, AD, Irani, S, Mutuku, S, Spotbeen, X, Bagadi, M, Waltregny, D, Moldovan, M, Dehairs, J, Vanderhoydonc, F, Bloch, K, Das, R, Stahl, J, Kench, J, Gevaert, T, Derua, R, Waelkens, E, Nassar, ZD, Selth, LA, Trim, PJ, Snel, MF, Lynn, DJ, Tilley, WD, Horvath, LG, Centenera, MM & Swinnen, JV 2020, 'Lipidomic profiling of clinical prostate cancer reveals targetable alterations in lipid composition'.

Principal Author

Name of Principal Author (Candidate)	Lisa M Butler		
Contribution to the Paper	Conceptualization, Methodology, Data acquisition, Analysis and Interpretation of data, Investigation, Supervision, Writing – Original and draft preparation, Writing – Review and editing		
Signature		Date:	01/04/2021

Co-Author Contributions

By signing the Statement of Authorship, each author certifies that:

i. the candidate's stated contribution to the publication is accurate (as detailed above);
ii. permission is granted for the candidate to include the publication in the thesis; and
iii. the sum of all co-author contributions is equal to 100% less than the candidate's stated contribution.

Name of Co-Author	Chui Yan Mah		
Contribution to the Paper	Acquisition of data, Analysis and Interpretation of data, Investigation, Visualisation, Writing – Review and editing		
Overall Percentage (%)	15 %		
Signature		Date:	26/03/2021

Name of Co-Author	Jelle Machiels		
Contribution to the Paper	Methodology, Acquisition of data, Writing – Review and editing		
Signature	Jelle Machiels (Signature) Digitaal ondertekend door Jelle Machiels (Signature) Datum: 2021.03.22 10:10:14 +01'00'	Date:	22/03/2021

Name of Co-Author	Andrew D Vincent		
Contribution to the Paper	Analysis and Interpretation of data, Writing – Review and editing		
Signature		Date:	22/3/21
Name of Co-Author	Swati Irani		
Contribution to the Paper	Acquisition of data, Writing – Review and editing		
Signature		Date:	30/03/2021
Name of Co-Author	Shadrack Mutuku		
Contribution to the Paper	Methodology, Acquisition of data, Writing – Review and editing		
Signature		Date:	22 Mar 2021
Name of Co-Author	Xander Spotbeen		
Contribution to the Paper	Methodology, Acquisition of data, Writing – Review and editing		
Signature		Date:	01/04/2021
Name of Co-Author	Muralidhararao Bagadi		
Contribution to the Paper	Writing – Review and editing		
Signature		Date:	01/04/2021
Name of Co-Author	David Waltregny		
Contribution to the Paper	Analysis and Interpretation of data, Writing – Review and editing		
Signature		Date:	
Name of Co-Author	Max Moldovan		
Contribution to the Paper	Analysis and Interpretation of data, Writing – Review and editing		
Signature		Date:	24 Mar 2021
Name of Co-Author	Jonas Dehairs		
Contribution to the Paper	Methodology, Analysis and Interpretation of data, Writing – Review and editing		
Signature		Date:	22/03/2021

Name of Co-Author	Frank Vanderhoydonc		
Contribution to the Paper	Acquisition of data, Writing – Review and editing		
Signature		Date:	01/04/2021

Name of Co-Author	Katarzyna Bloch		
Contribution to the Paper	Acquisition of data, Writing – Review and editing		
Signature		Date:	01/04/2021

Name of Co-Author	Rajdeep Das		
Contribution to the Paper	Methodology, Pathology of patient samples, Acquisition of data, Writing – Review and editing		
Signature		Date:	March- 24th, 2021

Name of Co-Author	Jurgen Stahl		
Contribution to the Paper	Pathology of patient samples, Writing – Review and editing		
Signature		Date:	01/04/2021

Name of Co-Author	James Kench		
Contribution to the Paper	Pathology of patient samples, Writing – Review and editing		
Signature		Date:	23/3/2021

Name of Co-Author	Thomas Gevaert		
Contribution to the Paper	Writing – Review and editing		
Signature		Date:	01/04/2021

Name of Co-Author	Rita Derua		
Contribution to the Paper	Methodology, Pathology of patient samples, Writing – Review and editing		
Signature		Date:	01/04/2021

Name of Co-Author	Etienne Waelkens		
Contribution to the Paper	Methodology, Writing – Review and editing		
Signature		Date:	March 24, 2021

Name of Co-Author	Zeyad D Nassar		
Contribution to the Paper	Analysis and Interpretation of data, Writing – Review and editing		
Signature		Date:	26/03/2021

Name of Co-Author	Luke A Selth		
Contribution to the Paper	Analysis and Interpretation of data, Writing – Review and editing		
Signature		Date:	22/03/2021

Name of Co-Author	Paul J Trim		
Contribution to the Paper	Methodology, Supervision, Analysis and Interpretation of data, Writing – Review and editing		
Signature		Date:	23/03/2021

Name of Co-Author	Marten F Snel		
Contribution to the Paper	Methodology, Supervision, Analysis and Interpretation of data, Writing – Review and editing		
Signature		Date:	23/3/21

Name of Co-Author	David J Lynn		
Contribution to the Paper	Supervision, Analysis and Interpretation of data, Writing – Review and editing		
Signature		Date:	22/3/21

Name of Co-Author	Wayne D Tilley		
Contribution to the Paper	Analysis and Interpretation of data, Writing – Review and editing		
Signature		Date:	01/04/2021

Name of Co-Author	Lisa G Horvath		
Contribution to the Paper	Analysis and Interpretation of data, Writing – Review and editing		
Signature		Date:	01/04/2021

Name of Co-Author	Margaret M Centenera	
Contribution to the Paper	Conceptualization, Methodology, Data acquisition, Analysis and Interpretation of data, Supervision, Writing – Original and draft preparation, Writing – Review and editing	
Signature		Date: 30/03/2021

Name of Co-Author	Johannes V Swinnen	
Contribution to the Paper	Conceptualization, Methodology, Analysis and Interpretation of data, Supervision, Writing – Original and draft preparation, Writing – Review and editing	
Signature		Date: **22 March 2021**

Chapter 6

Lipidomic profiling of clinical prostate cancer reveals targetable alterations in membrane lipid composition

Lisa M. Butler[1,2]*, Chui Yan Mah[1,2], Jelle Machiels[3], Andrew D. Vincent[1,2], Swati Irani[1,2], Shadrack Mutuku[1,2], Xander Spotbeen[2,3], Muralidhararao Bagadi[3], David Waltregny[4], Max Moldovan[2], Jonas Dehairs[3], Frank Vanderhoydonc[3], Katarzyna Bloch[3], Rajdeep Das[1,5], Jurgen Stahl[6], James Kench[7], Thomas Gevaert[8], Rita Derua[9], Etienne Waelkens[9], Zeyad D. Nassar[1,2], Luke A. Selth[1,5], Paul J. Trim[2], Marten F. Snel[2], David J. Lynn[2,10], Wayne D. Tilley[1,5], Lisa G. Horvath[7,11,12,13], Margaret M. Centenera[1,2]* and Johannes V. Swinnen[3]*

[1]Adelaide Medical School and Freemasons' Foundation Centre for Men's Health, University of Adelaide, Adelaide SA 5005, Australia
[2]South Australian Health and Medical Research Institute, Adelaide SA 5000, Australia
[3]Laboratory of Lipid Metabolism and Cancer, LKI – Leuven Cancer Institute, KU Leuven, B-3000 Leuven, Belgium
[4]Department of Urology and GIGA Cancer Center, University Hospital of Liege, B-4000 Liege, Belgium
[5]Dame Roma Mitchell Cancer Research Laboratories, University of Adelaide, Adelaide SA 5005, Australia
[6]Clinpath Laboratories, Adelaide SA 5000, Australia
[7]Garvan Institute of Medical Research, Darlinghurst, NSW 2010, Australia
[8]Department of Urology, UZ Leuven, B-3000 Leuven, Belgium
[9]Department of Molecular Cell Biology and ProMeta Center, KU Leuven, B-3000 Leuven, Belgium
[10]College of Medicine and Public Health, Flinders University, Bedford Park, SA 5042, Australia
[11]Chris O'Brien Lifehouse, Camperdown, NSW 2050, Australia
[12]University of Sydney, Camperdown, NSW 2006, Australia
[13]University of New South Wales, Sydney, NSW 2052, Australia

Running title: Phospholipid profiling of prostate tumors

Conflicts of Interest: The authors declare no potential conflicts of interest

Key words: lipidomics, fatty acid synthesis, saturation, elongation, cancer

*Equal contribution

Corresponding Author: Lisa M. Butler, University of Adelaide Medical School, South Australian Health and Medical Research Institute, Adelaide SA 5000, email: lisa.butler@adelaide.edu.au

6.2 Abstract

Dysregulated lipid metabolism is a prominent feature of prostate cancer that is driven by androgen receptor (AR) signalling. Herein, we used quantitative mass spectrometry to define the “lipidome” in prostate tumors with matched benign tissues (n=21), independent tissues (n=47), and primary prostate explants cultured with a clinical AR antagonist, enzalutamide (n=43). Significant differences in lipid composition were detected and spatially visualized in tumors compared to matched benign samples. Notably, tumors featured higher proportions of monounsaturated lipids overall and elongated fatty acid chains in phosphatidylinositol and phosphatidylserine lipids. Significant associations between lipid profile and malignancy were validated in unmatched samples, and PL composition was characteristically altered in patient tissues that responded to AR inhibition. Importantly, targeting of altered tumor-related lipid features, via inhibition of acetyl CoA carboxylase 1, significantly reduced cellular proliferation in tissue explants (n=13). This first characterization of the prostate cancer lipidome in clinical tissues revealed enhanced fatty acid synthesis, elongation and desaturation as tumor-defining features, with potential for therapeutic targeting.

6.3 Introduction

With more than 1 million deaths annually, prostate cancer remains a major cause of mortality and morbidity for men worldwide (1). The clinical implementation of systemic androgen receptor (AR) targeting agents such as enzalutamide and apalutamide has increased the available therapeutic options beyond androgen deprivation, but development of resistance to these strategies remains inevitable. To more effectively combat this disease, there is a need for alternative targets for intervention and a thorough understanding of the molecular changes that accompany cancer development, progression and therapy. The advent of parallel 'omic' approaches has led to the identification of previously unsuspected cancer subtypes and therapeutic targets. However, in contrast to the genome, transcriptome, and proteome, the cancer "lipidome" remains inadequately characterized (2). As building blocks of cellular membranes, lipids affect numerous cellular processes including signal transduction, ion transport, cell proliferation, energy metabolism and cell death mechanisms, which are all involved in the development and progression of cancer (3,4). For prostate cancer, the lipidomic changes that accompany malignancy are of particular interest due to the unique metabolic profile of this cancer, whereby the normal cellular production of citrate is instead utilized in the TCA cycle for oxidative phosphorylation and biosynthetic processes such as lipogenesis (5,6). Moreover, lipid metabolism is a highly androgen-sensitive process in prostate cancer cells (7) and lipid composition may therefore be a unique cellular readout of both androgen targeting and tumorigenesis. While panels of circulating plasma lipids have previously been associated with prostate cancer risk (8), diagnosis (9) and patient outcome (10), analysis of the prostate tumor lipidome has largely been confined to cell line-based studies (11-13), which lack clinical relevance. The recent evidence of malignancy-related changes in lipid composition of prostate tumors provided by mass spectrometry-based imaging studies (14-17) supports undertaking a more detailed and quantitative study of the clinical prostate cancer lipidome. Moreover, treatment-related changes in the lipidome, which may reveal new resistance-related vulnerabilities, remain completely unexplored.

To gain insight into the potentially targetable changes in the lipid composition of prostate cancer, we employed a quantitative mass spectrometry-based lipidomics approach coupled with mass spectrometry imaging to robustly analyze and visualize a wide range of intact phospholipid (PL) species in malignant and matched non-malignant tissues. Our results provide the first comprehensive picture of the lipidomic landscape in a clinical cancer context and reveal robust associations with malignancy. We further demonstrate treatment-related changes in the lipidome accompanying response to enzalutamide, an AR antagonist widely used in the management of prostate cancer, in patient-derived explants (PDEs) of clinical prostate tissues. Finally, we report that an inhibitor of acetyl CoA carboxylase was effective in pharmacologically targeting the most recurrent lipidomic alterations observed.

6.4 Results

6.4.1 Tumor-specific lipid profiles are evident in clinical prostate tumors

Spatial variation in PL composition was initially assessed in a set of clinical prostate tumors that contained discrete benign and malignant areas of epithelium within the same tissue section, using MALDI-mass spectrometry imaging (MALDI-MSI). Shown in ***Figure 1A*** is a representative tumor in which comparison of spectral data from these regions revealed a tumor-specific PL composition that was distinct from that detected in pathologically benign epithelium or a region of high-grade prostatic intraepithelial neoplasia (PIN) from the same patient (***Figure 1B***; Supplementary ***Figure 1A***). Distinct PL mass spectra and specific masses (eg m/z 756.53, Figure 1A) were consistently detected in multiple independent tumor regions assessed across 3 individual PCa patients (Supplementary Figure 1B,C), consistent with recent reports (16,17) that characteristic changes in lipid composition accompany prostate tumorigenesis.

In light of these findings, we undertook a more detailed examination and quantification of tumor-related changes in PL composition using shotgun lipidomics incorporating electrospray tandem mass spectrometry in pathologist-microdissected regions of prostate tumor and matched benign tissues from 21 prostate cancer patients (***Figure 1C***). Clinicopathological data for the patients are summarized in Supplementary Table S1. Using this methodology, a total of 108 PL species of the four most abundant subclasses (PC, PE, PS and PI) could be detected and quantified. PL profiles of both cancer and normal tissues were dominated by PC species, and the total proportion of PC lipids was greater in tumor than in benign tissues for this cohort (Supplementary Figure 2A; $p<0.05$). There was a significant tumor-specific increase in the collective abundance of PL species with 1 or 2 double bonds, most evident in the PC lipids (***Figure 1D***). As these mainly represent species with one or two monounsaturated fatty acyl (MUFA) chains, this shift altered PL composition towards a greater overall proportion of MUFAs in the tumors, consistent with a lipogenic tumor phenotype (11).

Shown in ***Figure 1E*** is a circle plot summarizing the individual tumor-related lipidomic changes for this cohort of patients. PL are annotated by “lipid subclass”

followed by the “total fatty acyl chain length:total number of unsaturated bonds” (eg PC34:1). The species in each PL class are ordered from fully saturated to highly polyunsaturated and, within each subgroup, from shortest to longest (combined) acyl chain length. When considering the relative abundance of individual PL species, consistent patterns of change in PL saturation groups were more evident within certain lipid classes (***Figure 1E***, outer circle). Most notably, PC species had tumor-related increases in fatty acyl chains containing 1 or 2 double bonds, indicative of MUFAs, accompanied by relative decreases in polyunsaturated (PUFA; ≥3 double bonds) and fully saturated (0 double bonds) species. In PS species, however, marked increases in long PUFA species were evident across multiple saturation groups in tumor compared to benign tissue.

Consistent changes across patients were also detected in the fatty acyl chain lengths of tumor PLs. To most optimally visualize altered acyl chain length, we expressed the abundance of each PL species in tumors and matching benign tissue relative to the shortest PL species of each saturation subclass (***Figure 1E***, inner circle; denoted “elongation index”). Whereas substantial heterogeneity in fatty acyl chain length existed between individual patients for PC and PE lipids (Supplementary Figure 2B), almost every tumor exhibited increased combined acyl chain length over multiple saturation groups of the PI and PS classes compared to normal tissue, particularly for polyunsaturated species (***Figure 1D***; Supplementary Figure 2B). This was validated within the cohort as a significant increase in average chain length for polyunsaturated PI and PS lipids (Supplementary Figure 2C).

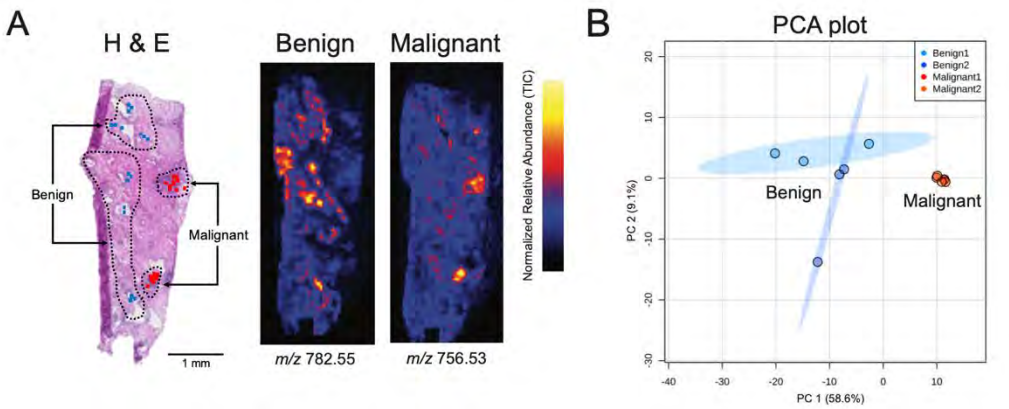
A
H & E
Benign
Malignant
Benign
Malignant
1 mm
Benign
Malignant
m/z 782.55
m/z 756.53
Normalized Relative Abundance (TIC)
B
PCA plot
Benign1
Benign2
Malignant1
Malignant2
Benign
Malignant
PC 2 (9.1%)
PC 1 (58.6%)

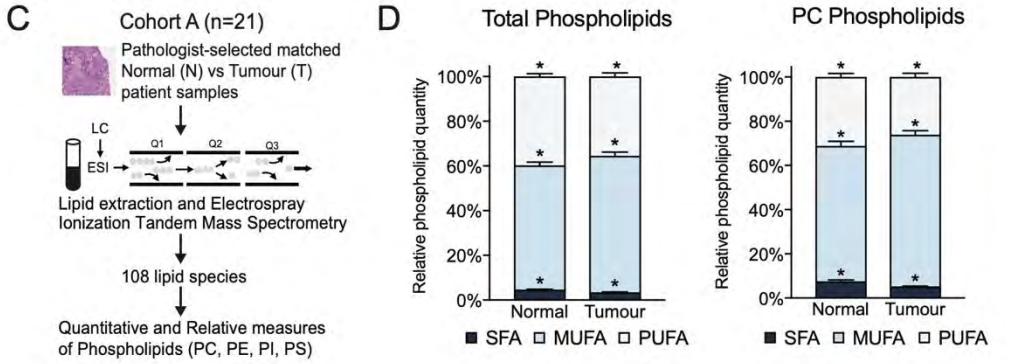
C
Cohort A (n=21)
Pathologist-selected matched Normal (N) vs Tumour (T) patient samples
LC
ESI
Q1
Q2
Q3
Lipid extraction and Electrospray Ionization Tandem Mass Spectrometry
108 lipid species
Quantitative and Relative measures of Phospholipids (PC, PE, PI, PS)
D
Total Phospholipids
PC Phospholipids
Relative phospholipid quantity
Normal
Tumour
SFA
MUFA
PUFA

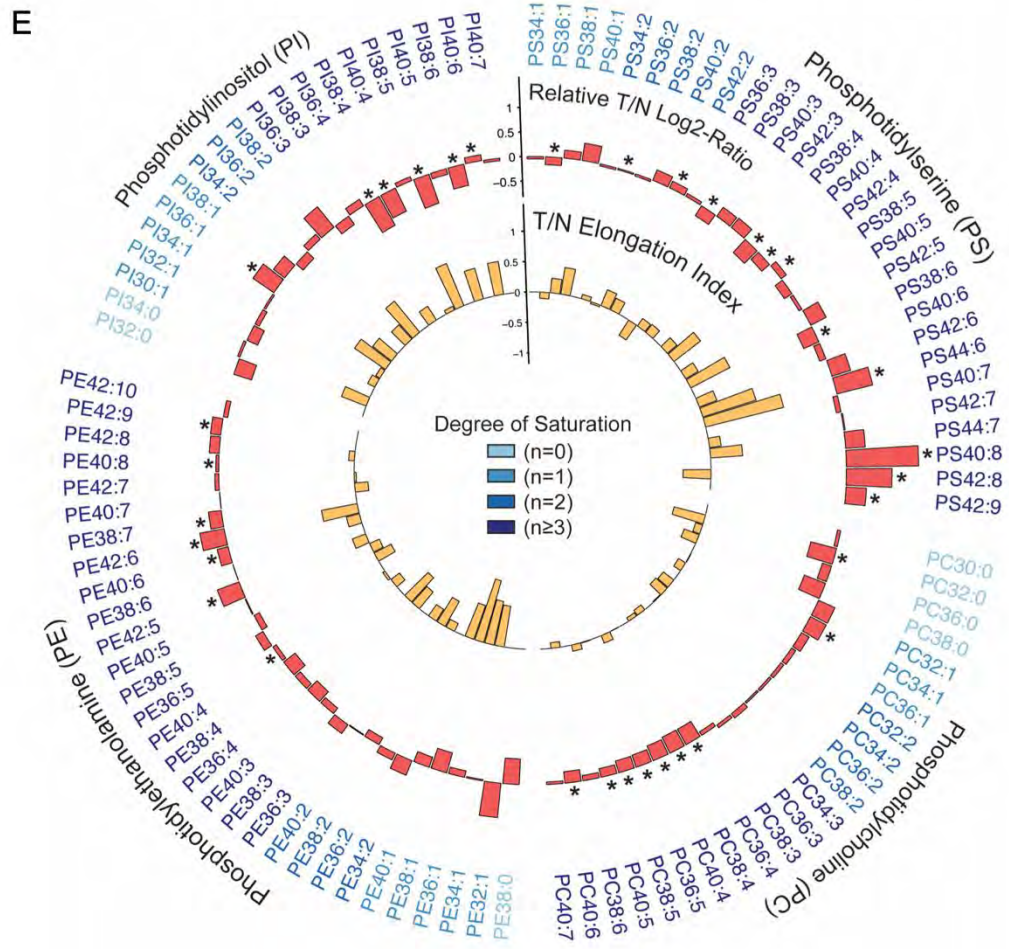
E
Phosphotidylinositol (PI)
Phosphotidylserine (PS)
Phosphotidylethanolamine (PE)
Phosphotidylcholine (PC)
Relative T/N Log2-Ratio
T/N Elongation Index
Degree of Saturation
(n=0)
(n=1)
(n=2)
(n≥3)

Figure 6.1 Evidence for a tumor-associated phospholipidome in clinical prostate cancer. A. MALDI-mass spectrometry imaging of pathologically heterogeneous prostate tissue, including ion maps of two representative examples of histology-restricted lipid masses. **B.** principal component analysis of the top 25 mass features distinguishing benign from malignant regions of tissue. **C.** Workflow for shotgun lipidomics analysis of matched normal and tumor tissues from 21 prostate cancer patients. **D.** Relative proportions of phospholipids containing 0 (SFA), 1 or 2 (MUFA), or 3 or greater (PUFA) unsaturations in benign versus tumor specimens. **E.** Circle plot of tumor-related lipidomic changes in relative abundance and fatty acyl chain elongation across the patient cohort. The outer circle represents the ratio of median-adjusted normalized abundance of individual lipid species in tumor versus benign tissues. * reflects significant association with tumor tissues. The inner circle represents fatty acid elongation index in tumor versus benign tissues. PL are annotated using “lipid subclass” followed by the “total fatty acyl chain length:total number of unsaturated bonds”.

6.4.2 Associations between Lipid Profiles and Malignancy

Based on the above observations, we investigated whether there were associations between any lipid measures and sample malignancy status. Linear mixed effects models regressed PL measures from malignant samples onto the equivalent values from benign samples, adjusting for age and batch. We specifically considered i) abundance of individual PL species, ii) saturation group abundance and iii) fatty acyl chain length per saturation group. The permutation analysis indicated that there were associations between lipid profile and malignancy beyond what would be expected by chance (Supplementary Figure 3A; permutation $p<0.001$). Of the 51 lipid features most strongly associated with malignant versus benign prostate tissue, 34 were individual lipid species (***Figure 2A*** & Supplementary Table S2), five were mean chain lengths within saturation groups and 12 were overall saturation group abundance (Supplementary Figure 3B & Table S2). As expected, certain individual species cross-correlated within and across head group classes (***Figure 2B***).

We subsequently assessed whether similar malignancy-associated lipidomic profiles would also be evident in an independent collection of 47 non-patient matched tissue specimens comprising 26 tumors and 21 benign samples (***Figure 2C***). A greater range of lipids were measured in this cohort (n=248), and included sphingomyelins (SM), ceramides (Cer) and lysoPLs (containing only 1 fatty acyl chain) in addition to the main four PL classes analyzed above. Using the same criteria as for the paired cohort, a substantial signal was again detected in terms of FDR for significant associations between lipid features and sample malignancy (Supplementary Figure 3A). Associations were detected for 64 lipid features, including 44 individual lipid species (FDR=0.03; permutation $p<0.001$; Supplementary Figures 3C,D,E and Supplementary Table S3).

There was considerable overlap in the lipid features identified in both cohorts, and by combining data from both cohorts, we identified a series of lipids that robustly associated with prostate tumor malignancy (Table 1). Shown in ***Figure 2D*** are representative examples of these lipids demonstrating concordant associations with malignancy across the individual cohorts and batches, which included the abundance of monounsaturated PC lipids (PC1 SA), individual lipids PE42:6 and

PI36:4, and chain length in monounsaturated PI lipids (PI1 CL). Consistent with these data, MALDI-MSI on two patient tissues imaged in negative ion mode revealed the expected changes in relative abundance of masses corresponding to PE42:6 (m/z 818.5) and PI36:4 (m/z 857.5) in malignant versus non-malignant regions of the tissues (***Figure 2E***; box plots of normalized mass intensity shown adjacent to ion map images; Supplementary Figure 4).

While the tumour cohort size limited our ability to detect associations with clinical parameters such as serum PSA (Supplementary Figure 5B; permutation p=0.79) and Gleason Score (Supplementary Figure 5B,C; permutation p=0.24), there was evidence for weak associations between lipid profile and TMPRSS2-ERG subtype (Supplementary Figure 5B,D,E and Table S4; permutation p=0.05) and proliferation (Ki67 positivity index) in malignant samples (Supplementary Figure 5A,F and Table S5; permutation p=0.10).

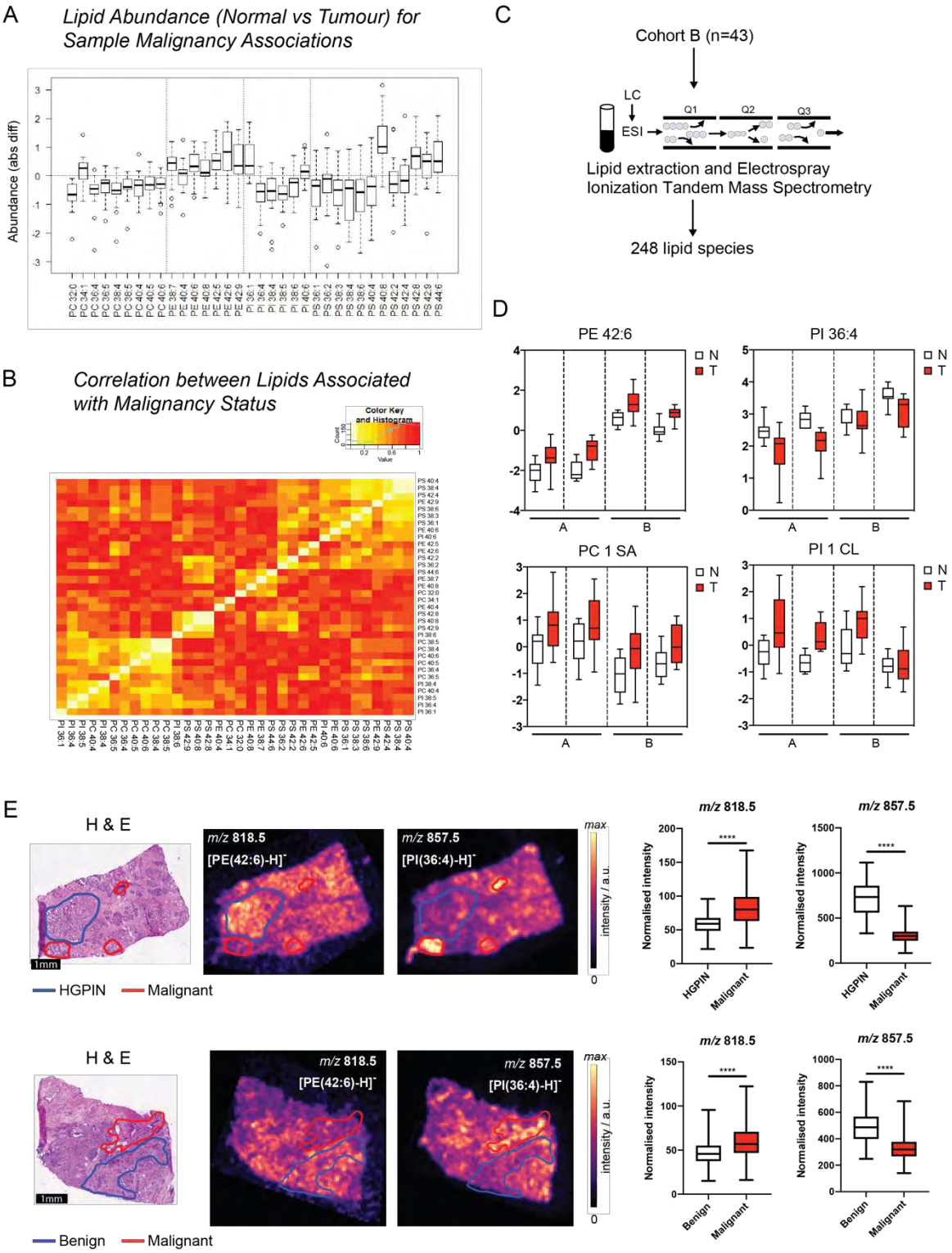
A
Lipid Abundance (Normal vs Tumour) for Sample Malignancy Associations
Abundance (abs diff)
B
Correlation between Lipids Associated with Malignancy Status
Color Key and Histogram
C
Cohort B (n=43)
LC
ESI
Q1
Q2
Q3
Lipid extraction and Electrospray Ionization Tandem Mass Spectrometry
248 lipid species
D
PE 42:6
PI 36:4
PC 1 SA
PI 1 CL
N
T
A
B
E
H & E
m/z 818.5
[PE(42:6)-H]-
m/z 857.5
[PI(36:4)-H]-
max
intensity / a.u.
1mm
HGPIN
Malignant
Benign
Normalised intensity
****

Figure 6.2 Associations of phospholipid profile with malignancy. A. Phospholipid variables significantly associated with tumor versus matched benign tissues in Cohort A. **B.** Correlation plot of individual phospholipid species significantly associated with sample malignancy in Cohort A. **C.** Workflow for lipidomics analysis of unmatched patient tissue cohort B (n=47). **D.** Box plots of representative examples of different phospholipid variables significantly associated with sample malignancy across both patient cohorts A and B. **E.** MALDI-mass spectrometry imaging of ion masses corresponding to PE42:6 (*m/z* 818.5) and PI36:4 (*m/z* 857.5) in 2 independent prostate cancer tissues, with box plots of normalized ion intensity between non-malignant and malignant tissues regions adjacent to the images.

6.4.3 Lipid profile is altered by AR inhibition in patient-derived tumor explants

From the cohort of 47 unmatched samples analyzed above, 43 of the samples were also cultured *ex vivo* as patient-derived explants (PDEs) in the absence and presence of the clinical antiandrogen, enzalutamide (ENZ; n=24 cultured with 10μM ENZ, n=19 cultured with 10μM and 50μM ENZ; ***Figure 3A***). This provided the unique opportunity to examine dynamic, treatment-related changes in lipid composition using patient-matched samples. *Ex vivo* culture alone had a minimal effect on lipid profile; 80% of lipid species had a correlation >0.5 between uncultured and cultured tissues (Supplementary Figure 6A). Transcript profiling and gene set enrichment analysis performed on a subset of these samples (n=12) confirmed significant downregulation by ENZ (10μM) of androgen signalling and multiple pathways associated with metabolism (***Figure 3B***). Independent qPCR validation confirmed the decrease in expression of canonical AR target genes *kallikrein 3* (encoding prostate specific antigen) and kallikrein 2 gene across the majority of samples (Supplementary Figure 6B). As expected based on clinical trial outcomes (18,19), the PDEs showed substantial heterogeneity in proliferative response to ENZ, measured as change in Ki67 proliferative index from matched vehicle-treated tissue (***Figure 3C***). The above features of the ENZ-treated PDEs were conducive to analysis of treatment-related dynamic changes in PL profile, and associations with decreased Ki67 index in individual samples. ENZ-related changes in 18 PL variables (including 15 individual species, featuring long-chain PC and PE lipids) were associated with Ki67 proliferation index (Supplementary Figure 6C and Supplementary Table S6; ***Figure 3D***). MALDI-MSI analysis of a subset of PDE tissues indicated that the majority of individual response-related lipids identified reflected the epithelial regions of the tumors, and treatment-related changes in abundance were evident (example of PC34:1 shown in ***Figure 3E***, boxplots in Supplementary Figure 6D). Dynamic changes in PL profile were therefore associated with response to AR inhibition across this cohort of PDEs.

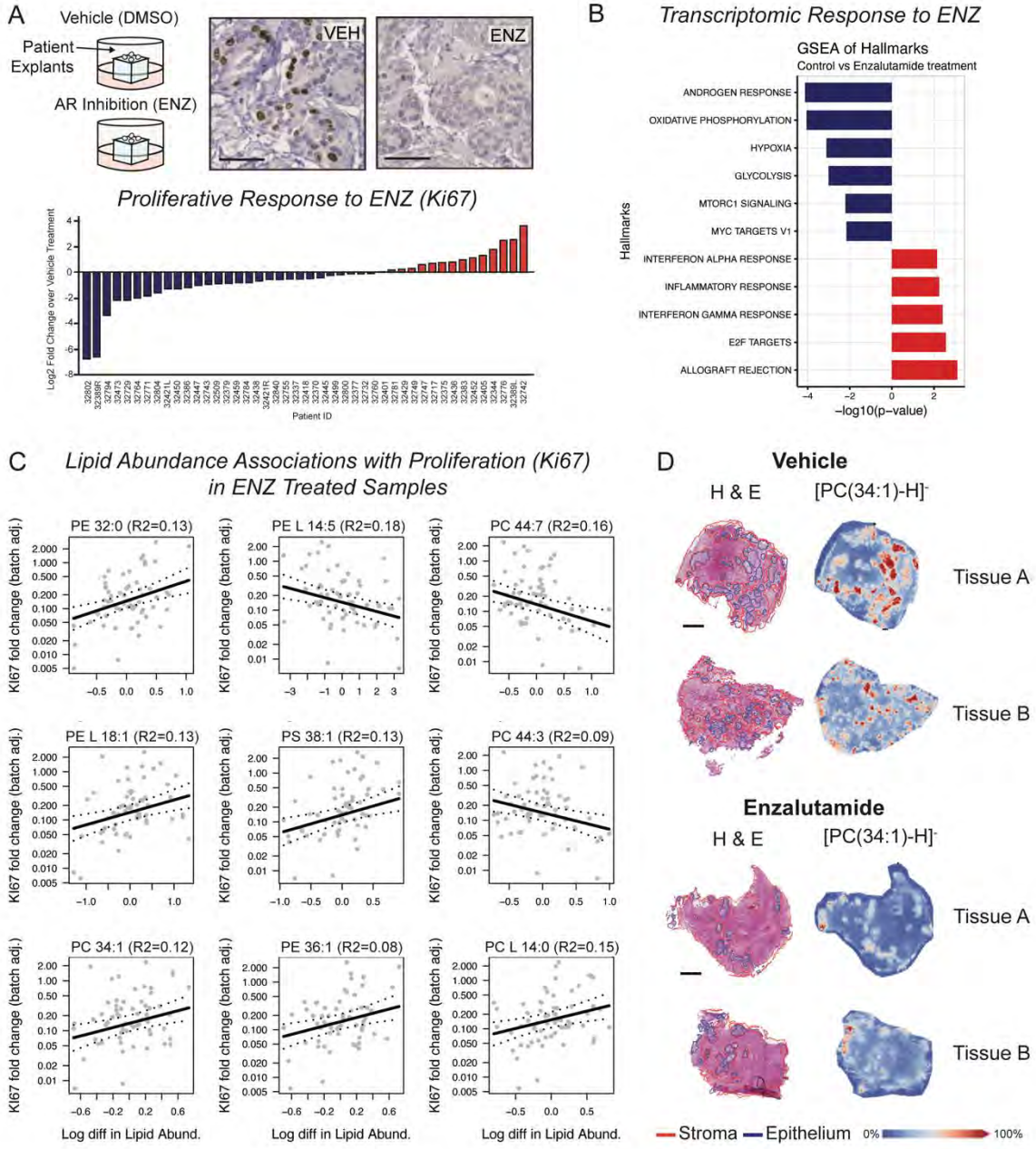
A
Vehicle (DMSO)
Patient Explants
AR Inhibition (ENZ)
VEH
ENZ
Proliferative Response to ENZ (Ki67)
Log2 Fold Change over Vehicle Treatment
Patient ID
B
Transcriptomic Response to ENZ
GSEA of Hallmarks
Control vs Enzalutamide treatment
ANDROGEN RESPONSE
OXIDATIVE PHOSPHORYLATION
HYPOXIA
GLYCOLYSIS
MTORC1 SIGNALING
MYC TARGETS V1
INTERFERON ALPHA RESPONSE
INFLAMMATORY RESPONSE
INTERFERON GAMMA RESPONSE
E2F TARGETS
ALLOGRAFT REJECTION
Hallmarks
−log10(p−value)
C
Lipid Abundance Associations with Proliferation (Ki67) in ENZ Treated Samples
PE 32:0 (R2=0.13)
PE L 14:5 (R2=0.18)
PC 44:7 (R2=0.16)
PE L 18:1 (R2=0.13)
PS 38:1 (R2=0.13)
PC 44:3 (R2=0.09)
PC 34:1 (R2=0.12)
PE 36:1 (R2=0.08)
PC L 14:0 (R2=0.15)
Ki67 fold change (batch adj.)
Log diff in Lipid Abund.
D
Vehicle
H & E
[PC(34:1)-H]⁻
Tissue A
Tissue B
Enzalutamide
H & E
[PC(34:1)-H]⁻
Tissue A
Tissue B
Stroma
Epithelium
0%
100%

Figure 6.3 Associations between phospholipid profile and tumor response to the clinical antiandrogen enzalutamide (ENZ). A. Variation in proliferative response of prostate tissues to ENZ across cohort B. Upper panel: Patient-derived explant culture setup for prostate tissue from Cohort B and Ki67 immunohistochemistry in a representative set of patient samples. Lower panel: Waterfall plot of individual patient response to ENZ, measured as log2fold change in Ki67 proliferative index. **B.** Gene set enrichment analysis for transcriptomic data from enzalutamide treated versus vehicle control tissues (n=12 patients). **C.** Correlation plots of phospholipid species whose change in abundance is significantly associated with response (change in Ki67 index) to ENZ ($p<0.01$). **D.** MALDI-mass spectrometry imaging of ion mass corresponding to PC34:1-H+ in 2 independent prostate cancer tissue cores from a single patient, showing epithelial localization and ENZ-related change in abundance.

6.4.4 Targeting lipidomic changes in clinical tumors suppresses cellular proliferation

To determine whether the cancer-associated alterations in PL composition directly influence cellular proliferation, or merely accompany tumorigenesis, we pharmacologically targeted two of the key lipidomic changes we detected (i.e. enhanced lipogenesis and elongation of fatty acyl chains in the PLs) in patient-derived explants (PDEs) of clinical prostate tissues. Inhibition of acetyl CoA carboxylase (ACC1/2), which depletes the cellular content of malonyl CoA, was selected as a strategy to simultaneously inhibit both synthesis and elongation of fatty acids (***Figure 4A***). We utilized PF-05175157, an ACC1/2 inhibitor (20), as a proof of principle tool. Culture of PDEs with PF-05175157 (50μM) for 48 or 72 hours (***Figure 4B***) markedly suppressed epithelial cell proliferation in the tumors (n=13) compared to matched, vehicle-treated control tissues (***Figure 4C***). Enhanced epithelial staining of pACC1, a marker of ACC inhibition by PF-05175157 in prostate cancer cells (Supplementary Figure 7B), confirmed that the agent was effectively targeting ACC activity in the tumors ($p<0.01$; ***Figure 4D***). Moreover, PL profiling by mass spectrometry revealed a pronounced shortening of PL fatty acyl chains in the majority of PF-05175157-treated tumors (***Figure 4E***; Supplementary Figure 7). Together, these data link the efficacy of PF-05175157 to ACC1 inhibition in the tissues.

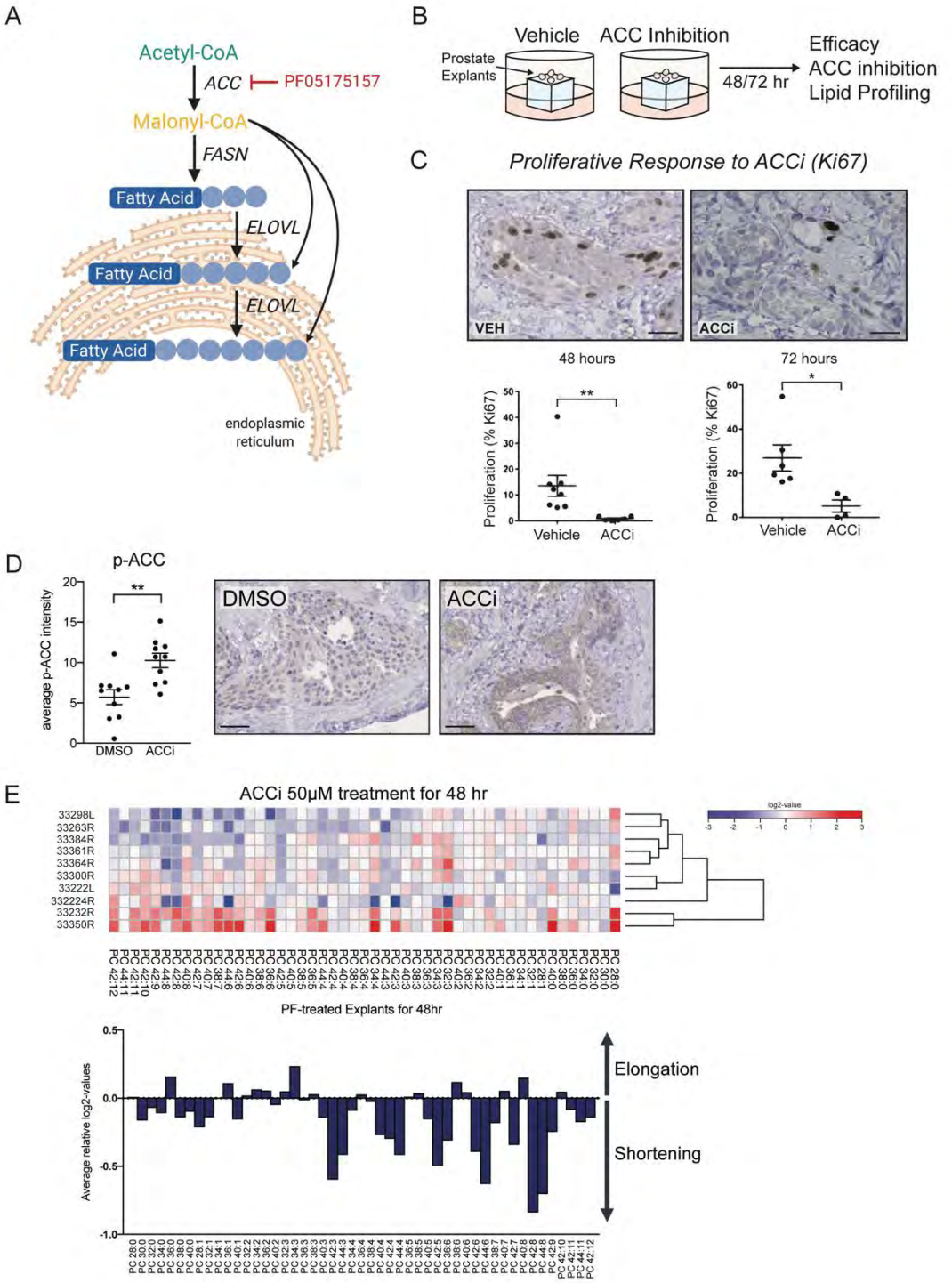
A
Acetyl-CoA
ACC
PF05175157
Malonyl-CoA
FASN
Fatty Acid
ELOVL
Fatty Acid
ELOVL
Fatty Acid
endoplasmic reticulum
B
Vehicle
ACC Inhibition
Prostate Explants
48/72 hr
Efficacy
ACC inhibition
Lipid Profiling
C
Proliferative Response to ACCi (Ki67)
VEH
ACCi
48 hours
72 hours
Proliferation (% Ki67)
Vehicle
ACCi
D
p-ACC
average p-ACC intensity
DMSO
ACCi
E
ACCi 50μM treatment for 48 hr
log2-value
PF-treated Explants for 48hr
Average relative log2-values
Elongation
Shortening

Figure 6.4 Efficacy of acetyl CoA carboxylase inhibition in patient-derived prostate explants. A. The ACC1/2 inhibitor PF-05175157 targets fatty acid synthesis and chain elongation. **B.** Patient-derived explant culture setup and workflow. **C.** Antiproliferative activity, measured by Ki67 proliferative index, of PF-05175157 (50μM) compared to vehicle-treated matched control tissue in patient-derived explants (PDEs; n=13 patients). **D.** Immunohistochemical detection and quantification of pACC1 intensity in PDEs cultured in the absence and presence of PF-05175157. **E.** Treatment-induced alterations (expressed as log2-fold change in the heatmap) in PC phospholipid abundance for PDEs cultured with PF-05175157. Altered relative fatty acyl chain length for the upper cluster of PDEs are further visualized graphically.

6.5 Discussion

Using mass spectrometry-based lipidomics to sensitively quantify and visualize PL species in clinical tissues, we have provided new insight into the changes in lipid composition that accompany prostate cancer development. Moreover, this is the first report of dynamic, treatment-related changes in lipidomic profiles and the efficacy of targeting lipid metabolic enzymes in a clinical tissue context. This study therefore moves beyond previous cell-line based approaches to demonstrate that, despite the observed heterogeneity at the level of individual lipid species, recurrent and clinically-actionable changes in PL metabolism can be detected in tumors; some of which may represent common vulnerabilities. Lipidomic profiling of prostate tumor biopsies, possibly guided by imaging approaches as highlighted in several recent reports (16,17), has the potential to provide new information about disease features and, potentially, patient responsiveness to therapeutics such as enzalutamide.

While robustly associated with sample malignancy, PL profile was only weakly linked to the most common clinicopathological characteristics of prostate cancer; PSA levels and Gleason score. While this may reflect limitations in the sample size of our cohorts, it also raises the possibility that lipidomic profiling may provide independent information regarding tumor biology and prognosis. Moreover, the associations we detected between lipid profiles and the TMPRSS2-ERG molecular subtype and Ki67 proliferative index are interesting observations that warrant further investigation in larger independent tissue cohorts, particularly in light of our recent report of Ki67 status in localized prostate cancer being a significant predictive biomarker of subsequent metastatic relapse (21).

Despite differences in the breadth and scope of lipid classes measured, certain key cancer-related changes in PL profile reported here support the findings of previous imaging-based studies, notably for altered abundance and/or elongation of PC and PI-based lipids and ceramides (reviewed in (2,22)). While the functional consequences of individual lipid changes remain to be elucidated, PI lipids are of fundamental importance in cancer cells as they form the membrane scaffold for kinase and phosphatase activity that supports oncogenic signalling. Moreover,

altered acyl chain length of PI-based lipids has been linked to p53 mutational status (23), a common genomic alteration in clinical prostate cancer. The results are also largely consistent with our earlier observed overexpression of lipid synthetic enzymes, such as FASN, in cancer cells, which correlates with a shift towards MUFA-containing species, at the expense of PUFA-containing species (11). Similarly, the tumor-related shift from saturated to monounsaturated PC species that we found to be significantly associated with sample malignancy is concordant with the earlier observed overexpression of SCD in certain cancer tissues (24-27). The novel changes in acyl chain length and head group switches that we detected may be related to reported alterations in enzymes involved in acyl chain elongation including ELOVL enzymes, modulators of malonyl-CoA levels including ACC, FASN and malonyl-CoA decarboxylase and head group-modifying enzymes including PS decarboxylase (28-32). Tumor-specific activation/inactivation patterns of these individual enzymes, most likely driven by tumor-specific oncogenic signalling (33-38), may lead to the unique phospholipid profile that is characteristic for every individual tumor. In view of the evidence that the lipid composition of cellular membranes affects numerous aspects of cell biology (reviewed in (39)), including membrane fluidity and curvature, vesicle formation, signal transduction (40), ion channel activity (41,42), susceptibility to lipid peroxidation (11), resistance to oxidative stress (11), energy metabolism (43), and uptake and response to chemotherapeutics (11), even subtle changes within the lipidome may be critical to support the cancer phenotype and treatment resistance. Given the lipidome is an integration of oncogenic events and an effector of numerous cancer-related processes, it is expected that the tumor lipidome holds significant potential for biomarker discovery and identification of novel targets that may be used in a theranostic setting (44).

While inter-patient heterogeneity was evident in PL profiles from clinical prostate tissues in the current study, particularly at the individual lipid species level, more consistent changes in broader lipid metabolic processes were evident. Notable among these were proportionally higher fatty acid monounsaturation, and elongation of the PL fatty acyl chains. Considering these phenotypes, inhibition of acetyl CoA carboxylase (ACC) presented an appealing approach to simultaneously target de novo biosynthesis and elongation of intracellular fatty acids by restricting

production of the substrate for long chain fatty acid biosynthesis, malonyl CoA (45,46). To date, the focus for development of ACC inhibitors has been their ability to inhibit *de novo* lipogenesis and increase fatty acid oxidation, thereby reducing lipid accumulation and improving insulin sensitivity in patients with diabetes or non-alcoholic liver steatosis. There has, however, been considerable interest in repurposing these agents for oncology, particularly for lipogenic tumors such as prostate and breast, in which potential side-effects would be less of a concern. Here, as proof of principle, we utilized a spiroketone derivative ACC1/2 inhibitor, PF-05175157, developed by Pfizer as a clinical agent for treatment of Type 2 diabetes and non-alcoholic hepatic steatosis (20). Our results show marked efficacy for this agent in reversing the chain elongation phenotype and reducing epithelial cell proliferation in clinical PDEs, raising the promise that this class of agents may be efficacious in clinical prostate cancer. While the possibility of off-target effects of this compound contributing to its antiproliferative effects cannot be discounted, we have used two lines of evidence to associate efficacy with ACC inhibition in the tissues. First, we assessed the tissue levels of Ser79-phosphorylated ACC1, which is the inactive form of ACC1, the predominant isoform in prostate cells. This phosphorylation was induced by PF-05175157 treatment of prostate cancer cells and in PDEs. Second, our PL profiling of the treated tissues revealed consistent shortening of the fatty acyl chains, indicative of decreased elongation reactions. Taken together, our findings provide the first evidence that ACC inhibition can be achieved in the context of a complex tumor microenvironment and provide impetus for further investigation of ACC inhibition in prostate cancer. In light of the marked tumor-associated changes in fatty acyl chain saturation, and particularly monounsaturation, future studies targeting desaturases such as SCD1, shown recently to be a promising therapeutic target in prostate cancer (47), would also distinguish causality from association for this alteration.

In summary, the cancer-related changes in PL profiles we have detected in clinical tissues strengthen the case for lipidomics as a source of novel molecular cancer biomarkers and therapeutic targets, as well as an indicator of the underlying biology from which PL profiles are derived. Defining subtypes of lipid profile in tumors, rather than immortalized cell lines, and the underlying mechanisms in this and other association-based studies are all critical future endeavors if key components of lipid

metabolism are to be effectively targeted in clinical disease. The heterogeneity of PCa evident from our work reinforces the concept that such approaches must also be personalized to the individual patient's biology. Our findings warrant further functional investigation of lipidomes in other cancer types, to unravel the molecular mechanisms underlying these changes and to explore the impact on membrane functioning and, ultimately, on cancer development and progression.

6.6 Materials and Methods

6.6.1 Tissue collection

A. Matched normal/tumor cohort. Prostate tumor tissues with matching normal samples were obtained from patients who had undergone radical prostatectomy (Centre Hospitalier Universitaire de Liège, Belgium). Samples were snap-frozen and stored at -80°C for lipid and protein extractions. Normal and tumor tissues were identified by histological analysis of adjacent tissue, Gleason scores were determined, and the percentage of cancer was estimated (48). All tumor samples used for lipidomics were verified to contain at least 75% prostate adenocarcinoma by histological examination. The Local Commission for Medical Ethics and Clinical Studies at the University of Liège approved the use of clinical samples. Approval to perform lipidomics analysis on clinical samples was obtained from the local Ethical Committee of KU Leuven.

B. Unmatched patient tissue cohort. Prostate tissues were collected with written informed consent from patients undergoing radical prostatectomy at St Andrew's Hospital, Adelaide, Australia. A longitudinal section of each tissue was removed prior to *ex vivo* culture (described below). Half was snap frozen and the remainder fixed in formalin and paraffin embedded for assessment by a pathologist. Ethical approval for tissue collection and experimentation was obtained from St Andrew's and the University of Adelaide Human Research Ethics committees. Histopathologic features of all tumors used in this study are detailed in Supplementary Table 1; an additional 5 patients with only benign prostatic hyperplasia and no evidence of cancer were also analyzed with this cohort.

6.6.2 *Ex vivo* culture of primary prostate tissues

Prostate specimens were dissected and cultured as patient-derived explants for 48 hours in the presence and absence of enzalutamide (ENZ; Selleckchem; 10 or 50μM) or the ACC1/2 inhibitor PF-05175157 (Pfizer; 50μM), as previously described (49). In each case, following culture, tissue was either formalin-fixed and paraffin embedded for histology or snap frozen for lipidomics and/or RNA extraction.

6.6.3 MALDI mass spectrometry imaging

Frozen sections of prostate tissue (10µm) were thaw-mounted on super-frost ultraplus microscope slides and matrix (10mg/ml α-CHCA in methanol) applied to tissue sections by sublimation. The sections were analyzed on a MALDI SYNAPT HDMS Mass Spectrometer (Waters Corporation, Manchester, UK). The laser raster-size was set at 60µm (x,y) and off-tissue areas provided QC spots for data filtering. MALDI raw spectrum files were converted to MSI data files by high definition imaging (HDI) software (Waters Corporation, Manchester, UK). The data processing settings were resolution 8,000 full-width half-height (FWHM) at mass window of 0.02 Da at a (restricted) mass range of *m/z* 400-990 Da. The top 1000 mass features were selected for processing and statistical analysis was carried out using the web-based *MetaboAnalyst* R package (48). The MSI ion map were overlaid or aligned to adjacent pathologically annotated histopathology images to identify morphological regions of interest (ROIs). Equivalent number of data points (3 pixels/mass spectra) from multifocal adenocarcinoma areas and off-tissue regions were selected. The data points were then exported as a single .csv file in the form of ROI's vs mass features with relative intensity (abundance) as the variable. Before import into *MetaboAnalyst*, the data was filtered in R studio 3.4.4 using baseline packages. The pre-filtered .csv files were uploaded into *MetaboAnalyst* R in the format of spectral bins, data filtering was done by inter-quantile range and data was normalized by log transformation and pareto scaling. Heatmaps were generated by hierarchical clustering and top 25 mass features (identified by ANOVA) were visualized. Principal component analysis (PCA) score plots indicated the relative variation of multifocal ROI's based on distribution of lipid species. For negative ion mode imaging, the methodology was adapted as follows: Norharmane matrix (7 mg/mL) (Sigma-Aldrich) in CHCl3:MeOH (7:3 v/v) was applied to the tissue sections with a SunCollect sprayer (SunChrom, Friedrichsdorf, Germany). Data processing settings were resolution 8,000 FWHM at mass window of 0.02 Da at a (restricted) mass range of *m/z* 50-990 Da. Full-scan MSI data was imported into Python and a custom script used for ROI selection. All images, mass spectra and boxplots were generated after total ion current normalization of the acquired data.

For validation of ESI-MS/MS data in patient-derived explants, we conducted MALDI imaging using a timsTOF FleX mass spectrometer (Bruker Daltonik, Bremen, Germany). Briefly 10µm thick frozen tissue sections were thaw mounted onto ITO slides, spray coated with *ca* 500 µL of 7 mg/mL αCHCA matrix using a SunCollect MALDI sprayer (Sunchrom GmbH, Friedrichsdorf, Germany). Data were acquired with a 20 µm pixel size and a 20 µm laser step-size over *m/z* 50-1250. Imaging data was imported into SCiLS Lab 2020a (Bruker Daltonik, Bremen, Germany). Spectra were normalised to total ion count, with weak denoising, and segmentation analysis was preformed using bisecting k-means algorithm with correlation distance metric in SCiLS Lab. Segments which aligned with the epithelia in matched H&E stained sections were selected for each tissue. Box plots of the relative intensity of *m/z* of interest were generated from these segments.

6.6.4 ESI-MS/MS-based lipidomics

Lipid extracts were generated by homogenizing approximately 40mg of tissue in 800µl PBS with a Dounce or a Precellys (Bertin Technologies) homogenizer. An aliquot of 100µl was set aside for DNA quantification. The remaining 700µl was transferred to a glass tube with Teflon liner and 900µl 1N HCl:CH_3OH 1:8 (v/v), 800µl $CHCl_3$ and 500µg of the antioxidant 2,6-di-tert-butyl-4-methylphenol (BHT) (Sigma, St. Louis, MO) were added. DNA concentration was measured using Hoechst 33258 reagent (Calbiochem, La Jolla, CA). The appropriate lipid standards (Avanti Polar Lipids Inc., Alabaster, AL) were added based on the amount of DNA of the original sample (per mg DNA: 150nmol PC26:0; 50nmol PC28:0; 150nmol PC40:0; 75nmol PE28:0; 8.61nmol PI25:0 and 3nmol PS28:0). After mixing for 5 min in a rotary shaker and phase separation (by centrifugation at 17300xg, for 5 min at 4°C), the lower organic fraction was collected using a glass Pasteur pipette and evaporated using a Savant Speedvac spd111v (Thermo Fisher Scientific, Waltham, MA). The remaining lipid pellet was covered with argon gas and stored at -20 °C. Before ESI-MS/MS measurement, lipid pellets were reconstituted in diluent (CH_3OH:$CHCl_3$:NH_4OH; 90:10:1.25, v/v/v) according to the amount of DNA in the original cell sample (1µl diluent / 1µg DNA). Phospholipid species were analyzed by ESI-MS/MS on a hybrid quadrupole linear ion trap mass spectrometer (4000 QTRAP system; Applied Biosystems, Foster City, CA) equipped with an Advion

TriVersa robotic nanosource for automated sample injection (Advion Biosciences). For quantification of individual phospholipid species, the system was operated in multiple reaction monitoring (MRM) mode. MRM transitions were built based on the release of the phospholipid head group as ion or as neutral species during tandem MS experiments. Analysis was performed using Rapid Lipid Profiling v2.2. Data were corrected for carbon isotope effects. Blank samples consisting of only diluent were measured to determine background signals. Only phospholipid species with an intensity > 5-fold the intensity of the blank were considered true signals. PL were annotated using “lipid subclass” and the “C followed by the total fatty acyl chain length:total number of unsaturated bonds”. The circle plot of lipidomic alterations was generated using the circlize R package (50).

6.6.5 RNA extraction and sequencing

RNA was extracted from cultured PDE tissues as previously described (51). Total RNA samples were treated with Ribo-Zero to deplete rRNA prior to library construction with the Illumina TruSeq RNA kit. Sequencing was performed on an Illumina NextSeq 500 to generate 1×100bp single-end reads. Library preparation and sequencing were performed at the Genomics Facility of the South Australian Health and Medical Research Institute (Adelaide, Australia). The quality and number of reads for each sample were assessed with FastQC v0.11.3. Adaptors were trimmed from reads, and low-quality bases, with Phred scores < 28, were trimmed from ends of reads, using Trimgalore v0.4.4. Trimmed reads of < 20 nucleotides were discarded. Reads passing all quality control steps were aligned to the hg38 assembly of the human genome using TopHat v2.1.1 (52) allowing for up to two mismatches. Reads not uniquely aligned to the genome were discarded. HTSeq-count v0.6.1 (53) was used with the union model to assign uniquely aligned reads to Ensembl Hg38.86-annotated genes. Data were normalized across libraries by the trimmed mean of M-values (TMM) normalization method, implemented in the R v3.5.0, using Bioconductor v3.6 EdgeR v3.20.9 package (54). Only genes expressed at a count-per-million above 0.5 for at least 18 out of 36 samples were analysed for evidence of differential gene expression. Differentially expressed genes were identified using the quasi-likelihood negative binomial generalized log-linear model implemented in EdgeR and were defined as having an FDR adjusted

P value of < 0.05. Gene Set Enrichment Analysis (GSEA) was undertaken using camera() function in the R limma v3.34.9 package.

6.6.6 Immunohistochemical staining

Sections (3 µm) of paraffin-embedded cultured patient-derived explants were immunostained essentially as described previously (49). Briefly, antigen retrieval was performed using Tris-EDTA buffer, pH 6.5 using a Biocare Medical Nexgen decloaker at 115°C for 15 min. Tissue slides were then incubated at room temperature with 10% goat serum block. Primary antibody against Ki67 (DAKO, M7240; 1:200), ERG (Abcam, ab92513; 1:400) or pACC1 (Cell Signaling, 3661S; 1:400) was applied and slides incubated overnight at 4°C. Secondary antibody anti-rabbit (DAKO E0432, Lot #20027287) was applied for one hour, followed by HRP-conjugated streptavidin (DAKO, P0397, Lot #20040879) at 1:500 for one hour and visualization by DAB.

6.6.7 Statistical analysis

Matched patient tissues: *Cohort A*. In the n=21 sample with matched tumour and disease free tissue a mixed effects regression of the within individual difference in lipid variable adjusting for lipid variable in normal tissue sample and individuals age. A random intercept was included per batch, error variance was allowed to differ with batch, and a compound symmetry correlation structure for errors within batches (R package nlme). Restricted maximum likelihoods of this full model is compared with a reduced model without the error variance and correlation structure and the full model chosen only when 2 times the difference in log likelihoods exceeded the 95th percentile of $\chi 2(df=1)=3.84$. The lipid variables consisted of log2 transformed species abundance, saturation group abundance and saturation group mean chain length. Prior to these calculations lipid species abundances in each sample were standardized to the median abundance across all samples (ref Dieterle et al 2006).

Unmatched patient tissues: *Cohort B*. In the cohort of n=47 with single tissue samples per individual, for associations with sample malignancy similar mixed effects regression to those described above (same random effects structure) were constructed for each lipid variable as outcome, however the only fixed effect

covariate was age. In the subset of 28 individuals with malignant samples associations between lipid variables and serum PSA employed the same mixed effects regression models with sample malignancy replaced by log transformed PSA as a fixed effect and sample Gleason score included as an additional covariate.

Proliferation associations. For associations with Ki67 both in Day 0 samples and in vehicle vs ENZ treated samples we analyze repeated count data across fields of view within a sample using a beta-binomial mixed effects regression (R package glmmTMB). In the Day 0 analyses, the lipid variables are the primary predictors of interest with batch and age being included as fixed effect covariates. In the treated samples, the primary predictor of interest is the batch-adjusted difference between ENZ and vehicle, with batch, age and lipid variable vehicle as fixed effects. In all models, a random intercept is included per individual, with a logit link for the mean Ki67 cell positivity prevalence.

For each set of outcomes the distribution of p-values for the species abundance associations is assessed to determine the presence of a signal (deviation from the uniform distribution) (55) and the FDR reported for the number of significant associations defined as $p<0.01$. To address concerns that an apparent signal may be due to a combination of insufficient comparisons and clustering between lipid species, we perform a permutation test with 1000 permutations of the clinical outcome, and define the fraction of significant associations are beyond that observed in the original cohort as the permutation p-value. These permutation analyses are performed within batches and where appropriate within malignancy groups, and by design retain the between lipid correlation structure.

Other statistical analyses. Statistical analysis for lipid or immunostaining quantification and PDE *ex vivo* culture experiments, was carried out using GraphPad Prism software v7.02 (2016, GraphPad Software). Significance was measured by two-tailed unpaired t-test or One-way ANOVA with Dunnett's multiple comparison test as indicated. Significance is expressed as $*P < 0.05$, $**P < 0.01$ and $***P < 0.001$.

Table 6.1 Conserved lipid associations with malignancy in clinical prostate samples.

Variable	Lipid ID	Est [95% CI]	p-value
Lipid Abundance	PI 38:6	-0.35 [-0.36, -0.33]	6.52E-19
	PI 40:6	0.19 [0.18, 0.21]	1.78E-14
	PS 40:8	1.10 [1.00, 1.20]	6.40E-14
	PC 36:4	-0.56 [-0.64, -0.49]	3.51E-11
	PC 34:1	0.17 [0.14, 0.20]	5.81E-10
	PC 40:4	-0.45 [-0.57, -0.33]	1.18E-06
	PI 38:5	-0.68 [-0.89, -0.48]	4.51E-06
	PS 42:8	0.70 [0.50, 0.90]	2.20E-05
	PS 42:2	-0.26 [-0.35, -0.16]	4.08E-05
	PS 42:4	-0.23 [-0.32, -0.14]	8.25E-05
	PE 42:6	0.75 [0.44, 1.06]	0.000149
	PI 36:4	-0.68 [-0.96, -0.39]	0.000203
	PE 42:5	0.51 [0.29, 0.74]	0.000255
	PS 38:4	-0.66 [-0.96, -0.36]	0.000399
	PC 38:4	-0.52 [-0.77, -0.27]	0.000693
	PS 36:2	-0.32 [-0.48, -0.16]	0.000753
	PS 36:1	-0.46 [-0.68, -0.23]	0.000789
	PC 32:0	-0.66 [-0.98, -0.33]	0.000832
	PS 38:3	-0.72 [-1.08, -0.36]	0.000942
	PC 40:6	-0.36 [-0.55, -0.18]	0.001045
	PS 38:6	-0.82 [-1.24, -0.40]	0.001116
	PE 40:4	0.042 [0.02, 0.065]	0.001414
	PC 38:5	-0.38 [-0.59, -0.18]	0.001489
	PE 38:7	0.36 [0.17, 0.56]	0.001681
	PI 38:4	-0.50 [-0.80, -0.20]	0.001944
	PC 36:5	-0.40 [-0.60, -0.20]	0.002105
	PS 44:6	0.52 [0.23, 0.81]	0.002306
	PI 36:1	0.51 [0.22, 0.80]	0.00274
	PS 42:9	0.47 [0.19, 0.75]	0.003707
	PS 40:4	-0.48 [-0.77, -0.20]	0.003719
	PE 42:9	0.45 [0.16, 0.73]	0.005855
	PE 40:6	0.36 [0.13, 0.60]	0.006456
	PE 40:8	0.28 [0.10, 0.46]	0.006487
	PC 40:5	-0.30 [-0.50, -0.10]	0.008872
Mean Chain Length	PE 3	-0.13 [-0.14, -0.12]	7.43E-14
	PS 1	0.13 [0.07, 0.18]	0.000187
	PE 6	0.11 [0.06, 0.15]	0.000209
	PI 1	0.19 [0.11, 0.27]	0.000231
	PS 3	0.096 [0.048, 0.144]	0.000948
Saturation Abundance	PC 6	-0.0021 [-0.0024, -0.0017]	6.10E-10
	PI 2	0.013 [0.01, 0.015]	2.16E-08
	PE 3	0.0029 [0.0022, 0.0037]	9.74E-07
	PS 8	0.0036 [0.0026, 0.0046]	1.82E-06
	PS 9	0.00078 [0.00048, 0.00108]	6.25E-05
	PC 4	-0.038 [-0.056, -0.021]	0.00046
	PC 1	0.066 [0.033, 0.098]	0.000959
	PC 5	-0.0071 [-0.0107, -0.0034]	0.001172
	PI 5	-0.0016 [-0.0025, -7e-04]	0.002608
	PS 3	-0.0088 [-0.0139, -0.0036]	0.003266
	PC 0	-0.013 [-0.021, -0.005]	0.004081
	PS 4	-0.0079 [-0.0133, -0.0025]	0.009611

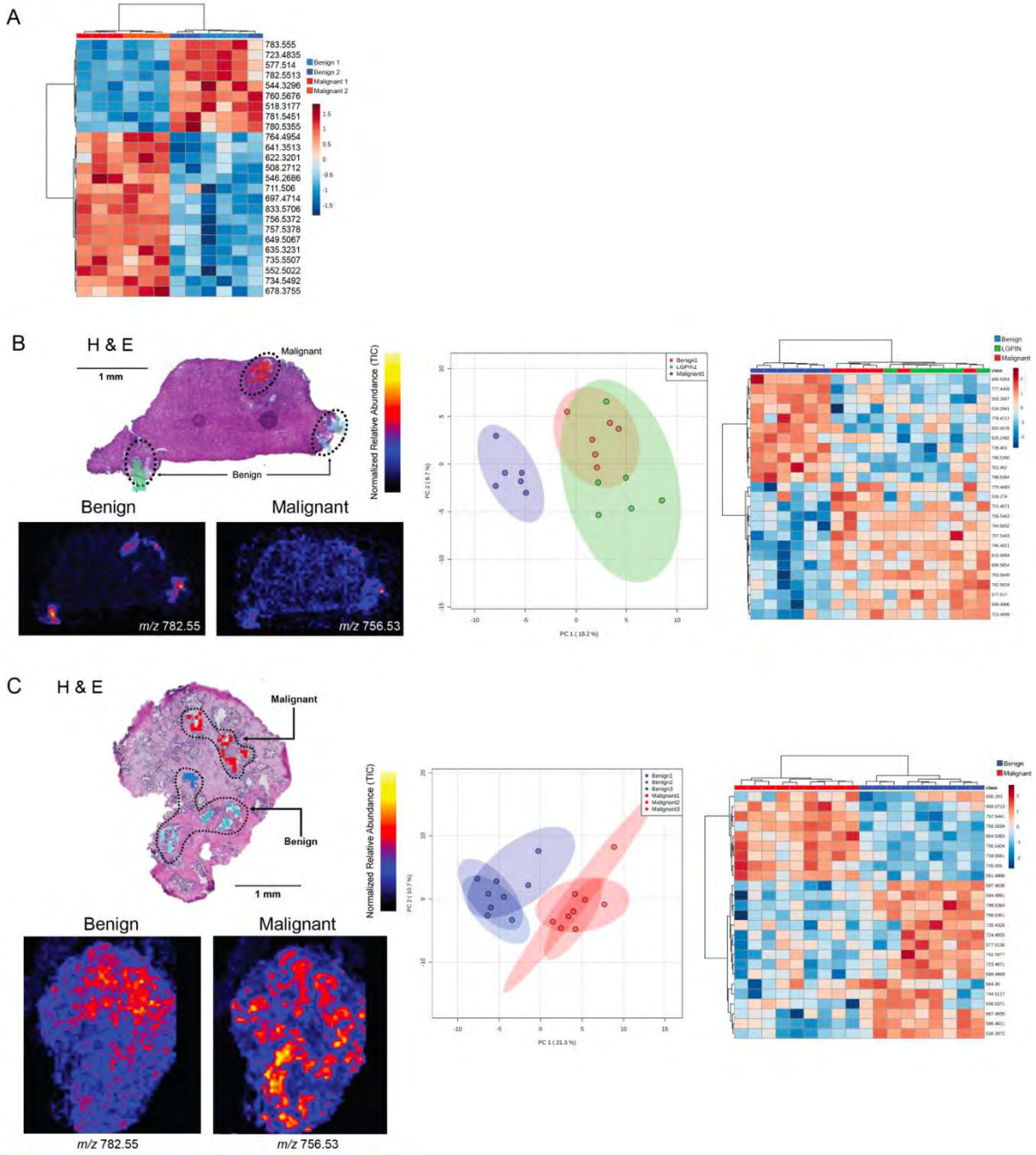

Supplementary Figure 6.1 MALDI-mass spectrometry imaging of regions of interest in pathologically heterogeneous prostate tissue from 3 individual prostate cancer patients, including ion maps of two representative examples of histology-restricted lipid masses, principal component and heatmap analysis of the top 25 mass features distinguishing benign from malignant regions of tissue for each patient.

A

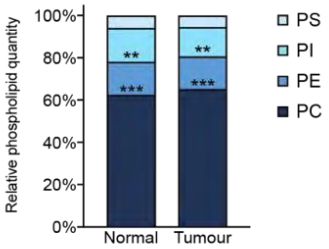

B *Phospholipid Elongation in PI and PS*

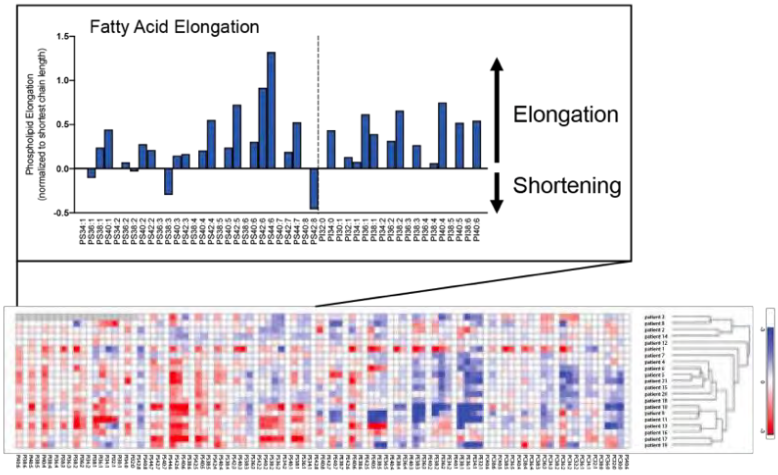

C *Average Chain Length in Normal vs Tumour*

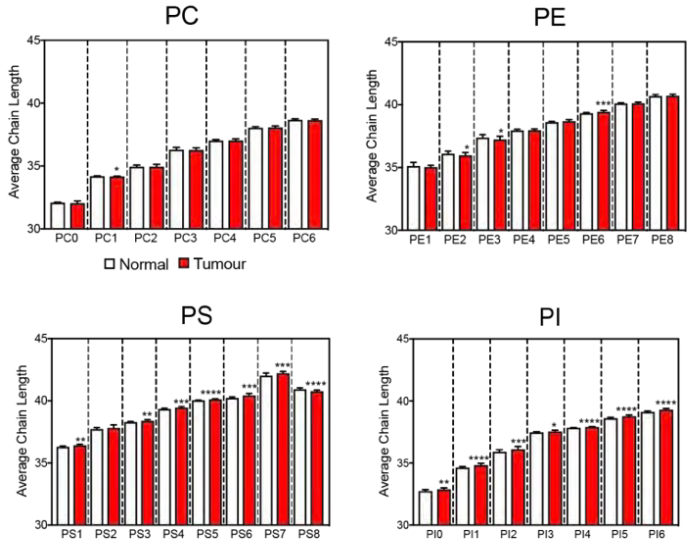

Supplementary Figure 6.2 Cancer-related changes in phospholipid composition in matched non-malignant and malignant tissues from prostate cancer patients (n=21). A. Relative proportions of PC, PE, PS and PI phospholipid classes across the patient cohort. **B.** Heatmap clustering of changes in PI, PS, PE and PC fatty acid chain length and saturation in prostate tumours versus matched non-malignant tissue. Each row represents a patient, and each column represents a different phospholipid species. The elongation can be observed as vertical striation patterns of increased chain lengths for each saturation group and is represented graphically for the PS and PI species in the inset box. **C.** Tumor-related changes in average chain length for each main phospholipid class.

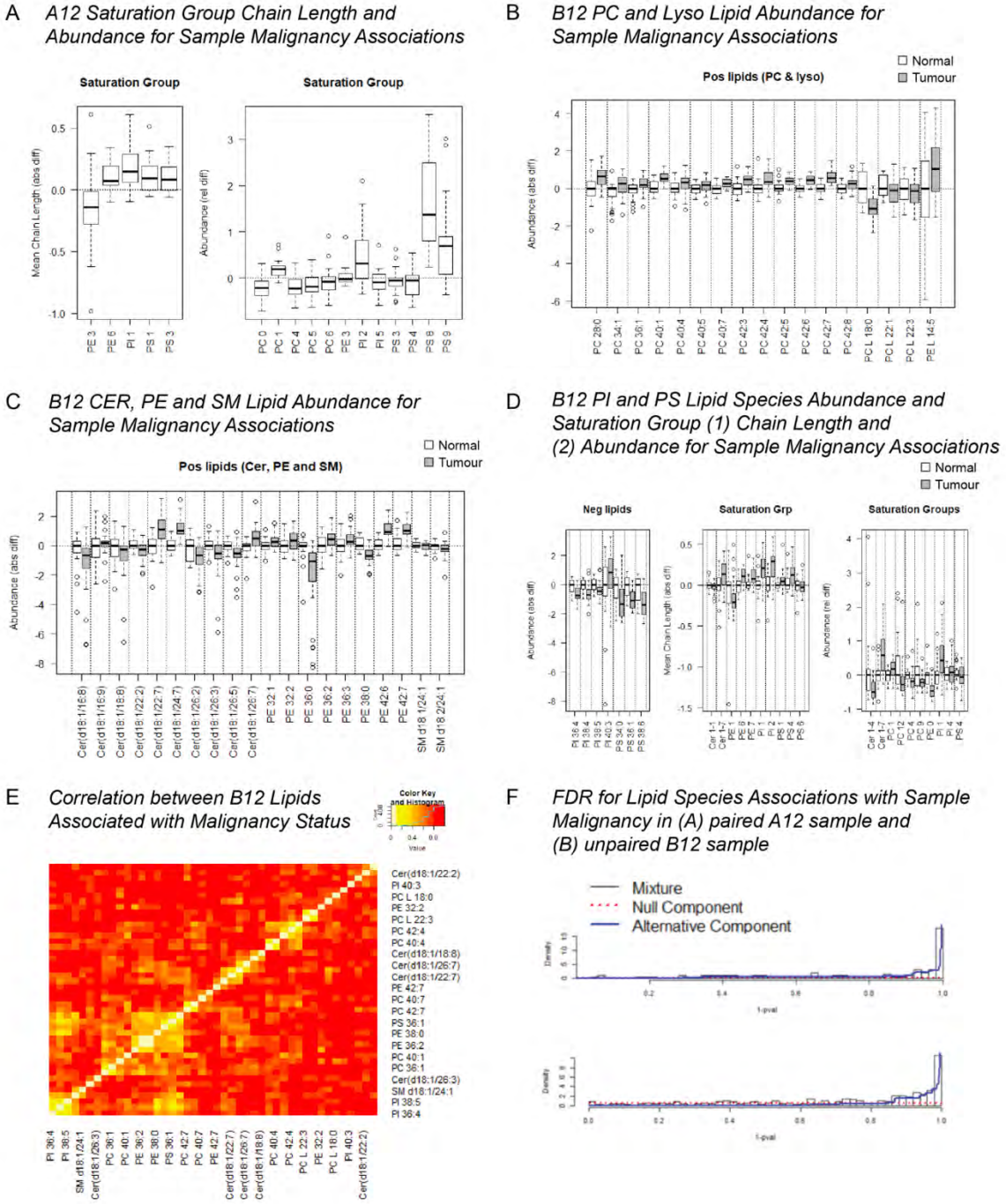

Supplementary Figure 6.3 Phospholipid species associations with malignancy. A. FDR for PL associations with malignancy in Cohorts A and B. **B.** Saturation group chain length and abundance associations with malignancy in Cohort A. **C, D, E.** PL abundance associations with malignancy in Cohort B. **F.** Correlation plot of individual phospholipid species significantly associated with sample malignancy in Cohort B.

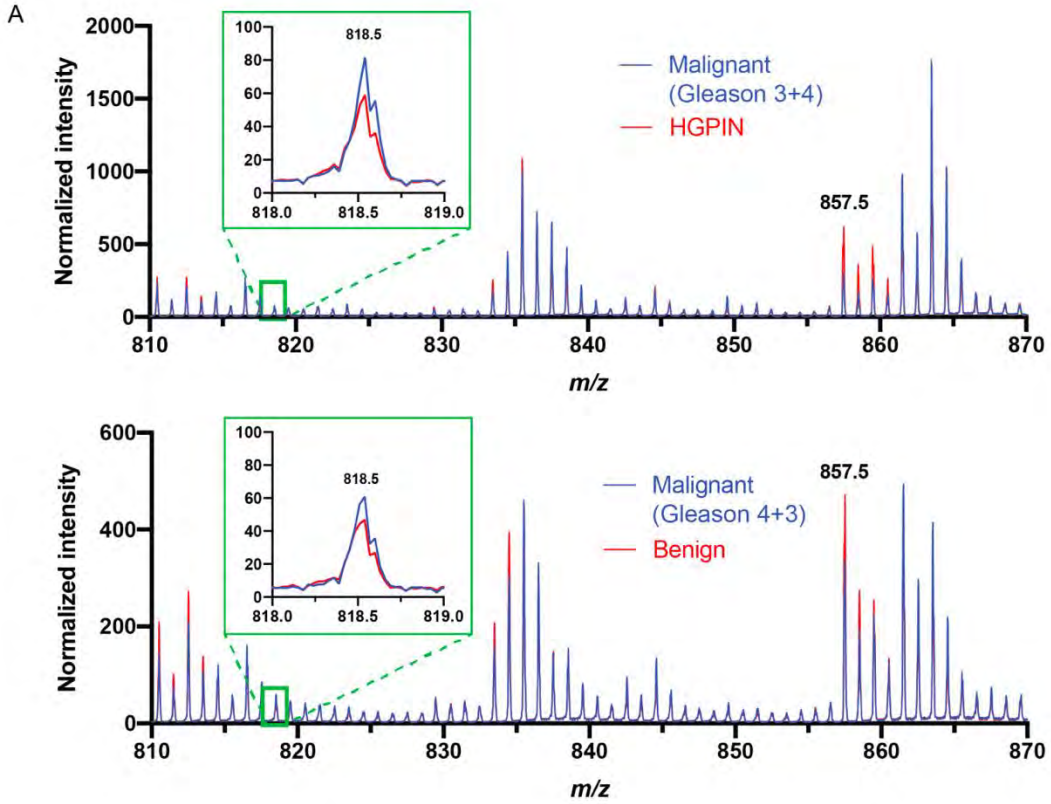

Supplementary Figure 6.4 MALDI-mass spectrometry imaging-derived spectra of discrete histological foci (non-malignant versus malignant as indicated) in 2 independent prostate cancer patients.

A *p-value distribution for lipid species associations with Ki67 in (A) A12 Malignant Samples and (B) A12 Non-malignant Samples*

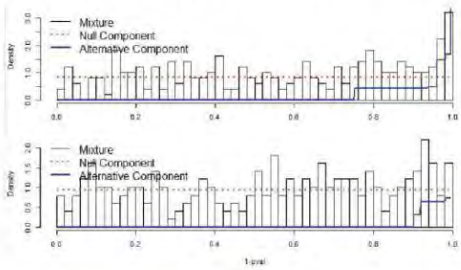

B *p-value distribution for lipid species associations with (A) PSA; (B) GS and (C) ERG respectively.*

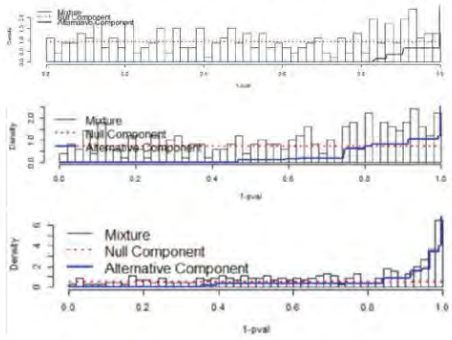

C *Lipids Associated with Sample Gleason Score in samples (1) without tumour and (2) with tumour*

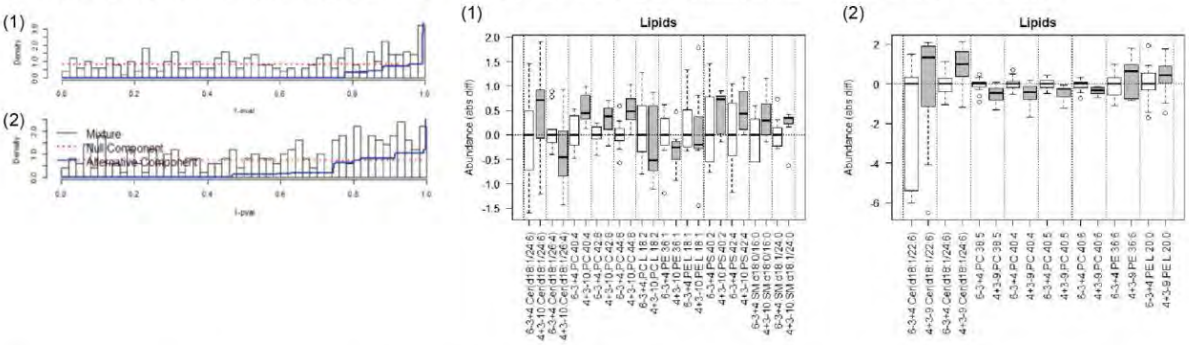

D *Lipid Abundance Associated with ERG Status (p<0.01)*

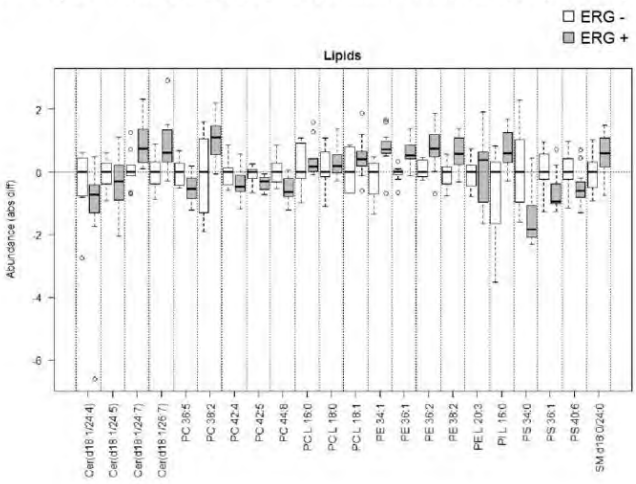

E *Lipid Saturation Groups Associated with ERG Status (p<0.01)*

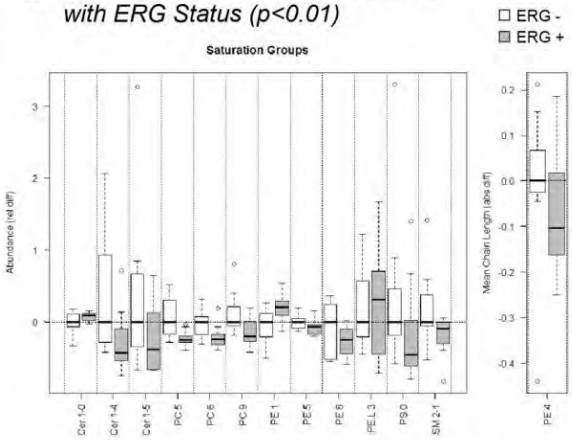

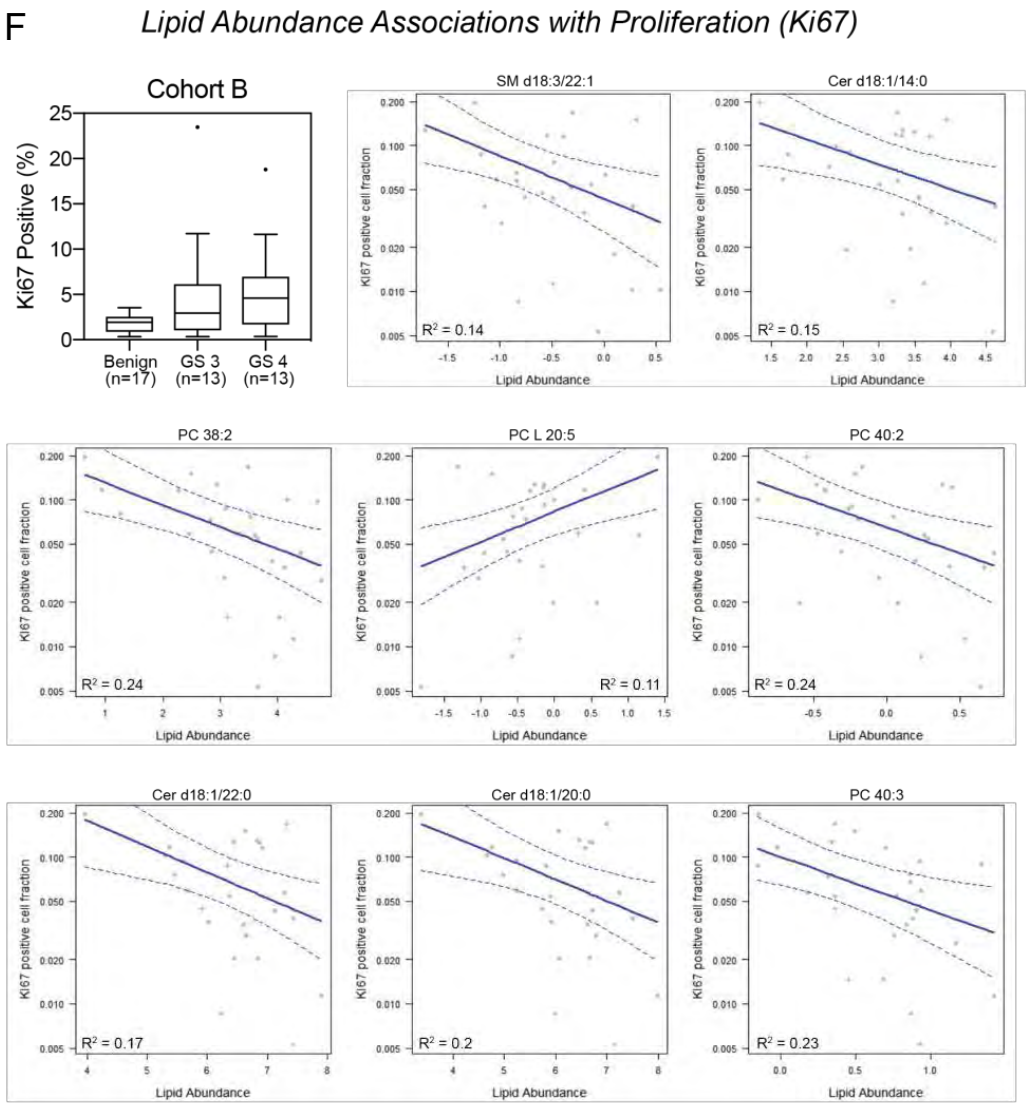

Supplementary Figure 6.5 Associations of lipid measures with tumor clinicopathological features. p-value distribution for associations of lipid species with **A.** Ki67 proliferative index, and **B.** serum prostate specific antigen levels, tumor Gleason score, and ERG positivity. **C.** PL abundance associations with original tumor pathology. **D, E.** PL associations with ERG positivity status. **F.** PL associations with Ki67 positivity.

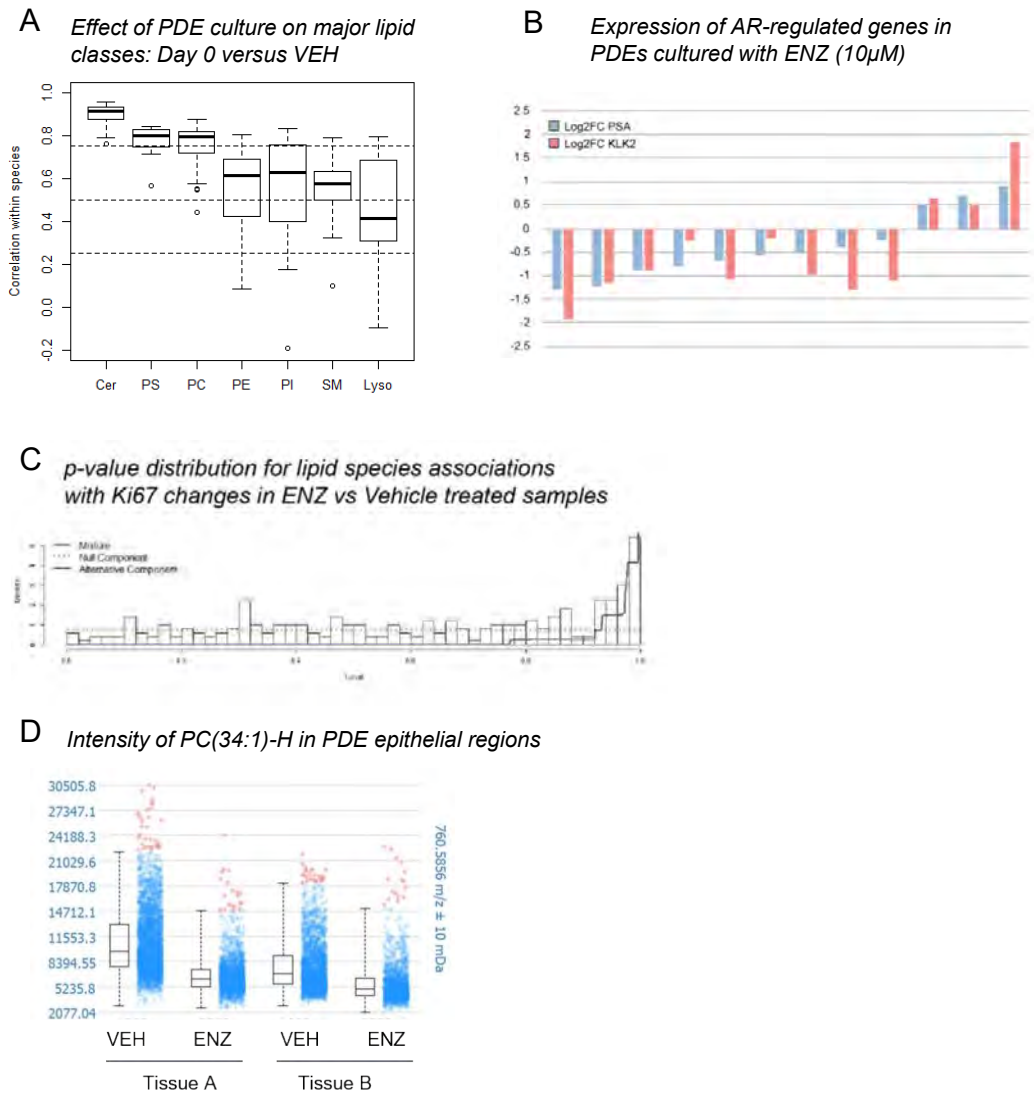

Supplementary Figure 6.6 Associations of lipid measures with response to the AR antagonist enzalutamide in patient-derived explants of clinical prostate tissues. A. Effect of *ex vivo* culture on PL profiles in prostate tissues, demonstrated by correlations in lipids between uncultured and vehicle-cultured samples. **B.** Treatment-related changes in mRNA expression of the AR-target genes, *KLK3* (prostate specific antigen) and *KLK2*. **C.** P-value distribution for PL associations with proliferative response to enzalutamide. **D.** Box plots of normalized ion intensity for PC34:1-H+ in epithelial regions of enzalutamide-treated versus vehicle-treated explants from two separate tissue cores.

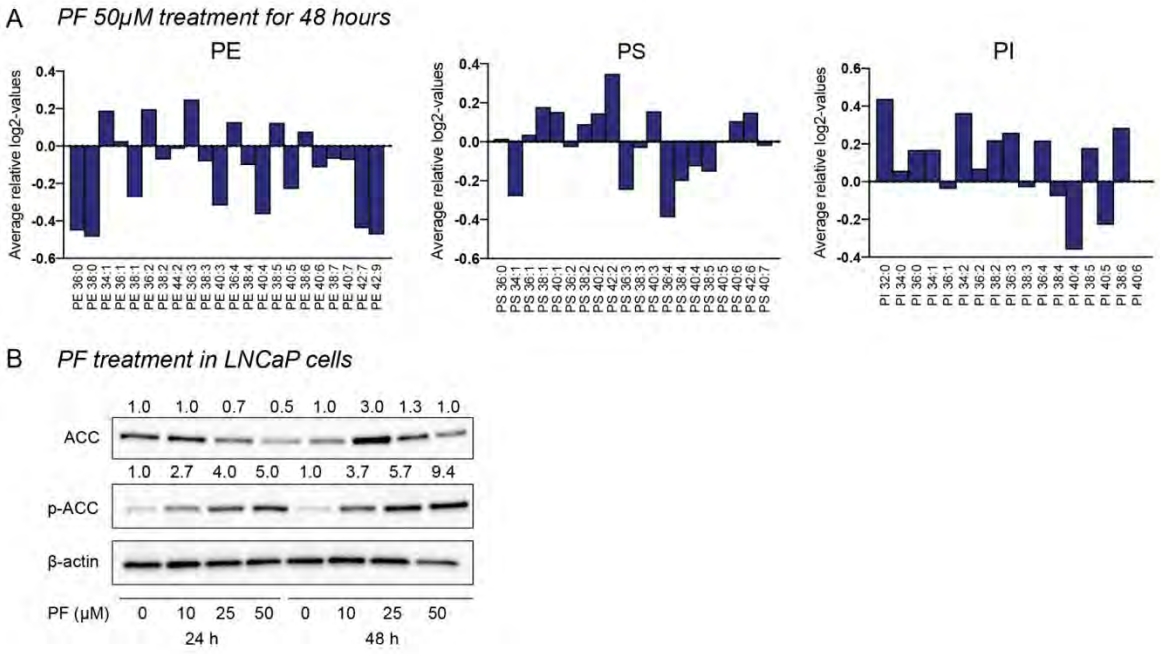

Supplementary Figure 6.7 A. Altered fatty acyl chain length for PE, PS and PI lipids in patient-derived explants cultured in the ACC inhibitor PF-05175157 compared to vehicle control. **B.** Dose-dependent increase in pACC1/ACC1 levels in LNCaP prostate cancer cells cultured with PF-05175157 (50μM) for 24 or 48 hours.

Supplementary Table 6.1 Histopathologic features of all tumors used in this study.

				SURGICAL SPECIMEN			LIPIDOMICS SAMPLE				
	Patient ID	Age at RP	Pre-RP PSA	1° Gleason	2° Gleason	Total Gleason	1° Gleason	2° Gleason	Total Gleason	ERG +	Pathological Staging
BATCH 1	32326	73.7	35.2	3	4	7	3	4	7	YES	PT3A
	32337	70.7	7.1	4	5	9	4	4	8	YES	PT3B
	32344	65.3	9.3	3	4	7	3	4	7	YES	PT3A
	32370	64.2	6.3	3	4	7			benign	N/A	PT2C
	32375	77.1	8	4	3	7			benign	N/A	PT3A
	32377	64.4	14.2	3	4	7	4	3	7	YES	PT3A
	32379	64.8	4.9	4	4	8	4	4	8	YES	PT3B
	32383	59.9	4.4	3	4	7			benign	N/A	PT3A
	32386	67.2	6.2	4	3	7	4	4	8	N/A	PT3B
	32389	59.5	9.3	4	3	7	3	3	6	NO	PT3A
	32401	58	4.5	3	4	7	3	4	7	YES	PT3A
	32405	63.6	4.4	3	4	7			benign	N/A	PT2A
	32418	72.4	3.9	5	4	9	3	4	7	YES	PT2C
	32419	63.5	7.6	4	4	8	3	3	6	NO	PT3A
	32421	69.2	13	3	4	7	3	4	7	NO	PT3B
	32429	66	5.2	3	4	7	3	3	6	NO	PT2C
	32436	74.5	17.8	4	3	7	3	5	8	YES	PT3A
	32438	71.4	10	5	5	10	5	4	9	YES	PT3B
	32445	78.7	31	4	3	7			benign	N/A	PT3B
	32447	64.2	8.6	3	4	7	3	3	6	NO	PT3A
	32450	71.6	6.2	4	4	8	4	5	9	NO	PT3A
	32452	71.4	6	4	3	7	4	3	7	NO	PT3A
	32459	66.6	5.8	3	4	7			benign	N/A	PT3A
	32473	63.2	5.4	3	4	7	4	3	7	YES	PT3A
	32499	61.3	6.6	3	4	7	4	3	7	YES	PT2C
	32509	66.2	6.9	3	4	7	3	4	7	YES	PT3A
BATCH 2	32717	70.7	16	3	4	7			benign	N/A	PT2C
	32729	66.8	18	4	4	8	4	4	8	NO	PT3B
	32732	66.7	7	3	4	7			benign	N/A	PT3A
	32742	69	8.3	4	3	7			benign	N/A	PT3A
	32743	67.3	18.6	4	4	8			benign	N/A	PT3A
	32747	57.6	6.9	3	4	7			benign	N/A	PT2C
	32749	61.6	7.9	3	3	6	4	3	7	YES	PT3A
	32755	64.2	5.6	3	3	6			benign	N/A	PT3A
	32760	70.6	6.5	3	4	7	3	4	7	YES	PT2C
	32764	67.1	8.1	3	4	7	4	3	7	NO	PT3A
	32771	66.5	5.7	3	4	7	3	3	6	N/A	PT2C
	32776	55.8	17.6	5	4	9	4	5	9	NO	PT3B
	32781	60.8	4.1	3	4	7			benign	N/A	PT3A
	32784	55.5	4.4	4	3	7	3	3	6	NO	PT2C
	32794	58.8	13.5	4	3	7	4	3	7	YES	PT2C
	32800	59.2	1.8	3	4	7			benign	N/A	PT2C
	32802	69.1	7	4	3	7			benign	N/A	PT3A
	32804	70.3	7.9	4	3	7			benign	N/A	PT3A
	32840	50.6	8.6	3	4	7	4	4	8	N/A	PT2C

Supplementary Table 6.2 Phospholipid measures from the paired cohort (Cohort A) that were associated with sample malignancy (p<0.01).

Variable	Lipid ID	Est [95%CI]	p-value
Lipid abundance	PI 38:6	-0.35 [-0.36, -0.33]	6.52E-19
	PI 40:6	0.19 [0.18, 0.21]	1.78E-14
	PS 40:8	1.10 [1.00, 1.20]	6.40E-14
	PC 36:4	-0.56 [-0.64, -0.49]	3.51E-11
	PC 34:1	0.17 [0.14, 0.20]	5.81E-10
	PC 40:4	-0.45 [-0.57, -0.33]	1.18E-06
	PI 38:5	-0.68 [-0.89, -0.48]	4.51E-06
	PS 42:8	0.70 [0.50, 0.90]	2.20E-05
	PS 42:2	-0.26 [-0.35, -0.16]	4.08E-05
	PS 42:4	-0.23 [-0.32, -0.14]	8.25E-05
	PE 42:6	0.75 [0.44, 1.06]	0.000149
	PI 36:4	-0.68 [-0.96, -0.39]	0.000203
	PE 42:5	0.51 [0.29, 0.74]	0.000255
	PS 38:4	-0.66 [-0.96, -0.36]	0.000399
	PC 38:4	-0.52 [-0.77, -0.27]	0.000693
	PS 36:2	-0.32 [-0.48, -0.16]	0.000753
	PS 36:1	-0.46 [-0.68, -0.23]	0.000789
	PC 32:0	-0.66 [-0.98, -0.33]	0.000832
	PS 38:3	-0.72 [-1.08, -0.36]	0.000942
	PC 40:6	-0.36 [-0.55, -0.18]	0.001045
	PS 38:6	-0.82 [-1.24, -0.40]	0.001116
	PE 40:4	0.042 [0.02, 0.065]	0.001414
	PC 38:5	-0.38 [-0.59, -0.18]	0.001489
	PE 38:7	0.36 [0.17, 0.56]	0.001681
	PI 38:4	-0.50 [-0.80, -0.20]	0.001944
	PC 36:5	-0.40 [-0.60, -0.20]	0.002105
	PS 44:6	0.52 [0.23, 0.81]	0.002306
	PI 36:1	0.51 [0.22, 0.80]	0.00274
	PS 42:9	0.47 [0.19, 0.75]	0.003707
	PS 40:4	-0.48 [-0.77, -0.20]	0.003719
	PE 42:9	0.45 [0.16, 0.73]	0.005855
	PE 40:6	0.36 [0.13, 0.60]	0.006456
	PE 40:8	0.28 [0.10, 0.46]	0.006487
	PC 40:5	-0.30 [-0.50, -0.10]	0.008872
Mean Chain Length	PE 3	-0.13 [-0.14, -0.12]	7.43E-14
	PS 1	0.13 [0.07, 0.18]	0.000187
	PE 6	0.11 [0.06, 0.15]	0.000209
	PI 1	0.19 [0.11, 0.27]	0.000231
	PS 3	0.096 [0.048, 0.144]	0.000948
Saturation Abundance	PC 6	-0.0021 [-0.0024, -0.0017]	6.10E-10
	PI 2	0.013 [0.01, 0.015]	2.16E-08
	PE 3	0.0029 [0.0022, 0.0037]	9.74E-07
	PS 8	0.0036 [0.0026, 0.0046]	1.82E-06
	PS 9	0.00078 [0.00048, 0.00108]	6.25E-05
	PC 4	-0.038 [-0.056, -0.021]	0.00046
	PC 1	0.066 [0.033, 0.098]	0.000959
	PC 5	-0.0071 [-0.0107, -0.0034]	0.001172
	PI 5	-0.0016 [-0.0025, -7e-04]	0.002608
	PS 3	-0.0088 [-0.0139, -0.0036]	0.003266
	PC 0	-0.013 [-0.021, -0.005]	0.004081
	PS 4	-0.0079 [-0.0133, -0.0025]	0.009611

For Mean Chain Length and Saturation Abundance, lipids are named by subclass and total number of unsaturations.

Supplementary Table 6.3 Phospholipid measures from the unpaired cohort (Cohort B) associated with sample malignancy (p<0.01).

Variable	Lipid ID	Est [95%CI]	p-value
Lipid Abundance	Cer(d18:1/26:5)	-0.59 [-0.71, -0.48]	2.99E-13
	PI 38:4	-0.77 [-0.95, -0.60]	1.52E-11
	Cer(d18:1/26:3)	-0.79 [-0.99, -0.60]	1.94E-10
	Cer(d18:1/18:8)	-0.73 [-0.94, -0.51]	2.64E-08
	PC 42:7	0.60 [0.40, 0.80]	2.67E-08
	PE 42:6	0.84 [0.55, 1.12]	5.49E-07
	Cer(d18:1/24:7)	0.97 [0.61, 1.32]	2.12E-06
	PC 42:8	0.31 [0.19, 0.42]	2.13E-06
	Cer(d18:1/22:7)	1.10 [0.60, 1.60]	7.02E-05
	Cer(d18:1/26:7)	0.61 [0.33, 0.90]	8.04E-05
	PC 42:6	0.32 [0.17, 0.48]	0.000142
	PE 42:7	0.46 [0.24, 0.69]	0.000174
	Cer(d18:1/22:2)	-0.40 [-0.60, -0.20]	0.000199
	PC 40:1	0.36 [0.18, 0.54]	0.000212
	SM d18:2/24:1	-0.21 [-0.31, -0.10]	0.000236
	PC 40:5	0.21 [0.10, 0.32]	0.000296
	PI 38:5	-0.49 [-0.74, -0.23]	0.000429
	PC 40:7	0.30 [0.10, 0.50]	0.00044
	PE 32:1	0.27 [0.13, 0.41]	0.000492
	PC L 22:1	-0.37 [-0.57, -0.17]	0.000571
	Cer(d18:1/26:2)	-0.97 [-1.51, -0.44]	0.000646
	PE 32:2	0.55 [0.24, 0.87]	0.001055
	PC 42:3	0.34 [0.14, 0.53]	0.001414
	PE 36:2	0.51 [0.21, 0.81]	0.001584
	PE L 14:5	1.10 [0.40, 1.70]	0.001594
	PC L 18:0	-0.47 [-0.76, -0.19]	0.001872
	Cer(d18:1/16:8)	-0.71 [-1.14, -0.28]	0.001924
	Cer(d18:1/16:9)	0.46 [0.18, 0.74]	0.002174
	PE 36:3	0.51 [0.19, 0.82]	0.002183
	PE 38:0	-0.51 [-0.82, -0.19]	0.002252
	PC 28:0	0.60 [0.20, 1.00]	0.003476
	PC L 22:3	-0.35 [-0.58, -0.12]	0.003681
	PC 42:5	0.28 [0.09, 0.46]	0.003975
	PC 40:4	0.23 [0.08, 0.38]	0.004354
	PC 42:4	0.33 [0.11, 0.56]	0.004794
	PC 36:1	0.36 [0.12, 0.61]	0.005118
	PE 36:0	-0.41 [-0.69, -0.13]	0.005191
	PI 36:4	-0.40 [-0.70, -0.10]	0.005688
	PI 40:3	0.98 [0.30, 1.65]	0.005736
	PS 34:0	-0.90 [-1.50, -0.30]	0.006216
	PS 38:6	-0.68 [-1.17, -0.19]	0.008117
	PC 34:1	0.47 [0.13, 0.82]	0.008694
	SM d18:1/24:1	-0.11 [-0.20, -0.03]	0.008839
	PS 36:1	-0.46 [-0.80, -0.12]	0.009917
Mean Chain Length	PE 7	0.12 [0.07, 0.16]	2.05E-06
	PS 4	0.12 [0.07, 0.16]	3.64E-06

	Cer 1-1	-0.038 [-0.06, -0.015]	0.001637
	PS 6	0.078 [0.031, 0.125]	0.001773
	PS 1	0.076 [0.029, 0.124]	0.002483
	PE 6	0.088 [0.029, 0.146]	0.004439
	Cer 1-7	0.15 [0.05, 0.25]	0.004768
	PI 2	0.16 [0.05, 0.27]	0.005542
	PE 1	-0.086 [-0.146, -0.025]	0.007031
	PI 1	0.12 [0.03, 0.21]	0.00791
Saturation Abundance	Cer 1-4	-0.012 [-0.015, -0.009]	5.61E-09
	PS 4	-0.012 [-0.018, -0.006]	0.000292
	Cer 1-7	0.012 [0.006, 0.018]	0.000354
	PE 0	-0.0051 [-0.0078, -0.0023]	0.000654
	PC 9	-0.00034 [-0.00056, -0.00013]	0.002216
	PC 1	0.06 [0.02, 0.10]	0.004828
	PI 4	-0.036 [-0.061, -0.012]	0.005076
	PC 12	-0.00071 [-0.0012, -0.00023]	0.005235
	PI 1	0.019 [0.005, 0.032]	0.008837
	PC 4	-0.037 [-0.064, -0.009]	0.009926

For Mean Chain Length and Saturation Abundance, lipids are named by subclass and total number of unsaturations.

Supplementary Table 6.4 Phospholipid measures from Cohort B associated with sample ERG status (p<0.01).

Variable	Lipid ID	Est [95%CI]	p-value
Lipid Abundance	Cer(d18:1/24:4)	-0.88 [-1.01, -0.75]	4.66E-07
	Cer(d18:1/24:5)	-0.61 [-0.73, -0.50]	4.84E-06
	PC 44:8	-0.58 [-0.80, -0.37]	8.40E-06
	PC L 18:0	0.25 [0.17, 0.33]	1.50E-05
	PC 42:4	-0.45 [-0.59, -0.32]	2.17E-05
	PE 36:1	0.57 [0.33, 0.80]	3.63E-05
	Cer(d18:1/24:7)	0.75 [0.47, 1.03]	4.99E-05
	Cer(d18:1/26:7)	0.41 [0.24, 0.58]	0.0001159
	PE 34:1	0.94 [0.44, 1.43]	0.000403975
	PC L 16:0	0.39 [0.21, 0.57]	0.000437926
	PS 34:0	-1.50 [-2.40, -0.60]	0.000905376
	PE 38:2	0.69 [0.27, 1.10]	0.00148699
	PC 38:2	1.30 [0.50, 2.10]	0.002281809
	PE L 20:3	-0.65 [-0.89, -0.40]	0.002457796
	PE 36:2	0.69 [0.23, 1.16]	0.003388082
	PC 36:5	-0.53 [-0.90, -0.17]	0.004195823
	PI L 16:0	1.20 [0.40, 2.00]	0.004216038
	PC L 18:1	0.57 [0.20, 0.94]	0.004737572
	PC 42:5	-0.30 [-0.50, -0.10]	0.005471192
Mean Chain Length	PE 4	-0.092 [-0.135, -0.048]	0.000784549
Saturation Abundance	PE 1	0.056 [0.031, 0.081]	0.000124795
	SM 2-1	-0.016 [-0.023, -0.009]	0.000142232
	PC 5	-0.016 [-0.024, -0.008]	0.000240119
	PE 5	-0.0084 [-0.0126, -0.0042]	0.000361836
	PC 9	-0.00018 [-0.00027, -9e-05]	0.000404002
	PS 0	-0.00074 [-0.00112, -0.00036]	0.000684119
	Cer 1-5	-0.002 [-0.003, -0.001]	0.000806838
	Cer 1-4	-0.0058 [-0.0092, -0.0024]	0.001361804
	PE 8	-0.00071 [-0.00116, -0.00026]	0.002055687
	PE.L 3	-0.0042 [-0.0065, -0.0018]	0.003138887
	Cer 1-0	0.071 [0.026, 0.117]	0.005062845
	PC 6	-0.0061 [-0.0101, -0.002]	0.005428866

For Mean Chain Length and Saturation Abundance, lipids are named by subclass and total number of unsaturations.

Supplementary Table 6.5 Phospholipid measures from Cohort B associated with malignant samples Ki67 cell positivity (p<0.01).

Variable	Lipid ID	Est [95%CI]	p-value
Lipid Abundance	PC 38:2	-0.35 [-0.56, -0.13]	0.001137415
	PC L 20:5	0.48 [0.16, 0.79]	0.002488468
	PC 40:2	-0.81 [-1.36, -0.26]	0.00304984
	Cer(d18:1/22:0)	-0.40 [-0.70, -0.10]	0.003552997
	Cer(d18:1/20:0)	-0.34 [-0.57, -0.10]	0.004787576
	PC 40:3	-0.84 [-1.44, -0.24]	0.004928755
	SM d18:3/22:1	-0.68 [-1.17, -0.19]	0.005400972
	Cer(d18:1/14:0)	-0.39 [-0.69, -0.09]	0.008881727
Mean Chain Length	Cer 1-3	59.90 [22.70, 97.20]	0.001286395
	PE 8	84.60 [31.90, 137.30]	0.001335494
	PC 6	66.50 [23.50, 109.50]	0.001985756
	PE 5	35.50 [12.40, 58.60]	0.002132982
	PC 5	33.20 [11.20, 55.20]	0.002523195
	Cer 1-4	61.90 [19.10, 104.70]	0.003803916
	Cer 1-0	-4.70 [-8.00, -1.40]	0.004346096
	Cer 1-2	40.70 [11.00, 70.40]	0.006064642
	PC 7	193.64 [50.55, 336.74]	0.006798926
	PC 9	850.99 [202.46, 1499.52]	0.008681164

For Mean Chain Length and Saturation Abundance, lipids are named by subclass and total number of unsaturations.

Supplementary Table 6.6 Phospholipid measures from PDEs associated with change in Ki67 cell positivity in ENZ and vehicle treated samples (p<0.01).

Variable	Lipid ID	Est [95%CI]	p-value
Lipid Abundance	PE 32:0	1.0 [0.5, 1.5]	0.000101448
	PE L 14:5	-0.22 [-0.35, -0.09]	0.000625325
	PC 44:7	-0.8 [-1.2, -0.3]	0.000674426
	PE L 18:1	0.59 [0.24, 0.95]	0.000794281
	PS 38:1	0.8 [0.3, 1.4]	0.001499912
	PC 44:3	-0.8 [-1.3, -0.3]	0.002054796
	PC 34:1	1.0 [0.3, 1.6]	0.002532567
	PE 36:1	1.0 [0.3, 1.7]	0.002561362
	PC L 14:0	0.8 [0.3, 1.4]	0.003165986
	Cer(d18:1/24:0)	0.50 [0.14, 0.87]	0.005589286
	SM d18:1/18:1	-0.6 [-1.0, -0.2]	0.007073325
	Cer(d18:1/22:3)	-0.33 [-0.57, -0.08]	0.00756436
	PE 38:4	0.8 [0.2, 1.5]	0.008528304
	PE 36:2	0.7 [0.2, 1.2]	0.008596447
	PC 44:2	-0.48 [-0.84, -0.11]	0.008750496
Mean Chain Length	PC.L 0	-2.4 [-4.1, -0.7]	0.005447759
Saturation Abundance	Cer 1-3	-90 [-139, -41]	0.00022117
	Cer 1-4	-74 [-121, -27]	0.00154786

For Mean Chain Length and Saturation Abundance, lipids are named by subclass and total number of unsaturations.

6.7 References

1. Bray F, Ferlay J, Soerjomataram I, Siegel RL, Torre LA, Jemal A. Global cancer statistics 2018: GLOBOCAN estimates of incidence and mortality worldwide for 36 cancers in 185 countries. CA Cancer J Clin 2018;68(6):394-424.

2. Butler LM, Perone Y, Dehairs J, Lupien LE, de Laat V, Talebi A, et al. Lipids and cancer: Emerging roles in pathogenesis, diagnosis and therapeutic intervention. Adv Drug Deliv Rev 2020.

3. Hanahan D, Weinberg RA. Hallmarks of cancer: the next generation. Cell 2011;144(5):646-74.

4. Koundouros N, Poulogiannis G. Reprogramming of fatty acid metabolism in cancer. Br J Cancer 2020;122(1):4-22.

5. Bader DA, McGuire SE. Tumour metabolism and its unique properties in prostate adenocarcinoma. Nat Rev Urol 2020;17(4):214-31.

6. Zadra G, Loda M. Metabolic Vulnerabilities of Prostate Cancer: Diagnostic and Therapeutic Opportunities. Cold Spring Harb Perspect Med 2018;8(10).

7. Butler LM, Centenera MM, Swinnen JV. Androgen control of lipid metabolism in prostate cancer: novel insights and future applications. Endocr Relat Cancer 2016;23(5):R219-27.

8. Crowe FL, Appleby PN, Travis RC, Barnett M, Brasky TM, Bueno-de-Mesquita HB, et al. Circulating fatty acids and prostate cancer risk: individual participant metaanalysis of prospective studies. J Natl Cancer Inst 2014;106(9).

9. Patel N, Vogel R, Chandra-Kuntal K, Glasgow W, Kelavkar U. A novel three serum phospholipid panel differentiates normal individuals from those with prostate cancer. PLoS One 2014;9(3):e88841.

10. Lin HM, Mahon KL, Weir JM, Mundra PA, Spielman C, Briscoe K, et al. A distinct plasma lipid signature associated with poor prognosis in castration-resistant prostate cancer. Int J Cancer 2017;141(10):2112-20.

11. Rysman E, Brusselmans K, Scheys K, Timmermans L, Derua R, Munck S, et al. De novo lipogenesis protects cancer cells from free radicals and chemotherapeutics by promoting membrane lipid saturation. Cancer Res 2010;70(20):8117-26.

12. Sorvina A, Bader CA, Caporale C, Carter EA, Johnson IRD, Parkinson-Lawrence EJ, et al. Lipid profiles of prostate cancer cells. Oncotarget 2018;9(85):35541-52.

13. Burch TC, Isaac G, Booher CL, Rhim JS, Rainville P, Langridge J, et al. Comparative Metabolomic and Lipidomic Analysis of Phenotype Stratified Prostate Cells. PLoS One 2015;10(8):e0134206.

14. Goto T, Terada N, Inoue T, Kobayashi T, Nakayama K, Okada Y, et al. Decreased expression of lysophosphatidylcholine (16:0/OH) in high resolution imaging mass spectrometry independently predicts biochemical recurrence after surgical treatment for prostate cancer. Prostate 2015;75(16):1821-30.

15. Goto T, Terada N, Inoue T, Nakayama K, Okada Y, Yoshikawa T, et al. The expression profile of phosphatidylinositol in high spatial resolution imaging mass spectrometry as a potential biomarker for prostate cancer. PLoS One 2014;9(2):e90242.

16. Morse N, Jamaspishvili T, Simon D, Patel PG, Ren KYM, Wang J, et al. Reliable identification of prostate cancer using mass spectrometry metabolomic imaging in needle core biopsies. Laboratory Investigation 2019.

17. Randall EC, Zadra G, Chetta P, Lopez BGC, Syamala S, Basu SS, et al. Molecular Characterization of Prostate Cancer with Associated Gleason Score Using Mass Spectrometry Imaging. Mol Cancer Res 2019;17(5):1155-65.

18. Beer TM, Armstrong AJ, Rathkopf DE, Loriot Y, Sternberg CN, Higano CS, et al. Enzalutamide in metastatic prostate cancer before chemotherapy. N Engl J Med 2014;371(5):424-33.

19. Scher HI, Fizazi K, Saad F, Taplin ME, Sternberg CN, Miller K, et al. Increased survival with enzalutamide in prostate cancer after chemotherapy. N Engl J Med 2012;367(13):1187-97.

20. Griffith DA, Kung DW, Esler WP, Amor PA, Bagley SW, Beysen C, et al. Decreasing the rate of metabolic ketone reduction in the discovery of a clinical acetyl-CoA carboxylase inhibitor for the treatment of diabetes. J Med Chem 2014;57(24):10512-26.

21. Zhang AY, Chiam K, Haupt Y, Fox S, Birch S, Tilley W, et al. An analysis of a multiple biomarker panel to better predict prostate cancer metastasis after radical prostatectomy. Int J Cancer 2019;144(5):1151-59.

22. Bandu R, Mok HJ, Kim KP. Phospholipids as cancer biomarkers: Mass spectrometry-based analysis. Mass Spectrom Rev 2018;37(2):107-38.

23. Naguib A, Bencze G, Engle DD, Chio, II, Herzka T, Watrud K, et al. p53 mutations change phosphatidylinositol acyl chain composition. Cell Rep 2015;10(1):8-19.

24. Falvella FS, Pascale RM, Gariboldi M, Manenti G, De Miglio MR, Simile MM, et al. Stearoyl-CoA desaturase 1 (Scd1) gene overexpression is associated with genetic predisposition to hepatocarcinogenesis in mice and rats. Carcinogenesis 2002;23(11):1933-6.

25. Fritz V, Benfodda Z, Rodier G, Henriquet C, Iborra F, Avances C, et al. Abrogation of de novo lipogenesis by stearoyl-CoA desaturase 1 inhibition interferes with oncogenic signaling and blocks prostate cancer progression in mice. Mol Cancer Ther 2010;9(6):1740-54.

26. Griffitts J, Tesiram Y, Reid GE, Saunders D, Floyd RA, Towner RA. In vivo MRS assessment of altered fatty acyl unsaturation in liver tumor formation of a TGF alpha/c-myc transgenic mouse model. J Lipid Res 2009;50(4):611-22.

27. Li J, Ding SF, Habib NA, Fermor BF, Wood CB, Gilmour RS. Partial characterization of a cDNA for human stearoyl-CoA desaturase and changes in its mRNA expression in some normal and malignant tissues. Int J Cancer 1994;57(3):348-52.

28. Romanuik TL, Ueda T, Le N, Haile S, Yong TM, Thomson T, et al. Novel biomarkers for prostate cancer including noncoding transcripts. Am J Pathol 2009;175(6):2264-76.

29. Tamura K, Makino A, Hullin-Matsuda F, Kobayashi T, Furihata M, Chung S, et al. Novel lipogenic enzyme ELOVL7 is involved in prostate cancer growth through saturated long-chain fatty acid metabolism. Cancer Res 2009;69(20):8133-40.

30. Wang HW, Wu YH, Hsieh JY, Liang ML, Chao ME, Liu DJ, et al. Pediatric primary central nervous system germ cell tumors of different prognosis groups show characteristic miRNome traits and chromosome copy number variations. BMC Genomics 2010;11:132.

31. Marien E, Meister M, Muley T, Fieuws S, Bordel S, Derua R, et al. Non-small cell lung cancer is characterized by dramatic changes in phospholipid profiles. Int J Cancer 2015;137(7):1539-48.

32. Swinnen JV, Vanderhoydonc F, Elgamal AA, Eelen M, Vercaeren I, Joniau S, et al. Selective activation of the fatty acid synthesis pathway in human prostate cancer. Int J Cancer 2000;88(2):176-9.

33. Swinnen JV, Heemers H, Deboel L, Foufelle F, Heyns W, Verhoeven G. Stimulation of tumor-associated fatty acid synthase expression by growth factor activation of the sterol regulatory element-binding protein pathway. Oncogene 2000;19(45):5173-81.

34. Van de Sande T, De Schrijver E, Heyns W, Verhoeven G, Swinnen JV. Role of the phosphatidylinositol 3'-kinase/PTEN/Akt kinase pathway in the overexpression of fatty acid synthase in LNCaP prostate cancer cells. Cancer Res 2002;62(3):642-6.

35. Moreau K, Dizin E, Ray H, Luquain C, Lefai E, Foufelle F, et al. BRCA1 affects lipid synthesis through its interaction with acetyl-CoA carboxylase. J Biol Chem 2006;281(6):3172-81.

36. Kinlaw WB, Church JL, Harmon J, Mariash CN. Direct evidence for a role of the "spot 14" protein in the regulation of lipid synthesis. J Biol Chem 1995;270(28):16615-8.

37. Sabbisetti V, Di Napoli A, Seeley A, Amato AM, O'Regan E, Ghebremichael M, et al. p63 promotes cell survival through fatty acid synthase. PLoS One 2009;4(6):e5877.

38. Swinnen JV, Ulrix W, Heyns W, Verhoeven G. Coordinate regulation of lipogenic gene expression by androgens: evidence for a cascade mechanism involving sterol regulatory element binding proteins. Proceedings of the National Academy of Sciences of the United States of America 1997;94(24):12975-80.

39. Harayama T, Riezman H. Understanding the diversity of membrane lipid composition. Nat Rev Mol Cell Biol 2018;19(5):281-96.

40. Rogers KR, Kikawa KD, Mouradian M, Hernandez K, McKinnon KM, Ahwah SM, et al. Docosahexaenoic acid alters epidermal growth factor receptor-related signaling by disrupting its lipid raft association. Carcinogenesis 2010;31(9):1523-30.

41. Gillet L, Roger S, Bougnoux P, Le Guennec JY, Besson P. Beneficial effects of omega-3 long-chain fatty acids in breast cancer and cardiovascular diseases: voltage-gated sodium channels as a common feature? Biochimie 2011;93(1):4-6.

42. Jude S, Roger S, Martel E, Besson P, Richard S, Bougnoux P, et al. Dietary long-chain omega-3 fatty acids of marine origin: a comparison of their protective effects on coronary heart disease and breast cancers. Prog Biophys Mol Biol 2006;90(1-3):299-325.

43. Kiebish MA, Han X, Cheng H, Chuang JH, Seyfried TN. Cardiolipin and electron transport chain abnormalities in mouse brain tumor mitochondria: lipidomic evidence supporting the Warburg theory of cancer. Journal of lipid research 2008;49(12):2545-56.

44. Hilvo M, Denkert C, Lehtinen L, Muller B, Brockmoller S, Seppanen-Laakso T, et al. Novel theranostic opportunities offered by characterization of altered membrane lipid metabolism in breast cancer progression. Cancer Res 2011;71(9):3236-45.

45. Beckers A, Organe S, Timmermans L, Scheys K, Peeters A, Brusselmans K, et al. Chemical inhibition of acetyl-CoA carboxylase induces growth arrest and cytotoxicity selectively in cancer cells. Cancer Res 2007;67(17):8180-7.

46. Brusselmans K, De Schrijver E, Verhoeven G, Swinnen JV. RNA interference-mediated silencing of the acetyl-CoA-carboxylase-alpha gene induces growth inhibition and apoptosis of prostate cancer cells. Cancer Res 2005;65(15):6719-25.

47. Peck B, Schug ZT, Zhang Q, Dankworth B, Jones DT, Smethurst E, et al. Inhibition of fatty acid desaturation is detrimental to cancer cell survival in metabolically compromised environments. Cancer Metab 2016;4:6.

48. Waltregny D, Alami Y, Clausse N, de Leval J, Castronovo V. Overexpression of the homeobox gene HOXC8 in human prostate cancer correlates with loss of tumor differentiation. Prostate 2002;50(3):162-9.

49. Centenera MM, Hickey TE, Jindal S, Ryan NK, Ravindranathan P, Mohammed H, et al. A patient-derived explant (PDE) model of hormone-dependent cancer. Mol Oncol 2018;12(9):1608-22.

50. Gu Z, Gu L, Eils R, Schlesner M, Brors B. circlize Implements and enhances circular visualization in R. Bioinformatics 2014;30(19):2811-2.

51. Armstrong HK, Gillis JL, Johnson IRD, Nassar ZD, Moldovan M, Levrier C, et al. Dysregulated fibronectin trafficking by Hsp90 inhibition restricts prostate cancer cell invasion. Sci Rep 2018;8(1):2090.

52. Kim D, Pertea G, Trapnell C, Pimentel H, Kelley R, Salzberg SL. TopHat2: accurate alignment of transcriptomes in the presence of insertions, deletions and gene fusions. Genome Biol 2013;14(4):R36.

53. Anders S, Pyl PT, Huber W. HTSeq--a Python framework to work with high-throughput sequencing data. Bioinformatics 2015;31(2):166-9.

54. Robinson MD, McCarthy DJ, Smyth GK. edgeR: a Bioconductor package for differential expression analysis of digital gene expression data. Bioinformatics 2010;26(1):139-40.

55. Strimmer K. A unified approach to false discovery rate estimation. BMC Bioinformatics 2008;9:303.

Chapter 7: General Discussion

This Chapter summarises the main findings in this thesis and highlights new discussion points that were not covered in Chapters 3 to 6. This Chapter builds on the discussion for some of the results and suggests new areas for investigation in addition to providing implications for our findings.

7.1 Summary of findings

Altered lipid metabolism is a well-established hallmark of prostate cancer (Mah et al. 2020; Wu et al. 2014). In support of this, Chapter 6 provides an overview of the lipidomic changes that accompany prostate cancer development in clinical tissues in addition to treatment-related changes in lipid profiles. Despite observed inter-patient heterogeneity at the level of lipid species, our data revealed consistent changes in broader lipid metabolic processes such as increased lipid elongation and monounsaturation. Notably, these key cancer-related changes in phospholipid profiles support the findings of previous studies and may represent common tumour-specific vulnerabilities. We also provide first line evidence for the efficacy of targeting these phenotypes using a clinically available ACC inhibitor in clinical prostate cancer tissues. Taken together, our findings highlight the importance of studying the lipidome to understand cancer development and progression and revealed lipid metabolism as sources of novel molecular biomarkers and therapeutic targets.

This dissertation primarily focuses on fatty acid oxidation as an underexplored facet of lipid metabolism and promising therapeutic avenue to overcome prostate cancer progression and treatment resistance. Fatty acid oxidation (FAO) is the dominant bioenergetic pathway in prostate cancer (Liu 2006) and hence, represents a metabolic vulnerability that may be exploited for therapeutic intervention. This thesis critically advances existing knowledge on the role of FAO (mitochondrial and peroxisomal) in prostate cancer oncogenesis and identifies two key enzymes, DECR1 and DECR2, as novel therapeutic candidates for advanced disease. Finally, this thesis also explores the potential of FAO as an adaptive survival pathway to support CRPC development and treatment resistance.

In **Aim 1**, we aimed to identify new therapeutic targets of FAO for the treatment of prostate cancer. In Chapter 3, 2,4-Dienoyl-CoA Reductase 1 (DECR1; a mitochondrial auxiliary enzyme involved in polyunsaturated fatty acid (PUFA) oxidation) was identified as a key survival factor in prostate cancer cells. Interrogation of clinical datasets showed that DECR1 is robustly overexpressed in prostate cancer tissues and associated with shorter relapse-free survival rates.

DECR1 targeting significantly suppressed prostate cancer cell proliferation and migration *in vitro*, and tumour growth and metastasis *in vivo*. DECR1 was selective for PUFA oxidation; DECR1 depletion resulted in PUFA accumulation and increased mitochondrial oxidative stress, ultimately leading to lipid peroxidation and cell death by ferroptosis. Moreover, DECR1 is an androgen-repressed gene which may promote prostate cancer cell survival by upregulating its expression in response to ADT or AR-targeted therapies, suggesting PUFA oxidation as an adaptive survival response that may contribute to development of CRPC and treatment resistance. In Chapter 4, 2,4-Dienoyl-CoA Reductase 2 (DECR2; a peroxisomal β-oxidation enzyme) was identified as a novel therapeutic target for advanced metastatic prostate cancer. DECR2 was significantly upregulated in prostate cancer tissues, particularly metastatic/CRPC samples and its overexpression was associated with poor overall survival rates. Phenotypically, DECR2 targeting in CRPC and enzalutamide-resistant cells significantly suppressed prostate cancer oncogenesis and migration *in vitro.* Furthermore, DECR2 depletion led to profound changes in lipid content and composition, suggestive of a potential link between mitochondrial and peroxisomal β-oxidation to promote prostate cancer cell survival. Finally, attenuation of prostate cancer cell viability after DECR2 knockdown was associated with inhibition of cell cycle progression, and sensitised prostate cancer cells to the CDK4/6 inhibitor, ribociclib. Taken together, these findings provide compelling evidence for targeting (mitochondrial and peroxisomal) fatty acid oxidation in prostate cancer by inhibiting DECR1 and DECR2.

Aim 2, investigated the potential of FAO as an adaptive survival pathway in the context of treatment resistance. In Chapter 5, FAO was discovered as a survival pathway that is activated in clinical tumours in response to heat shock protein 90 (HSP90) inhibition. Co-treatment of prostate cancer cells with AUY922 and FAO inhibitors (including etomoxir and perhexiline) showed sensitisation of prostate cancer cells to AUY922 treatment. Moreover, we demonstrated that the combination treatment significantly inhibited cellular proliferation and induced apoptosis in our preclinical patient-derived prostate tumour models more effectively than individual treatments alone. In Chapter 4, we also report a close link between peroxisomal metabolism and resistance to AR-targeted therapies. We demonstrated that peroxisomal β-oxidation inhibition (either via DECR2 targeting or pharmacological

inhibition by thioridazine) could sensitise prostate cancer cells, and particularly enzalutamide-resistant cells to enzalutamide treatment. Overall, this suggests that FAO is not only an important source of energy, but also an adaptive survival pathway that is enhanced in response to drug treatments to support cancer cell survival and resistance.

In summary, this thesis identified new molecular targets of key facets of FAO and previously unexplored FAO enzymes that are critical for prostate cancer cell survival, CRPC development and treatment resistance.

7.2 Fatty acid oxidation and molecular heterogeneity

In Chapters 3 and 4, the efficacy of mitochondrial and peroxisomal β- oxidation inhibition (etomoxir and thioridazine) was demonstrated using our laboratory's preclinical patient-derived prostate tumour models. To our knowledge, this is the first clinically relevant evidence that targeting these FAO pathways is efficacious. Intriguingly, the data revealed patient heterogeneity in response to etomoxir or thioridazine treatments, whereby some patients responded more strongly to the treatments compared to others. This raised the question: what are the factors that may contribute to the variation in treatment response?

Prostate cancer is a highly heterogenous and multifocal disease. This is reflected in the metabolic plasticity of prostate tumours, potentially driven by genomic aberrations such as mutations in tumour suppressor genes (ie. PTEN, RB1, TP53) or oncogenes (AR, ERG, MYC) (Peitzsch et al. 2020). Recently, few studies have revealed that prostate tumours actively rewire their metabolism to support tumour progression (Lin et al. 2017; Schöpf et al. 2020), including lipid metabolism (Balaban et al. 2019). In a broader context, one aspect that needs to be considered is the expression of lipid metabolism enzymes across different tumour types and molecular subclassifications. One such example is long-chain acyl-CoA synthetase 3 (ACSL3) where its expression is overexpressed in androgen-dependent and castrate-resistant prostate cancer but is downregulated in triple-negative breast cancers (TNBC) (Migita et al. 2017; Wright et al. 2017). Similarly, DECR1 expression is significantly upregulated in prostate cancer to promote cancer cell survival whereas another study found that DECR1 expression is markedly decreased in primary human breast cancers (Ursini-Siegel et al. 2007; Nassar et al. 2020). What about the differences in FAO during cancer progression? A study in prostate cancer cells highlighted striking heterogeneity in the intracellular handling of FAs (Balaban et al. 2019). For example, castrate-resistant C4-2B cells exhibited higher rates of FAO compared to androgen-independent PC3 cells. In the context of molecular heterogeneity, using findings from studies in breast cancers as an example, gene expression analysis comparing receptor-positive breast cancer (RPBC) and TNBC has revealed marked differences with respect to lipid homeostasis (Monaco 2017). For instance, RPBCs are associated with a gene

signature comprising of elevated *de novo* lipogenesis, fatty acid mobilisation and oxidation; whereas TNBC upregulates genes involved in lipid uptake and storage. This is further compounded by genomic alterations or upstream regulators that modulate lipid metabolism. A recent study reported a metabolic dependency for FAO in MYC-overexpressing TNBC cells (Camarda et al. 2016). The authors proceeded to confirm its selectivity for MYC-driven breast tumours and demonstrated sensitisation of MYC-overexpressing TNBC cells to FAO inhibition (via etomoxir) both *in vitro* and *in vivo*, but not MYC-low TNBCs or RPBCs. A previous study investigated the changes in metabolic phenotypes using untargeted metabolomics of human prostate cancers in response to different oncogenic drivers, specifically the AKT and MYC oncogenes. They reported that AKT activation was associated with glycolysis and glucose-related pathways (including pentose phosphate pathways and fructose metabolism). On the other hand, MYC overexpression was associated with dysregulation of lipid metabolism pathways, in particular, an enrichment of pathways involved in the synthesis and degradation of membrane lipids. Of particular interest, the authors showed elevated levels of omega-3 and omega-6 fatty acids (FAs) in MYC-high prostate tumours compared to AKT-high tumours suggesting uptake of unsaturated FAs during early transformation (Priolo et al. 2014).

We should not rule out the possibility of off-target effects of pharmacological modulators of FAO pathways. For instance, etomoxir (ETX), the most widely used carnitine palmitoyltransferase 1 (CPT1) inhibitor was reported to exhibit off-target effects such as inhibition of complex I of the electron transport chain and induction of oxidative stress via elevated reactive oxygen species (ROS) production (Yao et al. 2018; O'Connor et al. 2018). Similarly, trimetazidine and ranolazine, partial FAO inhibitors targeting the enzyme 3-ketoacyl-coA thiolase (3-KAT; a component of the trifunctional protein complex that catalyses the last three steps of mitochondrial β-oxidation) was reported to interfere with other cellular processes such as ion channels to exert their clinical benefits (Cavar et al. 2016; Antzelevitch et al. 2004; Nie et al. 2019; Guarnieri et al. 1997). A recent study assessed the anti-FAO activities of several FAO inhibitors (including etomoxir, perhexiline, trimetazidine and ranolazine) and found that, with the exception of etomoxir, these compounds did not significantly inhibit FAO in the cells (Ma et al. 2020). Unlike mitochondrial

FAO, peroxisomal FAO has attracted very little research attention. In Chapter 4, we introduced a peroxisomal β-oxidation inhibitor, thioridazine (TDZ) (Van den Branden and Roels 1985; Shi et al. 2012). TDZ was reported to block dopamine receptor 2 (DRD2) (Feinberg et al. n.d.) and is also a substrate of the cytochrome P450 enzymes (Gervasini et al. 2013; Daniel et al. 2001). It is plausible that TDZ may inhibit FAO via its inhibitory effects on cytochrome P450 enzymes (Shen et al. 2020), given that cytochrome P450 enzymes were suggested to play a role in polyunsaturated fatty acid metabolism (Konkel and Schunck 2011; Sarparast et al. 2020). Taken together, more work is needed to investigate the specificities, potencies, and metabolic impact of these FAO inhibitors. Moreover, this warrants further investigation into developing more specific and selective targets/inhibitors of FAO for anti-cancer therapy as proposed throughout Chapters 3 and 4 in this dissertation.

7.3 Crosstalk between mitochondria and peroxisomes

In Chapter 4, mitochondrial respiration or oxidative phosphorylation remained active after inhibition of peroxisomal β-oxidation via DECR2 knockdown. Furthermore, in Supplementary Chapter 3, RNA-seq analysis found that peroxisome KEGG pathway genes were negatively enriched in DECR1 knockdown cells. This suggests a potential and previously unexplored link between mitochondrial and peroxisomal β-oxidation that may have functional relevance in prostate cancer.

The interplay of peroxisomes with mitochondria is essential for subsequent metabolism of peroxisomal β-oxidation end products such as acetyl-CoA, NADH, and chain-shortened fatty acyl-CoAs (Wanders et al. 2015). For peroxisomal β-oxidation to proceed, it requires the conversion of NADH (reduced form; end product of peroxisomal FAO) to NAD^+ (oxidised form) (Wanders et al. 2015). This can only be achieved in the mitochondria where NADH is oxidised via the electron transport chain to generate energy/ATP through oxidative phosphorylation. Intriguingly, a study reported that monocarboxylate transporter 2 (MCT2; a metabolic enzyme that regulates pyruvate for lactate exchange) was found to localise to the peroxisome. MCT2 is a redox shuttle system that exists across the peroxisomal (also found on mitochondria) membrane to re-oxidise NADH to fuel peroxisomal β-oxidation and

promote ROS production (McClelland et al. 2003). Indeed, increased peroxisomal localisation of MCT2 is associated with malignant transformation of prostate cancer cells and knockdown inhibits prostate cancer cell growth and proliferation (Valença et al. 2015; Valença et al. 2020; Pertega-Gomes et al. 2015). In addition to its role in supporting β-oxidation and energy production, NAD^+ is also required for the maintenance of intracellular redox homeostasis, glycolysis, and several other non-redox processes such as DNA repair, cell signalling, post-translational modifications, senescence and apoptosis (Navas and Carnero 2021). In non-redox reactions, NAD^+ is consumed as a substrate by different types of enzymes including sirtuins and poly (ADP-ribose) polymerases (PARPs) (Anderson et al. 2017; Langelier et al. 2018; Kim et al. 2005). On the contrary, DECR1/2 are NADH-dependent auxiliary enzymes that play key roles in polyunsaturated fatty acid (PUFA) oxidation. It is not surprising that higher NAD^+/NADH ratios are found in cancer cells compared to non-malignant cells (Moreira et al. 2016). Therefore, it can be speculated that mitochondrial and peroxisomal β-oxidation work together to maintain the intricate balance between NAD^+ and NADH levels to support tumour cell proliferation and biomass production. However, further research is needed to elucidate the exact mechanism on how mitochondria are coupled to the transfer of peroxisomal redox equivalents.

Crosstalk of mitochondrial and peroxisomal metabolism may also occur at the transcriptional level (Sargsyan and Thoms 2020). For instance, the peroxisome proliferator-activated receptor (PPAR) transcription factors are key regulators of peroxisomal β-oxidation and proliferation. PPARs have been implicated in regulating the expression of genes involved in mitochondrial β-oxidation and biogenesis (Fransen et al. 2017). In addition, PPAR co-activator PGC-1α, a regulator of peroxisomal biogenesis, was reported to promote mitochondrial biogenesis and metabolism, oxidative phosphorylation, and antioxidant protection (Fransen et al. 2017). There are only a limited number of studies that have examined how perturbations in mitochondrial β-oxidation influence peroxisomal metabolism. Some studies showed that mitochondrial β-oxidation inhibition (via pharmacological inhibition or genetic knockouts) increased the expression of genes involved in peroxisomal β-oxidation pathways (Vickers 2009; Zhang et al. 2007; Lee et al. 2017). Notably, one study demonstrated that inhibition of mitochondrial β-oxidation in

muscle cells led to a compensatory increase in peroxisomal β-oxidation (Wicks et al. 2015). Therefore, it is also plausible that mitochondrial OXPHOS remains active or upregulated to compensate for peroxisomal β-oxidation inhibition or more specifically, DECR2 knockdown to prevent toxic lipid accumulation or maintain mitochondrial TCA cycle, thereby supporting tumour survival.

DECR1 inhibition results in mitochondrial ROS production and elevated oxidative stress. One can speculate that DECR1 knockdown would result in downregulation of peroxisomal metabolism to reduce excessive ROS production from peroxisomal β-oxidation. In addition, it is possible that very long chain fatty acid synthesis in the endoplasmic reticulum (ER) via fatty acid elongation (Kihara 2012) may be inhibited due to excess PUFA accumulation after DECR1 knockdown (Barelli and Antonny 2016). This would explain, in part, why peroxisomal metabolism was negatively enriched in DECR1 knockdown cells according to our RNA-seq results.

Another interesting aspect to consider is that the mitochondria and peroxisomes share isoforms of various metabolic enzymes. For instance, AMACR (peroxisomal enzyme responsible for branched chain FAO) is an established biomarker of prostate cancer and is expressed in both the mitochondria and peroxisome (Jiang et al. 2013; Amery et al. 2000). Moreover, increasing evidence suggests that glucose metabolism enzymes such as GAPDH, 3-phosphoglycerate kinase, and lactate dehydrogenase are partially localised in peroxisomes (Cipolla and Lodhi 2017). Furthermore, it is possible that the mitochondria are able to compensate for the decrease in peroxisomal β-oxidation and vice versa through the exchange of fatty acid substrates (Houten et al. 2020). From a biochemical perspective, these findings further challenge the conventional idea that the mitochondria and peroxisomes can only oxidise distinct pools of fatty acids.

7.4 Ferroptosis and polyunsaturated fatty acid metabolism

In Chapter 3, we uncovered a novel mechanism of DECR1 and polyunsaturated fatty acid (PUFA) oxidation and hypothesise that DECR1 is overexpressed in prostate cancer cells to prevent accumulation of PUFAs and protect the cancer cells from lipid peroxidation-induced cell death, called ferroptosis.

Ferroptosis is an iron-dependent form of cell death induced by excessive lipid peroxidation. This process relies on several key components, mainly PUFA-containing membrane phospholipids, metal iron (Fe^{2+}), and ROS. PUFAs are highly susceptible to lipid peroxidation due to their multiple double bonds and are the key drivers of ferroptosis. Previous studies have shown that PUFAs are esterified into membrane phospholipids, particularly phosphatidylethanolamine (PE)-containing phospholipids (arachidonic acid and adrenic acid) which generate lipid peroxides and trigger ferroptosis (Tang and Kroemer 2020). Several mechanisms of regulation of ferroptosis exists: (1) cysteine uptake via the System Xc- cysteine/glutamate anti-transporter; (2) glutathione peroxidase 4 (GPX4; ROS-scavenging protein that inhibits the formation of lipid peroxides; (3) intra- or inter- cellular signalling processes and environmental stresses that impact ferroptosis by regulating cellular metabolism and ROS levels (ie. iron levels, lipogenesis, mitochondrial TCA cycle, p53 and AMPK signalling pathways) (Jiang et al. 2021). The current operational definition of ferroptosis is a form of cell death process suppressed by both iron depletion and lipophilic antioxidants such as ferrostatin-1 (Jiang et al. 2021; Stockwell et al. 2017). Both requirements should be taken into account as there are also iron-dependent cell death mechanisms distinct from ferroptosis (Jiang et al. 2021). To this end, several ferroptosis inducers and inhibitors (including iron chelators) were employed to provide evidence of ferroptosis-induced cell death and sensitisation in DECR1 knockdown cells. Furthermore, lipid peroxidation was directly detected using fluorescent dyes such as BODIPY-C11. In addition to PUFA accumulation, few studies have linked mitochondrial oxidative metabolism to ferroptosis. Recent studies reported glutamine (or glutaminolysis) to be essential for cysteine deprivation-induced (CDI) ferroptosis via activation of the mitochondrial TCA cycle and ETC, thereby increasing mitochondrial respiration and ROS production to initiate ferroptosis (Gao et al. 2015; M. Gao et al. 2019). In a follow-up study, the authors also demonstrated that cancer cells deficient of the tumour suppressor fumarate hydratase are resistant to CDI ferroptosis (M. Gao et al. 2019), providing the basis for potential ferroptosis-inducing therapeutic approaches like DECR1. More recently, glucose starvation has been shown to inhibit ferroptosis. This was mediated by AMP activated kinase (AMPK) activation and subsequent downstream inhibitory phosphorylation of ACC1, leading to inhibition of lipid biosynthesis, which in turn protects cells from lipid peroxide accumulation and

ferroptosis (Lee et al. 2020; Li et al. 2020). DECR1 depleted cells exhibited increased glycolysis, which is accompanied by decreases in glycolytic intermediates, most likely to sustain TCA cycle intermediate levels. This poses critical questions for future research, whether glucose which serves as a major fuel of the TCA cycle regulates ferroptosis in DECR1 knockdown cells (as one would predict that inhibition of PUFA oxidation would attenuate ROS production and delay ferroptosis)? How does mitochondrial metabolism contribute to ferroptosis after DECR1 inhibition? Nevertheless, these findings reveal a multifaceted role of mitochondrial metabolism in the regulation of ferroptosis: generation of lipids or lipid precursors for phospholipid synthesis or via production of ROS (by-products of oxidative metabolism). More importantly, this study highlighted a previously unknown role of FAO in ferroptosis.

In Chapter 4, we observed a significant increase in MUFAs and PUFAs after DECR2 knockdown, as well as increases in several phospholipid species. This prompts the novel question – do peroxisomes also contribute to ferroptosis? Recently, a study identified peroxisomes as critical contributors to ferroptosis through biosynthesis of ether phospholipids (or plasmalogens) for lipid peroxidation (Zou et al. 2020). The authors performed a genome-wide CRISPR-Cas9 screen to identify genes that regulate the susceptibility of human renal and ovarian cancer cell lines to GPX4 inhibitor-induced ferroptosis (RSL3 and ML210). They found a significant enrichment of peroxisome-related genes, including peroxisomal enzymes involved in synthesis of ether lipids such as alkylglycerone phosphate synthase (AGPS), fatty acyl-CoA reductase 1 (FAR1), and glyceronephosphate O-acyltransferase (GNPAT); depletion of which increased cellular viability and resistance to ferroptosis. In contrast, knockout of peroxisomal enzymes, SOD1 and CAT, unrelated to ether lipid metabolism showed no effect. Notably, lipidomic analysis showed downregulation of ether phospholipids (ePLs), especially polyunsaturated ether phospholipids (PUFA-ePLs) in peroxisome-depleted cells. Furthermore, the provision of liposomal nanoparticles containing PUFA-ePLs (arachidonic acid and docosahexaenoic acid) was sufficient to confer sensitivity to ferroptosis by lipid peroxidation, but not MUFA-ePLs, highlighting the importance of PUFAs (and by inference MUFA:PUFA ratios) in ferroptosis sensitisation. Finally, the authors investigated the role of peroxisomes in promoting ferroptosis sensitivity *in vivo*.

While most GPX4 knockout cancer cells failed to survive *in vivo*, those that survive and developed tumours proliferated rapidly despite lack of GPX4 expression. Further analysis showed that such GPX4$^{-/-}$ cells downregulated synthesis of PUFA-ePLs, thus conferring resistance to ferroptosis.

Intriguingly, a study demonstrated that exogenous MUFAs induced a ferroptosis-resistant state in cells in an ACSL3-dependent manner (Magtanong et al. 2019). The authors proposed that exogenous MUFAs activated by acyl-CoA synthetase long-chain family member 3 (ACSL3; enzymes that convert free fatty acids to fatty acyl-CoA and incorporated into glycerophospholipids) displace PUFAs from plasma membrane phospholipids to reduce lipid ROS accumulation following GPX4 inhibition. This was supported by one other study in KRAS-driven lung tumours showing RAS-driven ACSL3 expression driving MUFA-containing lysophospholipid uptake to confer resistance to ferroptosis (Kamphorst et al. 2013). Overall, this suggests a close interaction between MUFA and PUFA metabolism and ferroptosis in influencing tumour cell survival or cell death – whether this is applicable to DECR2 knockdown cells remains elusive. Consistent with this idea, in Chapter 6, phospholipid profiling of clinical prostate tumours revealed significant changes in lipid composition relative to matched normal tissues whereby prostate tumours exhibit markedly elevated levels of MUFAs compared to SFA and PUFAs. This further supports the notion that tumour cells are protected from ferroptosis or lipotoxicity (discussed below).

7.5 Cell cycle and lipid metabolism

In Chapter 4, DECR2 knockdown or inhibition of peroxisomal β-oxidation attenuates prostate cancer cell viability via inhibition of cell cycle progression.

7.5.1 Interplay of oncogenic signalling, cell cycle and metabolism

Cell cycle regulators such as CDK4, cyclin D1 or Rb have been implicated in metabolic rewiring associated with proliferation (Lopez-Mejia and Fajas 2015; Huber et al. 2020). For instance, it was demonstrated that cyclin-dependent kinase 9 (CDK9; key regulator of RNA-polymerase II) inhibition markedly decreased FAO in prostate cancer cells (Itkonen et al. 2019). So far, the effects of DECR2 knockdown on cell cycle arrest may be attributed, at least in part, to Rb signalling. It was shown that Rb loss significantly decreased mitochondrial oxidative phosphorylation (OXPHOS) capacity and increased sensitivity to mitochondrial OXPHOS inhibitors (Nicolay et al. 2015). On the other hand, this study showed that Rb reactivation by CDK4/6 inhibition (CDK4/6i) reversed this effect, in turn, activating mitochondrial function and sensitising cells to glucose withdrawal and mitochondrial stress (Franco et al. 2016). Similarly, in DECR2 knockdown cells a reduction in pRb signalling contributing to cell cycle arrest and sustained mitochondrial OXPHOS. In light of this, it was interesting that DECR2 knockdown sensitised prostate cancer cells to the CDK4/6 inhibitor, ribociclib. This suggests that the effect may be context-dependent and further experimentation may be needed to study the effects of CDK4/6i on mitochondrial function in prostate cancer. Additionally, it is possible that DECR2 knockdown exhibits distinct endpoints with CDK4/6 inhibition by ribociclib. For instance, MEK inhibitors in combination with CDK4/6i enhance accumulation of mitochondria and OXPHOS to promote cell cycle arrest with features of senescence (Franco et al. 2016). In contrast, mTOR inhibitors restricted glycolytic metabolism and OXPHOS induced by CDK4/6i and suppressed tumour growth (Franco et al. 2016). What about cell cycle-dependent control of lipid metabolism? Rb was reported to suppress tumorigenesis by altering lipid composition (Muranaka et al. 2017), suggesting cell cycle regulation of lipid composition. One study reported that cell cycle stages can dictate changes in lipid composition in metazoan cells such as the production of key phospholipids, PC and PE (Sanchez-Alvarez et al. 2015). Moreover, a study in marine diatoms showed that cells arrested in G1 phase

accumulate TAGs and upregulate genes involved in *de novo* lipogenesis (Kim et al. 2017).

This prompts the question of whether cell cycle progression is influenced as a consequence of lipid accumulation/remodelling in DECR2 knockdown cells or vice versa? Certain lipid species have been implicated in cell cycle progression. For example, the long chain PUFA, docosahexaenoic acid (DHA) has been shown to influence cell cycle progression and hence, cancer cell viability and proliferation (Newell et al. 2017). Moreover, sphingolipids and ceramides which serves as bioactive molecules with key roles in cancer cell signalling and proliferation, are critical mediators of cell cycle arrest (Ogretmen and Hannun 2004; Ogretmen 2018).

7.5.2 Possible mechanism for peroxisomal metabolism in cell cycle regulation

mTORC1 is a protein complex that controls protein synthesis in a variety of cellular processes such as cell growth, proliferation, and autophagy in response to nutrient sensing, energy, and redox status. A study by Zhang et al in 2012 identified peroxisomes as a signalling organelle involved in the regulation of mammalian target of rapamycin complex (mTORC1). This was attributed to the localisation of tuberous sclerosis complex (TSC) signalling node (composed of TSC1, TSC2 and Rheb) to the peroxisomes where it represses mTORC1 in response to ROS (Zhang et al. 2013). In addition, cytoplasmic ATM (serine/threonine kinase) which responds to ROS to activate AMPK and TSC2 was also previously found to localise to peroxisomes (Alexander et al. 2010; Watters et al. 1999; Zhang et al. 2015). The connection between mTORC1 and cell cycle regulation have been described (Huber et al. 2020). For instance, a recent study found that cyclin D1-CDK4/6 activates mTORC1 via phosphorylation and inhibition of TSC2, thereby promoting cell proliferation directly via phosphorylation of Rb signalling and indirectly by enhancing cell growth (Romero-Pozuelo et al. 2020). Similarly, ATM is also known to play key roles in cell cycle control and DNA damage pathways. Consistent with this idea, GSEA correlation analysis showed that DECR2 is positively correlated with DNA repair pathways (Figure 7.1). Overall, these findings link peroxisomal metabolism to cell cycle control and opens up possible avenues for further investigation.

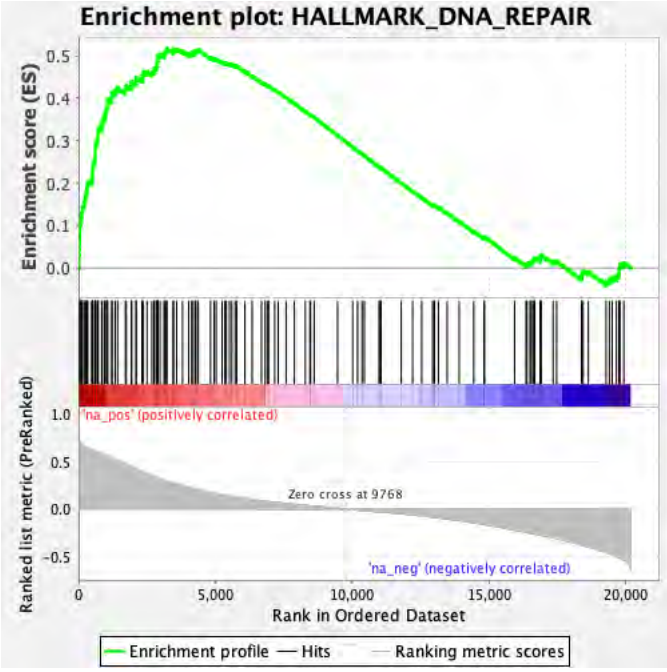

Figure 7.1 GSEA correlation analysis of DECR2 revealed significant positive correlation with hallmark DNA repair pathway.

7.6 Lipid accumulation and remodelling: protects or kills?

Chapter 3 identified a mechanism whereby excess PUFA accumulation in response to DECR1 (PUFA oxidation) inhibition leads to the induction of ferroptosis in prostate cancer cells. Likewise in Chapter 4, DECR2 knockdown (peroxisomal β-oxidation inhibition) led to overall lipid accumulation, particularly in lipid droplet content, and elevated MUFA/PUFA levels.

A study found that fatostatin (inhibitor of *de novo* lipogenesis via repression of SREBP) induced cell cycle arrest and apoptosis in ER+ breast cancer cells and tumours. This involves the activation of endoplasmic reticulum (ER) stress and lipid accumulation. Apoptosis was attributed to elevated ceramide levels mediated by ER stress, while accumulation of PUFA-TAGs promoted an anti-apoptotic response. Previous studies have reported saturated fatty acid (SFA)-induced apoptotic lipotoxicity (Li et al. 2018; Bobrovnikova-Marjon et al. 2008). This can be overcome by channelling SFAs into neutral lipids for storage in lipid droplets (Listenberger et al. 2003) or by exogenous MUFA uptake (Magtanong et al. 2019). Studies from peroxisomal disorders have shed light on the roles of lipid metabolic intermediates of peroxisomal metabolism in lipotoxicity (Wanders et al. 2010). In addition to

serving as a fuel source, lipid droplets can also protect cells from lipotoxicity and sustain mitochondrial OXPHOS during starvation-induced autophagy (Nguyen et al. 2017; Rambold et al. 2015; Benador et al. 2018). Moreover, a recent study has found that peroxisomes are tightly associated with lipid droplets to direct fatty acid trafficking (Chang et al. 2019). Consistently, DECR2 knockdown cells significantly induced lipid accumulation, particularly lipid droplet contents, and MUFA/PUFA lipids suggesting lipid partitioning, possibly as a protective mechanism against anti-tumour effects such as ROS.

Arguably, other mechanisms exist that involve lipid accumulation and suppression of cell growth, for instance ferroptosis (as discussed above) and cellular senescence. Senescent cells prompt DNA damage response signalling to the cell cycle inhibitor $p21^{CIP1}$, leading to increased expression of CDK4/6 inhibitor $p16^{INK4a}$ to halt cell cycle in G1 phase (Lee and Schmitt 2019). Moreover, senescence is associated with the induction of p53 and Rb pathways (Lee and Schmitt 2019). A study showed that deregulation of lipid metabolism may initiate a positive feedback loop that serves to maintain cells in senescence, independent of DNA damage (Flor et al. 2017). Proteomics and systems analysis identified enrichment of several lipid metabolism pathways marked by increased lipid uptake and accumulation, including upregulation of mitochondrial and peroxisomal β-oxidation enzymes. Additionally, the authors identified lipid peroxidation and production of reactive lipid aldehydes as key factors regulating cellular senescence (Flor et al. 2017). Intriguingly, mitochondrial CPT1C was recently identified as a critical regulator of cancer cell senescence by prevent lipotoxicity (Zhang et al. 2020). In light of these findings, we can speculate that DECR2 inhibition may lead to cellular senescence.

7.7 Epigenetics and lipid metabolism

In Chapter 4, fluctuations in the protein expression of histone H3 acetylation in DECR2 knockdown and TDZ treated cells were observed, proposing a potential link between FAO and epigenetic mechanisms potentially driven by acetyl-CoA availability.

While the link between glucose and histone acetylation have been well-studied, it was reported that *de novo* lipogenesis and histone acetylation use the same pool of acetyl-CoA. This study demonstrated that knockdown of the rate limiting enzyme of fatty acid synthesis, acetyl-CoA carboxylase 1 (ACC1) resulted in histone hyperacetylation (Galdieri and Vancura 2012). This is because ACC is the nexus between histone acetylation and fatty acid synthesis where these two processes compete for acetyl-CoA. Another study reported that lipid oxidation (mitochondrial and peroxisomal) -derived acetyl-CoA is the predominant contributor to the global acetyl-CoA pool, leading to increased histone acetylation (McDonnell et al. 2016). Furthermore, the authors showed that histone acetylation is accompanied by activation of a lipid-specific gene expression program, which differs from glucose or HDACi induced histone acetylation (McDonnell et al. 2016). On the other hand, a previous study identified FAO-induced histone deacetylation resulting in increased acetyl-CoA and mitochondrial protein hyperacetylation, and downregulation of ACC2 to promote tumour cell adaption to acidic conditions (Corbet et al. 2016). In contrast, a study in colorectal cancer found that butyrate (short chain FA) inhibits histone deacetylation to increase the expression of cell cycle arrest genes and induction of apoptosis (Han et al. 2018). Interestingly, a recent study demonstrated that CPT1A supports prostate cancer progression by supplying acetyl groups, thereby regulating histone acetylation and cell growth (Joshi et al. 2019). Peroxisomal metabolism may also influence histone acetylation through peroxisome-derived acetyl moieties, which can also serve as substrates for ACC (Hunt et al. 2014). In view of the limited knowledge on the connection between peroxisomal metabolism and epigenetics in cancer, we can speculate a link based on studies in human peroxisomal disorders. It was previously reported that phytanic acid, a substrate of peroxisomal alpha-oxidation, enhances HDAC activity *in vitro* and induces cell death as a result of reduced histone acetylation in neuronal cells (Nagai 2015). Furthermore, it was proposed that restoration of sirtuin 1 (SIRT1; NAD^+ dependent histone deacetylase) could rescue the effects of *Abcd*$^{-/-}$ (peroxisomal fatty acid transporter protein) mice and peroxisomal disease X-linked adrenoleukodystrophy (X-ALD) (Morató et al. 2015). More recently, it was demonstrated that knockdown of acyl-CoA oxidase 4 (ACX4; peroxisomal β-oxidation enzyme) in *Arabidopsis* suppressed histone acetylation and increased

DNA methylation at specific genomic loci, suggesting a link between peroxisomal β-oxidation and nuclear epigenetic modifications (Wang et al. 2019).

Besides acetyl-CoA availability, it is also important to note that histone (de)acetylation is markedly influenced by other factors such as energetic and redox state of the cell (i.e. cellular NAD^+/NADH ratio) and availability of metabolic intermediates such as free CoA, CoA-derivatives, NADPH and butyrate (Farr et al. 2016). All of which are influenced directly or indirectly by changes in mitochondrial or peroxisomal activity. Moreover, acetyl-CoA is present ubiquitously in the cell in distinct pools, including mitochondria, peroxisome, endoplasmic reticulum, cytosolic and nuclear compartments (Kinnaird et al. 2016). Although it is believed that acetyl-CoA cannot readily cross organelle membranes, it is plausible that compartmentalisation of acetyl-CoA may not be as rigid as one thought. Interestingly, this study found that labelling of octanoate carbon into acetyl-CoA were consistent with labelling in histone acetylation and other key metabolites synthesised from acetyl-CoA, regardless of compartment (McDonnell et al. 2016).

Taken together, these studies demonstrated that reprogramming of fatty acid metabolism, specifically FAO are associated with changes in epigenetic modifications. More extensive research is needed to determine how metabolic and epigenetic processes work together to ensure the appropriate cellular response and how these are perturbed in cancer.

7.8 A role for DECR1/2 in neuroendocrine prostate cancer

In Chapters 3 and 4, we described how DECR1/2 are potentially involved in CRPC development and resistance to AR targeted therapies. Notably, there was a discrepancy in the expression of DECR1/2 across different prostate cancer cell lines (androgen-dependent or independent). CRPC and NEPC (neuroendocrine prostate cancer) are lethal forms of prostate cancer that remains incurable. After long-term ADT, 25-30% of emergent CRPC will acquire an aggressive neuroendocrine (NE) phenotype that is AR-negative and lacks any targeted therapy (Sainio et al. 2018). Therefore, new treatment options to overcome resistance to ADT and treat incurable stages of the disease are urgently sought.

Tumour metabolic profiles vary between stages of the disease. For instance, few studies have reported an increased aerobic glycolytic phenotype in advanced stages of prostate cancer, taking into consideration differences between androgen-dependent and androgen-independent prostate cancer (Vaz et al. 2012; Li et al. 2016). However, it is known that early prostate tumorigenesis is accompanied by a low glycolytic rate, which is why prostate cancers are poorly detected by FDG-PET. A recent study using a multi-omics approach compared metabolic profiles between androgen-dependent LNCaP and SCNC LASCPC-01 prostate cancer cells (B. Gao et al. 2019). Consistent with literature, the authors found that LNCaP cells exhibit increased citrate levels accompanied by increased expression of ACLY and FASN compared to LASCPC-01 SCNC cells, suggesting *de novo* lipogenesis. Of particular interest, they found elevated levels of carnitine and short-chain acylcarnitines (including propionylcarnitine, C3) in LASCPC-01 SCNC cells compared to LNCaP cells. This suggests upregulation of FAO in the more aggressive SCNC cells to support rapid tumour growth and proliferation and highlights a potential for targeting FAO in high-grade aggressive neuroendocrine prostate cancer. In light of these findings, it is possible to speculate the contribution of peroxisomal β-oxidation in SCNC cells as propionyl-CoA is one of the major end products of peroxisomal β-oxidation (Jakobs and Wanders 1995; Westin et al. 2008). In support of this, several peroxisomal β-oxidation enzymes were found to be elevated in androgen-independent PC3 cells (ACOX1 and PECI). Consistently, DECR1/2 expression was significantly upregulated in neuroendocrine prostate cancer (NEPC) tissues. On the other hand, the fact that some isoforms of glycolytic enzymes are found to partially reside in peroxisomes prompts us to rethink about importance of peroxisomes in aggressive prostate cancer. In consideration of these observations, it would be worth evaluating the potential of targeting DECR1/2 and (mitochondrial or peroxisomal) fatty acid oxidation in the context of NEPC. However, the relevance of mitochondrial or peroxisomal metabolism at various tumour stages remains elusive.

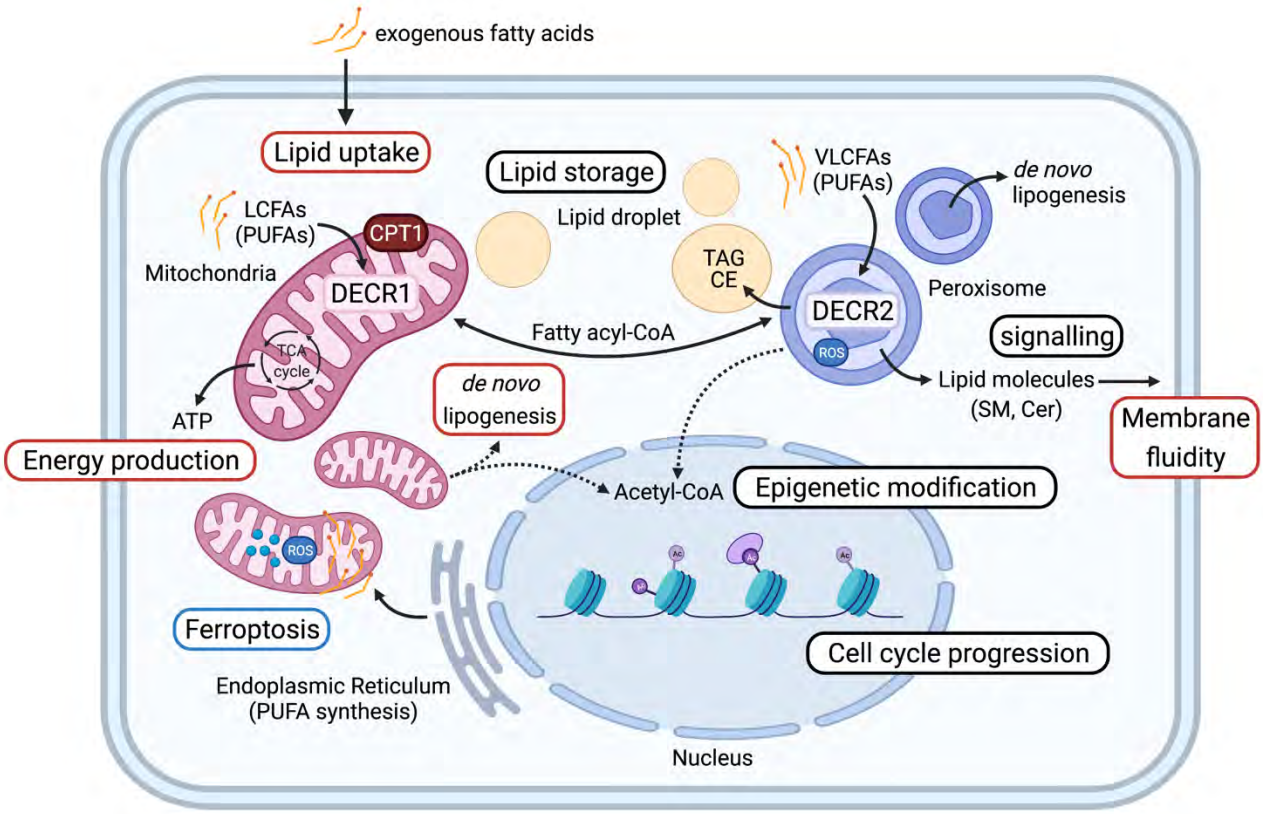

Figure 7.2 An overview of the findings discussed in Chapter 7.
Mitochondrial and peroxisomal fatty acid β-oxidation (FAO) pathways represent a metabolic vulnerability in prostate cancer. This illustration provides an overview of the implications in relation to mitochondrial and peroxisomal FAO as well as DECR1/2 inhibition. Lipids can be taken up exogenously or via de novo lipogenesis in both the mitochondria and peroxisomes. VLCFAs/PUFA-VLCFAs can be synthesised in the endoplasmic reticulum via fatty acid desaturation and elongation pathways. Mitochondrial DECR1 and peroxisomal DECR2 function to oxidise PUFA-LCFA and PUFA-VLCFAs respectively. Mitochondrial β-oxidation produces energy/ATP and ROS; whereas peroxisomal β-oxidation generates shortened fatty acyl-CoA (which is transported into the mitochondria via CPT1), acetyl-CoA and ROS. The exchange of metabolic substrates/intermediates (i.e., fatty acyl-CoAs) as well as co-factors (i.e., NAD+/NADH) illustrates the intimate relationship between the mitochondria and peroxisomes. Acetyl-CoA generated from the mitochondria and peroxisomes via FAO can be utilised in the nucleus for epigenetic modifications, for instance histone acetylation, thus altering gene transcription which, in turn, regulates numerous (oncogenic) signalling or metabolic pathways such as cell cycle progression. PUFAs can react with ROS to generate lipid peroxides, and its

accumulation (as a result of DECR1 inhibition) triggers ferroptosis (an iron-dependent form of cell death). DECR2 inhibition led to significant accumulation of multiple lipid classes, particularly in lipid droplet content (for storage), possibly to prevent ferroptosis or lipotoxicity, or as a source of energy (by mobilising lipid droplets). Certain lipid intermediates may serve as secondary messengers to influence signalling pathways. Changes in membrane lipid composition affects membrane fluidity (i.e., MUFA/PUFA ratio, cholesterol, or sphingolipid content). *Red border = upregulation; Blue border = downregulation, of pathway/process in prostate cancer. LCFA = long chain fatty acids; VLCFA = very long chain fatty acids; PUFA = polyunsaturated fatty acids; CPT1 = carnitine palmitoyltransferase 1; Ac = acetylation; TCA = tricarboxylic acid cycle/Kreb's cycle; ATP = adenosine triphosphate; ROS = reactive oxygen species; TAG = triacylglyceride; CE = cholesteryl ester; SM = sphingomyelin; Cer = ceramide.*

7.9 From bench to bedside: strategies for fatty acid oxidation inhibition

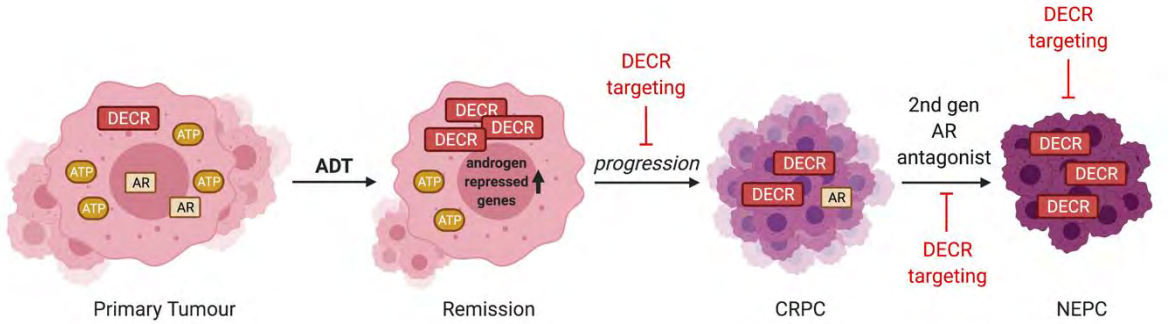

Figure 7.3 An overview of possible stages of prostate cancer where fatty acid oxidation inhibition would be beneficial. AR fuels prostate cancer with energy and drives prostate cancer progression. ADT may induce expression of androgen-repressed genes (i.e., DECR1) or other key FAO-related genes, and activate survival pathways to provide energy and promote survival. Targeting FAO in conjunction with ADT or AR-targeted therapies may enhance ADT efficacy and delay disease progression or treatment resistance to CRPC and NEPC. Alternatively, FAO inhibition could be beneficial in patients with CRPC and NEPC. *AR = androgen receptor; DECR = 2,4 dienoyl-CoA reductase; ATP = adenosine triphosphate; ADT = androgen deprivation therapy.*

Throughout this dissertation, we have incorporated the use of primary prostate cancer and CRPC or treatment-resistant models such as in cell lines (i.e., hormone-sensitive LNCaP cells, enzalutamide-resistant MR49F cells) and *ex vivo* patient-derived explant models representing primary disease. Our data and studies by other groups have demonstrated efficacy in targeting FAO in both primary and advanced stages of prostate cancer (Blomme et al. 2020; Gao et al. 2019; Kong et al. 2018; Flaig et al. 2017; Toren et al. 2016), including overcoming treatment resistance (Chapter 5). In Chapters 3 and 4, we identified DECR1 and DECR2, two enzymes involved in polyunsaturated fatty acid metabolism to be induced by ADT in prostate cancer cells and their expressions correlated with disease progression and overall survival. Hence, we propose that co-targeting of adaptive pathways like FAO that are induced by ADT or AR-targeting strategies may be essential to delay disease progression and promote a more durable therapeutic response.

7.10 Conclusion and future directions

The findings of this thesis provide new mechanistic insights into how fatty acid oxidation contributes to prostate cancer tumorigenesis, disease progression and treatment resistance. Notably, we identified and characterised two previously unexplored (mitochondrial and peroxisomal) FAO enzymes, DECR1 and DECR2, which represent novel and promising therapeutic targets for future clinical development. A novel role for FAO via DECR1 and PUFA oxidation in ferroptosis was also revealed. Moreover, we report that DECR1 is an androgen-repressed gene and proposed that upregulation of DECR1 may contribute to disease progression and CRPC. Furthermore, we explored the potential of targeting peroxisomal β-oxidation in advanced metastatic prostate cancer via DECR2 and pharmacological repurposing of clinically available peroxisomal β-oxidation inhibitors. In this study, the data revealed a novel link between epigenetics (acetyl-CoA availability) and lipid metabolism as well as the intimate association between mitochondrial and peroxisomal fatty acid metabolism, stimulating new mechanistic questions. Importantly, our work shows that FAO is a potential adaptive survival pathway to promote prostate cancer progression and treatment resistance. This supports the need for new and effective combination strategies to subvert resistance to AR targeted therapies as well as delay progression to CRPC. In addition, our data also provided a basis for biomarker discovery to facilitate patient stratification when metabolic therapies such as FAO inhibitors are considered as therapeutic approach. More importantly, these findings may be translatable to other cancers, as we have shown in Chapter 3 that DECR1 is also overexpressed in other tumour types apart from prostate cancer.

In future studies, the computational integration of omics (lipidomics, transcriptomics and proteomics) data would be beneficial to elucidate the interactions between cancer metabolism and signalling pathways. For instance, the activation status of proteins involved in cell cycle progression is heavily dependent on protein phosphorylation status. Moreover, it is becoming increasing clear that metabolism is closely associated with post-translational modifications (particularly lipids and proteins) and epigenetic modifications. Another important aspect to consider is tumour heterogeneity (as discussed in our review). We should consider

incorporating the use of patient-derived explants, xenograft models and potentially human prostate cancer organoids to provide more robust but clinically-relevant mechanistic insight.

Specific future directions relating to the respective Chapters are described below.

7.10.1 Small molecule inhibitors of DECR1

A previous study has solved the crystal structure of DECR1 and its active site (Alphey et al. 2005). Initial structure-based drug discovery identified thienodiazaborine as a potential ligand for DECR1. Subsequent induced-fit docking studies using a human DECR1-NADP-hexanoyl-CoA complex predicted that a D-2b18-NADP conjugate interacts strongly with several key amino acid residues in the binding pocket. Molecular Mechanics/Generalized Born Surface Area (MM/GBSA) calculations suggests that the conjugate binds with similar affinity as endogenous NADP. Future studies will evaluate the efficacy of this compound for DECR1 inhibition (via acylcarnitine measurement as described in Chapter 3) and prostate cancer cell viability using pre-clinical *ex vivo* and animal models.

7.10.2 Mechanistic insights of DECR2 and peroxisomal β-oxidation

More extensive work is needed to build upon the findings of Chapter 4. First and foremost, we will need to validate whether peroxisomal β-oxidation is indeed inhibited after targeting DECR2 or TDZ treatment. To elucidate the mechanism by which DECR2 may drive prostate cancer tumorigenesis, we aim to perform RNA-seq using stable DECR2 overexpression LNCaP cells. Why does DECR2 inhibition lead to total lipid accumulation, and what are the downstream consequences? What is the association between DECR2 or peroxisomal β-oxidation and mitochondrial phosphorylation? What are the upstream regulators that converge with DECR2 or peroxisomal β-oxidation to drive cell cycle arrest? Is cell cycle progression linked to lipid dysregulation after DECR2 knockdown or TDZ treatment? The new findings will shed light on the role of peroxisomal β-oxidation in prostate cancer which may be important for understanding fundamental biology and development of therapeutics.

Other relevant research questions to address going forward include: What stage(s) of disease is peroxisomal β-oxidation necessary to drive prostate cancer cell survival and treatment resistance? Is there a correlation between DECR2 or peroxisomal β-oxidation with specific molecular subtypes of prostate cancer? Taking into account patient heterogeneity, we will investigate the hallmarks of patients or their tumours which will indicate their dependence on mitochondrial or peroxisomal β-oxidation to determine their likelihood of response to therapy. Do androgens also regulate DECR2, and if not, what other pathway regulators influence DECR2 expression? As discussed above, some potential transcriptional regulators include PPAR and its co-activator PGC-1α, which warrants further investigation. Likewise, DECR1 is overexpressed in all stages of prostate cancer despite being an androgen-repressed gene which is suggestive of other mechanisms of regulation apart from AR.

Altogether, this work provides ground-breaking evidence for the significance of targeting FAO in prostate cancer and introduced two novel therapeutic targets for prostate cancer patients. The new findings here will spearhead treatment strategies that involve targeting mitochondrial or peroxisomal FAO to improve patient outcomes or delay treatment resistance and spur further discoveries to understand the role of mitochondrial and peroxisomal FAO in cancer.

Chapter 8: References

1. Albany, C. and Hahn, N.M. 2014. Heat shock and other apoptosis-related proteins as therapeutic targets in prostate cancer. *Asian Journal of Andrology* 16(3), pp. 359–363.

2. Alexander, A., Cai, S.-L., Kim, J., et al. 2010. ATM signals to TSC2 in the cytoplasm to regulate mTORC1 in response to ROS. *Proceedings of the National Academy of Sciences of the United States of America* 107(9), pp. 4153–4158.

3. Allain, E.P., Rouleau, M., Lévesque, E. and Guillemette, C. 2020. Emerging roles for UDP-glucuronosyltransferases in drug resistance and cancer progression. *British Journal of Cancer* 122(9), pp. 1277–1287.

4. Alphey, M.S., Yu, W., Byres, E., Li, D. and Hunter, W.N. 2005. Structure and reactivity of human mitochondrial 2,4-dienoyl-CoA reductase: enzyme-ligand interactions in a distinctive short-chain reductase active site. *The Journal of Biological Chemistry* 280(4), pp. 3068–3077.

5. Amery, L., Fransen, M., De Nys, K., Mannaerts, G.P. and Van Veldhoven, P.P. 2000. Mitochondrial and peroxisomal targeting of 2-methylacyl-CoA racemase in humans. *Journal of Lipid Research* 41(11), pp. 1752–1759.

6. Anderson, K.A., Madsen, A.S., Olsen, C.A. and Hirschey, M.D. 2017. Metabolic control by sirtuins and other enzymes that sense NAD+, NADH, or their ratio. *Biochimica et biophysica acta. Bioenergetics* 1858(12), pp. 991–998.

7. Anon Prostate cancer in Australia statistics | Cancer Australia [Online]. Available at: https://www.canceraustralia.gov.au/affected-cancer/cancer-types/prostate-cancer/prostate-cancer-australia-statistics [Accessed: 23 November 2020].

8. Antzelevitch, C., Belardinelli, L., Zygmunt, A.C., et al. 2004. Electrophysiological effects of ranolazine, a novel antianginal agent with antiarrhythmic properties. *Circulation* 110(8), pp. 904–910.

9. Attard, G., Parker, C., Eeles, R.A., et al. 2016. Prostate cancer. *The Lancet* 387(10013), pp. 70–82.

10. Bailey, A.P., Koster, G., Guillermier, C., et al. 2015. Antioxidant role for lipid droplets in a stem cell niche of drosophila. *Cell* 163(2), pp. 340–353.

11. Balaban, S., Nassar, Z.D., Zhang, A.Y., et al. 2019. Extracellular fatty acids are the major contributor to lipid synthesis in prostate cancer. *Molecular Cancer Research* 17(4), pp. 949–962.

12. Barelli, H. and Antonny, B. 2016. Lipid unsaturation and organelle dynamics.

Current Opinion in Cell Biology 41, pp. 25–32.

13. Barfeld, S.J., Itkonen, H.M., Urbanucci, A. and Mills, I.G. 2014. Androgen-regulated metabolism and biosynthesis in prostate cancer. *Endocrine-Related Cancer* 21(4), pp. T57-66.

14. Beloribi-Djefaflia, S., Vasseur, S. and Guillaumond, F. 2016. Lipid metabolic reprogramming in cancer cells. *Oncogenesis* 5, p. e189.

15. Benador, I.Y., Veliova, M., Mahdaviani, K., et al. 2018. Mitochondria Bound to Lipid Droplets Have Unique Bioenergetics, Composition, and Dynamics that Support Lipid Droplet Expansion. *Cell Metabolism* 27(4), p. 869–885.e6.

16. Bobrovnikova-Marjon, E., Hatzivassiliou, G., Grigoriadou, C., et al. 2008. PERK-dependent regulation of lipogenesis during mouse mammary gland development and adipocyte differentiation. *Proceedings of the National Academy of Sciences of the United States of America* 105(42), pp. 16314–16319.

17. de Bono, J.S., Logothetis, C.J., Molina, A., et al. 2011. Abiraterone and increased survival in metastatic prostate cancer. *The New England Journal of Medicine* 364(21), pp. 1995–2005.

18. Bray, F., Ferlay, J., Soerjomataram, I., Siegel, R.L., Torre, L.A. and Jemal, A. 2018. Global cancer statistics 2018: GLOBOCAN estimates of incidence and mortality worldwide for 36 cancers in 185 countries. *CA: A Cancer Journal for Clinicians* 68(6), pp. 394–424.

19. Butler, L.M., Centenera, M.M. and Swinnen, J.V. 2016. Androgen control of lipid metabolism in prostate cancer: novel insights and future applications. *Endocrine-Related Cancer* 23(5), pp. R219-27.

20. Camarda, R., Zhou, A.Y., Kohnz, R.A., et al. 2016. Inhibition of fatty acid oxidation as a therapy for MYC-overexpressing triple-negative breast cancer. *Nature Medicine* 22(4), pp. 427–432.

21. Carracedo, A., Cantley, L.C. and Pandolfi, P.P. 2013. Cancer metabolism: fatty acid oxidation in the limelight. *Nature Reviews. Cancer* 13(4), pp. 227–232.

22. Cavar, M., Ljubkovic, M., Bulat, C., et al. 2016. Trimetazidine does not alter metabolic substrate oxidation in cardiac mitochondria of target patient population. *British Journal of Pharmacology* 173(9), pp. 1529–1540.

23. Chang, C.-L., Weigel, A.V., Ioannou, M.S., et al. 2019. Spastin tethers lipid droplets to peroxisomes and directs fatty acid trafficking through ESCRT-III. *The Journal of Cell Biology* 218(8), pp. 2583–2599.

24. Cipolla, C.M. and Lodhi, I.J. 2017. Peroxisomal Dysfunction in Age-Related Diseases. *Trends in Endocrinology and Metabolism* 28(4), pp. 297–308.

25. Cookson, M.S., Lowrance, W.T., Murad, M.H., Kibel, A.S. and American Urological Association 2015. Castration-resistant prostate cancer: AUA guideline amendment. *The Journal of Urology* 193(2), pp. 491–499.

26. Corbet, C., Pinto, A., Martherus, R., Santiago de Jesus, J.P., Polet, F. and Feron, O. 2016. Acidosis Drives the Reprogramming of Fatty Acid Metabolism in Cancer Cells through Changes in Mitochondrial and Histone Acetylation. *Cell Metabolism* 24(2), pp. 311–323.

27. Crawford, E.D., Heidenreich, A., Lawrentschuk, N., et al. 2019. Androgen-targeted therapy in men with prostate cancer: evolving practice and future considerations. *Prostate cancer and prostatic diseases* 22(1), pp. 24–38.

28. Currie, E., Schulze, A., Zechner, R., Walther, T.C. and Farese, R.V. 2013. Cellular fatty acid metabolism and cancer. *Cell Metabolism* 18(2), pp. 153–161.

29. Daniel, W.A., Syrek, M., Ryłko, Z. and Kot, M. 2001. Effects of phenothiazine neuroleptics on the rate of caffeine demethylation and hydroxylation in the rat liver. *Polish journal of pharmacology* 53(6), pp. 615–621.

30. Davis, I.D., Martin, A.J., Stockler, M.R., et al. 2019. Enzalutamide with Standard First-Line Therapy in Metastatic Prostate Cancer. *The New England Journal of Medicine* 381(2), pp. 121–131.

31. Demarquoy, J. and Le Borgne, F. 2015. Crosstalk between mitochondria and peroxisomes. *World journal of biological chemistry* 6(4), pp. 301–309.

32. Ducker, G.S. and Rabinowitz, J.D. 2017. One-Carbon Metabolism in Health and Disease. *Cell Metabolism* 25(1), pp. 27–42.

33. Farese, R.V. and Walther, T.C. 2009. Lipid droplets finally get a little R-E-S-P-E-C-T. *Cell* 139(5), pp. 855–860.

34. Farr, R.L., Lismont, C., Terlecky, S.R. and Fransen, M. 2016. Peroxisome biogenesis in mammalian cells: The impact of genes and environment. *Biochimica et Biophysica Acta* 1863(5), pp. 1049–1060.

35. Feinberg, S.M., Fariba, K. and Saadabadi, A. Thioridazine. In: *StatPearls*. Treasure Island (FL): StatPearls Publishing.

36. Flor, A.C., Wolfgeher, D., Wu, D. and Kron, S.J. 2017. A signature of enhanced lipid metabolism, lipid peroxidation and aldehyde stress in therapy-induced senescence. *Cell death discovery* 3, p. 17075.

37. Franco, J., Balaji, U., Freinkman, E., Witkiewicz, A.K. and Knudsen, E.S. 2016. Metabolic reprogramming of pancreatic cancer mediated by CDK4/6 inhibition elicits unique vulnerabilities. *Cell reports* 14(5), pp. 979–990.

38. Fransen, M., Lismont, C. and Walton, P. 2017. The Peroxisome-Mitochondria Connection: How and Why? *International Journal of Molecular Sciences* 18(6).

39. Galdieri, L. and Vancura, A. 2012. Acetyl-CoA carboxylase regulates global histone acetylation. *The Journal of Biological Chemistry* 287(28), pp. 23865–23876.

40. Gao, B., Lue, H.-W., Podolak, J., et al. 2019. Multi-Omics Analyses Detail Metabolic Reprogramming in Lipids, Carnitines, and Use of Glycolytic Intermediates between Prostate Small Cell Neuroendocrine Carcinoma and Prostate Adenocarcinoma. *Metabolites* 9(5).

41. Gao, M., Monian, P., Quadri, N., Ramasamy, R. and Jiang, X. 2015. Glutaminolysis and transferrin regulate ferroptosis. *Molecular Cell* 59(2), pp. 298–308.

42. Gao, M., Yi, J., Zhu, J., et al. 2019. Role of mitochondria in ferroptosis. *Molecular Cell* 73(2), p. 354–363.e3.

43. Gervasini, G., Caballero, M.J., Carrillo, J.A. and Benitez, J. 2013. Comparative cytochrome p450 in vitro inhibition by atypical antipsychotic drugs. *ISRN pharmacology* 2013, p. 792456.

44. Guarnieri, C., Finelli, C., Zini, M. and Muscari, C. 1997. Effects of trimetazidine on the calcium transport and oxidative phosphorylation of isolated rat heart mitochondria. *Basic Research in Cardiology* 92(2), pp. 90–95.

45. Guillemette, C., Lévesque, É. and Rouleau, M. 2014. Pharmacogenomics of human uridine diphospho-glucuronosyltransferases and clinical implications. *Clinical Pharmacology and Therapeutics* 96(3), pp. 324–339.

46. Han, A., Bennett, N., Ahmed, B., Whelan, J. and Donohoe, D.R. 2018. Butyrate decreases its own oxidation in colorectal cancer cells through inhibition of histone deacetylases. *Oncotarget* 9(43), pp. 27280–27292.

47. Hiltunen, J.K. and Qin, Y. 2000. beta-oxidation - strategies for the metabolism of a wide variety of acyl-CoA esters. *Biochimica et Biophysica Acta* 1484(2–3), pp. 117–128.

48. Houten, S.M., Wanders, R.J.A. and Ranea-Robles, P. 2020. Metabolic interactions between peroxisomes and mitochondria with a special focus on acylcarnitine metabolism. *Biochimica et biophysica acta. Molecular basis of disease*

1866(5), p. 165720.

49. Huber, K., Mestres-Arenas, A., Fajas, L. and Leal-Esteban, L.C. 2020. The multifaceted role of cell cycle regulators in the coordination of growth and metabolism. *The FEBS Journal*.

50. Huggins, C. 1941. Studies on prostatic cancer. *Archives of Surgery* 43(2), p. 209.

51. Hunt, M.C., Tillander, V. and Alexson, S.E.H. 2014. Regulation of peroxisomal lipid metabolism: the role of acyl-CoA and coenzyme A metabolizing enzymes. *Biochimie* 98, pp. 45–55.

52. Hussain, M., Fizazi, K., Saad, F., et al. 2018. Enzalutamide in Men with Nonmetastatic, Castration-Resistant Prostate Cancer. *The New England Journal of Medicine* 378(26), pp. 2465–2474.

53. Itkonen, H.M., Poulose, N., Walker, S. and Mills, I.G. 2019. CDK9 Inhibition Induces a Metabolic Switch that Renders Prostate Cancer Cells Dependent on Fatty Acid Oxidation. *Neoplasia* 21(7), pp. 713–720.

54. Jakobs, B.S. and Wanders, R.J. 1995. Fatty acid beta-oxidation in peroxisomes and mitochondria: the first, unequivocal evidence for the involvement of carnitine in shuttling propionyl-CoA from peroxisomes to mitochondria. *Biochemical and Biophysical Research Communications* 213(3), pp. 1035–1041.

55. Jiang, N., Zhu, S., Chen, J., Niu, Y. and Zhou, L. 2013. A-methylacyl-CoA racemase (AMACR) and prostate-cancer risk: a meta-analysis of 4,385 participants. *Plos One* 8(10), p. e74386.

56. Jiang, X., Stockwell, B.R. and Conrad, M. 2021. Ferroptosis: mechanisms, biology and role in disease. *Nature Reviews. Molecular Cell Biology*.

57. Joshi, M., Stoykova, G.E., Salzmann-Sullivan, M., et al. 2019. CPT1A Supports Castration-Resistant Prostate Cancer in Androgen-Deprived Conditions. *Cells* 8(10).

58. Kamphorst, J.J., Cross, J.R., Fan, J., et al. 2013. Hypoxic and Ras-transformed cells support growth by scavenging unsaturated fatty acids from lysophospholipids. *Proceedings of the National Academy of Sciences of the United States of America* 110(22), pp. 8882–8887.

59. Karantanos, T., Corn, P.G. and Thompson, T.C. 2013. Prostate cancer progression after androgen deprivation therapy: mechanisms of castrate resistance and novel therapeutic approaches. *Oncogene* 32(49), pp. 5501–5511.

60. Kihara, A. 2012. Very long-chain fatty acids: elongation, physiology and related disorders. *Journal of Biochemistry* 152(5), pp. 387–395.

61. Kim, J., Brown, C.M., Kim, M.K., et al. 2017. Effect of cell cycle arrest on intermediate metabolism in the marine diatom Phaeodactylum tricornutum. *Proceedings of the National Academy of Sciences of the United States of America* 114(38), pp. E8007–E8016.

62. Kim, M.Y., Zhang, T. and Kraus, W.L. 2005. Poly(ADP-ribosyl)ation by PARP-1: “PAR-laying” NAD+ into a nuclear signal. *Genes & Development* 19(17), pp. 1951–1967.

63. Kinnaird, A., Zhao, S., Wellen, K.E. and Michelakis, E.D. 2016. Metabolic control of epigenetics in cancer. *Nature Reviews. Cancer* 16(11), pp. 694–707.

64. Konkel, A. and Schunck, W.-H. 2011. Role of cytochrome P450 enzymes in the bioactivation of polyunsaturated fatty acids. *Biochimica et Biophysica Acta* 1814(1), pp. 210–222.

65. Koundouros, N. and Poulogiannis, G. 2020. Reprogramming of fatty acid metabolism in cancer. *British Journal of Cancer* 122(1), pp. 4–22.

66. Kregel, S., Wang, C., Han, X., et al. 2020. Androgen receptor degraders overcome common resistance mechanisms developed during prostate cancer treatment. *Neoplasia* 22(2), pp. 111–119.

67. Langelier, M.-F., Zandarashvili, L., Aguiar, P.M., Black, B.E. and Pascal, J.M. 2018. NAD+ analog reveals PARP-1 substrate-blocking mechanism and allosteric communication from catalytic center to DNA-binding domains. *Nature Communications* 9(1), p. 844.

68. Lee, H., Zandkarimi, F., Zhang, Y., et al. 2020. Energy-stress-mediated AMPK activation inhibits ferroptosis. *Nature Cell Biology* 22(2), pp. 225–234.

69. Lee, J., Choi, J., Selen Alpergin, E.S., et al. 2017. Loss of Hepatic Mitochondrial Long-Chain Fatty Acid Oxidation Confers Resistance to Diet-Induced Obesity and Glucose Intolerance. *Cell reports* 20(3), pp. 655–667.

70. Lee, S. and Schmitt, C.A. 2019. The dynamic nature of senescence in cancer. *Nature Cell Biology* 21(1), pp. 94–101.

71. Li, C., Dong, X., Du, W., et al. 2020. LKB1-AMPK axis negatively regulates ferroptosis by inhibiting fatty acid synthesis. *Signal transduction and targeted therapy* 5(1), p. 187.

72. Li, N., Sancak, Y., Frasor, J. and Atilla-Gokcumen, G.E. 2018. A Protective

Role for Triacylglycerols during Apoptosis. *Biochemistry* 57(1), pp. 72–80.

73. Li, W., Cohen, A., Sun, Y., et al. 2016. The role of CD44 in glucose metabolism in prostatic small cell neuroendocrine carcinoma. *Molecular Cancer Research* 14(4), pp. 344–353.

74. Lin, D., Ettinger, S.L., Qu, S., et al. 2017. Metabolic heterogeneity signature of primary treatment-naïve prostate cancer. *Oncotarget* 8(16), pp. 25928–25941.

75. Listenberger, L.L., Han, X., Lewis, S.E., et al. 2003. Triglyceride accumulation protects against fatty acid-induced lipotoxicity. *Proceedings of the National Academy of Sciences of the United States of America* 100(6), pp. 3077–3082.

76. Liu, C.J., Yang, J.H., Huang, F.Z., et al. 2017. Glutathione-s-transferase A 4 (GSTA4) suppresses tumor growth and metastasis of human hepatocellular carcinoma by targeting AKT pathway. *American journal of translational research* 9(2), pp. 301–315.

77. Liu, L., Zhang, K., Sandoval, H., et al. 2015. Glial lipid droplets and ROS induced by mitochondrial defects promote neurodegeneration. *Cell* 160(1–2), pp. 177–190.

78. Liu, Y. 2006. Fatty acid oxidation is a dominant bioenergetic pathway in prostate cancer. *Prostate cancer and prostatic diseases* 9(3), pp. 230–234.

79. Lopez-Mejia, I.C. and Fajas, L. 2015. Cell cycle regulation of mitochondrial function. *Current Opinion in Cell Biology* 33, pp. 19–25.

80. Ma, Y., Temkin, S.M., Hawkridge, A.M., et al. 2018. Fatty acid oxidation: An emerging facet of metabolic transformation in cancer. *Cancer Letters* 435, pp. 92–100.

81. Ma, Y., Wang, W., Devarakonda, T., et al. 2020. Functional analysis of molecular and pharmacological modulators of mitochondrial fatty acid oxidation. *Scientific Reports* 10(1), p. 1450.

82. Magtanong, L., Ko, P.-J., To, M., et al. 2019. Exogenous Monounsaturated Fatty Acids Promote a Ferroptosis-Resistant Cell State. *Cell Chemical Biology* 26(3), p. 420–432.e9.

83. Mah, C.Y., Nassar, Z.D., Swinnen, J.V. and Butler, L.M. 2020. Lipogenic effects of androgen signaling in normal and malignant prostate. *Asian Journal of Urology* 7(3), pp. 258–270.

84. McClelland, G.B., Khanna, S., González, G.F., Butz, C.E. and Brooks, G.A.

2003. Peroxisomal membrane monocarboxylate transporters: evidence for a redox shuttle system? *Biochemical and Biophysical Research Communications* 304(1), pp. 130–135.

85. McDonnell, E., Crown, S.B., Fox, D.B., et al. 2016. Lipids reprogram metabolism to become a major carbon source for histone acetylation. *Cell reports* 17(6), pp. 1463–1472.

86. McNevin, C.S., Baird, A.-M., McDermott, R. and Finn, S.P. 2021. Diagnostic strategies for treatment selection in advanced prostate cancer. *Diagnostics (Basel)* 11(2).

87. Migita, T., Takayama, K.-I., Urano, T., et al. 2017. ACSL3 promotes intratumoral steroidogenesis in prostate cancer cells. *Cancer Science* 108(10), pp. 2011–2021.

88. Monaco, M.E. 2017. Fatty acid metabolism in breast cancer subtypes. *Oncotarget* 8(17), pp. 29487–29500.

89. Morató, L., Ruiz, M., Boada, J., et al. 2015. Activation of sirtuin 1 as therapy for the peroxisomal disease adrenoleukodystrophy. *Cell Death and Differentiation* 22(11), pp. 1742–1753.

90. Moreira, J. da V., Hamraz, M., Abolhassani, M., et al. 2016. The Redox Status of Cancer Cells Supports Mechanisms behind the Warburg Effect. *Metabolites* 6(4).

91. Muranaka, H., Hayashi, A., Minami, K., et al. 2017. A distinct function of the retinoblastoma protein in the control of lipid composition identified by lipidomic profiling. *Oncogenesis* 6(6), p. e350.

92. Nagai, K. 2015. Phytanic acid induces Neuro2a cell death via histone deacetylase activation and mitochondrial dysfunction. *Neurotoxicology and Teratology* 48, pp. 33–39.

93. Nagarajan, S.R., Butler, L.M. and Hoy, A.J. 2021. The diversity and breadth of cancer cell fatty acid metabolism. *Cancer & metabolism* 9(1), p. 2.

94. Nassar, Z.D., Mah, C.Y., Dehairs, J., et al. 2020. Human DECR1 is an androgen-repressed survival factor that regulates PUFA oxidation to protect prostate tumor cells from ferroptosis. *eLife* 9.

95. Navas, L.E. and Carnero, A. 2021. NAD+ metabolism, stemness, the immune response, and cancer. *Signal transduction and targeted therapy* 6(1), p. 2.

96. Newell, M., Baker, K., Postovit, L.M. and Field, C.J. 2017. A critical review on

the effect of docosahexaenoic acid (DHA) on cancer cell cycle progression. *International Journal of Molecular Sciences* 18(8).

97. Nguyen, T.B., Louie, S.M., Daniele, J.R., et al. 2017. DGAT1-Dependent Lipid Droplet Biogenesis Protects Mitochondrial Function during Starvation-Induced Autophagy. *Developmental Cell* 42(1), p. 9–21.e5.

98. Nicolay, B.N., Danielian, P.S., Kottakis, F., et al. 2015. Proteomic analysis of pRb loss highlights a signature of decreased mitochondrial oxidative phosphorylation. *Genes & Development* 29(17), pp. 1875–1889.

99. Nie, J., Duan, Q., He, M., et al. 2019. Ranolazine prevents pressure overload-induced cardiac hypertrophy and heart failure by restoring aberrant Na+ and Ca2+ handling. *Journal of Cellular Physiology* 234(7), pp. 11587–11601.

100. O'Connor, R.S., Guo, L., Ghassemi, S., et al. 2018. The CPT1a inhibitor, etomoxir induces severe oxidative stress at commonly used concentrations. *Scientific Reports* 8(1), p. 6289.

101. Ogretmen, B. 2018. Sphingolipid metabolism in cancer signalling and therapy. *Nature Reviews. Cancer* 18(1), pp. 33–50.

102. Ogretmen, B. and Hannun, Y.A. 2004. Biologically active sphingolipids in cancer pathogenesis and treatment. *Nature Reviews. Cancer* 4(8), pp. 604–616.

103. Peitzsch, C., Gorodetska, I., Klusa, D., et al. 2020. Metabolic regulation of prostate cancer heterogeneity and plasticity. *Seminars in Cancer Biology*.

104. Pertega-Gomes, N., Vizcaino, J.R., Felisbino, S., et al. 2015. Epigenetic and oncogenic regulation of SLC16A7 (MCT2) results in protein over-expression, impacting on signalling and cellular phenotypes in prostate cancer. *Oncotarget* 6(25), pp. 21675–21684.

105. Ponnusamy, S., He, Y., Hwang, D.-J., et al. 2019. Orally Bioavailable Androgen Receptor Degrader, Potential Next-Generation Therapeutic for Enzalutamide-Resistant Prostate Cancer. *Clinical Cancer Research* 25(22), pp. 6764–6780.

106. Priolo, C., Pyne, S., Rose, J., et al. 2014. AKT1 and MYC induce distinctive metabolic fingerprints in human prostate cancer. *Cancer Research* 74(24), pp. 7198–7204.

107. Pullar, B. and Shah, N. 2016. Prostate cancer. *Surgery (Oxford)* 34(10), pp. 505–511.

108. Rambold, A.S., Cohen, S. and Lippincott-Schwartz, J. 2015. Fatty acid

trafficking in starved cells: regulation by lipid droplet lipolysis, autophagy, and mitochondrial fusion dynamics. *Developmental Cell* 32(6), pp. 678–692.

109. Resh, M.D. 2006. Palmitoylation of ligands, receptors, and intracellular signaling molecules. *Science's STKE: Signal Transduction Knowledge Environment* 2006(359), p. re14.

110. Ricciardelli, C., Mayne, K., Sykes, P.J., et al. 1997. Elevated stromal chondroitin sulfate glycosaminoglycan predicts progression in early-stage prostate cancer. *Clinical Cancer Research* 3(6), pp. 983–992.

111. Ricciardelli, C., Quinn, D.I., Raymond, W.A., et al. 1999. Elevated levels of peritumoral chondroitin sulfate are predictive of poor prognosis in patients treated by radical prostatectomy for early-stage prostate cancer. *Cancer Research* 59(10), pp. 2324–2328.

112. Richter, E., Srivastava, S. and Dobi, A. 2007. Androgen receptor and prostate cancer. *Prostate cancer and prostatic diseases* 10(2), pp. 114–118.

113. Röhrig, F. and Schulze, A. 2016. The multifaceted roles of fatty acid synthesis in cancer. *Nature Reviews. Cancer* 16(11), pp. 732–749.

114. Romero-Pozuelo, J., Figlia, G., Kaya, O., Martin-Villalba, A. and Teleman, A.A. 2020. Cdk4 and Cdk6 Couple the Cell-Cycle Machinery to Cell Growth via mTORC1. *Cell reports* 31(2), p. 107504.

115. Sainio, M., Visakorpi, T., Tolonen, T., Ilvesaro, J. and Bova, G.S. 2018. Expression of neuroendocrine differentiation markers in lethal metastatic castration-resistant prostate cancer. *Pathology, Research and Practice* 214(6), pp. 848–856.

116. Sanchez-Alvarez, M., Zhang, Q., Finger, F., Wakelam, M.J.O. and Bakal, C. 2015. Cell cycle progression is an essential regulatory component of phospholipid metabolism and membrane homeostasis. *Open biology* 5(9), p. 150093.

117. Sargsyan, Y. and Thoms, S. 2020. Staying in Healthy Contact: How Peroxisomes Interact with Other Cell Organelles. *Trends in Molecular Medicine* 26(2), pp. 201–214.

118. Sarparast, M., Dattmore, D., Alan, J. and Lee, K.S.S. 2020. Cytochrome P450 metabolism of polyunsaturated fatty acids and neurodegeneration. *Nutrients* 12(11).

119. Scher, H.I., Fizazi, K., Saad, F., et al. 2012. Effect of MDV3100, an androgen receptor signaling inhibitor (ARSI), on overall survival in patients with prostate cancer postdocetaxel: Results from the phase III AFFIRM study. *Journal of Clinical*

Oncology 30(5_suppl), p. LBA1.

120. Schöpf, B., Weissensteiner, H., Schäfer, G., et al. 2020. OXPHOS remodeling in high-grade prostate cancer involves mtDNA mutations and increased succinate oxidation. *Nature Communications* 11(1), p. 1487.

121. Shen, S., Faouzi, S., Souquere, S., et al. 2020. Melanoma Persister Cells Are Tolerant to BRAF/MEK Inhibitors via ACOX1-Mediated Fatty Acid Oxidation. *Cell reports* 33(8), p. 108421.

122. Shi, R., Zhang, Y., Shi, Y., Shi, S. and Jiang, L. 2012. Inhibition of peroxisomal β-oxidation by thioridazine increases the amount of VLCFAs and Aβ generation in the rat brain. *Neuroscience Letters* 528(1), pp. 6–10.

123. Siegel, R.L., Miller, K.D. and Jemal, A. 2019. Cancer statistics, 2019. *CA: A Cancer Journal for Clinicians* 69(1), pp. 7–34.

124. Smith, M.R., Saad, F., Chowdhury, S., et al. 2018. Apalutamide Treatment and Metastasis-free Survival in Prostate Cancer. *The New England Journal of Medicine* 378(15), pp. 1408–1418.

125. Snaebjornsson, M.T., Janaki-Raman, S. and Schulze, A. 2020. Greasing the wheels of the cancer machine: the role of lipid metabolism in cancer. *Cell Metabolism* 31(1), pp. 62–76.

126. Stockwell, B.R., Friedmann Angeli, J.P., Bayir, H., et al. 2017. Ferroptosis: A regulated cell death nexus linking metabolism, redox biology, and disease. *Cell* 171(2), pp. 273–285.

127. Swinnen, J.V., Van Veldhoven, P.P., Timmermans, L., et al. 2003. Fatty acid synthase drives the synthesis of phospholipids partitioning into detergent-resistant membrane microdomains. *Biochemical and Biophysical Research Communications* 302(4), pp. 898–903.

128. Tai, S., Sun, Y., Squires, J.M., et al. 2011. PC3 is a cell line characteristic of prostatic small cell carcinoma. *The Prostate* 71(15), pp. 1668–1679.

129. Tan, M.H.E., Li, J., Xu, H.E., Melcher, K. and Yong, E. 2015. Androgen receptor: structure, role in prostate cancer and drug discovery. *Acta Pharmacologica Sinica* 36(1), pp. 3–23.

130. Tang, D. and Kroemer, G. 2020. Peroxisome: the new player in ferroptosis. *Signal transduction and targeted therapy* 5(1), p. 273.

131. Toren, P., Kim, S., Johnson, F. and Zoubeidi, A. 2016. Combined AKT and MEK Pathway Blockade in Pre-Clinical Models of Enzalutamide-Resistant Prostate

Cancer. *Plos One* 11(4), p. e0152861.

132. Turgeon, D., Chouinard, S., Belanger, P., et al. 2003. Glucuronidation of arachidonic and linoleic acid metabolites by human UDP-glucuronosyltransferases. *Journal of Lipid Research* 44(6), pp. 1182–1191.

133. Ursini-Siegel, J., Rajput, A.B., Lu, H., et al. 2007. Elevated expression of DecR1 impairs ErbB2/Neu-induced mammary tumor development. *Molecular and Cellular Biology* 27(18), pp. 6361–6371.

134. Valença, I., Ferreira, A.R., Correia, M., et al. 2020. Prostate cancer proliferation is affected by the subcellular localization of MCT2 and accompanied by significant peroxisomal alterations. *Cancers* 12(11).

135. Valença, I., Pértega-Gomes, N., Vizcaino, J.R., et al. 2015. Localization of MCT2 at peroxisomes is associated with malignant transformation in prostate cancer. *Journal of Cellular and Molecular Medicine* 19(4), pp. 723–733.

136. Van den Branden, C. and Roels, F. 1985. Thioridazine: a selective inhibitor of peroxisomal beta-oxidation in vivo. *FEBS Letters* 187(2), pp. 331–333.

137. Vaz, C.V., Alves, M.G., Marques, R., et al. 2012. Androgen-responsive and nonresponsive prostate cancer cells present a distinct glycolytic metabolism profile. *The International Journal of Biochemistry & Cell Biology* 44(11), pp. 2077–2084.

138. Vickers, A.E.M. 2009. Characterization of hepatic mitochondrial injury induced by fatty acid oxidation inhibitors. *Toxicologic Pathology* 37(1), pp. 78–88.

139. Wanders, R.J.A., Ferdinandusse, S., Brites, P. and Kemp, S. 2010. Peroxisomes, lipid metabolism and lipotoxicity. *Biochimica et Biophysica Acta* 1801(3), pp. 272–280.

140. Wanders, R.J.A., Waterham, H.R. and Ferdinandusse, S. 2015. Metabolic Interplay between Peroxisomes and Other Subcellular Organelles Including Mitochondria and the Endoplasmic Reticulum. *Frontiers in cell and developmental biology* 3, p. 83.

141. Wang, L., Wang, C., Liu, X., et al. 2019. Peroxisomal β-oxidation regulates histone acetylation and DNA methylation in Arabidopsis. *Proceedings of the National Academy of Sciences of the United States of America* 116(21), pp. 10576–10585.

142. Watson, P.A., Arora, V.K. and Sawyers, C.L. 2015. Emerging mechanisms of resistance to androgen receptor inhibitors in prostate cancer. *Nature Reviews. Cancer* 15(12), pp. 701–711.

143. Watters, D., Kedar, P., Spring, K., et al. 1999. Localization of a portion of extranuclear ATM to peroxisomes. *The Journal of Biological Chemistry* 274(48), pp. 34277–34282.

144. Westin, M.A.K., Hunt, M.C. and Alexson, S.E.H. 2008. Short- and medium-chain carnitine acyltransferases and acyl-CoA thioesterases in mouse provide complementary systems for transport of beta-oxidation products out of peroxisomes. *Cellular and Molecular Life Sciences* 65(6), pp. 982–990.

145. Wicks, S.E., Vandanmagsar, B., Haynie, K.R., et al. 2015. Impaired mitochondrial fat oxidation induces adaptive remodeling of muscle metabolism. *Proceedings of the National Academy of Sciences of the United States of America* 112(25), pp. E3300-9.

146. Wright, H.J., Hou, J., Xu, B., et al. 2017. CDCP1 drives triple-negative breast cancer metastasis through reduction of lipid-droplet abundance and stimulation of fatty acid oxidation. *Proceedings of the National Academy of Sciences of the United States of America* 114(32), pp. E6556–E6565.

147. Wu, X., Daniels, G., Lee, P. and Monaco, M.E. 2014. Lipid metabolism in prostate cancer. *American journal of clinical and experimental urology* 2(2), pp. 111–120.

148. Yao, C.-H., Liu, G.-Y., Wang, R., Moon, S.H., Gross, R.W. and Patti, G.J. 2018. Identifying off-target effects of etomoxir reveals that carnitine palmitoyltransferase I is essential for cancer cell proliferation independent of β-oxidation. *PLoS Biology* 16(3), p. e2003782.

149. Zadra, G., Photopoulos, C. and Loda, M. 2013. The fat side of prostate cancer. *Biochimica et Biophysica Acta* 1831(10), pp. 1518–1532.

150. Zhang, D., Liu, Z.-X., Choi, C.S., et al. 2007. Mitochondrial dysfunction due to long-chain Acyl-CoA dehydrogenase deficiency causes hepatic steatosis and hepatic insulin resistance. *Proceedings of the National Academy of Sciences of the United States of America* 104(43), pp. 17075–17080.

151. Zhang, H., Wang, Y., Guan, L., et al. 2020. Lipidomics reveals carnitine palmitoyltransferase 1C protects cancer cells from lipotoxicity and senescence. *Journal of Pharmaceutical Analysis*.

152. Zhang, J., Kim, J., Alexander, A., et al. 2013. A tuberous sclerosis complex signalling node at the peroxisome regulates mTORC1 and autophagy in response to ROS. *Nature Cell Biology* 15(10), pp. 1186–1196.

153. Zhang, J., Tripathi, D.N., Jing, J., et al. 2015. ATM functions at the peroxisome to induce pexophagy in response to ROS. *Nature Cell Biology* 17(10), pp. 1259–1269.

154. Zopf, C.J., Quinn, K., Zeidman, J. and Maheshri, N. 2013. Cell-cycle dependence of transcription dominates noise in gene expression. *PLoS Computational Biology* 9(7), p. e1003161.

155. Zou, Y., Henry, W.S., Ricq, E.L., et al. 2020. Plasticity of ether lipids promotes ferroptosis susceptibility and evasion. *Nature* 585(7826), pp. 603–608.

Chapter 9: Appendices

9.1 Appendix A: Nassar et al., 2018 BJU International

BJUI
BJU International

Review

Peri-prostatic adipose tissue: the metabolic microenvironment of prostate cancer

Zeyad D. Nassar*†‡, Adel T. Aref*†‡, Dushan Miladinovic§, Chui Yan Mah*†‡, Ganesh V. Raj¶, Andrew J. Hoy§ and Lisa M. Butler*†‡

*University of Adelaide Medical School, Adelaide, SA, Australia, †Freemasons Foundation Centre for Men's Health, Adelaide, SA, Australia, ‡South Australian Health and Medical Research Institute, Adelaide, SA, Australia, §Discipline of Physiology, School of Medical Sciences and Bosch Institute, Charles Perkins Centre, University of Sydney, Sydney, NSW, Australia, and ¶Departments of Urology and Pharmacology, UT Southwestern Medical Center at Dallas, Dallas, TX, USA

Z.D.N. and A.T.A. contributed equally to the work.

Emerging data have linked certain features of clinical prostate cancer (PCa) to obesity and, more specifically, increased adiposity. Whereas the large number of clinical studies and meta-analyses that have explored the associations between PCa and obesity have shown considerable variability, particularly in relation to prostate cancer risk, there is an accumulating weight of evidence consistently linking obesity to greater aggressiveness of disease. In probing this association mechanistically, it has been posited that peri-prostatic adipose tissue (PPAT), a significant component of the prostate microenvironment, may be a critical source of fatty acids and other mitogens and thereby influences PCa pathogenesis and progression. Notably, several recent studies have identified secreted factors from both PPAT and PCa that potentially mediate the two-way communication between these intimately linked tissues. In the present review, we summarize the available literature regarding the relationship between PPAT and PCa, including the potential biological mediators of that relationship, and explore emerging areas of interest for future research endeavours.

Keywords

adipocytes, obesity, peri-prostatic adipose tissue, prostate cancer, tumour microenvironment

Introduction

Prostate cancer (PCa) is the most commonly diagnosed cancer in men in developed countries and the second most common cancer worldwide [1]. The past 30 years have seen a progressive increase in the incidence of PCa, to an extent that cannot be explained solely by the implementation of PSA-based testing programmes. This increase in PCa incidence has largely mirrored the increase in the prevalence of obesity and metabolic syndrome [2,3]. While there are conflicting reports on the effect of obesity on PCa incidence [4], there is an increasing body of evidence demonstrating associations between obesity and more aggressive carcinoma, poor treatment outcome and higher risk of cancer-specific mortality for PCa [5,6]. A range of mechanisms have been proposed to underpin the effects of an obese environment on PCa behaviour, including increased systemic inflammation, hyperinsulinaemia, altered adipokine profiles and increased lipid availability [7,8]. Enhanced synthesis and uptake of lipids are key hallmarks of PCa and are regulated by androgen signalling (the key driver of PCa pathogenesis), reviewed in Butler et al. [9]. Taken together with observations that increased local adipose tissue amounts, specifically peri-prostatic adipose tissue (PPAT), may be associated with higher grade or aggressiveness of disease (Table 1), obesity-mediated change to the size of this lipid depot may be an important contributor to PCa pathobiology. In this review, we present the available data regarding the link between PPAT and PCa aggressiveness, drawing from both clinical studies and *in vitro* laboratory research, and consider potential mechanistic pathways by which PPAT may influence PCa.

Methodology

We searched PubMed, Medline, Scopus and Google Scholar using the following search terms: 'periprostatic', 'adipocytes', 'adipose tissue', 'prostate' and 'cancer' in various combinations. There was no limitation on the year of

© 2018 The Authors
BJU International © 2018 BJU International | doi:10.1111/bju.14173
Published by John Wiley & Sons Ltd. www.bjui.org

BJU Int 2018; **121:** Supplement 3, 9–21
wileyonlinelibrary.com

Table 1 Clinical studies investigating the association between the clinical features of peri-prostatic adipose tissue and prostate cancer.

References	Year	Method	*N*	Major findings	Analysis	OR (95%CI), *P*
[58]	2010	CT	725 patients who underwent brachytherapy	PPAT area and density were not associated with PCa aggressiveness.	Univariable logistic regression analysis.	1 (0.96–1.05), $P = 0.93$
[59]	2011	CT	932 patients who underwent brachytherapy or radiotherapy	Significant association between total PPAT area and density with high-risk PCa.	Multivariable logistic regression analysis	1.06 (1.04–1.08), $P < 0.001$
[67]	2012	TRUS	279 healthy controls 434 patients with PCa 218 patients with high-grade PCa	Increasing in PPAT thickness was a risk factor for detecting PCa and detecting high-grade PCa on biopsy. For each 1-mm increase in peri-prostatic fat thickness there was a 12% increase in odds detecting PCa and 20% in odds of detecting high-grade PCa.	Multivariable logistic regression analysis	PCa: 1.12, (1.02–1.23), $P \leq 0.02$ High grade PCa: 1.20 (1.07–1.34), $P \leq 0.002$
[63]	2014	MRI	184 patients who underwent radical retropubic prostatectomy	PPAT area and ratio (PPAT volume/ prostate volume) were associated with high-risk PCa.	Multivariable logistic regression analysis	PPAT area: 1(0.96–1.04), $P = 0.024$ PPAT ratio: 1.05(1.03–1.08), $P = 0.31$
[60]	2014	CT scan	308 patients who underwent radiotherapy	Visceral adipose tissue area and PPAT area were associated with aggressive PCa in black men but not in white men.	Multivariable logistic regression analysis	Visceral adipose tissue area: 4.23 (1.67–10.69), $P = 0.002$ PPAT area: 1.88 (0.80–4.44), $P = 0.135$
[61]	2015	MRI	190 patients who underwent MRI before prostatectomy	PPAT thickness was correlated with Gleason Score. PPAT was an independent predictive factor for high-grade PCa.	Multivariable logistic regression analysis	1.331 (1.063–1.666), $P \leq 0.013$
[62]	2016	MRI	234 patients who underwent different treatment methods	PPAT fat ratio (PPAT volume/ prostate volume) was associated with higher Gleason score.	Multivariable logistic regression analysis	3.45(1.69–7.06), $P \leq 0.001$
[56]	2017	CT scan	61 patients treated with 5ARIs for ≥12 months, and 117 patients without any exposure to 5ARIs	Weak significant correlation between the CAPRA score and the PPAT volume. In multivariate linear regression analysis adjusted for 5ARI use, PPAT was not predictive of the total CAPRA score.	Multivariable logistic regression analysis	PCa: 1.55, (1.03–1.84), $P \leq 0.001$. High grade PCa: 1.46 (1.20–1.73), $P \leq 0.001$
[65]	2017	MRI	371 PCa patients; 292 with high-grade disease	PPAT thickness was an independent predictor of PCa and high-grade PCa.	Multivariable logistic regression analysis	1.398 (1.037–1.883), $P = 0.028$
[66]	2017	MRI	162 patients who underwent MRI prior to prostatectomy	PPAT fat ratio (PPAT volume/ prostate volume) was associated with PCa aggressiveness (grade and stage).	Binary logistic regression analysis	$P = 0.18$

5ARI, 5α-reductase inhibitor; CAPRA, Cancer of the Prostate Risk Assessment; OR, odds ratio; PCa, prostate cancer; PPAT, peri-prostatic adipose tissue.

© 2018 The Authors

publication or the publication language. The reference lists of identified publications were also searched for additional material.

Obesity and Prostate Cancer

Epidemiological Evidence Linking Obesity and Prostate Cancer

Multiple epidemiological studies have identified associations between obesity (often measured as body mass index (BMI) and increased incidence of different types of cancer, including oesophageal, gynaecological and colorectal cancers [10–17]. Obesity has also been associated with poor treatment outcome and increased cancer-specific mortality [18]. Similar relationships have been observed for PCa, although the findings are inconsistent; some studies report an association between obesity and increased PCa incidence [19–23], whilst others have shown no or only modest associations with PCa incidence [24–26]. Meta-analyses designed to examine robustly the association between obesity and PCa incidence are equally inconclusive [4–6,19,27–29].

Several studies have, however, identified significant associations between obesity and the progression of PCa, most commonly with the presence of a more aggressive carcinoma and/or higher PCa-specific mortality [25,30–33], as well as increasing the risk of biochemical recurrence [34,35]. Unlike the data for PCa incident risk, meta-analyses have shown more consistent associations between obesity and more advanced stages of PCa as well as higher disease-related mortality [4–6,19,27–29].

In a study exploring the effect of pre-diagnostic BMI on PCa incidence in the Prostate, Lung, Colorectal, and Ovarian (PLCO) Cancer Screening Trial, BMI at the age of 50 years and at the study baseline was inversely associated with total incidence [36]. Interestingly, one meta-analysis found obesity to be associated with decreased risk of localized disease but an increased risk of a more advanced disease [37]. Several factors could be attributable for this finding including the lower PSA levels in obese men [38], the technical difficulties in examination, diagnostic procedures and treatment methods, as well as potential stage-specific interactions [39].

Proposed Mechanisms Linking Obesity and Prostate Cancer

Causative mechanisms that have been proposed as explanations for the potential link between obesity and PCa aggressiveness have largely focused on alterations in the host systemic milieu, such as increased circulating levels of insulin and other growth factors, altered inflammatory status and dyslipidaemia [7,8]. Alongside these systemic changes, it is also evident that cells of the surrounding or nearby tissue, such as stromal, endothelial, lymphocytes and adipose stem cells, contribute to a supportive tumour microenvironment [40]. Peri-tumoral adipose tissue and other adipose beds that support metastatic disease promote growth of a range of cancers through diverse mechanisms including the release of growth factors, inflammatory signalling activators, and the release of fatty acids as a source of potential usable energy [41]. Adipose tissue is a heterogeneous mix of cell types comprising resident immune cells, fibroblasts, the stem cell population termed 'pre-adipocytes' and mature adipocytes, with mature adipocytes alone able to promote tumour progression in several types of cancer [42–44]. These considerations, together with the close proximity of PPAT to the prostate, have understandably stimulated interest in this understudied adipose depot and its influence on PCa.

All Adipose Tissue Depots are not Equal

Adipose tissue is a metabolically active organ that can be broadly classified into visceral and subcutaneous adipose beds. Visceral adipose tissue releases more inflammatory and growth factors compared with subcutaneous adipose tissue [45], and a recent study by Lee et al. [46] reported that visceral adipose tissue, and the visceral to subcutaneous adipose tissue ratio, is an independent predictor for all-cause mortality. Moreover, in 2004 Von Hafe et al. [47] found that higher visceral fat identified by CT was associated with higher risk of PCa. To date, very few data exist on the phenotype of PPAT and how it relates to subcutaneous adipose tissue and other visceral adipose beds. Differences between the various adipose beds with respect to BMI highlight the need to analyse more accurately the associations between PCa incidence and aggressiveness with the actual differential fat content of the body using radiological methods.

Relationships Between Peri-Prostatic Adipose Tissue and Prostate Cancer Features

A range of studies have investigated the relationship between PPAT thickness and/or density and PCa clinical features, most during the past 4 years, and the impact of obesity on these measures (summarized in Table 1 and below). While there is no consistent definition of PPAT, it can be generally defined as the adipose bed that surrounds the prostatic surface (Fig. 1). Notably, the distribution of PPAT differs across the distinct surfaces of the prostate gland [48]. Whilst a fibro-muscular capsule normally separates the prostate gland from the surrounding PPAT, invasion of PCa into PPAT, resulting in the juxtaposition of PCa cells with cells of the adipose tissue, is defined as extracapsular extension and

© 2018 The Authors
BJU International © 2018 BJU International

Fig. 1 Matched intra-operative (top panel), MRI (middle panel) and CT (lower panel) images of peri-prostatic adipose tissue (PPAT) and its spatial relationship to the prostate for a representative patient. Right panels depict the prostate and PPAT as orange and blue regions, respectively.

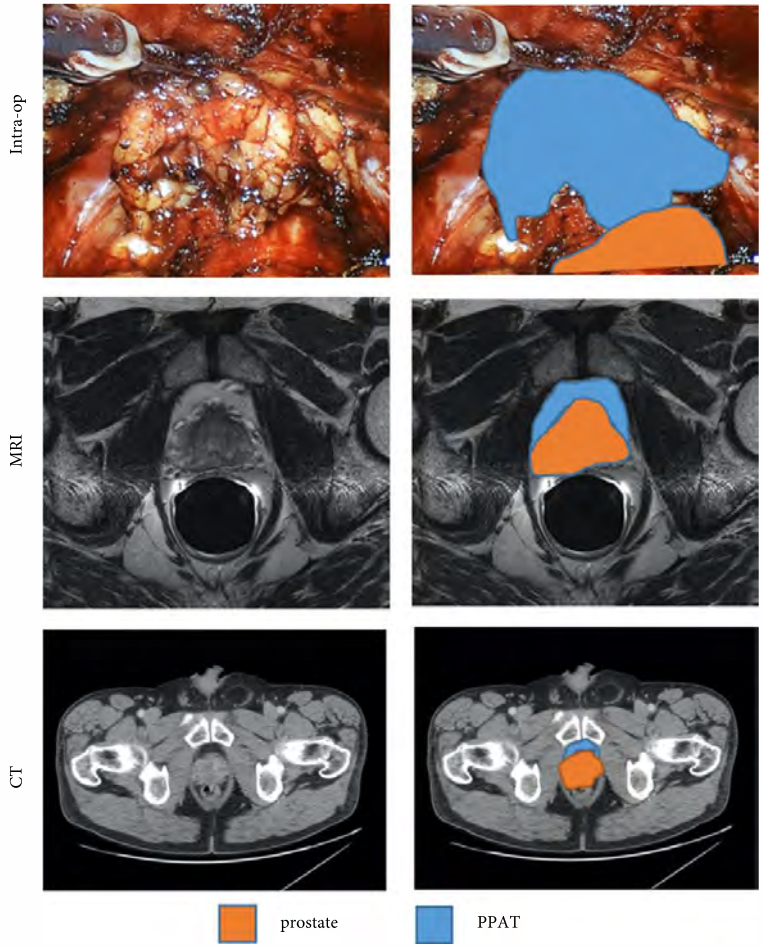

patients with this pathological feature have poorer prognostic outcomes [49–55].

Measurements of Peri-Prostatic Adipose Tissue using CT

A common approach used to measure PPAT thickness in PCa studies is CT. Most recently, Taussky et al. [56] defined PPAT as the adipose bed located only anteriorly to the prostate gland in a CT section at the level of the intervertebral space at the L4 and L5 level. The authors reported no significant correlation between BMI and PPAT volume and density, nor between PPAT and PCa aggressiveness, as defined by Cancer of the Prostate Risk Assessment (CAPRA) score. Similar observations were reported by Tiberi et al. [57], who defined PPAT as the contour at the level of the superior border of the symphysis pubis with exclusion of the tissue medial to the levator ani muscles on both the anterior and posterior aspects of the CT image, and van Roermund et al. [58], who defined PPAT in a transverse section at the level of the caput femoris and greater trochanter of the femur. In the study by van Roermund, 31% of patients with normal BMI had a high PPAT density (>75th percentile) and only 20% of the cohort population had high-grade disease [58]. Interestingly, these authors did report that total PPAT

© 2018 The Authors

area and PPAT density were associated with high-grade disease, whereas BMI was not associated with high-grade disease, using the same CT technique in a separate cohort of patients including a group of patients who received intensity-modulated radiotherapy, of whom 83% had high-risk disease [59]. These studies included only white populations.

Allott et al. [60] explored the association between PCa aggressiveness and visceral and subcutaneous adipose tissue or PPAT in black vs white patients who underwent radiotherapy. The three types of adipose tissue were identified by CT scan at the level of the symphysis pubis. BMI was associated with increased risk of aggressive PCa (in terms of Gleason score ≥7) in both black and white patients, while visceral adipose tissue was associated with aggressive PCa only in black patients. Obesity, measured by BMI, was associated with PPAT area ($r = 0.2$; $P < 0.001$) and visceral adipose tissue ($r = 0.65$; $P < 0.001$), but no significant association was found between PPAT and risk of aggressive PCa in either group of patients. One important observation in their study was that, despite there being no significant difference in BMI, black patients had significantly lower amounts of visceral adipose tissue and PPAT than white patients ($P < 0.001$ for both).

Measurements of Peri-Prostatic Adipose Tissue using MRI

A number of studies have measured PPAT volume using MRI [61–64]. For example, Salji et al. [64] assessed PPAT volume by delineating the first visible facial boundary laterally, the Denonvillier's facia posteriorly, and symphysis pubis anteriorly in a small group of patients with advanced PCa before commencing androgen deprivation therapy. In that study, higher PPAT volume was significantly associated with the development of castrate-resistant PCa. Adding PPAT volume to a predictive model improved the receiver-operating characteristic (ROC) sensitivity (area under the curve 0.9 with PPAT volume vs 0.8 without PPAT volume). Notably, there was no significant association in this study between PPAT volume, body weight or waist circumference.

Likewise, Woo et al. [61] found a significant correlation between PPAT, measured by MRI, and Gleason score; however, the correlation was low ($R = 0.0228$). Interestingly, there was no association between BMI and PPAT, although 62% of the study population were non-obese. Tan et al. [62] assessed the correlation between three separate measures in MRI images and aggressive PCa in 234 men; in this case, PPAT volume was measured by identifying the area of adipose on the MRI cut from the level of the base to the apex of the prostate. The PPAT ratio was calculated by dividing PPAT volume by prostate volume. Another measurement considered was the supra-pubic adipose thickness. PPAT volume and PPAT ratio were significantly associated with higher Gleason score, but the supra-pubic adipose was not. Of note, PPAT ratio did not show significant correlation with age, PSA level or BMI. Sensitivity analysis in this study showed that age, PSA and BMI were poor determinates of high Gleason score (0.56, 0.50 and 0.51, respectively), while PPAT ratio had the higher determinate in the ROC analysis (0.64). An important limitation of that study was that the TRUS biopsy result was used as the reference standard instead of the prostatectomy pathology result. Finally, Zhang et al. [63] reported similar results in a small group of patients ($n = 184$, 30% with high-risk disease) where PPAT area was identified by MRI transverse section at the level of the femoral head and greater trochanter of the femur. In their study, there were significant associations between PPAT area and both clinical stage and Gleason score, but not for BMI. Recently, two clinical studies have also shown that PPAT measured by MRI is an independent predictor for aggressive PCa [65,66].

Other Techniques to Measure Peri-Prostatic Adipose Tissue

Alongside CT and MRI, PPAT has also been determined from images obtained for TRUS-guided biopsy procedures. Using TRUS images, Bhindi et al. [67] used the shortest perpendicular line from the pubic bone to the prostate to determine PPAT thickness, which was associated with PCa, more aggressive cancer and BMI. Again, ROC curves had an area under the curve of 0.58 for PPAT to detect PCa, and 0.59 to detect high-grade PCa, which was comparable to PSA and DRE and age as determinates.

Peri-Prostatic Adipose Tissue and Prostate Cancer Outcome

The above studies collectively demonstrate that there is an association between PPAT and PCa aggressiveness. PPAT volume also predicts time to castrate-resistant PCa [64] but its influence on other oncological outcomes of PCa are yet to be reported. Interestingly, obesity increases the risk of biochemical recurrence [34,35]; however, these studies did not explore the contribution of PPAT. Further studies are required to explore this association.

Summary: Clinical Peri-Prostatic Adipose Tissue Studies

For detecting high-grade PCa, PPAT appears to have a promising degree of sensitivity, irrespective of the method used to determine the PPAT, and could be considered for risk stratification of patients in the future. Despite this finding, information about PPAT is still not included in PCa registries [68]. The inclusion of PPAT-related data in existing

© 2018 The Authors
BJU International © 2018 BJU International

registries and its prospective collection in biobanks will help to elucidate the influence of PPAT size and composition on PCa features, treatment outcomes and risk of recurrence.

Despite the range of approaches used to define PPAT, measuring PPAT at the retropubic region seems to be adequate, and the inconsistencies between the various study findings are probably influenced more by the study population than the method by which PPAT was identified. Considering that most patients with PCa are now having MRI as part of their staging and diagnosis evaluation, identifying the PPAT via MRI images would be the preferred method, being the most accurate and least operator-dependent.

By contrast, the correlation between PPAT and BMI is complex. There may be many reasons for this. Firstly, PPAT is correlated with prostate volume, which is influenced by age and may affect the association between BMI and PPAT. Furthermore, BMI is not a robust indicator of adiposity (neither subcutaneous nor visceral), and not all men with high BMI have more visceral adipose and PPAT, and vice versa. BMI only quantifies the relationship between height and mass, and thus provides no insight into body composition or metabolic health of obese adults. There is an obvious need to identify more relevant and detailed measurements of metabolic health when considering the role of obesity in PCa. Collectively, these studies highlight the complexity of the associations between PPAT, BMI and PCa measures, some of which may be influenced by racial differences.

Potential Mechanistic Links Between Peri-Prostatic Adipose Tissue and Prostate Cancer

The epidemiological evidence of an effect of obesity on PCa progression, and the associations found between PPAT thickness and PCa aggressiveness, suggest that expansion of local adipose tissue can influence PCa behaviour. These clinical findings have spurred laboratory-based studies of the mechanistic pathways that may underlie this association. In this section, we will describe the interactions observed between adipose tissue and PCa cells (summarized in Fig. 2).

Adipocytes in the Prostatic Microenvironment

Whereas intraprostatic adipocytes are extremely rare [69,70], the extracapsular extension of PCa into the PPAT promotes tumour-adipocyte cross-talk because of the close proximity of these cell populations. This cross-talk may be further amplified by the increased number of pre-adipocytes observed in PPAT from patients with PCa compared to patients with BPH [71,72], and PPAT being richer in adipocyte precursors than other visceral adipose tissue [71]. The reciprocal interaction between adipocytes and tumour cells re-programmes adipocytes to a less differentiated status referred to as cancer-associated adipocytes, a phenotype favourable to more aggressive tumours including PCa [73–77]. Multiple lines of evidence suggest that cancer-associated adipocytes, in turn, can enhance the malignant characteristics of the cancer cells, ultimately producing a vicious self-amplifying positive feedback circle [73,78,79]. *In vitro* Boyden chamber migration assays have shown that PCa cells or PCa conditioned media (CM) can attract pre-adipocytes, and to a significantly greater extent than non-malignant cells or their CM [72,80]. Importantly, this interaction is not limited to the close proximity of the prostate gland; in an elegant study, Lin et al. [80] showed that human PCa cells injected in the right flank of athymic nude mice can recruit pre-adipocytes transplanted into the opposite flank, and this migration of the pre-adipocytes enhances tumour growth and angiogenesis. The origin of the recruited adipocytes in clinical samples still lacks solid experimental evidence; while the PPAT is a likely source, some investigators have suggested that PCa cells can differentiate into adipocyte-like cells [81], while others have implicated mobilization of adipocytes from visceral adipose tissue through local vessels or systemic circulation [71,82], although this mechanism has been questioned as being incompatible with the chemo-physical properties of adipocytes [83].

Reciprocal Interactions Between Adipose Tissue and Prostate Cancer Cells

Culturing human PPAT with PC3 cell-derived CM enhances secretion by the PPAT of adipokines (8–11 kDa secreted proteins), TNF-α, interleukin (IL)-6 and osteopontin, and increases mitochondrial DNA copy number and metalloproteinase (MMP)-9 activity [73]. Moreover, pre-adipocytes primed with PCa CM undergo neoplastic-like transformation including genetic instability, mesenchymal-to-epithelial transition, and formation of prostate-like neoplastic lesions *in vivo* [84].

Prostate cancer is, in turn, influenced by adipocyte-secreted factors that enhance its ability to proliferate, migrate and/or invade [74,79,85–89]. Punch biopsies of human prostate specimens or PPAT collected after prostatectomy revealed a strong concentration gradient of the adipokine CCL7, suggesting that the PPAT secretome passively diffuses from PPAT into the tumour tissues to enhance the directed migration of PCa cells [74]. The CM of PPAT contains higher MMP activity compared with peri-peritoneal visceral adipose tissue [79], and this MMP activity degrades extracellular matrix proteins and promotes invasion of

© 2018 The Authors

Fig. 2 Model of how peri-prostatic adipose tissue (PPAT) may promote prostate cancer (PCa) aggressiveness and the influence of obesity. The reciprocal interaction between adipocytes and tumour cells re-programmes adipocytes to a less differentiated status, referred to as cancer-associated adipocytes (CAAs). In turn, CAAs secrete several adipokines, cytokines, hormones, enzymes and growth factors that may boost PCa cell growth and metastasis. Fatty acids are also translocated from PPAT into the PCa cells, increasing energy production. Obesity drives inflammation within the PPAT, and modifies PPAT constituents, transcriptomic, metabolic and endocrine profiles, potentially augmenting their secretome. These effects on the PPAT, taken together with the documented systemic effects of obesity, may underpin the emerging associations between obesity and increasing PCa aggressiveness.

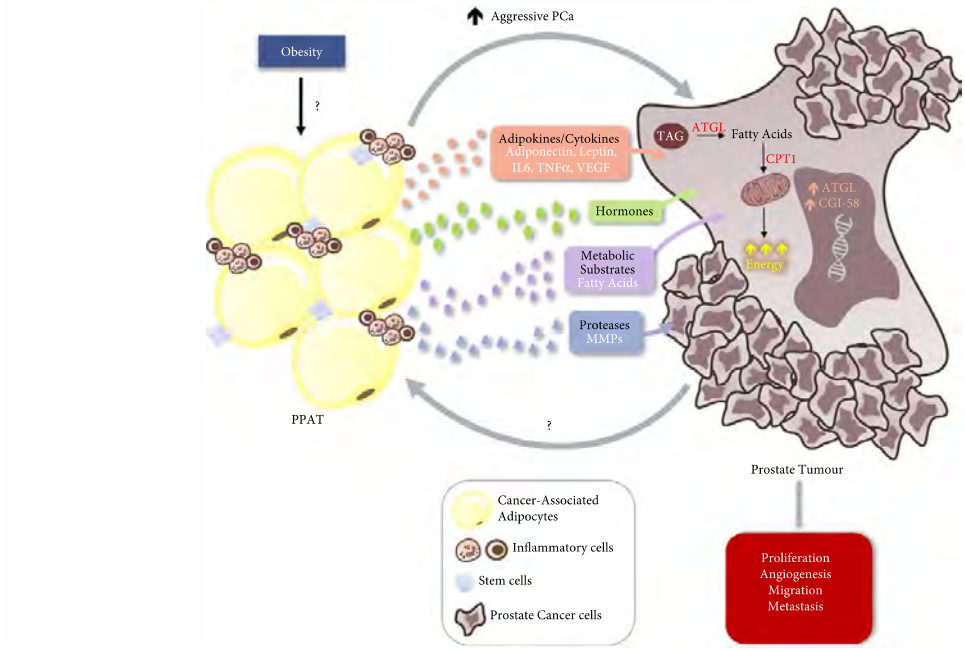

cancer cells into the surrounding tissues [90]. Direct adipocyte-prostate cell cross-talk has been detected in co-culture models of prostate cells with adipocytes. Mature rat epididymal adipocytes influenced the growth and differentiation of normal rat prostatic epithelium [91] or human PCa [92,93] when co-cultured in a three-dimensional collagen gel matrix. These effects were accompanied by increased expression of the cytokines VEGF and PdGF 20-fold [92], and activation of the PI3K pathway [93] in the PC3 PCa cell line. However, these studies have shown considerable variability; while PPAT CM showed a stimulatory effect on PC3 and LNCaP cell migration in one study [79], the effect was not significant in another [88]. Similarly, co-culturing rat epididymal adipocytes with PC3 cells increased PC3 proliferation in one study [92] but not in a later study [93]. These differences probably reflect the nature of the cell lines and experimental methodologies used; a critical issue discussed in detail below. Nevertheless, the functional significance of adipocyte–PCa interactions is highlighted by a study using a subcutaneous *in vivo* tumour model, in which co-injection of PCa cells with pre-adipocytes resulted in larger tumours than injection of unaccompanied PCa cells [94].

Pro-Inflammatory Effects of Adipose Tissue on Prostate Cancer Cells

Obesity can be considered a state of chronic inflammation that is characterized by increased secretion of inflammatory proteins by adipose tissues [95]. Adipose tissues produce many inflammatory and pro-mitogenic molecules, including leptin, adiponectin, IL-6, IL-8, MCP-1, VEGF, CCL5, CCL7, visfatin and TNF-α. At least some of these factors may also be produced by infiltrating immune cells such as macrophages. Strikingly, ~30% of the 100 most significantly expressed genes in adipose tissues that are correlated with body mass encode inflammation-related genes [96]; however, the interaction between inflammatory markers, insulin resistance, obesity and metabolic syndrome is complex [97–100] and the current lack of detailed metabolic phenotyping of patients with PCa makes it challenging to determine the extent to which PPAT inflammation is a consequence of obesity or metabolic syndrome.

© 2018 The Authors
BJU International © 2018 BJU International

These inflammatory markers are also associated with PCa promotion and progression both in clinical and *in vitro* studies [101–103]. Notably, IL-6 secreted by PPAT from patients with PCa was present at >375 times greater concentration than in the matched patient serum, and significantly with the disease pathological grade [86]. In a recent study, PPAT inflammation defined by the presence of crown-like structures was found to be associated with larger adipocyte size, higher circulating levels of insulin and triglycerides, and with high-grade PCa [104].

Adipose Tissue and its Constituents Modify Prostate Cancer Cell Metabolism

Adipose tissues serve as reservoirs for triglycerides, and adipocytes mobilize and locally release stored fatty acids via lipolysis to the surrounding and distant organs [105]. Lipolysis is catalysed through a sequence of lipases, initiated by adipose triglyceride lipase. Cancer cells cause metabolic changes in the adipocyte that lead to activation of lipolytic pathways and thus use adipocytes as source of energy, a condition defined as cachexia [106]. This is consistent with the increased expression of the lipolytic enzymes adipose triglyceride lipase and CGI-58 detected in high grade PCa [107]. Gazi et al. [108] have shown in a study using Fourier transform infrared spectroscopy that there is strong evidence of lipid translocation between adipocyte and PCa cells. This phenomenon has been also reported for ovarian cancer [109] and breast cancer [110], but there is little known about the role of adipocyte-derived fatty acids as metabolic substrates for PCa.

In addition to the potential for enhanced fatty acid release and transfer to PCa cells, the composition of fatty acids in the PPAT is commonly altered in PCa compared to benign prostatic tissue [111,112]. For example, Quiroga et al. [111] studied 23 patients (12 with PCa and 11 with BPH) and showed that PPAT from patients with PCa had significantly higher levels of palmitic and dihomo-gammalinolenic acids, and lower levels of arachidonic acid. Similarly, Iordanescu et al. [112] used magnetic resonance spectroscopy to show that PPAT from patients with more aggressive PCa has a higher ratio of monounsaturated/saturated fatty acids. However, this relationship was not observed with high Gleason scores (7 vs 6), which may be attributable in part to those patients with Gleason score 7 being a mixed population of 4 + 3 (only four patients) and 3 + 4 (13 patients). As fatty acids are quantitatively important sources of energy for PCa cells compared with glucose and glutamine, studies of the uptake and differential utilization of these various fatty acids by PCa cells, and their impact on PCa biology in a clinical setting of obesity, remain important gaps in our understanding and potential avenues for therapeutic intervention.

Hormonal Influences of Peri-Prostatic Adipose Tissue on Prostate Cancer Progression

Adipose tissues are endocrine organs with capacity to synthesize, secrete and metabolize steroid hormones from circulating precursors. While less is known about PPAT than other adipose beds, adipose tissue contains multiple androgens and androgen precursors, including testosterone, dihydrotestosterone, androstenedione, progesterone and dehydroepiandrosterone [113,114], which, in the case of PPAT, provide a credible local extragonadal source of androgens that may support PCa growth and metastasis. PPAT also expresses aromatase enzymes, which convert androgens to oestrogens [77], and abundant historical data support the suggestion of a promoting role for oestradiol in PCa pathogenesis and progression, and as a modifier of racial differences in PCa incidence [115]. Age-related increases in oestradiol/testosterone ratio in men predispose to PCa [116], and a high ratio has been associated with increased risk of aggressive PCa among male-to-female transsexuals [117]. In addition, oestrogen can activate both wild-type and mutated androgen receptors [118]. More detailed analyses of sex steroid production and secretion in PPAT vs other visceral and subcutaneous adipose, and the influence of PPAT size and composition on these measures, are important areas for future investigation.

Peri-Prostatic Adipose Tissue may Influence Obesity-Induced Prostate Cancer Progression

Obesity modifies the metabolic and endocrine profiles of multiple adipose tissues, resulting in increased release of growth factors, hormones, adipokines and mobilization of lipids and free fatty acids [74,119–123]. In addition, obesity increases the rate of pre-adipocyte migration from white adipose tissue, which may contribute to the obesity-induced promotion of PCa progression [82,124,125]. Given the consistent correlation between PPAT and aggressive PCa, increasing attention has focused on obesity-related changes in PPAT composition.

Venkatasubramanian et al. [126] reported that PPAT tissue composition differs from that of the subcutaneous adipose tissue in obese vs lean patients (obesity defined by BMI >30 kg/m^2). Specifically, the PPAT of obese men had increased monounsaturated/saturated lipid ratio compared to subcutaneous fat. In addition, obesity alters the PPAT gene expression profile to favour hypercellularity and reduced immune surveillance, thereby promoting a conducive environment for PCa progression [78]. PPAT in obese men is more metabolically and secretorily active than PPAT in lean men. PPAT in obese men had higher MMP-9 activity [79], and CM from these tissues induced PC3 PCa cell line and endothelial cell proliferation more than CM from tissues in

© 2018 The Authors

lean men [127]. PPAT from obese men exhibited increased angiogenic capacity compared with that from lean men, as evidenced by *ex vivo* measurement of T2 relaxation time [127]. Obese patients with PCa exhibited increased expression of the chemokine CXCL1, a concentration gradient of which is needed for obesity-dependent recruitment of pre-adipocytes [128].

Importance of Experimental Model Systems

Progress in understanding the biology and functional consequences of adipocyte–PCa cross-talk has been hampered by a lack of consistency in experimental conditions and model systems used, resulting in substantial variability between studies and laboratories. The choice of *in vitro* interaction models between PCa cells and adipocytes, in particular, has a significant impact on the observed effects on both cell types. For instance, adipocyte co-culture using Boydon chambers enhances RM1 PCa cell proliferation more than when RM1 cells are exposed directly to the adipocyte CM [85]. Another important factor is the use of isolated adipocytes rather than adipose tissue. The adipose tissue is a heterogeneous mixture of cells consisting of mature adipocytes, pre-adipocytes (stem cells), immune cells and fibroblasts, and thus the observed effects might be caused or modified, at least partly, by cell types other than adipocytes, or could be attributed to interactions between these different cell populations. In addition, adipose tissues are often sourced from varying anatomical depots; some studies used visceral fats [73,88,127], while others used epididymal adipose tissue [91–93]. Distinct adipose depots exhibit different adipokine [45,129–131] and gene expression [132] profiles and have different cellular composition. Further, the metabolic activity of adipose beds differs, with omental adipose tissue having increased expression of proteins involved in lipid and glucose metabolism including HSP90, HSP70, GAPDH and fatty acid binding protein 5 compared with subcutaneous adipose [133]. PPAT in particular contains higher MMP-2 and MMP-9 activity compared with adipose tissue from the median pre-peritoneal visceral region [79], and higher *in vitro* pro-angiogenic responses and viability effects on PC3 cells than for subcutaneous adipose tissue [127]. Another important source of diversity is the intrinsic heterogeneity of the patients studied, their tumour subtypes and their individual metabolic profiles. PPAT from obese and overweight men exhibits overexpression of inflammatory adipogenic, anti-lipolytic, proliferative, anti-apoptotic, and mild immunoinflammatory genes compared with that from lean men [78]. Ideally, the influence of disease stage and metabolic profiles for PPAT and human PCa tissues should be taken into account in future studies, and incorporation of patient-derived explant or xenograft models offer the opportunity to study reciprocal PCa-adipose interactions in systems that more closely recapitulate the disease heterogeneity and complexity of the clinical tissue microenvironment [134,135].

Concluding Remarks

The accumulated weight of evidence to date supports an association between PPAT quantity and increased PCa aggressiveness, although the mechanistic basis of this association remains inconclusive and has limited the development of potential interventions. Measuring PPAT area or density showed more significant correlations with PCa aggressiveness than measuring general obesity markers BMI and waist circumference [59,61,63], while the correlation of PPAT thickness with BMI or weight was non-significant or weak [56–58,61,63,67]. Moreover, no association has been demonstrated between subcutaneous adipose thickness and PCa aggressiveness [59,61]; thus, PPAT measurements may serve as an independent predictor of PCa aggressiveness rather than as a surrogate measure for body adiposity. Incorporating PPAT-related measures into a PCa risk assessment model may improve PCa prognostication and identify patients who may be in need of more aggressive treatment methods. To facilitate this, large prospective studies are required that take into consideration the assessment of obesity, subcutaneous fat, visceral fat and PPAT in determining risk of PCa incidence and aggressiveness. Ideally, these would be accompanied by *ex vivo* studies to examine functional readouts, such as the secretome, of the PPAT from these patients and provide a more robust mechanistic basis by which PPAT may influence PCa pathogenesis.

Acknowledgements

Lisa M. Butler and Andrew J. Hoy acknowledge grant support from The Movember Foundation/Prostate Cancer Foundation of Australia (MRTA3). Zeyad D. Nassar is supported by the Freemason's Foundation Centre for Men's Health at the University of Adelaide and an Early Career Fellowship from the National Health and Medical Research Council of Australia (ID 1138648); Adel T. Aref is supported by an International PhD Scholarship from the University of Adelaide and the Freemason's Foundation Centre for Men's Health at the University of Adelaide; Chui Yan Mah is supported by a MPhil Scholarship from the University of Adelaide and the Freemason's Foundation Centre for Men's Health at the University of Adelaide; Ganesh V. Raj is the Paul Peters endowed chair of Urology and is supported by grants from the Department of Defense, Cancer Prevention Research Institute of Texas, the National Institutes of Health, the John and Mimi Cole Foundation and the Thompson family foundation; Andrew J. Hoy is supported by a Helen and Robert Ellis Postdoctoral Research Fellowship from the Sydney Medical School Foundation and funding from the University of Sydney; Lisa M. Butler is supported by a Future Fellowship from the Australian Research Council (FT130101004).

© 2018 The Authors
BJU International © 2018 BJU International

Conflict of Interest

None declared.

References

1 **Zhou CK, Check DP, Lortet-Tieulent J et al.** Prostate cancer incidence in 43 populations worldwide: An analysis of time trends overall and by age group. *Int J Cancer* 2016; 138: 1388–400

2 **Arnold M, Karim-Kos HE, Coebergh JW et al.** Recent trends in incidence of five common cancers in 26 European countries since 1988: Analysis of the European Cancer Observatory. *Eur J Cancer* 2015; 51: 1164–87

3 **Arnold M, Leitzmann M, Freisling H et al.** Obesity and cancer: An update of the global impact. *Cancer Epidemiol* 2016; 41: 8–15

4 **Golabek T, Bukowczan J, Chlosta P, Powroznik J, Dobruch J, Borowka A.** Obesity and prostate cancer incidence and mortality: a systematic review of prospective cohort studies. *Urol Int* 2014; 92: 7–14

5 **Zhong S, Yan X, Wu Y et al.** Body mass index and mortality in prostate cancer patients: a dose-response meta-analysis. *Prostate Cancer Prostatic Dis* 2016; 19: 122–31

6 **Hu MB, Liu SH, Jiang HW, Bai PD, Ding Q.** Obesity affects the biopsy-mediated detection of prostate cancer, particularly high-grade prostate cancer: a dose-response meta-analysis of 29,464 patients. *PLoS ONE* 2014; 9: e106677

7 **Zadra G, Photopoulos C, Loda M.** The fat side of prostate cancer. *Biochim Biophys Acta* 2013; 1831: 1518–32

8 **Grossmann M, Wittert G.** Androgens, diabetes and prostate cancer. *Endocr Relat Cancer* 2012; 19: F47–62

9 **Butler LM, Centenera MM, Swinnen JV.** Androgen control of lipid metabolism in prostate cancer: novel insights and future applications. *Endocr Relat Cancer* 2016; 23: R219–27

10 **Bianchini F, Kaaks R, Vainio H.** Overweight, obesity, and cancer risk. *Lancet Oncol* 2002; 3: 565–74

11 **Calle EE, Kaaks R.** Overweight, obesity and cancer: epidemiological evidence and proposed mechanisms. *Nat Rev Cancer* 2004; 4: 579–91

12 **Cobb LP, Secord AA.** Association between obesity and clinical outcomes in gynecologic cancer. *Curr Obstet Gynecol Rep* 2015; 4: 240–8

13 **Lee J, Meyerhardt JA, Giovannucci E, Jeon JY.** Association between body mass index and prognosis of colorectal cancer: a meta-analysis of prospective cohort studies. *PLoS ONE* 2015; 10: e0120706

14 **McTiernan A.** Obesity and cancer: the risks, science, and potential management strategies. *Oncology (Williston Park, NY)* 2005;19:871–81; discussion 81-2, 85-6.

15 **Nead KT, Sharp SJ, Thompson DJ et al.** Evidence of a causal association between insulinemia and endometrial cancer: a Mendelian randomization analysis. *J Natl Cancer Inst* 2015;107:djv178.

16 **Pan SY, Johnson KC, Ugnat A-M, Wen SW, Mao Y, Group CCRER.** Association of obesity and cancer risk in Canada. *Am J Epidemiol* 2004; 159: 259–68

17 **Allott EH, Hursting SD.** Obesity and cancer: mechanistic insights from transdisciplinary studies. *Endocr Relat Cancer* 2015; 22: R365–86

18 **Parekh N, Chandran U, Bandera EV.** Obesity in cancer survival. *Annu Rev Nutr* 2012; 32: 311–42

19 **MacInnis RJ, English DR.** Body size and composition and prostate cancer risk: systematic review and meta-regression analysis. *Cancer Causes Control* 2006; 17: 989–1003

20 **Park J, Cho SY, Lee SB, Son H, Jeong H.** Obesity is associated with higher risk of prostate cancer detection in a biopsy population in Korea. *BJU Int* 2014; 114: 891–5

21 **Masuda H, Kagawa M, Kawakami S et al.** Body mass index influences prostate cancer risk at biopsy in Japanese men. *Int J Urol* 2013; 20: 701–7

22 **Freedland SJ, Wen J, Wuerstle M et al.** Obesity is a significant risk factor for prostate cancer at the time of biopsy. *Urology* 2008; 72: 1102–5

23 **Barrington WE, Schenk JM, Etzioni R, et al.** Difference in Association of Obesity with Prostate Cancer Risk Between US African American and Non-Hispanic White Men in the Selenium and Vitamin E Cancer Prevention Trial (SELECT). *JAMA Oncol* 2015; 1: 342–9

24 **Stocks T, Hergens MP, Englund A, Ye W, Stattin P.** Blood pressure, body size and prostate cancer risk in the Swedish Construction Workers cohort. *Int J Cancer* 2010; 127: 1660–8

25 **Bassett JK, Severi G, Baglietto L et al.** Weight change and prostate cancer incidence and mortality. *Int J Cancer* 2012; 131: 1711–19

26 **Haggstrom C, Stocks T, Ulmert D et al.** Prospective study on metabolic factors and risk of prostate cancer. *Cancer* 2012; 118: 6199–206

27 **Cao Y, Ma J.** Body mass index, prostate cancer-specific mortality, and biochemical recurrence: a systematic review and meta-analysis. *Cancer Prev Res (Phila)* 2011; 4: 486–501

28 **Bergstrom A, Pisani P, Tenet V, Wolk A, Adami HO.** Overweight as an avoidable cause of cancer in Europe. *Int J Cancer* 2001; 91: 421–30

29 **Renehan AG, Tyson M, Egger M, Heller RF, Zwahlen M.** Body-mass index and incidence of cancer: a systematic review and meta-analysis of prospective observational studies. *Lancet* 2008; 371: 569–78

30 **De Nunzio C, Freedland SJ, Miano L, Finazzi Agro E, Banez L, Tubaro A.** The uncertain relationship between obesity and prostate cancer: an Italian biopsy cohort analysis. *Eur J Surg Oncol* 2011; 37: 1025–9

31 **Allott EH, Masko EM, Freedland SJ.** Obesity and prostate cancer: weighing the evidence. *Eur Urol* 2013; 63: 800–9

32 **Engeland A, Tretli S, Bjorge T.** Height, body mass index, and prostate cancer: a follow-up of 950000 Norwegian men. *Br J Cancer* 2003; 89: 1237–42

33 **Moller H, Roswall N, Van Hemelrijck M et al.** Prostate cancer incidence, clinical stage and survival in relation to obesity: a prospective cohort study in Denmark. *Int J Cancer* 2015; 136: 1940–7

34 **Bai PD, Hu MB, Xu H et al.** Body mass index is associated with higher Gleason score and biochemical recurrence risk following radical prostatectomy in Chinese men: a retrospective cohort study and meta-analysis. *World J Surg Oncol* 2015; 13: 311

35 **Hu MB, Xu H, Bai PD, Jiang HW, Ding Q.** Obesity has multifaceted impact on biochemical recurrence of prostate cancer: a dose-response meta-analysis of 36,927 patients. *Med Oncol* 2014; 31: 829

36 **Kelly SP, Graubard BI, Andreotti G, Younes N, Cleary SD, Cook MB.** Prediagnostic body mass index trajectories in relation to prostate cancer incidence and mortality in the PLCO cancer screening trial. *J Natl Cancer Inst* 2016; 109: djw225

37 **Discacciati A, Orsini N, Wolk A.** Body mass index and incidence of localized and advanced prostate cancer–a dose-response meta-analysis of prospective studies. *Ann Oncol* 2012; 23: 1665–71

38 **Grubb RL 3rd, Black A, Izmirlian G et al.** Serum prostate-specific antigen hemodilution among obese men undergoing screening in the Prostate, Lung, Colorectal, and Ovarian Cancer Screening Trial. *Cancer Epidemiol Biomarkers Prev* 2009; 18: 748–51

39 **Bandini M, Gandaglia G, Briganti A.** Obesity and prostate cancer. *Curr Opin Urol* 2017; 27: 415–421

40 **Strong AL, Burow ME, Gimble JM, Bunnell BA.** Concise review: The obesity cancer paradigm: exploration of the interactions and crosstalk with adipose stem cells. *Stem Cells* 2015; 33: 318–26

41 **Iyengar NM, Gucalp A, Dannenberg AJ, Hudis CA.** Obesity and cancer mechanisms: Tumor microenvironment and inflammation. *J Clin Oncol* 2016; 34: 4270–6

42 **Incio J, Liu H, Suboj P et al.** Obesity-Induced Inflammation and Desmoplasia Promote Pancreatic Cancer Progression and Resistance to Chemotherapy. *Cancer Discov* 2016; 6: 852

© 2018 The Authors

43 **Wang YY, Lehuede C, Laurent V et al.** Adipose tissue and breast epithelial cells: a dangerous dynamic duo in breast cancer. *Cancer Lett* 2012; 324: 142–51

44 **Hoy AJ, Balaban S, Saunders DN.** Adipocyte-tumor cell metabolic crosstalk in breast cancer. *Trends Mol Med* 2017; 23: 381–92

45 **Fain JN, Madan AK, Hiler ML, Cheema P, Bahouth SW.** Comparison of the release of adipokines by adipose tissue, adipose tissue matrix, and adipocytes from visceral and subcutaneous abdominal adipose tissues of obese humans. *Endocrinology* 2004; 145: 2273–82

46 **Lee SW, Son JY, Kim JM, Hwang SS, Han JS, Heo NJ.** Body fat distribution is more predictive of all-cause mortality than overall adiposity. *Diabetes Obes Metab* 2017; 20: 141–147

47 **von Hafe P, Pina F, Perez A, Tavares M, Barros H.** Visceral fat accumulation as a risk factor for prostate cancer. *Obes Res* 2004; 12: 1930–5

48 **Hong H, Koch MO, Foster RS et al.** Anatomic distribution of periprostatic adipose tissue: a mapping study of 100 radical prostatectomy specimens. *Cancer* 2003; 97: 1639–43

49 **Byar DP, Mostofi FK.** Carcinoma of the prostate: prognostic evaluation of certain pathologic features in 208 radical prostatectomies. Examined by the Step-Section Technique. *Cancer* 1972; 30: 5–13

50 **Zincke H, Bergstralh EJ, Blute ML et al.** Radical prostatectomy for clinically localized prostate cancer: long-term results of 1,143 patients from a single institution. *J Clin Oncol* 1994; 12: 2254–63

51 **Epstein JI, Partin AW, Sauvageot J, Walsh PC.** Prediction of progression following radical prostatectomy. A multivariate analysis of 721 men with long-term follow-up. *Am J Surg Pathol* 1996; 20: 286–92

52 **McNeal JE, Villers AA, Redwine EA, Freiha FS, Stamey TA.** Capsular penetration in prostate cancer. Significance for natural history and treatment. *Am J Surg Pathol* 1990; 14: 240–7

53 **Zagars GK, Geara FB, Pollack A, von Eschenbach AC.** The T classification of clinically localized prostate cancer. An Appraisal Based on Disease Outcome After Radiation Therapy. *Cancer* 1994; 73: 1904–12.

54 **Kapoor J, Namdarian B, Pedersen J et al.** Extraprostatic extension into periprostatic fat is a more important determinant of prostate cancer recurrence than an invasive phenotype. *J Urol* 2013; 190: 2061–6

55 **Cheng L, Darson MF, Bergstralh EJ, Slezak J, Myers RP, Bostwick DG.** Correlation of margin status and extraprostatic extension with progression of prostate carcinoma. *Cancer* 1999; 86: 1775–82

56 **Taussky D, Barkati M, Campeau S et al.** Changes in periprostatic adipose tissue induced by 5alpha-reductase inhibitors. *Andrology* 2017; 5: 511–515.

57 **Tiberi D, Gruszczynski N, Meissner A, Delouya G, Taussky D.** Influence of body mass index and periprostatic fat on rectal dosimetry in permanent seed prostate brachytherapy. *Radiat Oncol* 2014; 9: 93

58 **van Roermund JG, Bol GH, Witjes JA, Ruud Bosch JL, Kiemeney LA, van Vulpen M.** Periprostatic fat measured on computed tomography as a marker for prostate cancer aggressiveness. *World J Urol* 2010; 28: 699–704

59 **van Roermund JG, Hinnen KA, Tolman CJ et al.** Periprostatic fat correlates with tumour aggressiveness in prostate cancer patients. *BJU Int* 2011; 107: 1775–9

60 **Allott EH, Howard LE, Song HJ et al.** Racial differences in adipose tissue distribution and risk of aggressive prostate cancer among men undergoing radiotherapy. *Cancer Epidemiol Biomarkers Prev* 2014; 23: 2404–12

61 **Woo S, Cho JY, Kim SY, Kim SH.** Periprostatic fat thickness on MRI: correlation with Gleason score in prostate cancer. *AJR Am J Roentgenol* 2015; 204: W43–7

62 **Tan WP, Lin C, Chen M, Deane L.** Periprostatic fat: a risk factor for prostate cancer? *Urology* 2016; 98: 107–112

63 **Zhang Q, Sun LJ, Qi J, Yang ZG, Huang T, Huo RC.** Periprostatic adiposity measured on magnetic resonance imaging correlates with prostate cancer aggressiveness. *Urol J* 2014; 11: 1793–9

64 **Salji M, Hendry J, Patel A, Ahmad I, Nixon C, Leung HY.** Peri-prostatic fat volume measurement as a predictive tool for castration resistance in advanced prostate cancer. *Euro Urol Focus* 2017; in press

65 **Cao Y, Cao M, Chen Y et al.** The combination of prostate imaging reporting and data system version 2 (PI-RADS v2) and periprostatic fat thickness on multi-parametric MRI to predict the presence of prostate cancer. *Oncotarget* 2017; 8: 44040–9

66 **Dahran N, Szewczyk-Bieda M, Wei C, Vinnicombe S, Nabi G.** Normalized periprostatic fat MRI measurements can predict prostate cancer aggressiveness in men undergoing radical prostatectomy for clinically localised disease. *Sci Rep* 2017; 7: 4630

67 **Bhindi B, Trottier G, Elharram M et al.** Measurement of peri-prostatic fat thickness using transrectal ultrasonography (TRUS): a new risk factor for prostate cancer. *BJU Int* 2012; 110: 980–6

68 **Evans SM, Nag N, Roder D et al.** Development of an International Prostate Cancer Outcomes Registry. *BJU Int* 2016; 117(Suppl 4): 60–7

69 **Nazeer T, Kee KH, Ro JY et al.** Intraprostatic adipose tissue: a study of 427 whole mount radical prostatectomy specimens. *Hum Pathol* 2009; 40: 538–41

70 **Billis A.** Intraprostatic fat: does it exist? *Hum Pathol* 2004; 35: 525

71 **Ribeiro R, Monteiro C, Silvestre R et al.** Human periprostatic white adipose tissue is rich in stromal progenitor cells and a potential source of prostate tumor stroma. *Exp Biol Med (Maywood)* 2012; 237: 1155–62

72 **Xie H, Li L, Zhu G et al.** Infiltrated pre-adipocytes increase prostate cancer metastasis via modulation of the miR-301a/androgen receptor (AR)/TGF-beta1/Smad/MMP9 signals. *Oncotarget* 2015; 20: 12326–39

73 **Ribeiro RJ, Monteiro CP, Cunha VF et al.** Tumor cell-educated periprostatic adipose tissue acquires an aggressive cancer-promoting secretory profile. *Cell Physiol Biochem* 2012; 29: 233–40

74 **Laurent V, Guerard A, Mazerolles C et al.** Periprostatic adipocytes act as a driving force for prostate cancer progression in obesity. *Nat Commun* 2016; 12: 10230

75 **Dirat B, Bochet L, Dabek M et al.** Cancer-associated adipocytes exhibit an activated phenotype and contribute to breast cancer invasion. *Cancer Res* 2011; 01: 2455–65

76 **Bochet L, Lehuede C, Dauvillier S et al.** Adipocyte-derived fibroblasts promote tumor progression and contribute to the desmoplastic reaction in breast cancer. *Cancer Res* 2013; 15: 5657–68

77 **Nieman KM, Romero IL, Van Houten B, Lengyel E.** Adipose tissue and adipocytes support tumorigenesis and metastasis. *Biochim Biophys Acta* 2013; 1831: 1533–41

78 **Ribeiro R, Monteiro C, Catalan V et al.** Obesity and prostate cancer: gene expression signature of human periprostatic adipose tissue. *BMC Med* 2012; 10: 108

79 **Ribeiro R, Monteiro C, Cunha V et al.** Human periprostatic adipose tissue promotes prostate cancer aggressiveness in vitro. *J Exp Clin Cancer Res* 2012; 31: 32

80 **Lin G, Yang R, Banie L et al.** Effects of transplantation of adipose tissue-derived stem cells on prostate tumor. *Prostate* 2010; 70: 1066–73

81 **Zhau HE, He H, Wang CY et al.** Human prostate cancer harbors the stem cell properties of bone marrow mesenchymal stem cells. *Clin Cancer Res* 2011; 17: 2159–69

82 **Zhang Y, Daquinag AC, Amaya-Manzanares F, Sirin O, Tseng C, Kolonin MG.** Stromal progenitor cells from endogenous adipose tissue contribute to pericytes and adipocytes that populate the tumor microenvironment. *Cancer Res* 2012; 72: 5198–208

83 **Watt MJ, Taylor RA.** Fat talks: a new role for adipose tissue in promoting prostate cancer in obesity. *Transl Cancer Res* 2016; 5: S129–32

84 **Abd EZ, Yang Y, Thomas R et al.** Neoplastic reprogramming of patient-derived adipose stem cells by prostate cancer cell-associated exosomes. *Stem Cells (Dayton, Ohio)* 2014; 32: 983–97

© 2018 The Authors
BJU International © 2018 BJU International

85 **Moreira A, Pereira SS, Costa M et al.** Adipocyte secreted factors enhance aggressiveness of prostate carcinoma cells. *PLoS ONE* 2015; 10: e0123217

86 **Finley DS, Calvert VS, Inokuchi J et al.** Periprostatic adipose tissue as a modulator of prostate cancer aggressiveness. *J Urol* 2009; 182: 1621–7

87 **Onuma M, Bub JD, Rummel TL, Iwamoto Y.** Prostate cancer cell-adipocyte interaction: leptin mediates androgen-independent prostate cancer cell proliferation through c-Jun NH2-terminal kinase. *J Biol Chem* 2003; 278: 42660–7

88 **Sacca PA, Creydt VP, Choi H et al.** Human periprostatic adipose tissue: its influence on prostate cancer cells. *Cell Physiol Biochem* 2012; 30: 113–22

89 **Ito Y, Ishiguro H, Kobayashi N et al.** Adipocyte-derived monocyte chemotactic protein-1 (MCP-1) promotes prostate cancer progression through the induction of MMP-2 activity. *Prostate* 2015; 75: 1009–19

90 **Duffy MJ, Maguire TM, Hill A, McDermott E, O'Higgins N.** Metalloproteinases: role in breast carcinogenesis, invasion and metastasis. *Breast Cancer Res* 2000; 2: 252–7

91 **Tokuda Y, Toda S, Masaki Z, Sugihara H.** Proliferation and differentiation of rat dorsal prostatic epithelial cells in collagen gel matrix culture, focusing upon effects of adipocytes. *Int J Urol* 1999; 6: 509–19

92 **Tokuda Y, Satoh Y, Fujiyama C, Toda S, Sugihara H, Masaki Z.** Prostate cancer cell growth is modulated by adipocyte-cancer cell interaction. *BJU Int* 2003; 91: 716–20

93 **Kaneko A, Satoh Y, Tokuda Y, Fujiyama C, Udo K, Uozumi J.** Effects of adipocytes on the proliferation and differentiation of prostate cancer cells in a 3-D culture model. *Int J Urol* 2010; 17: 369–76

94 **Prantl L, Muehlberg F, Navone NM et al.** Adipose tissue-derived stem cells promote prostate tumor growth. *Prostate* 2010; 70: 1709–15

95 **Divella R, De Luca R, Abbate I, Naglieri E, Daniele A.** Obesity and cancer: the role of adipose tissue and adipo-cytokines-induced chronic inflammation. *J Cancer* 2016; 7: 2346–59

96 **Weisberg SP, McCann D, Desai M, Rosenbaum M, Leibel RL, Ferrante AW Jr.** Obesity is associated with macrophage accumulation in adipose tissue. *J Clin Invest* 2003; 112: 1796–808

97 **Furukawa S, Fujita T, Shimabukuro M et al.** Increased oxidative stress in obesity and its impact on metabolic syndrome. *J Clin Invest* 2004; 114: 1752–61

98 **Zeyda M, Stulnig TM.** Obesity, inflammation, and insulin resistance–a mini-review. *Gerontology* 2009; 55: 379–86

99 **Grandl G, Wolfrum C.** Hemostasis, endothelial stress, inflammation, and the metabolic syndrome. *Semin Immunopathol* 2017; 40: 215–224

100 **Kaur J.** A comprehensive review on metabolic syndrome. *Cardiol Res Pract* 2014; 2014: 943162

101 **Yu D, Zhong Y, Li X et al.** ILs-3, 6 and 11 increase, but ILs-10 and 24 decrease stemness of human prostate cancer cells in vitro. *Oncotarget* 2015; 6: 42687–703

102 **Sharma J, Gray KP, Harshman LC et al.** Elevated IL-8, TNF-α, and MCP-1 in men with metastatic prostate cancer starting androgen-deprivation therapy (ADT) are associated with shorter time to castration-resistance and overall survival. *Prostate* 2014; 74: 820–8

103 **Xu H, Hu MB, Bai PD et al.** Proinflammatory cytokines in prostate cancer development and progression promoted by high-fat diet. *Biomed Res Int* 2015; 2015: 249741

104 **Gucalp A, Iyengar NM, Zhou XK et al.** Periprostatic adipose inflammation is associated with high-grade prostate cancer. *Prostate Cancer Prostatic Dis* 2017; 20: 418–423

105 **Arner P.** Insulin resistance in type 2 diabetes: role of fatty acids. *Diabetes Metab Res Rev* 2002; 18(Suppl 2): S5–9

106 **Tisdale MJ.** Cachexia in cancer patients. *Nat Rev Cancer* 2002; 2: 862–71

107 **Novakovic K, Fitchev P, Brendler C et al.** Active triacylglycerol metabolism and increased infiltrating adipocyte density in high grade prostate cancer. *J Urol* 2012; 187: e127

108 **Gazi E, Gardner P, Lockyer NP, Hart CA, Brown MD, Clarke NW.** Direct evidence of lipid translocation between adipocytes and prostate cancer cells with imaging FTIR microspectroscopy. *J Lipid Res* 2007; 48: 1846–56

109 **Nieman KM, Kenny HA, Penicka CV et al.** Adipocytes promote ovarian cancer metastasis and provide energy for rapid tumor growth. *Nat Med* 2011; 17: 1498–503

110 **Balaban S, Shearer RF, Lee LS et al.** Adipocyte lipolysis links obesity to breast cancer growth: adipocyte-derived fatty acids drive breast cancer cell proliferation and migration. *Cancer Metab* 2017; 5: 1

111 **Careaga Quiroga VP, Sacca PA, Mazza ON et al.** Fatty acid composition of human periprostatic adipose tissue from Argentine patients and its relationship to prostate cancer and benign prostatic hyperplasia. *Research In Cancer and Tumor* 2015; 4: 1–6

112 **Iordanescu G, Brendler C, Crawford SE, Wyrwicz AM, Venkatasubramanian PN, Doll JA.** MRS measured fatty acid composition of periprostatic adipose tissue correlates with pathological measures of prostate cancer aggressiveness. *J Magn Reson Imaging* 2015; 42: 651–7

113 **Blouin K, Veilleux A, Luu-The V, Tchernof A.** Androgen metabolism in adipose tissue: recent advances. *Mol Cell Endocrinol* 2009; 301: 97–103

114 **Arai S, Shibata Y, Koike H et al.** Androgen production in periprostatic adipose tissue in prostate cancer patients. *J Urol* 2012; 187: e389–90

115 **Di Zazzo E, Galasso G, Giovannelli P et al.** Prostate cancer stem cells: the role of androgen and estrogen receptors. *Oncotarget* 2016; 7: 193–208

116 **Rahman HP, Hofland J, Foster PA.** In touch with your feminine side: how oestrogen metabolism impacts prostate cancer. *Endocr Relat Cancer* 2016; 23: R249–66

117 **Gooren L, Morgentaler A.** Prostate cancer incidence in orchidectomised male-to-female transsexual persons treated with oestrogens. *Andrologia* 2014; 46: 1156–60

118 **Susa T, Ikaga R, Kajitani T et al.** Wild-type and specific mutant androgen receptor mediates transcription via 17beta-estradiol in sex hormone-sensitive cancer cells. *J Cell Physiol* 2015; 230: 1594–606

119 **Tourniaire F, Romier-Crouzet B, Lee JH et al.** Chemokine expression in inflamed adipose tissue is mainly mediated by NF-κB. *PLoS ONE* 2013; 8: e66515

120 **Huber J, Kiefer FW, Zeyda M et al.** CC chemokine and CC chemokine receptor profiles in visceral and subcutaneous adipose tissue are altered in human obesity. *J Clin Endocrinol Metab* 2008; 93: 3215–21

121 **Capurso C, Capurso A.** From excess adiposity to insulin resistance: the role of free fatty acids. *Vascul Pharmacol* 2012; 57: 91–7

122 **de Ferranti S, Mozaffarian D.** The perfect storm: obesity, adipocyte dysfunction, and metabolic consequences. *Clin Chem* 2008; 54: 945–55

123 **Ebbert JO, Jensen MD.** Fat depots, free fatty acids, and dyslipidemia. *Nutrients* 2013; 5: 498–508

124 **Zhang Y, Daquinag A, Traktuev DO et al.** White adipose tissue cells are recruited by experimental tumors and promote cancer progression in mouse models. *Cancer Res* 2009; 69: 5259–66

125 **Klopp AH, Zhang Y, Solley T et al.** Omental adipose tissue-derived stromal cells promote vascularization and growth of endometrial tumors. *Clin Cancer Res* 2012; 18: 771–82

126 **Venkatasubramanian PN, Crawford SE, Fitchev PS et al.** Periprostatic fat from obese patients promotes prostate cancer growth. In: Proceedings of the 103rd Annual Meeting of the American Association for Cancer Research; 2012 Mar 31–Apr 4; Chicago, IL. Philadelphia (PA): AACR; Cancer Res 2012; 72(8 Suppl):Abstract nr: 1499

127 **Venkatasubramanian PN, Crawford SE, Fitchev PS et al.** Abstract 1499: Periprostatic fat from obese patients promotes prostate cancer growth. *Can Res* 2012; 72: 1499

128 **Zhang T, Tseng C, Zhang Y et al.** CXCL1 mediates obesity-associated adipose stromal cell trafficking and function in the tumour microenvironment. *Nat Commun* 2016; 7: 11674

129 **Ouchi N, Parker JL, Lugus JJ, Walsh K.** Adipokines in inflammation and metabolic disease. *Nat Rev Immunol* 2011; 11: 85–97

© 2018 The Authors

130 **Yamashita AS, Lira FS, Rosa JC et al.** Depot-specific modulation of adipokine levels in rat adipose tissue by diet-induced obesity: the effect of aerobic training and energy restriction. *Cytokine* 2010; 52: 168–74

131 **Tchkonia T, Thomou T, Zhu Y et al.** Mechanisms and metabolic implications of regional differences among fat depots. *Cell Metab* 2013; 17: 644–56

132 **Dolinkova M, Dostalova I, Lacinova Z et al.** The endocrine profile of subcutaneous and visceral adipose tissue of obese patients. *Mol Cell Endocrinol* 2008; 291: 63–70

133 **Perez-Perez R, Ortega-Delgado FJ, Garcia-Santos E et al.** Differential proteomics of omental and subcutaneous adipose tissue reflects their unalike biochemical and metabolic properties. *J Proteome Res* 2009; 8: 1682–93

134 **Centenera MM, Gillis JL, Hanson AR et al.** Evidence for efficacy of new Hsp90 inhibitors revealed by ex vivo culture of human prostate tumors. *Clin Cancer Res* 2012; 18: 3562–70

135 **Centenera MM, Raj GV, Knudsen KE, Tilley WD, Butler LM.** Ex vivo culture of human prostate tissue and drug development. *Nat Rev Urol* 2013; 10: 483–7

Correspondence: Andrew J. Hoy, Discipline of Physiology, School of Medical Sciences & Bosch Institute, Charles Perkins Centre, University of Sydney, NSW 2006, Australia.

e-mail: andrew.hoy@sydney.edu.au

and

Lisa M. Butler, University of Adelaide Medical School, South Australian Health and Medical Research Institute, Adelaide, SA 5000, Australia.

e-mail: lisa.butler@adelaide.edu.au

Abbreviations: BMI, body mass index; CM, conditioned media; IL, interleukin; MMP, metalloproteinase; PCa, prostate cancer; PPAT, peri-prostatic adipose tissue; ROC, receiver-operating characteristic.

© 2018 The Authors
BJU International © 2018 BJU International

9.2 Appendix B: Centenera et al., 2021 Cancer Research

Published OnlineFirst February 5, 2021; DOI: 10.1158/0008-5472.CAN-20-2511

CANCER RESEARCH | METABOLISM AND CHEMICAL BIOLOGY

ELOVL5 Is a Critical and Targetable Fatty Acid Elongase in Prostate Cancer

Margaret M. Centenera[1,2,3], Julia S. Scott[1,2,3], Jelle Machiels[4], Zeyad D. Nassar[1,2,3], Deanna C. Miller[1,2,3], Irene Zinonos[1,5], Jonas Dehairs[4], Ingrid J.G. Burvenich[6,7], Giorgia Zadra[8], Paolo M. Chetta[8,9], Clyde Bango[8], Emma Evergren[10], Natalie K. Ryan[1,3], Joanna L. Gillis[1,3], Chui Yan Mah[1,2,3], Terence Tieu[11,12], Adrienne R. Hanson[1], Ryan Carelli[13], Katarzyna Bloch[4], Vasilios Panagopoulos[1,3], Etienne Waelkens[14], Rita Derua[14], Elizabeth D. Williams[15], Andreas Evdokiou[1,5], Anna Cifuentes-Rius[11], Nicolas H. Voelcker[11,12,16], Ian G. Mills[10,17], Wayne D. Tilley[1,2], Andrew M. Scott[6,7,18,19], Massimo Loda[13], Luke A. Selth[1,2,20], Johannes V. Swinnen[4], and Lisa M. Butler[1,2,3]

ABSTRACT

The androgen receptor (AR) is the key oncogenic driver of prostate cancer, and despite implementation of novel AR targeting therapies, outcomes for metastatic disease remain dismal. There is an urgent need to better understand androgen-regulated cellular processes to more effectively target the AR dependence of prostate cancer cells through new therapeutic vulnerabilities. Transcriptomic studies have consistently identified lipid metabolism as a hallmark of enhanced AR signaling in prostate cancer, yet the relationship between AR and the lipidome remains undefined. Using mass spectrometry–based lipidomics, this study reveals increased fatty acyl chain length in phospholipids from prostate cancer cells and patient-derived explants as one of the most striking androgen-regulated changes to lipid metabolism. Potent and direct AR-mediated induction of ELOVL fatty acid elongase 5 (ELOVL5), an enzyme that catalyzes fatty acid elongation, was demonstrated in prostate cancer cells, xenografts, and clinical tumors. Assessment of mRNA and protein in large-scale data sets revealed ELOVL5 as the predominant ELOVL expressed and upregulated in prostate cancer compared with nonmalignant prostate. ELOVL5 depletion markedly altered mitochondrial morphology and function, leading to excess generation of reactive oxygen species and resulting in suppression of prostate cancer cell proliferation, 3D growth, and *in vivo* tumor growth and metastasis. Supplementation with the monounsaturated fatty acid cis-vaccenic acid, a direct product of ELOVL5 elongation, reversed the oxidative stress and associated cell proliferation and migration effects of ELOVL5 knockdown. Collectively, these results identify lipid elongation as a protumorigenic metabolic pathway in prostate cancer that is androgen-regulated, critical for metastasis, and targetable via ELOVL5.

Significance: This study identifies phospholipid elongation as a new metabolic target of androgen action that is critical for prostate tumor metastasis.

Introduction

Prostate cancer is the most common cancer diagnosed in men from the developed world and is a major cause of mortality (1). Androgens acting through the androgen receptor (AR) transcription factor drive prostate cancer initiation and progression. Accordingly, androgen deprivation therapy (ADT) has remained the first-line treatment strategy for advanced prostate cancer since the 1940s. Although initially effective, ADT fails to achieve an enduring remission, and patients ultimately develop castration-resistant prostate cancer, which has a poor prognosis despite the clinical implementation of new AR-directed agents (2). Underpinning the development of more effective therapeutic strategies is a more detailed understanding of the critical

[1]University of Adelaide Medical School, Adelaide, SA, Australia. [2]Freemasons Foundation Centre for Men's Health, Adelaide, SA, Australia. [3]South Australian Health and Medical Research Institute, Adelaide, SA, Australia. [4]Department of Oncology, Laboratory of Lipid Metabolism and Cancer, KU Leuven, Leuven, Belgium. [5]Basil Hetzel Institute, Queen Elizabeth Hospital, SA, Australia. [6]Tumour Targeting Laboratory, Olivia Newton-John Cancer Research Institute, Melbourne, VIC, Australia. [7]School of Cancer Medicine, La Trobe University, Melbourne, VIC, Australia. [8]Dana-Farber Cancer Institute, Boston, Massachusetts. [9]University of Milan, Milan, Italy. [10]Patrick G Johnston Centre for Cancer Research, Queen's University Belfast, Belfast, UK. [11]Drug Delivery, Disposition and Dynamics, Monash University, Parkville, VIC, Australia. [12]Commonwealth Scientific and Industrial Research Organisation (CSIRO), Clayton, VIC, Australia. [13]Department of Pathology and Laboratory Medicine, Weill Cornell Medicine, New York-Presbyterian Hospital, New York, New York. [14]Department of Cellular and Molecular Medicine, KU Leuven, Leuven, Belgium. [15]Australian Prostate Cancer Research Centre - Queensland, Queensland University of Technology (QUT), Princess Alexandra Hospital, Translational Research Institute, Brisbane, QLD, Australia. [16]Melbourne Centre for Nanofabrication, Victorian Node of the Australian National Fabrication Facility, Clayton, VIC, Australia. [17]Nuffield Department of Surgical Sciences, University of Oxford, Oxford, UK. [18]Department of Medicine, University of Melbourne, Melbourne, VIC, Australia. [19]Department of Molecular Imaging and Therapy, Austin Health, Melbourne, VIC, Australia. [20]Flinders Health and Medical Research Institute, Flinders University, Bedford Park, South Australia, Australia.

Note: Supplementary data for this article are available at Cancer Research Online (http://cancerres.aacrjournals.org/).

Current address for P.M. Chetta: Boehringer-Ingelheim RCV GmbH & Co KG, Vienna, Austria.

L.M. Butler and J.V. Swinnen jointly supervised this work.

Corresponding Authors: Lisa M. Butler, South Australian Health and Medical Research Institute, University of Adelaide, Medical School and Freemasons Foundation Centre for Men's Health, Adelaide, SA 5001, Australia. Phone: 61-8-8128-4360; E-mail: lisa.butler@adelaide.edu.au; and Johannes V. Swinnen, Laboratory of Lipid Metabolism and Cancer, KU Leuven, O&N I Herestraat 49, Box 818, Leuven 3000, Belgium. Phone: 32-16-33-05-33; E-mail: j.swinnen@kuleuven.be

Cancer Res 2021;81:1704–18

doi: 10.1158/0008-5472.CAN-20-2511

©2021 American Association for Cancer Research.

Downloaded from cancerres.aacrjournals.org on April 1, 2021. © 2021 American Association for Cancer Research.

Published OnlineFirst February 5, 2021; DOI: 10.1158/0008-5472.CAN-20-2511

cellular processes through which androgens regulate prostate tumor biology and promote cancer cell survival.

It is well established that androgens have a major stimulatory effect on *de novo* lipogenesis in prostate cancer cells (3). This synthesis of fatty acids is activated in the majority of prostate cancers, and is associated with poor prognosis (4, 5). Approximately 80% of *de novo* synthesized fatty acids are utilized for the production of phospholipids, the dominant component of cellular membranes, and is linked to the tumor cell's increased demand for cellular membranes and their protection from oxidative stress (6). This biology has elicited major efforts to target lipid synthesis therapeutically via inhibition of the key lipogenesis enzyme, fatty acid synthase (*FASN*). FASN is directly and indirectly regulated by the AR, and although FASN inhibitors have proved promising in the preclinical setting, off-target effects, poor solubility, and pharmacokinetics have prevented their clinical development (7).

It is known that androgens stimulate expression of over 20 enzymes involved in lipid synthesis, binding, uptake, metabolism and transport (8, 9); however, the precise regulatory mechanisms and influence of these factors on lipid composition and metabolism in prostate tumor cells remain largely undefined. The aim of this study was to gain insight into regulation of the prostate tumor lipidome by androgens in prostate cancer cells, and ultimately identify novel metabolic effectors of androgen action for therapeutic intervention.

Materials and Methods

Cell culture and treatments

Human prostate cancer cell lines LNCaP (clone FGC), 22Rv1, and LAPC4 were from the ATCC. All cell lines were authenticated by short tandem repeat profiling at Cell Bank Australia (NSW, Australia) in July 2016 and again in July 2020. Cell lines were cultured in RPMI-1640 medium (Life Technologies) containing 10% fetal bovine serum (FBS) and 2 mmol/L L-glutamine (Life Technologies). For androgen treatment, cells were initially seeded in medium containing 5% dextran charcoal coated FBS (dcc-FBS), and after 24 hours, 1 nmol/L mibolerone or DHT added and cells cultured for an additional 72 hours. For antiandrogen treatment, LNCaP cells were cultured in growth medium containing 1 μmol/L enzalutamide for 72 hours.

Patient-derived explant tissue culture

Patient-derived explant (PDE) experiments were conducted according to Declaration of Helsinki principles. Prostate tumor specimens were obtained with written informed consent through the Australian Prostate Cancer Bioresource from men undergoing robotic radical prostatectomy at St. Andrew's Hospital (Adelaide, Australia). Tumors were cultured as PDEs for 48 hours in the presence or absence of 10 μmol/L enzalutamide, as previously described (10). Half was formalin-fixed and paraffin-embedded for histology and half was snap frozen for lipidomics.

Electrospray ionization tandem mass spectrometry–based lipidomics

Cells or tissues were homogenized in ice-cold 800 μL phosphate-buffered saline (PBS). Cell/explant lysate (100 μL) was set aside to quantify DNA for normalization then lipids extracted using a modified Bligh-Dyer protocol by adding 800 μL $CHCl_3$, 900 μL 1N HCl:CH_3OH 1:8 (v/v), and 500 μg of the antioxidant 2,6-di-tert-butyl-4-methylphenol (Sigma). Following centrifugal phase separation, the lower organic fraction was collected, evaporated, and the lipid pellet stored under argon gas at −20°C. Lipid pellets were reconstituted in diluent (CH_3OH:$CHCl_3$:NH_4OH; 90:10:1.25, v/v/v) according to DNA quantification (1 μL diluent/1 μg DNA). Phospholipids were analyzed by electrospray ionization tandem mass spectrometry (ESI-MS/MS) on a hybrid quadrupole linear ion trap mass spectrometer (4000 QTRAP system, AB SCIEX) equipped with a TriVersa NanoMate robotic nanosource (Advion Biosciences) as described previously (6).

Quantitative real-time PCR

RNA was extracted using the PureLink total RNA purification system (Life Technologies) according to the manufacturer's instructions, and concentration assessed using a NanoDrop DM-1000 spectrophotometer (NanoDrop Technologies). RNA was reverse transcribed using Superscript II RT and random hexamer primers according to the manufacturer's instructions (Invitrogen). RT-qPCR was performed on a 7500 Fast Real-Time system (Applied Biosystems) using primer sequences detailed in Supplementary Table S1. Expression levels were normalized against 18S, GUSB, or L19 as reference genes.

Gene set enrichment analysis

Gene set enrichment analysis (GSEA) was implemented using the Broad Institute's public GenePattern server essentially as described previously (11). Briefly, the correlation between expression levels of *ELOVL2, ELOVL5, ELOVL7*, and 26,447 genes was calculated using data from a cohort of 131 patients from Memorial Sloan-Kettering Cancer Center (MSKCC; ref. 12). Genes were subsequently ranked according to Pearson correlation coefficient (r) value, and this ranked gene list was used for GSEA pre-ranked analysis.

Analysis of published chromatin immunoprecipitation sequencing data

AR chromatin immunoprecipitation sequencing (ChIP-seq) data from clinical specimens (7 normal prostate and 13 primary tumors; ref. 13) were obtained from GEO (GSE56288). Mean signals from normal and tumor samples were generated using the Integrated Genome Browser (14).

Chromatin immunoprecipitation

LNCaP cells were seeded at 3×10^6 cells/plate in 15 cm plates in RPMI-1640 containing 10% dcc-FBS for 3 days and then treated for 4 hours with 10 nmol/L DHT or vehicle (ethanol). AR ChIP was performed as described previously (15).

Transient RNA interference

ON-TARGET plus human small interfering RNAs (siRNA) and a control siRNA (D-001810-01-20 ON-TARGET plus Nontargeting siRNA #1) were from Dharmacon. The most effective siRNA from a pool of four was selected for targeting ELOVL2 (J-009531-10; J-009531-11), ELOVL5 (J-009260-10; J-009260-12), ELOVL7 (J-028493-09; J-028493-11), and SREBP1 (J-006891-07) and reverse transfected at a concentration of 5 nmol/L using Lipofectamine RNAiMAX transfection reagent (Invitrogen) according to the manufacturer's instructions.

Fluorescence IHC of human prostate cancer tissue microarray

Five tissue microarrays (TMA) comprised of 1-mm triplicate tumor cores, and single/duplicate benign tissue cores were used for evaluation of ELOVL5 expression. TMAs were constructed from a cohort of 249 radical prostatectomy prostate cancer patients who had archival tissue available through the Gelb Center at Dana-Farber Cancer Institute (Boston, MA). Human studies were conducted according to Declaration of Helsinki principles under institutional review board. A written informed consent was received from participants prior to inclusion in the study.

Downloaded from cancerres.aacrjournals.org on April 1, 2021. © 2021 American Association for Cancer Research.

Published OnlineFirst February 5, 2021; DOI: 10.1158/0008-5472.CAN-20-2511

A multiplex tyramine signal amplification (TSA) method was performed on 4-μm TMA sections for the detection of ELOVL5 protein, with pan-Cytokeratin and p63 for masking the tumor and benign epithelium, respectively. Staining was performed on a Leica Bond Rx automated immunostainer, using a protocol for sequential TSA-amplified immunofluorescence labels, with DAPI as the nuclear counterstain. Slides were incubated for 30 minutes with antibodies against ELOVL5 (HPA047752, Sigma, 1:2,000), pan-Cytokeratin CAM5.2 (452M, Cell Marque, 1:500), and an HMWCK-P63 cocktail comprised of p63 (4892, Cell Signaling Technology, 1:100) and cytokeratin 5/4 (API3025AA, Biocare, ready-to-use), followed by 15-minute incubation with TSA-conjugated Opal dye (Opal 690 for ELOVL5, Opal 520 for pan-Cytokeratin, Opal 570 for HMWCK and p63). A tissue and cell segmentation algorithm was developed in PerkinElmer InForm software and applied to the TMAs. All images were reviewed by a pathologist and manually edited for accuracy before the final segmentation data were generated. Cores with major folding or staining artifacts were excluded. Signal was expressed as fluorescent count normalized to exposure time. Per-cell ELOVL5 cytoplasmic signal was normalized to nuclear DAPI signal before comparison between tumor and benign glands. Unpaired *t* test was used when variances were equal; otherwise, nonparametric Mann–Whitney was applied.

Dendrimer functionalized porous silicon nanoparticle knockdown of ELOVL5

Alexa Fluor-488 labeled PAMAM(G4)-porous silicon nanoparticles (pSiNP) were prepared as described previously (16), and loaded with either siCTRL or siELOVL5 overnight prior to experimental day. On the day of PDE treatment, loaded NPs were washed 2× in RNase-free water and added to explant culture media at a concentration of 200 μg/mL. Explants were prepared in triplicate as described above and cultured in a 24-well plate containing 500 μL NPsiCTRL or NPsiELOVL5 containing growth medium or growth medium without any NPs as a control. After 24 hours, an additional 50 μL of NP containing media was added, and explants were cultured for an additional 48 hours, making a total culture time of 72 hours. At the end of the experiment, explants were formalin-fixed and paraffin-embedded prior to immunostaining with antibodies for ELOVL5 (HPA047752, Sigma, 1: 2,000) or Ki67 (M7240, DAKO, 1:200), as described previously (10). Slides were scanned with an Axio Z.1 Scanner (Carl Zeiss Pty. Ltd.) using 40× objective, and images captured using Zen Blue 2.6 Software (Carl Zeiss Pty. Ltd.). Ki67 positivity was manually counted, as described previously (10). ELOVL5 staining intensity was measured using ImageJ software.

Generation of shELOVL5 and hELOVL5 LNCaP cells

For shELOVL5, LNCaP cells were transduced with universal negative control shRNA lentivirus [pLenti-H1-shRNA(Neg-Control)-Rsv (Puro)] or ELOVL5 shRNA lentivirus [pLenti-H1-shRNA (hELOVL5)-Rsv(Puro)], while for hELOVL5, cells were transduced with universal null control hRNA lentivirus [pLenti-TetCMV(hRNA (Null-Control))-Rsv(GFP-Puro)] or ELOVL5 hRNA lentivirus [pLenti-TetCMV(hRNA(ELOVL5))-Rsv(GFP-Puro)]. All lentiviruses were designed by GenTarget Inc., according to the manufacturer's instructions. Briefly, $1–5\times10^5$ cells were seeded in 24-well plates overnight and then treated with hexadimethrine bromide (8 μg/mL) and transduced at MOI of 5. After 3 days, cell selection was undertaken using 4 μg/mL puromycin dihydrochloride (Gibco). ELOVL5 downregulation or upregulation was confirmed by Western blot as described previously (17).

Cell viability assay

LNCaP or 22Rv1 cells were transfected with siRNA overnight in 24-well plates at a density of 2×10^4 cells/well, then treated as indicated for 6 days and counted as previously described (17). Fatty acids, arachidonic acid (AA), docosahexaenoic acid (DHA), or cis-vaccenic acid (cVA) were supplemented as indicated for rescue studies.

3D spheroid growth assay

LNCaP cells transfected with siRNA in 6-well plates were collected after 48 hours and suspended at 7.5×10^4 cells/mL in RPMI-1640 containing 10% FBS. Cell suspensions (1,500 cells in 20 μL) were pipetted inside the lid of a petri dish and 10–15 mL PBS added to the base. Dishes were reassembled and incubated at 37°C. After 5 days, the formed spheres were imaged, and sphere volume was determined using the equation $V = (L \times W2)/2$.

Transwell migration assay

LNCaP/22Rv1 cells transfected with siRNA were seeded into the upper chamber of 24-well polycarbonate transwell inserts (3422, Sigma-Aldrich) at a density of $3.5 \times 10^4/2 \times 10^5$ cells/well in RMPI-1640 containing 1% bovine serum albumin. The bottom chamber was filled with 650 μL of RPMI-1640 containing 5% FBS and cells incubated at 37°C for 48 hours. Transwell membranes were then collected, washed with PBS, and nonmigrated cells were scraped from the upper face. The membranes were fixed in 4% paraformaldehyde for 30 minutes, stained with 1% crystal violet for 1 hour and mounted using permount mounting medium. The number of migrated cells was counted microscopically. Results are reported as the number of migrated cells normalized to the number of viable cells counted in a viability assay at the same time point. For rescue experiments, cells were seeded in serum-free RPMI-1640 containing fatty acids as indicated, and data are presented as number of migrated cells.

Electron microscopy

LNCaP cells transfected with siRNA were fixed after 72 hours in 1.25% glutaraldehyde, 4% sucrose, 4% paraformaldehyde in PBS (pH 7.2) for 1 hour at room temperature, post-fixed in 1% osmium tetraoxide in water, dehydrated in a graded ethanol series, and embedded in epoxy resin Embed812 (Electron Microscopy Science). Ultrathin sections (70 nm) were cut on a Leica UCT6 ultramicrotome, collected on formvar-coated copper-iridium slot grids, counterstained with 2% uranylacetate and Reynold's lead citrate, and imaged in an FEI Tecnai G2 Spirit transmission electron microscope at 80 kV.

Cellular reactive oxygen species measurement

LNCaP cells were transfected with siRNA for 6 days in 24-well plates. For negative controls, cells were treated with 500 μmol/L Trolox (Sapphire Bioscience, NSW, Australia) 24 hours prior to collection, followed by treatment with 200 μmol/L tert-butyl hydroperoxide (TBHP; Thermo Fisher Scientific) for 1 hour prior to collection. For positive controls, cells were treated with 200 μmol/L TBHP for 1 hour prior to collection. Cells were collected into fluorescence-activated sorting tubes and stained with 500 nmol/L CellROX Orange Reagent (Thermo Fisher Scientific) for 1 hour at 37°C. Cells were centrifuged, washed with PBS, and then stained with 1 μmol/L CellROX Orange Reagent (Thermo Fisher Scientific) for 15 minutes on ice. The samples were then read on a BD LSRFortessa X20 flow cytometer.

Colony formation assay

ELOVL5 stable downregulated (shELOVL5), overexpressing (hELOVL5), or negative control cells (shCTRL) were plated in 6-well

Downloaded from cancerres.aacrjournals.org on April 1, 2021. © 2021 American Association for Cancer Research.

Published OnlineFirst February 5, 2021; DOI: 10.1158/0008-5472.CAN-20-2511

plates (3–500 cells/well) and were incubated for up to 3 weeks at 37°C, with medium replenished every 4–7 days. Cells were then washed with PBS, fixed with 4% paraformaldehyde, and stained with 1% crystal violet for 30 minutes. Colonies with >50 cells were counted manually in a blinded manner.

Subcutaneous LNCaP xenograft model

Subcutaneous xenograft studies were approved by the Austin Health Animal Ethics Committee (approval number A2015/05311). LNCaP cells (5×10^6 cells in 50 μL RPMI-1640 containing 10% FBS) were coinjected subcutaneously with 50 μL Matrigel in 5- to 6-week-old NOD/SCID Gamma male mice (Bioresource Facility, Austin Health). When tumors reached ~200 mm^3, mice were randomized to three treatment groups; untreated ($n = 5$), vehicle control (10% DMSO/PBS; $n = 5$), and enzalutamide (10 mg/kg enzalutamide in 10% DMSO/PBS, $n = 5$). Five of the ten castrated mice were treated daily with enzalutamide (10 mg/kg MDV3100 in 10% DMSO/PBS) by oral gavage for 7 days, beginning 5 days after surgery. After the animals were sacrificed, half the tumor was formalin-fixed and paraffin-embedded, and half was analyzed for lipidomics.

shELOVL5 animal studies

Subcutaneous and intraprostatic xenograft studies were approved by the University of Adelaide Animal Ethics Committee (approval number M-2016-160). Eight-week-old male NOD/SCID mice (Animal Resources Centre, Western Australia) received intraprostatic injections (1×10^6 shCTRL or shELOVL5 LNCaP cells in 10 μL of PBS) or subcutaneous flank injections (2×10^6 shCTRL or shELOVL5 LNCaP cells in 50 μL of PBS mixed with 50 μL Matrigel-HC). Each study used 7 animals per group. Noninvasive, whole-body imaging to monitor luciferase-expressing cells was performed at the time of injection and once weekly using the IVIS Spectrum *In Vivo* Imaging System (PerkinElmer) as described previously (18). Caliper measurements were taken regularly throughout the study. After the animals were sacrificed, internal organs and prostate glands were excised for *ex vivo* imaging using the IVIS system.

Histologic staining of mouse lung metastatic lesions

Hematoxylin and eosin (H&E) staining was performed on 2-μm sections that were stained with hematoxylin (Australian Biostain), blued with 1% acid alcohol, and counterstained with eosin (Australian Biostain). IHC was performed on 2-μm sections that were blocked for endogenous peroxidase before being subjected to heat-induced epitope retrieval. Sections were blocked in 10% normal goat serum (Sigma) and incubated with AR primary antibody (1:200, Abcam ab108341) overnight, biotinylated anti-rabbit secondary antibody (1:400, DAKO) for 1 hour, and streptavidin-horseradish peroxidase complex (1:500, DAKO) for 1 hour. Positive cells were visualized with DAB and counterstained with hematoxylin (Australian Biostain). Images were captured on a NanoZoomer digital slide scanner (Hamamatsu).

Statistical analysis

Statistical analysis was carried out using GraphPad Prism software v7.02 (2016, GraphPad Software), and data are representative of at least two independent experiments. Bar graphs represent the mean ± SEM of at least three biological replicates unless otherwise indicated. Dot plots represent the mean ± SEM of individually counted cells, spheroids, or lipid droplets from at least three biological replicates unless otherwise indicated. Box plots represent the mean ± interquartiles, and whiskers represent minimum and maximum values. For cell line and animal studies, significance was measured by two-tailed unpaired *t* test or one-way ANOVA with Dunnett multiple comparison test as indicated. For clinical data, significance was measured using Mann–Whitney *U* test. Significance is expressed as *, $P < 0.05$; **, $P < 0.01$; ***, $P < 0.001$. Heat maps, hierarchical clustering, and Pearson correlations were generated using GENE-E (www.broadinstitute.org/cancer/software/GENE-E/). All heat maps shown are row-normalized for presentation purposes. Pearson correlation with average linkage was used for clustering.

Results

Androgens induce fatty acyl chain elongation of phospholipids in prostate cancer cell lines

To investigate the influence of androgens on the prostate cancer lipidome, lipids extracted from androgen-treated AR-positive LNCaP prostate cancer cells were subjected to quantitative lipidomic profiling by tandem mass spectrometry (**Fig. 1A**). In cells treated with low (1 nmol/L) and high (10 nmol/L) physiologic doses of the synthetic androgen mibolerone, total phospholipid abundance increased dose dependently compared with vehicle-treated cells (**Fig. 1B**). Analysis of the four major phospholipid classes, phosphatyidyl-choline (PC), -ethanolamine (PE), -inositol (PI), and -serine (PS), revealed an increase in PC abundance with the low dose of 1 nmol/L mibolerone, and marked increases in abundance across all four classes with the high dose of 10 nmol/L mibolerone compared with vehicle (**Fig. 1C**). Androgen treatment did not alter saturated fatty acid (SFA) levels but significantly increased the abundance of monounsaturated fatty acids (MUFA; defined as phospholipids containing 1–2 unsaturations, i.e., one for each fatty acid tail) and polyunsaturated fatty acids (PUFA; defined as phospholipids containing 3 or more unsaturations) at the high dose of 10 nmol/L mibolerone compared with vehicle (**Fig. 1D**).

The most prominent effect of androgens on the lipidome was elongation of MUFAs and PUFAs across all four phospholipid classes analyzed. Elongation was evident as decreased abundance of short chain phospholipid species and a concomitant increase in long-chain phospholipids with a given number of double bonds, and was observed in LNCaP cells treated with either 1 nmol/L mibolerone compared with vehicle (Supplementary Fig. S1) or 1 nmol/L of the native androgen 5α-dihydrotestosterone (DHT; **Fig. 1E**; Supplementary Fig. S1). The opposite effect on phospholipid chain length was observed in LNCaP cells treated with the clinical AR antagonist enzalutamide (**Fig. 1E**; Supplementary Fig. S1). Androgen-induced elongation was also observed in AR-positive LAPC4 and 22Rv1 prostate cancer cells, but not in AR-negative PC-3 prostate cancer cells (Supplementary Fig. S2A), which is consistent with the low level of ELOVL5 expression observed in PC-3 cells compared with AR-positive cell lines (Supplementary Fig. S2B). The clinical relevance of this androgenic effect was addressed by undertaking phospholipidomic profiling in matched prostate cancer PDEs treated with enzalutamide or vehicle ($n = 19$; **Fig. 1F**). The major trend observed for the majority (17/19; 89.4%) of enzalutamide-treated PDEs was inhibition of fatty acid chain elongation in MUFAs and PUFAs with up to 4 unsaturations (**Fig. 1G**; Supplementary Fig. S3). Taken together, we have demonstrated that androgens have a significant effect on phospholipid composition in prostate cancer cells and tumors, whereby androgens induce and enzalutamide inhibits fatty acid chain elongation (**Fig. 1H**).

AR directly regulates genes involved in fatty acid chain elongation

Consistent with the effects of androgens on fatty acyl chain length, we observed androgenic induction of three ELOVL fatty acid elongases

Downloaded from cancerres.aacrjournals.org on April 1, 2021. © 2021 American Association for Cancer Research.

Published OnlineFirst February 5, 2021; DOI: 10.1158/0008-5472.CAN-20-2511

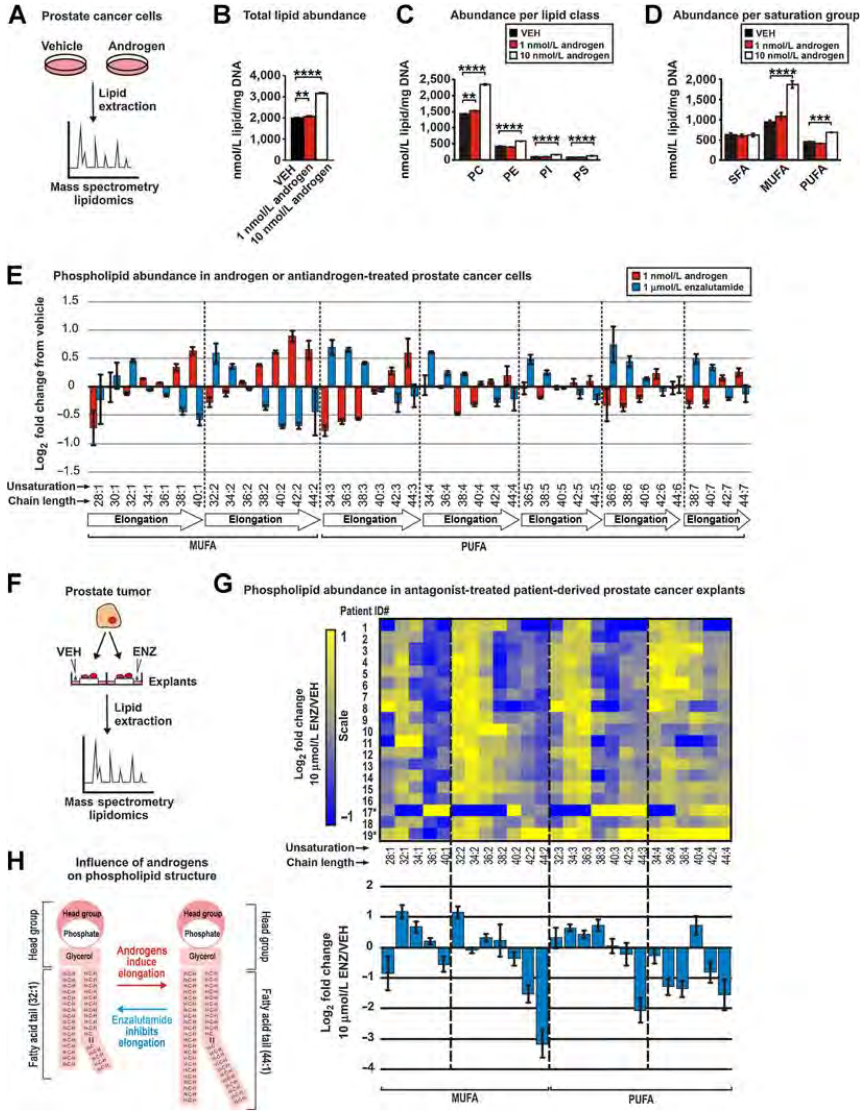

Figure 1.

Androgens influence fatty acid chain elongation of phospholipids in prostate cancer. **A,** Schematic diagram of experimental design. Phospholipids were extracted from prostate cancer cells and treated ± androgens for 72 hours prior to mass spectrometry-based lipidomics. **B–D,** Phospholipidomic changes in total lipid abundance, abundance per lipid class, and saturation in LNCaP cells following treatment with synthetic androgen mibolerone. Data, mean ± SEM of triplicate wells. **, $P < 0.01$; ***, $P < 0.001$; ****, $P < 0.0001$; ANOVA treatment versus vehicle. **E,** Phospholipidomic changes in LNCaP cells following treatment with androgen 5α-dihydrotestosterone (DHT), or AR antagonist enzalutamide (Enz). Data, $\log_2$-fold change in relative abundance of phosphatidylethanolamine lipid species in treated versus control cells ($n = 3$). Lipids are labeled along the *x*-axis as XX:Y, where XX denotes the total number of fatty acid carbons and Y the total number of unsaturations in the fatty acyl chains. Lipids are grouped according to degree of unsaturation (groups separated by dashed lines). Within each saturation group, lipids are ordered from left to right by increasing acyl chain length. **F,** Schematic diagram of experimental design. Phospholipids were extracted from patient-derived prostate cancer explants treated ± enzalutamide for 48 hours prior to mass spectrometry-based lipidomics. **G,** Hierarchical clustered heat map represents $\log_2$-fold change in relative abundance of select PC species in enzalutamide-treated explants compared with vehicle ($n = 19$). Average $\log_2$-fold change in PC abundance depicted in histogram to highlight inhibition of elongation by enzalutamide in patient-derived prostate cancer explants. **H,** Androgens significantly influence phospholipid structure by inducing elongation of its fatty acyl tails, whereas enzalutamide shortens phospholipid fatty acid tails.

Downloaded from cancerres.aacrjournals.org on April 1, 2021. © 2021 American Association for Cancer Research.

Published OnlineFirst February 5, 2021; DOI: 10.1158/0008-5472.CAN-20-2511

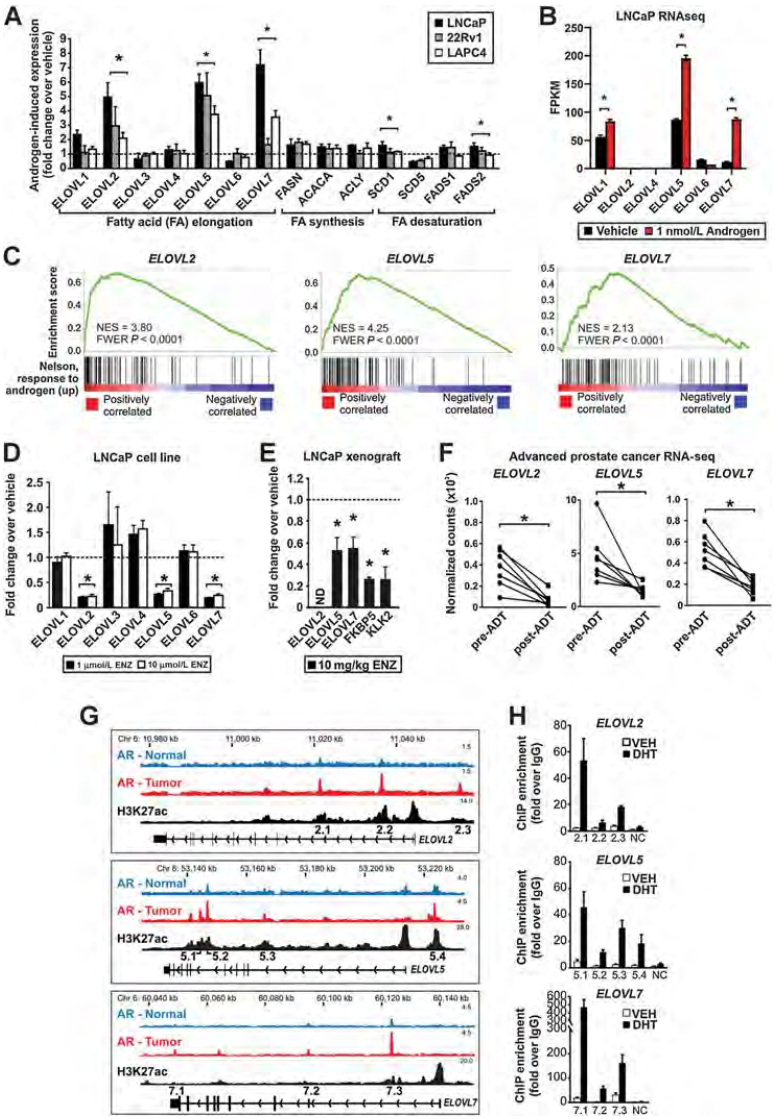

Figure 2.
AR regulates genes involved in fatty acid elongation. **A,** qRT-PCR analysis of key genes involved in lipid metabolism in LNCaP, 22Rv1, and LAPC4 prostate cancer cells stimulated with androgen (1 nmol/L mibolerone). Data, mean ± SEM of triplicate wells. *, $P < 0.05$; ANOVA treatments versus vehicle. **B,** Bar graph representing RNA-seq analysis of *ELOVL* genes in LNCaP cells treated with androgen (1 nmol/L R1881) or vehicle control. Data, mean ± SEM of triplicate wells. *, $P < 0.05$; ANOVA treatments versus vehicle. **C,** ELOVL2, ELOVL5, and ELOVL7 expression is positively correlated with genes induced by DHT in prostate cancer cells, as assessed by GSEA. DHT-induced genes in the ordered data set are shown as black lines in the middle, and the running enrichment score is plotted at the top. **D,** qRT-PCR analysis of all ELOVL genes in LNCaP cells stimulated with the AR antagonist enzalutamide (1 μmol/L and 10 μmol/L) compared with vehicle control-treated cells. Data, mean ± SEM of triplicate wells. *, $P < 0.05$; ANOVA treatment versus vehicle. **E,** qRT-PCR analysis of ELOVL2 (ND, not detected), ELOVL5, ELOVL7, and known androgen-regulated genes FKBP5 and KLK2 in subcutaneous LNCaP xenograft tumors obtained from mice treated with vehicle control ($n = 5$) or enzalutamide (ENZ; $n = 5$). *, $P < 0.05$; ANOVA treatments versus vehicle. **F,** RNA-seq analysis of ELOVL2, ELOVL5, and ELOVL7 expression in prostate cancer patient material pre- and post-treatment with ADT. **G,** AR binding sites proximal to the *ELOVL2, ELOVL5*, and *ELOVL7* genes in normal prostate tissues (mean ChIP-seq signal of seven samples) and prostate tumors (mean ChIP-seq signal of 13 samples). **H,** Validation of three putative AR binding sites (highlighted below the ChIP-seq tracks in **Fig. 3B**) by ChIP-qPCR. NC, negative control. Data, mean ± SEM of triplicate wells.

(ELOVL) in LNCaP, LAPC4, and 22Rv1 prostate cancer cells, as well as induction of the known AR-regulated gene *FASN* (**Fig. 2A**). The most marked androgen-induced increases were observed for *ELOVL2, ELOVL5*, and *ELOLV7*, which was also evident in an independent, published LNCaP RNA-seq data set (**Fig. 2B**; ref. 19). Expression of these three ELOVLs was strongly associated with androgen-induced prostate cancer gene sets (Nelson, **Fig. 2C**; Wang, Supplementary Fig. S4A; refs. 20, 21). As expected, the AR antagonist enzalutamide significantly decreased *ELOVL2, ELOVL5*, and *ELOLV7* expression compared with vehicle in LNCaP cell lines (**Fig. 2D**) and LNCaP xenograft tumors (**Fig. 2E**). Expression of *ELOVL2* was not detected in the LNCaP xenografts. Importantly, *ELOVL2, ELOVL5*, and *ELOVL7* were repressed by androgen deprivation in prostatic biopsies from patients with locally advanced or metastatic prostate cancer after short-term neoadjuvant ADT ($n = 7$; **Fig. 2F**; ref. 22), and in radical prostatectomy samples from neoadjuvant intense ADT patients ($n = 18$; Supplementary Fig. S4B; ref. 23). Previous studies suggested that androgens may mediate ELOVL expression indirectly through activation of the master lipogenic transcription factor, sterol regulatory element-binding protein (SREBP1; ref. 24), or directly via AR transcriptional activity (25). To explore regulation through SREBP1, we knocked down SREBP1 in LNCP cells in the presence and absence of

Downloaded from cancerres.aacrjournals.org on April 1, 2021. © 2021 American Association for Cancer Research.

Published OnlineFirst February 5, 2021; DOI: 10.1158/0008-5472.CAN-20-2511

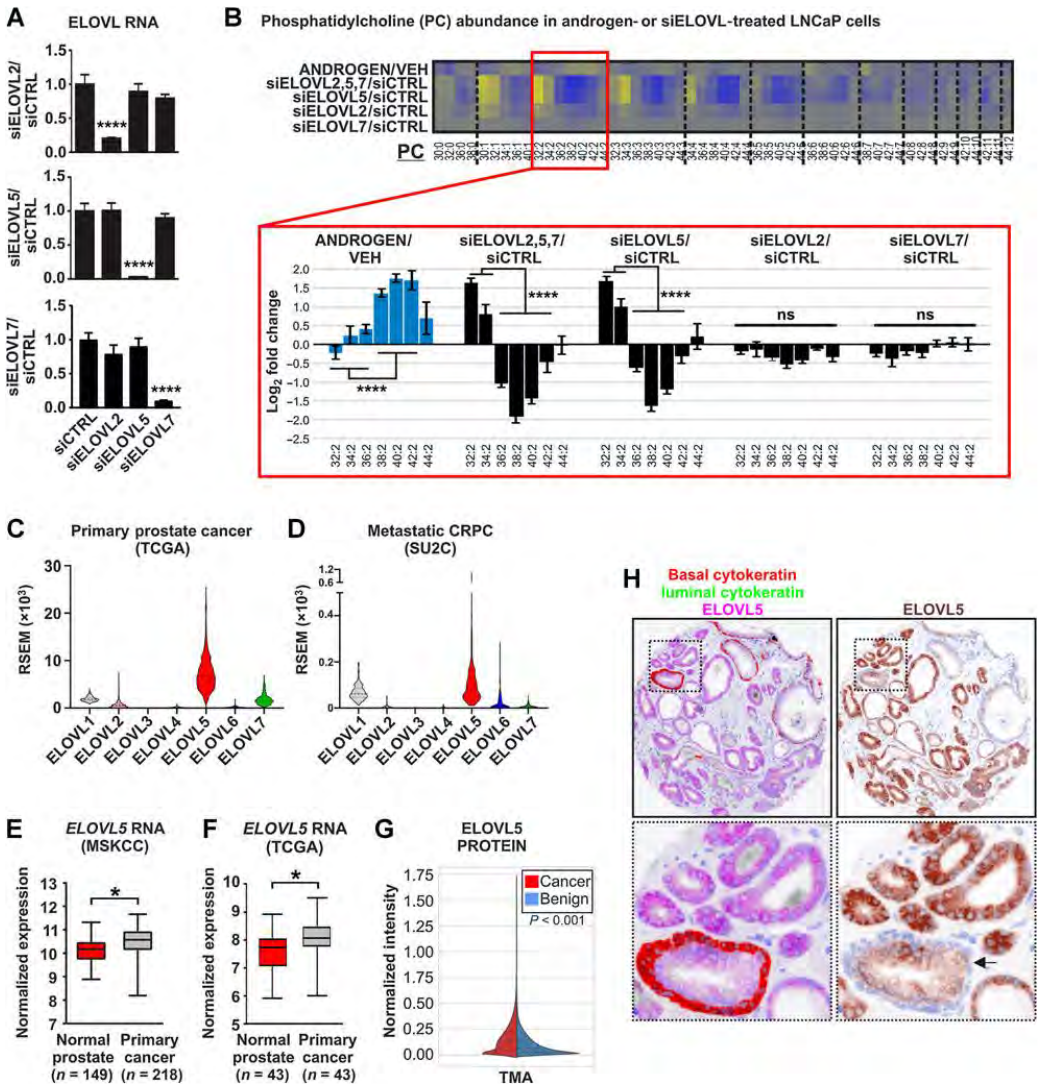

Figure 3.

ELOVL5 is the predominant elongase in prostate cells and is overexpressed in prostate cancer. **A,** qRT-PCR analysis to determine specificity of siRNA directed to *ELOVL2, ELOVL5,* or *ELOVL7* in LNCaP cells. Data are presented as fold change over siCTRL, and error bars represent mean ± SEM of triplicate wells. ****, $P < 0.05$ ANOVA; siELOVL versus siCTRL. **B,** Phospholipidomic changes in LNCaP cells subjected to knockdown of ELOVL2, ELOVL5, and ELOVL7 alone or in combination, in the presence of androgen (1 nmol/L mibolerone). Heat maps represent the $\log_2$-fold change in relative abundance of all measured PC species in androgen- or siELOVL-treated cells ($n = 3$). Red box depicts one unsaturation group as a bar graph to highlight effects of siELOVL on elongation. Data, mean ± SEM of triplicate wells. ****, $P < 0.0001$ ANOVA; short acyl chain lengths versus long acyl chain length; ns, not significant for any comparison. **C** and **D,** RNA-seq analysis of *ELOVL* expression in primary prostate tumors (TCGA) and metastatic castration-resistant prostate tumors (SU2C). **E** and **F,** ELOVL5 transcript levels in normal prostate tissue compared with prostate cancer in two independent data sets (MSKCC and TCGA). Data, normalized ELOVL5 expression. Boxplots show interquartiles with mean values; whiskers represent minimum and maximum values. *, $P < 0.05$; Mann–Whitney test. **G,** ELOVL5 protein expression in cancer compared with benign prostate clinical tissues in five primary prostate cancer tissue microarrays ($n = 249$). Violin plots are presented using normalized intensity units. *, $P < 0.001$; Mann–Whitney *U* test. **H,** Representative ELOVL5 immunostaining. Left, multiplex fluorescence staining of ELOVL5 (magenta) in malignant glands as indicated by the absence of basal cells (red stain). Luminal cells are stained green. Chromogenic staining of ELOVL5 (brown stain) is shown on the right. Black arrow, benign prostate gland.

Downloaded from cancerres.aacrjournals.org on April 1, 2021. © 2021 American Association for Cancer Research.

Published OnlineFirst February 5, 2021; DOI: 10.1158/0008-5472.CAN-20-2511

androgens (Supplementary Fig. S4C; 84% decrease in gene expression with siSREBP1 compared with siCTRL). As expected, siSREBP1 inhibited androgen induction of FASN expression, but was unable to suppress androgen induction of ELOVL2, *ELOVL5, or ELOVL7* (Supplementary Fig. S4C), which indicates that SREBP1 is not the primary mediator of androgen-induced ELOVL expression. To explore direct AR regulation, we examined AR ChIP-seq data from clinical samples (13). Multiple AR binding sites proximal to the *ELOVL2, ELOVL5*, and *ELOVL7* genes were evident in human prostatic tissues, many of which were enriched in malignant compared with normal tissues (**Fig. 2G**; Supplementary Fig. S5). Supporting their relevance, these AR binding sites were coincident with histone H3 lysine 27 acetylation (H3K27ac), a mark of active promoters and enhancers. We provide evidence of these AR binding sites in many published ChIP-seq data sets using ChIP-Atlas (Supplementary Fig. S6A–S6C), and validated AR binding at a subset of these sites by ChIP-qPCR in LNCaP cells (**Fig. 2H**). Collectively, these data indicate that AR binds to multiple sites proximal to the transcriptional start sites of the *ELOVL2, ELOVL5*, and *ELOVL7* genes, supporting a direct mode of AR-mediated transcriptional regulation.

ELOVL5 is the major elongase in the prostate and is overexpressed in prostate cancer

To assess the relative contributions of *ELOVL2, ELOVL5*, and *ELOVL7* to the androgen-induced elongation phenotype, siRNA-mediated knockdown of all three ELOVLs in combination or alone was performed in LNCaP cells. Two independent siRNAs were tested per *ELOVL* gene in LNCaP cells, each achieving at least 80% knockdown within 48 hours (Supplementary Fig. S7A). We observed no evidence of *ELOVL2, ELOVL5*, or *ELOVL7* knockdown alone causing compensatory increases in expression of the other *ELOVLs* (**Fig. 3A**). When compared with siCTRL, complete reversal of the androgen-mediated increase in longer fatty acid chains was observed in all four phospholipid classes with simultaneous knockdown of *ELOVL2/5/7* in LNCaP cells (**Fig. 3B**; Supplementary Fig. S7B). Notably, almost identical changes to the combined *ELOVL2/5/7* knockdown were achieved by *ELOVL5* knockdown alone (**Fig. 3B**; Supplementary Fig. S7B). *ELOVL2* and *ELOVL7* knockdown showed no discernible effect, implicating *ELOVL5* as the primary contributor to androgen regulation of phospholipid fatty acyl chain elongation in LNCaP cells. Supporting *ELOVL5* as the major elongase in prostate cancer, *ELOVL5* was the most highly expressed of all seven *ELOVL* genes in two independent transcriptomic data sets, derived from 419 localized primary prostate tumors generated by The Cancer Genome Atlas (TCGA) Research Network (http://cancergenome.nih.gov/; **Fig. 3C**) and 118 metastatic castration-resistant prostate tumors from the Stand Up to Cancer (SU2C) data set (**Fig. 3D**). Given the high level of *ELOVL5* expression in prostate cancer, we investigated whether this is aberrant expression compared with normal prostate tissue. Data from three clinical cohorts were evaluated, including transcriptomic data sets from MSKCC (**Fig. 3E**), TCGA (**Fig. 3F**), and a proteomic data set from Tampere University Hospital (Supplementary Fig. S8A; ref. 26). In all three cohorts, *ELOVL5* expression was significantly higher in prostate cancer compared with normal/benign prostatic hyperplasia. Further supporting these observations, ELOVL5 protein levels were analyzed by IHC in five tissue microarrays (TMA) comprised of 249 primary prostate cancer samples. DAPI-normalized ELOVL5 intensity was significantly increased in tumor compared with adjacent benign prostate epithelial cells in the entire cohort (**Fig. 3G** and **H**), or when each TMA was independently evaluated (Supplementary Fig. S8B).

ELOVL5 targeting inhibits prostate cancer cell proliferation

The significant role of ELOVL5 in modifying the cellular lipidome suggests that it may contribute to cellular proliferation and energetic processes. Indeed, transient knockdown of *ELOVL5* by two independent siRNAs in LNCaP (Supplementary Fig. S7A) and 22Rv1 cells (Supplementary Fig. S8C) significantly attenuated viability of both prostate cancer cell lines (**Fig. 4A** and **B**), but did not induce death (**Fig. 4A** and **B**) or apoptosis (Supplementary Fig. S8D). In contrast, constitutive overexpression of ELOVL5 (hELOVL5$^+$) in LNCaP cells significantly increased viable cell number compared with control cells (hCTRL; **Fig. 4C**). LNCaP colony formation was affected in a similar manner, where stable knockdown of ELOVL5 with short hairpin RNA (shELOVL5$^-$) significantly reduced colony formation (**Fig. 4D**) while stable overexpression of ELOVL5 increased colony formation (**Fig. 4E**). Given we observed no impact of ELOVL5 depletion on cell death, we evaluated proliferation as the driver of ELOVL5-mediated increase in cell viability. Transient knockdown of ELOVL5 with siRNA significantly attenuated LNCaP and 22Rv1 cell proliferation compared with control siRNA, as determined by a Cyquant assay (**Fig. 4F**), which was associated with cell-cycle arrest at the G_1–S phase (**Fig. 4G**). Encouraged by the antiproliferative effects of ELOVL5 knockdown in prostate cancer cell lines, we again used our PDE model to determine efficacy of ELOVL5 targeting in clinical prostate tumors. Significant ELOVL5 depletion (44.7%) was achieved in PDE tissues using siRNA-loaded nanoparticles (**Fig. 4H**; Supplementary Fig. S8E), and this resulted in a marked decrease in expression of the proliferative marker ki67 from 52.9% in siCTRL PDE tissues to 21.06% in siELOVL5 PDE tissues (**Fig. 4H**; Supplementary Fig. S8E). Finally, reduced spheroid growth was observed in siELOVL5-depleted LNCaP cells compared with siCTRL (**Fig. 4I**), and constitutively expressing shELOVL5 LNCaP cells showed significantly reduced capacity for tumor growth compared with shCTRL cells when grown subcutaneously in NOD/SCID mice ($n = 7$ mice/treatment; **Fig. 4J**).

ELOVL5 elongation of the monounsaturated fatty acid cis-vaccenic acid is critical for prostate cancer cell viability

Published phenotypic studies of ELOVL5 knockout mice demonstrate that hepatic steatosis induced by ELOVL5 knockout can be rescued by supplementation with the PUFAs AA (C20:4, n-6) and docosahexaenoic acid (DHA; C22:6, n-3; ref. 27), as these PUFAs are reliant on ELOVL5 for synthesis (**Fig. 5A**). We found that although AA and DHA levels were reduced in ELOVL5-depleted LNCaP cells (Supplementary Fig. S9A), supplementation with AA or DHA did not alter ELOVL5 knockdown-mediated changes in cell viability (**Fig. 5B**). Also distinct from the mouse model, ELOVL5 knockdown caused no induction of key lipid metabolism enzymes (SREBP1, FASN, ACACA, and ATGL; Supplementary Fig. S9B), nor any alteration to cellular lipid content, as determined by the number of lipid droplets observed per cell by electron microscopy (Supplementary Fig. S9C). These findings indicated that the role of ELOVL5 in prostate cells differs substantially from those in the liver. In considering other known products of ELOVL5, we tested an omega-7 MUFA, cis-vaccenic acid (cVA; C18:1, n-7), which has previously been implicated in ELOVL5 action (**Fig. 5A**; ref. 28). Remarkably, supplementation with cVA completely reversed the inhibitory effect of ELOVL5 knockdown on cell viability (**Fig. 5C**), indicating MUFA elongation as a key ELOVL5 function in prostate cancer.

ELOVL5 activity regulates mitochondrial respiratory function and oxidative stress

Electron microscopy examination of ELOVL5-depleted LNCaP cells showed a marked increase in the size and length of the cellular

Downloaded from cancerres.aacrjournals.org on April 1, 2021. © 2021 American Association for Cancer Research.

Published OnlineFirst February 5, 2021; DOI: 10.1158/0008-5472.CAN-20-2511

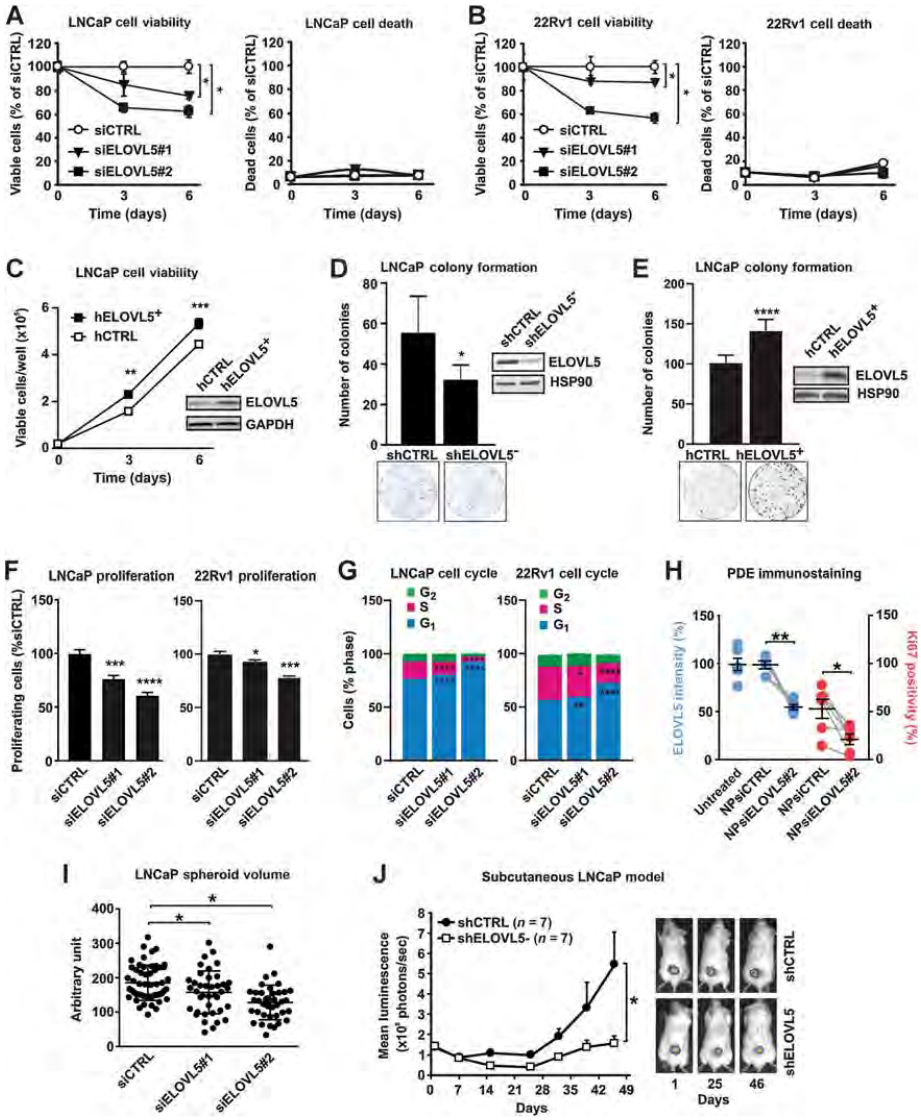

Figure 4.

ELOVL5 knockdown inhibits prostate cancer cell growth, associated with impaired mitochondrial respiration, and ROS production. **A** and **B,** Prostate cancer cell lines subjected to siRNA-mediated ELOVL5 knockdown (siELOVL5) or scrambled siRNA control (siCTRL) were analyzed using the Trypan blue dye exclusion assay for LNCaP cell viability and death (**A**) and 22Rv1 cell viability and death (**B**). **C,** LNCaP cells with stable overexpression of ELOVL5 (hELOVL5$^+$) were analyzed for cell viability compared with control cells (hCTRL). **D** and **E,** LNCaP colony formation was evaluated in cells with stable shRNA ELOVL5 knockdown (shELOVL5) or stable ELOVL5 overexpression (hELOVL5$^+$). **F,** LNCaP and 22Rv1 cell proliferation was evaluated by Cyquant assay following siRNA-mediated ELOVL5 knockdown. **G,** LNCaP and 22Rv1 cell-cycle distribution was evaluated by flow cytometric analysis 72 hours after siRNA-mediated ELOVL5 knockdown. **H,** Immunostaining for ELOVL5 and proliferative marker Ki67 in untreated, NPsiCTRL-treated, or NPsiELOVL5-treated PDEs. A decrease in proliferative marker Ki67 expression can be seen when PDE tissues are treated with NPsiELOVL5 ($n = 6$). **I,** LNCaP spheroid volume was evaluated in LNCaP cells subjected to siRNA-mediated ELOVL5 knockdown, compared with siCTRL. **J,** Inhibition of subcutaneous tumor growth in stable ELOVL5 knockdown LNCaP cells (shELOVL5$^-$; $n = 7$) compared with shCTRL LNCaP cells ($n = 7$) and representative bioluminescent tumor images. All *in vivo* data are representative of at least three independent experiments. Data, mean ± SEM of triplicate wells unless otherwise indicated. *, $P < 0.05$; **, $P < 0.01$; ***, $P < 0.001$; ****, $P < 0.0001$; ANOVA ELOVL5 knockdown versus control.

Downloaded from cancerres.aacrjournals.org on April 1, 2021. © 2021 American Association for Cancer Research.

Published OnlineFirst February 5, 2021; DOI: 10.1158/0008-5472.CAN-20-2511

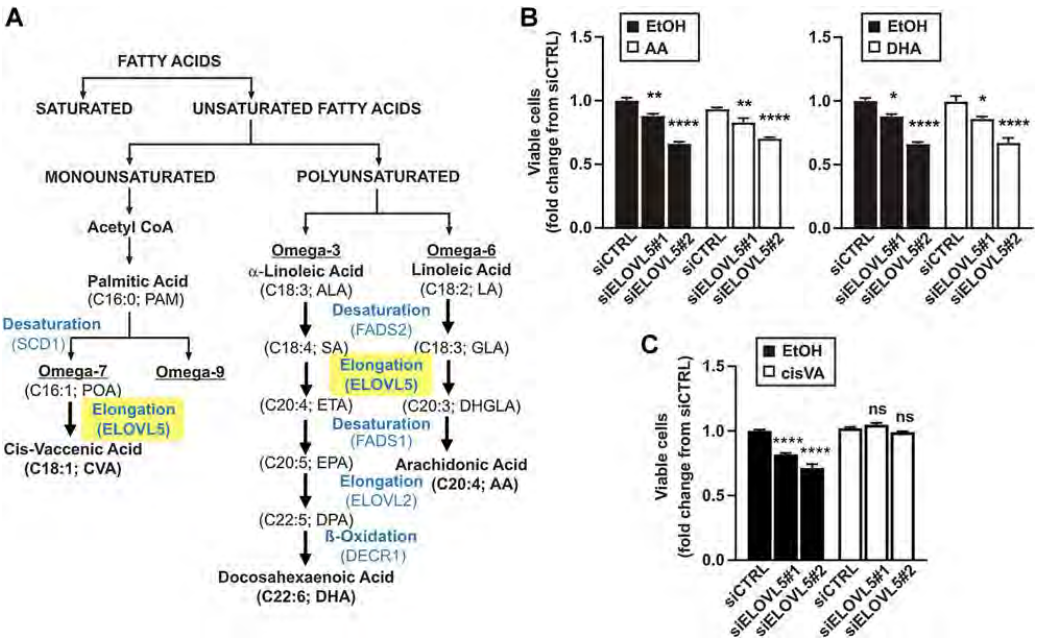

Figure 5.

Proliferative effects of ELOVL5 knockdown are rescued by cis-vaccenic acid. **A,** Schematic pathway of MUFA and PUFA synthesis showing elongation and desaturation steps of fatty acids regulated by ELOVL5 that result in production of AA, DHA, and cVA. **B** and **C,** LNCaP cell viability rescue experiments for ELOVL5 knockdown-related changes in response to AA (C20:4;omega-6), DHA (C22:6;omega-3), and cVA (C18:1;omega-7) products of ELOVL5 (5–10 μmol/L). Data are representative of at least three independent experiments and are presented as mean ± SEM of triplicate wells. ns, not significant; *, $P < 0.05$; **, $P < 0.01$; ****, $P < 0.0001$; ANOVA ELOVL5 knockdown versus control.

mitochondria compared with control cells, as well as darker and denser cristae (**Fig. 6A**), indicative of cellular stress. Further investigation of the mitochondria was undertaken using the Seahorse mitochondrial stress test assay. Decreased basal and maximal respiration rates were observed in ELOVL5-depleted LNCaP cells (**Fig. 6B**), whereas ELOVL5 overexpression increased maximal mitochondrial respiration (**Fig. 6C**). A decrease in mitochondrial respiration, as observed upon ELOVL5 knockdown, is a strong indicator of mitochondrial dysfunction and can result in aberrant generation of reactive oxygen species (ROS; ref. 29). The fluorogenic dye CellROX Orange was used to investigate whether ELOVL5 targeting influences ROS production. Markedly increased ROS levels were observed upon ELOVL5 knockdown in LNCaP cells, which was completely reversed by the potent antioxidant/ROS scavenger Trolox (**Fig. 6D**). Trolox also rescued the inhibitory effects of ELOVL5 depletion on LNCaP cell viability (**Fig. 6E**), revealing ROS production as a key antiproliferative mechanism for ELOVL5 targeting. Consistent with these results, ELOVL5-mediated changes in ROS production were also rescued by supplementation with cVA (**Fig. 6E**). Confirming that ROS induction was not part of a generalized stress response, stable overexpression of ELOVL5 markedly reduced ROS levels in LNCaP cells (**Fig. 6F**).

ELOVL5 promotes prostate tumor growth and metastasis

Having established a critical role for ELOVL5 in prostate cancer cell proliferation, we next investigated its influence on metastatic tumor features *in vitro* and *in vivo*. ELOVL5 knockdown significantly reduced transwell migration through Matrigel in both LNCaP (**Fig. 7A**) and 22Rv1 cells (**Fig. 7B**), whereas ELOVL5 overexpression promoted LNCaP migration (**Fig. 7C**). Importantly, supplementation of ELOVL5-depleted LNCaP cells with cVA reversed the migratory phenotype (**Fig. 7D**), reinforcing a critical role for this MUFA in prostate cancer. To determine whether ELOVL5 influences spontaneous metastasis, we used an orthotopic assay in which LNCaP cells were injected directly into the prostate (i.e., intraprostatic xenografts). Weekly monitoring of the mice revealed that tumor incidence was 100% for both shELOVL5 and shCTRL cells, but the shELOVL5 tumors grew significantly more slowly and measured almost 40% smaller than shCTRL tumors after 50 days (**Fig. 7E**). *Ex vivo* bioluminescent imaging of the major organs following intraprostatic tumor growth revealed that shCTRL cells spread to major visceral organs, most notably the lungs, in 4 of 7 mice (**Fig. 7F**). Histologic evidence of LNCaP tumor metastases to the lung was demonstrated by staining for AR and H&E (**Fig. 7F**). Significantly, no overt metastasis by shELOVL5 cells was detected in any mice (**Fig. 7F**).

Discussion

The advent of high-throughput "omics" approaches has revolutionized the molecular characterization of cancer, but in contrast to the genome, transcriptome and proteome, the lipidome remains largely underexplored. We utilized tandem mass spectrometric analysis to

Downloaded from cancerres.aacrjournals.org on April 1, 2021. © 2021 American Association for Cancer Research.

Published OnlineFirst February 5, 2021; DOI: 10.1158/0008-5472.CAN-20-2511

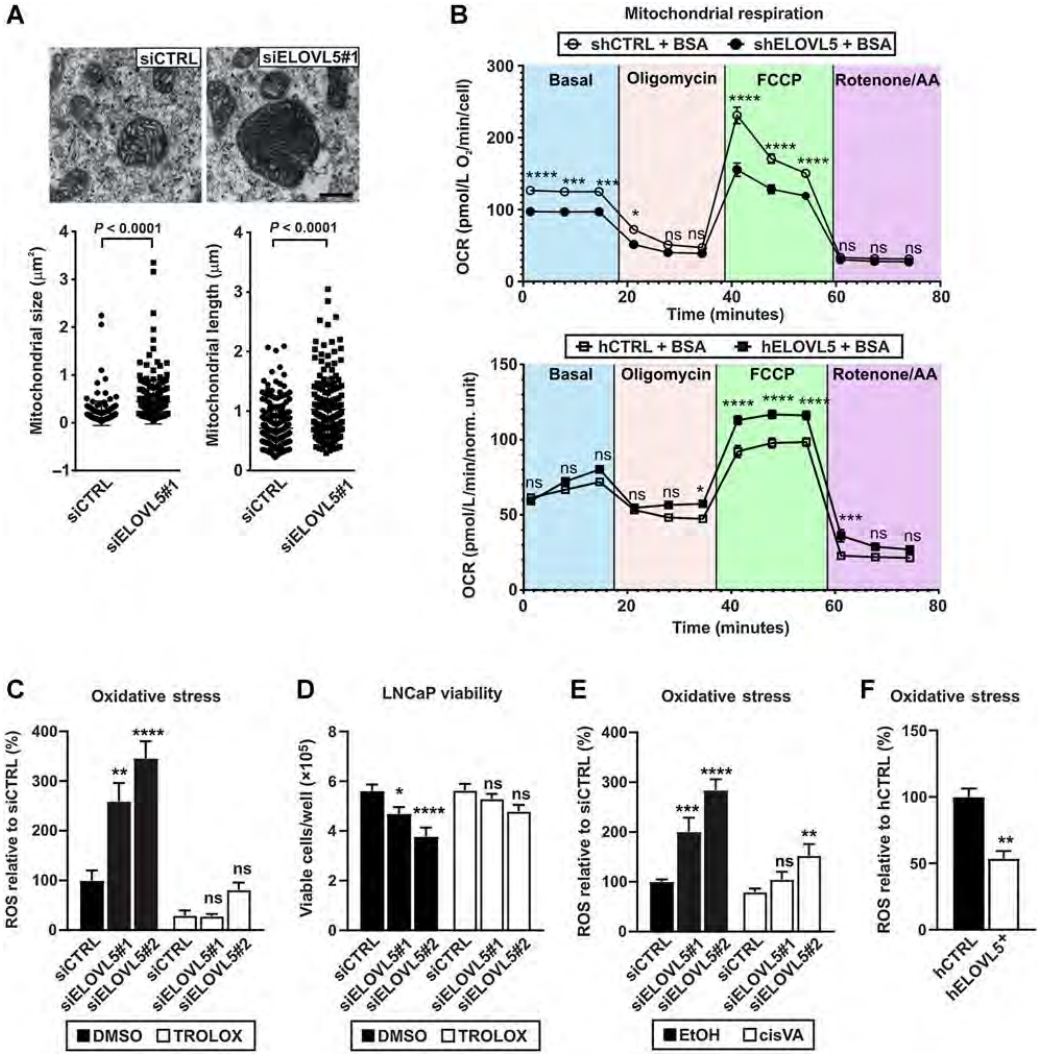

Figure 6.

ELOVL5 knockdown alters mitochondrial morphology, respiration, and ROS production. **A,** Mitochondrial phenotype changes related to ELOVL5 knockdown in LNCaP cells revealed by electron microscopy, with significant increases in mitochondrial size and length detected. *, $P < 0.0001$ *t* test, siELOVL5 versus siCTRL. **B,** Seahorse analysis of mitochondrial respiration in ELOVL5-depleted LNCaP cells (top) and ELOVL5-overexpressing LNCaP cells (bottom). Basal and maximal respiration, ATP production, and mitochondrial spare capacity are shown and compared with BSA control. Data are representative of three independent experiments and are presented as mean ± SEM of triplicate wells. *, $P < 0.05$; ***, $P < 0.001$; ****, $P < 0.0001$; ANOVA ELOVL5 knockdown versus control; ns, not significant. **C,** ROS production induced by ELOVL5 knockdown and rescue using antioxidant trolox (100 μmol/L) by flow cytometric measurement of CellROX Orange Reagent. **D,** LNCaP cell viability rescue experiments for ELOVL5 knockdown-related changes in response to 100 μmol/L trolox. **E,** ROS produced by ELOVL5 knockdown in LNCaP cells and rescue in the presence of MUFA cVA (10 μmol/L) by flow-cytometric measurement of CellROX Orange Reagent. **F,** ROS inhibition upon ELOVL5 overexpression in LNCaP cells. All data are representative of at least three independent experiments and are presented as mean ± SEM of triplicate wells. *, $P < 0.05$; **, $P < 0.01$; ***, $P < 0.001$; ****, $P < 0.0001$; ANOVA ELOVL5 knockdown versus control; ns, not significant.

profile the androgen-regulated lipidome of prostate cancer cell lines and PDEs and uncovered ubiquitous increases in fatty acyl chain elongation mediated by the fatty acid elongase, *ELOVL5*. Molecular targeting of ELOVL5 reversed fatty acyl chain elongation in prostate cancer cells, which through induction of mitochondrial oxidative stress, significantly reduced prostate tumorigenesis and metastatic

Downloaded from cancerres.aacrjournals.org on April 1, 2021. © 2021 American Association for Cancer Research.

Published OnlineFirst February 5, 2021; DOI: 10.1158/0008-5472.CAN-20-2511

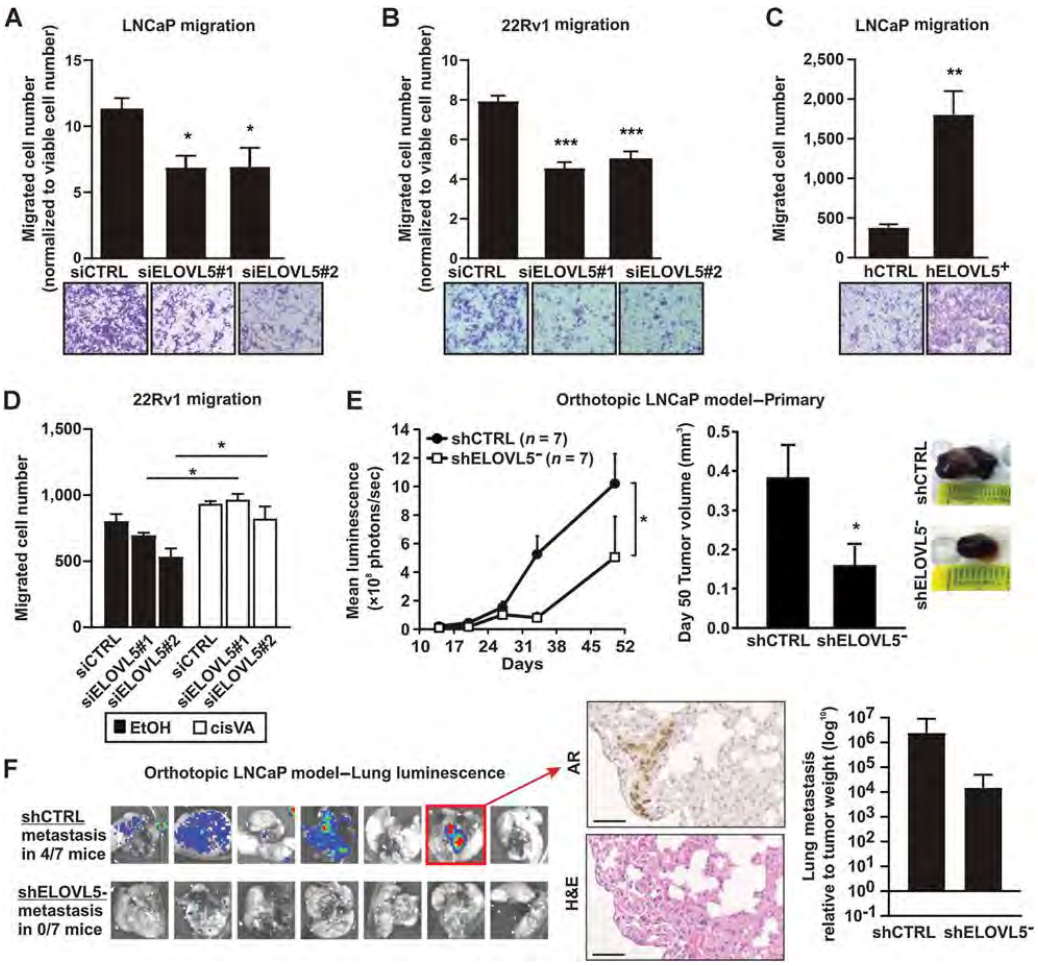

Figure 7.

ELOVL5 knockdown inhibits cell migration, prostate tumor growth, and metastasis. **A** and **B,** LNCaP and 22Rv1 prostate cancer cell lines subjected to siRNA-mediated ELOVL5 knockdown were analyzed for cell migration through Matrigel. Data are representative of at least two independent experiments and are presented as mean ± SEM of triplicate wells. *, $P < 0.05$; ***, $P < 0.001$ ANOVA, siELOVL5#1/#2 versus siCTRL. **C,** LNCaP cells with stable overexpression of ELOVL5 were analyzed for cell migration through Matrigel. Data are representative of two independent experiments and are presented as mean ± SEM of triplicate wells. **, $P < 0.01$, ANOVA, shELOVL5⁻ versus shCTRL. **D,** 22Rv1 migration rescue experiments for ELOVL5 knockdown-related changes in response to 10 μmol/L cVA. Data are representative of three independent experiments and are presented as mean ± SEM of triplicate wells. *, $P < 0.05$; ANOVA, cVA versus vehicle control. **E,** LNCaP cells constitutively expressing shRNA directed to ELOVL5 ($n = 7$) or control ($n = 7$) were analyzed for orthotopic LNCaP tumor growth in mice. Data, mean ± SEM. *, $P < 0.05$; *t* test, shELOVL5⁻ versus shCTRL. **F,** Bioluminescent images of metastatic spread to the lungs of all shCTRL ($n = 7$) and shELOVL5⁻ ($n = 7$) mice from **E.** Representative H&E staining and AR immunostaining of shCTRL mouse lung boxed in red, showing histologic evidence of metastatic human LNCaP cells in the mouse lung. Metastasis of orthotopic tumors to the lungs presented as lung luminescence normalized to primary tumor weight.

potential *in vitro* and *in vivo*. Moreover, we demonstrate that the monounsaturated fatty acid product of ELOVL5 activity, cVA, is a critical modulator of ELOVL5-induced oxidative stress and survival in prostate cancer. Our findings provide new insights into the downstream metabolic actions of AR in prostate cancer cells, beyond the previous almost exclusive focus on *de novo* lipogenesis, and identify fatty acid elongation as a critical target of androgen action for therapeutic intervention.

Elongation is a critical step in the production of fatty acids with a chain length of more than 16 carbons, and is a stepwise process whereby carbon units are added to the carboxyl terminal of fatty acid chains (30). The reaction is catalyzed by enzymes called elongases,

Downloaded from cancerres.aacrjournals.org on April 1, 2021. © 2021 American Association for Cancer Research.

Published OnlineFirst February 5, 2021; DOI: 10.1158/0008-5472.CAN-20-2511

encoded by a family of seven ELOVL genes (ELOVL1–7) that display distinct tissue distribution and substrate preference (31). *ELOVL5* is most highly expressed in the adrenal glands, testis, and prostate (32). Increasing evidence suggests that ELOVL expression is frequently altered in cancer. ELOVL6 is the most commonly studied, with reported overexpression in hepatocellular cancer (33), lung cancer (34), and breast cancer (35). In prostate cancer, ELOVL7 has been reported as overexpressed in hormone-naïve prostate cancer (36, 37), with influences on cell viability, xenograft tumor growth, and potentially *de novo* steroidogenesis (36, 38); however, we found its abundance in clinical prostate tumors to be very low. When directly comparing all seven ELOVL family members at both the RNA and protein levels, ELOVL5 was the most highly expressed in both primary and castration-resistant clinical prostate tumors, and was overexpressed in malignant compared with nonmalignant prostate. In published overexpression studies in primary rat hepatocytes, adenoviral overexpression of ELOVL5 induced elongation of C20 PUFAs and gave rise to altered hepatic fatty acid content (39). The reverse was observed in *ELOVL5* knockout mice where inhibition of C20 and C22 PUFA elongation and concomitant increase in C18 PUFAs was observed, and resulted in development of hepatic steatosis (27). Unfortunately, the effect of ELOVL5 ablation on the mouse prostate was not reported, but we likewise observed inhibition of fatty acid elongation in prostate cancer cells with ELOVL5 knockdown. Phenotypically, targeting ELOVL5 had profound effects on prostate cancer cell proliferation, colony formation, spheroid growth, and invasion through Matrigel, in preclinical models that range from typical cell lines to complex 3D cultures and PDEs. The latter provides the most physiologically and clinically relevant preclinical model currently available, as the critical tumor microenvironment remains intact (10). The therapeutic efficacy of ELOVL5 depletion was also significant *in vivo* where primary tumor growth was suppressed, and spontaneous metastasis to distant sites was restricted by the knockdown.

Demonstrated in this study is a previously unknown relationship between ELOVL5-driven lipid elongation in prostate cancer, mitochondrial homeostasis, and intracellular ROS levels. ELOVL5′s dual effects on mitochondrial respiratory activity and intracellular ROS levels are consistent, given mitochondria are a major source of intracellular ROS (40). Importantly, our data indicate that ROS induction is not a nonspecific cellular stress response to ELOVL5 targeting, as ectopic ELOVL5 overexpression markedly suppresses ROS production. It is well established that ROS production is elevated in cancer cells, as a consequence of increased metabolic demand, mutation rate, and hypoxia, as a means of promoting cancer cell proliferation and tumor progression (41). Although these effects are beneficial for cancer cell growth and survival, the increase in baseline ROS also represents a vulnerability to further oxidative stress, as high levels of ROS are cytotoxic (42). Unlike their benign counterparts with low baseline ROS levels, small increases in ROS production can push cancer cells over the "cytotoxic ROS threshold" (41) to suppress cell survival and/or induce cell death. The role of ELOVL5 in prostate cancer appears to be, at least in part, as a regulator of cellular redox homeostasis, to ensure that prostate cancer cells do not exceed this "cytotoxic ROS threshold," whilst maintaining appropriate ROS production to drive tumorigenesis. Although an increasing number of cancer treatments target ROS as a therapeutic strategy, including both chemotherapies and molecular targeted agents (43), specific targeting of lipid metabolism through ELOVL5 now provides a new avenue for ROS induction as a treatment for prostate cancer.

One of the most significant findings of this study was rescue of ELOVL5-mediated proliferation, metastasis, and ROS induction by supplementation with the monounsaturated product of ELOVL5, cis-vaccenic acid, but not by supplementation with long-chain polyunsaturated fatty acids. This was an unexpected, because ELOVL5 was previously considered to be mainly involved in production of PUFAs rather than MUFAs, and the main hepatic phenotype of the ELOVL5 knockout mouse was fully rescued by PUFA supplementation. In light of recent reports of the critical importance of MUFAs in maintaining redox homeostasis in cancer cells (44), our data suggest that cis-vaccenic acid production underpins this aspect of ELOVL5 activity, and may serve to reduce oxidation of ELOVL5-derived PUFAs. Although it is the least studied of ELOVL5′s products, cis-vaccenic acid has been reported to be linked to coronary heart disease risk when incorporated into red blood cell membranes (45), has displayed antilipogenic effects in bovine adipocytes (46) and its ratio with its precursor has been suggested as an indicator of biotin deficiency (47). A study undertaken in HepG2 (kidney) cells suggested that *cis*-vaccenic was the mediator of ELOVL5 regulation of the mTORC2–Akt–FOXO1 pathway (28). Importantly, its role in metabolism is largely unknown (46) and there is little to no published data on its role in cancer, highlighting this as an important focus for future investigations.

Important for the potential of ELOVL5 as a therapeutic target, the murine ELOVL5 knockout was not lethal. This is in contrast to the master fatty acid synthesis enzyme FASN, which is lethal when knocked out in mice (48), and suggests that targeted inhibition of ELOVL5 could have a higher therapeutic window than inhibition of FASN—currently the most widely studied metabolic target in cancer. Moreover, loss of ELOVL5 did not elicit changes to the expression of other ELOVL family members, key lipid synthetic enzymes, or to cellular fatty acid content. These findings further highlight the potential of ELOVL5 as a therapeutic target, as compensatory adaptive responses that can mitigate efficacy have frequently been observed with investigative metabolic drugs and limit their clinical application. For example, FASN inhibitors target *de novo* lipid synthesis but can result in compensatory increases in uptake of exogenous dietary lipids or expression of genes in the fatty acid synthesis pathway including ACACA, ACLY, as well as FASN itself, to satisfy the cell's demand for fatty acids (49, 50).

Transcriptomic studies have suggested for many years that lipid synthesis is enriched by AR activity in prostate cancer but the explicit details of how this contributes to tumorigenicity have remained unclear. Herein we provide a specific new functional role for the AR in maintaining lipid homeostasis via ELOVL5-mediated elongation of fatty acids, and demonstrate the significant impact of elongation on prostate cancer cell malignancy and metastasis. The antimetastatic effects of ELOVL5 knockdown are particularly notable given that metastatic prostate cancer remains a major clinical challenge and is associated with a high rate of death despite multiple new drug approvals in recent years. Based on the findings in this study, targeting specific lipidomic features of prostate tumor cells such as elongation is a promising therapeutic strategy that warrants further investigation.

Authors' Disclosures

M.M. Centenera reports grants from Prostate Cancer Foundation of Australia during the conduct of the study. J. Machiels reports a patent for WO2012038525 licensed. I.J. Burvenich reports grants from Movember Foundation and Prostate Cancer Foundation of Australia during the conduct of the study. C.C. Bango reports other employment from Glaxosmithkline outside the submitted work. A.M. Scott reports other funding from AbbVie, EMD Serono, ITM, Medimmune, AVID, Telix, Adalta, Cyclotek, and Theramyc, and personal fees from Life Science Pharmaceuticals

Downloaded from cancerres.aacrjournals.org on April 1, 2021. © 2021 American Association for Cancer Research.

Published OnlineFirst February 5, 2021; DOI: 10.1158/0008-5472.CAN-20-2511

and Imagion, outside the submitted work. L.A. Selth reports grants from Cancer Council SA during the conduct of the study. J.V. Swinnen reports grants from Prostate Cancer Foundation of Australia, Research Foundation–Flanders, Stichting tegen Kanker, KU Leuven, and Interreg V-A EMR23 "EURLIPIDS" during the conduct of the study; in addition, J.V. Swinnen had a patent for WO2012038525 issued. L.M. Butler reports grants from Movember Australia, Australian Research Council, Cancer Council South Australia, Prostate Cancer Foundation of Australia, and U.S. Department of Defense during the conduct of the study. No disclosures were reported by the other authors.

Authors' Contributions

M.M. Centenera: Conceptualization, investigation, writing–original draft, writing–review and editing. **J.S. Scott:** Investigation. **J. Machiels:** Investigation. **Z.D. Nassar:** Investigation. **D.C. Miller:** Investigation. **I. Zininos:** Investigation. **J. Dehairs:** Investigation. **I.J.G. Burvenich:** Investigation. **G. Zadra:** Investigation. **P.M. Chetta:** Investigation. **C. Bango:** Validation and investigation. **E. Evergren:** Validation and investigation. **N.K. Ryan:** Investigation. **J.L. Gillis:** Investigation. **C.Y. Mah:** Investigation. **T. Tieu:** Investigation. **A.R. Hanson:** Investigation. **R. Carelli:** Investigation. **K. Bloch:** Investigation. **V. Panagopoulos:** Investigation. **E. Waelkens:** Investigation. **R. Derua:** Investigation. **E.D. Williams:** Investigation. **A. Evdokioou:** Investigation. **A. Cifuentes-Rius:** Writing–review and editing. **N.H. Voelcker:** Writing–review and editing. **I.G. Mills:** Writing–review and editing. **W.D. Tilley:** Writing–review and editing. **A.M. Scott:** Writing–review and editing. **M. Loda:** Writing–review and editing. **L.A. Selth:** Investigation, writing–review and editing. **J.V. Swinnen:** Conceptualization, supervision, writing–review and editing. **L.M. Butler:** Conceptualization, supervision, writing–review and editing.

Acknowledgments

The authors thank the study participants, urologists, nurses, histopathologists, and the South Australian Coordinator of the Australian Prostate Cancer Bioresource; Jessica Savage, who assisted in the recruitment and collection of patient material and information; Swati Irani for assistance with explant tissue culture and analysis; Dr. Ying Huang for immunostaining the tissue microarrays; the University of Adelaide Microscopy facility for technical assistance with electron microscopy. The authors acknowledge financial support from the Movember Foundation and Prostate Cancer Foundation of Australia (MRTA3 to L.M. Butler, J.V. Swinnen, W.D. Tilley, A.M. Scott, L.A. Selth, M.M. Centenera; MRTA1 to E.D. Williams), Prostate Cancer Foundation of Australia (NDDA2711 to L.M. Butler, M.M. Centenera, J.V. Swinnen; NCG1816 to L.M. Butler, A. Cifuentes-Rius, N.H. Voelcker), the Research Foundation–Flanders (FWO G.0841.15 to J.V. Swinnen), the Stichting tegen Kanker (to J.V. Swinnen), KU Leuven (C16/15/073 and C32/17/052 to J.V. Swinnen), Interreg V-A (EMR23 to J.V. Swinnen and E. Waelkens), the National Health and Medical Research Council (1121057 to W.D. Tilley and L.A. Selth), the National Institute of Health (RO1CA131945 to M. Loda), the NCI (P50CA211024 to M. Loda), the Prostate Cancer Foundation (to M. Loda), the United States Department of Defense (PC150263 to G. Zadra; PC160357 to M. Loda; PC180582 to M. Loda, L.M. Butler, J.V. Swinnen), and the Dana-Farber Cancer Institute (Claudia Adams Barr Award in Innovative Basic Cancer Research to G. Zadra). M.M. Centenera was supported by a Prostate Cancer Foundation of Australia Young Investigator Award (YIG0412). Z.D. Nassar was supported by National Health and Medical Research Center Early Career Fellowship (1138648) and Prostate Cancer Foundation of Australia John Mills Young Investigator Award (YI1417). T. Tieu and N.H. Voelcker acknowledge support from the Office of the Chief Executive and CSIRO Manufacturing. T. Tieu acknowledges support of an Australian Government RTP scholarship. A. Cifuentes-Rius was supported by a National Health and Medical Research Council Early Career Fellowship (1112432). L.M. Butler was supported by an ARC Future Fellowship (130101004). L.M. Butler and L.A. Selth are supported by Principal Cancer Research Fellowships awarded by Cancer Council's Beat Cancer project on behalf of its donors, the state government through the Department of Health, and the Australian Government through the Medical Research Future Fund (PRF1117 and PRF2919).

The costs of publication of this article were defrayed in part by the payment of page charges. This article must therefore be hereby marked *advertisement* in accordance with 18 U.S.C. Section 1734 solely to indicate this fact.

Received July 23, 2020; revised December 17, 2020; accepted January 29, 2021; published first February 5, 2021.

References

1. Siegel RL, Miller KD, Jemal A. Cancer statistics, 2016. CA Cancer J Clin 2016;66:7–30.
2. Attard G, Parker C, Eeles RA, Schroder F, Tomlins SA, Tannock I, et al. Prostate cancer. Lancet 2016;387:70–82.
3. Swinnen JV, Esquenet M, Goossens K, Heyns W, Verhoeven G. Androgens stimulate fatty acid synthase in the human prostate cancer cell line LNCaP. Cancer Res 1997;57:1086–90.
4. Nguyen PL, Ma J, Chavarro JE, Freedman ML, Lis R, Fedele G, et al. Fatty acid synthase polymorphisms, tumor expression, body mass index, prostate cancer risk, and survival. J Clin Oncol 2010;28:3958–64.
5. Swinnen JV, Roskams T, Joniau S, Van Poppel H, Oyen R, Baert L, et al. Overexpression of fatty acid synthase is an early and common event in the development of prostate cancer. Int J Cancer 2002;98:19–22.
6. Rysman E, Brusselmans K, Scheys K, Timmermans L, Derua R, Munck S, et al. De novo lipogenesis protects cancer cells from free radicals and chemotherapeutics by promoting membrane lipid saturation. Cancer Res 2010;70:8117–26.
7. Zadra G, Photopoulos C, Loda M. The fat side of prostate cancer. Biochim Biophys Acta 2013;1831:1518–32.
8. Swinnen JV, Heemers H, van de Sande T, de Schrijver E, Brusselmans K, Heyns W, et al. Androgens, lipogenesis and prostate cancer. J Steroid Biochem Mol Biol 2004;92:273–9.
9. Sharma NL, Massie CE, Ramos-Montoya A, Zecchini V, Scott HE, Lamb AD, et al. The androgen receptor induces a distinct transcriptional program in castration-resistant prostate cancer in man. Cancer Cell 2013;23:35–47.
10. Centenera MM, Hickey TE, Jindal S, Ryan NK, Ravindranathan P, Mohammed H, et al. A patient-derived explant (PDE) model of hormone-dependent cancer. Mol Oncol 2018;12:1608–22.
11. Selth LA, Das R, Townley SL, Coutinho I, Hanson AR, Centenera MM, et al. A ZEB1-miR-375-YAP1 pathway regulates epithelial plasticity in prostate cancer. Oncogene 2017;36:24–34.
12. Taylor BS, Schultz N, Hieronymus H, Gopalan A, Xiao Y, Carver BS, et al. Integrative genomic profiling of human prostate cancer. Cancer Cell 2010;18:11–22.
13. Pomerantz MM, Li F, Takeda DY, Lenci R, Chonkar A, Chabot M, et al. The androgen receptor cistrome is extensively reprogrammed in human prostate tumorigenesis. Nat Genet 2015;47:1346–51.
14. Freese NH, Norris DC, Loraine AE. Integrated genome browser: visual analytics platform for genomics. Bioinformatics 2016;32:2089–95.
15. Paltoglou S, Das R, Townley SL, Hickey TE, Tarulli GA, Coutinho I, et al. Novel androgen receptor coregulator GRHL2 exerts both oncogenic and antimetastatic functions in prostate cancer. Cancer Res 2017;77:3417–30.
16. Tieu T, Dhawan S, Haridas V, Butler LM, Thissen H, Cifuentes-Rius A, et al. Maximizing RNA loading for gene silencing using porous silicon nanoparticles. ACS Appl Mater Interfaces 2019;11:22993–3005.
17. Centenera MM, Gillis JL, Hanson AR, Jindal S, Taylor RA, Risbridger GP, et al. Evidence for efficacy of new Hsp90 inhibitors revealed by ex vivo culture of human prostate tumors. Clin Cancer Res 2012;18:3562–70.
18. Panagopoulos V, Leach DA, Zinonos I, Ponomarev V, Licari G, Liapis V, et al. Inflammatory peroxidases promote breast cancer progression in mice via regulation of the tumour microenvironment. Int J Oncol 2017;50:1191–200.
19. Spans L, Helsen C, Clinckemalie L, Van den Broeck T, Prekovic S, Joniau S, et al. Comparative genomic and transcriptomic analyses of LNCaP and C4-2B prostate cancer cell lines. PLoS One 2014;9:e90002.
20. Nelson PS, Clegg N, Arnold H, Ferguson C, Bonham M, White J, et al. The program of androgen-responsive genes in neoplastic prostate epithelium. Proc Natl Acad Sci U S A 2002;99:11890–5.
21. Wang G, Jones SJ, Marra MA, Sadar MD. Identification of genes targeted by the androgen and PKA signaling pathways in prostate cancer cells. Oncogene 2006;25:7311–23.
22. Rajan P, Sudbery IM, Villasevil ME, Mui E, Fleming J, Davis M, et al. Next-generation sequencing of advanced prostate cancer treated with androgen-deprivation therapy. Eur Urol 2014;66:32–9.

Downloaded from cancerres.aacrjournals.org on April 1, 2021. © 2021 American Association for Cancer Research.

Published OnlineFirst February 5, 2021; DOI: 10.1158/0008-5472.CAN-20-2511

23. Sowalsky AG, Ye H, Bhasin M, Van Allen EM, Loda M, Lis RT, et al. Neoadjuvant-intensive androgen deprivation therapy selects for prostate tumor foci with diverse subclonal oncogenic alterations. Cancer Res 2018; 78:4716–30.
24. Heemers HV, Verhoeven G, Swinnen JV. Androgen activation of the sterol regulatory element-binding protein pathway: current insights. Mol Endocrinol 2006;20:2265–77.
25. Chan SC, Selth LA, Li Y, Nyquist MD, Miao L, Bradner JE, et al. Targeting chromatin binding regulation of constitutively active AR variants to overcome prostate cancer resistance to endocrine-based therapies. Nucleic Acids Res 2015; 43:5880–97.
26. Latonen L, Afyounian E, Jylha A, Nattinen J, Aapola U, Annala M, et al. Integrative proteomics in prostate cancer uncovers robustness against genomic and transcriptomic aberrations during disease progression. Nat Commun 2018; 9:1176.
27. Moon YA, Hammer RE, Horton JD.Deletion of ELOVL5 leads to fatty liver through activation of SREBP-1c in mice. J Lipid Res 2009;50:412–23.
28. Tripathy S, Jump DB. Elovl5 regulates the mTORC2-Akt-FOXO1 pathway by controlling hepatic cis-vaccenic acid synthesis in diet-induced obese mice. J Lipid Res 2013;54:71–84.
29. Murphy MP. How mitochondria produce reactive oxygen species. Biochem J 2009;417:1–13.
30. Kihara A. Very long-chain fatty acids: elongation, physiology and related disorders. J Biochem 2012;152:387–95.
31. Jakobsson A, Westerberg R, Jacobsson A. Fatty acid elongases in mammals: their regulation and roles in metabolism. Prog Lipid Res 2006;45:237–49.
32. Leonard AE, Bobik EG, Dorado J, Kroeger PE, Chuang LT, Thurmond JM, et al. Cloning of a human cDNA encoding a novel enzyme involved in the elongation of long-chain polyunsaturated fatty acids. Biochem J 2000;350Pt 3:765–70.
33. Matsuzaka T, Atsumi A, Matsumori R, Nie T, Shinozaki H, Suzuki-Kemuriyama N, et al. Elovl6 promotes nonalcoholic steatohepatitis. Hepatology 2012;56: 2199–208.
34. Marien E, Meister M, Muley T, Gomez Del Pulgar T, Derua R, Spraggins JM, et al. Phospholipid profiling identifies acyl chain elongation as a ubiquitous trait and potential target for the treatment of lung squamous cell carcinoma. Oncotarget 2016;7:12582–97.
35. Feng YH, Chen WY, Kuo YH, Tung CL, Tsao CJ, Shiau AL, et al. Elovl6 is a poor prognostic predictor in breast cancer. Oncol Lett 2016;12:207–12.
36. Tamura K, Makino A, Hullin-Matsuda F, Kobayashi T, Furihata M, Chung S, et al. Novel lipogenic enzyme ELOVL7 is involved in prostate cancer growth through saturated long-chain fatty acid metabolism. Cancer Res 2009;69: 8133–40.
37. Tolkach Y, Merseburger A, Herrmann T, Kuczyk M, Serth J, Imkamp F. Signatures of adverse pathological features, androgen insensitivity and metastatic potential in prostate cancer. Anticancer Res 2015;35:5443–51.
38. Han W, Gao S, Barrett D, Ahmed M, Han D, Macoska JA, et al. Reactivation of androgen receptor-regulated lipid biosynthesis drives the progression of castration-resistant prostate cancer. Oncogene 2018;37:710–21.
39. Wang Y, Torres-Gonzalez M, Tripathy S, Botolin D, Christian B, Jump DB. Elevated hepatic fatty acid elongase-5 activity affects multiple pathways controlling hepatic lipid and carbohydrate composition. J Lipid Res 2008; 49:1538–52.
40. Rodic S, Vincent MD. Reactive oxygen species (ROS) are a key determinant of cancer's metabolic phenotype. Int J Cancer 2018;142:440–8.
41. Nogueira V, Hay N. Molecular pathways: reactive oxygen species homeostasis in cancer cells and implications for cancer therapy. Clin Cancer Res 2013;19:4309–14.
42. Hayes JD, Dinkova-Kostova AT, Tew KD. Oxidative stress in cancer. Cancer Cell 2020;38:167–97.
43. Perillo B, Di Donato M, Pezone A, Di Zazzo E, Giovannelli P, Galasso G, et al. ROS in cancer therapy: the bright side of the moon. Exp Mol Med 2020;52: 192–203.
44. Magtanong L, Ko PJ, To M, Cao JY, Forcina GC, Tarangelo A, et al. Exogenous monounsaturated fatty acids promote a ferroptosis-resistant cell state. Cell Chem Biol 2019;26:420–32.
45. Djousse L, Matthan NR, Lichtenstein AH, Gaziano JM. Red blood cell membrane concentration of cis-palmitoleic and cis-vaccenic acids and risk of coronary heart disease. Am J Cardiol 2012;110:539–44.
46. Burns TA, Kadegowda AK, Duckett SK, Pratt SL, Jenkins TC. Palmitoleic (16:1 cis-9) and cis-vaccenic (18:1 cis-11) acid alter lipogenesis in bovine adipocyte cultures. Lipids 2012;47:1143–53.
47. Liu YY, Shigematsu Y, Bykov I, Nakai A, Kikawa Y, Fukui T, et al. Abnormal fatty acid composition of lymphocytes of biotin-deficient rats. J Nutr Sci Vitaminol 1994;40:283–8.
48. Chirala SS, Chang H, Matzuk M, Abu-Elheiga L, Mao J, Mahon K, et al. Fatty acid synthesis is essential in embryonic development: fatty acid synthase null mutants and most of the heterozygotes die in utero. Proc Natl Acad Sci U S A 2003;100: 6358–63.
49. Sankaranarayanapillai M, Zhang N, Baggerly KA, Gelovani JG. Metabolic shifts induced by fatty acid synthase inhibitor orlistat in non-small cell lung carcinoma cells provide novel pharmacodynamic biomarkers for positron emission tomography and magnetic resonance spectroscopy. Mol Imaging Biol 2013;15:136–47.
50. Alwarawrah Y, Hughes P, Loiselle D, Carlson DA, Darr DB, Jordan JL, et al. Fasnall, a selective FASN inhibitor, shows potent anti-tumor activity in the MMTV-neu model of HER2(+) breast cancer. Cell Chem Biol 2016;23:678–88.

Downloaded from cancerres.aacrjournals.org on April 1, 2021. © 2021 American Association for Cancer Research.

Published OnlineFirst February 5, 2021; DOI: 10.1158/0008-5472.CAN-20-2511

Cancer Research
The Journal of Cancer Research (1916–1930) | The American Journal of Cancer (1931–1940)

AACR American Association for Cancer Research

ELOVL5 Is a Critical and Targetable Fatty Acid Elongase in Prostate Cancer

Margaret M. Centenera, Julia S. Scott, Jelle Machiels, et al.

Cancer Res 2021;81:1704-1718. Published OnlineFirst February 5, 2021.

Updated version	Access the most recent version of this article at: doi:10.1158/0008-5472.CAN-20-2511
Supplementary Material	Access the most recent supplemental material at: http://cancerres.aacrjournals.org/content/suppl/2021/02/02/0008-5472.CAN-20-2511.DC1

Cited articles	This article cites 50 articles, 15 of which you can access for free at: http://cancerres.aacrjournals.org/content/81/7/1704.full#ref-list-1

E-mail alerts	Sign up to receive free email-alerts related to this article or journal.
Reprints and Subscriptions	To order reprints of this article or to subscribe to the journal, contact the AACR Publications Department at pubs@aacr.org.
Permissions	To request permission to re-use all or part of this article, use this link http://cancerres.aacrjournals.org/content/81/7/1704. Click on "Request Permissions" which will take you to the Copyright Clearance Center's (CCC) Rightslink site.

Downloaded from cancerres.aacrjournals.org on April 1, 2021. © 2021 American Association for Cancer Research.

9.3 Appendix C: Butler et al., 2021 Cancer Research

Published OnlineFirst August 6, 2021; DOI: 10.1158/0008-5472.CAN-20-3863

CANCER RESEARCH | METABOLISM AND CHEMICAL BIOLOGY

Lipidomic Profiling of Clinical Prostate Cancer Reveals Targetable Alterations in Membrane Lipid Composition

Lisa M. Butler[1,2], Chui Yan Mah[1,2], Jelle Machiels[3], Andrew D. Vincent[1,2], Swati Irani[1,2], Shadrack M. Mutuku[1,2], Xander Spotbeen[2,3], Muralidhararao Bagadi[3], David Waltregny[4], Max Moldovan[2], Jonas Dehairs[3], Frank Vanderhoydonc[3], Katarzyna Bloch[3], Rajdeep Das[1,5,6], Jurgen Stahl[7], James G. Kench[8,9,10], Thomas Gevaert[11], Rita Derua[12], Etienne Waelkens[12], Zeyad D. Nassar[1,2], Luke A. Selth[1,5,13], Paul J. Trim[2], Marten F. Snel[2], David J. Lynn[2,13], Wayne D. Tilley[1,5], Lisa G. Horvath[9,10,14,15], Margaret M. Centenera[1,2], and Johannes V. Swinnen[3]

ABSTRACT

Dysregulated lipid metabolism is a prominent feature of prostate cancer that is driven by androgen receptor (AR) signaling. Here we used quantitative mass spectrometry to define the "lipidome" in prostate tumors with matched benign tissues ($n = 21$), independent unmatched tissues ($n = 47$), and primary prostate explants cultured with the clinical AR antagonist enzalutamide ($n = 43$). Significant differences in lipid composition were detected and spatially visualized in tumors compared with matched benign samples. Notably, tumors featured higher proportions of monounsaturated lipids overall and elongated fatty acid chains in phosphatidylinositol and phosphatidylserine lipids. Significant associations between lipid profile and malignancy were validated in unmatched samples, and phospholipid composition was characteristically altered in patient tissues that responded to AR inhibition. Importantly, targeting tumor-related lipid features via inhibition of acetyl-CoA carboxylase 1 significantly reduced cellular proliferation and induced apoptosis in tissue explants. This characterization of the prostate cancer lipidome in clinical tissues reveals enhanced fatty acid synthesis, elongation, and desaturation as tumor-defining features, with potential for therapeutic targeting.

Significance: This study identifies malignancy and treatment-associated changes in lipid composition of clinical prostate cancer tissues, suggesting that mediators of these lipidomic changes could be targeted using existing metabolic agents.

Introduction

With more than 1 million deaths annually, prostate cancer remains a major cause of mortality and morbidity for men worldwide (1). The clinical implementation of systemic androgen receptor (AR) targeting agents such as enzalutamide and apalutamide has increased the available therapeutic options beyond androgen deprivation, but development of resistance to these strategies remains inevitable. To more effectively combat this disease, there is a need for alternative targets for intervention and a thorough understanding of the molecular changes that accompany cancer development, progression, and therapy. The advent of parallel "omic" approaches has led to the identification of previously unsuspected cancer subtypes and therapeutic targets. However, in contrast to the genome, transcriptome, and proteome, the cancer "lipidome" remains inadequately characterized (2). As building blocks of cellular membranes, lipids affect numerous cellular processes including signal transduction, ion transport, cell proliferation, energy metabolism, and cell death mechanisms, which are all involved in the development and progression of cancer (3, 4).

For prostate cancer, the lipidomic changes that accompany malignancy are of particular interest due to the unique metabolic profile of this cancer, whereby the normal cellular production of citrate is instead utilized in the tricarboxylic acid cycle for oxidative phosphorylation and biosynthetic processes such as lipogenesis (5, 6). Moreover, lipid metabolism is a highly androgen-sensitive process in prostate cancer cells (7) and lipid composition may therefore be a unique cellular readout of both androgen targeting and tumorigenesis. While panels of circulating plasma lipids have previously been associated with prostate cancer risk (8), diagnosis (9) and patient outcome (10), analysis of the prostate tumor lipidome has largely been confined to cell line–based studies (11–13), which lack clinical relevance. The recent evidence of malignancy-related changes in lipid composition of prostate tumors provided by mass spectrometry (MS)-based imaging studies (14–17) supports undertaking a more detailed and quantitative study of the clinical prostate cancer lipidome. Moreover, treatment-related

[1]Adelaide Medical School and Freemasons Centre for Male Health and Wellbeing, University of Adelaide, Adelaide, Australia. [2]South Australian Health and Medical Research Institute, Adelaide, Australia. [3]Laboratory of Lipid Metabolism and Cancer, LKI – Leuven Cancer Institute, KU Leuven, Leuven, Belgium. [4]Department of Urology, University Hospital of Liège, Liege, Belgium. [5]Dame Roma Mitchell Cancer Research Laboratories, University of Adelaide, Adelaide, Australia. [6]Northwestern University, Feinberg School of Medicine, Comprehensive Transplant Center, Chicago, Illinois. [7]Clinpath Laboratories, Adelaide, Australia. [8]Department of Tissue Pathology and Diagnostic Oncology, Royal Prince Alfred Hospital, NSW Health Pathology, Camperdown, New South Wales, Australia. [9]Garvan Institute of Medical Research, Darlinghurst, New South Wales, Australia. [10]University of Sydney, Camperdown, New South Wales, Australia. [11]Department of Urology, UZ Leuven, Leuven, Belgium. [12]Department of Cellular and Molecular Medicine and SyBioMa Center, KU Leuven, Leuven, Belgium. [13]Flinders Health and Medical Research Institute, Flinders University, Adelaide, Australia. [14]Chris O'Brien Lifehouse, Camperdown, New South Wales, Australia. [15]University of New South Wales, Sydney, New South Wales, Australia.

Note: Supplementary data for this article are available at Cancer Research Online (http://cancerres.aacrjournals.org/).

L.M. Butler, M.M. Centenera, and J.V. Swinnen contributed equally to this article.

Corresponding Author: Lisa M. Butler, Adelaide Medical School and Freemasons Centre for Male Health and Wellbeing, University of Adelaide, South Australian Health and Medical Research Institute, Adelaide, South Australia 5001, Australia. Phone: 618-8128-4360; E-mail: lisa.butler@adelaide.edu.au

Cancer Res 2021;81:4981–93

doi: 10.1158/0008-5472.CAN-20-3863

©2021 American Association for Cancer Research

Downloaded from cancerres.aacrjournals.org on October 20, 2021. © 2021 American Association for Cancer Research.

Published OnlineFirst August 6, 2021; DOI: 10.1158/0008-5472.CAN-20-3863

changes in the tumor lipidome, which may reveal new resistance-related vulnerabilities, remain completely unexplored.

To gain insight into the potentially targetable changes in the lipid composition of prostate cancer, we employed a quantitative MS-based lipidomics approach coupled with MS imaging (MSI) to robustly analyze and visualize a wide range of intact phospholipid (PL) species in malignant and matched nonmalignant tissues. Our results provide the first comprehensive picture of the lipidomic landscape in a clinical cancer context and reveal robust associations with malignancy. We further demonstrate treatment-related changes in the lipidome accompanying response to enzalutamide, an AR antagonist widely used in the management of prostate cancer, in patient-derived explants (PDE) of clinical prostate tissues. Finally, we report that an inhibitor of acetyl-CoA carboxylase (ACC) was effective in pharmacologically targeting the most recurrent tumor-related lipidomic alterations.

Materials and Methods

Tissue collection

Matched normal/tumor cohort

Prostate tumor tissues with matching normal samples were obtained from previously untreated patients who had undergone radical prostatectomy (Centre Hospitalier Universitaire de Liège, Liège, Belgium). Samples were snap frozen and stored at −80°C for lipid and protein extractions. Normal and tumor tissues were identified by histologic analysis of adjacent tissue, Gleason scores were determined, and the percentage of cancer was estimated (18). All tumor samples used for lipidomics were verified to contain at least 75% prostate adenocarcinoma by histologic examination. The Local Commission for Medical Ethics and Clinical Studies at the University of Liège (Liège, Belgium) approved the use of clinical samples. Approval to perform lipidomics analysis on clinical samples was obtained from the local Ethical Committee of KU Leuven (Leuven, Belgium).

Unmatched patient tissue cohort

Prostate tissues were collected with written informed consent from previously untreated patients undergoing radical prostatectomy at St Andrew's Hospital, Adelaide, Australia, through the Australian Prostate Cancer BioResource. A longitudinal section of each tissue was removed prior to *ex vivo* culture (described below). Half was snap frozen and the remainder fixed in formalin and paraffin embedded for assessment by a pathologist. Ethical approval for tissue collection and experimentation was obtained from St Andrew's and the University of Adelaide Human Research Ethics committees and all experiments with patient material were performed in accordance with the National Health and Medical Research Council of Australia guidelines. Histopathologic features of all tumors used in this study are detailed in Supplementary Table S1; an additional 5 patients with only benign prostatic hyperplasia and no evidence of cancer were also analyzed with this cohort.

Ex vivo culture of primary prostate tissues

Prostate specimens were dissected and cultured as PDEs in RPMI medium containing 10% FCS for 48 hours in the presence and absence of enzalutamide (Selleckchem; 10 or 50 μmol/L) or the ACC1/2 inhibitor PF-05175157 (Pfizer; 10, 25, or 50 μmol/L), as described previously (19). In each case, following culture, tissue was formalin fixed and paraffin embedded for histology or snap frozen for lipidomics and/or RNA extraction.

MALDI-MSI

Frozen sections of prostate tissue (10 μm) were thaw mounted on Superfrost Ultra Plus microscope slides and matrix (10 mg/mL α-CHCA in methanol) applied to tissue sections by sublimation. The sections were analyzed on a MALDI SYNAPT HDMS Mass Spectrometer (Waters Corporation). The laser raster size was set at 60 μm (*x,y*) and off-tissue areas provided QC spots for data filtering. MALDI raw spectrum files were converted to MSI data files by high definition imaging software (Waters Corporation). The data processing settings were resolution 8,000 full-width half-height (FWHM) at mass window of 0.02 Da at a (restricted) mass range of *m/z* 400–990 Da. The top 1,000 mass features were selected for processing and statistical analysis was carried out using the web-based *MetaboAnalyst R* package (www.metaboanalyst.ca; ref. 20). The MSI ion map were overlaid or aligned to adjacent pathologically annotated histopathology images to identify morphologic regions of interest (ROI). Equivalent number of data points (3 pixels/mass spectra) from multifocal adenocarcinoma areas and off-tissue regions were selected. The data points were then exported as a single .csv file in the form of ROI's versus mass features with relative intensity (abundance) as the variable. Before import into *MetaboAnalyst*, the data were filtered in R studio 3.4.4 using baseline packages. The prefiltered .csv files were uploaded into *MetaboAnalyst R* in the format of spectral bins, data filtering was done by interquantile range and data was normalized by log transformation and pareto scaling. Heatmaps were generated by hierarchical clustering and top 25 mass features (identified by ANOVA) were visualized. Principal component analysis (PCA) score plots indicated the relative variation of multifocal ROI's based on distribution of lipid species. For negative ion mode imaging, the methodology was adapted as follows: Norharmane matrix (7 mg/mL; Sigma-Aldrich) in CHCl3:MeOH [7:3 volume for volume (v/v)] was applied to the tissue sections with a SunCollect sprayer (SunChrom). Data processing settings were resolution 8,000 FWHM at mass window of 0.02 Da at a (restricted) mass range of *m/z* 50–990 Da. Full-scan MSI data were imported into Python and a custom script used for ROI selection. All images, mass spectra and boxplots were generated after total ion current normalization of the acquired data.

For validation of ESI-MS/MS data in patient-derived explants, we conducted MALDI imaging using a timsTOF FleX mass spectrometer (Bruker Daltonik). Briefly, 10-μm-thick frozen tissue sections were thaw mounted onto indium tin oxide slides, spray coated with approximately 500 μL of 7 mg/mL α-CHCA matrix using a SunCollect MALDI sprayer (Sunchrom GmbH). Data were acquired with a 20 μm pixel size and a 20 μm laser step size over *m/z* 50–1,250. Imaging data were imported into SCiLS Lab 2020a (Bruker Daltonik). Spectra were normalized to total ion count, with weak denoising, and segmentation analysis was preformed using bisecting k-means algorithm with correlation distance metric in SCiLS Lab. Segments that aligned with the epithelia in matched hematoxylin and eosin–stained sections were selected for each tissue. Boxplots of the relative intensity of *m/z* of interest were generated from these segments.

ESI-MS/MS–based lipidomics

Lipid extracts were generated by homogenizing approximately 40 mg of tissue in 800 μL PBS with a Dounce or a Precellys 24 (Bertin Technologies) homogenizer. An aliquot of 100 μL was set aside for DNA quantification. The remaining 700 μL was transferred to a glass tube with Teflon liner and 900 μL 1N HCl:CH_3OH 1:8 (v/v), 800 μL $CHCl_3$ and 500 μg of the antioxidant 2,6-di-tert-butyl-4-methylphenol (Sigma) were added. DNA concentration was measured using Hoechst 33258 reagent (Calbiochem). The appropriate lipid standards (Avanti

Downloaded from cancerres.aacrjournals.org on October 20, 2021. © 2021 American Association for Cancer Research.

Published OnlineFirst August 6, 2021; DOI: 10.1158/0008-5472.CAN-20-3863

Polar Lipids Inc.) were added on the basis of the amount of DNA of the original sample (per mg DNA: 150 nmol PC26:0; 50 nmol PC28:0; 150 nmol PC40:0; 75 nmol PE28:0; 8.61 nmol PI25:0 and 3 nmol PS28:0). After mixing for 5 minutes in a rotary shaker and phase separation (by centrifugation at 17,300 × *g*, for 5 minutes at 4°C), the lower organic fraction was collected using a glass Pasteur pipette and evaporated using a Savant Speedvac spd111v (Thermo Fisher Scientific). The remaining lipid pellet was covered with argon gas and stored at −20°C. Before ESI-MS/MS measurement, lipid pellets were reconstituted in diluent (CH_3OH:$CHCl_3$:NH_4OH; 90:10:1.25, v/v/v) according to the amount of DNA in the original cell sample (1 μL diluent/1 μg DNA). PL species were analyzed by ESI-MS/MS on a hybrid quadrupole linear ion trap mass spectrometer (4000 QTRAP system; Applied Biosystems) equipped with an Advion TriVersa robotic nanosource for automated sample injection (Advion Biosciences). For quantification of individual PL species, the system was operated in multiple reaction monitoring (MRM) mode. MRM transitions were built based on the release of the PL head group as ion or as neutral species during tandem MS experiments. Analysis was performed using Rapid Lipid Profiling v2.2. Data were corrected for carbon isotope effects. Blank samples consisting of only diluent were measured to determine background signals. Only PL species with an intensity > 5-fold the intensity of the blank were considered true signals. PL were annotated using "lipid subclass," with an "L" denoting the lyso form, and the "C" followed by the total fatty acyl chain length:total number of unsaturated bonds." The circos plot of lipidomic alterations was generated using the circlize R package (21).

RNA extraction and sequencing

RNA was extracted from cultured PDE tissues as described previously (22). Total RNA samples were treated with Ribo-Zero to deplete rRNA prior to library construction with the Illumina TruSeq RNA kit. Sequencing was performed on an Illumina NextSeq 500 to generate 1 × 100 bp single-end reads. Library preparation and sequencing were performed at the Genomics Facility of the South Australian Health and Medical Research Institute (Adelaide, Australia). The quality and number of reads for each sample were assessed with FastQC v0.11.3. Adaptors were trimmed from reads, and low-quality bases, with Phred scores < 28, were trimmed from ends of reads, using Trimgalore v0.4.4. Trimmed reads of <20 nucleotides were discarded. Reads passing all quality control steps were aligned to the hg38 assembly of the human genome using TopHat v2.1.1 (23) allowing for up to two mismatches. Reads not uniquely aligned to the genome were discarded. HTSeq-count v0.6.1 (24) was used with the union model to assign uniquely aligned reads to Ensembl Hg38.86-annotated genes. Data were normalized across libraries by the trimmed mean of M-values normalization method, implemented in the R v3.5.0, using Bioconductor v3.6 EdgeR v3.20.9 package (25). Only genes expressed at a count per million above 0.5 for at least 18 of 36 samples were analyzed for evidence of differential gene expression. Differentially expressed genes were identified using the quasi-likelihood negative binomial generalized log-linear model implemented in EdgeR and were defined as having an FDR-adjusted *P* value of < 0.05. Gene set enrichment analysis (GSEA) was undertaken using camera function in the R limma v3.34.9 package. RNA sequencing data are available through NCBI's Gene Expression Omnibus as GSE180628.

IHC staining

Sections (3 μm) of paraffin-embedded cultured PDEs were immunostained essentially as described previously (19). Briefly, antigen retrieval was performed using Tris-EDTA buffer, pH 6.5 using a Biocare Medical Nexgen decloaker at 115°C for 15 minutes. Tissue slides were then incubated at room temperature with 10% goat serum block. Primary antibody against the proliferative marker Ki67 (DAKO, M7240; 1:200), ERG (Abcam, ab92513; 1:400), PIN-4 antibody cocktail (mixture of p63, 34 beta E12 and AMACR; Biocare medical - Metagene Pty Ltd.) or pACC1 (Ser79, Cell Signaling Technology, 3661S; 1:400) was applied and slides incubated overnight at 4°C. Secondary antibody anti-rabbit (DAKO E0432, lot no. 20027287) was applied for 1 hour, followed by horseradish peroxidase–conjugated streptavidin (DAKO, P0397, lot no. 20040879) at 1:500 for 1 hour and visualization by 3,3′-diaminobenzidine (DAB).

Statistical analysis

Matched patient tissues: cohort A

In the $n = 21$ cohort with matched tumor and disease-free tissue, a mixed effects regression of the within individual difference in lipid variables was constructed, adjusting for lipid variable in normal tissue sample and individuals' age. A random intercept was included per batch, error variance was allowed to differ with batch, and a compound symmetry correlation structure for errors within batches (R package nlme). Restricted maximum likelihoods of this full model is compared with a reduced model without the error variance and correlation structure and the full model chosen only when two times the difference in log likelihoods exceeded the 95th percentile of $\chi^2(\mathrm{df} = 1) = 3.84$. The lipid variables consisted of $\log_2$-transformed species abundance, saturation group abundance, and saturation group mean chain length. Prior to these calculations, lipid species abundances in each sample were standardized to the median abundance across all samples (26).

Unmatched patient tissues: cohort B

In the cohort of $n = 47$ with single-tissue samples per individual, for associations with sample malignancy or ERG status similar mixed effects regression to those described above (same random effects structure) were constructed for each lipid variable as outcome; however, the only fixed effect covariate was age. In the subset of 28 individuals with malignant samples, associations between lipid variables and serum prostate-specific antigen (PSA) employed the same mixed effects regression models with sample malignancy replaced by log-transformed PSA as a fixed effect and sample Gleason score included as an additional covariate.

Proliferation associations

For associations with Ki67 both in day 0 samples and in vehicle-treated versus enzalutamide-treated samples, we analyze repeated count data across fields of view within a sample using a beta-binomial mixed effects regression (R package glmmTMB). In the day 0 analyses, the lipid variables are the primary predictors of interest with batch and age being included as fixed effect covariates. In the treated samples, the primary predictor of interest is the batch-adjusted difference between enzalutamide and vehicle, with batch, age and lipid variable vehicle as fixed effects. In all models, a random intercept is included per individual, with a logit link for the mean Ki67 cell positivity prevalence.

For each set of outcomes, the distribution of *P* values for the species abundance associations is assessed to determine the presence of a signal (deviation from the uniform distribution; ref. 27) and the FDR reported for the number of significant associations defined as $P < 0.01$. To address concerns that an apparent signal may be due to a combination of insufficient comparisons and clustering between lipid species, we perform a permutation test with 1,000 permutations of the clinical outcome, and define the fraction of significant associations

Downloaded from cancerres.aacrjournals.org on October 20, 2021. © 2021 American Association for Cancer Research.

Published OnlineFirst August 6, 2021; DOI: 10.1158/0008-5472.CAN-20-3863

are beyond that observed in the original cohort as the permutation P value. These permutation analyses are performed within batches and where appropriate within malignancy groups, and by design retain the between lipid correlation structure.

Other statistical analyses

Statistical analysis for lipid or immunostaining quantification and PDE culture experiments, was carried out using GraphPad Prism software v7.02 (2016, GraphPad Software). Significance was measured by two-tailed unpaired t test or one-way ANOVA with Dunnett multiple comparison test as indicated. Significance is expressed as *, $P < 0.05$; **, $P < 0.01$; and ***, $P < 0.001$.

Results

Tumor-specific lipid profiles are evident in clinical prostate tumors

Spatial variation in PL composition was initially assessed in a set of clinical prostate tumors that contained discrete benign and malignant areas of epithelium within the same tissue section, using MALDI-MSI. Shown in **Fig. 1A** is a representative tumor in which comparison of spectral data from these regions revealed a tumor-specific PL composition that was distinct from that detected in pathologically benign epithelium or a region of high-grade prostatic intraepithelial neoplasia (PIN) from the same patient (**Fig. 1B**; Supplementary Fig. S1A). Distinct PL MS and specific masses (e.g., m/z 756.53; **Fig. 1A**) were consistently detected in multiple independent tumor regions assessed across 3 individual patients with prostate cancer (Supplementary Fig. S1B and S1C), consistent with recent reports that characteristic changes in lipid composition accompany prostate tumorigenesis (16, 17).

In light of these findings, we undertook a more detailed examination and quantification of tumor-related changes in PL composition using shotgun lipidomics incorporating electrospray tandem MS in pathologist-microdissected regions of prostate tumor and matched benign tissues from 21 patients with prostate cancer (**Fig. 1C**). Clinicopathologic data for the patients are summarized in Supplementary Table S1. Using this methodology, a total of 108 PL species of the four most abundant subclasses (PC, PE, PS, and PI) could be detected and quantified. PL profiles of both cancer and normal tissues were dominated by PC species, and the total proportion of PC lipids was greater in tumor than in benign tissues for this cohort (Supplementary Fig. S2A; $P < 0.05$). There was a significant tumor-specific increase in the collective abundance of PL species with one or two double bonds, most evident in the PC lipids (**Fig. 1D**). As these mainly represent species with one or two monounsaturated fatty acyl (MUFA) chains, this shift altered PL composition towards a greater overall proportion of MUFAs in the tumors, consistent with a lipogenic tumor phenotype (11).

Shown in **Fig. 1E** is a circos plot summarizing the individual tumor-related lipidomic changes for this cohort of patients. PL are annotated by "lipid subclass" followed by the "total fatty acyl chain length:total number of unsaturated bonds" (e.g., PC 34:1). The species in each PL class are ordered from fully saturated to highly polyunsaturated and, within each subgroup, from shortest to longest (combined) acyl chain length. When considering the relative abundance of individual PL species, consistent patterns of change in PL saturation groups were more evident within certain lipid classes (**Fig. 1E**, outer circle). Most notably, PC species had tumor-related increases in fatty acyl chains containing one or two double bonds, indicative of MUFAs, accompanied by relative decreases in polyunsaturated fatty acyl (PUFA; ≥3 double bonds) and fully saturated (0 double bonds) species. In PS species, however, marked increases in long PUFA species were evident across multiple saturation groups in tumor compared with benign tissue.

Consistent changes across patients were also detected in the fatty acyl chain lengths of tumor PLs. To most optimally visualize altered acyl chain length, we expressed the abundance of each PL species in tumors and matching benign tissue relative to the shortest PL species of each saturation subclass (**Fig. 1E**, inner circle; denoted "elongation index"). Whereas substantial heterogeneity in fatty acyl chain length existed between individual patients for PC and PE lipids (Supplementary Fig. S2B), almost every tumor exhibited increased combined acyl chain length over multiple saturation groups of the PI and PS classes compared to normal tissue, particularly for polyunsaturated species (**Fig. 1D**; Supplementary Fig. S2B). This was validated within the cohort as a significant increase in average chain length for polyunsaturated PI and PS lipids (Supplementary Fig. S2C).

Associations between lipid profiles and malignancy

On the basis of the above observations, we investigated whether there were associations between any lipid measures and sample malignancy status. Linear mixed effects models regressed lipid measures from malignant samples onto the equivalent values from benign samples, adjusting for age and batch. We specifically considered (i) abundance of individual lipid species, (ii) saturation group abundance, and (iii) fatty acyl chain length per saturation group. The permutation analysis indicated that there were associations between lipid profile and malignancy beyond what would be expected by chance (Supplementary Fig. S3A; permutation $P < 0.001$). Of the 51 lipid features most strongly associated with malignant versus benign prostate tissue, 34 were individual lipid species (**Fig. 2A**; Supplementary Table S2), five were mean chain lengths within saturation groups and 12 were overall saturation group abundance (Supplementary Fig. S3B; Supplementary Table S2). As expected, certain individual species cross-correlated within and across head group classes (**Fig. 2B**).

We subsequently assessed whether similar malignancy-associated lipidomic profiles would also be evident in an independent collection of 47 non-patient-matched tissue specimens comprising 26 tumors and 21 benign samples (**Fig. 2C**). A greater range of lipids were measured in this cohort ($n = 248$), and included sphingomyelins, ceramides (Cer) and lysoPLs (containing only one fatty acyl chain) in addition to the main four PL classes analyzed above. Using the same criteria as for the paired cohort, a substantial signal was again detected in terms of FDR for significant associations between lipid features and sample malignancy (Supplementary Fig. S3A). Associations were detected for 64 lipid features, including 44 individual lipid species (FDR = 0.03; permutation $P < 0.001$; Supplementary Fig. S3C–S3E; Supplementary Table S3), and for this cohort cross-correlation within and across head group classes was again evident for certain species (Supplementary Fig. S3F).

There was considerable overlap in the lipid features identified in both cohorts, and by combining data from both cohorts, we identified a series of lipids that robustly associated with prostate tumor malignancy (**Table 1**). Shown in **Fig. 2D** are representative examples of these lipids demonstrating concordant associations with malignancy across the individual cohorts and batches, which included the abundance of monounsaturated PC lipids (PC1 SA), individual lipids PE 42:6 and PI 36:4, and chain length in monounsaturated PI lipids (PI1 CL). Consistent with these data, MALDI-MSI on two patient tissues imaged

Downloaded from cancerres.aacrjournals.org on October 20, 2021. © 2021 American Association for Cancer Research.

Published OnlineFirst August 6, 2021; DOI: 10.1158/0008-5472.CAN-20-3863

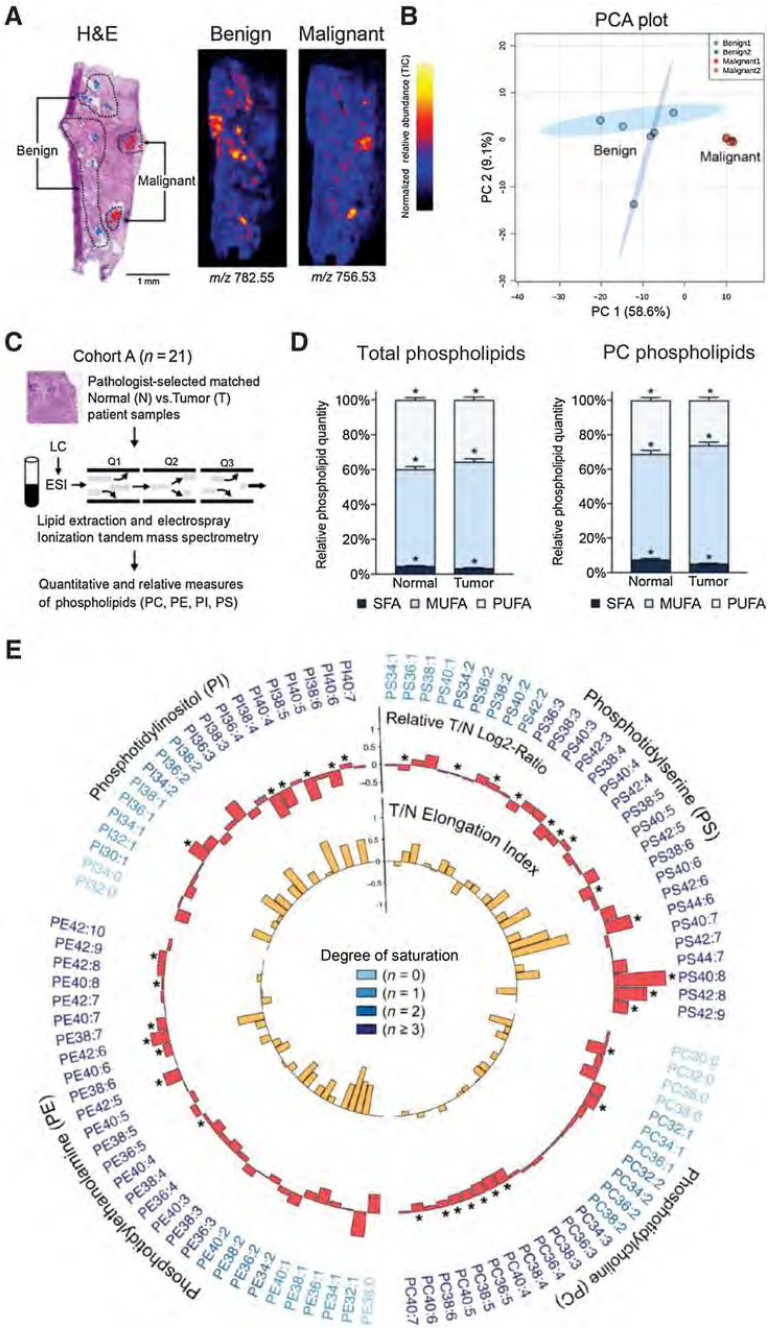

Figure 1.
Evidence for a tumor-associated lipidome in clinical prostate cancer. **A,** MALDI-MSI of pathologically heterogeneous prostate tissue, including ion maps of two representative examples of histology-restricted lipid masses within a single tissue [i.e., benign versus malignant localization; pathology annotation in hematoxyin and eosin (H&E) panel on left]. **B,** PCA of the top 25 mass features distinguishing benign from malignant regions of tissue. **C,** Workflow for shotgun lipidomics analysis of matched normal and tumor tissues from 21 patients with prostate cancer. **D,** Relative proportions of phospholipids containing 0 (SFA), 1 or 2 (MUFA), or 3 or greater (PUFA) unsaturations compared in benign versus tumor specimens. *, $P < 0.05$. **E,** Circos plot of tumor-related lipidomic changes in relative abundance and fatty acyl chain elongation across the patient cohort. The outer circle represents the ratio of median-adjusted normalized abundance of individual lipid species in tumor versus benign tissues. *, reflects significant association with malignancy ($P < 0.01$). The inner circle represents fatty acid elongation index in tumor versus benign tissues. Lipids are annotated using "lipid subclass," followed by the "total fatty acyl chain length:total number of unsaturated bonds."

Downloaded from cancerres.aacrjournals.org on October 20, 2021. © 2021 American Association for Cancer Research.

Published OnlineFirst August 6, 2021; DOI: 10.1158/0008-5472.CAN-20-3863

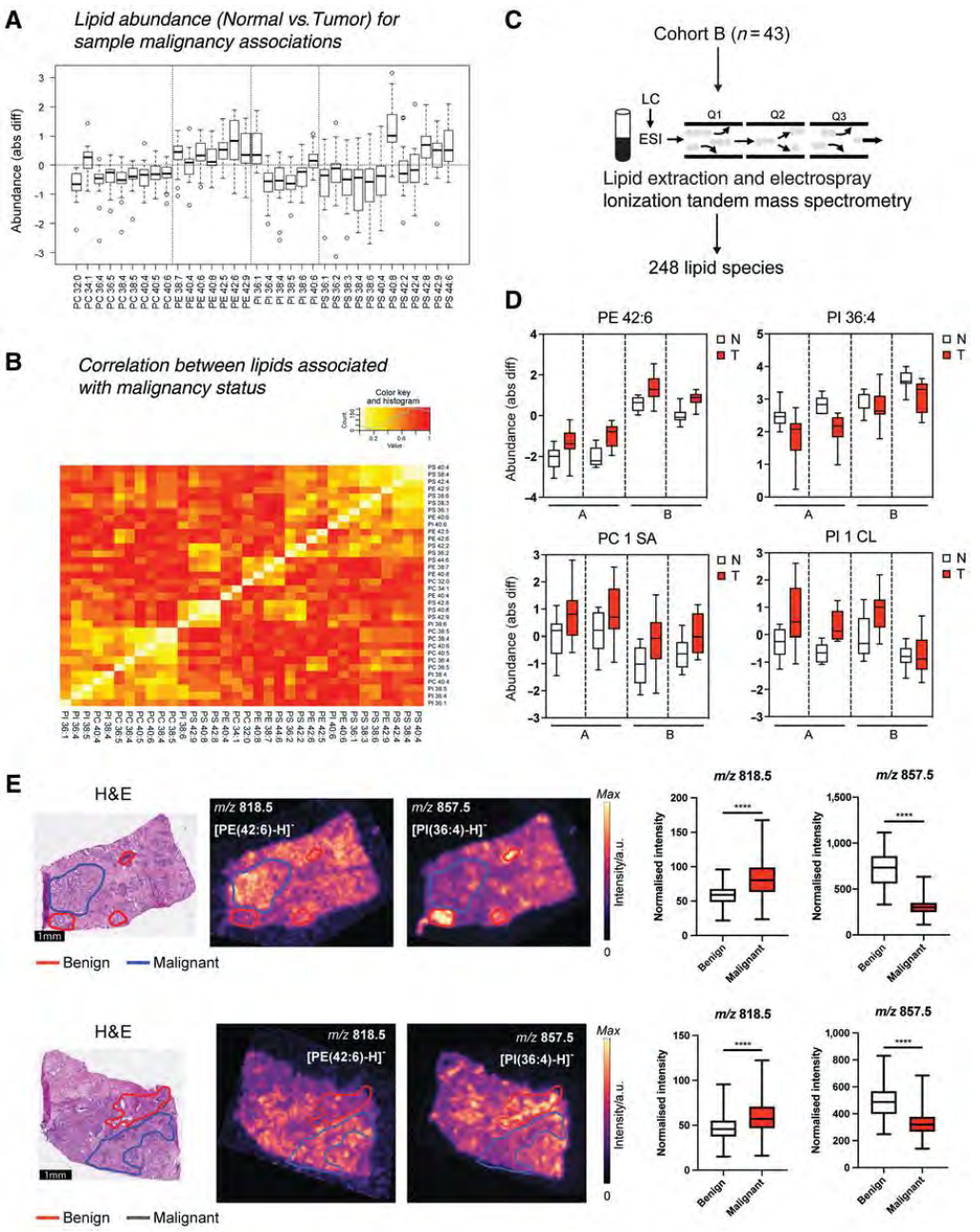

Figure 2.

Associations of lipid profile with malignancy. **A,** Lipid variables significantly associated with tumor versus matched benign tissues in cohort A ($P < 0.01$). **B,** Spearman correlation plot of individual phospholipid species significantly associated with sample malignancy in cohort A. **C,** Workflow for lipidomics analysis of unmatched patient tissue cohort B ($n = 47$). **D,** Boxplots of representative examples of different phospholipid variables significantly associated with sample malignancy across both patient cohorts A and B. **E,** MALDI-MSI of ion masses corresponding to PE 42:6 (*m/z* 818.5) and PI 36:4 (*m/z* 857.5) in two independent prostate cancer tissues, with boxplots of normalized ion intensity between nonmalignant and malignant tissues regions adjacent to the images. ****, $P < 0.001$. H&E, hematoxylin and eosin.

Downloaded from cancerres.aacrjournals.org on October 20, 2021. © 2021 American Association for Cancer Research.

Published OnlineFirst August 6, 2021; DOI: 10.1158/0008-5472.CAN-20-3863

Table 1. Conserved lipid associations with malignancy in clinical prostate samples.

Variable	Lipid ID	Est [95% CI]	*P*
Lipid abundance	PI 38:6	−0.35 [−0.36, −0.33]	6.52E-19
	PI 40:6	0.19 [0.18–0.21]	1.78E-14
	PS 40:8	1.10 [1.00–1.20]	6.40E-14
	PC 36:4	−0.56 [−0.64, −0.49]	3.51E-11
	PC 34:1	0.17 [0.14–0.20]	5.81E-10
	PC 40:4	−0.45 [−0.57, −0.33]	1.18E-06
	PI 38:5	−0.68 [−0.89, −0.48]	4.51E-06
	PS 42:8	0.70 [0.50–0.90]	2.20E-05
	PS 42:2	−0.26 [−0.35, −0.16]	4.08E-05
	PS 42:4	−0.23 [−0.32, −0.14]	8.25E-05
	PE 42:6	0.75 [0.44–1.06]	0.000149
	PI 36:4	−0.68 [−0.96, −0.39]	0.000203
	PE 42:5	0.51 [0.29–0.74]	0.000255
	PS 38:4	−0.66 [−0.96, −0.36]	0.000399
	PC 38:4	−0.52 [−0.77, −0.27]	0.000693
	PS 36:2	−0.32 [−0.48, −0.16]	0.000753
	PS 36:1	−0.46 [−0.68, −0.23]	0.000789
	PC 32:0	−0.66 [−0.98, −0.33]	0.000832
	PS 38:3	−0.72 [−1.08, −0.36]	0.000942
	PC 40:6	−0.36 [−0.55, −0.18]	0.001045
	PS 38:6	−0.82 [−1.24, −0.40]	0.001116
	PE 40:4	0.042 [0.02–0.065]	0.001414
	PC 38:5	−0.38 [−0.59, −0.18]	0.001489
	PE 38:7	0.36 [0.17–0.56]	0.001681
	PI 38:4	−0.50 [−0.80, −0.20]	0.001944
	PC 36:5	−0.40 [−0.60, −0.20]	0.002105
	PS 44:6	0.52 [0.23–0.81]	0.002306
	PI 36:1	0.51 [0.22–0.80]	0.00274
	PS 42:9	0.47 [0.19–0.75]	0.003707
	PS 40:4	−0.48 [−0.77, −0.20]	0.003719
	PE 42:9	0.45 [0.16–0.73]	0.005855
	PE 40:6	0.36 [0.13–0.60]	0.006456
	PE 40:8	0.28 [0.10–0.46]	0.006487
	PC 40:5	−0.30 [−0.50, −0.10]	0.008872
Mean chain length	PE 3	−0.13 [−0.14, −0.12]	7.43E-14
	PS 1	0.13 [0.07–0.18]	0.000187
	PE 6	0.11 [0.06–0.15]	0.000209
	PI 1	0.19 [0.11–0.27]	0.000231
	PS 3	0.096 [0.048–0.144]	0.000948
Saturation abundance	PC 6	−0.0021 [−0.0024, −0.0017]	6.10E-10
	PI 2	0.013 [0.01–0.015]	2.16E-08
	PE 3	0.0029 [0.0022–0.0037]	9.74E-07
	PS 8	0.0036 [0.0026–0.0046]	1.82E-06
	PS 9	0.00078 [0.00048–0.00108]	6.25E-05
	PC 4	−0.038 [−0.056, −0.021]	0.00046
	PC 1	0.066 [0.033–0.098]	0.000959
	PC 5	−0.0071 [−0.0107, −0.0034]	0.001172
	PI 5	−0.0016 [−0.0025, −7e-04]	0.002608
	PS 3	−0.0088 [−0.0139, −0.0036]	0.003266
	PC 0	−0.013 [−0.021, −0.005]	0.004081
	PS 4	−0.0079 [−0.0133, −0.0025]	0.009611

Note: Analyses represent data from two cohorts of patients, with individual tissue samples taken from each patient in the cohort. For mean chain length and saturation abundance, lipids are grouped by saturation number.

in negative ion mode revealed the expected changes in relative abundance of masses corresponding to PE 42:6 (*m/z* 818.5) and PI 36:4 (*m/z* 857.5) in malignant versus nonmalignant regions of the tissues (**Fig. 2E**; boxplots of normalized mass intensity shown adjacent to ion map images; Supplementary Fig. S3G).

Characteristic lipid profiles are evident in ERG-positive tumors

We did not detect robust associations with standard clinical parameters for prostate cancer such as serum PSA (Supplementary Fig. S4A; permutation $P = 0.79$) and Gleason Score (Supplementary Fig. S4A; permutation $P = 0.24$), but there was evidence for weak associations between lipid profile and proliferation (Ki67 marker positivity index) in malignant samples (Supplementary Fig. S4B and S4C; Supplementary Table S4; permutation $P = 0.10$). The very low frequency of genomic alterations in clinically localized prostate cancer constrained our ability to associate lipids with genomic features. Nevertheless, we detected associations between the most common clinical aberration (∼50%; *TMPRSS2-ERG* fusion, detected by ERG immunoreactivity; **Fig. 3A**) and tumor lipid profile in our cohort (Supplementary Fig. S4A and S4D; Supplementary Table S5; permutation $P = 0.05$). ERG-positive tumors featured altered abundance of PC, PE, and ceramide species across multiple saturation groups (**Fig. 3B**; Supplementary Fig. S4D).

Lipid profile is altered by AR inhibition in patient-derived tumor explants

From the cohort of 47 unmatched samples analyzed above, 43 of the samples were also cultured *ex vivo* as PDEs in the absence and presence of the clinical antiandrogen, enzalutamide ($n = 24$ cultured with 10 μmol/L enzalutamide, $n = 19$ cultured with 10 and 50 μmol/L enzalutamide; **Fig. 4A**). This provided the unique opportunity to examine dynamic, treatment-related changes in lipid composition using patient-matched samples. *Ex vivo* culture alone had a minimal effect on lipid profile; 80% of lipid species had a correlation >0.5 between uncultured and cultured tissues (Supplementary Fig. S5A). Transcript profiling and GSEA performed on a subset of these samples ($n = 12$) confirmed significant downregulation by enzalutamide (10 μmol/L) of androgen signaling and multiple pathways associated with metabolism (**Fig. 4B**). Independent qPCR validation confirmed the decrease in expression of canonical AR target genes *kallikrein 3* (encoding PSA) and *kallikrein 2* gene across the majority of samples (Supplementary Fig. S5B). As expected on the basis of clinical trial outcomes (28, 29), the PDEs showed substantial heterogeneity in proliferative response to enzalutamide, measured as change in Ki67 proliferative index from matched vehicle-treated tissue (**Fig. 4A**). The above features of the enzalutamide-treated PDEs were conducive to analysis of treatment-related dynamic changes in PL profile, and associations with decreased Ki67 index in individual samples. Enzalutamide-related changes in 18 PL variables (including 15 individual species, enriched for long-chain PC and PE lipids that were also identified as malignancy-related lipids) were associated with change in Ki67 proliferation index (Supplementary Fig. S5C; Supplementary Table S6; **Fig. 4C**). MALDI-MSI analysis of a subset of PDE tissues indicated that the majority of individual response-related lipids identified reflected the epithelial regions of the tumors, and treatment-related changes in abundance were evident (example of PC34:1, also a malignancy-associated lipid, shown in **Fig. 4D**, boxplots in Supplementary Fig. S5D). Dynamic changes in PL profile were therefore associated with response to AR inhibition across this cohort of PDEs.

Targeting lipidomic changes in clinical tumors suppresses cellular proliferation

To determine whether the malignancy-associated alterations in PL composition directly influence cellular proliferation, or merely accompany tumorigenesis, we pharmacologically targeted two of the key lipidomic changes we detected (i.e., enhanced lipogenesis and elongation of fatty acyl chains in the PLs). Inhibition of ACC (ACC1/2),

Downloaded from cancerres.aacrjournals.org on October 20, 2021. © 2021 American Association for Cancer Research.

Published OnlineFirst August 6, 2021; DOI: 10.1158/0008-5472.CAN-20-3863

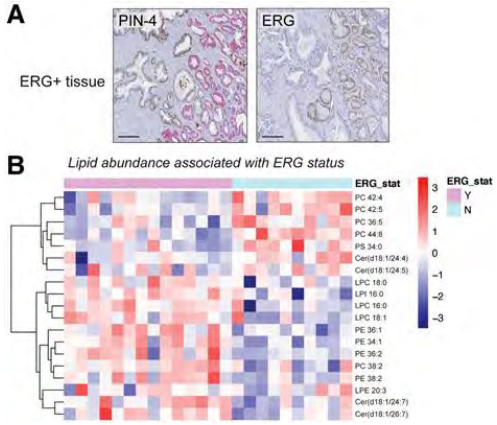

Figure 3.
Association of lipid profile with *TMPRSS2-ERG* gene fusion in clinical prostate tumors. **A,** Detection of *TMPRSS2-ERG* fusion via positive immunoreactivity for ERG in AMACR-positive (tumor) regions of tissues stained with PIN-4 triple antibody cocktail. **B,** Heatmap of individual lipid species significantly associated with ERG fusion status in individual patient tumors.

which depletes the cellular content of malonyl CoA, was selected as a strategy to simultaneously inhibit both synthesis and elongation of fatty acids (**Fig. 5A**). We utilized PF-05175157, an ACC1/2 inhibitor (30), as a proof of principle tool and evaluated its efficacy in PDEs. Culture of PDEs with PF-05175157 (10–50 μmol/L) for 48 hours (**Fig. 5B**) markedly suppressed epithelial cell proliferation and induced apoptosis ($n = 13$) compared with matched, vehicle-treated control tissues (**Fig. 5C**; Supplementary Fig. S6A). Enhanced epithelial staining of pACC1(Ser 79), a marker of ACC inhibition by PF-05175157 in prostate cancer cells (Supplementary Fig. S6B), confirmed that the agent was effectively targeting ACC activity ($P < 0.01$; **Fig. 5D**). Moreover, PL profiling by MS revealed a pronounced shortening of PL fatty acyl chains in the majority of PF-05175157-treated tumors (**Fig. 5E**; Supplementary Fig. S6C), confirmed as significant decreases in average chain length across all four main lipid classes (Supplementary Fig. S6D). Together, these data link the efficacy of PF-05175157 to ACC1 inhibition in the tissues.

Discussion

Using MS-based lipidomics to sensitively quantify and visualize PL species in clinical tissues, we have provided new insight into the changes in lipid composition that accompany prostate cancer development. Moreover, this is the first report of dynamic, treatment-related changes in lipidomic profiles and the efficacy of targeting lipid metabolic enzymes in a clinical tissue context. This study therefore moves beyond previous laboratory cell line–based approaches to demonstrate that, despite the observed heterogeneity at the level of individual lipid species, recurrent and clinically actionable changes in PL metabolism can be detected in tumors, some of which may represent common vulnerabilities. Lipidomic profiling of prostate tumor biopsies, possibly guided by imaging approaches as highlighted in several recent reports (16, 17), has the potential to provide new information about disease features and, potentially, patient responsiveness to therapeutics such as enzalutamide.

While robustly associated with sample malignancy, PL profile was only weakly linked to the most common clinicopathologic characteristics of prostate cancer; PSA levels and Gleason score. While this may reflect limitations in the sample size of our cohorts, it also raises the possibility that lipidomic profiling provides new and independent information regarding tumor biology and prognosis. Moreover, the associations we detected between lipid profile and Ki67 proliferative index are particularly interesting in light of our recent report of Ki67 status in localized prostate cancer being a significant predictive biomarker of subsequent metastatic relapse (31). Notably, ERG-fusion status of the tumors in our cohort was reflected in characteristic altered lipid profiles, providing further evidence that this early genomic aberration, which ultimately promotes disease progression, may be intimately linked to altered metabolism (32–34). As the first exploratory lipidomic study of this tumor subtype, an intriguing implication of our data is that the reduced PUFA and increased MUFA content of phospholipids we detected in ERG-positive cancers could render these tumors resistant to lipid peroxidation and ferroptosis, thereby enhancing their survival. Further exploration of this association in larger independent tissue cohorts is likely to reveal novel interventional strategies and biological insights based on tumor subtype-specific lipid metabolism.

Despite differences in the breadth and abundance of individual lipids measured, certain broader cancer-related changes in PL profile reported here support the findings of previous imaging-based studies in a range of cancers, notably for altered abundance and/or elongation of PC- and PI-based lipids and ceramides (reviewed in refs. 2, 35). While the functional consequences of individual lipid/pathway changes remain to be elucidated, PI lipids are of fundamental importance in cancer cells as they form the membrane scaffold for kinase and phosphatase activity that supports oncogenic signaling. Moreover, altered acyl chain length of PI-based lipids has been linked to p53 mutational status (36), a common genomic alteration in clinical prostate cancer, and altered PI abundance and signaling is characteristic of tumor hypoxia (37). The results are also largely consistent with our earlier observed overexpression of lipid synthetic enzymes, such as FASN, in cancer cells, which correlates with a shift towards MUFA-containing species, at the expense of PUFA-containing species (11). Similarly, the tumor-related shift from saturated to monounsaturated PC species that we found to be significantly associated with sample malignancy is concordant with the earlier observed overexpression of SCD in certain cancer tissues (38–41).

The novel changes in acyl chain length and head group switches detected in this study may be related to reported alterations in enzymes involved in acyl chain elongation including ELOVL enzymes, modulators of malonyl-CoA levels including ACC, FASN and malonyl-CoA decarboxylase and head group-modifying enzymes including PS decarboxylase (42–47). Tumor-specific activation/inactivation patterns of these individual enzymes, most likely driven by tumor-specific oncogenic signaling (48–53), may lead to the unique phospholipid profile that is characteristic for every individual tumor. In view of the evidence that the lipid composition of cellular membranes affects numerous aspects of cell biology (reviewed in ref. 54), including membrane fluidity and curvature, vesicle formation, signal transduction (55), ion channel activity (56, 57), susceptibility to lipid peroxidation (11), resistance to oxidative stress (11), energy metabolism (58), and uptake and response to chemotherapeutics (11), even subtle changes within the lipidome may be critical to support the cancer phenotype and treatment resistance. By utilizing clinical specimens and *ex vivo* culture, the current data provide information on which changes are a common feature of malignancy and which are patient

Downloaded from cancerres.aacrjournals.org on October 20, 2021. © 2021 American Association for Cancer Research.

Published OnlineFirst August 6, 2021; DOI: 10.1158/0008-5472.CAN-20-3863

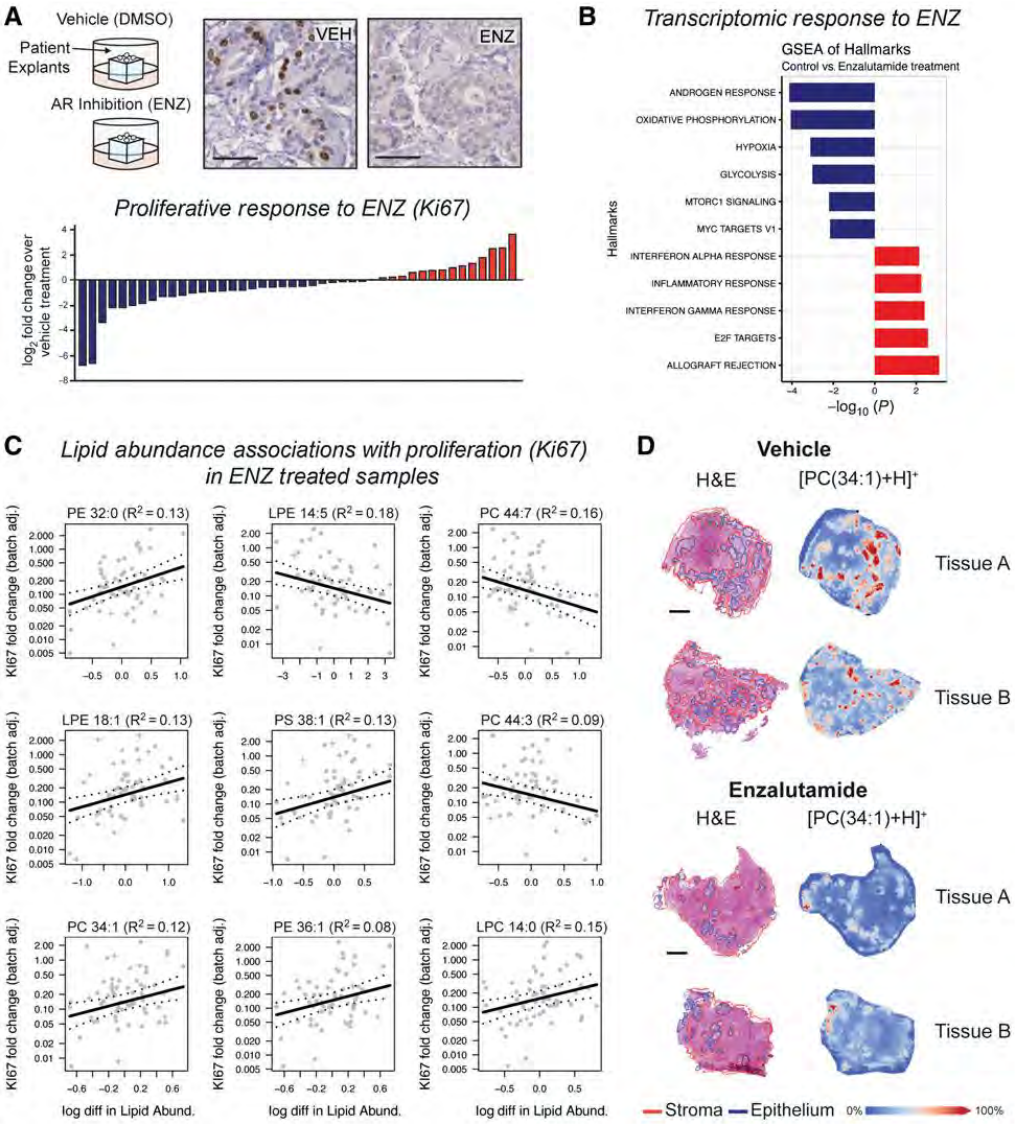

Figure 4.

Associations between lipid profile and tumor response to enzalutamide. **A,** Variation in proliferative response of prostate tissues to enzalutamide (ENZ) across cohort B. Top, PDE culture setup for prostate tissue from cohort B and Ki67 IHC in a representative sample. Bottom, waterfall plot of individual sample response to enzalutamide, measured as $\log_2$-fold change in Ki67 proliferative index. **B,** GSEA for transcriptomic data from enzalutamide versus vehicle-treated tissues ($n = 12$ patients). Blue pathways indicate reduced expression, while red indicates increased expression in response to enzalutamide. **C,** Correlation plots of lipid species whose change in abundance is significantly associated with response (change in Ki67 index) to enzalutamide ($P < 0.01$). **D,** MALDI-MSI of ion mass corresponding to $[PC(34:1)+H]^+$ in two independent samples from a single patient, showing epithelial localization and enzalutamide-related change in abundance. H&E, hematoxylin and eosin.

Downloaded from cancerres.aacrjournals.org on October 20, 2021. © 2021 American Association for Cancer Research.

Published OnlineFirst August 6, 2021; DOI: 10.1158/0008-5472.CAN-20-3863

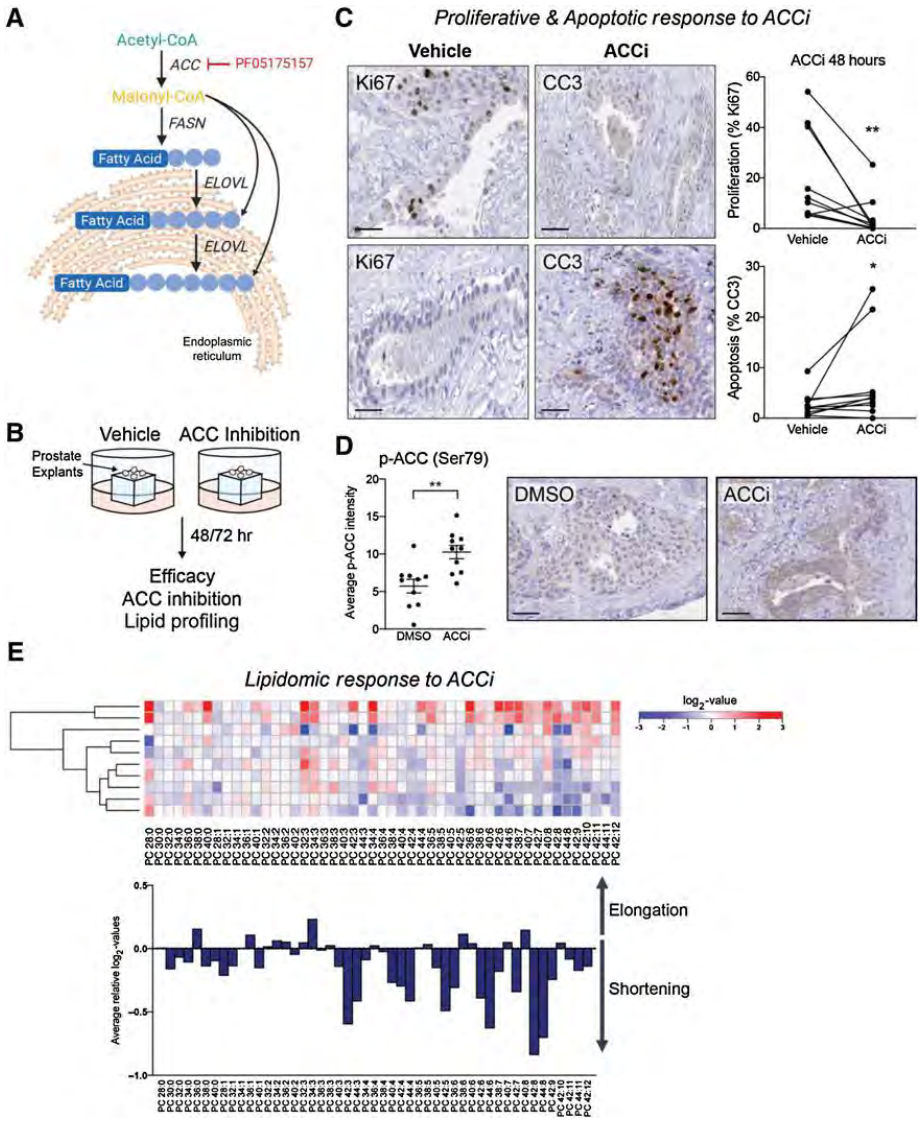

Figure 5.

Efficacy of acetyl CoA carboxylase inhibition in patient-derived prostate explants. **A,** The ACC1/2 inhibitor PF-05175157 targets fatty acid synthesis and chain elongation. **B,** PDE culture setup and workflow. **C,** Antiproliferative activity, measured by Ki67 proliferative index, and apoptosis, measured by cleaved caspase-3 positivity, of PF-05175157 (50 μmol/L) compared with vehicle-treated matched control tissue in PDEs cultured for 48 hours ($n = 13$ patients). **D,** IHC detection and quantification of pACC1 (Ser79) intensity in PDEs cultured in the absence and presence of PF-05175157. **E,** Treatment-induced alterations (expressed as $\log_2$-fold change in the heatmap) in PC phospholipid abundance for PDEs cultured with PF-05175157 compared with vehicle. Altered relative fatty acyl chain length for the lower cluster of PDEs is further visualized graphically. *, $P < 0.05$; **, $P < 0.01$.

specific, and also identifies clinical tumor lipidomic responses to a standard-of-care AR-targeted therapy. Interestingly, with the exception of a subset of PC- and PE-based species, the detected malignancy-associated lipid associations were mostly distinct from those for response to AR targeting in PDEs, but hold significant potential for biomarker discovery and identification of novel targets that may be used in a theranostic setting (59). Given the potential for culture media-derived lipids to influence tissue lipid metabolism and/or

Downloaded from cancerres.aacrjournals.org on October 20, 2021. © 2021 American Association for Cancer Research.

Published OnlineFirst August 6, 2021; DOI: 10.1158/0008-5472.CAN-20-3863

contribute to the lipidome in PDEs, the treatment response data provide a well-controlled, patient-matched baseline for future targeted validation in clinical trial specimens. This information is critical if such therapeutic strategies are to be tested in a clinical setting as, to date, therapies aimed at major metabolic processes have resulted in highly variable and noncurative responses in patients. It is likely to be more clinically impactful to precisely target the enzymes and pathways on which cancer cells are dependent, in a tissue- or patient-individualized manner, and anticipate likely redundancy pathways that may be activated.

While interpatient heterogeneity was evident in PL profiles from clinical prostate tumors in the current study, particularly at the individual lipid species level, more consistent changes in broader lipid metabolic processes were evident. Notable among these were proportionally higher fatty acid monounsaturation, and elongation of the PL fatty acyl chains. Considering these phenotypes, inhibition of ACC presented an appealing approach to simultaneously target *de novo* biosynthesis and elongation of intracellular fatty acids by restricting production of the substrate for long-chain fatty acid biosynthesis, malonyl CoA (60, 61). To date, the focus for development of ACC inhibitors has been their ability to inhibit *de novo* lipogenesis and increase fatty acid oxidation, thereby reducing lipid accumulation and improving insulin sensitivity in patients with diabetes or nonalcoholic liver steatosis. There has, however, been considerable interest in repurposing these agents for oncology, particularly for lipogenic tumors such as prostate and breast, in which potential side effects would be less of a concern. Here, as proof of principle, we utilized a spiroketone derivative ACC1/2 inhibitor, PF-05175157, developed by Pfizer as a clinical agent for treatment of type 2 diabetes and nonalcoholic hepatic steatosis (30). Our results show marked efficacy for this agent in reversing the chain elongation phenotype and reducing epithelial cell proliferation in clinical PDEs, raising the promise that this class of agents may be efficacious in clinical prostate cancer. While the possibility of off-target effects of this compound contributing to its antiproliferative effects cannot be discounted, we have used two lines of evidence to associate efficacy with ACC inhibition in the tissues. First, we assessed the tissue levels of Ser79-phosphorylated ACC1, which is the inactive form of ACC1, the predominant isoform in prostate cells. This phosphorylation was induced by PF-05175157 treatment of prostate cancer cells and in PDEs. Second, our PL profiling of the treated tissues revealed consistent shortening of the fatty acyl chains, indicative of decreased elongation reactions. Taken together, our findings provide the first evidence that ACC inhibition can be achieved in the context of a complex tumor microenvironment and provide impetus for further investigation of ACC inhibition in prostate cancer. Notably, there was little overlap in the lipidomic changes elicited in the tissues by ACC inhibition compared to AR targeting by enzalutamide; indeed, selectively targeting malignancy-associated lipid alterations achieved more consistent antiproliferative effects across patients in this preclinical context. In line with this notion, we recently reported that selective targeting of the main fatty acid elongase in prostate cancer, ELOVL5, consistently inhibits proliferation of prostate cancer cells in PDEs (47). In light of the marked tumor-associated changes in fatty acyl chain saturation, and particularly monounsaturation, detected here, future studies targeting desaturases such as SCD1, shown recently to be a promising therapeutic target in prostate cancer (62), would also distinguish causality from association for this alteration.

In summary, the cancer-related changes in PL profiles we have detected in clinical tissues strengthen the case for lipidomics as a source of novel molecular cancer biomarkers and therapeutic targets, as well as an indicator of the underlying biology from which PL profiles are derived. Defining subtypes of lipid profile in tumors, rather than immortalized cell lines, and the underlying mechanisms in this and other association-based studies are all critical future endeavors if key components of lipid metabolism are to be effectively targeted in clinical disease. The heterogeneity of prostate cancer evident from our work reinforces the concept that such approaches must also be personalized to the individual patient's biology. Our findings warrant further functional investigation of lipidomes in other cancer types, to unravel the molecular mechanisms underlying these changes and to explore the impact on membrane functioning and, ultimately, on cancer development and progression.

Authors' Disclosures

L.M. Butler reports grants from Movember Foundation, Prostate Cancer Foundation of Australia, U.S. Department of Defense, Cancer Council South Australia, and Cancer Australia during the conduct of the study. J. Machiels reports a patent for WO2012038525 licensed. E. Waelkens reports grants from European Community during the conduct of the study. L.A. Selth reports grants from Cancer Council SA and Movember/Prostate Cancer Foundation of Australia during the conduct of the study. P.J. Trim reports other support from University of Adelaide during the conduct of the study. M.F. Snel reports other support from University of Adelaide (L.M. Butler, main author) during the conduct of the study. L.G. Horvath reports other support from Exelexis, MSD, Pfizer, Eli-Lilly, Amgen, Novartis, Bristol Myers Squibb, Beigene, and Antagene outside the submitted work. M.M. Centenera reports grants from Prostate Cancer Foundation of Australia and Movember Foundation during the conduct of the study. J.V. Swinnen reports grants from The Movember Foundation/Prostate Cancer Foundation of Australia, Research Foundation - Flanders, Stichting tegen Kanker, Interreg V-A EMR23 "EURLIPIDS," Kom op tegen kanker, and Fondation Fournier-Majoie pour l'Innovation; grants and other support from KU Leuven during the conduct of the study; in addition, J.V. Swinnen has a patent for phospholipid profiling issued. No disclosures were reported by the other authors.

Authors' Contributions

L.M. Butler: Conceptualization, resources, data curation, supervision, funding acquisition, investigation, writing–original draft, project administration, writing–review and editing. **C.Y. Mah:** Data curation, formal analysis, investigation, visualization, writing–review and editing. **J. Machiels:** Formal analysis, investigation, visualization, methodology, writing–review and editing. **A.D. Vincent:** Data curation, software, formal analysis, validation, methodology, writing–review and editing. **S. Irani:** Investigation, writing–review and editing. **S.M. Mutuku:** Investigation, visualization, methodology, writing–review and editing. **X. Spotbeen:** Investigation, visualization, methodology, writing–review and editing. **M. Bagadi:** Investigation, methodology, writing–review and editing. **D. Waltregny:** Investigation, methodology, writing–review and editing. **M. Moldovan:** Data curation, formal analysis, investigation, writing–review and editing. **J. Dehairs:** Resources, data curation, software, formal analysis, investigation, methodology, writing–review and editing. **F. Vanderhoydonc:** Investigation, writing–review and editing. **K. Bloch:** Investigation, methodology, writing–review and editing. **R. Das:** Data curation, investigation, writing–review and editing. **J. Stahl:** Data curation, investigation, writing–review and editing. **J.G. Kench:** Data curation, investigation, writing–review and editing. **T. Gevaert:** Data curation, investigation, writing–review and editing. **R. Derua:** Investigation, methodology, writing–review and editing. **E. Waelkens:** Investigation, methodology, writing–review and editing. **Z.D. Nassar:** Supervision, writing–review and editing. **L.A. Selth:** Investigation, visualization, writing–review and editing. **P.J. Trim:** Supervision, investigation, visualization, methodology, writing–review and editing. **M.F. Snel:** Supervision, investigation, visualization, methodology, writing–review and editing. **D.J. Lynn:** Data curation, software, formal analysis, supervision, writing–review and editing. **W.D. Tilley:** Resources, funding acquisition, writing–review and editing. **L.G. Horvath:** Resources, funding acquisition, writing–review and editing. **M.M. Centenera:** Conceptualization, data curation, funding acquisition, investigation, visualization, methodology, writing–original draft, project administration, writing–review and editing. **J.V. Swinnen:** Conceptualization, resources, data curation, supervision, funding acquisition, investigation, visualization, methodology, writing–original draft, project administration, writing–review and editing.

Downloaded from cancerres.aacrjournals.org on October 20, 2021. © 2021 American Association for Cancer Research.

Published OnlineFirst August 6, 2021; DOI: 10.1158/0008-5472.CAN-20-3863

Acknowledgments

This research was supported by The Movember Foundation/Prostate Cancer Foundation of Australia (MRTA3); The Prostate Cancer Foundation of Australia (NDDA-4711); The U.S. Department of Defense (PC180582); The National Health and Medical Research Council (NHMRC) of Australia (1121057, 1130077, 1138242, 1145777); Cancer Australia (1138766); the Australian Cancer Research Foundation (Centre for Integrated Cancer Systems Biology); a Movember/NBCF Collaborative Linkage Grant (MNBCF-17-012), KU Leuven grants C1 (C16/15/073) and C3 (C32/17/052); Research Foundation - Flanders (FWO) grants G.841.15 and G0E0817N; Interreg V-A EMR23 EURLIPIDS; Stichting tegen Kanker; Kom op tegen Kanker; and the Fondation Fournier-Majoie pour l'Innovation. L.M. Butler was supported by a Future Fellowship from the Australian Research Council (FT130101004), and L.M. Butler and L.A. Selth are supported by Principal Cancer Research Fellowships (PRF1117 and PRF2919, respectively) awarded by Cancer Council's Beat Cancer project on behalf of its donors, the state Government through the Department of Health and the Australian Government through the Medical Research Future Fund. C.Y. Mah, R. Das, and S.M. Mutuku were supported by PhD Scholarships from the University of Adelaide, and C.Y. Mah and R. Das received Top-Up Scholarships from the Freemasons Centre for Male Health and Wellbeing at the University of Adelaide; Z.D. Nassar is supported by an Early Career Fellowship from the National Health and Medical Research Council of Australia (1138648); X. Spotbeen is supported by a Fellowship from the Research Foundation Flanders (FWO); D.J. Lynn is supported by an EMBL Australia group leader award; L.G. Horvath is supported by an Investigator Award from the National Health and Medical Research Council of Australia (1196225). The authors are grateful to the Belgian and Australian study participants, as well as the urologists, nurses, and histopathologists who assisted in the recruitment and collection of patient samples and clinical information.

The costs of publication of this article were defrayed in part by the payment of page charges. This article must therefore be hereby marked *advertisement* in accordance with 18 U.S.C. Section 1734 solely to indicate this fact.

Received November 24, 2020; revised June 7, 2021; accepted August 3, 2021; published first August 6, 2021.

References

1. Bray F, Ferlay J, Soerjomataram I, Siegel RL, Torre LA, Jemal A. Global cancer statistics 2018: GLOBOCAN estimates of incidence and mortality worldwide for 36 cancers in 185 countries. CA Cancer J Clin 2018;68:394–424.
2. Butler LM, Perone Y, Dehairs J, Lupien LE, de Laat V, Talebi A, et al. Lipids and cancer: emerging roles in pathogenesis, diagnosis and therapeutic intervention. Adv Drug Deliv Rev 2020;159:245–93.
3. Hanahan D, Weinberg RA. Hallmarks of cancer: the next generation. Cell 2011; 144:646–74.
4. Koundouros N, Poulogiannis G. Reprogramming of fatty acid metabolism in cancer. Br J Cancer 2020;122:4–22.
5. Bader DA, McGuire SE. Tumour metabolism and its unique properties in prostate adenocarcinoma. Nat Rev Urol 2020;17:214–31.
6. Zadra G, Loda M. Metabolic vulnerabilities of prostate cancer: diagnostic and therapeutic opportunities. Cold Spring Harb Perspect Med 2018;8: a030569.
7. Butler LM, Centenera MM, Swinnen JV. Androgen control of lipid metabolism in prostate cancer: novel insights and future applications. Endocr Relat Cancer 2016;23:R219–27.
8. Crowe FL, Appleby PN, Travis RC, Barnett M, Brasky TM, Bueno-de-Mesquita HB, et al. Circulating fatty acids and prostate cancer risk: individual participant meta-analysis of prospective studies. J Natl Cancer Inst 2014;106: dju240.
9. Patel N, Vogel R, Chandra-Kuntal K, Glasgow W, Kelavkar U. A novel three serum phospholipid panel differentiates normal individuals from those with prostate cancer. PLoS One 2014;9:e88841.
10. Lin HM, Mahon KL, Weir JM, Mundra PA, Spielman C, Briscoe K, et al. A distinct plasma lipid signature associated with poor prognosis in castration-resistant prostate cancer. Int J Cancer 2017;141:2112–20.
11. Rysman E, Brusselmans K, Scheys K, Timmermans L, Derua R, Munck S, et al. *De novo* lipogenesis protects cancer cells from free radicals and chemotherapeutics by promoting membrane lipid saturation. Cancer Res 2010;70:8117–26.
12. Sorvina A, Bader CA, Caporale C, Carter EA, Johnson IRD, Parkinson-Lawrence EJ, et al. Lipid profiles of prostate cancer cells. Oncotarget 2018;9:35541–52.
13. Burch TC, Isaac G, Booher CL, Rhim JS, Rainville P, Langridge J, et al. Comparative metabolomic and lipidomic analysis of phenotype stratified prostate cells. PLoS One 2015;10:e0134206.
14. Goto T, Terada N, Inoue T, Kobayashi T, Nakayama K, Okada Y, et al. Decreased expression of lysophosphatidylcholine (16:0/OH) in high resolution imaging mass spectrometry independently predicts biochemical recurrence after surgical treatment for prostate cancer. Prostate 2015;75:1821–30.
15. Goto T, Terada N, Inoue T, Nakayama K, Okada Y, Yoshikawa T, et al. The expression profile of phosphatidylinositol in high spatial resolution imaging mass spectrometry as a potential biomarker for prostate cancer. PLoS One 2014; 9:e90242.
16. Morse N, Jamaspishvili T, Simon D, Patel PG, Ren KYM, Wang J, et al. Reliable identification of prostate cancer using mass spectrometry metabolomic imaging in needle core biopsies. Lab Invest 2019;99:1561–71.
17. Randall EC, Zadra G, Chetta P, Lopez BGC, Syamala S, Basu SS, et al. Molecular characterization of prostate cancer with associated Gleason score using mass spectrometry imaging. Mol Cancer Res 2019;17:1155–65.
18. Waltregny D, Alami Y, Clausse N, de Leval J, Castronovo V. Overexpression of the homeobox gene HOXC8 in human prostate cancer correlates with loss of tumor differentiation. Prostate 2002;50:162–9.
19. Centenera MM, Hickey TE, Jindal S, Ryan NK, Ravindranathan P, Mohammed H, et al. A patient-derived explant (PDE) model of hormone-dependent cancer. Mol Oncol 2018;12:1608–22.
20. Chong J, Xia J. MetaboAnalystR: an R package for flexible and reproducible analysis of metabolomics data. Bioinformatics 2018;34:4313–4.
21. Gu Z, Gu L, Eils R, Schlesner M, Brors B. Circlize implements and enhances circular visualization in R. Bioinformatics 2014;30:2811–2.
22. Armstrong HK, Gillis JL, Johnson IRD, Nassar ZD, Moldovan M, Levrier C, et al. Dysregulated fibronectin trafficking by Hsp90 inhibition restricts prostate cancer cell invasion. Sci Rep 2018;8:2090.
23. Kim D, Pertea G, Trapnell C, Pimentel H, Kelley R, Salzberg SL. TopHat2: accurate alignment of transcriptomes in the presence of insertions, deletions and gene fusions. Genome Biol 2013;14:R36.
24. Anders S, Pyl PT, Huber W. HTSeq–a Python framework to work with high-throughput sequencing data. Bioinformatics 2015;31:166–9.
25. Robinson MD, McCarthy DJ, Smyth GK. edgeR: a Bioconductor package for differential expression analysis of digital gene expression data. Bioinformatics 2010;26:139–40.
26. Dieterle F, Ross A, Schlotterbeck G, Senn H. Probabilistic quotient normalization as robust method to account for dilution of complex biological mixtures. Application in 1H NMR metabonomics. Anal Chem 2006;78:4281–90.
27. Strimmer K. A unified approach to false discovery rate estimation. BMC Bioinformatics 2008;9:303.
28. Beer TM, Armstrong AJ, Rathkopf DE, Loriot Y, Sternberg CN, Higano CS, et al. Enzalutamide in metastatic prostate cancer before chemotherapy. N Engl J Med 2014;371:424–33.
29. Scher HI, Fizazi K, Saad F, Taplin ME, Sternberg CN, Miller K, et al. Increased survival with enzalutamide in prostate cancer after chemotherapy. N Engl J Med 2012;367:1187–97.
30. Griffith DA, Kung DW, Esler WP, Amor PA, Bagley SW, Beysen C, et al. Decreasing the rate of metabolic ketone reduction in the discovery of a clinical acetyl-CoA carboxylase inhibitor for the treatment of diabetes. J Med Chem 2014;57:10512–26.
31. Zhang AY, Chiam K, Haupt Y, Fox S, Birch S, Tilley W, et al. An analysis of a multiple biomarker panel to better predict prostate cancer metastasis after radical prostatectomy. Int J Cancer 2019;144:1151–9.
32. Meller S, Meyer HA, Bethan B, Dietrich D, Maldonado SG, Lein M, et al. Integration of tissue metabolomics, transcriptomics and immunohistochemistry reveals ERG- and Gleason score-specific metabolomic alterations in prostate cancer. Oncotarget 2016;7:1421–38.
33. Hansen AF, Sandsmark E, Rye MB, Wright AJ, Bertilsson H, Richardsen E, et al. Presence of TMPRSS2-ERG is associated with alterations of the metabolic profile in human prostate cancer. Oncotarget 2016;7:42071–85.
34. Dudka I, Thysell E, Lundquist K, Antti H, Iglesias-Gato D, Flores-Morales A, et al. Comprehensive metabolomics analysis of prostate cancer tissue in relation to tumor aggressiveness and TMPRSS2-ERG fusion status. BMC Cancer 2020; 20:437.

Downloaded from cancerres.aacrjournals.org on October 20, 2021. © 2021 American Association for Cancer Research.

Published OnlineFirst August 6, 2021; DOI: 10.1158/0008-5472.CAN-20-3863

35. Bandu R, Mok HJ, Kim KP. Phospholipids as cancer biomarkers: mass spectrometry-based analysis. Mass Spectrom Rev 2018;37:107–38.
36. Naguib A, Bencze G, Engle DD, Chio II, Herzka T, Watrud K, et al. p53 mutations change phosphatidylinositol acyl chain composition. Cell Rep 2015;10:8–19.
37. Saliakoura M, Rossi Sebastiano M, Pozzato C, Heidel FH, Schnöder TM, Savic Prince S, et al. PLCγ1 suppression promotes the adaptation of KRAS-mutant lung adenocarcinomas to hypoxia. Nat Cell Biol 2020;22:1382–95.
38. Falvella FS, Pascale RM, Gariboldi M, Manenti G, De Miglio MR, Simile MM, et al. Stearoyl-CoA desaturase 1 (Scd1) gene overexpression is associated with genetic predisposition to hepatocarcinogenesis in mice and rats. Carcinogenesis 2002;23:1933–6.
39. Fritz V, Benfodda Z, Rodier G, Henriquet C, Iborra F, Avances C, et al. Abrogation of *de novo* lipogenesis by stearoyl-CoA desaturase 1 inhibition interferes with oncogenic signaling and blocks prostate cancer progression in mice. Mol Cancer Ther 2010;9:1740–54.
40. Griffitts J, Tesiram Y, Reid GE, Saunders D, Floyd RA, Towner RA. *In vivo* MRS assessment of altered fatty acyl unsaturation in liver tumor formation of a TGF alpha/c-myc transgenic mouse model. J Lipid Res 2009;50:611–22.
41. Li J, Ding SF, Habib NA, Fermor BF, Wood CB, Gilmour RS. Partial characterization of a cDNA for human stearoyl-CoA desaturase and changes in its mRNA expression in some normal and malignant tissues. Int J Cancer 1994;57:348–52.
42. Romanuik TL, Ueda T, Le N, Haile S, Yong TM, Thomson T, et al. Novel biomarkers for prostate cancer including noncoding transcripts. Am J Pathol 2009;175:2264–76.
43. Tamura K, Makino A, Hullin-Matsuda F, Kobayashi T, Furihata M, Chung S, et al. Novel lipogenic enzyme ELOVL7 is involved in prostate cancer growth through saturated long-chain fatty acid metabolism. Cancer Res 2009;69:8133–40.
44. Wang HW, Wu YH, Hsieh JY, Liang ML, Chao ME, Liu DJ, et al. Pediatric primary central nervous system germ cell tumors of different prognosis groups show characteristic miRNome traits and chromosome copy number variations. BMC Genomics 2010;11:132.
45. Marien E, Meister M, Muley T, Fieuws S, Bordel S, Derua R, et al. Non-small cell lung cancer is characterized by dramatic changes in phospholipid profiles. Int J Cancer 2015;137:1539–48.
46. Swinnen JV, Vanderhoydonc F, Elgamal AA, Eelen M, Vercaeren I, Joniau S, et al. Selective activation of the fatty acid synthesis pathway in human prostate cancer. Int J Cancer 2000;88:176–9.
47. Centenera MM, Scott JS, Machiels J, Nassar ZD, Miller DC, Zininos I, et al. ELOVL5 is a critical and targetable fatty acid elongase in prostate cancer. Cancer Res 2021;81:1704–18.
48. Swinnen JV, Heemers H, Deboel L, Foufelle F, Heyns W, Verhoeven G. Stimulation of tumor-associated fatty acid synthase expression by growth factor activation of the sterol regulatory element-binding protein pathway. Oncogene 2000;19:5173–81.
49. Van de Sande T, De Schrijver E, Heyns W, Verhoeven G, Swinnen JV. Role of the phosphatidylinositol 3′-kinase/PTEN/Akt kinase pathway in the overexpression of fatty acid synthase in LNCaP prostate cancer cells. Cancer Res 2002;62:642–6.
50. Moreau K, Dizin E, Ray H, Luquain C, Lefai E, Foufelle F, et al. BRCA1 affects lipid synthesis through its interaction with acetyl-CoA carboxylase. J Biol Chem 2006;281:3172–81.
51. Kinlaw WB, Church JL, Harmon J, Mariash CN. Direct evidence for a role of the "spot 14" protein in the regulation of lipid synthesis. J Biol Chem 1995;270:16615–8.
52. Sabbisetti V, Di Napoli A, Seeley A, Amato AM, O'Regan E, Ghebremichael M, et al. p63 promotes cell survival through fatty acid synthase. PLoS One 2009;4:e5877.
53. Swinnen JV, Ulrix W, Heyns W, Verhoeven G. Coordinate regulation of lipogenic gene expression by androgens: evidence for a cascade mechanism involving sterol regulatory element binding proteins. Proc Natl Acad Sci U S A 1997;94:12975–80.
54. Harayama T, Riezman H. Understanding the diversity of membrane lipid composition. Nat Rev Mol Cell Biol 2018;19:281–96.
55. Rogers KR, Kikawa KD, Mouradian M, Hernandez K, McKinnon KM, Ahwah SM, et al. Docosahexaenoic acid alters epidermal growth factor receptor-related signaling by disrupting its lipid raft association. Carcinogenesis 2010;31:1523–30.
56. Gillet L, Roger S, Bougnoux P, Le Guennec JY, Besson P. Beneficial effects of omega-3 long-chain fatty acids in breast cancer and cardiovascular diseases: voltage-gated sodium channels as a common feature? Biochimie 2011;93:4–6.
57. Jude S, Roger S, Martel E, Besson P, Richard S, Bougnoux P, et al. Dietary long-chain omega-3 fatty acids of marine origin: a comparison of their protective effects on coronary heart disease and breast cancers. Prog Biophys Mol Biol 2006;90:299–325.
58. Kiebish MA, Han X, Cheng H, Chuang JH, Seyfried TN. Cardiolipin and electron transport chain abnormalities in mouse brain tumor mitochondria: lipidomic evidence supporting the Warburg theory of cancer. J Lipid Res 2008;49:2545–56.
59. Hilvo M, Denkert C, Lehtinen L, Muller B, Brockmoller S, Seppanen-Laakso T, et al. Novel theranostic opportunities offered by characterization of altered membrane lipid metabolism in breast cancer progression. Cancer Res 2011;71:3236–45.
60. Beckers A, Organe S, Timmermans L, Scheys K, Peeters A, Brusselmans K, et al. Chemical inhibition of acetyl-CoA carboxylase induces growth arrest and cytotoxicity selectively in cancer cells. Cancer Res 2007;67:8180–7.
61. Brusselmans K, De Schrijver E, Verhoeven G, Swinnen JV. RNA interference-mediated silencing of the acetyl-CoA-carboxylase-alpha gene induces growth inhibition and apoptosis of prostate cancer cells. Cancer Res 2005;65:6719–25.
62. Peck B, Schug ZT, Zhang Q, Dankworth B, Jones DT, Smethurst E, et al. Inhibition of fatty acid desaturation is detrimental to cancer cell survival in metabolically compromised environments. Cancer Metab 2016;4:6.

Downloaded from cancerres.aacrjournals.org on October 20, 2021. © 2021 American Association for Cancer Research.

Published OnlineFirst August 6, 2021; DOI: 10.1158/0008-5472.CAN-20-3863

Cancer Research
The Journal of Cancer Research (1916–1930) | The American Journal of Cancer (1931–1940)

AACR American Association for Cancer Research

Lipidomic Profiling of Clinical Prostate Cancer Reveals Targetable Alterations in Membrane Lipid Composition

Lisa M. Butler, Chui Yan Mah, Jelle Machiels, et al.

Cancer Res 2021;81:4981-4993. Published OnlineFirst August 6, 2021.

Updated version	Access the most recent version of this article at: doi:10.1158/0008-5472.CAN-20-3863
Supplementary Material	Access the most recent supplemental material at: http://cancerres.aacrjournals.org/content/suppl/2021/08/05/0008-5472.CAN-20-3863.DC1

Cited articles	This article cites 62 articles, 16 of which you can access for free at: http://cancerres.aacrjournals.org/content/81/19/4981.full#ref-list-1

E-mail alerts	Sign up to receive free email-alerts related to this article or journal.
Reprints and Subscriptions	To order reprints of this article or to subscribe to the journal, contact the AACR Publications Department at pubs@aacr.org.
Permissions	To request permission to re-use all or part of this article, use this link http://cancerres.aacrjournals.org/content/81/19/4981. Click on "Request Permissions" which will take you to the Copyright Clearance Center's (CCC) Rightslink site.

Downloaded from cancerres.aacrjournals.org on October 20, 2021. © 2021 American Association for Cancer Research.